International Telecommunication Union

ITU-R

Radiocommunication Sector of ITU

Report ITU-R P.2346-3

(05/2019)

Compilation of measurement data relating to building entry loss

P Series

Radiowave propagation

International Telecommunication Union

Foreword

The role of the Radiocommunication Sector is to ensure the rational, equitable, efficient and economical use of the radio-frequency spectrum by all radiocommunication services, including satellite services, and carry out studies without limit of frequency range on the basis of which Recommendations are adopted.

The regulatory and policy functions of the Radiocommunication Sector are performed by World and Regional Radiocommunication Conferences and Radiocommunication Assemblies supported by Study Groups.

Policy on Intellectual Property Right (IPR)

ITU-R policy on IPR is described in the Common Patent Policy for ITU-T/ITU-R/ISO/IEC referenced in Resolution ITU-R 1. Forms to be used for the submission of patent statements and licensing declarations by patent holders are available from http://www.itu.int/ITU-R/go/patents/en where the Guidelines for Implementation of the Common Patent Policy for ITU-T/ITU-R/ISO/IEC and the ITU-R patent information database can also be found.

Series of ITU-R Reports

(Also available online at http://www.itu.int/publ/R-REP/en)

Series	Title
BO	Satellite delivery
BR	Recording for production, archival and play-out; film for television
BS	Broadcasting service (sound)
BT	Broadcasting service (television)
F	Fixed service
M	Mobile, radiodetermination, amateur and related satellite services
P	**Radiowave propagation**
RA	Radio astronomy
RS	Remote sensing systems
S	Fixed-satellite service
SA	Space applications and meteorology
SF	Frequency sharing and coordination between fixed-satellite and fixed service systems
SM	Spectrum management

***Note**: This ITU-R Report was approved in English by the Study Group under the procedure detailed in Resolution ITU-R 1.*

Electronic Publication
Geneva, 2019

REPORT ITU-R P.2346-3

Compilation of measurement data relating to building entry loss

(2015-2016-2017-2019)

Scope

This Report provides a compilation of data on building entry loss, and is intended to supplement the material in Recommendation ITU-R P.2040.

TABLE OF CONTENTS

1 Introduction

This Report provides a compilation of empirical data on building entry loss (BEL), and is intended to support the material in Recommendation ITU-R P.2040.

It is also expected that the material in this Report will be of value in the development of new propagation models.

Annex 1 provides information that has been found helpful in planning broadcast and other point-to-area radio services at frequencies below 3 GHz. The contents of this Annex encapsulate measurement data but do not report on a specific measurement campaign.

It should be noted that the measurements recorded in this report have been made using a wide variety of methods. In particular, the definition of BEL may differ from that given in Recommendation ITU-R P.2040. Readers are advised to evaluate the material carefully to ensure that it is appropriate for the purpose intended.

2 Building entry loss measurements (VHF & UHF, Europe)

Measurements have been carried out in Germany and the United Kingdom to determine values of BEL and other parameters to be used in planning indoor reception of broadcasting services.

The German measurements were made at two frequencies in the VHF band used for digital audio broadcasting and two frequencies in the UHF band. The median values of the BEL over all measurements made in buildings typical for Germany were 9.1 dB at 220 MHz, 8.5 dB at 223 MHz, 7.0 dB at 588 MHz and 8.5 dB at 756 MHz.

The penetration loss from the front of the building (the side with higher signal level) into a room on the opposite side has median values of 14.8 dB at 220 MHz, 13.3 dB at 223 MHz, 17.8 dB at 588 MHz and 16 dB at 756 MHz.

Over all measurements, the median values of the location variation standard deviations are 3.5 dB for the 220 and 223 MHz signals with 1.5 MHz bandwidth and 5.5 dB for the 588 and 756 MHz signals with 120 kHz bandwidth.

The United Kingdom measurements were made at a number of frequencies in the UHF band.

The median BEL at UHF was found to be 8.1 dB with a standard deviation of 4.7 dB. However, the value for rooms on the side of the building furthest from the transmitter was 10.3 dB, whereas the corresponding value for rooms on the side of the building nearest to the transmitter was 5.4 dB; a difference of about 5 dB.

A median value of 13.5 dB was measured for the outdoors height gain between 1.5 and 10 m. The locations of the measurements were suburban.

The median value of the difference in field strength between ground floor and first floor rooms was found to be 5.4 dB.

The standard deviation of the variation of field strength within rooms was about 3 dB.

The standard deviation of the variation of field strength measured for a floor of a house was about 4 dB.

Despite differences in the frequencies and bandwidths of the measurements, there is very good agreement between the German and United Kingdom measurements.

3 Building entry loss measurements (5.2 GHz, Japan)

Entry loss measurements were made in Japan on 12 office buildings at distances from the transmitter of up to 1 km.

The additional path loss to points within a building was measured relative to the outdoor field averaged along a path around the building at 1.5 m height. Note that the use of the fixed height reference differs from the definition of building entry loss given in Recommendation ITU-R P.2040, and will lead to negative values of entry loss for higher floors of the building.

The data from these measurements has been fitted by the following expression for excess path loss with respect to the averaged 1.5 m value:

$$\Delta Loss(\text{dB}) = 0.41 \cdot d - 0.5 \cdot h - 2.1 \cdot \log(f) - 0.8 \cdot LoS + 11.5 \quad (1)$$

where:

d : 0 to 20 m; the distance from the window (m)

h : 1.5 to 30 m; the height from the ground (m)

f : 0.8 to 8 GHz; the frequency (GHz)

LoS : 1 for line-of-sight, LoS = 0 for non-line-of-sight.

4 Exit loss measurements

Figure 1 shows a picture of the house used in the measurement. It is a typical bi-level frame house in Japan. The site is approximately 11 m × 12 m. The outer walls have two or three windows on each side. The outside of the exterior walls is covered by painted wooden boards and the inside of the walls are covered with plasterboard. Glass fibre insulation fills the space between inside the walls. A transmitting antenna is set near the centre of the lower floor. The antenna height above the floor level is 1.5 m. A 5.2-GHz continuous wave is transmitted from a vertically polarized dipole antenna. A receiver connected to a dipole antenna is set on a pushcart and moved around the house. The receiving antenna height is set at 2.2 m from the ground level to make it equal in height to the transmitting antenna. Before conducting outside measurements, the received level is measured at several points inside the house.

FIGURE 1

Photo of house

P.2040-29

4.1 Measured result

Figure 2 is a contour map of the received level. High levels are expressed as dark colour and low levels are expressed as light colours. The map shows that intense radiowaves spread out through the windows and propagate to relatively far distances. In this figure, the white part in the upper right corner indicates the location where we could not take measurements due to a barn. The other white part in the upper left side is due to a hedgerow.

FIGURE 2

Contour map of the received level

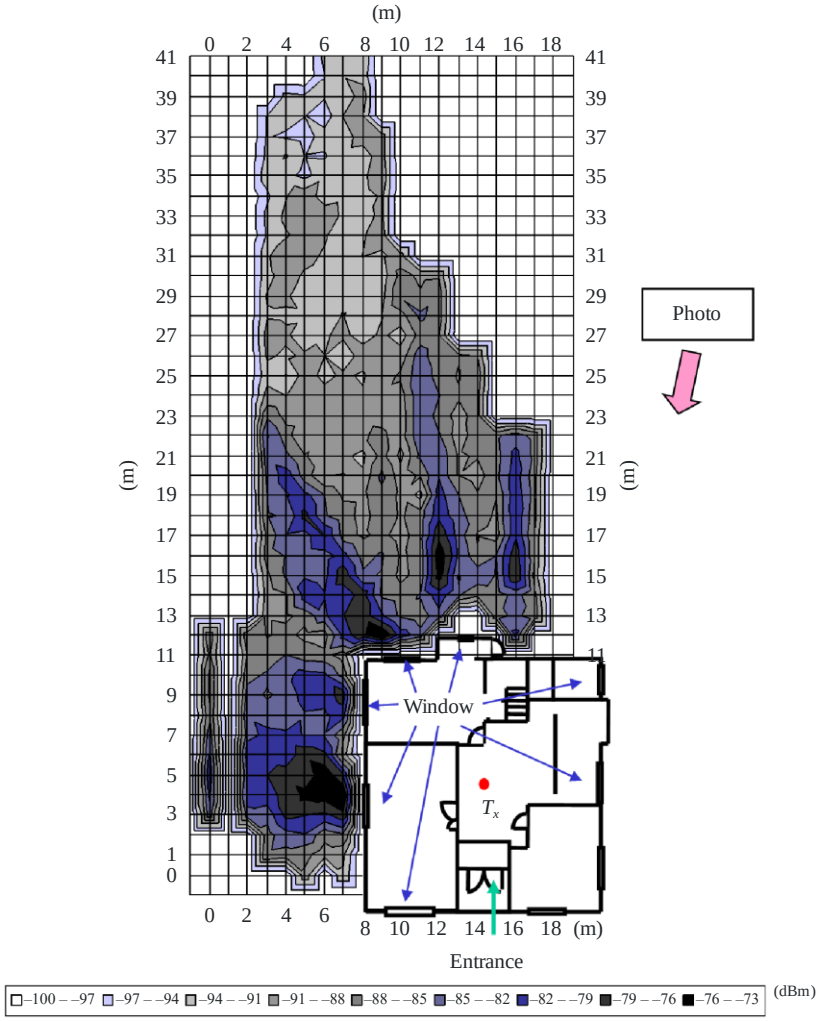

Figure 3 shows the distance dependency of the path loss. The abscissa is a linear scale. The blue circles represent outdoor data and the red triangles represent indoor data. The path loss is approximated by the following equation.

$$L(\text{dB}) = 20\log(f\,(\text{MHz})) + N\log(d(\text{m})) - 27.55 + L_f(\text{dB}) \quad (2)$$

where N is the attenuation coefficient for distance and L_f is the additional attenuation caused by wall penetration for example. When N and L_f equal 20 and 0, respectively, this equation expresses the free-space path loss.

Three calculated lines are shown in Fig. 3. The black dashed line is the free-space path loss at 5.2 GHz. The red solid line approximates the indoor data set. Its L_f equals zero but N equals 30 for a large decline compared to that for free space. The blue solid line has N = 20 and L_f = 15. The curve parallels that for free-space curve but with a drop of 15 dB. This result indicates that the path loss increases with a large N within the house and the increase becomes gradual after it exits the house. This feature is clearly observed in Fig. 3.

FIGURE 3

Distance dependencies of the path loss (linear scale)

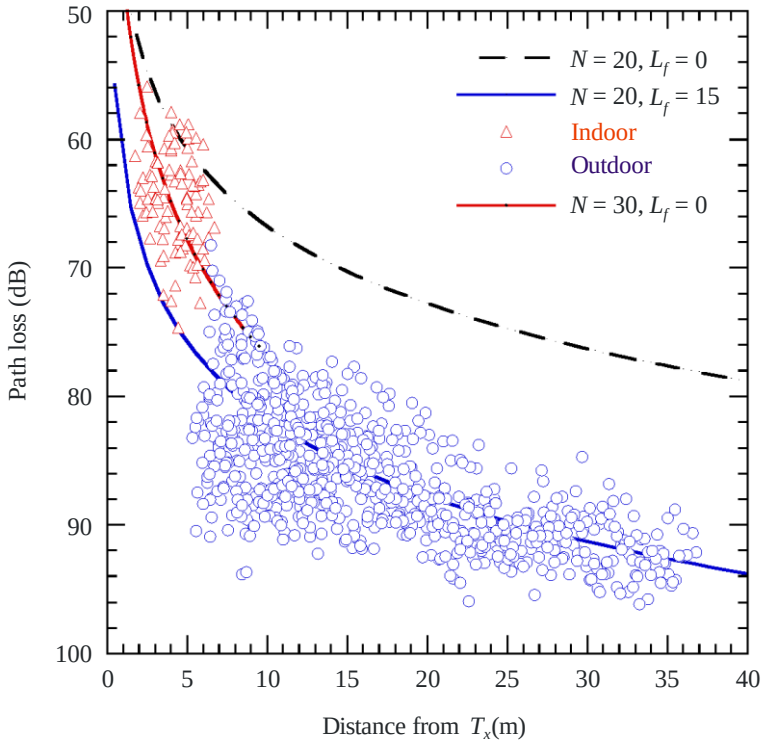

P.2040-31

Based on these data, cumulative probabilities of the path loss are derived in Fig. 4. The difference between these two probabilities is approximately 18 dB. This indicates that the radiowave exits from the house with an attenuation of approximately 18 dB and propagates with the same attenuation coefficient in distance as that for free space.

FIGURE 4

Cumulative probabilities of measured path loss data

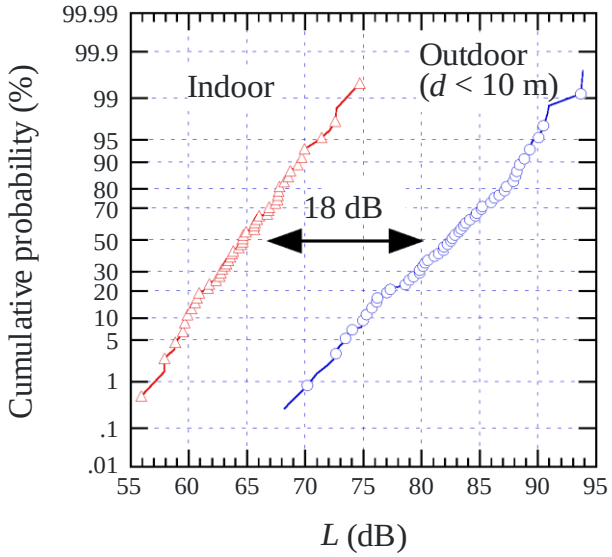

P.2040-32

5 Slant path measurements (500 MHz - 6 GHz)

5.1 UHF satellite signal measurements (860 MHz – 2.6 GHz)

Representative UHF satellite signal attenuation observed within rooms located near an exterior wall in timber-framed private homes is summarized in Table 1. For interior rooms, 0.6 dB must be added to the tabulated values. For timber-framed buildings the attenuation shows little variation with weather or path elevation angle but, as the Table illustrates, there is a systematic variation with frequency, polarization, construction materials, insulation and position within the structure. Some aluminium-backed insulating and construction materials contribute up to 20 dB of loss.

TABLE 1

UHF signal attenuation (dB) through timber-framed buildings*

Building condition		**Frequency (MHz) and polarization (Horizontal: H, Vertical: V)**			
Exterior	Insulation (non-metallic type)	860 H	860 V	1 550 V	2 569 V
Wood siding	Ceiling only	4.7	2.9	5.0	5.8
	Ceiling and wall	6.3	4.5	6.6	7.4
Brick veneer	Ceiling only	5.9	4.1	6.2	7.0
Bricks	Ceiling and wall	7.5	5.7	7.8	8.6

* The Table is for rooms located near to the exterior wall; for interior rooms, 0.6 dB should be added.

5.2 Slant-path measurements from towers or high rise buildings

Measurements of building entry loss using 18 to 20 m towers to simulate a satellite transmitter were performed in the bands 700 MHz to 1.8 GHz and 500 MHz to 3 GHz to determine the mean loss and spatial variability in a variety of buildings. There are insufficient data to give precise prediction methods, but the data in Tables 2 to 3 are indicative.

TABLE 2

Signal distributions at the average position and best position within buildings (over the frequency range 700 to 1 800 MHz)

Building number	Construction	Elevation angle	Average position		Best position	
			Mean loss (dB)	Standard deviation (dB)	Mean loss (dB)	Standard deviation (dB)
1	Corner office, large windows, single-story building. Concrete block, plasterboard, double-glazing. Concrete roof on steel beams	27.5° (LoS through window, azimuth angle between wall and LoS is 50°)	7.9	5.5	4.2	4.2
2	Small room with windows being 5/8 of exterior wall	18° (LoS through window, azimuth angle between wall and LoS is 50°)	9.1	4.4	5.4	3.7
3	Corner foyer, large reflective glass door in half of one exterior wall. External walls concrete, internal walls plasterboard on metal frame	16° (LoS through window, 45° azimuth angle between one wall and LoS, both exterior walls illuminated by transmitter)	15.4	8.4	9.7	6.7
4	Sheet metal shack with plywood interior. One small unscreened window on each of two sides, metal-covered door	25° (azimuth angle between wall and LoS is 60°)	9.7	6.3	5.2	4.9
5	Two-story wood-side house, rockwool insulation (walls and attic); gypsum board, no metallic heat-shield. No metallic screens on windows. Wood-shingled roof	25° (azimuth angle between wall and LoS is 45°)	9.0	4.5	5.4	3.7
6	Empty sheet-metal mobile trailer home, metal frame windows with metal screens	25° (azimuth angle between wall and LoS is 45°)	24.9	3.8	19.8	3.4

TABLE 3

Median loss at the average position and best position within buildings as a function of frequency (Construction details and elevation angle as in Table 2)

Building number	Average position	Best position
(As in Table 2)	750-1 750 MHz	750-1 750 MHz
1	5-11 dB	2-6 dB
2	5-14 dB	2-5 dB
3	17-18 dB	12-13 dB
4	9-11 dB	5-6 dB
5	5-11 dB	3-5 dB
6	20 to > 24 dB	16-22 dB

TABLE 4

Signal distributions at the average position within buildings (estimated over the frequency range 500-3 000 MHz)

Building number	Construction	Elevation angle (degrees)	Average position	
			Mean loss (dB)	Standard deviation (dB)
1	Entry lobby in single storey building – concrete tilt wall, tar roof	18	13	10
2	Office in single storey building – block brick, tar roof	38	9	7
3	Two-storey wood frame farmhouse, metal roof, no aluminium heat-shield	33	5	4
4	Hallway and living room of two-storey woodframe house, metal roof, aluminium heat-shield	41	19.5	12
5	Motel room in two-storey building, brick with composite roof	37	13	6
6	Lobby of two-storey building, glass and concrete, tar roof	26	12	5

In the first set of measurements (Tables 2 and 3), the first three buildings had elevation angles such that the room was illuminated through a window with a direct LoS from the transmitter. The elevation angles were below 30° to allow side illumination of the buildings.

In the case of building number 3 in these tables, losses through the reflective glass door were about 15 dB greater than when the door was open.

The results of another study are similar, with mean attenuation levels (in the frequency range 500 to 3 000 MHz) varying between 5 dB for a woodframe house with metal roof and no aluminium heat-shield, to 20 dB for a similar house with an aluminium heat-shield. Table 4 shows a summary of the measured mean attenuation values.

Note that for some of the measurements, values obtained near a window or an open door, are included in the averaging. In the motel (building 6), attenuation when the direct path penetrated a brick wall was 15 to 30 dB below the LoS value. Levels inside building 4 varied from 25 to 45 dB below the LoS value, due to the metal roof and aluminium heat-shield.

Note also that the measurements were on stationary paths. There is evidence that close-in multipath effects will give rise to fluctuations in received signal level should the transmitter or receiver move. This has implications particularly for low-Earth orbit (LEO) systems where the transmitter is moving rapidly with respect to the receiver.

The measurements indicate that attenuation increases with frequency by about 1 to 3 dB/GHz in buildings 1, 2, 4, and 6, by 6 dB/GHz in the least attenuating building (building 3), and shows almost no change with frequency in the glass-walled building 5. Since the values given above are averaged over the frequency range 500 MHz to 3 GHz, they are expected to be slightly optimistic for the 1 to 3 GHz range.

For the six buildings identified in Table 2, 1.6 GHz and 2.5 GHz measurements were performed and analysed to determine the median, 5% and 95% levels of relative signal loss when the antennas were moved horizontally over multiple 80 cm intervals. The buildings were illuminated from the side, and the signals received inside the outside wall (one-wall entry). Azimuthally omnidirectional antennas were used to receive the transmitted signals. Statistics derived from these measurements are summarized in Fig. 5. These data indicate the magnitude and variations of fading that are possible for signal transmission through building walls. Note that on occasions, multipath conditions yield relative signal levels in excess of 0 dB.

FIGURE 5

Median, 5% and 95% levels of building entry power loss relative to unobstructed LoS at 1.6 GHz and 2.5 GHz for the six buildings identified in Table 2 (designated by 1 to 6 in the Figure). For each building, the 1.6 GHz (L) and 2.5 GHz (S) statistics are shown separately

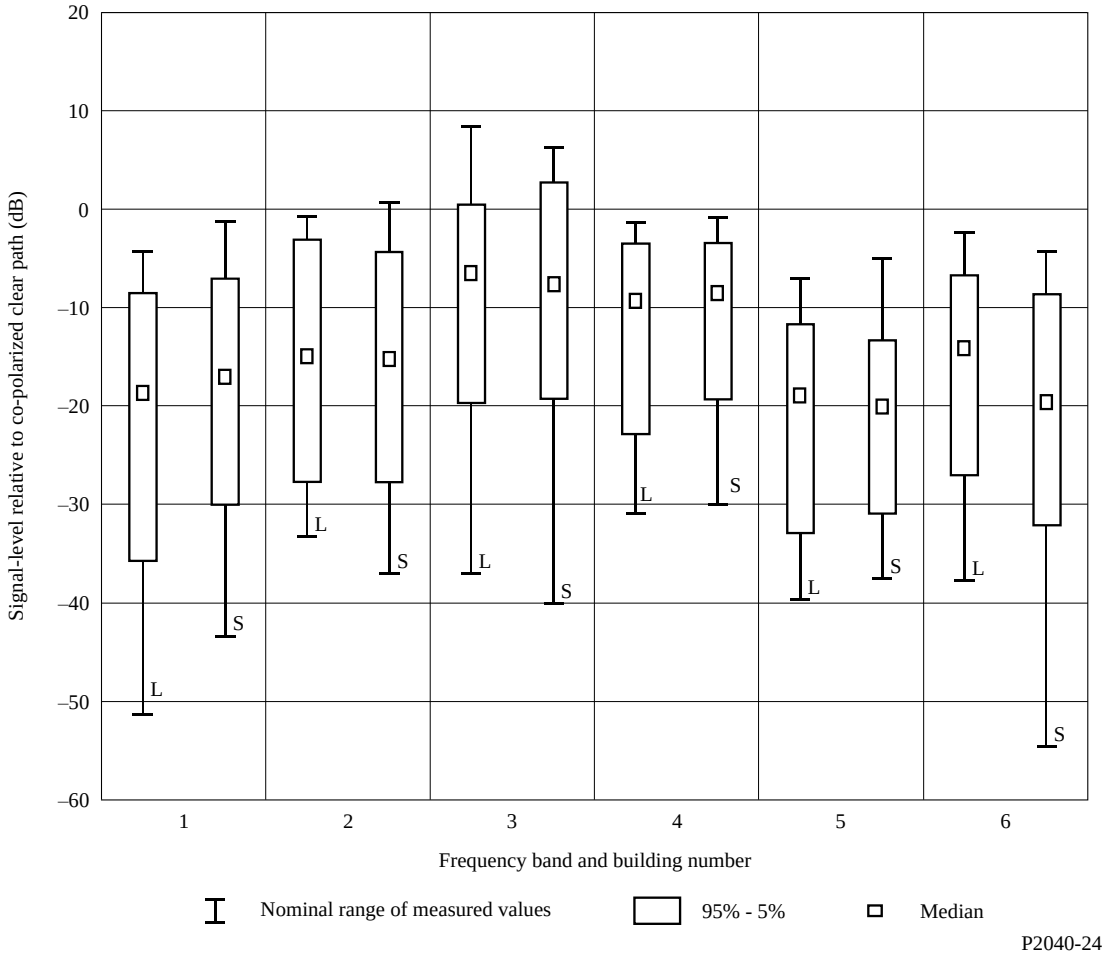

None of the available measurements at frequency bands below 3 GHz provides information for elevation angles above 41°. However, the large losses through metal structures (building 6 in Tables 2 and 3; building 4 in Table 3) suggest that attenuation for a direct path through a metal roof will be of the order of 20 dB. The losses of 15 to 30 dB for a brick wall in building 4 of Table 3 are relevant for higher elevation angles as well.

The elevation angle dependence of building entry loss was measured in the 5 GHz band at two different elevation angles by using high-rise buildings to simulate the reception of satellite signals. In an office-type room, the measured medians of the excess building entry loss were 20 dB and 35 dB for elevation angles of 15° and 55°, respectively.

5.3 Helicopter measurements to office building

The elevation and azimuth angle dependencies of building entry loss around 5 GHz were measured at different positions within an eight-storey building on three different floors. A helicopter was used to simulate a satellite transmitter. The received signal was continuously recorded, as well as the position of the helicopter by means of a differential global positioning system (GPS) receiver. The experimental conditions and averaged measurement results are summarized in Table 5. The behaviour of the building entry loss with respect to path elevation angle is shown in Fig. 6, and the behaviour with respect to azimuth in Fig. 7 for elevation angles of 15° and 30°.

FIGURE 6

Building entry loss at 5.1 GHz at sections 1, 2 and 3 for floors 2, 5 and 6. The angle Ψ_E is positive-defined when looking to the north and negative-defined to the south $|\Psi_E| = 90° - \varepsilon$ where ε is the elevation angle

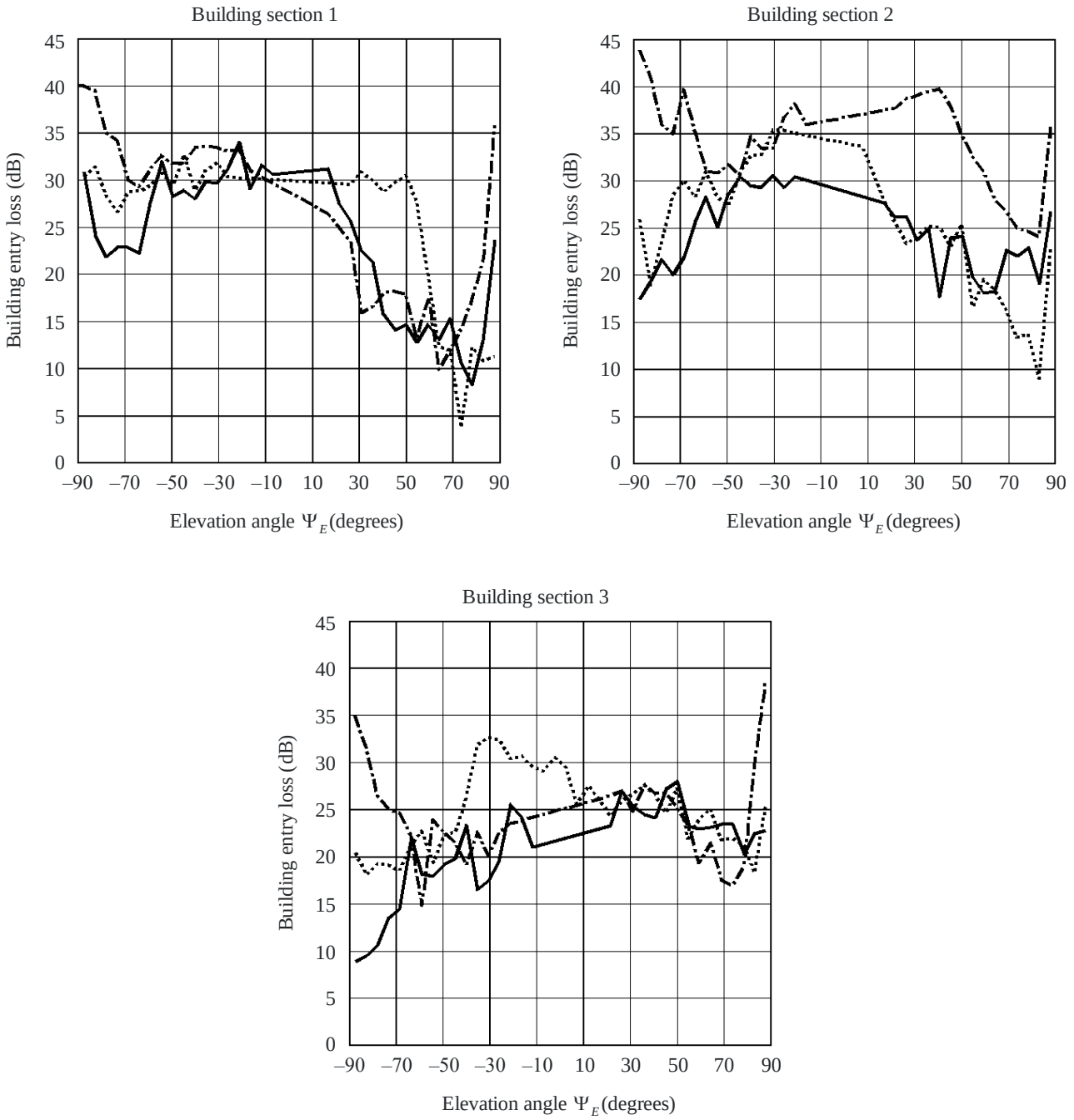

Building section 1: rooms with windows facing helicopter transmitter.

Building section 2: center of corridor.

Building section 3: rooms with windows not facing helicopter transmitter.

P.2040-25

FIGURE 7

Building entry loss at 5.1 GHz for elevation 15° and 30° at the four different indoor antenna positions. Numbers 1 and 2 are located close to an outer wall, whereas numbers 3 and 4 are located in the corridor

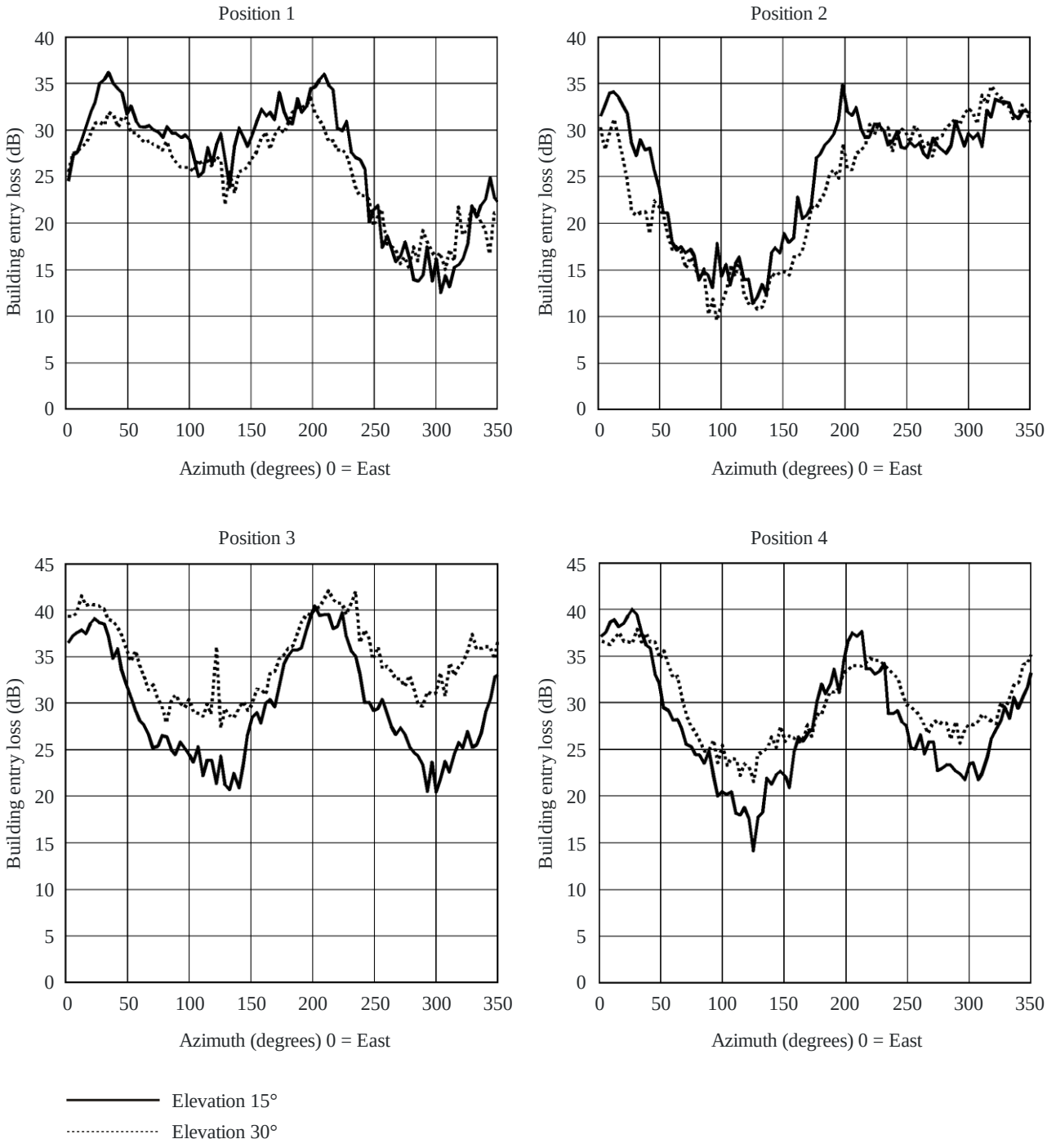

TABLE 5

Average median building entry loss and observed range of the median building entry loss measured at 5.1 GHz for different positions in an office building

	Type of measurements (helicopter trajectory)	Average of the median building entry loss for different receiver positions in the building (dB)	Observed range of the median building entry loss (dB)
Eight-storey building with seven storeys above ground and one extra storey placed on the former roof, brick-walls and windows placed in strips: behind the brick-wall there is a 10 cm thick concrete wall; windows made of two layers of plain non-thermal glass, storeys separated by 3.5 m with 2.5 m from floor to ceiling, two layers of plaster with wooden laths in between separate the rooms; interior walls facing the corridor are in most cases made of glass, rooms commonly furnished with desks and bookshelves; each storey has three sections, a corridor with office rooms at the sides	Elevation angle measurements (linear, perpendicular to the long side of the building)	19.1	~ 5-45
	Azimuth angle measurements (circular at elevation angles of 15° and 30°)	22.3	~ 10-42

Measurements at 2.57 GHz and 5.2 GHz using an igloo shaped flight pattern were performed inward to three different buildings, one of them in the Graz/Austria area, another two in the Vienna/Austria area, covering various building types. The transmitter was carried by a helicopter, on which a steerable helix antenna was mounted. The measurements were performed with a high resolution, pseudo random sequence based channel sounder with a chipping rate of 100 Mcps and 200 MHz bandwidth. The transmit antenna was right-hand circularly polarized (RHCP) while the receive antenna for the channel sounder case consisted of a set of patch antennas with two orthogonal linear polarizations covering a surface that approximates a semi-sphere.

Table 6 gives an overview of the inward building locations.

TABLE 6

Overview on buildings measured

Building		Location	#RX locations	Façade/roof material
Millennium Tower skyscraper	22nd floor 44th floor	Vienna	2 2	Metal grid and glass panels, coated glass with sun protective layer/Reinforced concrete
Graz airport	Gate Area Conference room	Feldkirchen near Graz	4 1	Steel, metal construction elements, coated glass with sun protective layer/Steel, metal sheets, layer of gravel
Office building FFG	Inner city office building, highest floor	Vienna	2	Reinforced concrete/coated windows

The building entry loss shown in Table 7 was calculated by subtracting the Average Power Delay Profile from an outdoor reference measurement from the Average Power Delay Profile measurement inside the buildings. The building entry loss for various distances to the window directed to the transmitter at 5.2 GHz is presented in Table 8.

TABLE 7

Entry loss (dB) for different elevation and relative azimuth angles at 2.57 and 5.2 GHz

Building	Relative azimuth to facade normal	2.57 GHz				5.2 GHz			
		Elevation				Elevation			
		15	30	45	60	15	30	45	60
Millennium Tower 44th floor	0	22.86	24.42	21.53	23.95	30.40	27.65	32.09	29.77
	–30	22.13	22.17	25.21	24.59	28.34	30.42	32.43	33.31
	–60	24.44	23.71	25.91	24.60	29.00	31.31	33.57	34.97
	–90	25.40	29.24	27.21	26.77	32.65	34.23	37.24	38.21
Millennium Tower 22nd floor	0	28.04	28.31	28.13	28.28	36.53	37.55	35.38	39.45
	–30	28.70	29.60	29.60	27.59	31.84	36.57	37.51	35.34
	–60	32.26	33.17	33.66	35.38	35.19	37.12	35.90	39.65
	–90	35.30	42.22	37.80	–	43.20	43.80	47.02	46.52
Office Building	0	21.69	29.23	26.18	31.40	26.52	31.13	34.13	35.28
	30	26.49	34.90	31.10	33.00	33.12	33.49	36.51	34.08
	60	27.43	–	35.90	36.13	34.29	34.16	36.30	35.73
	90	–	38.09	–	–	–	–	–	–
Airport – Gate Area	0	18.18	–	23.68	23.00	28.36	35.76	–	37.97
	–30	15.09	21.12	19.11	27.10	–	–	–	37.98
	–60	18.25	26.13	21.96	25.42	27.67	37.76	–	–
	–90	–	27.71	23.69	24.61	34.31	–	–	–
Airport – Conference Room	0	11.81	12.62	–	10.84	15.19	19.68	19.37	19.09
	–30	11.69	–	15.05	13.63	17.73	19.37	20.03	–
	–60	16.65	17.87	17.66	16.35	22.79	–	24.70	22.38
	–90	18.52	20.10	17.43	–	25.17	24.32	23.43	–

TABLE 8

Entry loss (dB) at 5.2 GHz for different elevation angles relative to the distance to the window directed to the transmitter located at 0 degrees relative azimuth angle to the façade normal

Building	Distance to window (m)	Elevation			
		15	30	45	60
Millenium Tower 44th floor	1.4	–	25.30	31.41	27.80
	2.4	–	27.34	31.16	27.81
	3.4	–	29.72	31.64	30.58
	4.4	–	25.6	32.19	28.88
	5.4	30.40	29.08	33.43	30.34
Airport – Gate Area	0.5	30.63	35.07	–	38.72
	2.5	30.28	35.01	–	37.09
	4.5	29.97	35.96	–	38.03
	6.5	16.40	36.85	–	–

5.4 Balloon measurements to domestic buildings (1-6 GHz)

Measurements have been made in the United Kingdom of building entry loss into a number of domestic buildings of traditional construction. These measurements were made at 1.4 GHz, 2.4 GHz and 5.8 GHz, and used a tethered balloon to explore a range of elevation angles.

Details of measurement locations are given in Table 9.

TABLE 9

Building	Date	Measurement locations
Small offices/flats (3 floors)	1985	Measurements in two offices (1st floor)
Detached house (3 floors)	1905	Kitchen (ground) and bedroom (1st floor)
Terraced house (2 floors and attic)	1880	Living room (ground), Bedroom (1st floor) and study (2nd floor)
Terraced house (2 floors)	1965	Dining room & living room (ground), hallway (1st floor)

The measurements were made using CW transmitters suspended from a tethered helium balloon, which allowed elevation angles up to around 70º to be explored. The receiver was switched between an indoor measuring antenna and an external reference antenna. The measuring antenna was moved along a 1 m track under computer control, to allow spatial averaging of measurements.

Omnidirectional antennas were used at both transmitter and receiver, and corrections were applied for antenna vertical radiation patterns, and the difference in free-space loss between the reference and measuring antennas.

Following the corrections described above, a data set giving the mean penetration loss for each test location was obtained. The cumulative distribution function (CDF) of these results is shown in Fig. 8, and represents the statistics of mean local loss with respect to all 11 receiver locations, at all elevation angles. The receiver locations were randomly chosen and were almost entirely NLoS to the balloon.

FIGURE 8

Overall statistics of building entry loss

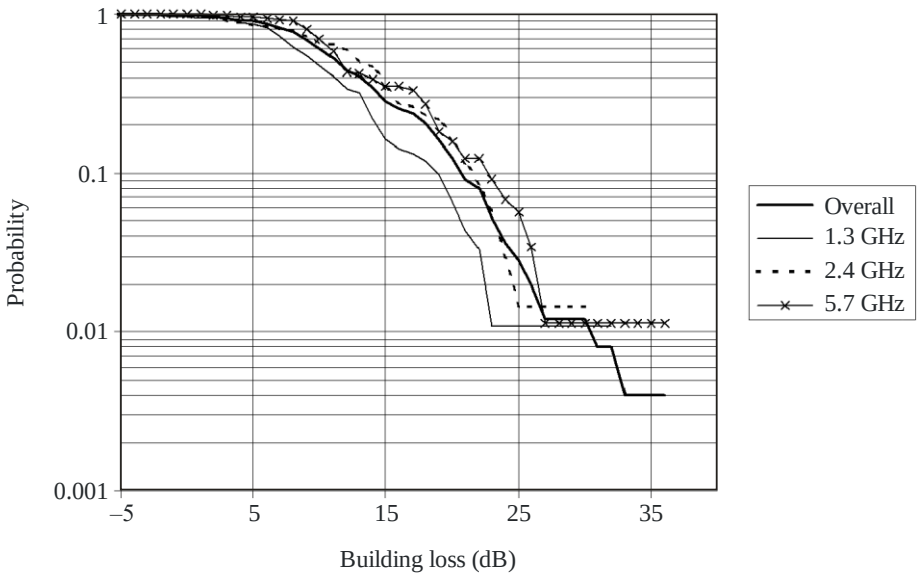

P.2040-27

The mean value of building entry loss, at all frequencies, is 11.2 dB. The results shown in Fig. 7 show a slight frequency dependence in the results. Mean values of penetration loss are 9.2 dB at 1.3 GHz, 11.2 dB at 2.4 GHz and 12.7 dB at 5.7 GHz.

Figure 9 shows the elevation dependence of the measurements (polynomial curves fitted to measurement points).

FIGURE 9

Mean values for each frequency compared

Dependence on path elevation

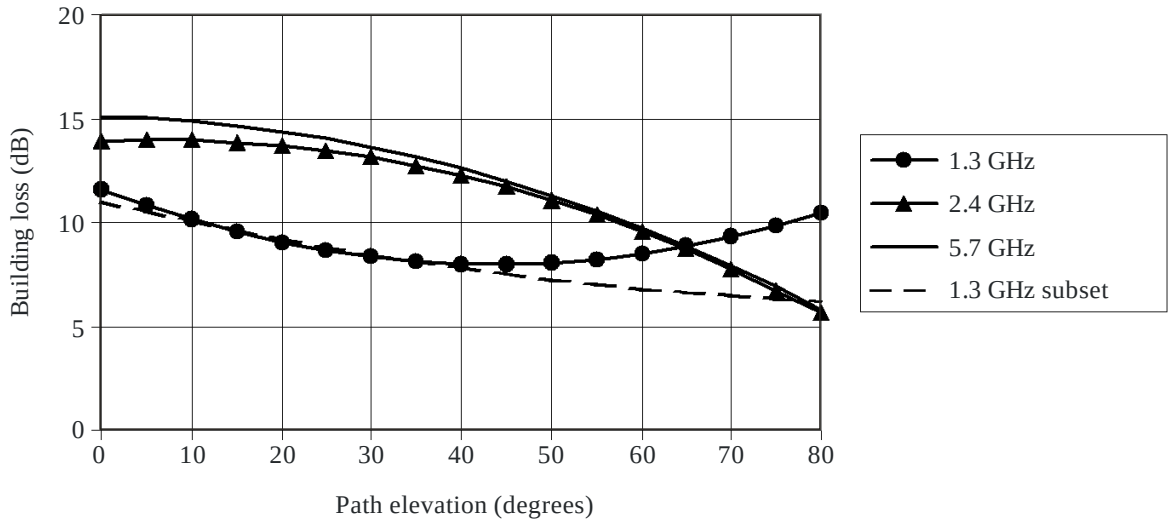

P.2040-28

The results at 1.3 GHz show an anomalous increase in the penetration loss for higher elevation angles. Examination of the measurement data shows that this effect is due to one set of measurements and the effect of excluding this data is shown in the dotted curve.

It can be seen that, except at the lowest frequency, there is a slight decrease in penetration loss for higher elevation angles. This decrease in building loss with elevation runs counter to the assumptions made in some previous models. It may be that this behaviour is characteristic of domestic buildings, where floors and ceilings are typically of light wooden construction.

Some dependence, of the averaged results, on the building floor is apparent, with the ground floor and first floor results generally showing some 5-8 dB greater loss than those for the second floor. It should be borne in mind, however, that only one set of measurements was made on a second floor, and the location was a converted roof space, used as a home office.

Building shadowing loss measurements

Measurements have been carried out in Australia to determine values of building shadowing loss to be used in planning frequency sharing between the fixed-satellite service and the fixed service.

The building shadowing loss is defined as transmission loss through a building.

The frequency is 11 GHz. Polarization is vertical and horizontal.

Table 10 shows the average results of measurements at 11 GHz through the different types of buildings.

TABLE 10

Mean and standard deviation of loss by polarization and building type

Test site	Avg. loss (V-Pol)	Std. dev.	Avg. loss (H-Pol)	Std. dev.
1 Wooden building (lengthways)	26.4 dB	7.1	–	–
1A Wooden building (widthways)	10.0 dB	7.0	8.3 dB	5.0
2 Concrete/brick building	30.1 dB	5.0	28.6 dB	5.5
3 Metal shed	36.4 dB	4.1	35.0 dB	3.2

The measurements show a high dependence on construction material in determining:

– the primary mode of propagation; and

– the amount of attenuation caused by the obstacle.

Wooden construction materials caused the lowest average attenuation of 10.0 to 25.0 dB, brick and concrete between 25.0 and 35.0 dB and metal between 35.0 and 40.0 dB. The primary mode of propagation for wooden and concrete structures was transmission, while the dominant mode of propagation for metal structures was propagation by diffraction.

During propagation by diffraction, there was a high dependence on diffraction angle. As the diffraction angle increased from the corners (i.e. towards the centre of the building shadow) the amount of attenuation due to diffraction increased (on the order of 5.0 to 10.0 dB).

Although there was dependence on polarization at each measurement point, there was little to no dependence on polarization or path length from the standpoint of averaged data. The average attenuation variation between horizontal and vertical polarizations was less than 1.5 dB.

Wooden construction materials caused the lowest average attenuation of 10.0 to 25.0 dB, brick and concrete between 25.0 and 35.0 dB and metal between 35.0 and 40.0 dB. The primary mode of propagation for wooden and concrete structures was transmission, while the dominant mode of propagation for metal structures was propagation by diffraction.

During propagation by diffraction, there was a high dependence on diffraction angle. As the diffraction angle increased from the corners (i.e. towards the centre of the building shadow) the amount of attenuation due to diffraction increased (on the order of 5.0 to 10.0 dB).

Although there was dependence on polarization at each measurement point, there was little to no dependence on polarization or path length from the standpoint of averaged data. The average attenuation variation between horizontal and vertical polarizations was less than 1.5 dB.

6 Impact of thermally-insulating materials (88 MHz – 5.8 GHz)

6.1 Introduction

A large body of measured data already exists and this study could add only a small amount to this. The focus was therefore on a careful assessment of the impact of well-characterised changes to building insulation.

A series of measurements have been undertaken on a small detached house; measurements of entry loss were made to the un-modified structure, with metalised windows and when fitted with foil-backed plasterboard. A further set of measurements was also made with window apertures covered in foil, as a diagnostic experiment, and to test the sensitivity to different incidence angles. Measurements were also made in a contrasting building – a much larger Victorian structure ('The Mansion').

Measurements made at five frequencies: 88 MHz, 217 MHz, 698 MHz, 2 410 MHz and 5 760 MHz; in the trials, a transmitter was carried so as to fully explore each room in a semi-random manner, with received field strength being logged at an outdoor receiver positioned some 30-50 m from the building. Each room in a building was characterised in terms of the median signal level, and this was related to the field immediately outside the building at the same height to determine the building entry loss.

6.2 Median building entry loss

Overall summary results are given in the figure below (in which 'win1' and 'win2' indicates the fitment of different metalised windows and 'FBP' of foil-backed plasterboard). All curves relate to measurements in the small, modern, house except for the single curve identified as 'mansion'.

FIGURE 10

Overall summary building entry loss results

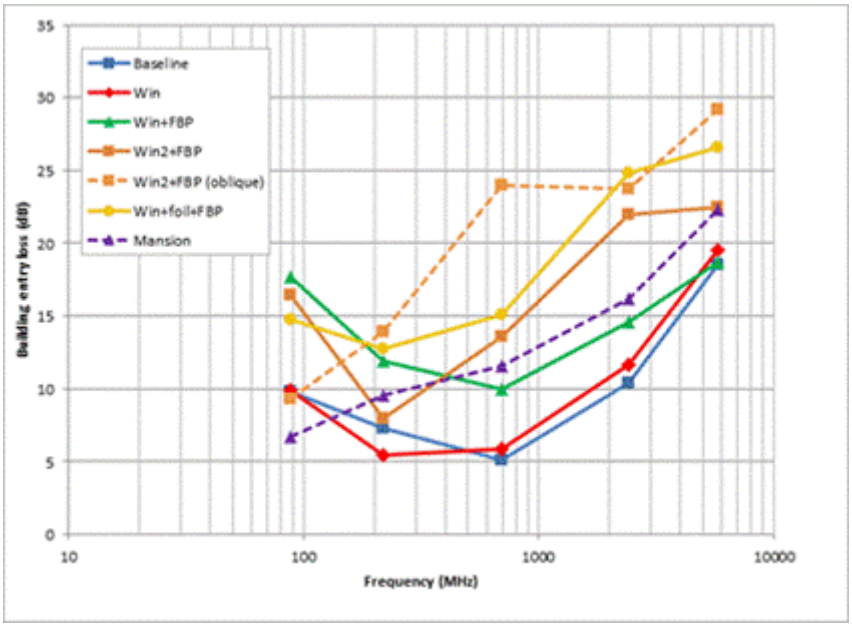

The relatively high losses seen at 88 MHz appear to be an anomalous feature of the small house; the effect was not seen when a path between terminals was more oblique with respect to the front wall of the house (although the results for 698 MHz now seem anomalous, illustrating the complexity of the mechanisms involved).

6.3 Variability of loss within a room

Data has also been gathered on signal variability, which is significantly higher inside buildings due almost entirely to multipath effects. Figure 10 shows time-series[1] of measurements at 88 MHz and 5.7 GHz (bottom), illustrating the variability of signals within one room of the house, compared with the variability measured over an equivalent outdoor area.

FIGURE 11

Measurements made indoors (blue) and outdoors (red) – see text

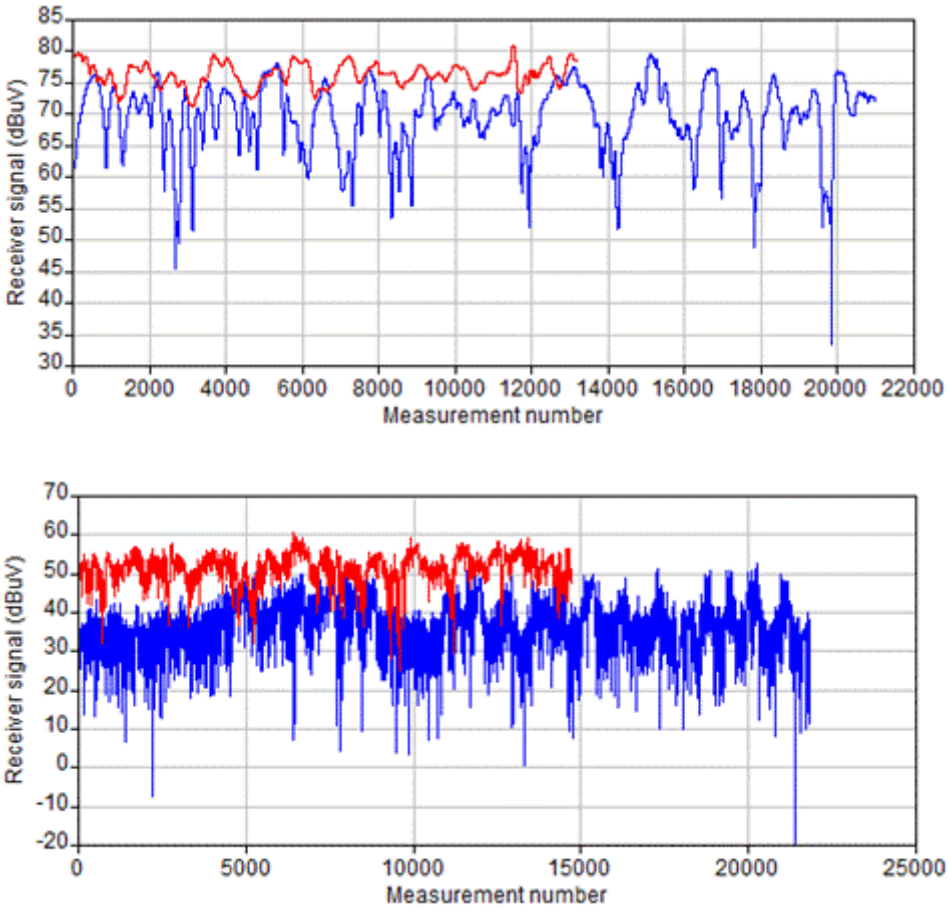

The results at both frequencies show similar trends. The inside signals are weaker on average due to the attenuation of the building. It is also clear that there is more variability on the measurements from inside the building. This is as expected because the inside environment is more rich in multipath than the outside environment. The standard deviations at 88 MHz are 5.5 dB (inside) and 1.8 dB (outside) and at 5.7 GHz are 6.8 dB (inside) and 3.8 dB (outside).

[1] Sampled at equal time-intervals; the faster pace of measurement outdoors resulted in fewer samples being collected.

These standard deviations relate mainly to signal variability due to multipath and a small contribution (less than a decibel) due to the path length variation over the measurement area.

6.4 Variability of loss from room-to-room

The standard deviation of the room median building entry loss values are shown in Fig. 12 for the different building configurations. There is no very useful frequency trend. The results for the small house configurations are reasonably consistent for type 1 glass, with type 2 glass and the artificial foil-over-windows cases showing some differences. The standard deviation is generally higher in the mansion.

FIGURE 12

Room to room standard deviation of building entry loss

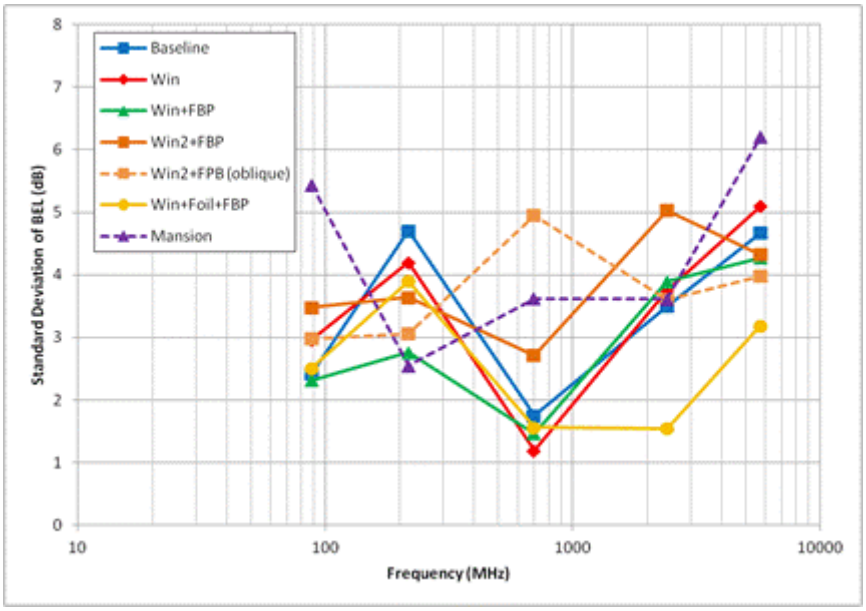

The room-to-room standard deviations are about half the values obtained for the signal variability within the living room alone. This is as expected because multipath has been removed in the room-to-room calculation. However the significant difference between the two buildings suggests that a good measure of 'variability' really needs to take account of a larger population of building types.

It is not clear that any adequate model yet exists to characterise this variability.

6.5 Impact of insulating materials on loss

The measurements show increasing levels of building entry loss as modern insulating materials are added to an uninsulated house (see Fig. 13).

FIGURE 13

Increase in BEL compared to baseline configuration

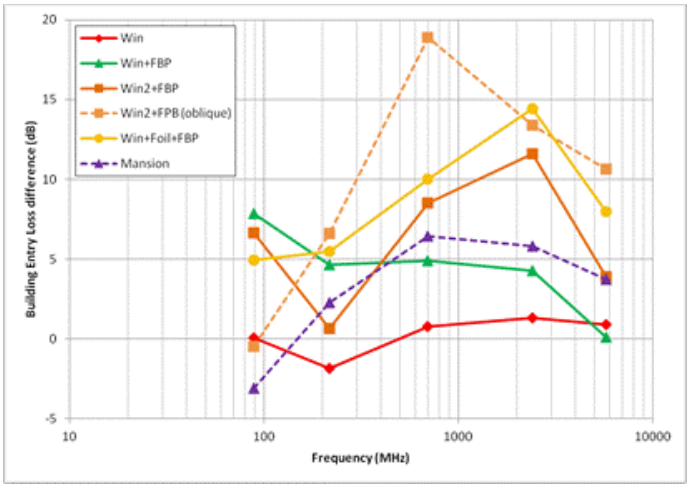

For a small house, a combination of foil-backed insulation and metalised double glazed windows (representative of a well-insulated property), added 5-10 dB to the building entry loss. The losses increase with frequency, but most of the increase is accounted for in the uninsulated configuration and the additional loss due to the insulating materials shows relatively weak frequency dependence. An additional 5 dB of screening was obtained when, in addition, all windows and door apertures were covered by foil; this might approximate to a 'worst case' whole building figure for building entry loss.

7 Measurements at 3.5 GHz

7.1 Environment

Concrete and glass are two typical materials for the building.

In this paper, these two materials are measured.

For the concrete material, 50 cm width * 100 cm length * 10 cm thickness concrete slab is tested. The test environment is an anechoic chamber in Tsinghua University, Beijing, China.

For the class material, the measurement field was located at the FIT building, Tsinghua University in Beijing, China. The FIT building is a typical office building full of coated glass, the overall window to wall ratio is more than 2:1. The building height is about 20 m. Coated glass offers enhanced benefits to buildings, partitions, skylights, curtain walls, and other applications. Annex 2 also provides similar material's building entry loss results.

The characteristics of the environment scenario are shown in Tables 11 and 12.

TABLE 11

Environment characteristics for the concrete scenario

Characteristics	
Location	Anechoic chamber in Tsinghua University
Building type	Basement room
Object of the measurement	Normal concrete slab
Thickness of the concrete slab	10 cm and 20 cm

The measurement object is the concrete slab in the middle of the transmitter and receiver antenna. The thickness is about 10 cm.

TABLE 12

Environment characteristics for the glass scenario

Characteristics	
Location	FIT building East hall, Tsinghua University, Beijing, China
Building type	Office
Object of the measurement	The coated glass between the FIT building hall and the centre garden
Thickness of the glass	Total 10 mm (two 2 mm glass plus 6 mm inner gap)
Height of buildings	About 20 m
Surrounding	Typical office building which full of glass, window-to-wall ratio is more than 2:1.

The measurement object is the glass between the FIT building hall and the centre garden. The glass is typical large two layer class in which the total thickness is about 10 mm including the inner gap. Note that 7 cm width metal pillars connect adjacent glass panels.

7.2 Measurement configuration

The measurement configuration parameters are shown in Table 13.

TABLE 13

Measurement configurations

Characteristics	
Centre frequency	3.34-3.66 GHz, granularity is 0.02 GHz
Bandwidth range	Total 300 MHz
Tx height for concrete scenario	43 cm above the ground, the ground height is 0 m
Rx height for concrete scenario	43 cm above the floor height, the floor height is 13.5 mm
Tx height for glass scenario	161 cm above the ground, the ground height is 0 cm
Rx height for glass scenario	147.5 cm above the floor height, the floor height is 13.5 cm

The Agilent E4438C ESG vector single generator operates at 3.34-3.66 GHz was applied to generate the transmit signal. The ROHDE&SCHWARZ spectrum analyser is used to conduct the building entry loss measurement. Incident angle is 0°.

7.3 Measurement results at 3.5 GHz

The measurement results are shown in Table 14.

TABLE 14

Loss due to coated glass and concrete slab at 0 incident angles

Frequency	Concrete slab (10 cm thickness)		Concrete slab (20 cm thickness)		Coated glass office (10 mm thickness)	
	Mean (dB)	Standard deviation (dB)	Mean (dB)	Standard deviation (dB)	Mean (dB)	Standard deviation (dB)
3.5 GHz	16	2.5	20	1.5	25	4

8 Measurements in Stockholm at 0.5 to 5 GHz

8.1 Configuration of the set-up

Figure 14 shows a map of the measurement area. The transmitter location is indicated with a circle on building 11. The outdoor measurement areas at buildings 27, 37 and 81 are marked with ellipses.

FIGURE 14

Map of the measurement area

Four separate CW (continuous wave) transmitters were used to transmit at f_1 = 460 MHz, f_2 = 881 MHz, f_3 = 1 859 MHz and f_4 = 5.11 GHz from a roof of a 29 metres tall building in an urban environment (Figs 1 and 2). This location was a few meters above the rooftops of the surrounding buildings (the transmitter location was on the roof of 30 m tall building and the surrounding buildings era around 25 m tall). The transmit power was between 23 dBm and 28 dBm. Vertical halfwave dipole antennas were used both at the receiver and the transmitter ensuring equal antenna pattern at all frequencies. A vector network analyser (VNA) was used to sample the receive signal at the different frequencies. In order to improve the sensitivity of the receiver a wideband LNA was used. Applying Doppler filtering in addition, based on 201 time samples taken at each frequency, made possible to measure path loss higher than 130 dB at all frequencies. The measurement routes covered corridors and other open areas.

8.2 General results

The cumulative distribution functions of excess path loss in all buildings are shown in Fig. 15 for the different frequencies. It is striking how small the general frequency dependency is in the band between 460-1 860 MHz. The mean is around 30 dB and the corresponding standard deviation is about 8 dB. In the band 1.8-5.1 GHz, however, the median excess loss increases more than 5 dB with frequency. This increase may partly be explained by shielding due to metallic window coating which attenuates the received signal substantially more at 5.1 GHz than at the other frequencies. This effect was indeed confirmed for building 27 by measuring the excess loss immediately behind the exterior wall facing the transmitter in line of sight (LoS) conditions. The resulting shielding loss of the exterior wall is 12, 16, 16 and 22 dB at carrier frequencies 460, 880, 1 860 and 5 100 MHz respectively. Buildings 11 and 32 also show an increase of excess loss at 5 GHz though the windows are not coated (as shown in Fig. 16). These buildings were located at short distance from the transmitter suggesting a corresponding enhancement of some frequency dependent propagation mechanisms. It was indeed possible to explain the frequency dependency as a diffraction effect in building 11.

FIGURE 15

Cumulative distribution functions of the excess path loss in all buildings

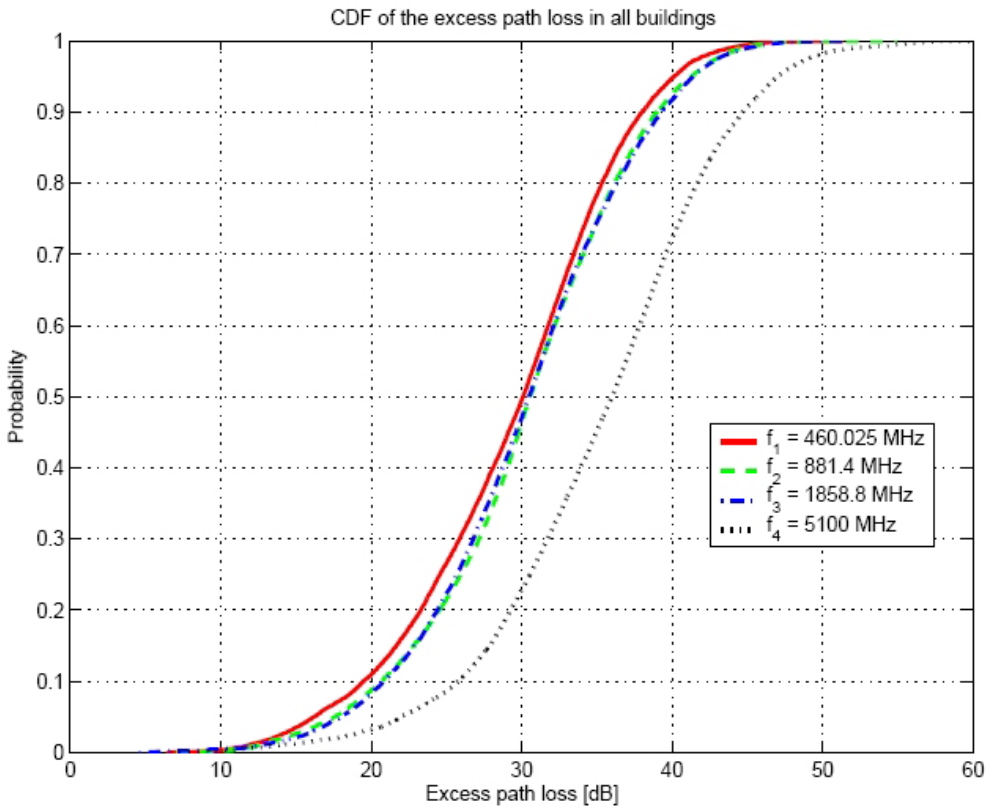

FIGURE 16

Mean excess path loss plotted against floor number for the different carrier frequencies in buildings 11, 27, 32, 37 and 81

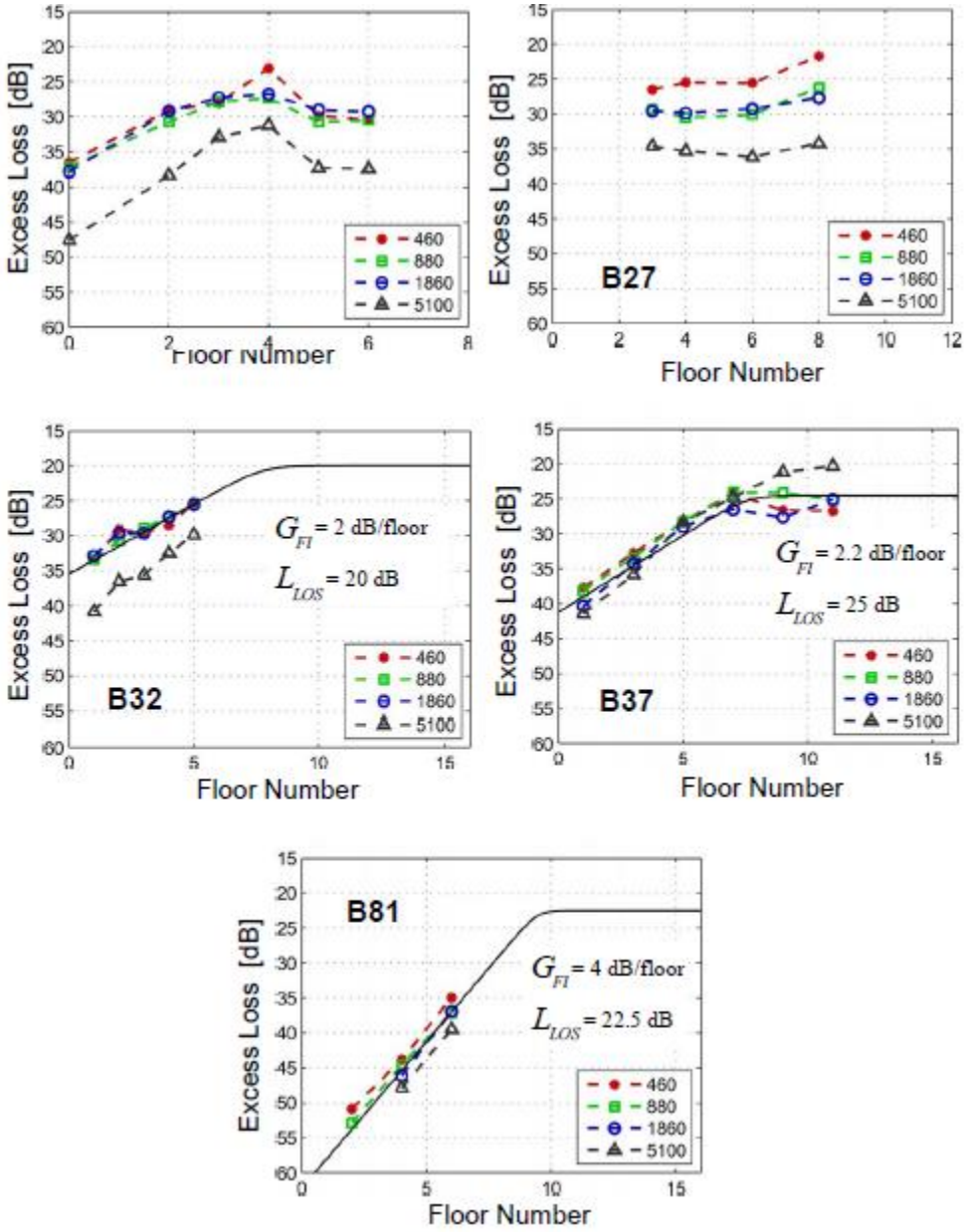

For further details refer to J. Medbo *et al.*, "Multi-Frequency Path Loss in an Outdoor to Indoor Macrocellular Scenario", EuCAP 2009, Berlin, Germany[2].

8.3 Average excess loss results

Building entry loss can be evaluated using two methods:

Method 1: Loss difference indoors and outdoors at ground level: $L_{out} - L_{in}$

Method 2: Excess loss at floor levels where building is LoS: $L_{FS} - L_{in}$

[2] Available: http://ieeexplore.ieee.org/stamp/stamp.jsp?tp=&arnumber=5068371.

FIGURE 17

Methods for evaluation of building entry loss (left = method 1, right = method 2)

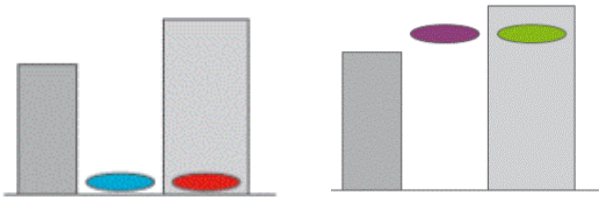

Penetration loss data for LoS conditions is not available in many cases since the buildings do not reach LoS height. For such buildings (e.g. building 81), L_{LoS} may be taken as the difference L_{Diff} between measured loss outdoors and indoors at ground level. This was done for buildings 27, 37 and 81 (see Table 15). For buildings 27 and 37 it is possible to compare the two methods. It turns out that L_{Diff} underestimates L_{LoS} in these two cases. The underestimation may be explained by the fact that the outdoor loss measurements were restricted to areas around the buildings which were not facing the transmitter (see Fig. 15) and thus giving higher loss. Since L_{LoS} is not known for building 81 the best one can do is assume $L_{LoS} = L_{Diff}$. The resulting floor number where LoS occurs, n_{Flb}, is around 9 which is consistent with visual inspection done at the transmitter location. The present results indicate that the two methods to determine the building entry loss give similar results. The outdoor measurement method is however uncertain due to large variations in shadowing suggesting the use of L_{LoS} whenever possible.

TABLE 15

Estimates of L_{LoS}

Building	Frequency (MHz)	Loss – Ground floor (dB)	Loss – Outdoors (dB)	Loss difference (dB)
81	460	48	27	21
	880	48	28	20
	1 860	51	26	25
	5 100	–	25	–
37	460	38	16	22
	880	38	21	17
	1 860	40	21	19
	5 100	41	22	20
27	460	26	3	23
	880	29	8	21
	1 860	30	8	22
	5 100	35	7	28

8.4 Method 1 versus Method 2 results

Method 2 gives typically 0-10 dB higher penetration loss.

There is one dominating direction in LoS conditions due to the angle-dependent penetration loss.

There is multipath in N_{LoS} conditions; often paths with perpendicular incidence.

Method 1 is not reliable if the outdoor area does not have uniform propagation conditions, e.g. partial LoS.

TABLE 16

Comparison of loss estimates

Building	Frequency (MHz)	Penetration loss Method 1 (dB) 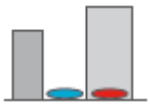	Penetration loss Method 2 (dB) 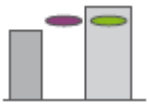	Diff
37	460	**22**	**27**	**5**
	880	**17**	**27**	**10**
	1 860	**19**	**25**	**6**
	5 100	**20**	**20**	**0**
27	460	**23**	**25**	**2**
	880	**21**	**30**	**9**
	1 860	**22**	**30**	**8**
	5 100	**28**	**35**	**7**

9 Building entry loss measurement at 3.5 GHz in Beijing

9.1 Measurement scenarios

Three typical office buildings in China are measured, named as building A, building B and building C, which have different structure and material. Building A is with reinforced concrete shear wall and one-way transparent glass which is with a thin metal coating. The thickness of the bearing wall is 35 cm ~ 38 cm. In addition, the building's exterior wall is being equipped with thermal insulation material whose structure is the foam polyethylene sheet and metal reflective layer. Building B is a modern building combined the toughened glass with the reinforced concrete. The toughened glass is laid in the wall which is known as a common toughened glass without metal coat. Building C is with reinforced concrete shear wall structure and one-way transparent glass.

9.1.1 Building A

Building A is with reinforced concrete shear wall structure, which has exterior load-bearing walls and some interior load-bearing walls. The thickness of the bearing walls is 35 cm ~ 38 cm. The glass of windows of the building is known as one-way transparent glass which has a good visibility from the inside to outside but a poor visibility from the outside to inside. This one-way transparent glass is with a thin metal coating, so it will reflect the electromagnetic wave and bring big penetration loss. In addition, the building’s exterior wall is being equipped with thermal insulation material whose structure is the foam polyethylene sheet and metal reflective layer.

The receiving antenna is on an outdoor platform which is on 4th floor. The pictures are shown in Fig. 18. Only two operators are on the platform during the test, and they stay away from the receiving

antenna. The height of the transmitting antenna is 2.3 m, and the height of the receiving antenna is 1.5 m.

The receiving point located on the 4th floor platform outdoor, the main receiving point is labelled as R1, marked as blue point in Fig. 19. Some transmitting points on the 4th floor indoor are marked as red points in Fig. 19. Other transmitting points on the 5th floor indoor are marked as red points shown in Fig. 20. Furthermore the receiving points and transmitting points are marked with coordinate values, R1 is the coordinate origin.

FIGURE 18

The outdoor platform of the building A: The building scene from the receiving point, the thermal insulation layer is adding to the exterior wall of the building A (Panoramic camera model, Middle image of the building is slightly bent)

FIGURE 19

The transmitting points indoor and the receiving points outdoor on the 4th floor, the length of the platform is 28 m

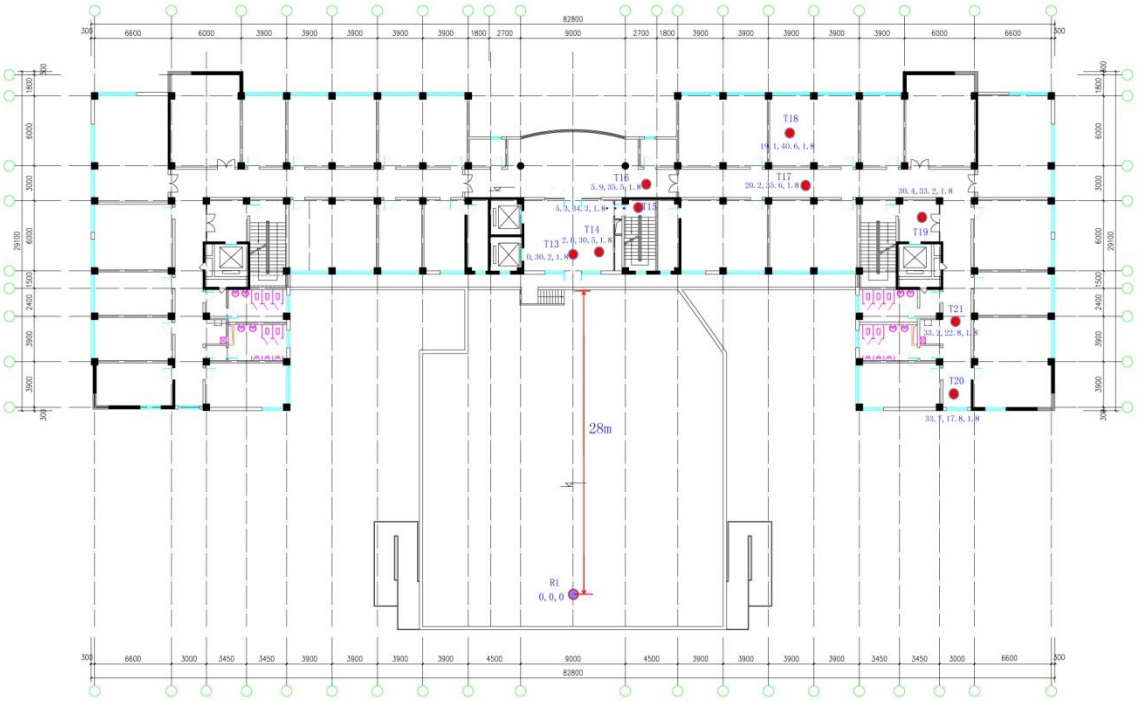

FIGURE 20

The transmitting points indoor on the 5th floor

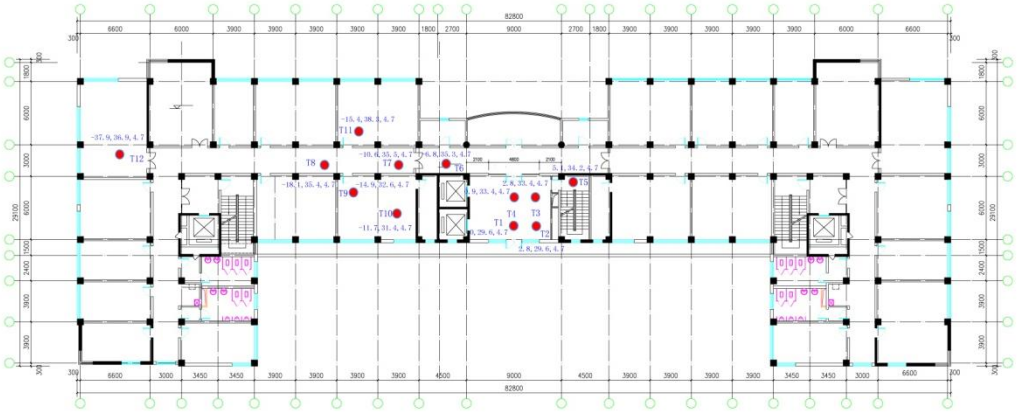

The coordinates of the receiving points and transmitting points in building A are shown in Table 17.

TABLE 17

The coordinates of the receiving points and transmitting points in building A (unit: m)

Points	x	y	z
R1	0	0	0
T1	0	29.6	4.7
T2	2.8	29.6	4.7
T3	2.8	33.4	4.7
T4	0.9	33.4	4.7
T5	5.1	34.2	4.7
T6	–6.8	35.3	4.7
T7	–10.6	35.5	4.7
T8	–18.1	35.4	4.7
T9	–14.9	32.6	4.7
T10	–11.7	31.4	4.7
T11	–15.4	38.3	4.7
T12	–37.9	36.9	4.7
T13	0	30.2	1.8
T14	2.8	30.5	1.8
T15	5.3	34.3	1.8
T16	5.9	35.5	1.8
T17	20.2	35.6	1.8
T18	19.1	40.6	1.8
T19	30.4	33.2	1.8
T20	33.7	17.8	1.8
T21	33.2	22.8	1.8

Some typical transmitting points' pictures in building A are shown in Figs 21 to 23.

FIGURE 21

The transmitting point in the corridor of the building A

FIGURE 22

The transmitting point by the glass door of the building A

FIGURE 23

The transmitting point in the stair channel of the building A

9.1.2 Building B

Building B is a modern building combining toughened glass with reinforced concrete. The toughened glass is laid in the wall which is known as a common toughened glass without metal coat. Part of exterior wall is equipped with a brown ceramic tile. There is a parking lot outside the building, the length of which is about 35 m. In order to avoid the influence of vehicle movement, the method is:

– The test is taken at the weekend to make sure there are few vehicles and staff.

– Make sure the receiving antenna is away from the vehicle.

– The height of the receiving antenna is set to 2.3 m to ensure that the connection between the transmitting antenna and the receiving antenna is not blocked by vehicles.

The main receiving point is R3, which is marked with blue point in Fig. 24, and the transmitting points on the 1st floor are marked with red points in Fig. 25. The transmitting points on the 2nd floor are marked with red points in Fig. 26. The transmitting points on the 3rd floor are marked with red points in Fig. 27. The height of the transmitting antenna is 2.3 m and the height of the receiving antenna is 2.3 m from the floors at that time.

FIGURE 24

Parking lot outside the building B: The building scene from the receiving point

FIGURE 25

The transmitting points indoor and the receiving point outdoor on the 1st floor in building B, the length of the outdoor parking lot is 35 m

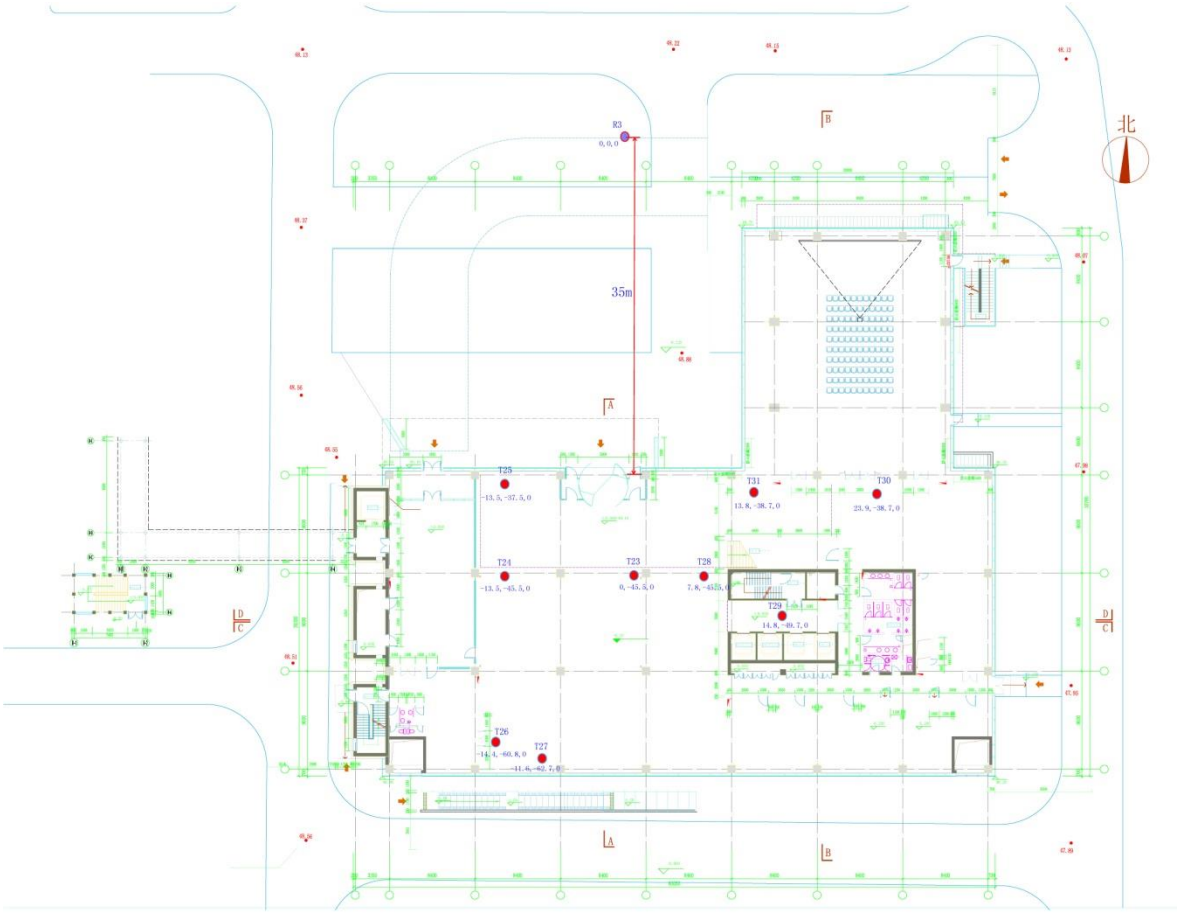

FIGURE 26

The transmitting points on the 2nd floor in building B

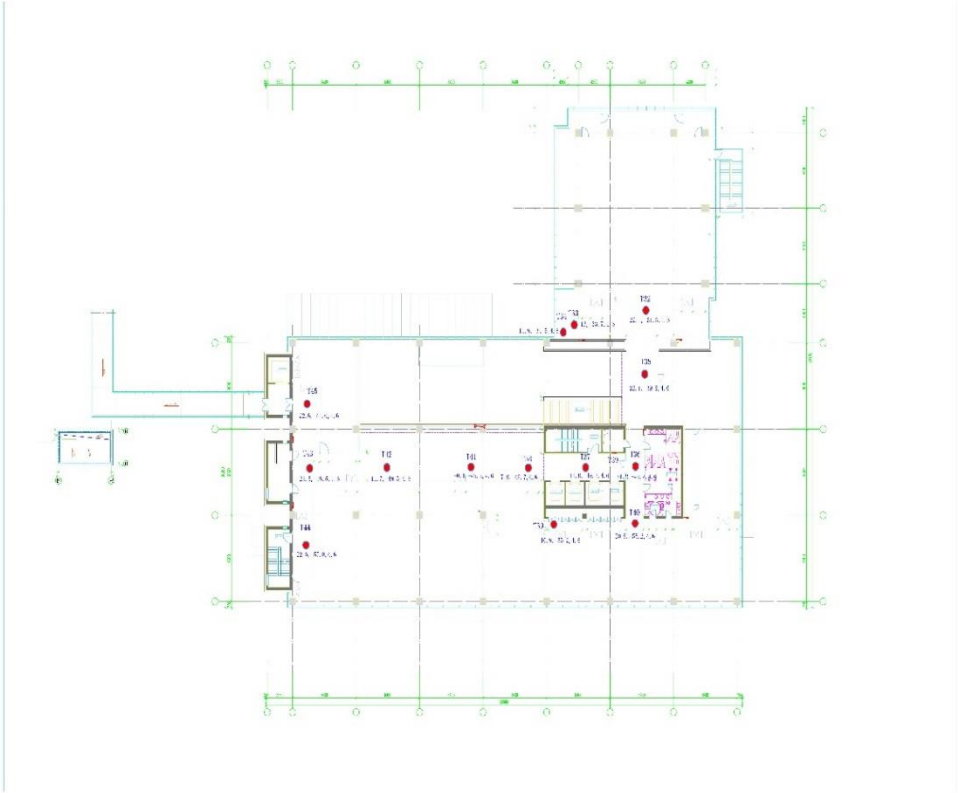

FIGURE 27

The transmitting points on the 3rd floor in building B

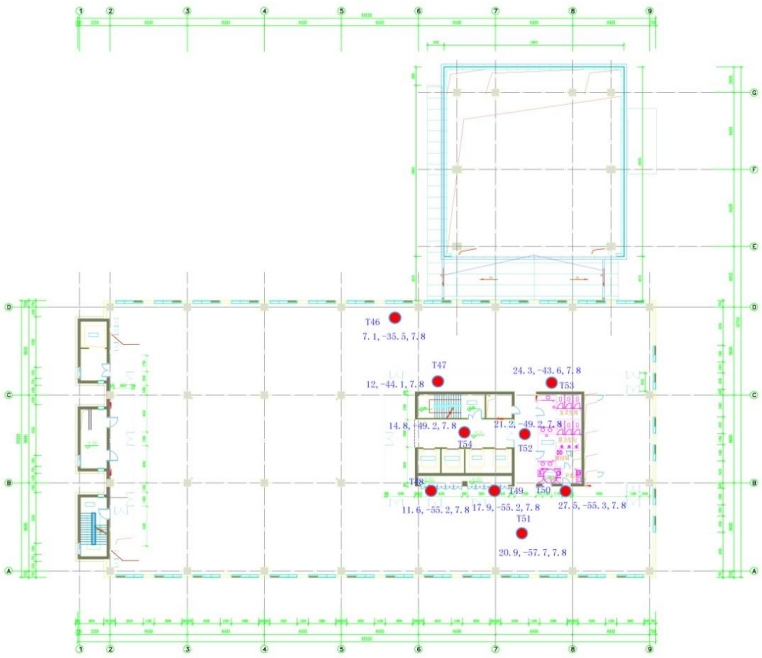

A coordinate system is formed with the R3 being a coordinate origin. The coordinates of the transmitting points and receiving point are shown in Table 18.

TABLE 18

The coordinates of the receiving points and transmitting points in building B (unit: m)

Points	***x***	***y***	***z***
R3	0.0	0.0	0.0
T23	0.0	–45.5	0.0
T24	–13.5	–45.5	0.0
T25	–13.5	–37.5	0.0
T26	–14.4	–60.8	0.0
T27	–11.6	–62.7	0.0
T28	7.8	–45.5	0.0
T29	14.8	–49.7	0.0
T30	23.9	–38.7	0.0
T31	13.8	–38.7	0.0
T32	22.1	–31.3	4.6
T33	13.0	–34.7	4.6
T34	11.9	–34.5	4.6
T35	22.1	–39.8	4.6
T36	21.2	–49.2	4.6
T37	14.8	–49.7	4.6
T38	7.8	–49.7	4.6
T39	10.9	–55.2	4.6
T40	20.8	–55.2	4.6
T41	–0.1	–49.5	4.6
T42	–11.7	–49.5	4.6
T43	–21.5	–49.5	4.6
T44	–22.6	–57.8	4.6
T45	–22.6	–41.6	4.6
T46	7.1	–35.5	7.8
T47	12.0	–44.1	7.8
T48	11.6	–55.2	7.8
T49	17.9	–55.2	7.8
T50	27.5	–55.3	7.8
T51	20.9	–57.0	7.8
T52	21.2	–49.2	7.8
T53	24.3	–43.6	7.8
T54	14.8	–49.2	7.8

Some typical transmitting points pictures in building B are shown in Figs 28-29.

FIGURE 28

The transmitting point in the lobby on the 1st floor in building B (in transmitting point the receiving point can be seen through glass)

FIGURE 29

The transmitting point next to the elevator on the 2nd floor in building B

9.1.3 Building C

Building C is with reinforced concrete shear wall structure. The glass of windows of the building is known as one-way transparent glass which has a good visibility from the inside to outside but a poor visibility from the outside to the inside. In the measurement only one transmitting location is selected, and the location is near the window, and 3 receiving locations are selected. From the outdoor level, the transmitting antenna height is 3.3 m, the receiving antenna height is 2.3 m, the horizontal distance from receiving point outdoor to transmitting point indoor is 9.65 m, 17.65 m and 29.65 m.

9.2 Test methodology

In building A and B, 11 frequency points are selected in 3.4 GHz to 3.6 GHz frequency band during the test, which are: 3 401 MHz, 3 421 MHz, 3 441 MHz, 3 461 MHz, 3 481 MHz, 3 501 MHz, 3 521 MHz, 3 541 MHz, 3 561 MHz, 3 581 MHz, 3 601 MHz.

In building C, 3 frequency points are selected: 3 401 MHz, 3 501 MHz, 3 599 MHz.

9.2.1 Measuring system and instrument

The devices of measuring system are shown in Table 19.

TABLE 19

The antenna selection consideration

Transmitting antenna	**Omni-directional vertical polarization antenna**
Receiving antenna	• In building A and B: Omni-directional vertical polarization antenna. • In building C: horn antenna with vertical polarization
Transmitter	Agilent E8267D signal generator
RF power amplifier	The output power in the test is set to 33 dBm
Receiver	Agilent N9030A signal analyzer

We have developed an automatic program in order to control instruments and record test data by LAN. In each location and frequency points, 500 continuous reading are obtained which will cost about 8 ~10 seconds.

9.2.2 Calculation method of building entry loss

The free space loss can be calculated as:

$$L_f = 32.45 + 20 \lg d_{(m)} + 20 \lg f_{(GHz)} \quad (3)$$

where d is defined in Fig. 30. f is carrier frequency (GHz). Set transmitted power be P_t (dBm) and received power be P_r (dBm), the building entry loss is expressed as L_E, transmitting antenna gain and receiving antenna gain in transmission path are expressed as G_t and G_r, relatively.

FIGURE 30

The location relationship between the receiving antenna and the transmitting antenna

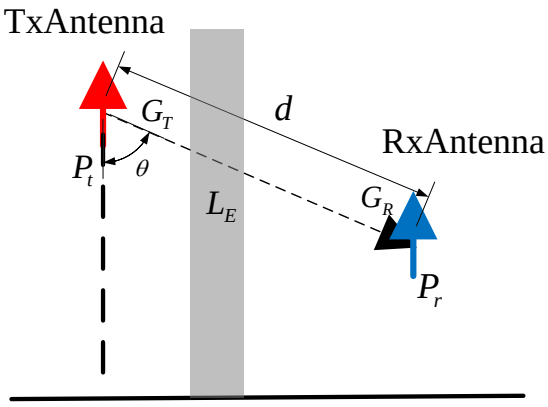

Then we can get equation (4).

$$P_{t(dBm)} + \left(G_t - L_f - L_E + G_r\right) = P_{r(dBm)} \tag{4}$$

And then the entry loss can be deduced from equation (5).

$$L_E = \left(P_{t(dBm)} - P_{r(dBm)}\right) - L_f + (G_t + G_r) \tag{5}$$

The omni-directional antenna used in the test is similar to half wave dipole antenna whose gain is 2.15 dB, and the normalized directivity function of electric field of half-wave dipole antenna is expressed as equation (6).

$$F(\theta) = sin\theta \tag{6}$$

Where θ is defined in Fig. 29. From equation (6) we can get equation (7).

$$G_t + G_r = 4.3 + 10\ \lg([F(\theta)]^4) = 4.3 + 10\ \lg(\sin^4\theta) \tag{7}$$

In the scenario of building C, for horn antenna is used as receiving antenna, so the receiving antenna gain is properly considered in calculation.

9.3 Measurement results

9.3.1 Measurement results and analysis of building A scenario

After processing the original test data the entry loss of building A can be obtained. Figure 31 shows an example of curve of readings in time domain and median value.

FIGURE 31

Measurement of building entry loss: readings in time domain and median value

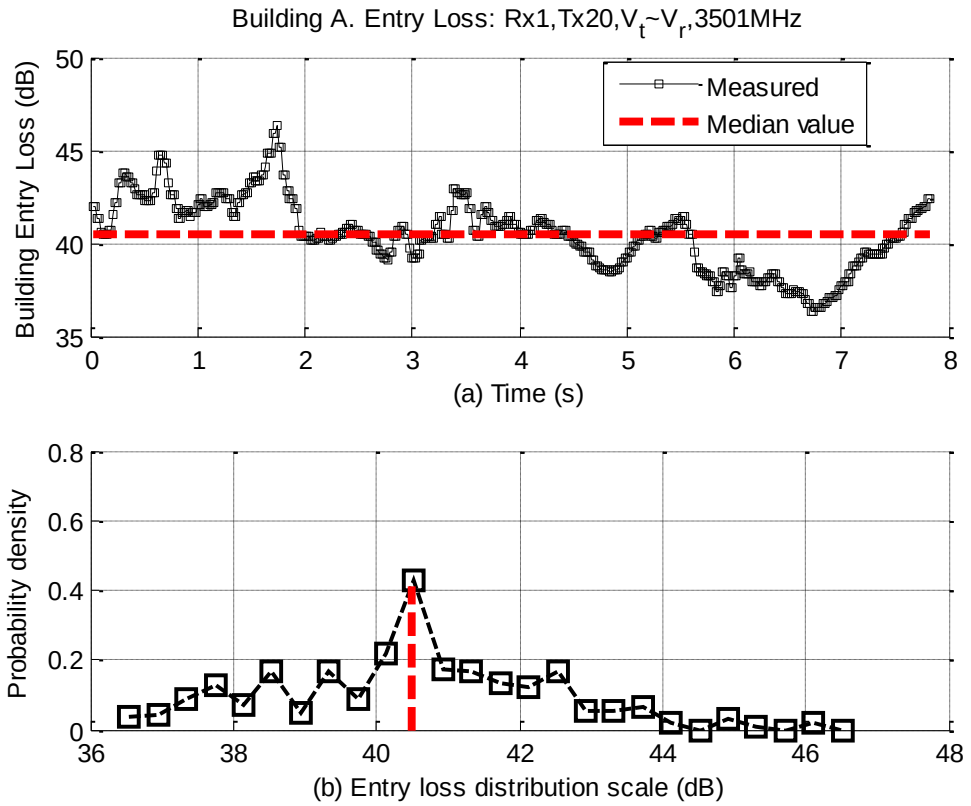

The median values of building entry loss measured above are shown in Table 20. The categories of all links from transmitters and receivers can be separated as four types:

– Category0: Outer-wall with one-way transparent glass
– Category1: Outer-wall+1 inner-wall
– Category2: Outer-wall+2 inner-wall
– Category3: Outer-wall+ elevator.

TABLE 20

The median value of entry loss (building A, unit: dB)

Frequency (MHz)	3 401	3 421	3 441	3 461	3 481	3 501	3 521	3 541	3 561	3 581	3 601	Category
Tx 1	27.3	20.2	36.9	29.5	28.7	32.1	37.7	24.5	28.4	45.0	38.5	0
Tx 2	20.0	19.5	19.7	19.9	22.1	29.1	16.1	20.7	18.1	17.6	28.0	0
Tx 3	21.2	25.8	22.3	21.1	25.0	22.9	27.4	25.1	23.8	23.4	28.1	0
Tx 4	34.3	26.7	24.4	25.7	23.1	26.8	25.9	27.6	22.0	24.0	27.4	0
Tx 5	46.3	45.1	56.5	41.4	40.3	44.2	45.1	36.6	37.9	41.3	42.9	1
Tx 6	44.5	40.6	38.3	42.0	43.0	37.7	43.2	41.2	47.0	49.7	56.6	3
Tx 7	42.6	44.4	49.2	44.7	71.3	44.1	41.0	44.2	42.7	39.9	39.0	3
Tx 8	39.1	45.8	45.7	42.8	43.3	46.5	48.0	49.0	51.4	53.6	53.0	1
Tx 9	27.6	36.1	26.5	21.8	36.7	37.2	20.1	31.8	32.9	24.1	31.8	0

TABLE 20 (*end*)

Frequency (MHz)	3 401	3 421	3 441	3 461	3 481	3 501	3 521	3 541	3 561	3 581	3 601	Category
Tx 10	19.2	24.8	27.4	25.8	26.1	42.1	30.2	26.9	23.0	24.2	29.8	0
Tx 11	51.9	57.7	65.4	60.2	53.0	64.3	62.9	63.9	59.7	56.3	51.9	2
Tx 12	60.3	53.6	63.0	56.2	54.1	51.1	51.1	55.1	55.4	57.4	58.4	2
Tx 13	27.1	34.5	33.3	34.9	50.2	28.7	29.0	36.7	32.1	39.2	40.9	0
Tx 14	40.2	35.7	38.1	30.2	26.4	32.4	28.1	33.3	35.4	40.9	30.1	0
Tx 15	53.0	50.7	55.5	49.1	41.6	44.3	57.5	46.7	66.3	56.6	53.1	3
Tx 16	50.5	53.1	60.3	55.6	46.9	50.8	47.2	52.5	57.0	69.0	57.1	2
Tx 17	51.9	52.1	55.5	61.1	44.1	52.7	43.5	50.0	42.1	46.3	49.8	2
Tx 18	60.0	66.2	76.1	68.9	66.8	75.0	69.9	74.0	65.8	70.6	61.7	2
Tx 19	58.3	63.5	64.2	58.3	65.0	66.5	73.2	61.5	60.9	64.1	64.6	2
Tx 20	31.8	33.7	33.7	33.4	32.5	40.5	45.3	43.4	35.3	36.9	33.7	1
Tx 21	43.3	54.5	52.8	50.9	55.2	47.9	59.9	52.6	44.2	50.8	43.2	1

Through analysis of median values of building entry loss (data in Table 20) at each frequency on each transmitter, we can get the CDF, as shown in Fig. 32. And, the mean of data in Table 18 is 42.8 dB and standard deviation is 14.3 dB.

FIGURE 32

Cumulative distribution function of median values of each Tx at each frequency

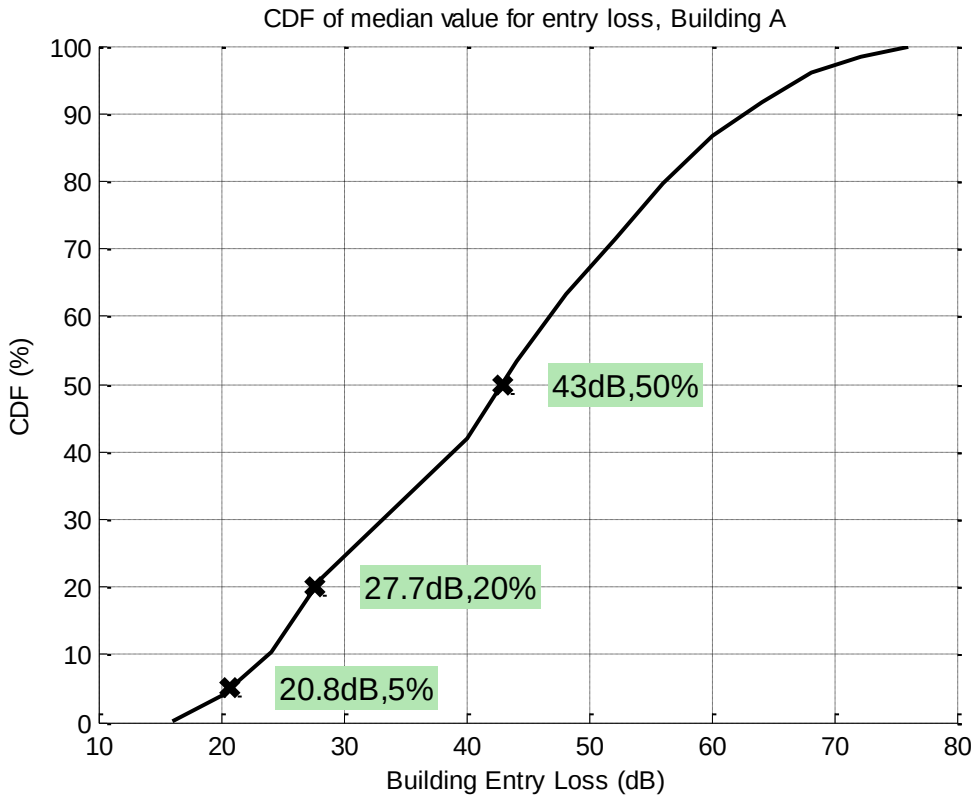

9.3.2 Measurement results and analysis of building B scenario

After processing the original test data the entry loss of building B can be obtained. The median value of the entry loss measurement above is shown in Table 21. The categories of all links from transmitters to receivers can be separated as four types:

– Category0: Outer-wall with glass
– Category1: Outer-wall+1 inner-wall
– Category2: Outer-wall+2 inner-wall
– Category1: Outer-wall+ elevator.

TABLE 21

The median value of the entry loss (building B, unit: dB)

Frequency (MHz)	3 401	3 421	3 441	3 461	3 481	3 501	3 521	3 541	3 561	3 581	3 601	Category
Tx 23	16.9	8.1	9.6	4.1	9.6	13.5	11.5	5.9	12.6	12.5	18.5	0
Tx 24	22.0	12.6	8.2	15.9	21.0	20.3	13.0	15.0	13.0	22.6	19.4	0
Tx 25	16.1	10.5	21.0	10.5	12.7	13.0	26.6	9.4	21.8	18.8	13.2	0
Tx 26	9.6	12.7	11.2	12.1	22.1	10.8	11.4	14.2	16.0	16.4	6.6	0
Tx 27	16.6	19.5	15.8	23.7	36.7	22.0	14.5	18.9	15.3	16.5	12.0	0
Tx 28	11.3	19.6	10.8	12.2	20.8	21.8	22.9	11.7	19.3	12.2	8.3	0
Tx 29	25.9	22.3	31.9	26.6	29.7	25.1	33.5	22.6	22.0	21.6	24.4	3
Tx 30	20.9	18.3	25.1	18.2	20.4	19.5	19.2	20.5	22.9	32.0	24.7	1
Tx 31	20.4	15.7	12.9	17.8	25.4	13.3	30.7	14.5	20.3	24.6	17.5	0
Tx 32	41.7	36.2	38.4	29.9	47.2	38.2	40.5	38.9	36.2	40.3	35.3	0
Tx 33	36.1	31.3	36.1	22.0	33.6	42.1	38.8	33.4	26.4	26.9	29.4	0
Tx 34	19.9	25.6	31.5	33.5	24.6	23.8	27.4	26.8	36.6	30.7	26.0	0
Tx 35	22.7	27.8	24.4	26.3	34.1	29.1	28.7	21.7	21.3	25.2	24.9	1
Tx 36	40.9	42.3	33.6	45.3	32.0	33.1	41.3	37.8	33.1	47.8	32.5	2
Tx 37	30.1	48.4	46.6	35.1	38.4	40.4	40.0	32.7	41.7	39.1	31.6	2
Tx 38	22.7	17.6	25.3	20.4	16.0	30.1	21.1	24.8	17.7	25.6	20.9	0
Tx 39	34.9	39.7	36.5	31.5	34.0	37.4	36.6	32.0	37.3	34.5	36.3	3
Tx 40	45.3	38.6	35.0	37.5	48.4	43.7	39.2	44.3	39.2	40.9	42.5	3
Tx 41	14.4	21.4	17.8	17.6	20.4	22.2	22.6	16.1	22.8	21.3	26.1	0
Tx 42	18.3	19.4	18.7	16.4	21.6	20.0	33.1	25.8	19.4	23.4	21.8	0
Tx 43	32.9	33.3	30.4	36.5	42.6	30.6	37.9	34.3	32.5	36.3	39.2	1
Tx 44	48.1	35.6	39.1	53.6	43.8	37.0	48.5	42.8	53.8	41.5	35.2	2
Tx 45	30.7	35.9	32.4	47.1	33.7	38.0	31.6	37.6	26.7	36.8	29.6	1
Tx 46	13.4	16.3	32.5	17.2	25.6	19.5	17.4	23.7	20.5	33.4	22.5	0
Tx 47	26.2	29.5	34.8	33.4	37.0	31.9	30.8	47.7	25.4	29.2	35.3	1
Tx 48	39.4	53.2	49.3	43.5	50.6	44.1	48.1	51.2	53.8	48.3	63.0	3
Tx 49	61.2	48.4	60.8	46.1	56.0	57.8	63.2	57.1	57.8	51.0	60.8	3

TABLE 21 (*end*)

Frequency (MHz)	3 401	3 421	3 441	3 461	3 481	3 501	3 521	3 541	3 561	3 581	3 601	Category
Tx 50	55.4	58.9	61.1	52.9	52.5	59.7	55.0	53.2	63.7	59.8	51.1	3
Tx 51	72.9	64.2	79.9	56.9	58.8	69.5	68.8	64.4	57.9	60.4	59.9	3
Tx 52	49.2	63.1	49.3	57.5	60.9	49.0	60.0	59.3	50.2	55.6	62.9	2
Tx 53	41.5	43.8	42.4	44.5	57.8	46.7	42.4	43.7	35.7	47.7	45.8	2
Tx 54	58.0	70.4	45.5	50.9	53.6	48.0	55.4	48.2	50.2	53.3	56.9	2

Through analysis of median values of building entry loss (data in Table 21) at each frequency on each transmitter, we can get the CDF, as shown in Fig. 33. And the mean of data in Table 19 is 32.8 dB and standard deviation is 15.3 dB.

FIGURE 33

Cumulative distribution function of median value of each Tx at each frequency

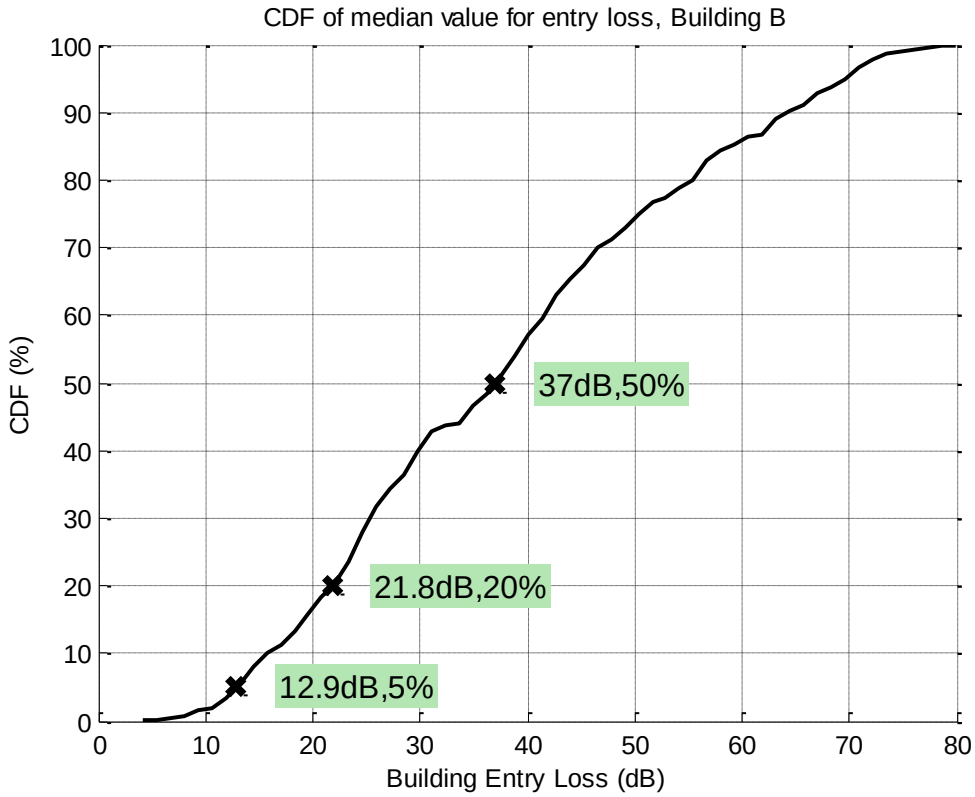

9.3.3 Measurement results and analysis of building C scenario

After processing the original test data the entry loss of building C can be obtained. The median value of the entry loss measurement above is shown in Table 22.

TABLE 22

The median value of the entry loss, One Tx vs 3 Rx (Building C, unit: dB)

Frequency (MHz)	3 401	3 501	3 599	Category
Rx 4	21.5	15.0	15.7	Outer wall with glass
Rx 5	18.4	22.3	20.9	Outer wall with glass
Rx 6	18.5	19.4	22.5	Outer wall with glass

Through analysis of median values of building entry loss (data in Table 22) at each frequency on each Rx, we can get the CDF, as shown in Fig. 34. And, the mean of data in Table 20 is 19.4 dB and standard deviation is 2.7 dB.

FIGURE 34

Cumulative distribution function of median value of each Rx at each frequency

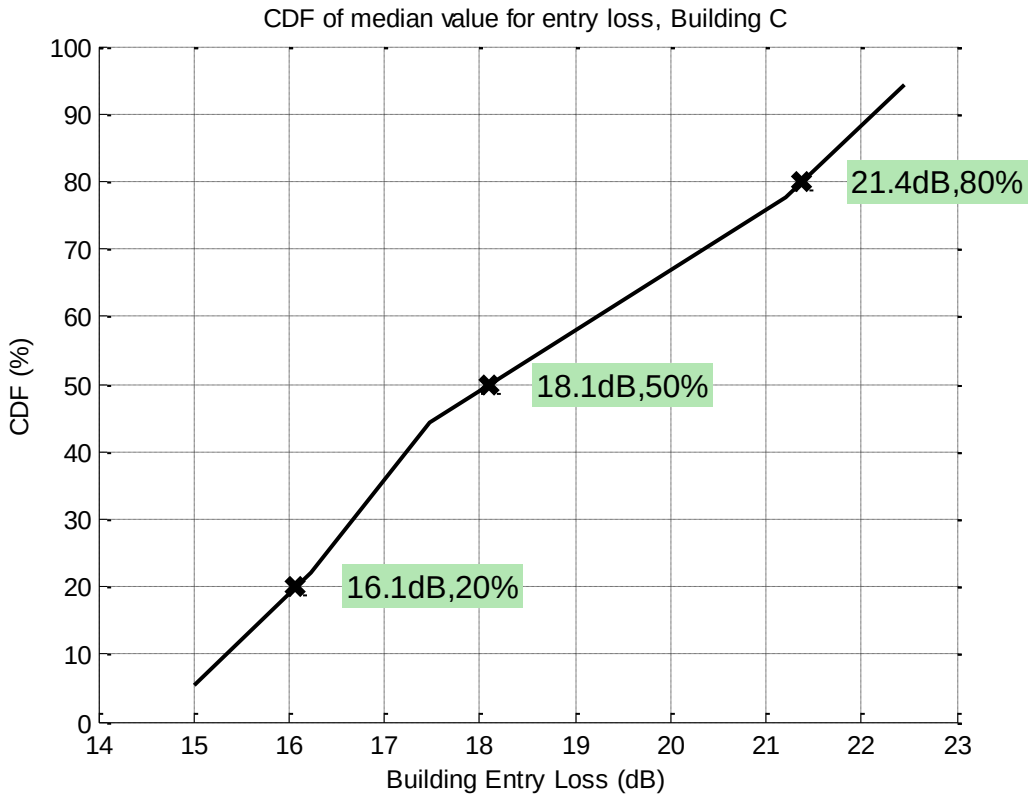

10 Building entry loss measurement at 3.5 GHz in UK

10.1 UK measurements

A limited campaign of measurements has been undertaken to gather 3.5 GHz entry loss data for UK buildings. The intention of this limited campaign was to inform discussions of BEL modelling within SG 3 and to develop and refine measurement methods. If the results are considered useful, it would be simple to extend the measurements, both within the UK and in other regions.

10.2 Methodology

The methodology adopted for the 3.5 GHz measurements closely follows that used in earlier UK studies (see 3J/90). A portable, handheld, transmitter is used to explore the building under test, with signals received at a transportable (vehicle-based) terminal located some tens of metres from the building (but in LoS). Figure 35 shows the arrangement.

FIGURE 35

Experimental arrangement

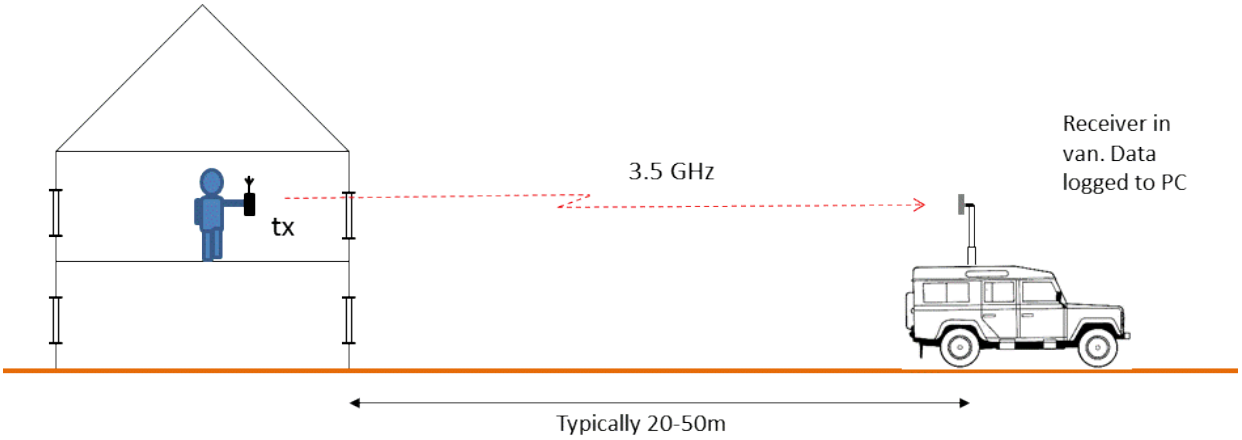

The pathloss measured from within the building is compared with that measured from outside the building, close to the wall facing the receiver. The ‘Building Entry Loss’ is then defined as the difference between the median values of the two distributions.

Given the enormous variation in entry loss seen at different points throughout a typical building (often around 30 dB), the measurements are broken down on a room-by-room basis. This seems to be the smallest degree of discretisation that is useful in practice; rooms may be characterised as, e.g. ‘first-floor, away from receiver’ or ‘ground-floor, facing receiver’. To attempt to define positions within rooms would rapidly become very complicated and building-specific and would be unlikely to aid statistical analysis.

A separate results file is recorded for each room in the building; within each room, the engineer will walk slowly around a semi-random route that explores the entire floor-area. It has been found that this method gives results repeatable to within about 1 dB.

An important point is that the intention is that the ‘outdoor reference’ measurements are made at the same height as the indoor measurements. This allows the modelling of building entry loss to be decoupled from the modelling of other local environmental effects, such as clutter loss due to surrounding buildings. It should be noted that this approach is not always followed in some of the studies reported in the literature.

In the ideal case, the receiver would be located sufficiently far from the building to ensure both a plane wavefront at the exterior wall and that the difference in free-space pathloss throughout the building is negligible. In practice, the latter may be up to 6 dB and needs to be corrected for in post-processing.

10.2.1 Hardware

The test source for the measurements is a small 2W transmitter operating at around 3.5 GHz. The transmitter feeds a handheld co-linear (omnidirectional) antenna, radiating an unmodulated carrier.

The vehicle-mounted receive system consists of a flat-plate antenna mounted on an extensible mast, feeding a Rohde & Schwarz FSP-13 spectrum analyser interfaced to a PC for data logging.

10.2.2 Software

The logging software recorded the received signal at a rate (1/80 ms) sufficient to capture the fast-fading (Rayleigh) statistics of the path. This fast fading is filtered from the results reported below, but could be explicitly included in the post-processing if required. Systematic analysis of this data would be difficult, however, as the speed with which the transmitter moves is not constant.

10.3 Test locations

Four test locations have been used in this brief campaign, comprising a small residential building, two large retail ‘superstores’ and a small office building. Measurements in a large modern office block are also planned but have not been completed at the time of writing.

In all cases, a clear LoS was available between the outdoor terminal and an exterior wall of the building under test.

10.3.1 Terraced house

This terraced family home (built in 1880) is of traditional brick construction, and has two rooms on the ground floor, three on the first floor and one attic room in the roof-space.

FIGURE 36

Terraced house

The receiver, in this instance, was not mounted in the vehicle but on a tripod in the garden behind the house, at a range of 13.5 m from the exterior wall.

10.3.2 Small office

A small office building of traditional brick constriction (built circa 1980) was measured with the receiver vehicle in two locations, to the front and rear of the building. The accommodation is on three floors.

FIGURE 37

Small office (Google Earth)

The measurements were made at ranges of 40 m (front) and 27 m (rear). The receiver locations and the building under test are shown in the plan view below.

FIGURE 38

Plan view of small office showing receiver locations (Google Earth)

10.3.3 Retail buildings

Measurements were made in two retail buildings, both of steel-frame, brick clad construction and both incorporating a large amount of metalwork in the interior fittings. The first, 'Retail A' was a technology store occupying an area of 40 m × 40 m, with the receiver located at 35 m distance. Measurements were made throughout the open-plan store, logged in 9 separate files representing paths in the front, middle and back of the store and the right, middle and left sides of the building (see Fig. 39, left).

The 'Retail B' building (a food supermarket) is significantly larger, and measurements were made in a 20 m × 40 m subset of the floor area, as shown in Fig. 39, right). Two receiver locations were used in this case, one at around 15° to the normal from the building and the other at around 40°. In both cases the range was around 90 m.

FIGURE 39

Measurement plans – 'Retail A' on left, 'Retail B' on right (Google Earth)

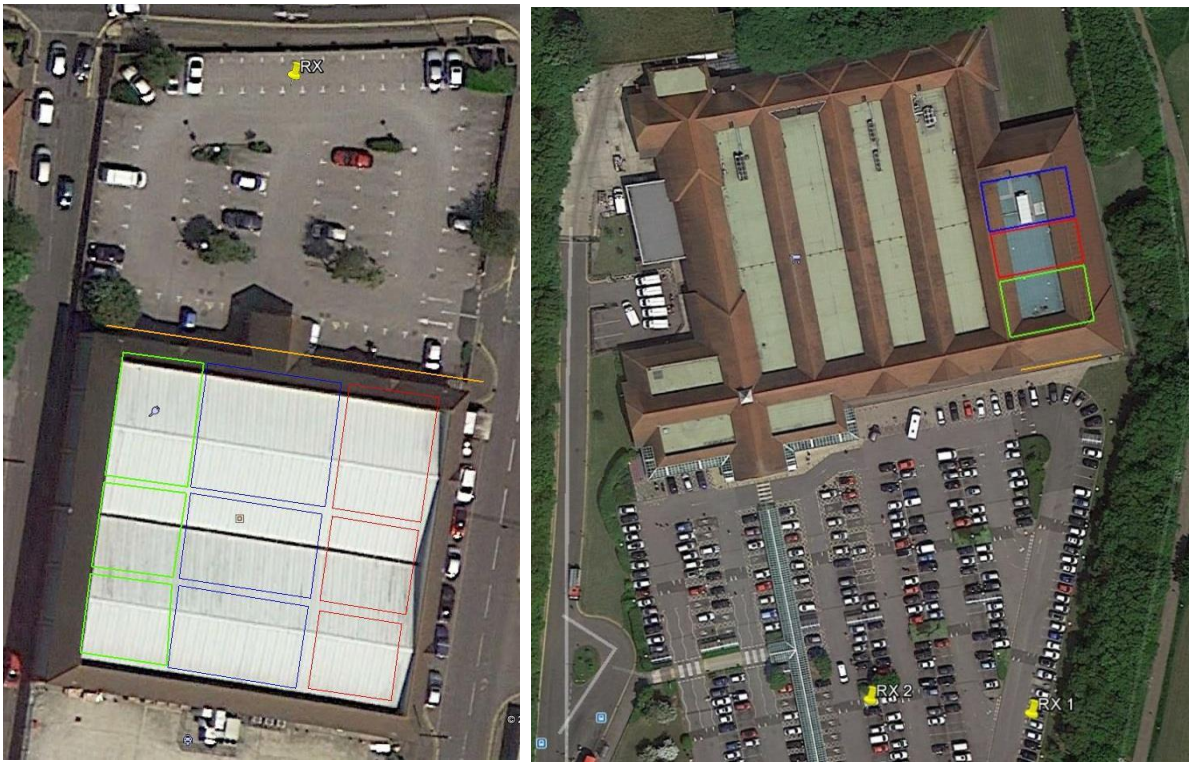

Figure 40 shows a view of 'Retail B' from the antenna[3] height at the second receiver location.

[3] The UHF log-periodic antenna seen in the picture is not the measurement antenna.

FIGURE 40

View of 'Retail B' building

10.4 Results

10.4.1 Building entry loss

In line with the definitions given in Recommendation ITU-R P.2040, BEL is taken to be the difference between the median field measured immediately outside the building and that measured within each room or subdivision of the building.

The BEL can be quickly estimated by inspecting the cumulative distributions of the power recorded at the outdoor receiver, as shown in Fig. 41, and comparing the indoor values with the outdoor reference at the 0.5 probability point.

FIGURE 41

Summary results for 'Retail B' measurements

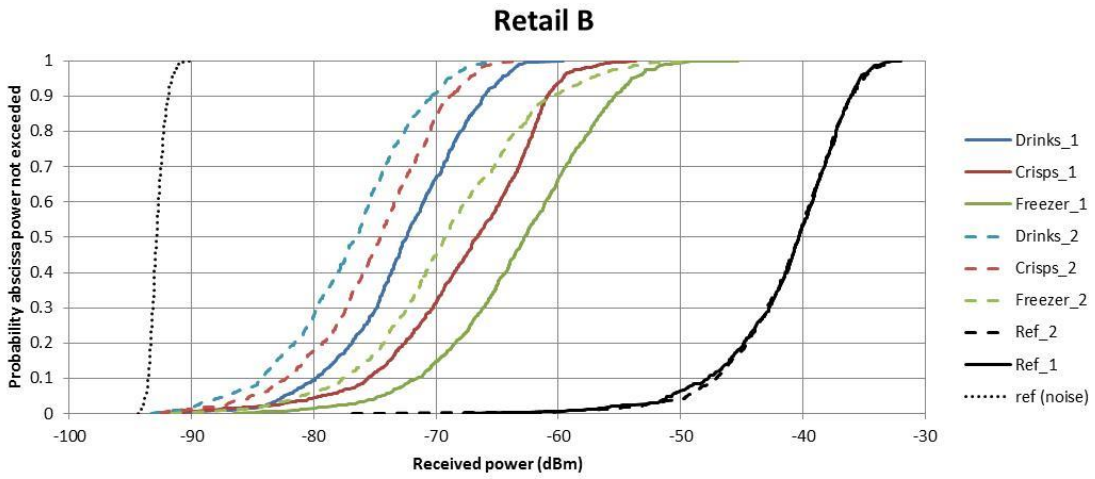

This figure shows that, as might be expected, the BEL increases (by 8-10 dB) as a function of depth within the building[4,5]. The loss to the 'outdoor reference' is almost identical from the two receiver locations, but it is interesting to note that the BEL values are greater for the more oblique 'RX2' measurements. This is in line with the Fresnel expressions for transmission loss through a plane surface at different angles, though the effect is surprisingly clear and may equally be due to other effects, such as diffraction loss from clutter within the store.

The results from the 'Retail A' building (Fig. 42) are very different in character, with smaller values of loss (as might be expected for a smaller, less cluttered, store). Most interesting, however, is the fact that there is very little dependence of BEL on penetration depth – possibly due to high levels of scattered energy within the building.

FIGURE 42

Summary results for 'Retail A' measurements

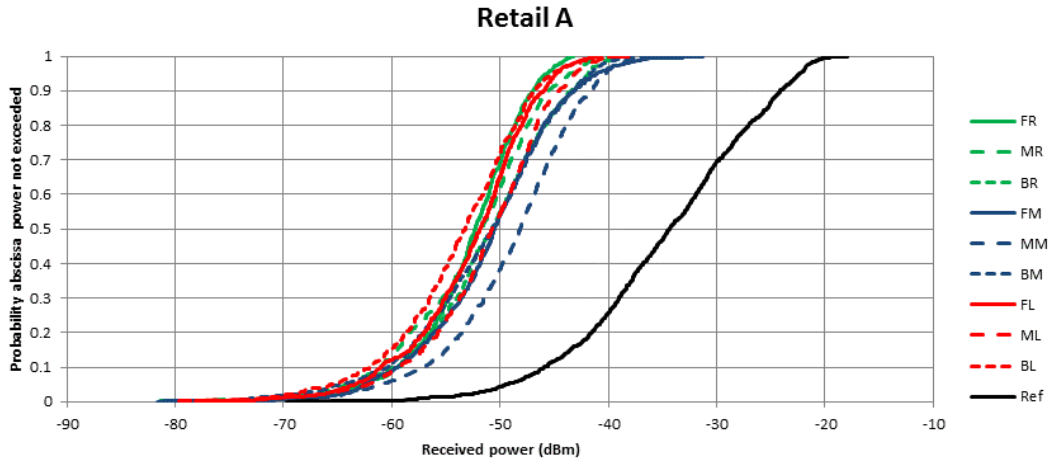

The repeatability of measurements is indicated in Fig. 43, which shows two independent sets of measurements for a single sub-section of the 'Retail A' building.

[4] The colour-coding of the traces follows that of the measurement areas in Fig. 39 (right).

[5] Note that BEL in the present definition includes both losses through the outer wall and additional losses within the building.

FIGURE 43

Showing repeatability of measurement

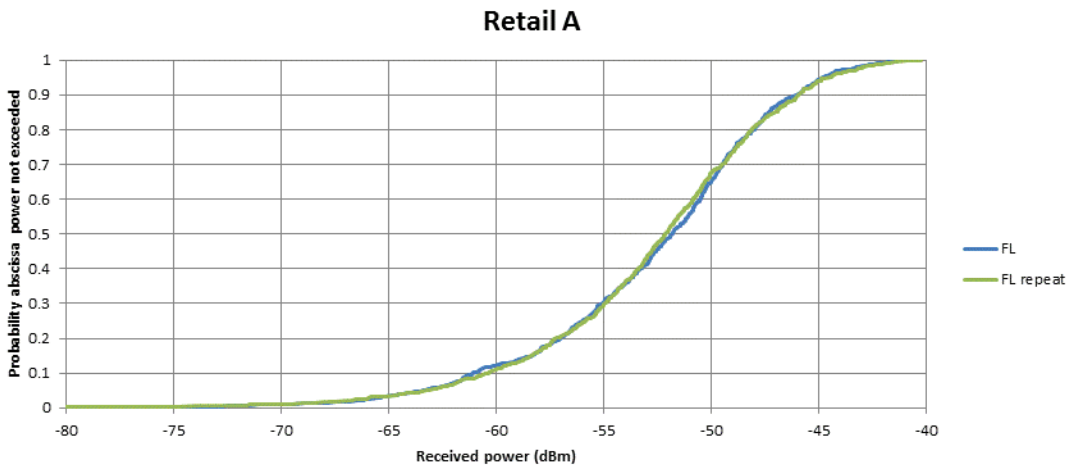

10.4.2 BEL Variability

Characterising the variability of pathloss into or out of buildings is a non-trivial problem. In the present context, we have defined variability to exclude multipath (selective fading) effects in line with the ITU-R definition of outdoor 'location variability'. This has the advantage of decoupling the statistics from consideration of radio system bandwidth, but imposes a requirement to undertake appropriate post-processing of the measured data.

As noted above, the simple nature of the present experimental arrangement[6], with data gathered at regular time intervals, but the terminal moving at arbitrary (walking) speed, precludes a very formal approach to such post-processing. For the results reported here, a 4-point moving average was applied to the data, which appears sufficient to remove the majority of selective fading while preserving the flat fading due to clutter and other effects.

With this averaging applied, the measured data is found to be reasonably fitted[7] by a lognormal distribution, as shown in the figures below, which are normalised to the median value. Given the current paucity of data, and the occasionally poor fit to the distribution tails (such as in Fig. 44a and c), it is suggested that BEL statistics should only be modelled between decile points.

---

[6] Such a simple approach is probably pragmatically necessary, to allow large amounts of data to be gathered rapidly.

[7] Although some skewing is always evident at the low-loss tail of the distribution and occasionally at both tails.

FIGURE 44

Sample loss distributions

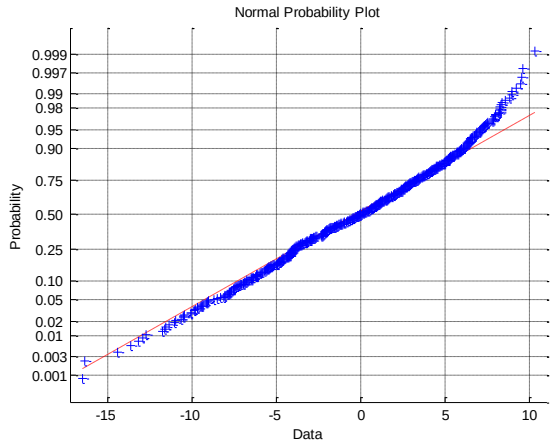

a: 'Small office' (Gnd floor kitchen, SD = 4.9 dB)

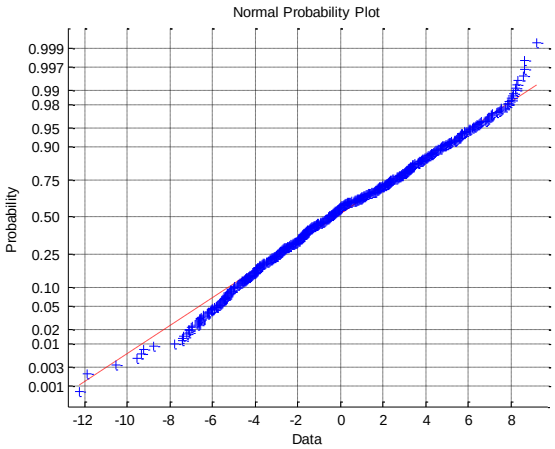

b: 'Retail B' (Back), SD = 3.7 dB)

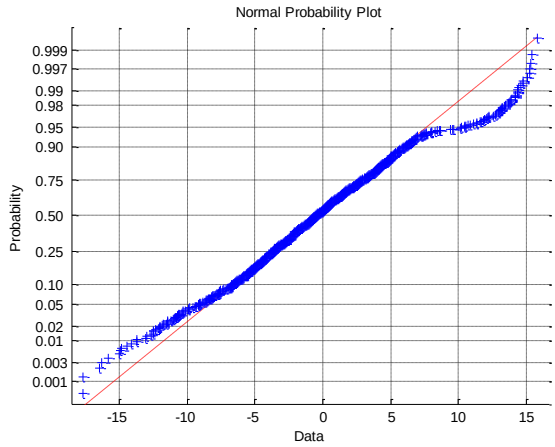

c: 'House' (study, SD = 5.5 dB)

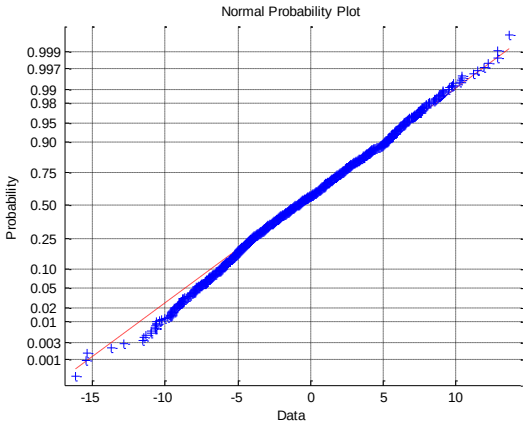

d: 'Retail A' (mid), SD = 4.4 dB)

11 Building entry loss measurements at 28 GHz

11.1 Scenario

The measurement scenario is shown in Fig. 44. The outdoor antenna was mounted on the roof of a parking garage 70 metres from the office, marked as point O in white, and the indoor antenna was mounted on a tripod on the third floor of an office building, marked yellow in Fig. 45.

FIGURE 45

Configuration of the antennas

The office has both standard and coated window glass as indicated in Fig. 46. The indoor distance between the walls with standard glass windows is 17 metres. The office landscape was empty apart from interior walls indicated in Fig. 46, and no people were accessing the area during the measurements. The weather-controlled textile outdoor blinds were not down during the first two measurements, but they were down occasionally during the long term measurement.

FIGURE 46

Drawing of the office landscape with type of glass marked, the black dot marks the spot for the long-term measurement. The distance between the walls with standard glass windows is 17 metres

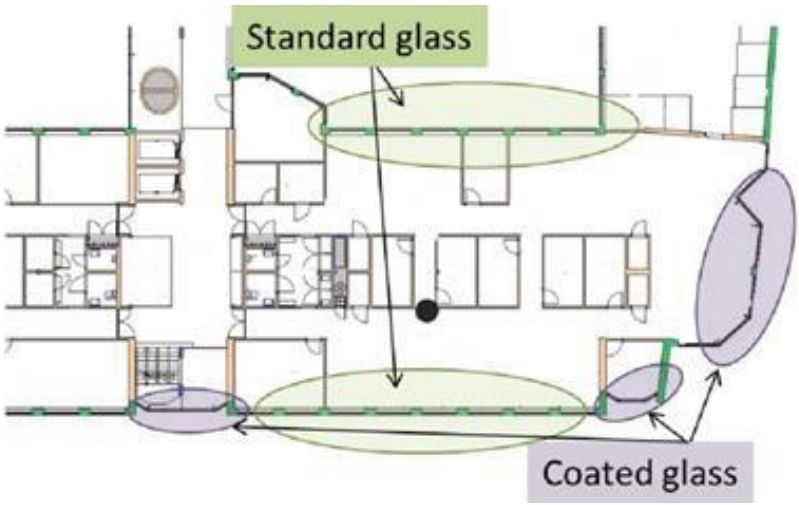

11.2 Experimental Set-up

The radio units used as transmitters and receivers in the measurements are commercially-available, all-outdoor single-carrier frequency division duplex (FDD) radio link units, operating in the 28 GHz band. They have a channel bandwidth of up to 50 MHz (56 MHz channel spacing) and modulation formats between 4 and 512 QAM, giving throughput between 94 and 406 Mbit/s at 50 MHz bandwidth. Adaptive modulation mode was enabled on the radios, which means that the modulation format depends on the mean square error detected by the radio, which in absence of additional interference can be referred to a threshold in received power.

At the indoor unit, a highly directive integrated antenna was used for all measurements. This antenna is a parabolic dish with diameter 0.24 m, 34 dBi gain, half-power beamwidth (HPBW) of 3.3 degrees, side-lobe level (SLL) below –20 dB and –30 dB at about 5 and 20 degrees, respectively. The

polarization of the antennas can be set to vertical or horizontal, and the cross-polarization discrimination (XPD) is better than 30 dB within two times the HPBW. The antenna was mounted 2 metres above floor level. At the outdoor unit, both the integrated 0.24 m antenna and a vertically-polarized wide-beam slot array antenna were used in two separate measurement setups. The wide-beam antenna has a gain of 22 dBi, a HPBW of 4.3 degrees in elevation, and about 60 degrees in azimuth. The XPD is better than 25 dB within the main beam.

The angular distributions at the indoor locations were determined by rotating the indoor antenna in the azimuth domain while continuously measuring the received power. This was done initially "by hand," but in a second campaign by using a motorized rotator to find the direction-of-arrival (DOA) to the strongest multipath components (MPCs). The set-up used for the second measurement campaign with the wide-beam outdoor antenna was also used for the long-term measurements. For the long-term measurements the indoor antenna was aligned for maximum received power.

The output power was always set to have an operating microwave link connection between the radios, though the transmitted power never exceeded +18 dBm. For the long-term measurements, an attempt was made to keep the power levels as realistic as possible, lowering the transmitted power of the indoor unit to minimize the regulated safety zone around the antenna. The transmitted power from the outdoor radio was +18 dBm on the roof and the indoor unit transmitted at –10 dBm.

11.3 Data collection/analysis

The transmitted and received powers of both radios, together with the capacity of the link in both directions, were collected during all measurements. The DOA angle of the maximum received power was also noted. To study the long-term stability of a potential radio link setup, a four-day measurement was conducted, with data collection every 30 seconds.

The excess loss in this paper is defined as the increase in loss relative to a measured reference LoS level at the indoor window location A, at 70 m LoS distance (see Fig. 47), with the window open.

FIGURE 47

Attenuation for the first scenario with narrow-beam antenna on both sides, with vertical polarization (left) and horizontal polarization (right). See Table 23 for the colour legend

TABLE 23

Colour legend used in Figs 47 and 48

Colour	Excess loss
	3-10 dB
	11-20 dB
	21-30 dB
	31-40 dB
	41-50 dB
	51-60 dB

11.4 Results

The measurement results are presented in Figs 47-49. At every measured point, an operating microwave link connection was established with a modulation format between 4 and 512 QAM. The capacity of the microwave link was in agreement with the predicted capacity for the actually received power and thus the link was usually not degraded due to multipath. At a couple of points there was evidence of frequency-selective fading, as the received powers differed between the up- and down-link directions. This was due to the separation of frequency in the FDD channel (1 008 MHz separation at 28 GHz). The indoor radio was in that case moved so that the received power in both directions became equal; the movement was less than 10 cm. Minor frequency-selective fading was expected, as the path differences for possible multipaths were small.

Figure 47 visualizes the excess loss for horizontal and vertical polarization when using a narrow antenna beam also at the outdoor unit. The reason for the steep increase in excess loss when moving backwards into the office, point A to C, is because the actual LoS path becomes partially blocked by the concrete pillars between the windows. From the measurement points further into the building, point D to F, the waves can either propagate through the interior wall or diffract/reflect around the interior cubical. Multiple MPCs with similar strengths were present.

Figure 48 shows the excess loss for vertical polarization with a sector antenna at the outdoor unit. The reason for the variation in excess loss along the corridor is due to the concrete pillars, as mentioned earlier, blocking the LoS path.

FIGURE 48

Attenuation in scenario two, with wide-beam antenna at the outdoor site. See Table 23 for colour legend

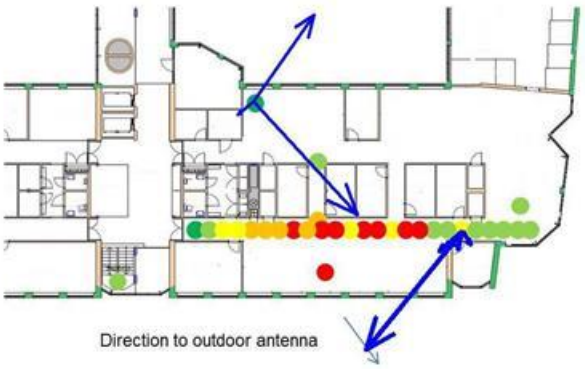

Figure 49 shows the received power and capacity from a long-term measurement during four days. The long-term measurement showed stable throughput and received power levels. The decrease in

received power, occurring every afternoon, was due to outdoor sun blinds going down automatically to cover the windows. In this scenario, any major time-dependent changes of the channel were not expected, as no person had access to the office landscape during the measurements and the outdoor weather during this period was without any precipitation. The difference in received power between the outdoor and indoor radio is due to the 28 dB difference in transmitted power mentioned earlier. The capacity of the links was 406/285 Mbit/s in down-/up-link, which correlates to a modulation format of 512/64 QAM. The up- and down-link radios are independent and can send data in different modulation formats. The modulation formats, as mentioned earlier, depend on the mean square error which, if no interference is present, is directly dependent on the received power. The capacities measured are in good agreement with the modulation format expected for the measured received power, indicating no degradation due to interference/multipath.

FIGURE 49

Received power and throughput over 4 days; the difference in received power is due to difference in transmitted power; the indoor unit transmitted 28 dB lower power

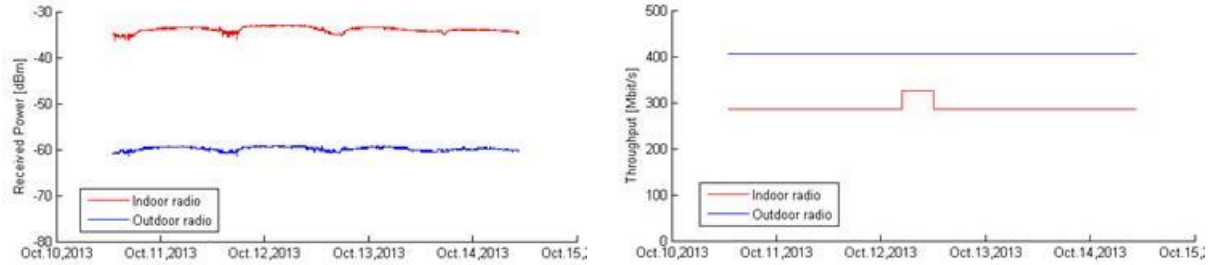

A loss of about 3-5 dB was measured in the standard glass window and about 30 dB in the coated window, which is in good agreement with other[8] observations.

At the indoor unit there was usually more than one incoming direction of waves. The attenuation in Figs 47 and 48 refers to the strongest path. If a LoS path was available, this was always the clearly dominating path, but in most other cases power was received from more than one incoming direction. Two examples of this are shown in Fig. 48. The lengths of the arrows indicate the linear relation between the received power in different DOA directions (a doubly-long arrow corresponds to 3 dB higher received power). The length of the arrows is normalized to the highest received power at that measured point and is not related to the length of the arrows at the other location. As can be seen at the top left point there is almost equal power from two directions. All waves seem to reach the point after passing through the narrow passage between the indoor cubicles, either through multiple reflection or diffraction. One path obviously also includes a reflection from the windows behind the measurement point. For the lower right measurement point, the paths are somewhat more difficult to explain. This case involves a concrete wall and an evacuation staircase with coated glass, blocking the LoS, which the signal is not penetrating so easily. As can be seen, the strongest path is propagating via a final diffraction on the edge of the blocking concrete wall in the proximity of the antenna. Regarding its path before the diffraction, it is not clear if it is reflection/diffraction on the concrete pillars between the windows or multiple reflections within the office space. Beyond this strongest path, 6 paths reaching the measurement point by reflection were also measured. Since these are about 10 dB below the strongest one, they are difficult to see in the picture.

---

[8] Zhao, H., *et al.*, "28 GHz Millimetre Wave Cellular Communication Measurements for Reflection and Penetration Loss in and around Buildings in New York City", Proc. IEEE International Conference on Communications (ICC 2013), June 2013.

11.5 Conclusion

The results show that attenuation/excess loss limits the coverage, rather than multipath interference. In the scenario studied, coverage was obtained at all measured locations with a loss between 3 and 60 dB above the reference level at 70 m LoS distance. If all windows in the office had been of the coated glass kind, then at least 20 dB higher excess loss would be expected and the coverage would be significantly more limited. Thus, the deployment opportunities strongly depend on the specific location and the kind of windows that are present.

It is concluded that the indoor environment at this location is not isolated from the outdoor cell. Thus, at many locations it will be possible to provide, for example, a backhaul link between an indoor wall-mounted high gain antenna and a similar outdoor antenna, even when the indoor excess loss is extensive.

12 Measurements at 5.2 GHz

The experimental results shown in Table 24 were obtained at 5.2 GHz through an external building wall made of brick and concrete with glass windows. The wall thickness was 60 cm and the window-to-wall ratio was about 2:1.

TABLE 24

Example of building entry loss

Frequency	**Office**	
	Mean	Standard deviation
5.2 GHz	12 dB	5 dB

Table 25 shows the results of measurements at 5.2 GHz through an external wall made of stone blocks, at incident angles from 0° to 75°. The wall was 400 mm thick, with two layers of 100 mm thick blocks and loose fill between. Particularly at larger incident angles, the loss due to the wall was extremely sensitive to the position of the receiver, as evidenced by the large standard deviation.

TABLE 25

Loss due to stone block wall at various incident angles

Incident angle (degrees)	0	15	30	45	60	75
Loss due to wall (dB)	28	32	32	38	45	50
Standard deviation (dB)	4	3	3	5	6	5

13 Building Entry Loss from 5-32 GHz

13.1 Introduction

This section presents measurements of outdoor-to-indoor propagation from 5-32 GHz. For this exercise three different buildings were measured. The first is a newer building (built in 2009) that is similar in construction to a modern residential home in the United States. The second is an older commercial office building (built in 1945). The last building is a very new commercial office building built using modern “green” building techniques. These two buildings allow for the measurement of

propagation losses through both modern and older materials such as glass/windows and exterior block and siding. The excess loss (with free space loss removed) for both buildings is presented in this document.

13.2 Experimental Setup

The signals used during this experiment were continuous wave (CW) at 5, 12, 25.5 and 32 GHz.

The antennas used for both the transmitter and receiver were identical dual ridge horn antennas (MVG Model Number: SH4000) with the following characteristics:

FIGURE 50

Picture of the antenna used for the experiment

TABLE 26

Transmit and receive antenna parameters

Antenna Gain	4.5-13 dBi (Frequency Dependent)
3 dB Beamwidth	80-40° (Frequency Dependent)
Gain Stability	±1 dB

The outdoor transmitter consisted of a signal generator (Anritsu MG3690C) connected to the dual ridge horn antenna, with an optional amplifier that was not used for this experiment but could be included for future measurements if necessitated by the expected free space loss. The receiver

consisted of an identical antenna connected to a spectrum analyzer (Agilent E4446A). Initially two identical receivers were setup with the intent on simultaneously measuring the outdoor reference and the indoor locations, as indicated by Recommendation ITU-R P.2040-1. However due to observed coupling between the two receive antennas, it was decided that the outdoor and indoor measurements would be conducted separately.

FIGURE 51

Block diagram of the receiver (left) and transmitter (right) used for the experiment

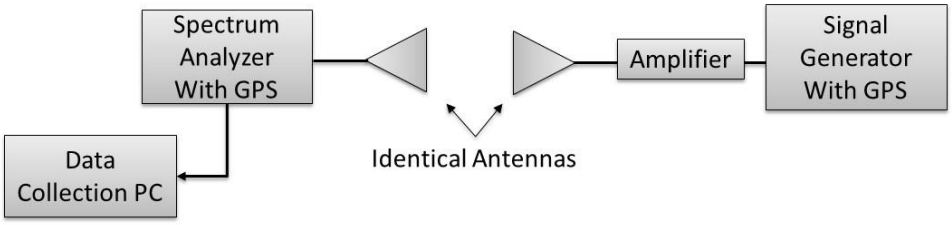

13.2.1 Building descriptions

The first building that was measured is a recently constructed building similar to a modern US residential building. The building's exterior is made up of vinyl siding followed by plywood sheeting with metal studs with fiberglass insulation in-between covered by final layer of drywall. The windows in the building are standard double pane low-emissivity windows used in most modern US construction.

The second building is an older commercial office building. The exterior walls are composed of 10.2 cm of brick on top of 20.3 cm of concrete block followed by 2.5 cm furring strips and 1.9 cm layer of plaster. The windows are older and made of double pane glazed glass with aluminium frames.

The third building is a new building that was constructed with a focus on environmental factors, e.g. a lot of recycled/energy efficient material and low E glass windows. There also is a reflective thermal coating on the windows to help keep the building cool in the summer and warm in the winter. This coating as well as the low E glass seems to have a large effect on the transmission of signals into/out of the building, as will be shown in the results that follow.

FIGURE 52

Photograph of the front of Building 1 (left) and Building 2 (right) and Building 3 (bottom)

13.2.2 Testing Locations

For each test point the transmitter was positioned so that the signal had normal incidence onto the face of the building. The receiver was then positioned in direct line of sight (LOS) at 0° azimuth with reference to the transmitter. The height of the transmitter and receiver were matched to eliminate any changes in the received signal level due gain deviations in the antenna patterns. Figure 53 shows the locations of each antenna during the experiment for both the reference measurement and the actual building measurement.

FIGURE 53

Depiction of experimental setup

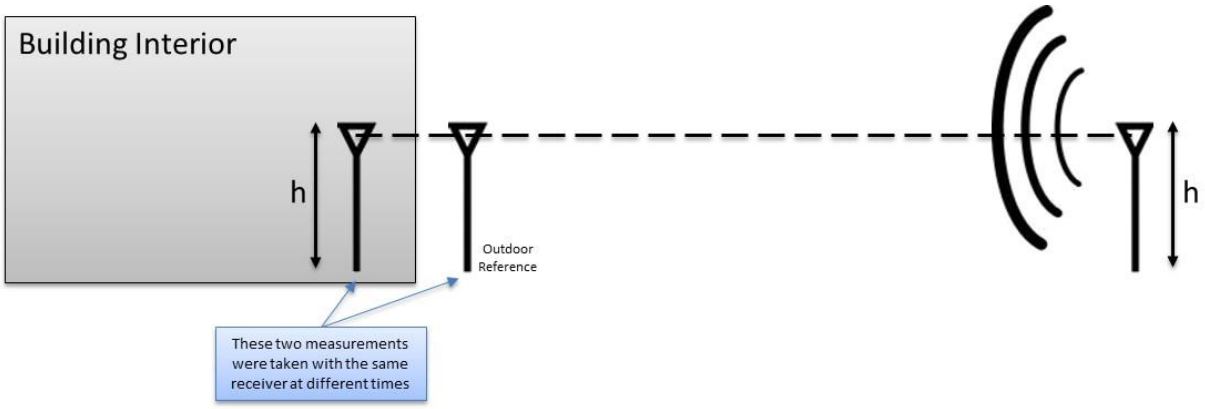

FIGURE 54

Photos of the transmitter and receiver during testing

After the outdoor reference measurement was taken, the receiver was moved into the building and positioned to again be a at 0° azimuth with reference to the transmitter and at the same height as both the outdoor measurement and the transmitter. A laser transit system was used to match the heights and to account for any changes in ground elevation. For each transmitter location the indoor measurements were stepped linearly, moving farther away from the transmitter at each test point taking care to ensure that the 0° azimuth with reference to the transmitter was maintained thought the experiment.

FIGURE 55

Diagram showing how receiver was linearly stepped into building

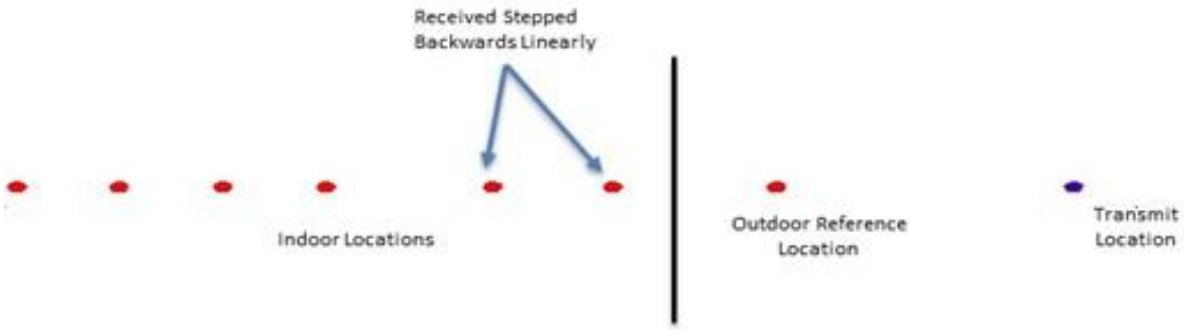

When the rear of the building was reached the transmitter was repositioned to the next location and the process was repeated. The transmitter was stepped across the face of the building to ensure that there was always normal incidence on the building face and so that the transmitter and receiver were always pointed boresight to reduce/eliminate signal level changes due to gain variations over the beamwidth. The floor plans and the testing locations of each building are shown in Figs 56-58.

The spatial density of points needs to be considered when conducting an experiment such as this. The testing locations were chosen to be somewhat uniformly distributed and to ensure that all of the unique aspects of the building were sampled (e.g. windows, doors, large wall sections, hallways, etc.). For Building 1 the spatial density was 1 point per 5 square meters, for Building 2 it was 1 point per 14 square meters, and for Building 3 it was 1 point per 27 square meters. The points were designated by

defining an arbitrary origin at a location inside the building, then referencing all spatial locations to that origin.

FIGURE 56

Floor plan and testing locations for Building 1

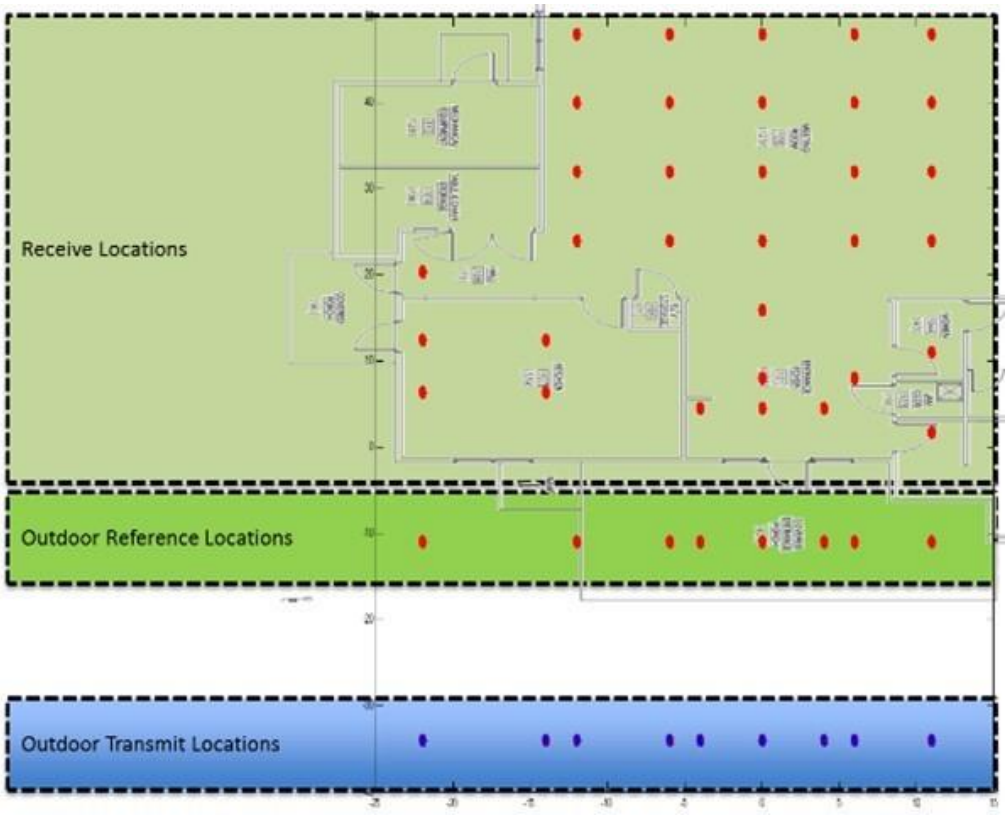

FIGURE 57

Floor plan and testing locations for Building 2

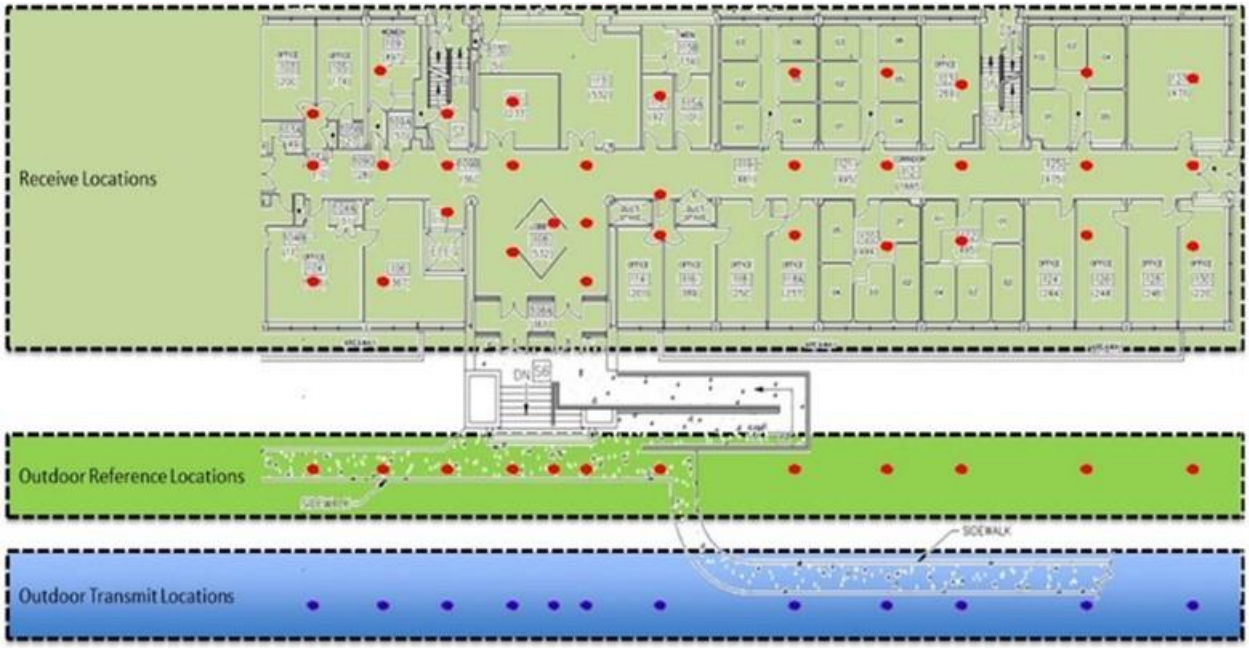

FIGURE 58

Floor plan and testing locations for Building 3

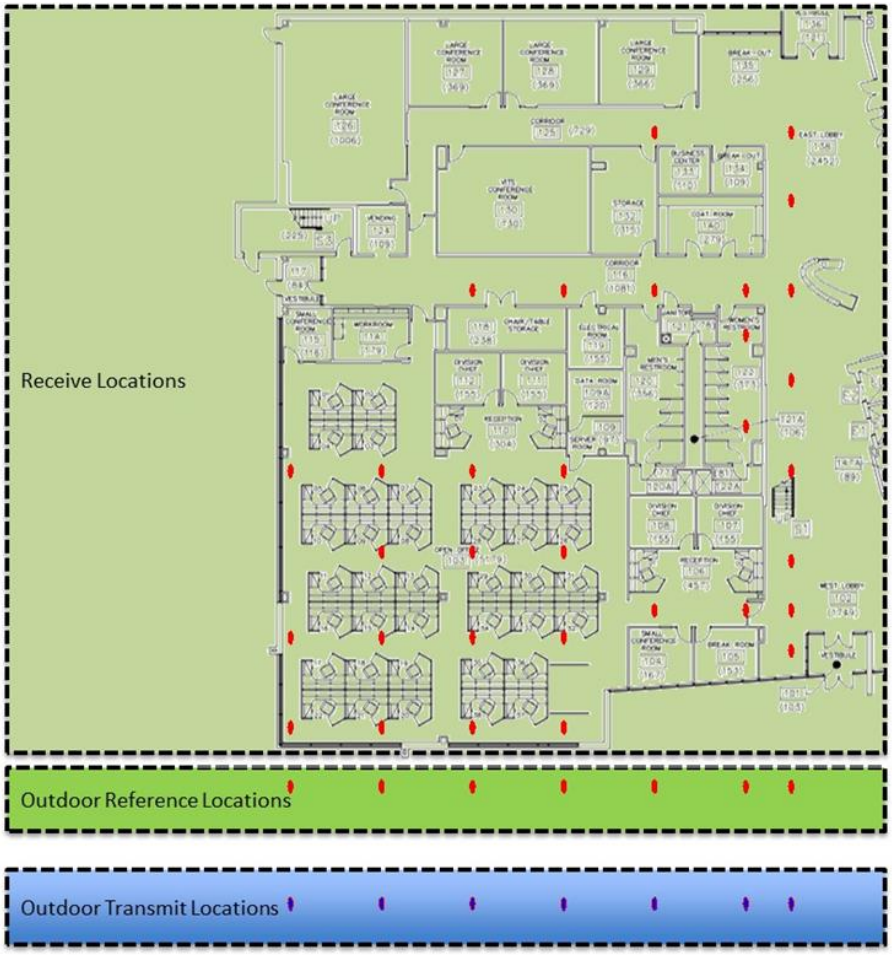

FIGURE 59

Photos of the interior testing points being laid out using tape measures to reference the defined origin

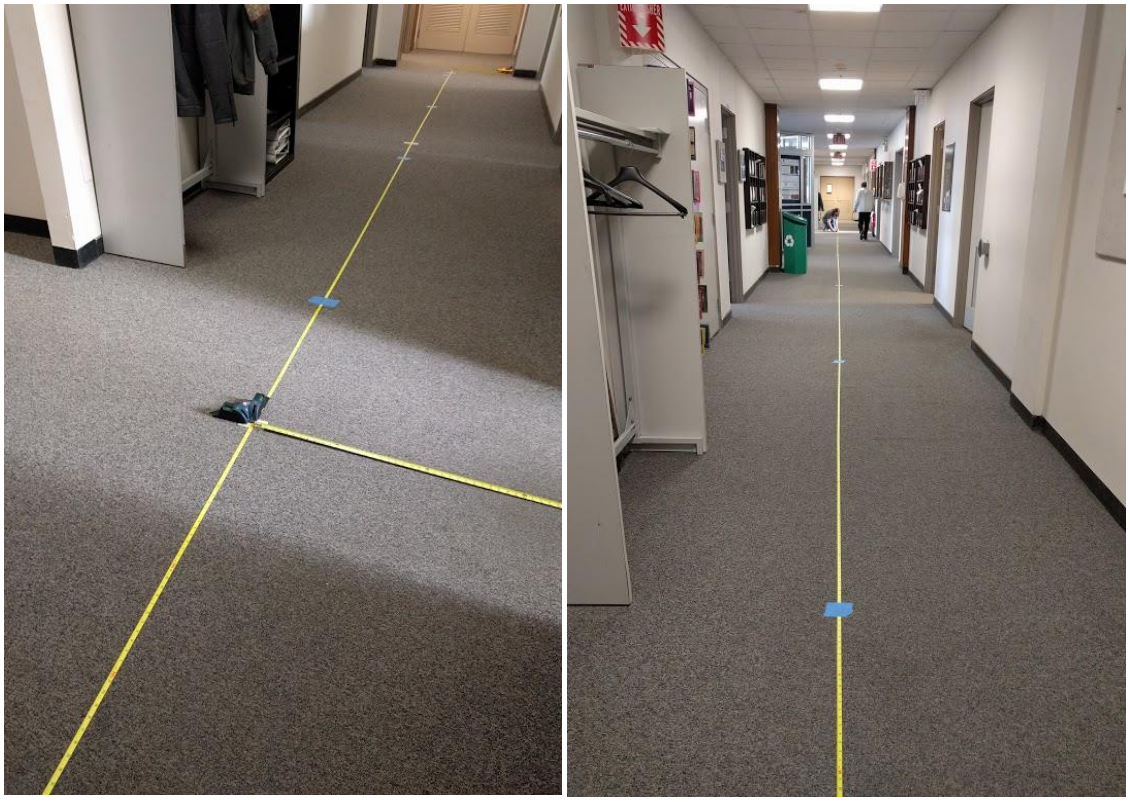

13.2.3 Data post processing

At each test point in the experiment a minimum of two minutes of data per frequency was collected at 1 Hz. In post processing the temporal data at each test point was subjected to a trimmed average by calculating the standard deviation (σ) of all the samples at a particular point and frequency then removing any outliers (defined as values exceeding ±3σ) then averaging the remaining points. The total number of outliers removed from the data set comprised less than 0.5% of the total samples collected.

The building entry loss in this paper is defined as:

$$BEL(x,y) = P_{ref}(x,y,t_0) - P_{indoor}(x,y,t_n) - L_{FS}(x,y)$$

Where BEL is the building entry loss, P_{ref} is the time averaged power received at the outdoor reference location, P_{indoor} is the received power at the indoor location and L_{FS} is the additional free space loss that occurred from the signal traveling past the reference point and into the building.

13.3 Results

The following sections contain the results of the measured building loss from each building. The results are analyzed and presented in several different ways, including: tabulated, visually with 2D maps and statistically.

13.3.1 Tabulated Results

The tabulated measurements results are presented in Tables 27 to 29. From the data in Tables 27 to 29, it can be seen that the range of building loss seen is quite large depending on the position inside the building. The minimum BEL seen was on the order of 1-2 dB with the maximum in excess of 50 dB. It is important to note that for each building the measurements were taken over the course of

a single evening and that during the time measurements were taken the temperatures deviation was less than 6°C. Additionally, there was no precipitation during testing.

TABLE 27

Tabulated Building Loss Results for Building 1

Frequency (GHz)	Minimum (dB)	Mean (dB)	Maximum (dB)	Standard deviation (dB)
5	1	8.5	27	6.5
12	.5	9.5	23.5	5.5
25.5	3.5	14	32	6
32	2.5	17	40	7.5

TABLE 28

Tabulated Building Loss Results for Building 2

Frequency (GHz)	Minimum (dB)	Mean (dB)	Maximum (dB)	Standard deviation (dB)
5	1	13.5	32.5	9.5
12	1	14	30	9.5
25.5	1.5	17.5	52.5	15
32	2.5	14.5	45	14.5

TABLE 29

Tabulated Building Loss Results for Building 3

Frequency (GHz)	Minimum (dB)	Mean (dB)	Maximum (dB)	Standard deviation (dB)
5	11.5	29	53	12
12	16	31	51.5	11
25.5	13	35.5	69	14.5
32	20.5	38	58.5	12

It is important to note that for each building the measurements were taken over the course of a single evening and that during the time measurements were taken the temperatures deviation was less than 6°C. Additionally, there was no precipitation during testing.

It is also important to note that all of the buildings presented a multipath rich environment. This created a substantial amount of variation in the received signal as a function of position. Multipath has the potential to be both constructive and destructive. When considering any single spatial point, the contribution of multipath should be taken into account, and therefore some of the minimum (and maximum) values in the above tables are likely influenced by multipath. Additionally, the reciprocal nature of the propagation path was not measured and therefore the measured building entry losses shown in Tables 27 to 29 may not necessarily be equated to building exit losses.

13.3.2 Coverage maps

A visualization of the building entry loss seen inside the building is shown in Figs 60 to 62. These figures were generated by taking the averaged data points and applying a 2D spline interpolation to approximate what the building entry loss values would be throughout the entire building. High levels of loss are expressed as warm colours (reds, yellows etc.) and lower levels of loss are cool colours (greens, blues etc.).

FIGURE 60

Interpolated building entry loss map of Building 1

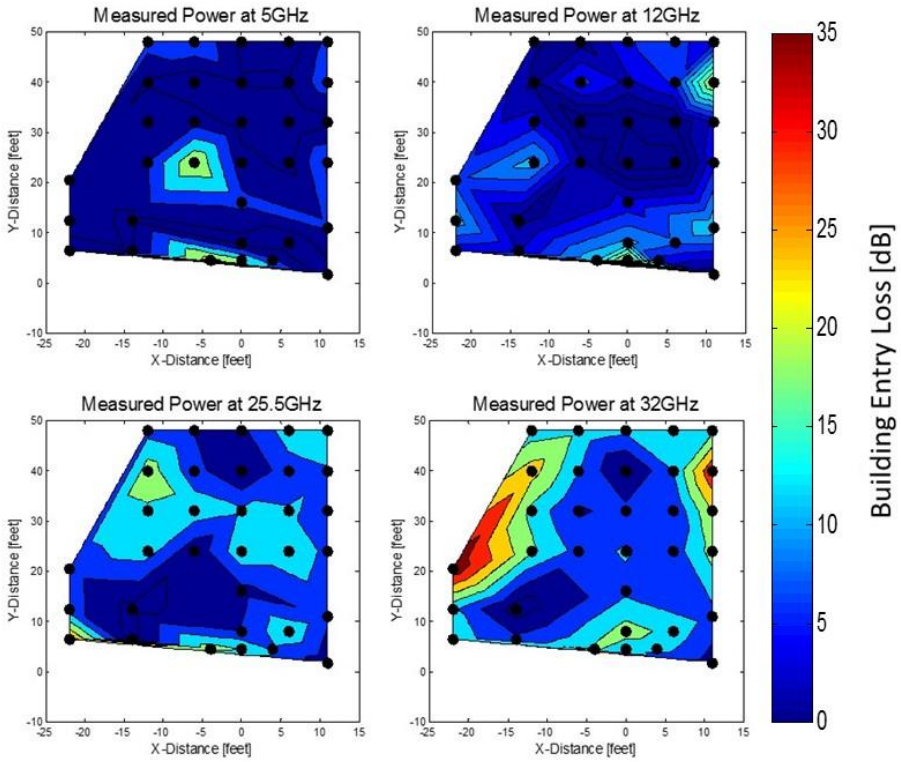

FIGURE 61

Interpolated building entry loss map of Building 2

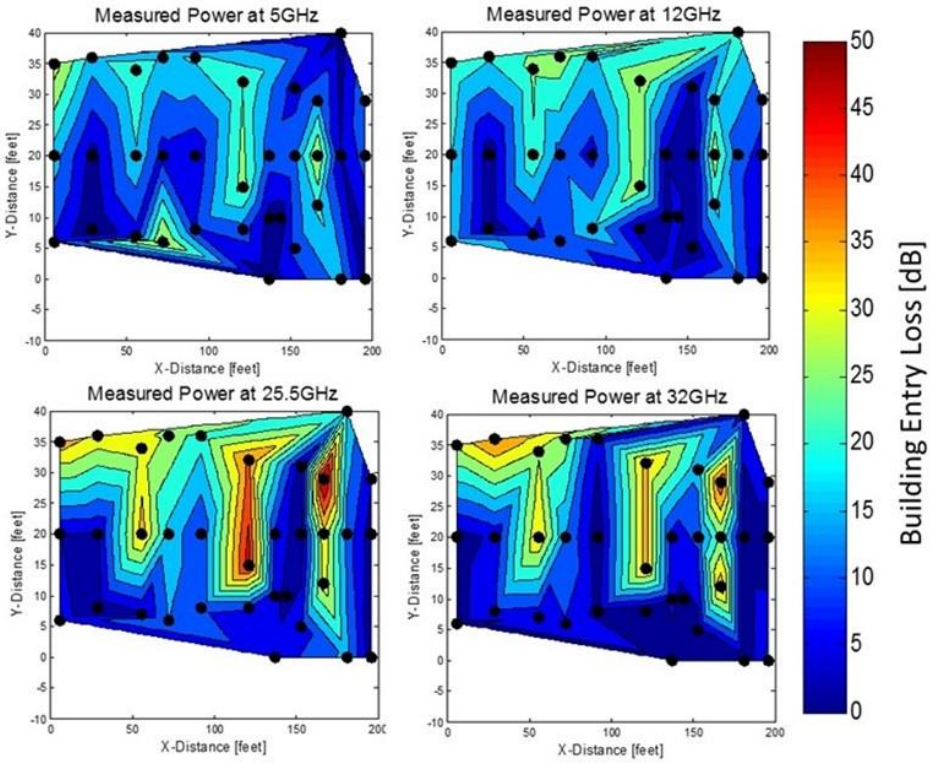

FIGURE 62

Interpolated building entry loss map of Building 3

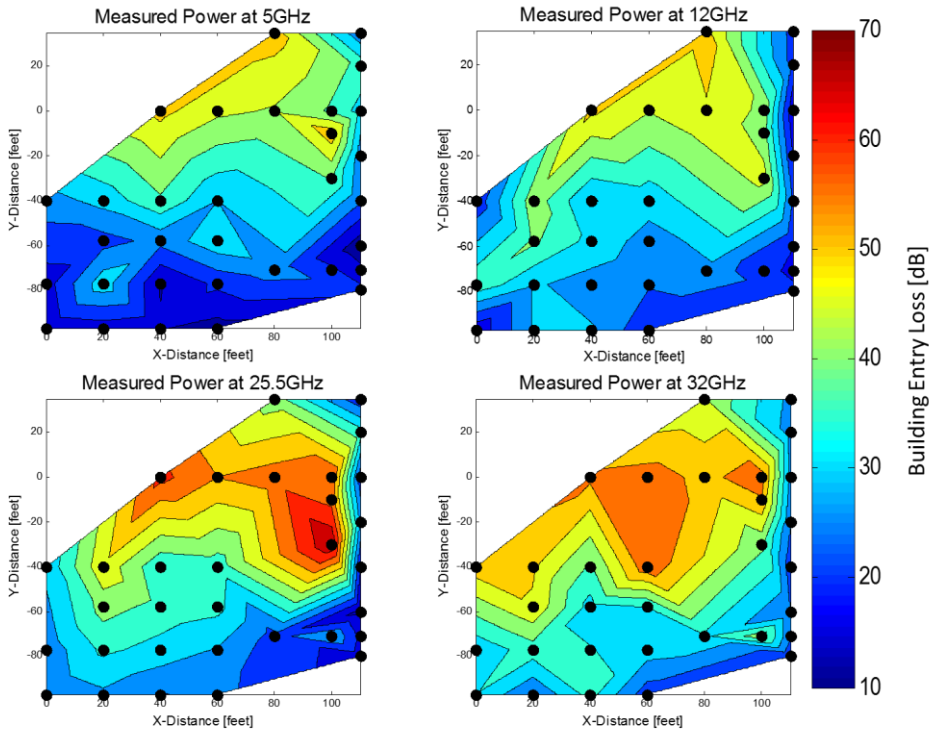

From these plots it appears that the measurement results are more uniform in Building 1. This is due to the open nature of the building, as seen from the floor plan. Once inside building one the majority of the area is contained inside one large "great room" with very few interior walls or furniture. Conversely, Building 2 and 3 are subdivided into many offices and those offices are further divided into individual cubicles each containing standard office furniture, desk, chairs, bookshelves, etc.

In both buildings there appeared to be a large amount of multipath as the signal diffracted/reflected off the building interior. For the purpose of this experiment the receivers were kept pointed boresight with the transmitter but a large amount of signal variation occurred with azimuth rotation. This effect needs to be explored further to characterize the overall role of multipath in building entry loss.

13.3.3 Distance dependency

The next three figures (Figs 63 to 65) show the relationship between the building entry loss and the distance from the transmitter, keeping in mind the all of the free space loss has been removed. There are four curves on each plot, corresponding to the four discrete frequencies that were tested. The 5, 12, 25.5 and 32 GHz curves are the dark blue, green, red and light blue curves respectively.

FIGURE 63

Building entry loss as a function of distance into Building 1

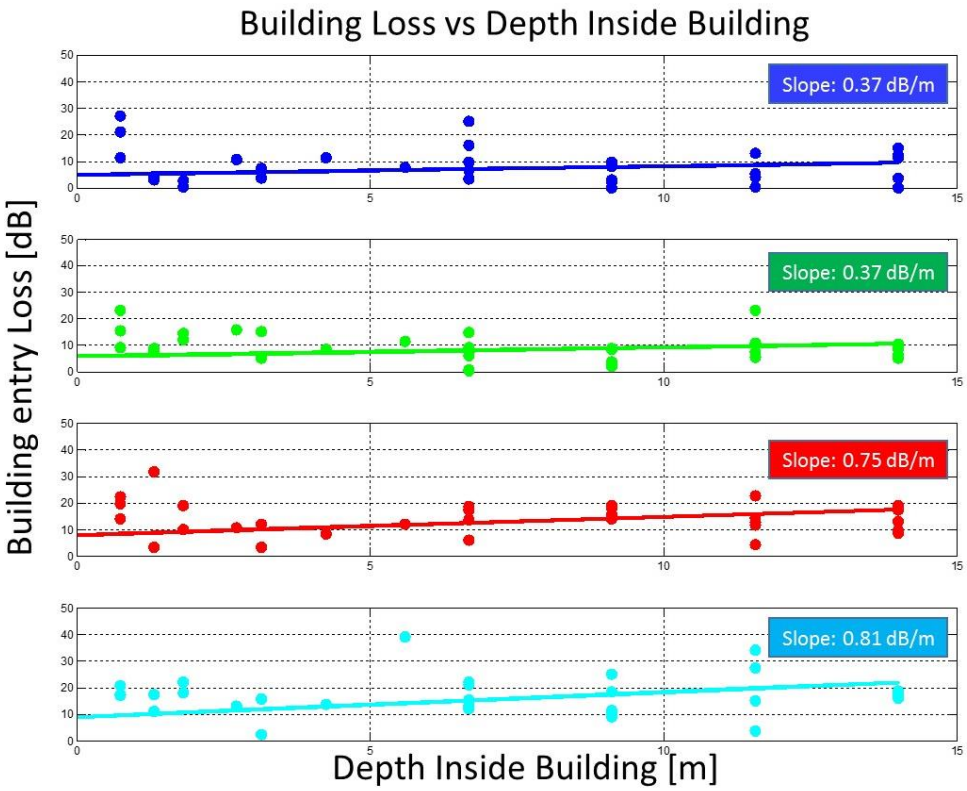

FIGURE 64

Building entry loss as a function of distance into Building 2

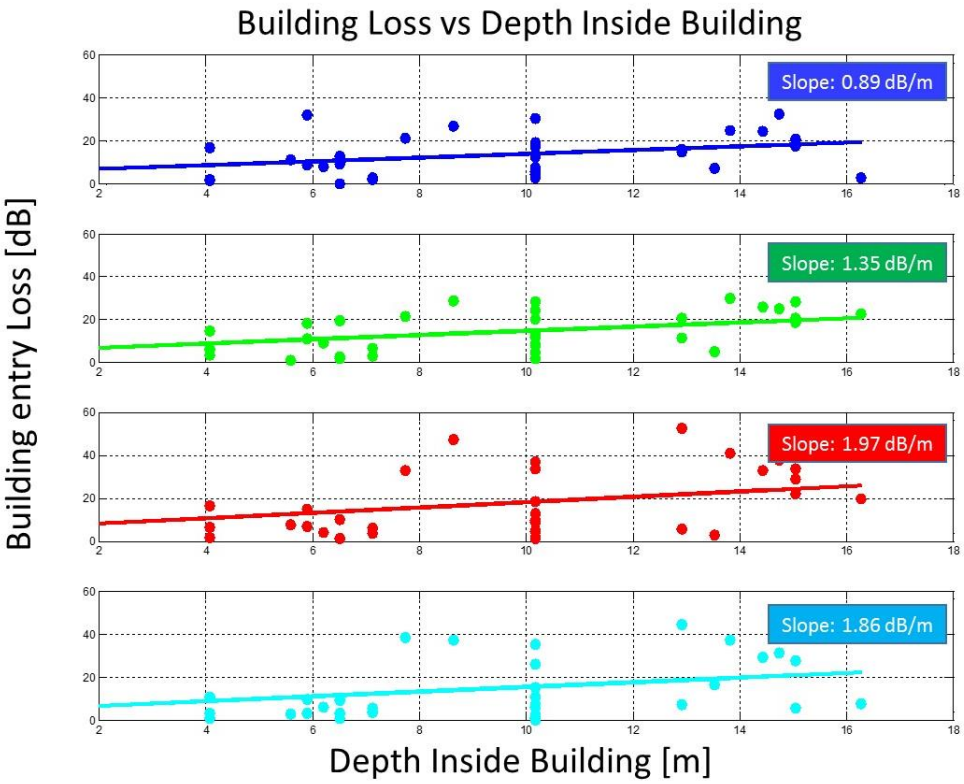

FIGURE 65

Building entry loss as a function of distance into Building 3

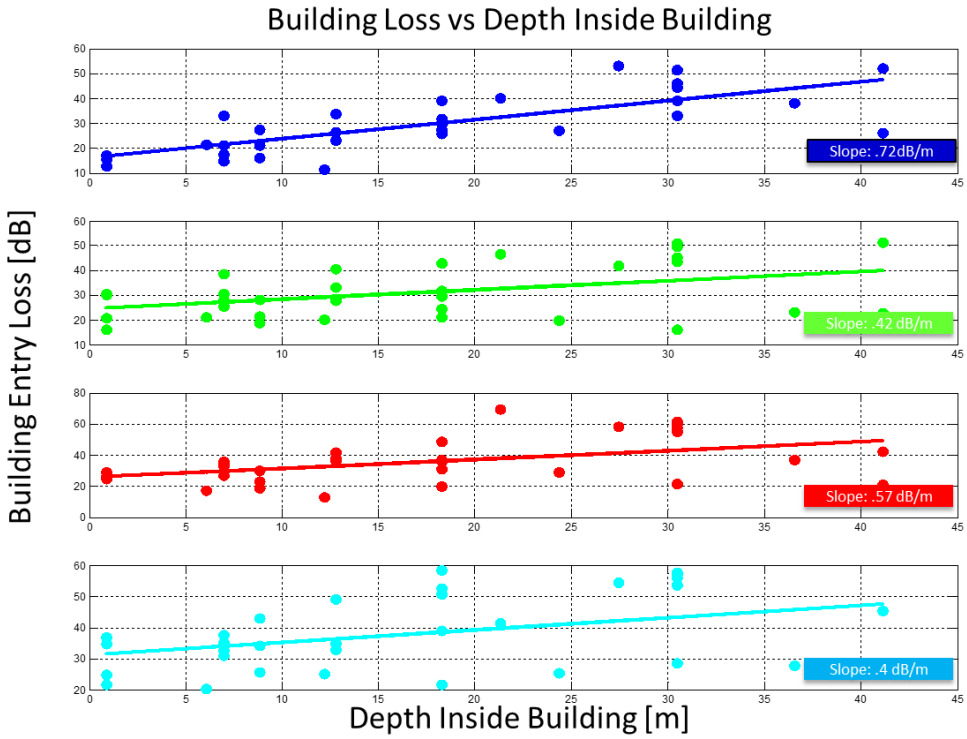

From the above Figures, it can be seen that there is an increasing trend in building entry loss as a function of distance inside of the building. This is due to the increase in different propagation mediums encountered as the signal travels into the building, e.g. interior walls, furnishings. This effect is more prevalent in Building 2 where the building had many interior walls and an abundance of furnishings.

13.3.4 PDF Distributions

Next the probability density functions (PDFs) of the data sets are considered. The distributions appear to be lognormal with the mean and standard deviation varying with frequency. Plotted alongside the actual PDF results are simulated lognormal PDFs using the means and standard deviations listed in Tables 27 and 28. The results from Building 1 more closely match the simulated log normal PDFs, this is most likely due to the open nature of the building with very few interior walls or furnishings. Additional data points for Buildings 2 and 3 could potentially enhance the PDF results and give a more accurate indication as to the PDF distributions.

More buildings will need to be measured in order to expand upon and examine these trends in more depth and confirm the conclusions about the distributions; but this information is promising for future modelling purposes.

FIGURE 66

PDF Distributions of Building 1

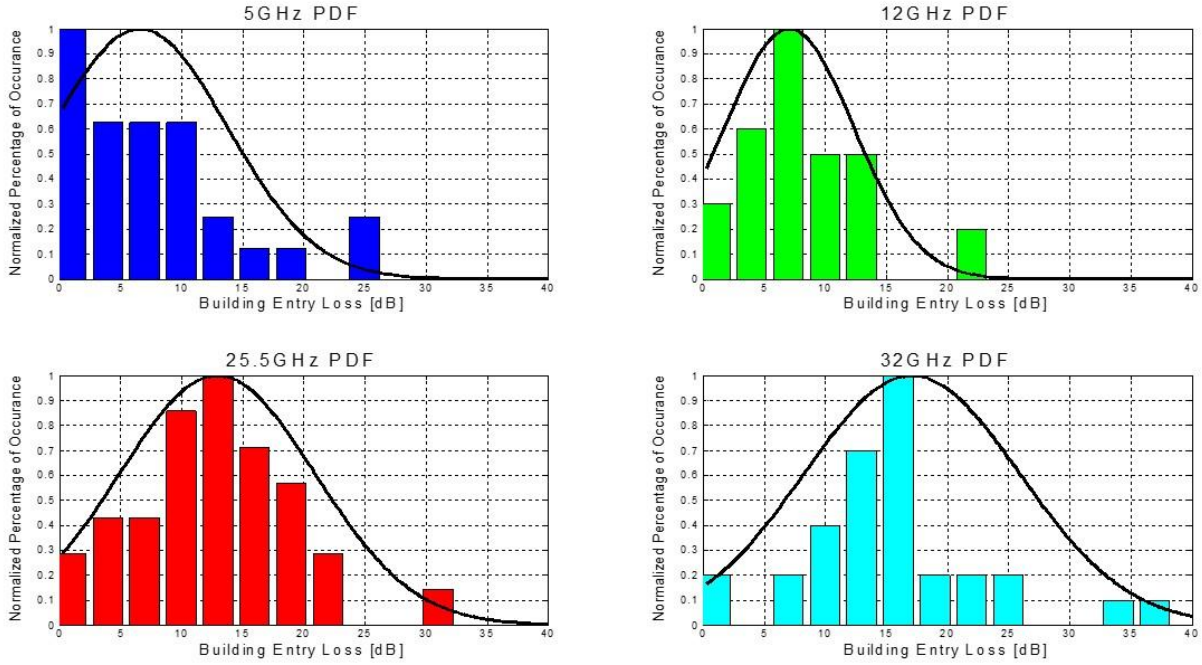

FIGURE 67

PDF distributions of Building 2

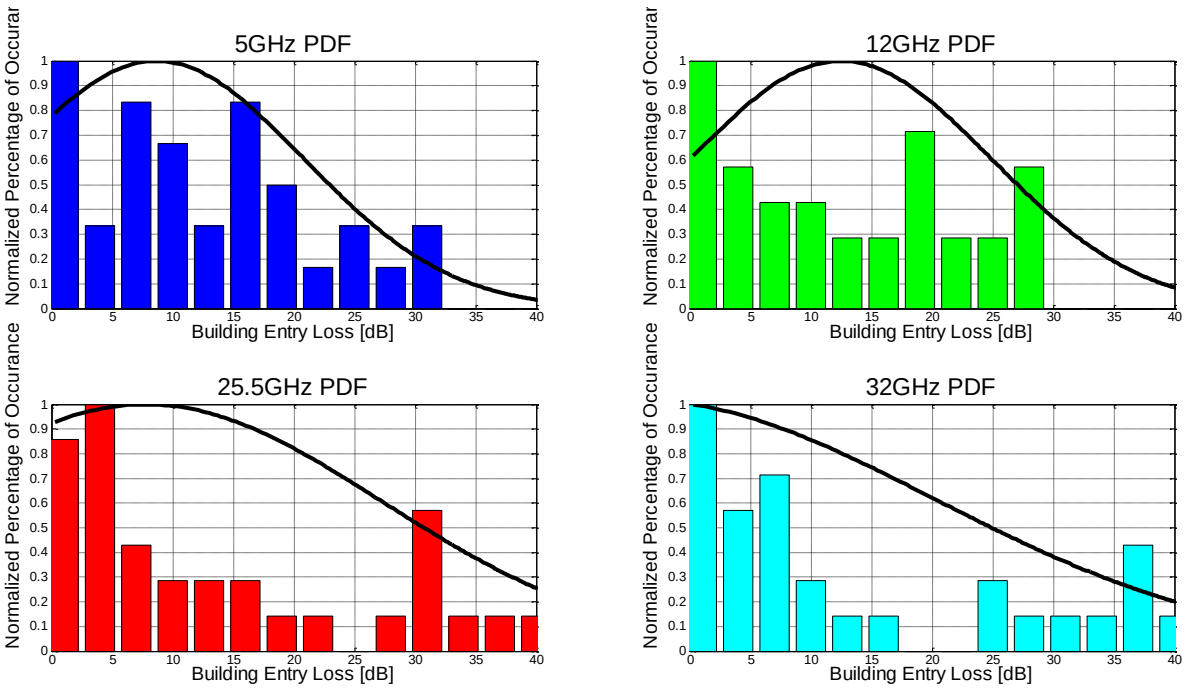

FIGURE 68

PDF distributions of Building 3

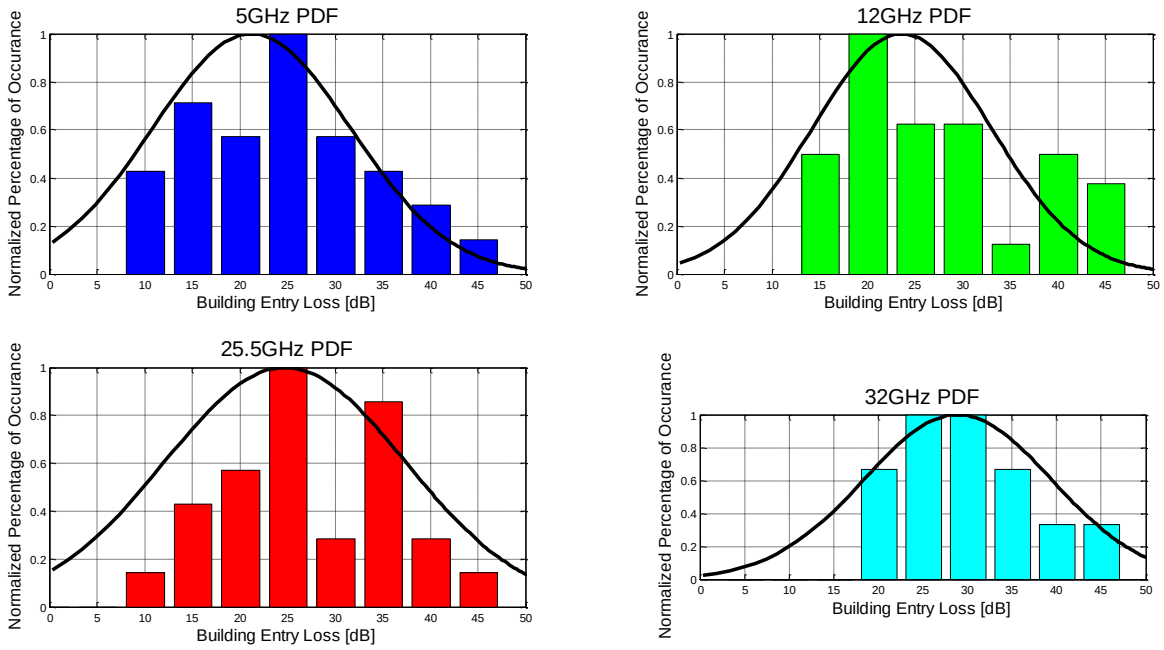

13.3.5 CDF Distributions

Finally the cumulative distribution functions (CDFs) are examined. The CDFs show that 90% of the time the loss contributed to the building was less than 26 dB for all frequencies in Building 1, however the higher frequencies saw increased loss in Building 2 with 90% of the overall building entry loss seen being less than 40 dB. Building 3 had the lowest minimum building entry loss seen over 10 dB however 90% of the measurements were still less than 40 dB.

FIGURE 69

CDF of building entry loss for Building 1

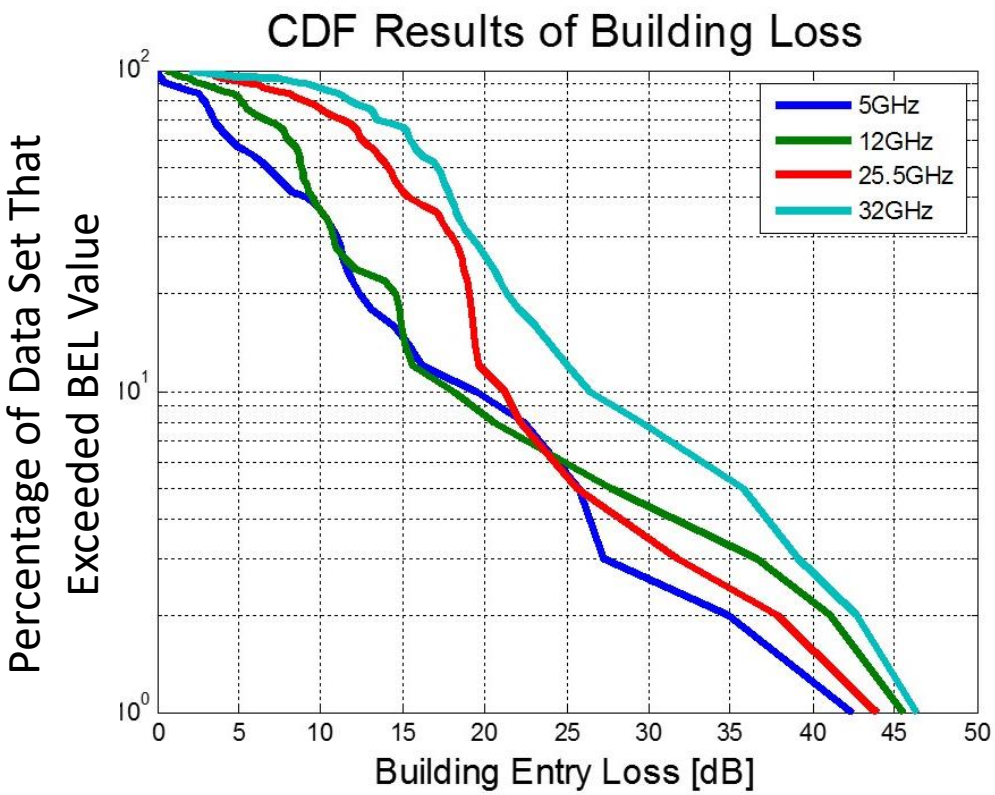

FIGURE 70

CDF of building entry loss for Building 2

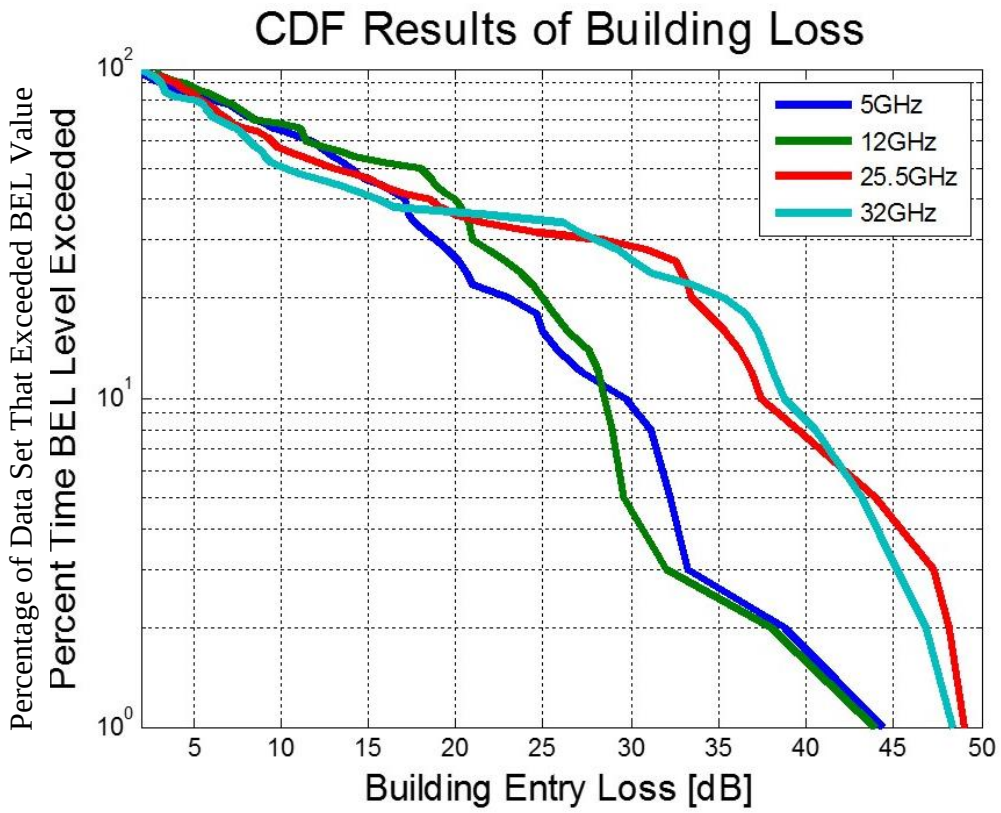

FIGURE 71

CDF of building entry loss for Building 3

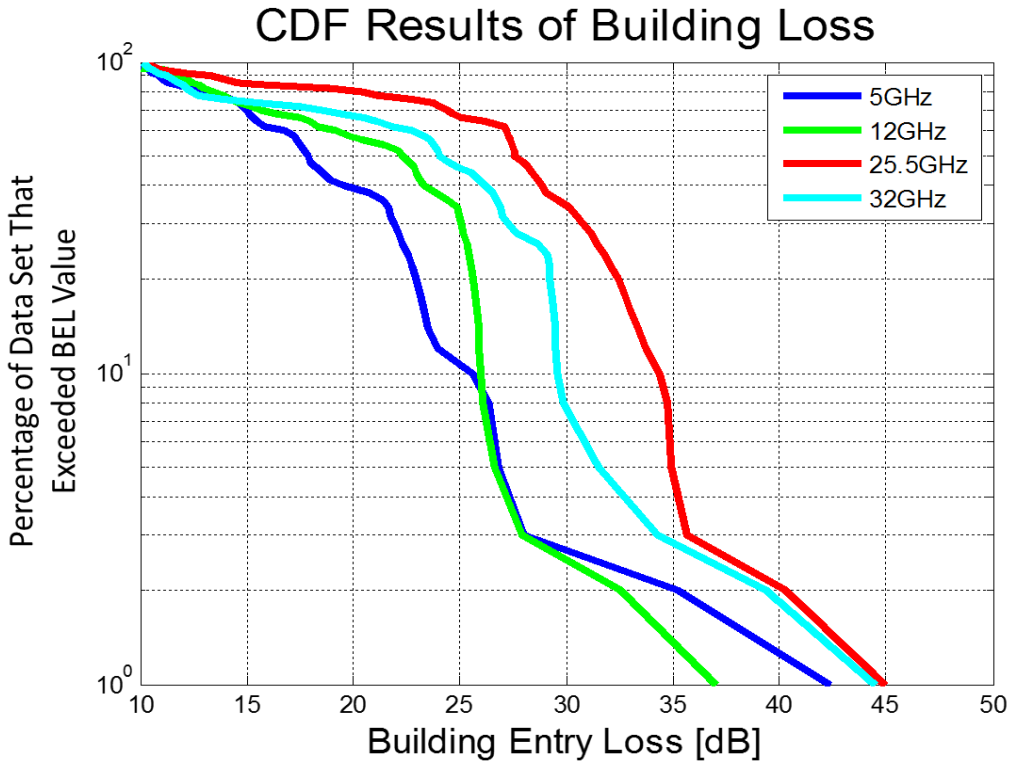

13.4 Tables of Building Parameters

Recommendation ITU-R P.2040 recommends the completion of the following Tables to identify pertinent details about the buildings testing and the measurements taken.

TABLE 30

Measurement parameters for Building 1

Frequency	**5, 12, 25.5 and 32 GHz**
Bandwidth of test signal	0 MHz
Surrounding environment	Suburban
Line of sight to building?	Yes
Averaging	Temporal averaging at each test point
Penetration depth	1 = indoor terminal in room/space with external wall facing outdoor terminal
Floor on which measurements made	Ground floor = 0
Area within which samples taken	180.88 m^2
Number of samples	42 spatial points with 100+ temporal samples at each location
Reference	1 = measured median signal
Distance of outdoor terminal from building	3.3528 m
Elevation angle of path	0°
Minimum azimuth with respect to normal to building face	0°
Maximum azimuth with respect to normal to building face	0°
Width	15.2 m
Length	15.2 m
Height	7.6 m
Total number of floors	1
Thickness of exterior walls	.152 m
Thickness of interior walls	.152 m
Thickness of floors	N/A
Proportion of building elevation area composed of windows/apertures	%
Window elements	2 = double
Window coating	0 = unknown
Metallic thermal insulation fitted?	0 = unknown
Floor material	3 = concrete
Primary Exterior wall material	5 = wooden
Secondary Exterior wall material	8 = metal
Internal walls	7 = Plasterboard (metal stud)
Roof materials	5 = wood with roofing felt

TABLE 31

Measurement parameters for Building 2

Frequency	**5, 12, 25.5 and 32 GHz**
Bandwidth of test signal	0 MHz
Surrounding environment	Suburban
Line of sight to building?	Yes
Averaging	Temporal averaging at each test point
Penetration depth	1 = indoor terminal in room/space with external wall facing outdoor terminal
Floor on which measurements made	Ground floor = 0
Area within which samples taken	700 m^2
Number of samples	50 spatial points with 100+ temporal samples at each location
Reference	1 = measured median signal
Distance of outdoor terminal from building	15.8 m
Elevation angle of path	0°
Minimum azimuth with respect to normal to building face	0°
Maximum azimuth with respect to normal to building face	0°
Width	12.1 m
Length	60.9 m
Height	7.6 m
Total number of floors	2
Thickness of exterior walls	.352 m
Thickness of interior walls	.152 m
Thickness of floors	N/A
Proportion of building elevation area composed of windows/apertures	%
Window elements	2 = double
Window coating	0 = unknown
Metallic thermal insulation fitted?	0 = unknown
Floor material	3 = concrete
Primary Exterior wall material	2 = brick
Secondary Exterior wall material	4 = lightweight block
Internal walls	7 = Plasterboard (metal stud)
Roof materials	9 = other

TABLE 32

Measurement parameters for Building 3

Frequency	5, 12, 25.5 and 32 GHz
Bandwidth of test signal	0 MHz
Surrounding environment	Suburban
Line of sight to building?	Yes
Averaging	Temporal averaging at each test point
Penetration depth	1 = indoor terminal in room/space with external wall facing outdoor terminal
Floor on which measurements made	Ground floor = 0
Area within which samples taken	1400 m^2
Number of samples	40 spatial points with 100+ temporal samples at each location
Reference	1 = measured median signal
Distance of outdoor terminal from building	11.5 m
Elevation angle of path	0°
Minimum azimuth with respect to normal to building face	0°
Maximum azimuth with respect to normal to building face	0°
Width	12.1 m
Length	46 m
Height	18 m
Total number of floors	3
Thickness of exterior walls	.352 m
Thickness of interior walls	.152 m
Thickness of floors	N/A
Proportion of building elevation area composed of windows/apertures	80%
Window elements	2 = double
Window coating	9 = other
Metallic thermal insulation fitted?	0 = unknown
Floor material	3 = concrete
Primary Exterior wall material	7 = glass
Secondary Exterior wall material	8 = metal
Internal walls	7 = Plasterboard (metal stud)
Roof materials	9 = other

13.5 Conclusion

The characterization of building entry loss is not a trivial task to undertake. There are many variables which must be isolated, such as free space loss, multipath, RF clutter, etc. This experiment sought to eliminate as many variables as possible and focus only of the actual loss introduced by the building

itself. The results of this study have shown that building entry loss is dependent upon the building which is being studied both in terms of its composition and its contents (interior walls, furniture, etc.). Within the two buildings studied, building entry loss as low as 0.5 dB and in excess of 50 dB was observed. However, even though the building results varied the PDF distributions of both appear to be lognormal, these results will be expanded upon and examined in more depth when additional buildings are completed.

14 Measurements at 3, 10 and 17 GHz

14.1 Measurement Campaign

This section presents a description of the measurement campaign from the considered scenarios to the setup parameters and the employed procedure to perform the measurements.

14.1.1 Scenario Description

The measurement scenario, displayed in Fig. 72 and Fig. 73, describes the O2I propagation scenario where the transmit antenna is located outside and mounted on top of a van (2.5 m above ground level). The receiver (RX) was located inside a building (Orange Labs premises in Belfort, France) at different location points where measurement data were collected. The location points refer to the different offices and corridors inside the building. The environment around the RX positions consisted of office and flat furniture in addition to the interior walls. The receive antenna height was kept at mobile user level (1.5 m). The distance between the transmitter (TX) and the exterior walls of the building was around 10 m.

FIGURE 72

Outdoor-to-Indoor Scenario. The TX is installed in the white measurement van and the RX is located inside the building marked out by the 2-sided orange arrow

FIGURE 73

Building Map and Room Pictures. Each number i corresponds with an RX position Ri. a) Corridor, b) Living Room, c) Small Office inside the Flat, d) Break Room, e) Large Office

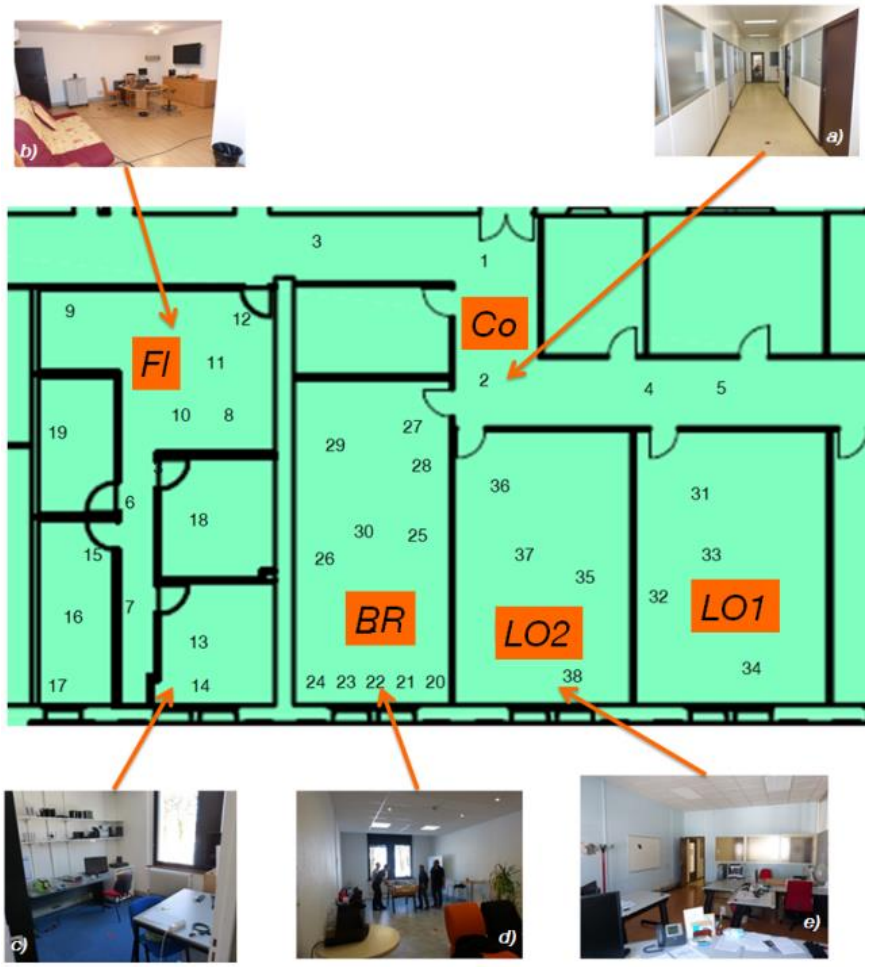

R21LoS, R23LoS and R14LoS will correspond with the RX positions at R21, R23 and R14 respectively, when the windows are opened, i.e. when the TX and the RX are in LoS conditions.

14.1.2 Setup and Procedure

The measurement campaign was conducted using a wideband channel sounding system [6] to characterize the propagation channel. The distance between the TX and the RX units was a few meters (10 to 25 m). An arbitrary waveform generator (AWG) generated successive 8192-length wideband sequences at 1 Gbps-rate with a 125 MHz channel bandwidth. The transmitted powers ranged from 23 to 30 dBm approximately, according to the frequency.

Depending on the RX antenna radiation patterns, the conducted measurements can be classified into two categories:

- Omnidirectional (Omni.) measurements: characterized by the use of omnidirectional RX antennas.
- Directional (Dir.) measurements: with the use of directional RX antennas.

Table 33 recapitulates the different measurement setup parameters.

TABLE 33

Measurement Setup Parameters

Setup Parameters	Omni.			Dir.
	3 GHz	**10 GHz**	**17 GHz**	**17 GHz**
Frequency bands (GHz)	3.6-3.725	10.5-10.625	17.3-17.425	
Tx Sequences	(8192-length, 1 Gbps-rate)			
Bandwidth	125 MHz			
TX Power	23-30 dBm			
RX Antenna gain (dBi)	1 dBi (Omni)	0 dBi (Omni)	0 dBi (Omni)	7 dBi (Dir)*
TX antenna gain (dBi)	1 dBi (Omni)	0 dBi (Omni)	7 dBi (Dir)*	7 dBi (Dir)*
TX and RX antenna Polarization	Vertical			
Antenna height	TX: 2.5 m and RX: 1.5 m (above ground level)			
Tigger time	100 ms			

(*) with 90° beam-width.

During the omnidirectional measurements, the RX antenna which was mounted on a rotating arm describing a circular trajectory. The radius of the trajectory was 2λ at 3 GHz, 4λ and 6λ at 10 and 17 GHz respectively.

However for the directional measurements, the directional RX antenna was pointing towards 4 different directions with 90° angular step (antenna beam-width) partitioning the space in 4 sectors. In each sector the antenna remained static while the data were being collected.

14.2 Data Processing

In this section, we describe the data processing and define channel metrics such as the building penetration losses L_{O2I} and the delay spread *DS*.

For the measurements performed with omnidirectional RX antennas at 3, 10 and 17 GHz, at a given RX position, let $h_n(\tau_m)$ be the propagation channel complex impulse response (CIR) of the n^{th} measurement snapshot and *N* the total number of measurement snapshots distributed along the circular trajectory.

Similarly for the directional measurements at 17 GHz, we will note $h_{n,k}(\tau_m)$ the channel CIR of the n^{th} measurement snapshot in the k^{th} sector and *K* the total number of sectors.

The measured channel CIRs are generally impacted by noise which can lead to a biased estimation of the penetration losses and the delay spread. The instantaneous dynamic range (difference between the CIR peak value and the noise level) ranged from 20 to 40 dB. Therefore, a single threshold of 20 dB was applied to all the CIRs allowing for a fair comparison between the different frequencies and scenarios. For example for the n^{th} measurement snapshot at a given RX position, only channel CIR samples τ compliant to the condition (8) were considered.

$$10 \cdot \log 10\left(\frac{\max_{\tau}\left(\left|h_n(\tau)\right|\right)}{\left|h_n(\tau)\right|} \right)^2 \leq 20 \tag{8}$$

For the omnidirectional measurements, the channel power delay profile (*PDP*) is given by (9):

$$PDP(\tau) = \frac{1}{N}\sum_{n=1}^{N}\left|h_n(\tau)\right|^2 \tag{9}$$

with τ the relative delay.

Regarding the directional measurements, the averaging of the measurement snapshots is done in the complex domain in order to remove the noise effects (10).

$$h_k(\tau) = \frac{1}{N}\sum_{k=1}^{K} h_{n,k}(\tau) \tag{10}$$

The *PDP* is then obtained by summing the power contributions of the *K* sectors (11).

$$PDP(\tau) = \sum_{k=1}^{K}\left|h_k(\tau)\right|^2 \tag{11}$$

This synthesizing procedure is similar to the method presented in [14].

The channel attenuations (A_{peak}, A_{av} and A_{max}), expressed in dB, are defined as following:

Let τ_{max} be the delay maximizing the *PDP*:

$$A_{\max} = -10 \cdot \log_{10}\left(PDP(\tau_{\max})\right) + G_{TX} + G_{RX} \tag{12}$$

$$A_{av} = -10 \cdot \log_{10}\left(\sum_{\tau} PDP(\tau)\right) + G_{TX} + G_{RX} \tag{13}$$

$$A_{peak}(n) = -10 \cdot \log_{10}\left(\left|h_n(\tau_{\max})\right|^2\right) + G_{TX} + G_{RX} \tag{14}$$

G_{TX} and G_{RX} are the TX and RX antenna gains respectively.

A_{max} and A_{peak} are defined to illustrate the LoS conditions and the multi-path fading phenomena and noise effects. The parameter A_{av} is an important characteristic since it expresses the average attenuation of the propagation channel.

The averaging procedure in (2) contributes to filter the small-scale fading effects caused by multiple propagation paths. These multipath fading effects can be noticed in Fig. 74 where the behavior of the channel peak-attenuation A_{peak} for a given RX position during the omnidirectional measurements at 17 GHz is shown.

FIGURE 74

Peak-Attenuation Variation at 17 GHz (Omni.) for R32

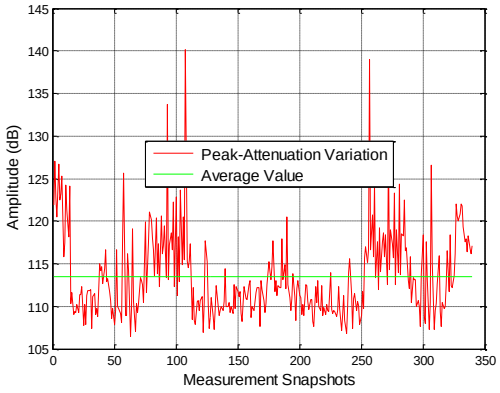

However, in Fig. 75, the small variations of the channel peak-attenuation during the directional measurements at 17 GHz are typical effects due the presence of noise. Hence the averaging in the complex domain, performed in (10), is more suited to cancel out these effects.

FIGURE 75

Peak-Attenuation Variation at 17 GHz (Dir.) for A5

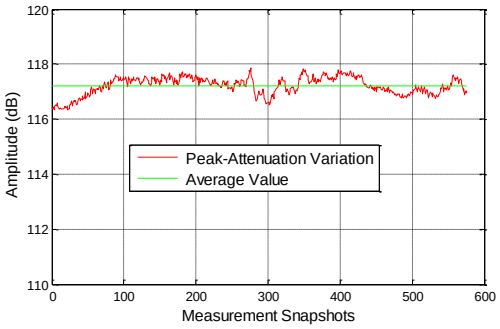

The dynamic range is also considerably improved as illustrated in Fig. 76 where it can be noticed that the noise level is significantly lower in the directional case than in the omnidirectional one.

FIGURE 76

PDP (Dir. Vs Omni.) 17 GHz for R24

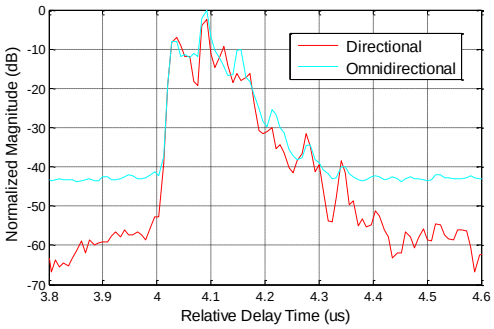

Figure 77 also shows the PDPs of the different sectors at a given RX position as well as the resulting synthesized PDP as described previously. This is representative of the channel characteristics assuming omnidirectional RX antennas.

FIGURE 77

PDPs from Dir. Measurements at 17 GHz for R7

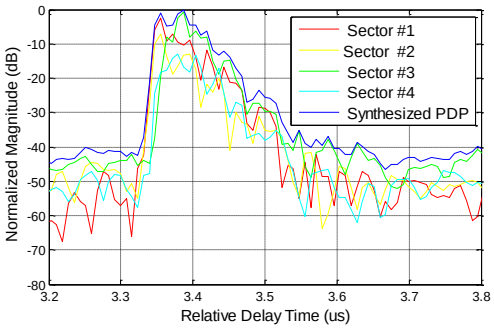

The building penetration losses, L_{O2I} (15), is defined as an additional attenuation compared to the theoretical free-space path loss (FSPL) L_{FS}.

$$L_{O2I} = A_{av} - L_{FS} \tag{15}$$

where $L_{FS} = -147.5 + 20 \cdot \log_{10}(f_c) + 20 \cdot \log_{10}(d)$.

L_{FS} is expressed in dB, f_c is the carrier frequency expressed in Hz and d the distance between TX and RX in m.

This parameter L_{O2I} takes into account the attenuation due to the penetration through external walls and/or windows and also the losses caused by the elements present in the indoor propagation environment.

Finally, the channel delay spread DS is quantified in (16).

$$DS = \sqrt{\frac{\sum_{\tau} (\tau_{mean} - \tau)^2 \cdot PDP(\tau)}{\sum_{\tau} PDP(\tau)}} \tag{16}$$

where:

$$\tau_{mean} = \frac{\sum_{\tau} \tau \cdot PDP(\tau)}{\sum_{\tau} PDP(\tau)}$$

14.3 Measurement results and analysis

14.3.1 Measurement validation (LoS cases)

In this section, it is proposed to determine the validity of the omnidirectional and directional measurements by verifying how close the attenuation A_{max} is to the FSPL L_{FS} in LoS conditions. Generally, in LoS conditions, there is a main path corresponding to the signal LoS component. Therefore, for the RX positions (R21LoS, R23LoS and R14LoS) considered as LoS cases, the attenuation value A_{max} should be equal to L_{FS}.

An up-sampling factor of 2 was applied to the channel CIRs in order to get a better estimation of A_{max} (peak-detection).

ϵ is defined as the gap between the two values of attenuation ($\epsilon = A_{max} - L_{FS}$) for the three RX positions (R21LoS, R23LoS and R14LoS). The computed values of attenuation for the three carrier frequencies are summarized in Table 34.

TABLE 34

Measurement Agreement with Free-Space Law

ϵ (dB)	Omni.			Dir.
	3 GHz	10 GHz	17 GHz	17 GHz
R21LoS	0	0	−2	−2
R23LoS	1	1	−1	−2
R14LoS	−1	2	2	2

These gaps around 2 dB revealed in Table 34 can be attributed to various factors:

– the impact of the multi-path fading phenomena: in Fig. 78, in at R23LoS, for the 10 GHz carrier frequency, e.g. A_{peak} displays strong variability along the circular trajectory, partly synonymous of secondary paths interfering with the signal LoS component. The same phenomenon is also observed at 3 and 17 GHz;

– the antenna maximum gain values used to calculate the channel attenuations in (12), (13) and (14) do not take into account the small variations due to different direction of arrival of the signal;

– the amplifier gain may also drift with temperature, biasing the estimations.

FIGURE 78

Channel Attenuation Values at 10 GHz for R23LoS

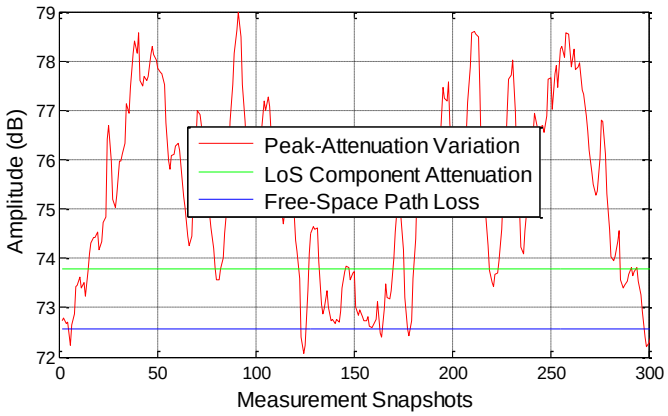

ϵ ranges between −2 and 2 dB suggesting that a difference of 2 dB between two measurement points may not have a physical meaning. A straightaway comparison between two different positions and/or carrier frequencies should be done cautiously.

14.3.2 Penetration Losses and Delay Spread

This section presents the penetration losses L_{O2I} and the delay spread *DS* of the propagation channel for the three frequency bands and the 38 different RX positions in non-line-of-sight (NLoS) conditions. As illustrated by Fig. 73 in § 14.1.1, the NLoS points include multiple RX locations (behind windows or walls, inside offices, corridors, etc.).

The computed L_{O2I} values from the measurement campaign for the different scenarios are summarized in Table 35.

α represents the incidence angle.

TABLE 35

Penetration loss values

Penetration loss (dB)	**Omni.**			**Dir.**
	3 GHz	**10 GHz**	**17 GHz**	**17 GHz**
CORRIDOR (Co)				
R1	18	18	18	22
R2	20	19	22	21
R3	18	20	21	17
R4	21	22	23	23
R5	21	22	21	-
AVERAGE	**20**	**20**	**21**	**21**
FLAT (Fl) – α=10°				
R6	27	31	33	31
R7	28	32	35	36
R8	29	30	33	37
R9	25	29	33	33
R10	28	31	30	34
R11	27	26	31	29
R12	25	29	32	27
R13	26	29	35	38
R14*	27	30	35	36
R15	27	31	35	37
R16	24	31	37	-
R17*	27	28	33	40
R18	29	31	33	38
R19	26	31	32	34
AVERAGE	**27**	**30**	**33**	**35**

TABLE 35 (*end*)

Penetration Loss (dB)	Omni.			Dir.
	3 GHz	**10 GHz**	**17 GHz**	**17 GHz**
BREAK ROOM (BR) – α=10°				
R20**	17	16	16	12
R21*	7	4	2	3
R22**	12	6	15	10
R23*	7	5	3	0
R24**	20	22	18	20
R25	5	3	2	-
R26	19	18	17	14
R27	9	4	2	-
R28	11	6	7	2
R29	12	12	8	9
R30	5	6	0	-
AVERAGE	**11**	**9**	**8**	**9**
LARGE OFFCICE 1 (LO1) – α=42°				
R31	17	21	22	19
R32	14	19	19	19
R33	17	20	22	-
R34*	8	8	8	17
AVERAGE	**14**	**17**	**18**	**18**
LARGE OFFICE 2 (LO2) – α=34°				
R35	20	19	22	-
R36	18	20	17	16
R37	20	24	19	-
R38*	23	25	27	32
AVERAGE	**20**	**22**	**21**	**24**

(*) RX locations just behind the building windows

(**) RX locations just behind the building walls

In BR, it was found that the attenuation behind the windows (R21, R23 and more or less R22) is lower than the attenuation when the RX is placed behind the walls (R20 and R24). The difference is approximately 15 dB. It can also be noticed in this scenario, for the RX positions which are located deeper inside the room (R25 to R30), that the signal attenuation is lower compared to the values observed just behind the walls. This could be explained by the fact that, at these positions, the RX has better visibility with the TX and/or the reflected paths hardly reach the positions just behind the walls.

The losses caused by the BR or LO1 windows (≈ 5 to 20 dB) are significantly lower than the losses recorded for the penetration through the Fl and the LO2 windows (≈ 20 to 40 dB). It is well known

that the attenuation depends on the incidence angle and the additional losses caused by the LO1 windows in comparison with the BR are consistent with this phenomenon. However, the window attenuation in Fl is totally unexpected since the incidence angle is almost the same as in the BR (normal incidence) and the window structures (two-layered glass) seem identical as well. An investigation is ongoing to determine the true composition of these windows.

The RX positions in Co provided attenuation values slightly higher than in the LO1, LO2 or BR depending on whether they were located behind the LO1, LO2 or BR respectively.

Similarly, Table 36 below presents the estimated *DS* values.

TABLE 36

Delay Spread Values

Delay Spread [ns]	**Omni.**			**Dir.**
	3 GHz	**10 GHz**	**17 GHz**	**17 GHz**
CORRIDOR (Co)				
R1	25	30	31	30
R2	42	30	42	36
R3	28	45	40	28
R4	48	35	35	40
R5	40	30	38	35
AVERAGE	**37**	**34**	**37**	**34**
FLAT (Fl)- α=10°				
R6	38	42	37	27
R7	45	40	37	44
R8	44	40	37	41
R9	38	35	37	33
R10	47	45	-	30
R11	47	31	35	26
R12	42	40	35	14
R13	35	33	45	51
R14*	35	42	37	41
R15	39	47	42	49
R16	40	35	47	-
R17*	45	23	40	30
R18	45	40	37	39
R19	36	40	35	27
AVERAGE	**41**	**38**	**39**	**35**

TABLE 36 (*end*)

Delay Spread [ns]	Omni.			Dir.
	3 GHz	**10 GHz**	**17 GHz**	**17 GHz**
BREAK ROOM (BR) - α=10°				
R20**	45	33	47	36
R21*	37	31	29	33
R22**	42	28	57	37
R23*	30	27	28	26
R24**	35	44	45	47
R25	26	14	20	-
R26	49	44	53	45
R27	24	28	33	-
R28	23	24	40	36
R29	37	39	28	32
R30	14	23	19	
AVERAGE	**33**	**30**	**36**	**38**
LARGE OFFICE 1 (LO1) - α=42°				
R31	28	40	37	40
R32	21	32	33	25
R33	37	30	40	
R34*	28	23	14	29
AVERAGE	**29**	**31**	**31**	**31**
LARGE OFFICE 2 (LO2) - α=34°				
R35	47	42	36	
R36	38	36	40	29
R37	44	42	33	
R38*	66	49	51	51
AVERAGE	**49**	**42**	**42**	**40**

(*) RX locations just behind the building windows

(**) RX locations just behind the building walls

1) **Omnidirectional Vs Directional at 17 GHz:** The two methods at 17 GHz provide similar estimates of L_{O2I} and DS. As indicated in Fig. 76 in § 14.2, a difference of 2 dB has been observed. Additional measurements must be proceeded to get a better understanding on these aspects.

2) **Frequency Dependence:** There is no clear frequency dependence of the L_{O2I} values with the carrier frequency, which has often been underlined in the literature [3], [9]. The PDPs for the three carrier frequencies represented in Fig. 79 illustrate this trend for a given RX position in NLoS conditions. The material composition as well as the indoor environment prove, however, to have major influences on these O2I propagation scenarios.

FIGURE 79

PDPs across the frequency bands for R33

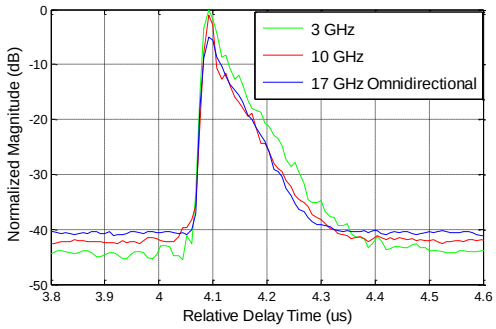

The *DS* values, lower than 50 ns for the most part (30 ns being approximately the delay spread in LoS conditions) do not seem to display any dependence regarding the carrier frequency as well. This observation is illustrated in Fig. 80 where the *PDPs* present overall the same shape.

FIGURE 80

Relative PDPs across the frequency bands for R33

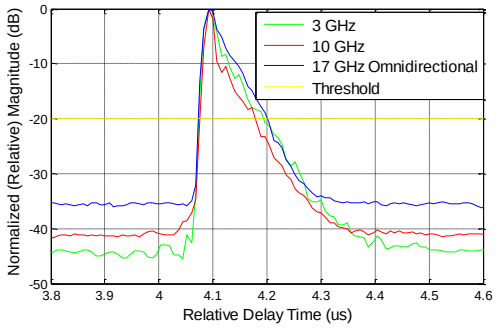

14.4 Conclusion

In this paper, the propagation channel properties at 3, 10 and 17 GHz were studied for mmW communication systems. For an O2I scenario, the building penetration losses and the channel delay spread were determined.

The results revealed a strong variation in signal attenuation (from 10–40 dB) depending on the room type and most definitely on the structure of the building exterior walls and/or windows. Differences within the window glass compositions may explain such variations. Regarding the frequency, the dependence is almost inexistent and is overshadowed by the variations caused by the materials. The delay spread values are pretty low and also uniformly distributed (below 50 ns in general for all the measurements) across the frequency bands.

At 17 GHz, the omnidirectional-equivalent characteristics (such as *PDPs*) obtained from directional channel measurements were found similar to the characteristics extracted directly from omnidirectional measurements. The utilized synthesizing procedure could be adopted at higher frequencies where the use of directional antennas is required to compensate for the increased propagation losses.

Measurements at higher frequency bands (60 GHz e.g.) are planned to extend the analysis of the frequency-dependence for the O2I penetration losses and the channel delay spread.

14.5 References

[1] T. S. Rappaport, G. R. MacCartney, Jr., M. K. Samimi, and S. Sun, “Wideband Millimeter-Wave Propagation Measurements and channel Models for future Wireless communication System Design,” IEEE Transactions on Communications, vol. 63, no. 9, pp. 3029-3056, Sept. 2015.

[2] R. J. Weiler, M. Peter, W. Keusgen, and M. Wisotzki, “Measuring the Busy Urban 60 GHz Outdoor Access Radio Channel,” IEEE International Conference on Ultra-Wideband (ICUWB), 2014.

[3] I. Rodriguez, H. C. Nguyen, N. T. K. Jorgensen, T. B. Sorensen and P. Mogensen, “Radio Propagation into Modern Buildings: Attenuation Measurements in the Range from 800 MHz to 18 GHz,” IEEE, 2014.

[4] C. Larson, F. Harrysson, B.-E. Olsson and J.-E. Berg, “An Outdoor-to-Indoor Propagation Scenario at 28 GHz,” IEEE European conference on antennas and Propagation (EuCAP), 2014.

[5] P. Okvist, H. Asplund, A. Simonsson, B. Halvarsson, J. Medbo and N. Seifi, “15 GHz Propagation Properties Assessed with 5G Radio access Prototype,” IEEE on Personal , Indoor and Mobile Radio Communications (PIMRC), 2015.

[6] J.-M. Conrat, P. Pajusco, and J. Y. Thiriet, "A Multibands Wideband Propagation Channel Sounder from 2 to 60 GHz," in *Instrumentation and Measurement Technology Conference (IMTC)*, Sorrento, 2006.

[7] S. Sun, G. R. MacCartney, M. K. Samimi, and T. S. Rappaport, “Synthesizing Omnidirectional Antenna Patterns, Received Power and Path Loss from directional Antennas for 5G Millimeter-Wave Communications,” in 2015 IEEE Global Communications Conference (GLOBECOM), Dec. 2015, pp. 3948-3953.

[8] A. Mitra, “Lecture Notes on Mobile Communications - Chapter 4: Free Space Radio Wave Propagation,” Nov. 2009.

[9] H. Okamoto, K. Kitai and S. Ichitsubo, “outdoor-to-Indoor Propagation Loss Prediction in 800-MHz to 8-GHz Band for an Urban Area,” IEEE Transactions on Vehicular Technology, vol. 58, no. 3, March. 2019.

15 Measurements in Stockholm in the 2-60 GHz frequency range

15.1 Introduction

In order to provide credible building entry loss modelling over the 5G frequency range, experimental data in the mmWave range is required. Until recently, the amount of measurement data available has been little. For this reason, an outdoor-to-indoor multi-frequency measurement campaign was conducted in an eight stories tall office building in Kista covering the frequency range 2 GHz to 60 GHz. Furthermore, Ericsson proposes a building entry loss model which is validated and calibrated based on the herein presented measurement data.

The research leading to these results received funding from the European Commission H2020 programme under grant agreement No 671650 (mmMAGIC project).

15.2 Measurement campaign

A building entry loss measurement campaign was performed in an ‘old type’ of office building in the Kista area of Stockholm, as depicted in Fig. 81. The transmitter was located in an open window at the upper floor of the building and the received signal was measured at 2 slightly shifted (30 cm) positions at 40 indoor locations across the inner yard on the same floor. Four different carrier frequencies between 2.44 GHz and 58.68 GHz were measured at three different measurement occasions over a few days. The basic details of the measurement set-up are given in Table 37. At the upper floor of the building, the exterior wall is covered with metal. The windows are, however, pure

glass without metallization. It should be noted that there are three layers of glass in the window frames resulting in some frequencies being substantially more attenuated than others with an oscillating trend over the measured frequency range.

TABLE 37

Basic data of measurement setup

Carrier frequency	2.44 GHz	5.8 GHz	14.8 GHz	58.68 GHz
Bandwidth	80 MHz	150 MHz	200 MHz	2 GHz
Transmit power	10 dBm	10 dBm	10 dBm	10 dBm
Antenna Tx (vert. polar.)	Patch ~7dBi	Patch ~7dBi	Open wave guide	Open wave guide
Antenna Rx (vert. polar.)	Omni 2dBi	Omni 2dBi	Omni 2dBi	Omni 2dBi
Tx Antenna height	1.5 m (ref : indoor floor)			
Rx Antenna height	1.5 m (ref : indoor floor)			

In order to avoid any bias due to the different bandwidths of the different frequencies, the measured impulse responses are filtered down to 80 MHz for all frequencies. For some locations and frequencies, 30 dB dynamic range was not possible to achieve. For these locations, the dynamic range of the carrier frequency having the smallest dynamic range is used for all carrier frequencies in order to avoid any frequency-dependent-bias.

FIGURE 81

Outdoor to indoor measurement scenario (left). The indoor Rx locations are marked with red-filled circles and the Tx location is marked with a blue-filled circle. On the right hand side, a photograph of the building is shown

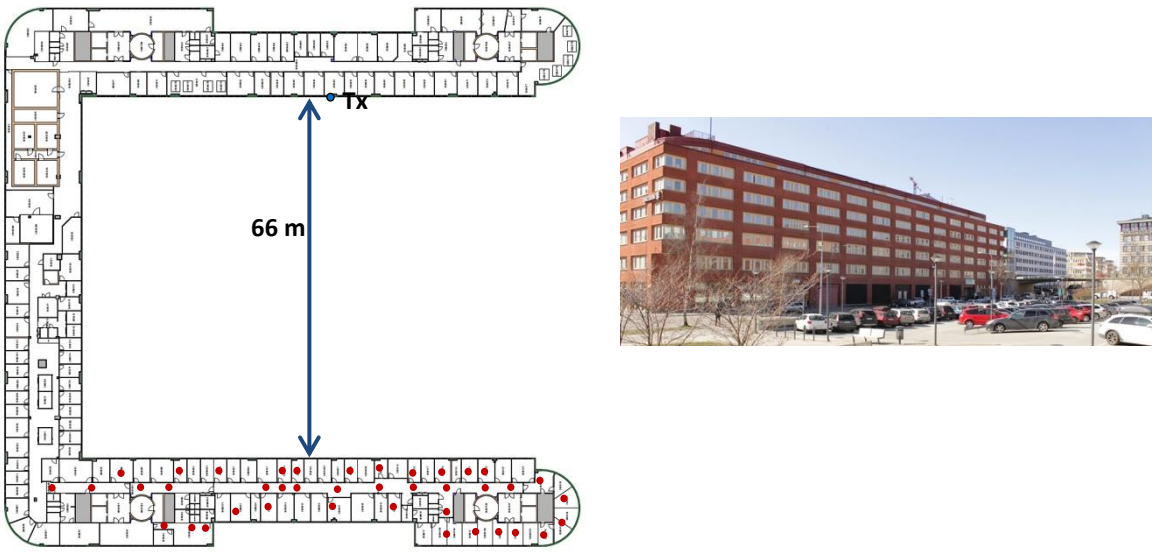

It can be observed from simulation and measurement, that for glass material, the penetration loss will increase slowly with the increase of frequency. But for concrete material, the penetration loss will increase sharply with the increase of the frequency.

Between 2.44 GHz and 14.8 GHz the building penetration loss ranges from around 0 dB up to 30 dB (Fig. 82). The lower end of penetration loss around 0 dB is similar for all frequencies while the highest losses around 45 dB occur only at 58.68 GHz. Between 2.44 GHz and 14.8 GHz the high end of penetration loss is between 25 dB and 30 dB. The proposed model (below) is based on the exterior wall loss, due to penetration of the exterior wall only, combined with additional loss due to further penetration into the building. Measurement locations of the Rx which are less than 4 m from the exterior wall facing the Tx experience exterior wall loss only, as there are no obstructing objects between the Rx and the exterior wall. It is clear from Fig. 82 that the corresponding exterior wall loss is in the range 0–20 dB over all frequencies.

FIGURE 82

Loss in excess of free space loss for the different frequencies in the outdoor to indoor measurements. On the left hand side, the CDFs are shown and on the right hand side the loss as function of distance from the exterior wall which is in LOS with respect to the transmitter is shown

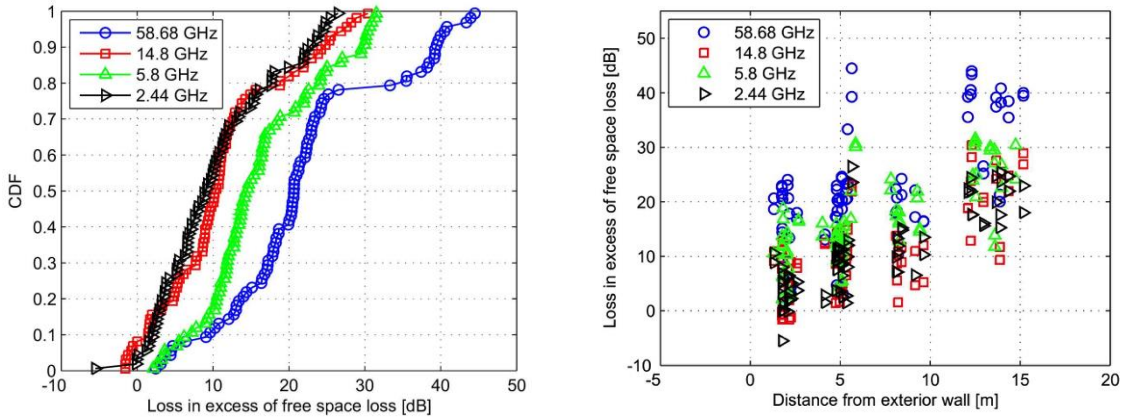

The spread is substantially larger for the higher frequencies. In particular, the exterior wall loss at 58.68 GHz is over 20 dB at the 90 percentile level i.e. 10% of the locations experience more than 20 dB exterior wall loss. For 2.44 GHz and 14.8 GHz the 90 percentile level is only about 10 dB. This difference may be explained by two effects. The first effect is interference due to multiple layers of glass in the windows. The corresponding loss is particularly severe at 5.8 GHz (see § 15.3). The other effect is blocking by venetian blinds and window frames. As the blinds are at the order of a couple of wavelengths at 58.68 GHz this effect becomes substantial at this frequency. At locations where high building entry loss is experienced at 58.68 GHz it is likely that either the blinds were down or that the window frame blocked line of sight. The window frame blocking might explain why the loss actually goes down only at 58.68 GHz when the distance to exterior wall increases.

FIGURE 83

Building penetration loss versus distance from exterior wall for the different frequencies at 10, 50 and 90 percentile levels

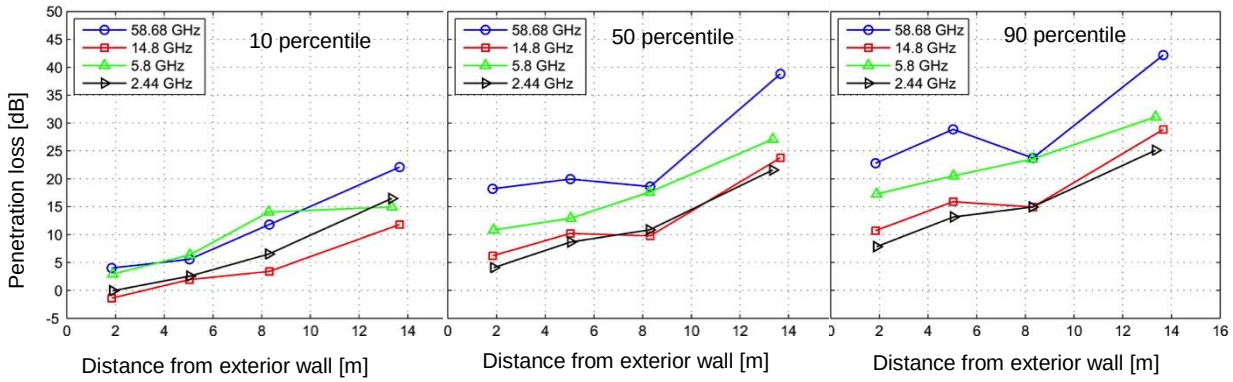

15.3 Monte Carlo simulation of multi-pane glass window transmission loss

To investigate the behaviour of how the multi-layered window glass impacts the frequency dependency, a simulation has been made for a two-glass window with varied airspace in a realistic interval. The result shows a strong frequency dependency and that the transmission loss (high or low) seems quite stable for specific frequency bands. How and if this should be reflected in the BEL model is still under consideration and may need more attention.

Simulation assumptions:

Two-pane layered standard glass with no metallization.

Airspace = 12-16 mm (uniformly distributed).

Glass thickness = 4 mm.

Relative permittivity of glass = 7.

Absorption loss of glass (tan δ) = 0.02.

Random polarization.

FIGURE 84

Median +/- standard deviation (error bars) for a two-layer window simulation

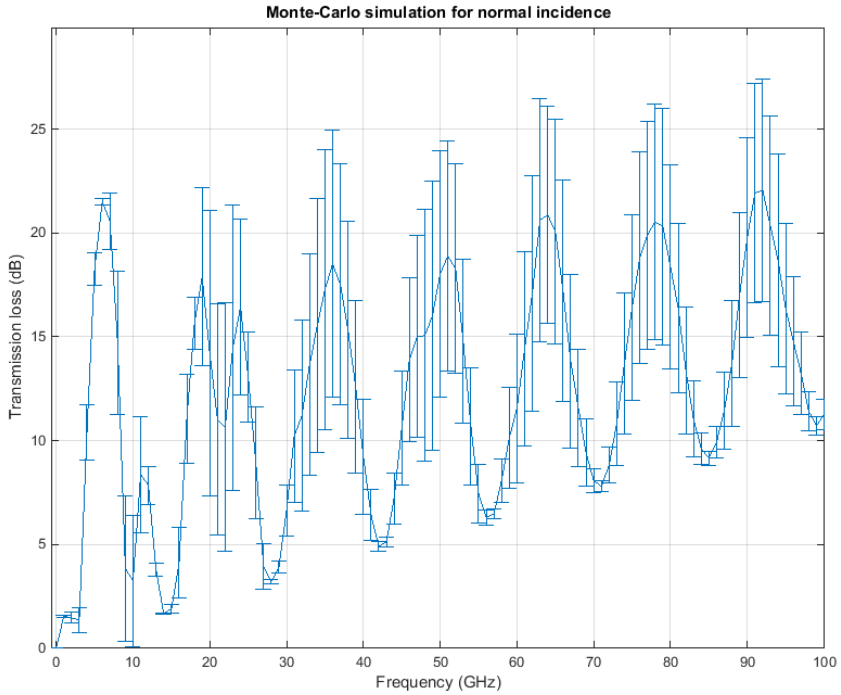

16 Measurements at 5-31 GHz in China

16.1 Measurement scenarios

Two office buildings in China are measured, named as Building A, Building B, which have different structure and material. Building A is with reinforced concrete shear wall and one-way transparent glass which is with a thin metal coating. The thickness of the bearing wall is 35 cm ~ 38 cm. In addition, the building's exterior wall is being equipped with thermal insulation material whose structure is the foam polyethylene sheet and metal reflective layer. Building B is a modern building combined the toughened glass with the reinforced concrete. The toughened glass is laid in the wall which is known as a common toughened glass without metal coat.

16.1.1 Building A

Building A is with reinforced concrete shear wall structure, whose have exterior load-bearing walls and some interior load-bearing walls. The thickness of the bearing walls is 35 cm ~ 38 cm. The glass of windows of the building is known as one-way transparent glass which has a good visibility from the inside to outside but a poor visibility from the outside to inside. This one-way transparent glass is with a thin metal coating, so it will reflect the electromagnetic wave and bring big penetration loss. In addition, the building's exterior wall is being equipped with thermal insulation material whose structure is the foam polyethylene sheet and metal reflective layer.

The receiving antenna is on an outdoor platform which is on 4th floor. The pictures are shown in Fig. 85. Only two operators are on the platform during the test, and they stay away from the receiving antenna. The height of the transmitting antenna is 2.3 m, and the height of the receiving antenna is 1.5 m.

The receiving point located on the 4th floor platform outdoor, the main receiving point is labelled as R1, marked as blue point in Fig. 86. Some transmitting points on the 4th floor indoor are marked as

red point in Fig. 86. Other transmitting points on the 5th floor indoor are marked as red point shown in Fig. 87. Furthermore the receiving points and transmitting points are marked with coordinate values. R1 is the coordinate origin.

FIGURE 85

The receiving antenna located on the platform of Building A, 4th floor

Figure 85: The outdoor platform of the Building A: The building scene from the receiving point, the thermal insulation layer is adding to the exterior wall of the Building A (Panoramic camera model. Middle image of the building is slightly bent). There are no any other obstacles, e.g. trees between the transmitter and receiver except the building.

FIGURE 86

The transmitting points indoor and the receiving points outdoor on the 4th floor, the length of the platform is 28 m

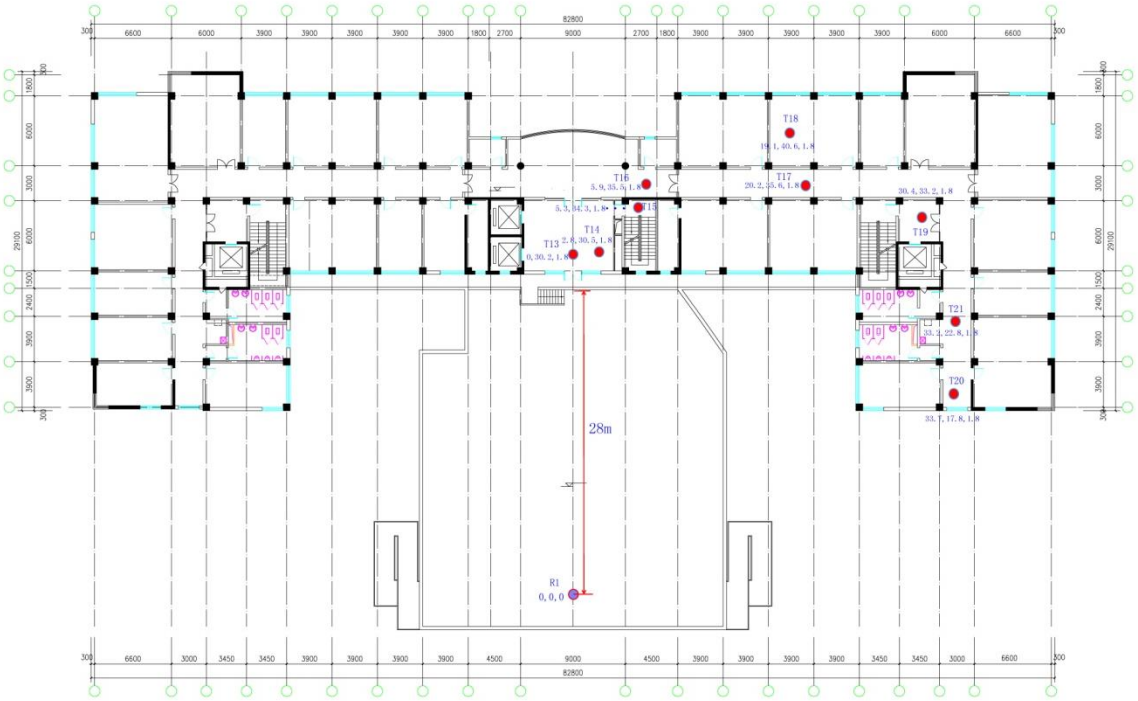

FIGURE 87

The transmitting points indoor on the 5th floor

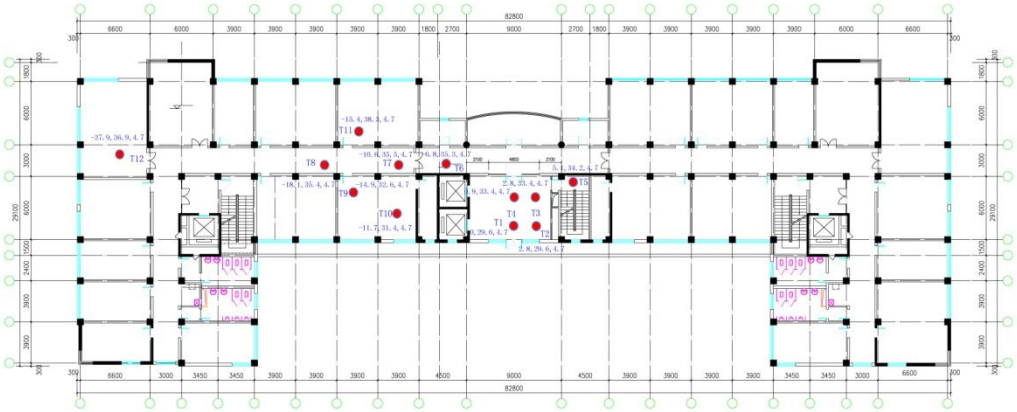

The coordinates of the receiving points and transmitting points in Building A are shown in Table 38.

TABLE 38

The coordinates of the receiving points and transmitting points in Building A (unit: m)

Points	x	y	z
R1	0	0	0
T1	0	29.6	4.7
T2	2.8	29.6	4.7
T3	2.8	33.4	4.7
T4	0.9	33.4	4.7
T5	5.1	34.2	4.7
T6	-6.8	35.3	4.7
T7	-10.6	35.5	4.7
T8	-18.1	35.4	4.7
T9	-14.9	32.6	4.7
T10	-11.7	31.4	4.7
T11	-15.4	38.3	4.7
T12	-37.9	36.9	4.7
T13	0	30.2	1.8
T14	2.8	30.5	1.8
T15	5.3	34.3	1.8
T16	5.9	35.5	1.8
T17	20.2	35.6	1.8
T18	19.1	40.6	1.8
T19	30.4	33.2	1.8
T20	33.7	17.8	1.8
T21	33.2	22.8	1.8

Some transmitting points' pictures in Building A are shown in Figs 88 to 90.

FIGURE 88

The transmitting point in the corridor of the Building A

FIGURE 89

The transmitting point by the glass door of the Building A

FIGURE 90

The transmitting point in the stair channel of the Building A

16.1.2 Building B

Building B is a modern building combined the toughened glass with the reinforced concrete. The toughened glass is laid in the wall which is known as a common toughened glass without metal coat. Part of exterior wall is equipped with a brown ceramic tile. There is a parking lot outside the building, the length of which is about 35 m. In order to avoid the influence of vehicle movement, the method is:

– The test is taken at the weekend to make sure there are few vehicles and staffs.

– Make sure the receiving antenna away from the vehicle.

– The height of the receiving antenna is set to 2.3 m to ensure that the connection between the transmitting antenna and the receiving antenna is not blocked by vehicles.

The main receiving point is R3, which is marked with blue point in Fig. 92, and the transmitting points on the 1st floor are marked with red point in Fig. 92. The transmitting points on the 2nd floor are marked with red points in Fig. 93. The transmitting points on the 3rd floor are marked with red point in Fig. 94. The height of the transmitting antenna is 2.3 m and the height of the receiving antenna is 2.3 m from the floors at that time.

FIGURE 91

Receiving antenna in the parking lot of Building B

Figure 91 Parking lot outside the Building B: The building scene from the receiving point. There are no any other obstacles, e.g. trees between the transmitter and receiver except the building.

FIGURE 92

The transmitting points indoor and the receiving point outdoor on the 1st floor in Building B, the length of the outdoor parking lot is 35 m

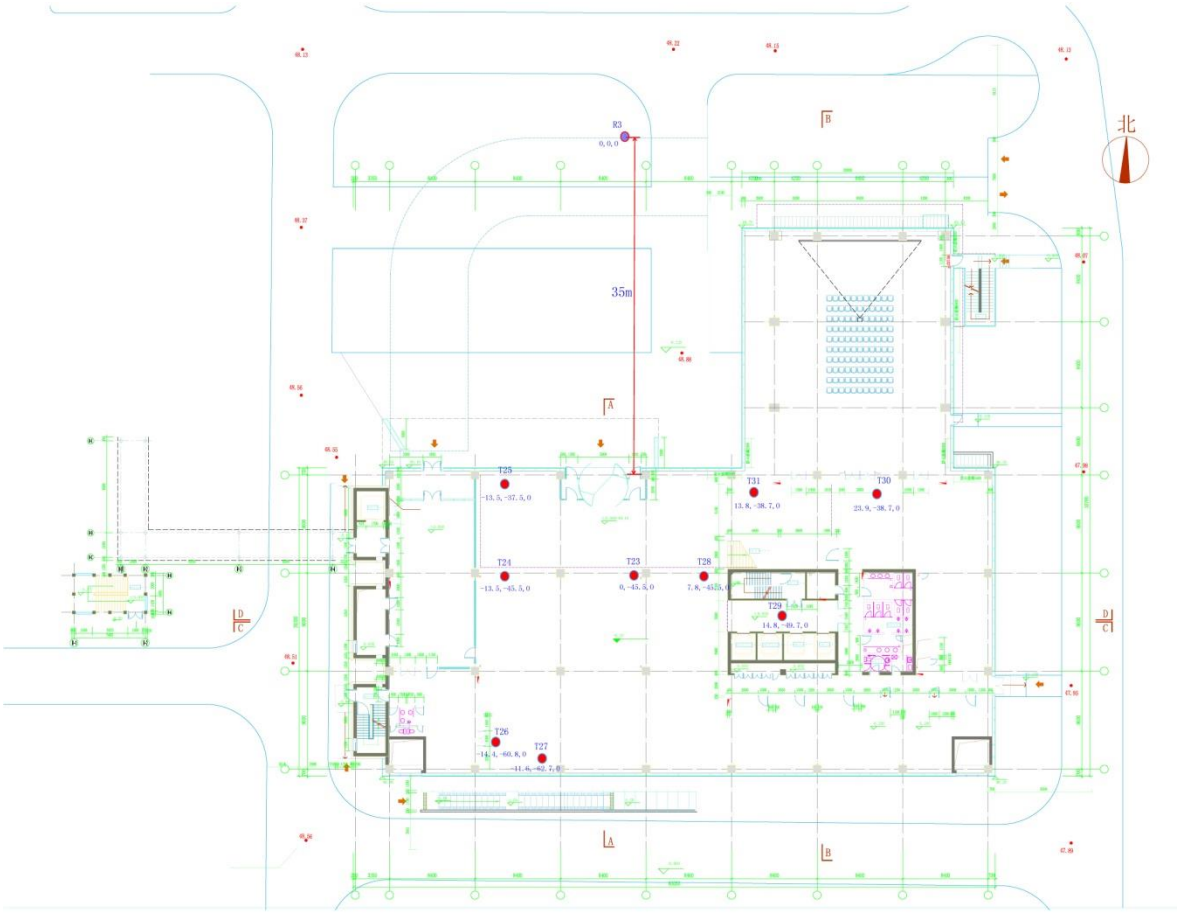

FIGURE 93

The transmitting points on the 2nd floor in Building B

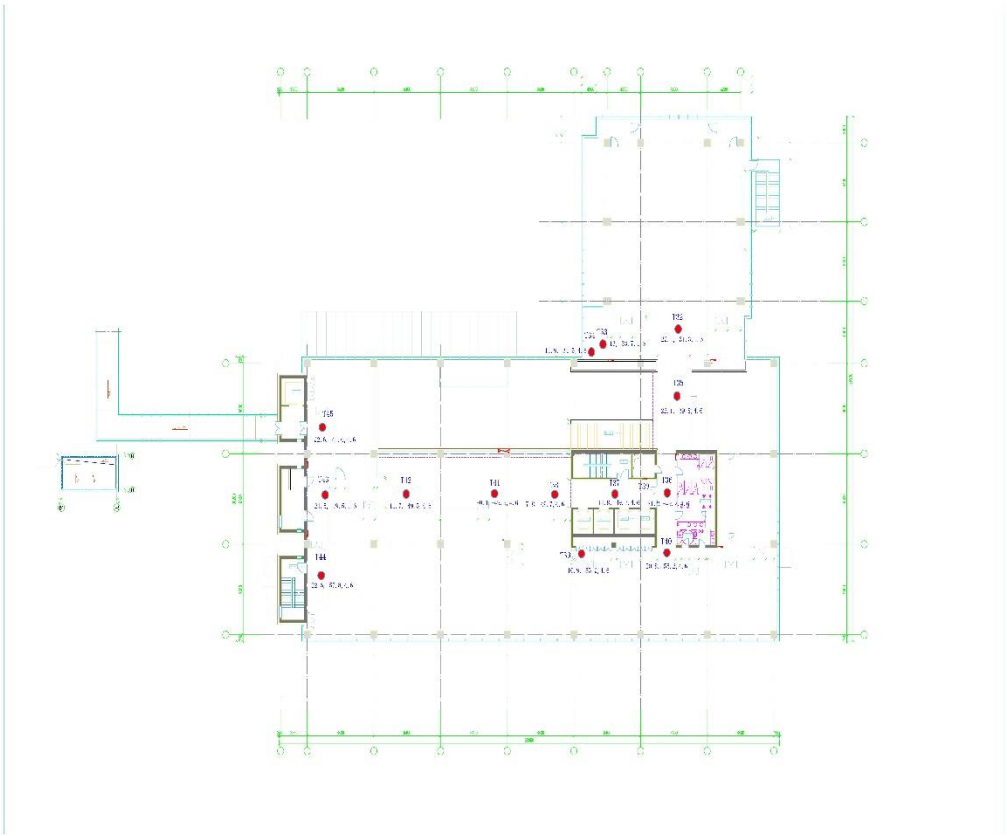

FIGURE 94

The transmitting points on the 3rd floor in Building B

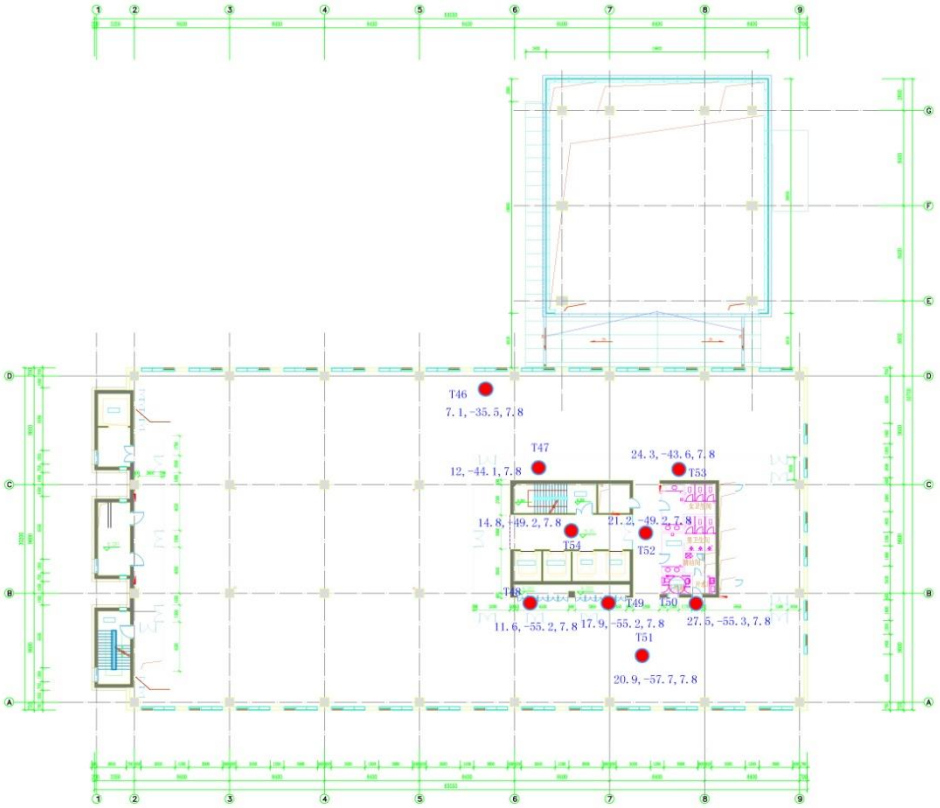

A coordinate system is formed with the R3 being a coordinate origin. The coordinates of the transmitting points and receiving point are shown in Table 39.

TABLE 39

The coordinates of the receiving points and transmitting points in Building B (unit: m)

Points	x	y	z
R3	0.0	0.0	0.0
T23	0.0	-45.5	0.0
T24	-13.5	-45.5	0.0
T25	-13.5	-37.5	0.0
T26	-14.4	-60.8	0.0
T27	-11.6	-62.7	0.0
T28	7.8	-45.5	0.0
T29	14.8	-49.7	0.0
T30	23.9	-38.7	0.0
T31	13.8	-38.7	0.0
T32	22.1	-31.3	4.6
T33	13.0	-34.7	4.6
T34	11.9	-34.5	4.6

TABLE 39 (*end*)

Points	x	y	z
T35	22.1	-39.8	4.6
T36	21.2	-49.2	4.6
T37	14.8	-49.7	4.6
T38	7.8	-49.7	4.6
T39	10.9	-55.2	4.6
T40	20.8	-55.2	4.6
T41	-0.1	-49.5	4.6
T42	-11.7	-49.5	4.6
T43	-21.5	-49.5	4.6
T44	-22.6	-57.8	4.6
T45	-22.6	-41.6	4.6
T46	7.1	-35.5	7.8
T47	12.0	-44.1	7.8
T48	11.6	-55.2	7.8
T49	17.9	-55.2	7.8
T50	27.5	-55.3	7.8
T51	20.9	-57.0	7.8
T52	21.2	-49.2	7.8
T53	24.3	-43.6	7.8
T54	14.8	-49.2	7.8

Some transmitting points' pictures in Building B are shown in Figs 95 to 96.

FIGURE 95

The transmitting point in the lobby on the 1st floor in Building B
(In transmitting point the receiving point can be seen through glass)

FIGURE 96

The transmitting point next to the elevator on the 2nd floor in Building B

16.2 Test methodology

In Building A and B, 11 frequency points are selected for each frequency band, e.g. 3.5 GHz, 5 GHz, 15 GHz, 24 GHz, 28 GHz and 31 GHz.

16.2.1 Measuring system and instrument

The devices of measuring system are shown in Table 40.

TABLE 40

The antenna selection consideration

Transmitting antenna	Omni-directional vertical polarization antenna (for 3.5 GHz) Horn vertical polarization antenna for 5-31 GHz band
Receiving antenna	Omni-directional vertical polarization antenna. (for 3.5 GHz) Horn vertical polarization antenna for 5-31 GHz band
Transmitter	Agilent E8267D signal generator
RF power amplifier	The output power in the test is set to 33 dBm for 3.5 and 20 dBm for 5-31 GHz band
Receiver	Agilent N9030A signal analyser

We have developed an automatic program in order to control instruments and record test data by LAN. In each location and frequency points, 500 continuous reading is got which will cost about 8 ~ 10 seconds.

16.3 Calculation method of building entry loss

The free space loss can be calculated as:

$$L_f = 32.45 + 20\lg d_{[m]} + 20\lg f_{[GHz]} \quad (17)$$

Where d is defined in Fig. 97. f is carrier frequency in GHz. Set transmitted power be P_t (dBm) and received power be P_r (dBm), the building entry loss is expressed as L_E, transmitting antenna gain and receiving antenna gain in transmission path are expressed as G_t and G_R, relatively.

FIGURE 97

The location relationship between the receiving antenna and the transmitting antenna

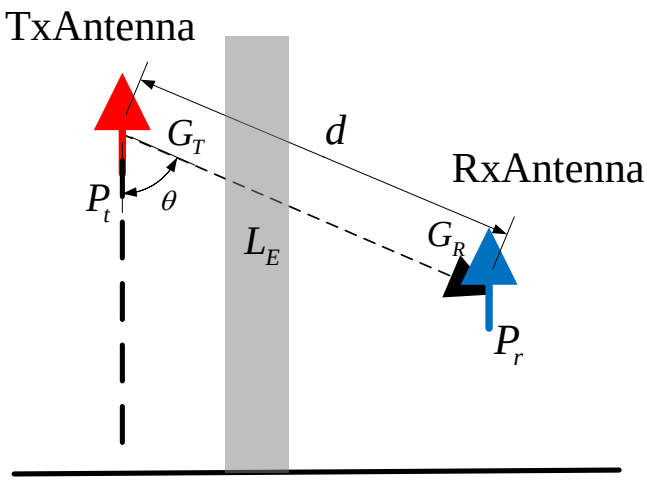

Then we can get equation (18).

$$P_{t[dBm]} + \left(G_t - L_f - L_E + G_r\right) = P_{r[dBm]} \quad (18)$$

And then equation (19) can be deduced from equation (18).

$$L_E = \left(P_{t[dBm]} - P_{r[dBm]}\right) - L_f + \left(G_t + G_r\right) \tag{19}$$

For Omni-directional antenna used in the 3.5 GHz test, the antenna pattern is similar to half wave dipole antenna whose gain is 2.15 dB, and the normalized directivity function of electric field of half-wave dipole antenna is expressed as equation (20).

$$F(\theta) = \sin\theta \tag{20}$$

Where θ is defined in Fig. 97. From equation (20), we can get equation (21).

$$G_t + G_r = 4.3 + 10\lg\left(\left[F(\theta)\right]^4\right) = 4.3 + 10\lg\left(\sin^4\theta\right) \tag{21}$$

For horn antenna case, the receiving antenna gain is properly considered in calculation.

16.4 Measurement results

The median values of building entry loss measured above are shown in Table 41. The categories of all links from transmitters and receivers can be separated as three types:

The ‘depth/penetration’ categories are as follows:

C1 Indoor terminal in a room/space with an external wall facing the outdoor terminal

C2 Indoor terminal in a room/space with no external walls (e.g. stairwell, corridor)

C3 Indoor terminal in a room/space with an external wall not facing the outdoor terminal

TABLE 41

The median value of entry loss (Building A, Unit: dB)

Frequency (GHz)	3.5	5	15	24	28	31
Tx 1	31.71	39.48	34.62	25.24	41.60	37.13
Tx 2	20.98	26.58	47.64	52.40	58.95	59.32
Tx 3	24.19	24.73	36.62	26.38	42.39	39.75
Tx 4	26.17	33.61	41.32	20.88	46.78	41.96
Tx 5	43.42	50.08	54.95	48.49	69.15	58.14
Tx 6	43.98	52.40	72.23	69.60	75.33	73.98
Tx 7	45.74	55.09	71.84	74.96	73.03	70.91
Tx 8	47.11	54.52	59.66	65.61	65.67	64.31
Tx 9	29.69	31.90	45.00	43.92	53.55	57.68
Tx 10	27.23	36.83	38.19	38.28	49.65	51.44
Tx 11	58.84	61.20	65.08	70.28	68.39	66.84
Tx 12	55.97	21.92	13.01	57.45	49.40	47.36
Tx 13	35.15	36.99	37.20	28.10	34.32	37.38
Tx 14	33.71	27.57	36.34	42.14	54.65	59.05
Tx 15	52.22	48.11	57.93	54.80	57.00	64.71
Tx 16	54.55	60.79	69.57	57.49	65.33	62.61
Tx 17	49.92	41.14	52.48	62.43	63.89	62.00

TABLE 41 (*end*)

Frequency (GHz)	3.5	5	15	24	28	31
Tx 18	68.64	57.09	60.54	65.79	65.88	64.82
Tx 19	63.65	34.25	22.26	81.56	81.02	79.45
Tx 20	36.38	21.28	12.77	53.86	54.86	62.33
Tx 21	50.48	18.32	10.90	51.50	58.28	64.28

16.4.1 Measurement results and analysis of Building B scenario

After processing the original test data the entry loss of Building B can be got. The median value of the entry loss measurement above is shown in Table 42. The categories of all links from transmitters to receivers are the same with Building A. It should be noted that 5 GHz and 15 GHz case is not been tested in this building.

TABLE 42

The median value of the Entry loss (Building B, Unit: dB)

Frequency (MHz)	3.5	24	28	31
Tx 23	11.16	15.39	13.27	13.86
Tx 24	16.64	22.77	21.19	20.22
Tx 25	15.78	19.39	22.80	22.39
Tx 26	13.01	25.66	27.96	23.92
Tx 27	19.23	40.02	37.99	39.28
Tx 28	15.54	16.64	28.19	28.50
Tx 29	25.96	32.94	33.56	37.14
Tx 30	21.97	35.31	38.82	38.24
Tx 31	19.37	27.52	34.49	35.57
Tx 32	38.44	47.51	52.72	52.21
Tx 33	32.37	49.57	49.76	49.40
Tx 34	27.85	43.51	45.59	45.74
Tx 35	26.02	43.97	43.63	49.92
Tx 36	38.15	44.04	46.34	49.41
Tx 37	38.55	65.28	66.76	64.40
Tx 38	22.02	26.78	34.14	22.88
Tx 39	35.52	50.71	60.16	61.95
Tx 40	41.33	49.01	53.45	58.04
Tx 41	20.25	18.00	22.00	27.15
Tx 42	21.63	24.79	32.64	31.94
Tx 43	35.14	42.81	51.34	47.96
Tx 44	43.55	56.37	61.69	60.83
Tx 45	34.55	41.43	42.92	45.21
Tx 46	22.00	28.74	27.41	28.53

TABLE 42 (*end*)

Frequency (MHz)	3.5	24	28	31
Tx 47	32.84	28.74	35.59	41.65
Tx 48	49.50	74.86	73.91	72.20
Tx 49	56.38	25.98	30.90	37.13
Tx 50	56.66	61.68	61.63	60.21
Tx 51	64.87	--	--	--
Tx 52	56.09	57.05	59.31	57.69
Tx 53	44.73	49.92	52.58	54.96
Tx 54	53.67	72.10	70.34	68.34

17 Measurements below 6 GHz in a modern office building

17.1 Method

The method adopted was the same as that used in the previous study and follows the recommendations given in § 4 of Recommendation ITU-R P.2040-1.

17.2 Locations

A major constraint in conducting measurements of building loss in urban areas is that it is very difficult to ensure that the measurement path has a clear line-of-sight to the building under investigation. If this condition is not met, the measured data will necessarily include an unknown element of local clutter loss.

The waterfront location of Ofcom (“Riverside House”) offered an opportunity to avoid this problem, and a building with a roof terrace was identified on the opposite side of the river, offering a clear line-of-sight to the front of the target offices.

FIGURE 98

Riverside House seen from receiver location

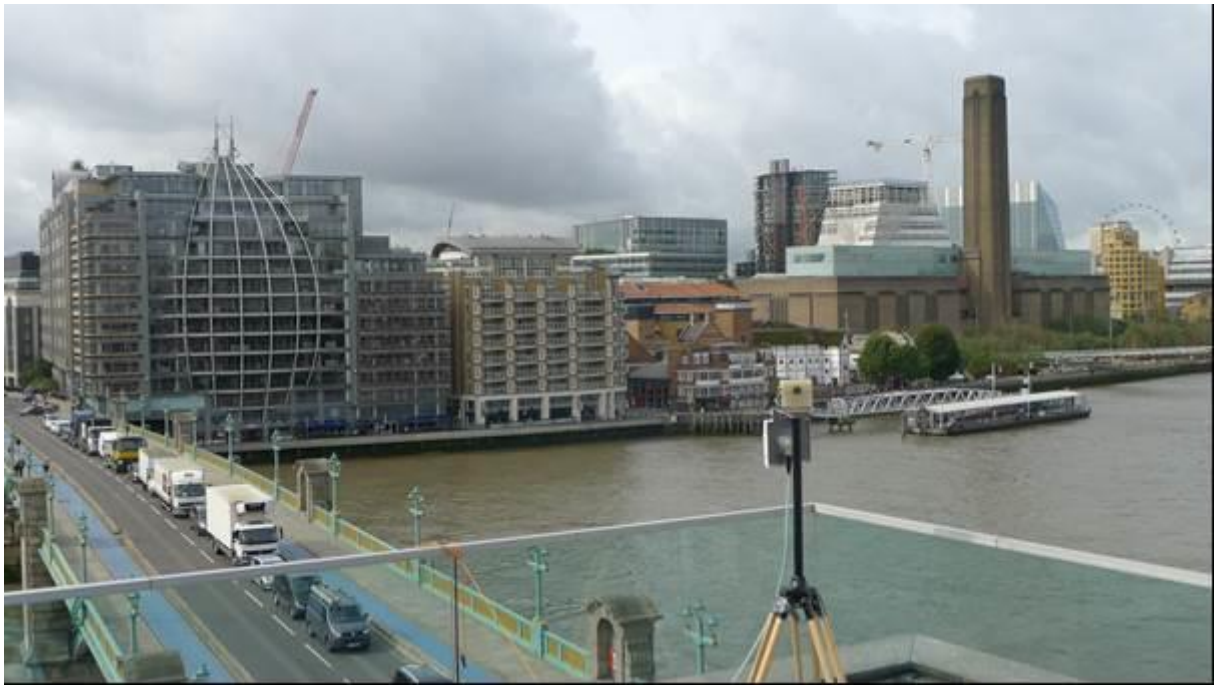

As for the earlier tests, the receiver was at the fixed outdoor location (simply because of the bulk of the spectrum analyser used), while the portable indoor terminal consisted of a set of compact CW transmitters developed for the earlier work.

FIGURE 99

View towards receiver site (arrowed) from Floor 11 of Riverside House

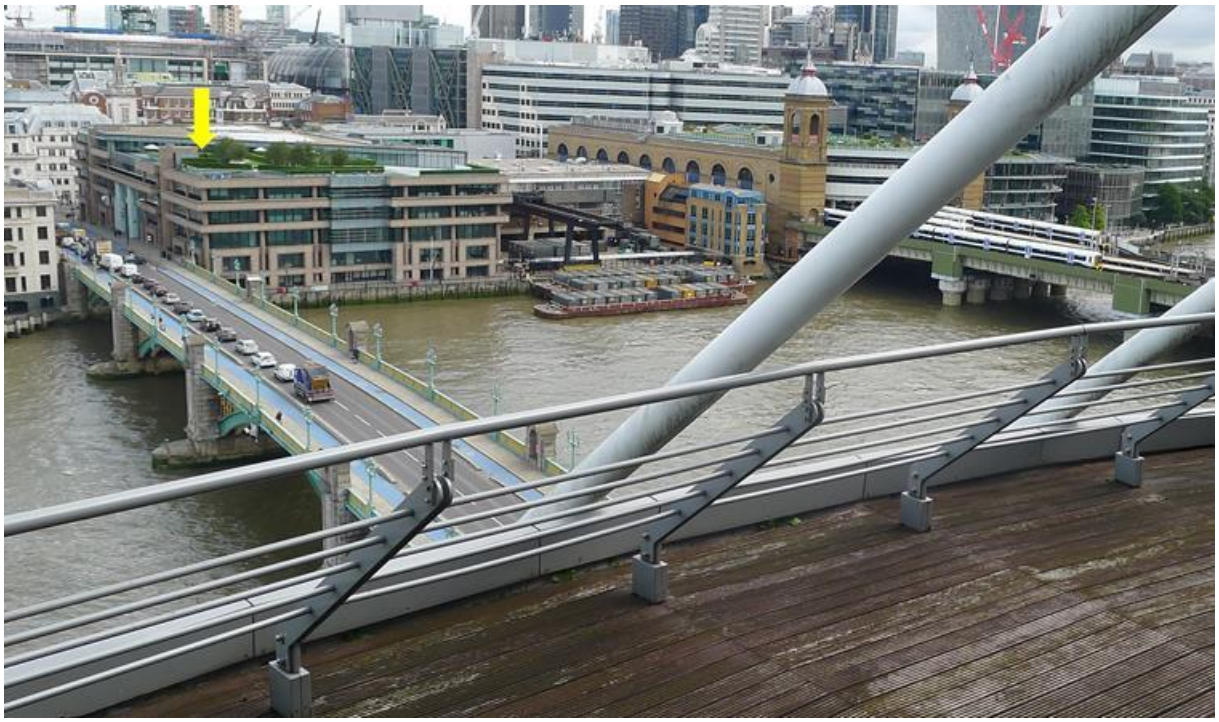

FIGURE 100

View towards receiver site (arrowed) from Floor 3 of Riverside House

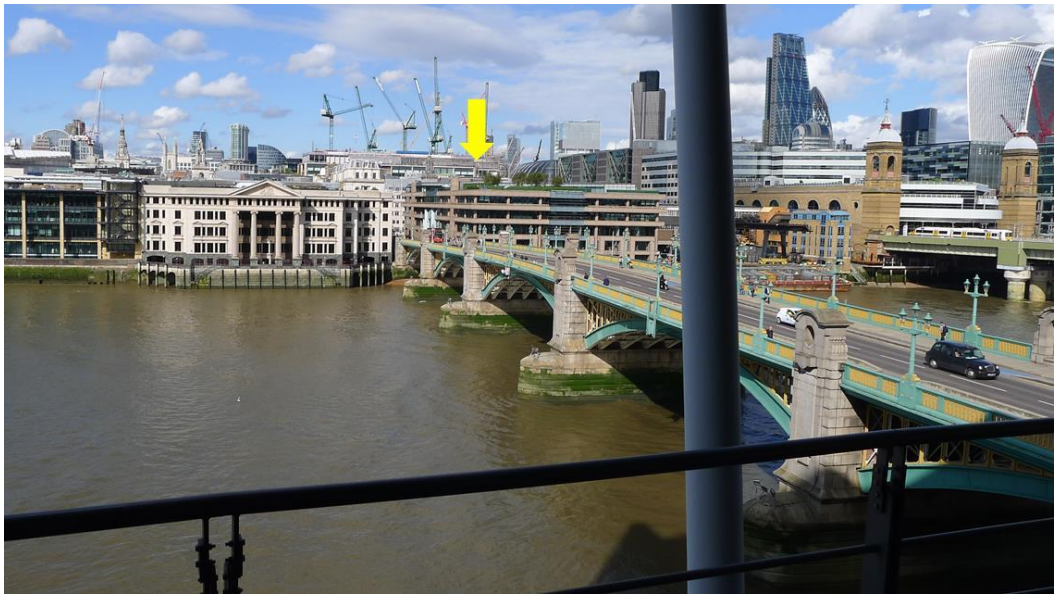

The receiver terminal was set up on the south-west corner of the terrace, with antennas supported on a 1.6 m tripod. The height above the river (wrt chart datum) was 24 metres.

The 230 metre path between the receiver and the front of riverside House is shown in Fig. 101.

FIGURE 101

Showing 230 metre path from Riverside House (south) to 10 Queen Street Place (north)

A sketch of the locations in elevation is shown in Fig. 102. This Figure also indicates the direct and river-reflected paths to a measurement location on the third floor of Riverside House (see discussion below). The height of the measurement antennas above river level (chart datum) was 23 m (floor 2), 26 m (floor 3) and 52 m (floor 11).

FIGURE 102

Sketch of locations (not to scale)

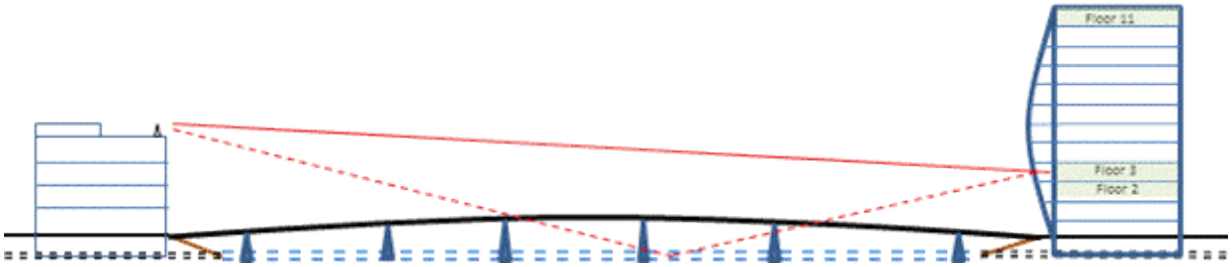

17.3 Measurement procedure

Measurements were made at five frequencies[9] , using the same equipment developed for the earlier measurements. The frequencies used were 87[10] MHz, 217 MHz, 690[11] MHz, 2 410 MHz and 5 760 MHz.

Following the Recommendation ITU-R P.2040 method, the measurement approach was statistical, in that no attempt was made to record the instantaneous position of the portable indoor terminal, Instead, the statistical distribution of received power was recorded in a series of small areas (‘zones’) within Riverside House. This will allow the parameterisation of building loss statistics in terms of depth within the building. The median received power in each zone is compared with a reference measurement made on the balcony of the relevant floor to derive the BEL.

Measurements were carried out on Floors 2, 3 and 11 of Riverside House. The two lower floors were each divided into eight measurement zones, while three zones were used on the upper floor. Plans showing the location of the zones are given in Annex C.

Measurements were made separately for each frequency, to avoid issues with antenna combining and interaction. The transmitter was carried around each zone in turn, with the receiver[12] logging received power at a sampling interval of 78 ms. No attempt was made to follow precisely the same path at different frequencies; earlier work has shown that median measured values are repeatable to within <1 dB using this method.

---

9 Measurements were also made at 3 550 MHz, using equipment funded under a separate study. The results of these measurements have been submitted to CG 3J-3K-3M

10 Changed from previous frequency (88.8 MHz) due to local FM radio services

11 Changed from previous frequency (698 MHz) due to local digital TV services

12 A Rohde & Schwarz FSP13 spectrum analyser

FIGURE 103

Indoor measurements (5.7 GHz)

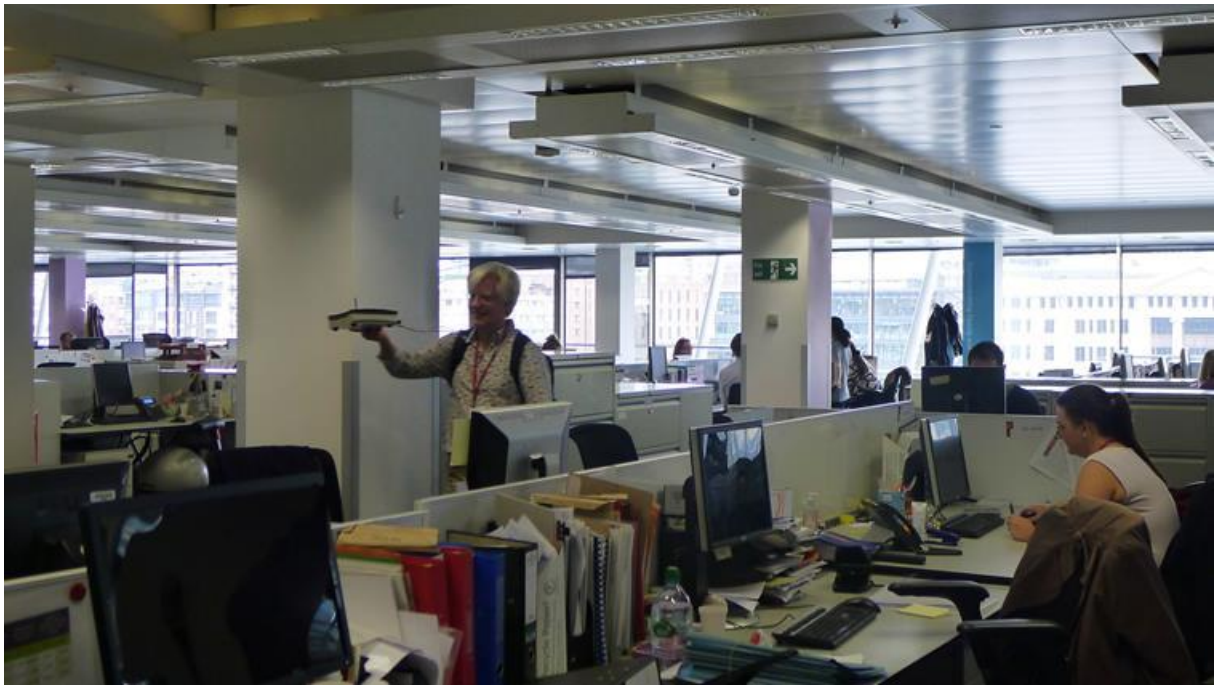

At a typical walking pace of 1 m/s, the receiver was sampling 44 times in a wavelength at 87 MHz and only 0.7 times at 5 760 MHz; reciprocally, only 23 wavelengths were explored at 87 MHz in a typical measurement length of 80 metres, but 1 428 wavelengths were covered at 5 760 MHz. The under-sampling at higher frequencies would be of concern if a record of median field along the path were required, but is acceptable in the context of deriving loss statistics for the each 'zone' as a whole.

FIGURE 104

Portion of data logged in Zone 5, floor 2 at low (left) and high (right) frequencies

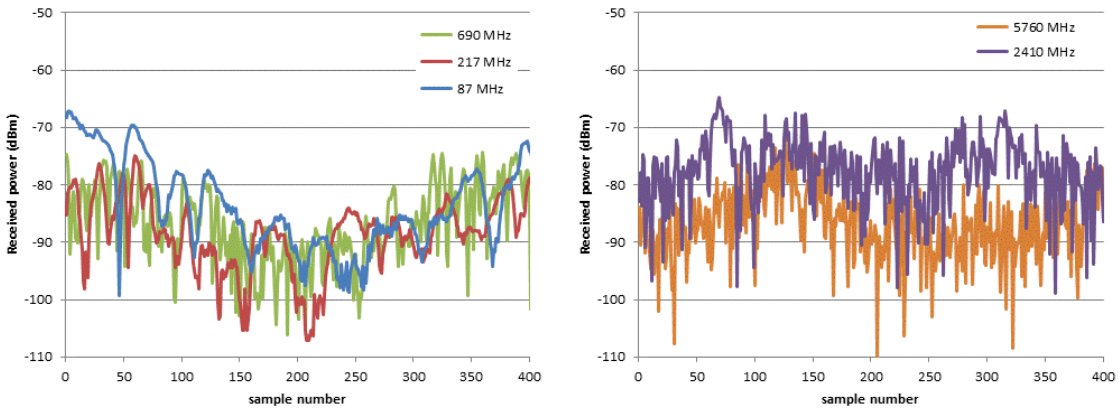

These very different sampling regimes have implications for data processing, and in particular limit the rigour with which multipath and shadow fading may be separated. In a more elaborate experiment sampling at a constant spatial or wavelength interval might be arranged, but this was not permitted by time and logistics. An alternative approach would be to employ a wideband channel sounder, but the bandwidth available would be very limited at the lower frequencies.

The path length to Riverside House is 230 m and the depth of the building is 50 m. This would correspond to an additional free space path loss of 1.7 dB. A small correction was made to each of the measured median entry loss values to account for this additional spreading loss[13].

17.4 Reference measurements

In line with the ITU-R Recommendation, and the measurements made in the earlier Ofcom study, the building entry loss is defined relative to the median field measured immediately outside the building, on the balcony of each floor.

These measurements were made by walking back and forth while holding the transmit antenna clear of local obstructions, and in clear sight of the receive location. These 'reference' measurements were made both before and after each set of indoor measurements as a check that no faults had developed with the transmit or receive systems.

FIGURE 105

Reference measurement on 11th floor balcony, showing receiver terminal location

It can be seen that there are a number of metallic obstructions on and around the balcony, and the received signal shows significant multipath effects as a result. As the intention is to confirm the strength of the field incident on the face of the building, rather than to observe local effects, the time-series record of received power was examined to identify portions where the received signal showed no sign of shadow fading, and a median was taken through the multipath (see Fig. 106). The value so derived should correspond to the free-space field (except, perhaps, at the lowest frequencies where coherent ground/water reflections might distort the results).

[13] 0.2 dB in zones 1 & 2, 0.4dB in zone 3, 0.5 dB in zones 4-6, 0.8 dB in stairwell, 0.9 dB in zone 7 and 1.4 dB in zone 8.

FIGURE 106

Balcony reference measurement (floor 3)

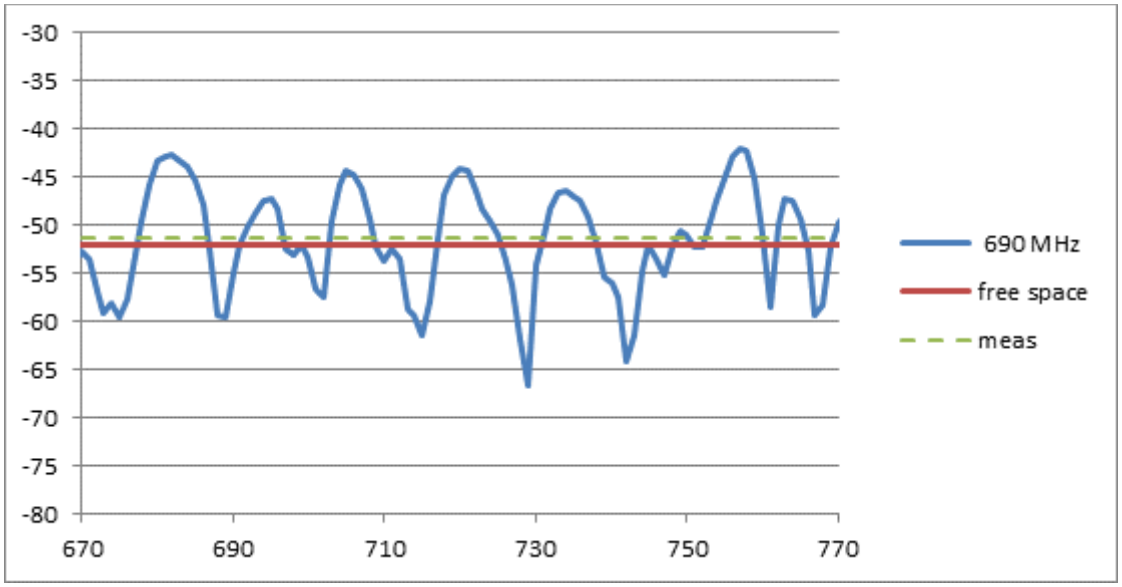

Link budgets are given in an annex, and a comparison between the predicted free-space power at the receiver and that actually measured is given in the Table below.

TABLE 43

Predicted and measured 'outdoor reference' powers

Frequency	87 MHz	217 MHz	690 MHz	2410 MHz	5760 MHz
RX power (free-space)	−29.1	−41.2	−52.0	−50.4	−55.7
Measured floor 11	−32.1	−45.0	−51.1	−54.5	−57.0
Measured floor 3	−34.1	−41.2	−51.3	−51.4	−56.5
Measured floor 2	−34.8	−41.1	−51.2	−51.4	−56.3

In all cases except at 87 MHz, the measured and predicted fields on the lower floors agree to within 1 dB. The significant discrepancy (5.0-5.7 dB) at the lowest frequency may be due to coupling between the transmit aerial and the large amount of metalwork on the balcony at distances less than a wavelength.

Another possibility is that of destructive interference between the direct and river-reflected rays sketched in Fig. 101. The impact of this is difficult to predict as the heights of the buildings relative to the river vary with the tide, and the reflection point may fall in the river or on the bridge (see Fig. 100). It is, nevertheless, instructive to plot the predicted path loss variation with terminal height at Riverside House (see Fig. 107), which suggests that for certain transmit terminal heights the field at the receiver may be more than 2 dB below free-space.

FIGURE 107

Loss as a function of transmitter height (87 MHz)

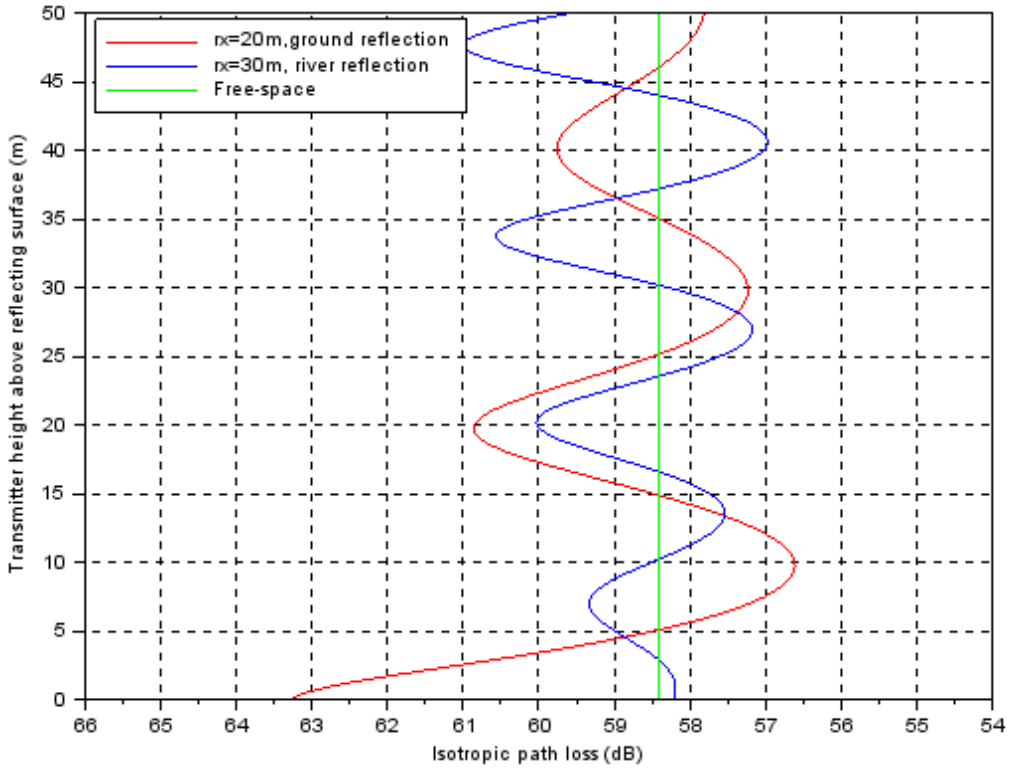

While the signals measured on the lower two balconies show a very close correspondence (with a maximum discrepancy of 0.7 dB between measurements made on floor 2 and floor 3), the same is not true for the 11th floor. In this case, only the 690 and 5 760 MHz results are close to those, and a 2-4 dB discrepancy at other frequencies. No explanation has been found for this – it cannot be attributed to the modest increase in elevation angle, as the vertical beamwidth of none of the antennas used would account for more than a fraction of one dB of additional attenuation.

Given the generally good agreement between prediction and the 'balcony reference' values, the latter will be used to determine the BEL values on each floor, as in the previous study and as recommended in Recommendation ITU-R P.2040. The uncertainties in the reference values at 87 MHz, and on the 11th floor should be borne in mind when examining the results, however.

17.5 Results

17.5.1 Building entry loss (median loss)

The 'headline' figure of interest is the difference between the median field that would be received in the absence of the building, and that actually measured.

The median signal level was determined for each of the measurements sets made in each zone, and these are plotted below.

FIGURE 108

Median loss values (floor 2)

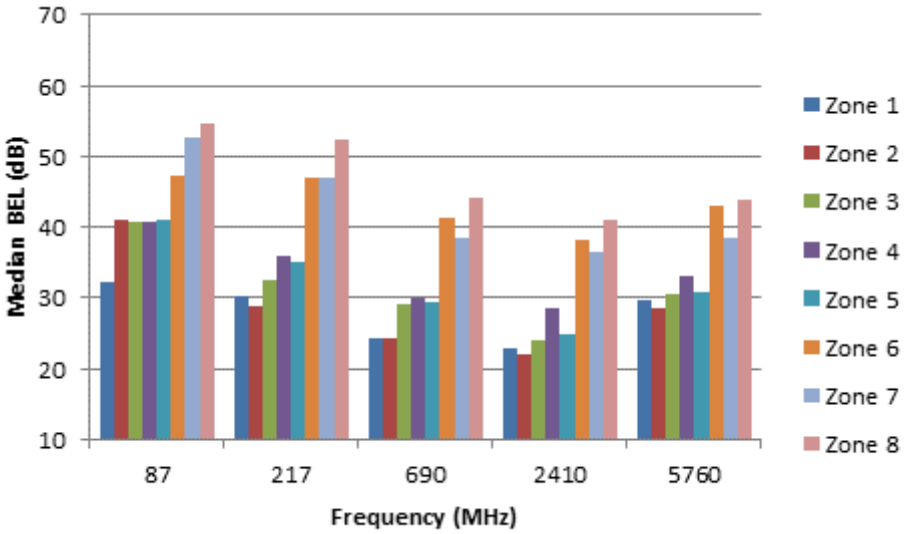

FIGURE 109

Median loss values (floor 3)

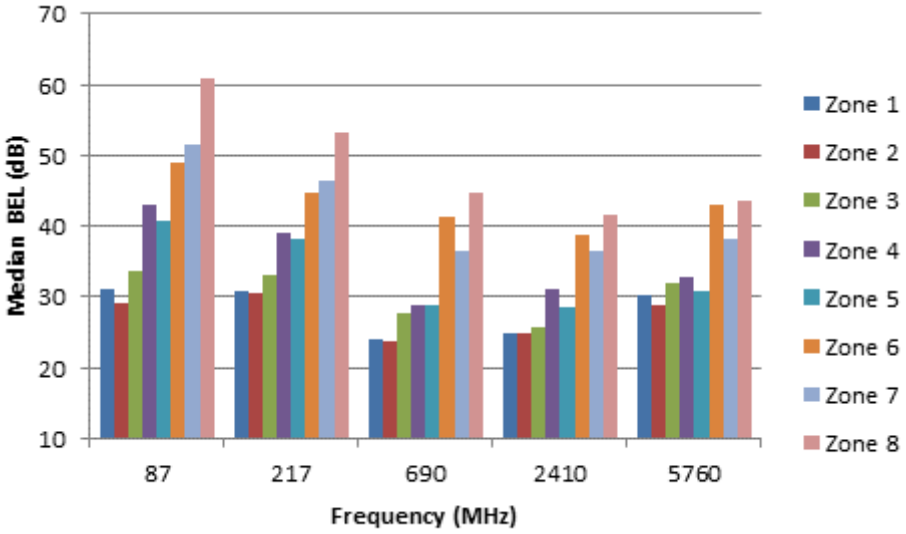

FIGURE 110

Median loss values (floor 11)

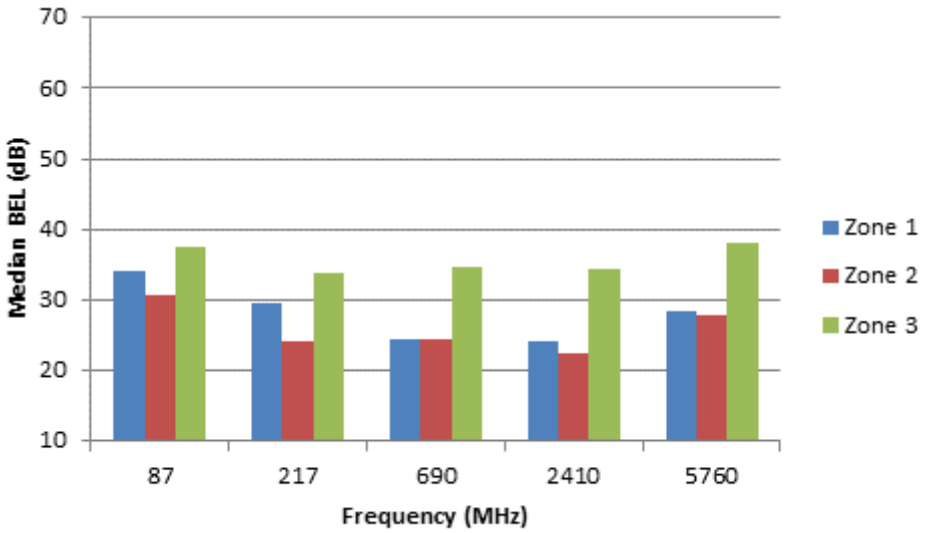

It can be seen that, as would be expected, the median loss increases as the mobile terminal moves further inside the building. In zone 1, by the windows facing the transmitter, losses are typically 20 dB less than at the back of the building.

The trend with frequency is interesting, with the highest losses seen at 87 MHz, falling to a minimum at 2.4 GHz and increasing again at the highest frequency. This trend is made more explicit in Fig. 111.

FIGURE 111

Trend of BEL with frequency

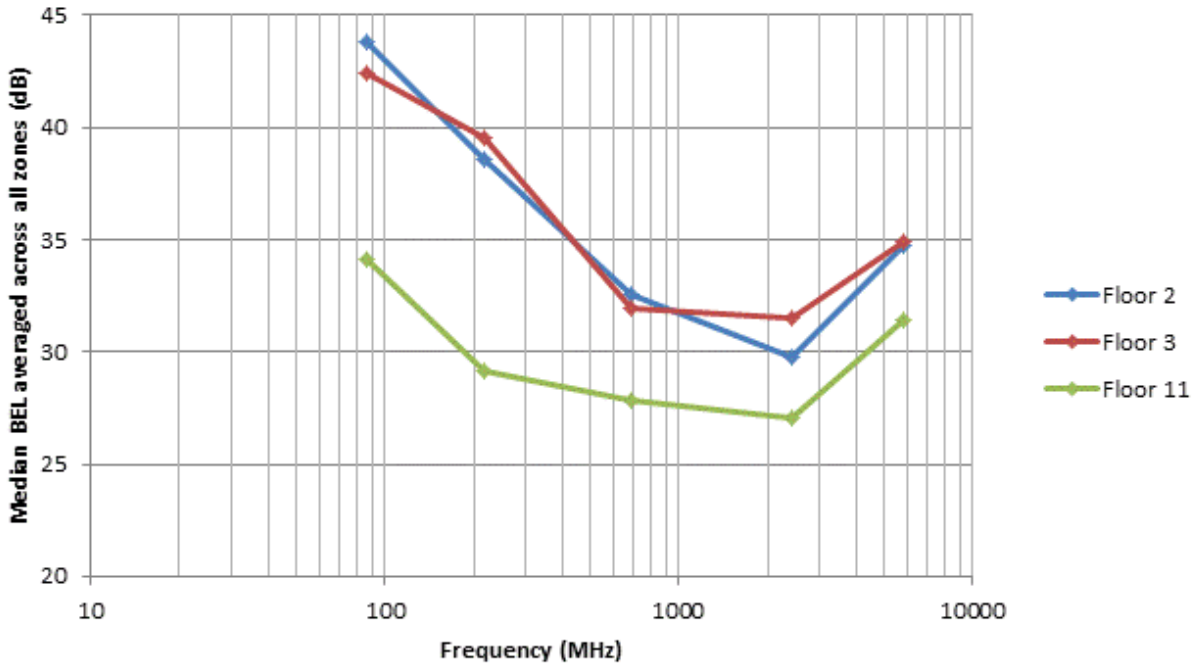

A similar non-monotonicity, although with the minimum around 217 MHz, was seen in the earlier measurements in domestic buildings, and can be explained qualitatively by observing that building

apertures are too small to permit efficient propagation at longer wavelengths, while higher frequencies will tend to suffer more absorption by building materials.

17.5.2 Building entry loss statistics

While the median loss value may be a useful 'headline' figure, a radio system designer concerned with ensuring the availability of a wanted signal, or protection from a potential interfere, will generally be interested in other points on the statistical distribution.

The measurements made in all zones on each floor have been aggregated and the cumulative distributions of the BEL derived (Fig. 112).

FIGURE 112

CDF of building entry loss (floors 2 and 3)

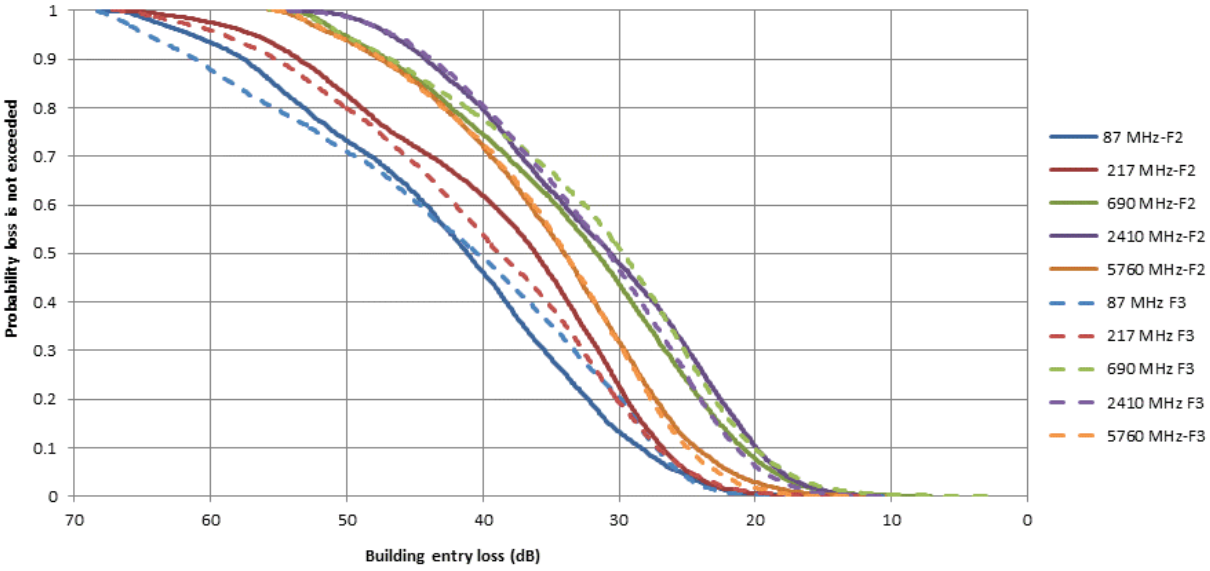

In the Figure, it can be seen that the results for the two floors are broadly similar, though with differences in detail. The interdecile range is about 30 dB at lower frequencies, falling to 20 dB at 5.7 GHz.

It should be borne in mind that these statistics include multipath fading, so the range of losses seen for wideband signals will be rather smaller; further processing should be undertaken to estimate the variability associated with flat fading (absorption and diffraction) alone.

The losses measured in the present study are significantly (20-30 dB) greater than those seen in the measurements made of domestic buildings, presumably due to a combination of the much greater depth of the building and the large amount of metalwork in the construction. Even in zones 1 and 2, immediately adjacent to the windows, losses are 10-20 dB greater than seen in either the terraced house or the mansion at BRE.

It would be expected that the office windows would be metallised for thermal efficiency, and these results would appear to confirm this; no data has yet been obtained on the characteristics of the glass, however.

17.6 Conclusions

The attenuation suffered by radio waves entering Riverside House is substantially greater than was the case for the domestic buildings measured previously.

Median entry loss was found to vary monotonically with depth within the building, but non-monotonically with frequency, with the highest losses observed at VHF frequencies and at 5.7 GHz. Evaluated over each floor of the building, 90% of losses were greater than 20 dB (690 MHz, 2.4 GHz) – 30 dB (87 MHz).

In making use of this measurement data it should be borne in mind that Riverside House may not be representative of the generality of urban office buildings.

17.7 Annex - link budgets

The Table below gives the link budgets for the equipment and reference locations used in the trials.

TABLE 44

Link budgets

Frequency	87 MHz	217 MHz	690 MHz	2410 MHz	5760 MHz
TX power (dBm)	27.0	19.0	18.4	25.4	27.5
Feeder loss (dB)	0.4	0.8	1.4	1.4	2.2
TX ant gain (dBi)	1.7	2.0	1.6	3.0	1.5
e.i.r.p. (dBm)	*28.3*	*20.2*	*18.6*	*27.0*	*26.8*
Isotropic path loss (dB)	58.5	66.4	76.5	87.3	94.8
RX ant gain (dBi)	1.3	5.3	6.4	11.0	14.0
Feeder loss (dB)	0.2	0.3	0.5	1.1	1.7
Free space Rx power (dBm)	*−29.1*	*−41.2*	*−52.0*	*−50.4*	*−55.7*

17.8 Annex - measurement zones at Riverside House

FIGURE 113

Floor 2 measurement zones

FIGURE 114

Floor 3 measurement zones

FIGURE 115

Floor 11 measurement zones

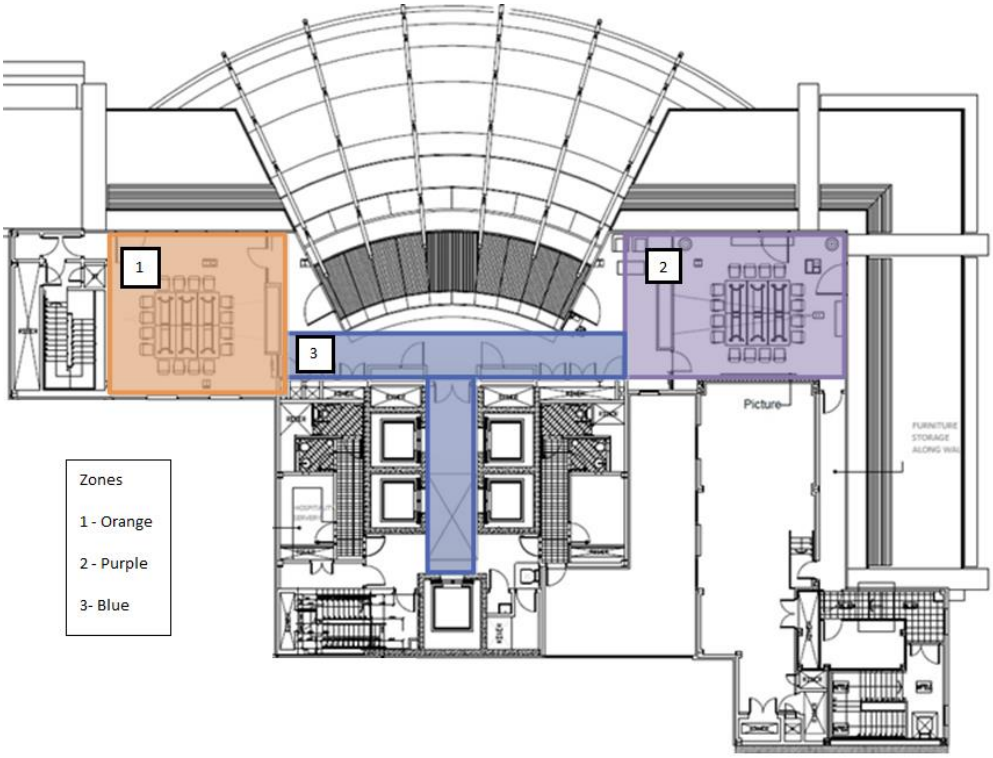

18 Building loss in an urban environment (Japan, 0.8-37 GHz)

Measurements have been made of the building entry loss to an office building at six frequencies between 0.8 and 37 GHz.

18.1 Measurement methods and parameters

This Section described the measurement method and parameters. Figures 116 to 118 respectively show photographs of the measurement area taken at one of the Tx positions, at a corridor inside the building and outdoor buildings. We regard as the glass window of the measurement route (marked yellow point) as an LOS environment from a Tx position in the measurement environment. The tall buildings surround the road in the measurement site. Figures 119 to 121 show the measurement route and Table 45 summarizes the measurement parameters. To analyse the frequency characteristics from microwave bands to millimeter wave bands, we set the measurement frequencies at 0.8, 2.2, 4.7, 8.4, 26.3 and 37.0 GHz, respectively. The continuous waves (CW) were simultaneously transmitted from the Tx antennas, which were set up on the roofs of cars positioned on the roadside outside as shown in Fig. 116. Rx antenna was located in the indoor building. The Tx antenna positions are shown as A1 and A2 in Fig. 119. We took repeated measurements on the 1st, 2nd, 4th, 6th and 8th floors (i.e. 1F, 2F, 4F, 6F and 8F). We also obtain the 3D incident angle characteristics described in Fig. 6. Tx antennas were located at A-1 and A-2. Tx antenna height was 2.5 m above the ground. The Rx antenna was set up on a hand truck inside the building, and measurements were carried out with the car running as shown in Figs 120 and 121. The Rx antenna height was 1.5 m above the floor. The radiation patterns of the Tx and Rx antennas are omni-directional in a horizontal plane. We note that vertically polarized waves were transmitted and received in these measurements. The median value of path loss calculated every 1 metre.

FIGURE 116

Building from Tx position

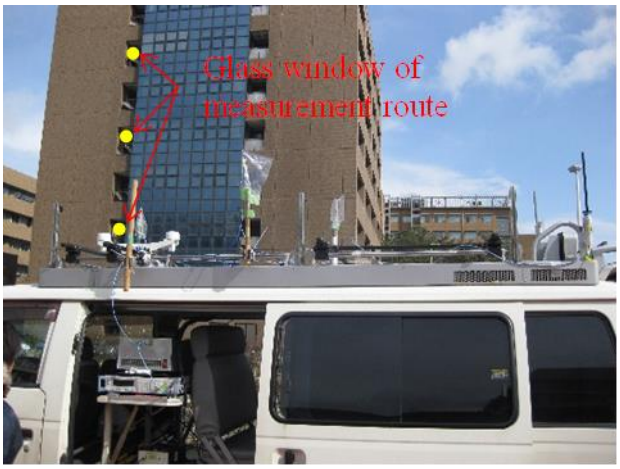

FIGURE 117

Measurement route at indoor corridor

FIGURE 118

Outdoor building from 6F

FIGURE 119

Outdoor building layout and Tx positions

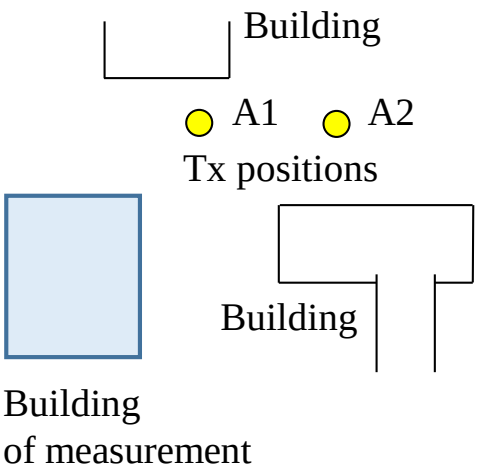

FIGURE 120

Top view of indoor environment and measurement route

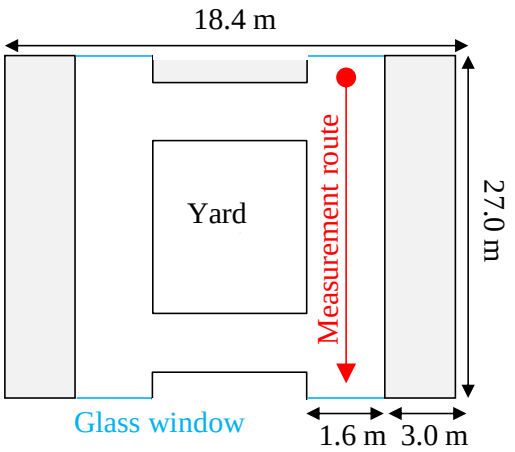

FIGURE 121

Vertical view of indoor environment and measurement route

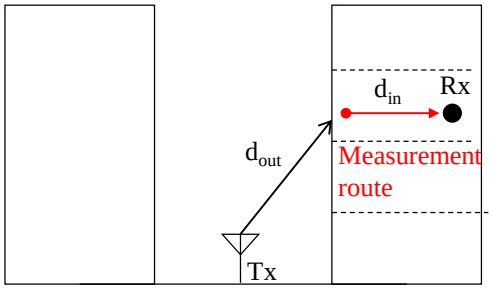

TABLE 45

Measurement parameters

Frequency (GHz)	0.8, 2.2, 4.7, 8.5, 26.4, 37.1
Tx antenna height	2.5 m
Rx antenna height	1.5 m
Floor number of measurement	1F, 2F, 4F, 6F and 8F
Tx/Rx antenna radiation pattern	Omni-directional

18.2 Measurement results from 0.8 to 37.1 GHz band

In this section, we describe the measured path loss characteristics from the 0.8 to the 37.1 GHz band. Figure 122 shows the path loss measurement results obtained at A-2 at 37.1 GHz for the route for floors 1F, 2F, 4F, 6F and 8F. The horizontal axis indicates Rx moving distance along the measurement route. The vertical axis indicates the normalized path loss. Figure 123 shows those path loss slope of measurement results for each floor. Figure 124 shows the measurement results obtained at A-2 on 8F for the 0.8, 2.2, 4.7, 8.5, 26.4 and 37.1 GHz frequency bands. Figure 125 shows the frequency dependence of measurement path loss. The horizontal axis indicates the median value of path loss. The vertical axis indicates the frequency. In order to analyse the path loss dependence on the

frequency and 3D incident angle, the building entry loss BEL_{meas} is normalized by subtracting free space loss PL_{free} from measurement path loss PL_{meas} by using equations (22) and (23) to follow.

$$BEL_{meas} = PL_{meas} - PL_{free} \tag{22}$$

$$PL_{free} = 20\log_{10}(d_{out} + d_{in}) + 20\log_{10} f_{GHz} + 32.4 \tag{23}$$

where d_{out} is the distance from Tx to the wall next to Rx, d_{in} is the perpendicular distance from the wall to Rx as shown in Fig. 121.

As Figs 122 and 123 show, the building entry loss slope tends to increase as the floor number increases. To illustrate, the values are about 0.2 dB/m at 1F and 0.8 dB/m at 8F. As Figs 124 and 125 show, building entry loss tends to increase as the frequency increases. Therefore, in order to construct a building entry loss model, it is necessary to take account of frequency and 3D incident angle characteristics.

FIGURE 122

Path loss measurement obtained at A-2 at 37.1 GHz for the route for floors 1F, 2F, 4F, 6F and 8F

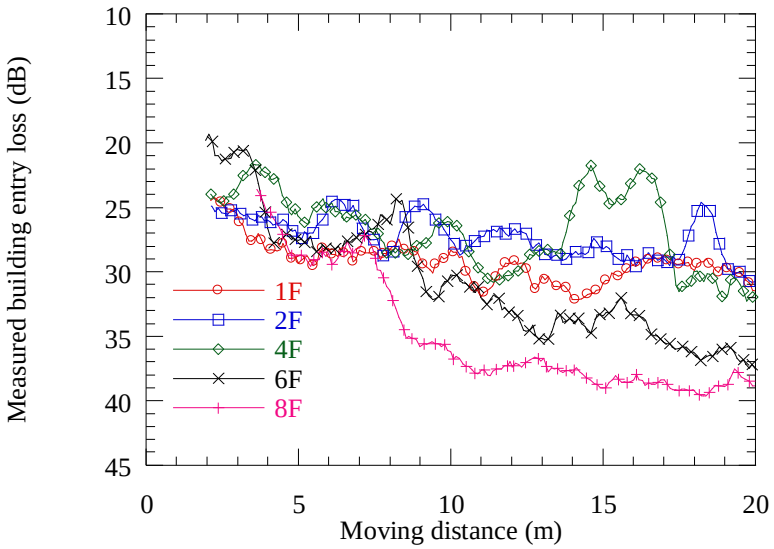

FIGURE 123

Normalized path loss slope for floors 1F, 2F, 4F, 6F and 8F

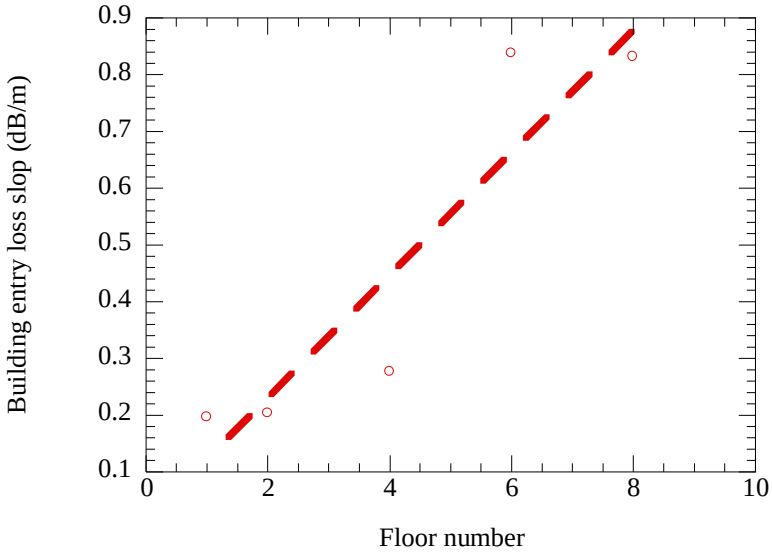

FIGURE 124

Path loss measurement obtained at A-2 on 8F for the 0.8, 2.2, 4.7, 8.5, 26.4 and 37.1 GHz frequency bands

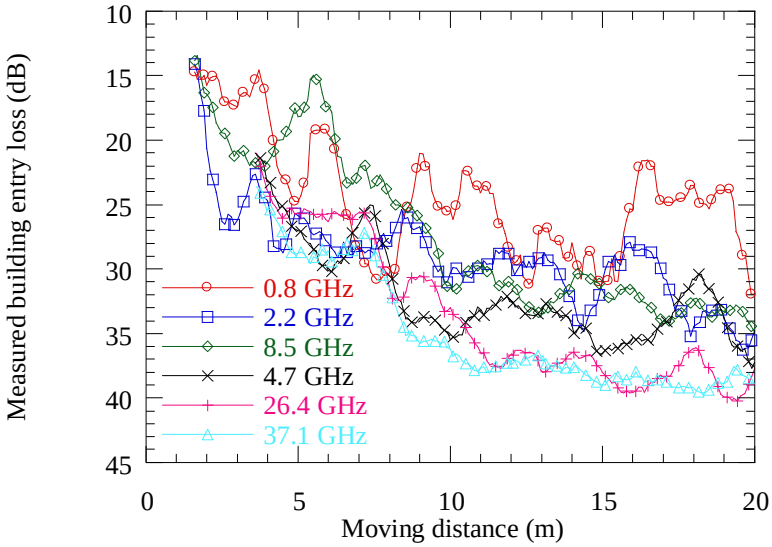

FIGURE 125

Frequency dependence of median value of normalized path loss for the 0.8, 2.2, 4.7, 8.5, 26.4 and 37.1 GHz frequency bands

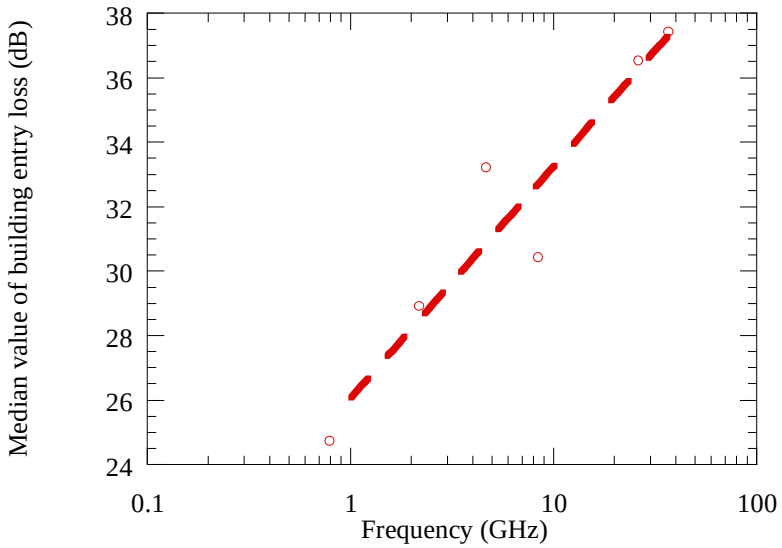

19 Multi-frequency sounder measurements in Canada (2.4 GHz, 3.5 GHz, 5.8 GHz, 13 GHz, 26 GHz, 38 GHz, and 61 GHz)

19.1 Introduction

This chapter describes propagation measurements which were conducted by Communications Research Centre Canada (CRC) at its Shirleys Bay campus in Ottawa, Canada.

The results concern BEL for a single building in the 13 GHz, 26 GHz, 38 GHz and 61 GHz frequency bands and building material losses for various types in the 2.4 GHz, 3.5 GHz, 5.8 GHz, 13 GHz, 26 GHz, 38 GHz and 61 GHz bands.

A wideband multi-frequency channel sounder was developed at CRC to enable double-directional propagation measurements to be performed over a range of frequency bands between approximately 2 and 60 GHz (see Table 46). This system is based around a VNA, which records frequency-domain channel response ($S_{21}(f)$) data. The measurement system employs frequency up- and down-converters, allowing for measurements outside the frequency range of the VNA. The directional scanning capabilities are obtained with the use of dual-polarized horn antennas, which are mechanically steered by precision pan-tilt units mounted on tripods. Switching between bands and polarizations is automated and controlled by software developed in-house, which also allows for real-time visualization of propagation data by overlaying measurement results on 360° panoramic photographs of the transmitter (Tx) and receiver (Rx) surroundings.

TABLE 46

Frequency bands used by the CRC Channel Sounder

Centre frequency (GHz)	Bandwidth (MHz)
2.450	100
3.4375	75
5.800	150
13.000	500
25.875	1250
38.000	1000
61.250	500

19.2 Building description

BEL data were collected on the second floor of CRC Building 76 (Fig. 126), which is of corrugated and smoother metal construction. It was built over 35 years ago, with closed offices connected via a corridor, but was recently refurbished into a semi-open office work environment with cubicles, a meeting room, laboratories, and a kitchen area. Most of the double-pane windows had no metal coating, with the exception of three of these on the second floor - but at the left end of the building face (labelled “Metal” in Fig. 126); this section of the building was not illuminated during our measurements, however. This building has corrugated metal ceilings on both floors with air ducts, electrical wiring and various pipes, all of these hidden from view by a floating ceiling (acoustic tiles) 1 m below.

FIGURE 126

General exterior view of Building 76 at CRC, with both smooth (beige) and corrugated metal siding (dark brown). The transmitting end of the channel sounder is mounted on a tripod at 1.5 m above ground, at location T_{x1}; the horn antennas are positioned to illuminate the area on the second floor surrounding the middle pillar

19.3 Description of the BEL measurements through Building 76

As seen in Fig. 126, the transmitter end of the channel sounder was deployed in front of CRC Building 76, at about 8.66 m from the building face ("Tx_1"); the VNA was left safely inside, at the bottom of the staircase on the first floor ("VNA"). A first set of measurements were taken with both the transmit and receive antennas on a tripod at 1.5 m above ground level (AGL) at both "Tx_1" and "Tx_2" locations. A second (limited) set of measurements was conducted only for the three locations closest to the VNA (A"- C" in Fig. 127) with the transmit antennas on top of a trailer at 4.4 m above ground at position "Tx_2" (see also Fig. 129); the receiving antennas were still on the tripod at 1.5 m above ground. Both linear polarizations (vertical and horizontal) were transmitted by the three horns, in sequence.

FIGURE 127

The first floor of Building 76 at CRC. (BEL measurements only took place on the second floor)

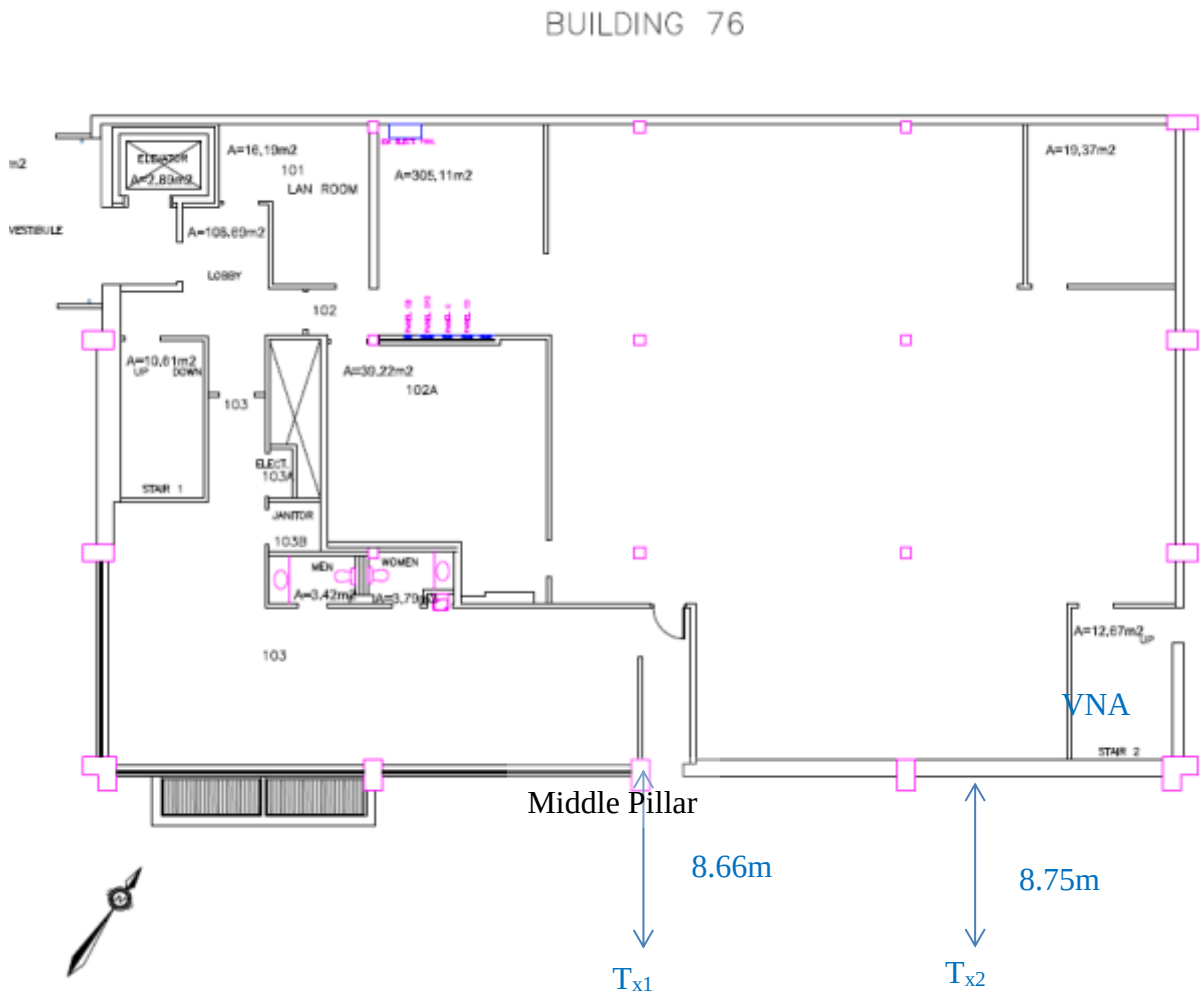

FIGURE 128

The second floor of Building 76. Three paths were considered for BEL: A-B-C, A'-B'-C' and A"-B"-C". The receiver position was changed from A to B, then C, it was not wheeled on the path

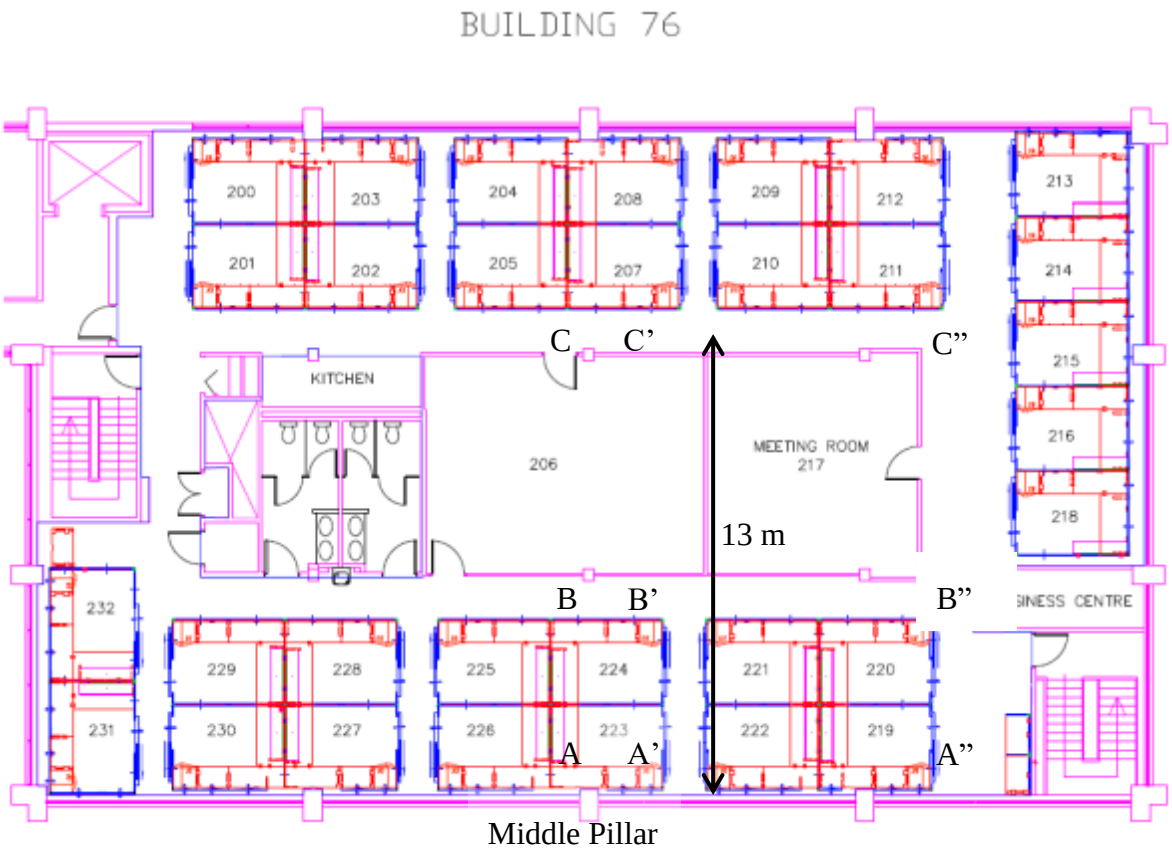

FIGURE 129

Setup for BEL measurements with the transmitter at 4.4 m above ground level (location T_{x2})

Single-directional scan measurements were conducted using the horns of the channel sounder at both ends of the link. The transmitting horns were kept in line of sight with the windows facing the receiving horns, the latter being scanned in azimuth and elevation, in order to retrieve angle-of-arrival data. The single-directional scan range at the receiving end was 360° in azimuth and from

−30° to +50° in elevation. Assuming that each measurement at a given angular position and polarization can be performed in about 7.3 s, each single-directional scan at a given location should take (36x9x4x7.3) seconds, thus about 2 hours and 37 minutes for all four polarization transmit and receive combinations (VV, VH, HV and HH). Only the co-polar data have been considered for this BEL study. Moreover, reference data were recorded once every 16 regular channel responses or, on average, approximately once per minute; they were taken between vertically-polarized horns, for fixed pointing directions corresponding to the strongest propagation path found during preliminary testing prior to the measurement.

The measurement plan is as follows, with steps 1-9 conducted with the transmit antenna set to 1.5 m AGL. (*Location T_{x1} was used for steps 1-6; location T_{x2} was used for steps 6-8*):

1. Measurements were first conducted in cubicle 223 (location "A", see Fig. 128), right behind the properly-labelled concrete middle pillar (Figs 128 and 130) with expected higher levels of BEL compared to a line-of-sight situation (see Step 2);
2. A second set of measurements was conducted in the same cubicle 223, this time right in front of the window (location A', see Fig. 128);
3. Thirdly, measurements were taken with the receiver located at B', deeper into the building (5.6 m from the window facing the transmitter), but still aligned with A';
4. Next, measurements were taken with the receiver at location B in Fig. 128, close to the door leading to room 206, and aligned with location A;
5. Without changing the position or the elevation / azimuth angles of the transmitting horns, BEL measurements were then conducted with the receiver located at C;
6. With the transmitter deployed at T_{x2}, BEL measurements were then taken with the receiver located at A";
7. *Without changing the setup at the transmitting antenna*, BEL measurements were taken with the receiver at location B" in Fig. 128;
8. *Without changing the setup at the transmitting antenna*, BEL measurements were taken with the receiver at location C" in Fig. 128;
9. Finally, BEL measurements were taken with the receiver at location C' in Fig. 128, with the transmitter returning to location T_{x1};
10. Steps 7-9 were repeated with the transmit antenna set at 4.4 m above ground. Unfortunately, locations A-C and A'- C' could not be measured with the transmit antennas at 4.4 m, due to restrictions in coaxial cable length (i.e. 25 m between the transmit antennas and the VNA; same cable length between the receive antennas and the VNA – see Fig. 129 again).

The various transmit antenna heights, elevation/ azimuth angles at the transmitter and distances into the room are given in Table 47 on the next page. Note that an azimuth of 0° corresponds to perpendicular incidence in that plane only.

FIGURE 130

View of the receiving end of the channel sounder at location A (see Fig. 128 again), 1.5 m behind the middle pillar

TABLE 47

Various geometric parameters of the BEL measurements conducted on the second floor of Building 76

BEL Measurement Number	Location (see Fig. 3)	Transmit Antenna Height (m AGL)	Elevation Angle at Transmit Antenna (°)	Azimuth Angle at Transmit Antenna (°)	Distance into the Room from the Window (m)
1	A	1.5	25	0	1.84
2	A’	1.5	25	4	1.83
3	B’	1.5	25	4	5.63
4	B	1.5	25	0	6.15
5	C	1.5	25	0	13.53
6	A”	1.5	28	0	1.63
7	B”	1.5	28	0	5.60
8	C”	1.5	28	0	13.11
9	C’	1.5	25	4	13.04
10	A”	4.4	10	0	1.63
11	B”	4.4	10	0	5.60
12	C”	4.4	10	0	13.11

These measurement locations were carefully selected to allow for various comparisons. A few examples are described next. BEL measurements taken with the receiver at locations A" – C" (Fig. 128) are progressively deeper into Building 76, but always in line-of-sight with the transmitter at T_{x2}, to help characterize how BEL varies with the distance inside this building without much additional scattering, reflection or absorption due to furniture. These measurements will be compared with those along the (A'-B'- C') path which include the effects of furniture and several layers of drywall, etc. The influence of the concrete pillar labelled in Fig. 128 on BEL can be assessed by comparing path (A-B-C) with path (A'-B'- C'). The dependence of BEL on transmitter height will be assessed by comparing measurements at locations A"-B"- C" with the transmitter at 1.5 m AGL with those taken at these same locations when the transmitter was deployed at 4.4 m AGL.

19.4 Methodology used for the estimation of BEL

The measured single-directional propagation data are shown overlaid on panoramic photographs taken from the receiving end of the channel sounder. Figure 131 shows one such "heat map" of data collected at location A", 38 GHz, using vertical polarization at both ends of the link. The transmitter was situated atop the trailer, at 4.4 m AGL (Fig. 129). These measured data are calibrated to correct for cable losses and delays as well as for other system gains and losses. All gain values shown in this input document represent overall gain between antenna ports and include both propagation loss *and* antenna gains. As a result, the actual propagation losses can be estimated by subtracting the antenna gains.

A cursory glance at Fig. 131 reveals the presence of a dominant ray with lower losses (i.e. a gain between antenna ports equal to −51.2 dB) at an elevation of −10° and an azimuth of arrival of −120°. Similar behaviour was observed over the bulk of the data set, which can be explained by the fact that signals enter this metal-clad building through the illuminated windows. Moreover, these windows are broad enough (1.1 m high; see Fig. 126 again) to provide full first-Fresnel zone clearance across the five highest bands (i.e. 5.8 to 61 GHz), even at locations C, C' and C". No diffraction losses are incurred across the seven bands at locations A, A', A", however.

Unfortunately, interference from Wi-Fi at 2.4 and 5.8 GHz and fixed wireless access (FWA) (3.5 GHz) corrupted some of the sounder data collected in the lower three bands. Fig. 132 is a case in point: a single, strong pixel is often surrounded by much weaker ones (e.g. at AoA = −160° and EoA = 30°), which is not representative of actual multipath components. In sharp contrast with Fig. 132, a dominant ray is evident in Fig. 131 at AoA = −120° and EoA = −10°, although spread out and blurred somewhat by the finite beamwidths of the horns, their imperfect sidelobes and finite cross-polarization isolations (XPI). In light of these interference issues, it was decided to focus on the estimation of BEL across the four highest frequency bands. BEL was estimated by computing the excess loss over free space (with the antenna gains removed) of the strongest ray found in each single-directional map.

FIGURE 131

Elevation and azimuth of arrival of the various multipath components measured at location A" (see Fig. 128), at 38 GHz, using vertical polarization at both ends of the link (VV)

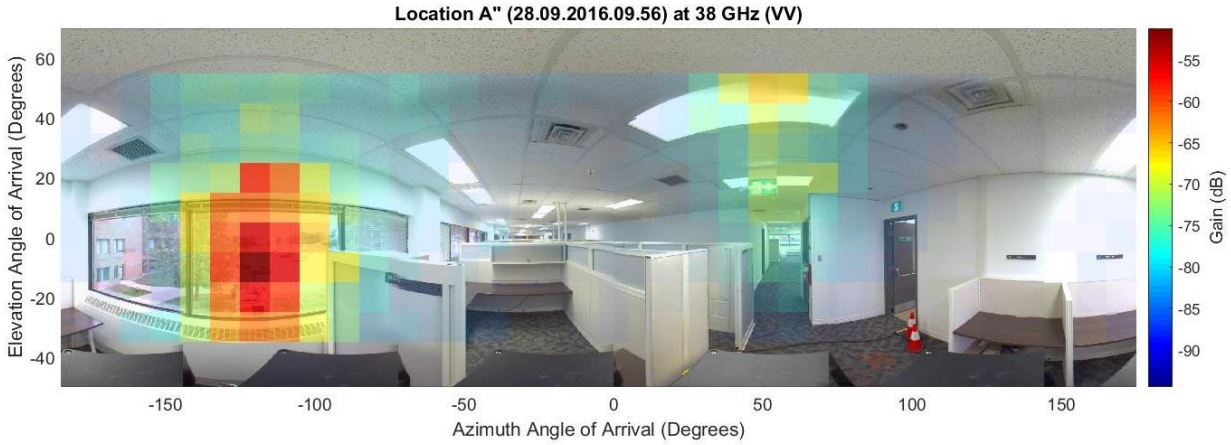

FIGURE 132

A case of interference from WiMax (3.5 GHz) measured at location A (see Fig. 128), in vertical polarization (VV)

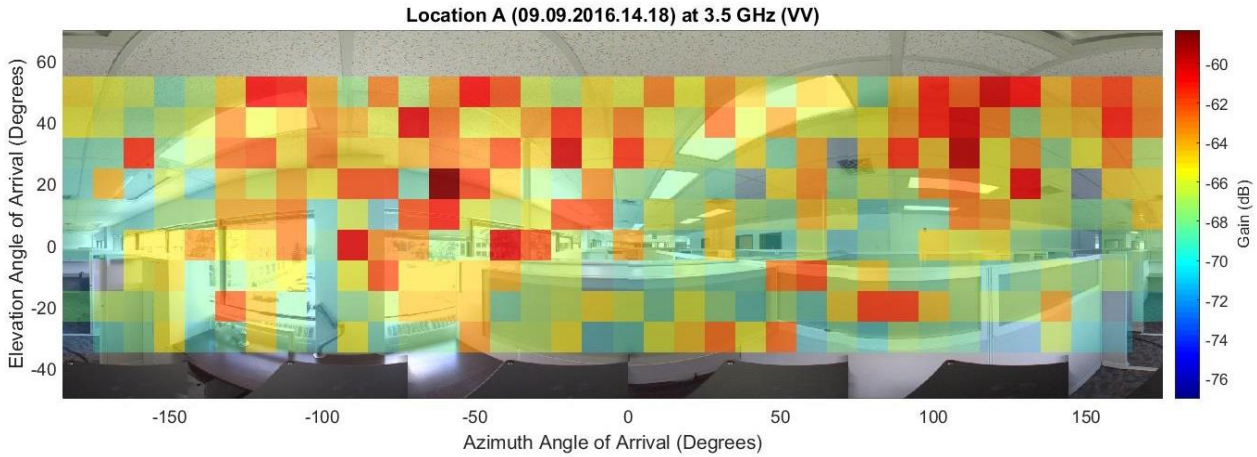

19.5 BEL measurement results and modelling

Various results will now be presented. Vertical and horizontal polarizations will be contrasted for each path. Figures 133 to 134 show plots of BEL as a function of distance across the room in the four highest bands (13-61 GHz) for paths A-B-C (with the sounder signals entering the building through the middle concrete pillar shown in Fig. 130), A'-B'-C' (with the signals entering through a regular double-pane window), and A"-B"-C" (much like the previous path, but through a corridor with much less clutter – see Fig. 128 again), respectively.

FIGURE 133

BEL measurements along path (A-B-C) around the middle pillar as a function of distance from the illuminated window (Figs 128 and 130) for the bands ranging from 13 to 61 GHz, using either vertical (left) or horizontal polarization (right) at both ends of the link

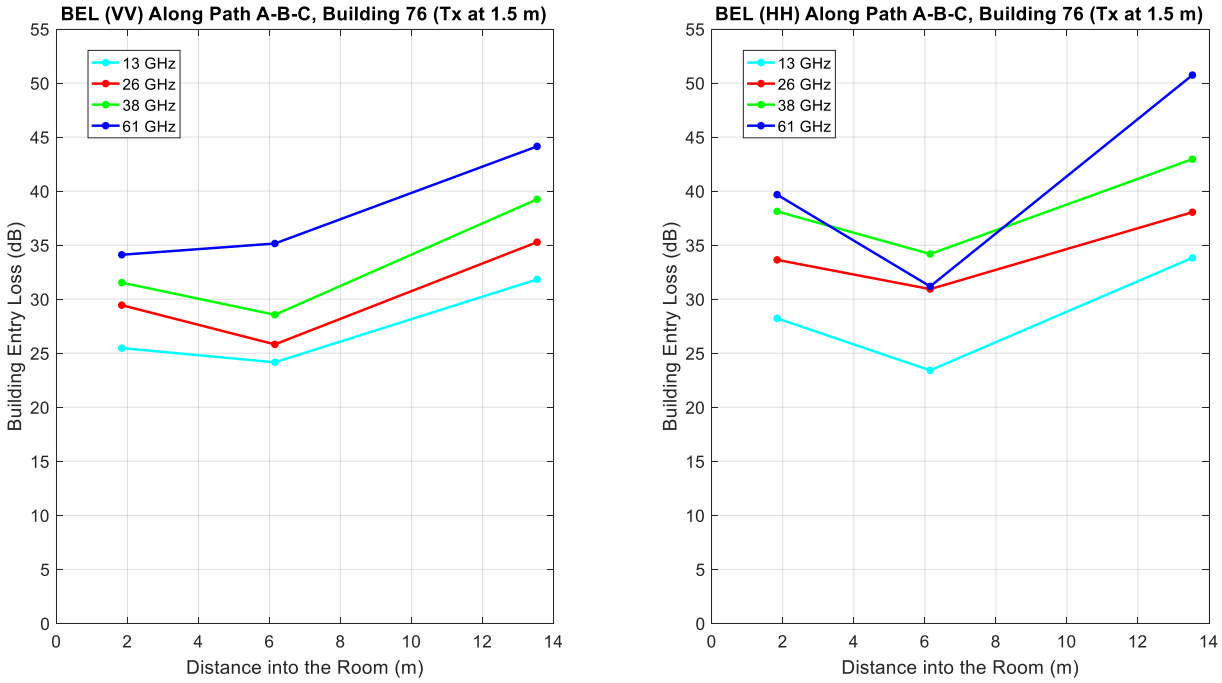

FIGURE 134

BEL measurements along path (A'-B'-C') as a function of distance from the illuminated window (Fig. 128) for the bands ranging from 13 to 61 GHz, using either vertical (left) or horizontal polarization (right)

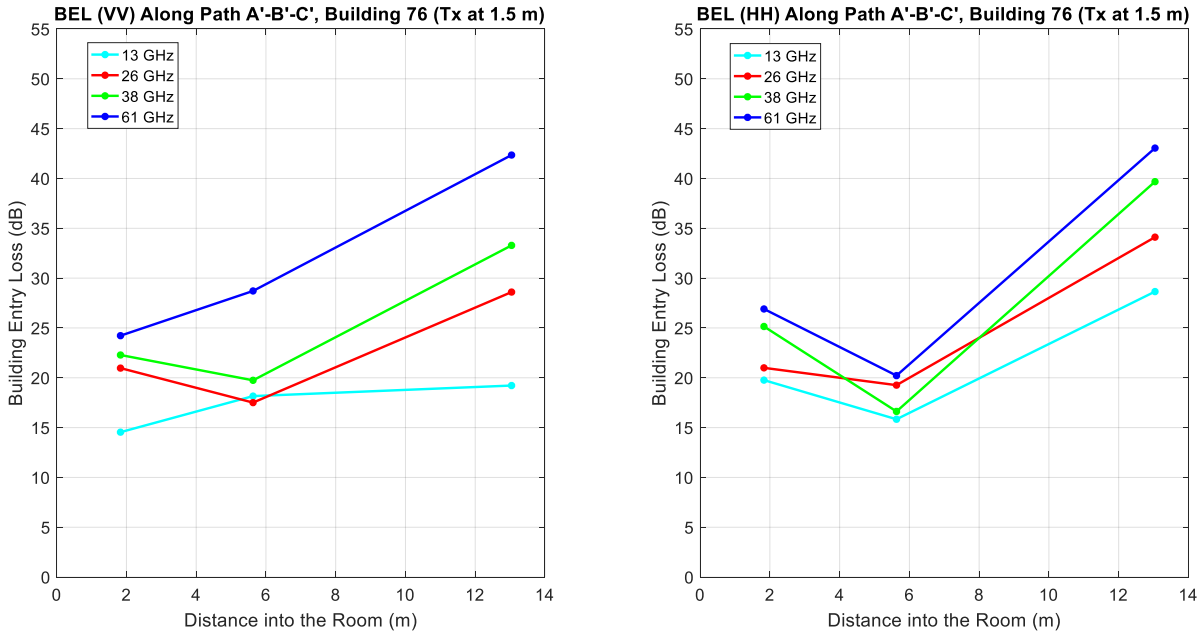

FIGURE 135

BEL measurements along path (A"-B"-C") as a function of distance from the illuminated window (Fig. 128) for two different transmitter heights, across four frequency bands (13-61 GHz), using either vertical (left) and horizontal polarization (right)

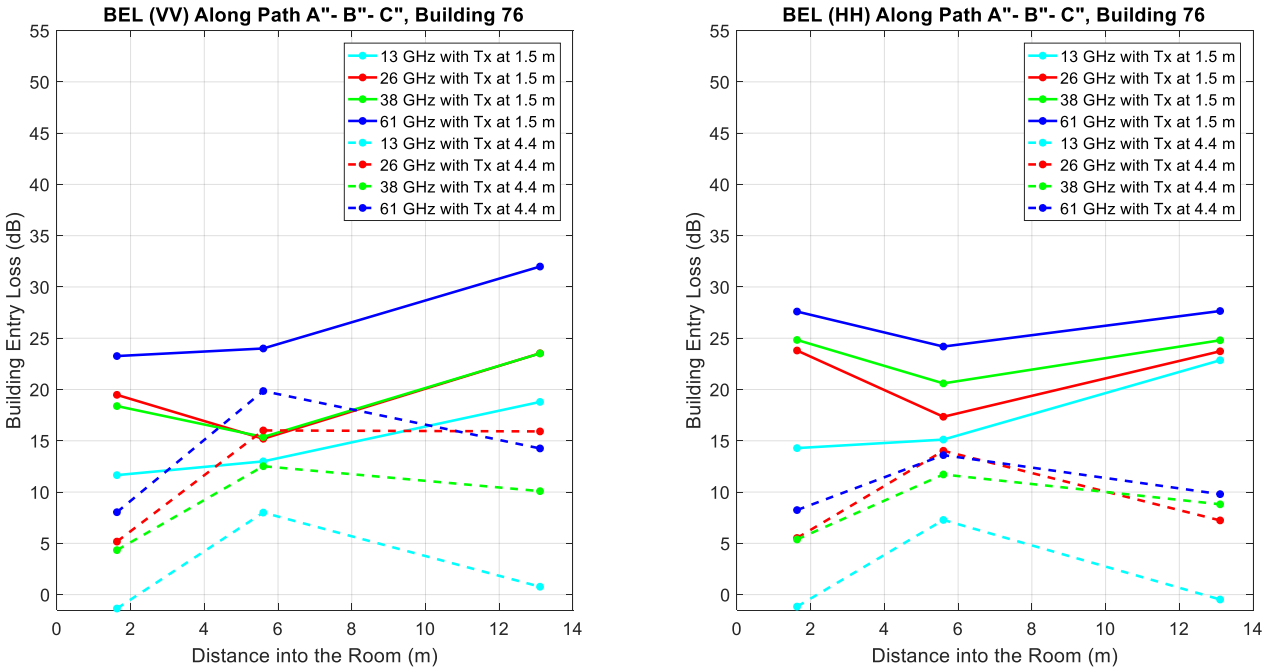

Several observations can be made by careful inspection of Figs 133-135:

- With a few exceptions at locations B, B', and B" (hallway), these building entry losses increase monotonically with frequency, much like losses through the various materials found along the radio path generally do. Diffraction losses through the window – another key propagation mechanism responsible for BEL [1] - do not come into play between 13 and 61 GHz, since full first Fresnel zone clearance is afforded through the windows;
- Building material loss measurements at CRC (described in § 6) confirmed that the acoustic tiles used as a low floating ceiling (as seen in Fig. 130) are very much transparent to microwaves and millimetre waves (see Fig. 143), unlike the corrugated *metallic* ceiling higher up, at 3.6 m. These construction details likely explain this drop in BEL at B, B' or B" when the transmitter is at 1.5 m AGL compared to locations A, A', or A": the link geometry is then such that the receiver can pick up rays which entered the building through the window at a steep angle and were reflected off the metallic ceiling, unimpeded by absorption and scattering due to cubicle partitions and furniture. These rays cannot reach the receiver at location A due to shadowing by the wall section under the window sill;
- Increasing the transmit antenna height to 4.4 m (dotted curves in Fig. 135) generally causes BEL to decrease; the impact of transmitter height on BEL is stronger in horizontal polarization than in vertical polarization. The slightly negative BEL values measured at 13 GHz at 4.4 m (dotted cyan curves in Fig. 135) are possibly due to constructive interference among multipath signals;
- The metal-covered concrete pillar (Figs 128 and 130) is completely opaque, but not wide enough (only 57 cm) to act as a perfect screen; indeed, the horns illuminate sizable areas of the windows on either side of it, especially across the lower frequency bands for which antenna beamwidths are larger. Therefore, shadowing due to the pillar explains the fact that BEL at location A (Fig. 128), i.e. through the middle pillar, but close to the window, are

approximately 8.5 to 11 dB higher in VV (and 8.5 to 13 dB in HH) than at location A'. Edge-diffraction from the sides of the pillar is one possible propagation mechanism: edge-diffracted rays are indeed visible inside the room at 38 and 61 GHz for both polarization and at 26 GHz in VV. Figure 136 shows such rays entering Building 76 at 61 GHz in HH, the strongest being at AoA = −80° and EoA = 10°, another one entering at AoA = −100° and EoA = 20°, etc.

FIGURE 136

Edge-diffracted rays entering the building around the middle pillar at 61 GHz in HH, at location A (Fig. 128)

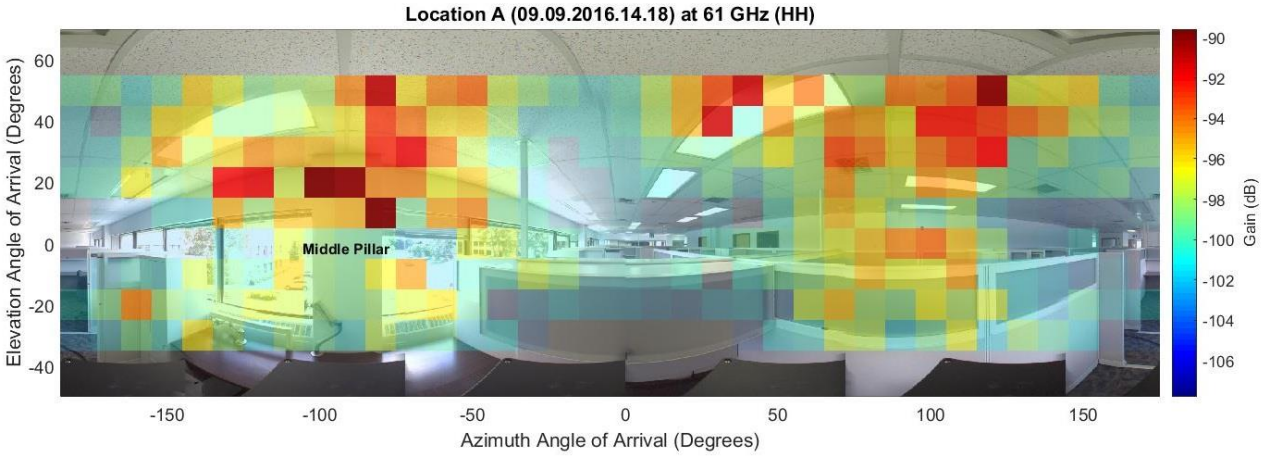

Modelling of BEL is discussed next. Figure 137 shows a scatter plot of the various BEL data collected with the transmit antenna at 1.5 m against distance in the room from the illuminated window. The four solid lines represent the median BEL computed for each of the three clusters, located at around 1.8, 5.6, and 13.1 m. Predicted median BEL values from the 3GPP model *without* the variability term $N(0, \sigma_{dB})$ are also shown in Fig. 137 (dotted lines). The following parameters gave a reasonable fit to the measured median BEL data at 13 GHz, in particular: $\beta = 0$ (old- type building), $\theta = 25°$, $L_{az} = 2$ dB, $\alpha = 1$ dB/m, $d_{room} = 6$ m, $d_{in} = [1.83, 5.63, 13.107]$ in m. These d_{in} values represent measured median distances in Building 76.

The variability of BEL *within the second floor* of Building 76 can be estimated by subtracting these median BEL values (solid lines in Fig. 137) from the measured BEL data (stars in Fig. 137). The resulting variability is approximately lognormal with a mean close to zero, as seen in Figs 138-139; a normal fit to the data in Figs 138-139 yielded the parameters shown in Table 48. The resulting fitted standard deviations of the distribution of BEL (often called "location variability" [2]) at these four frequencies were plotted in Fig. 140: this parameter can be adequately modelled by a linear regression with the logarithm of frequency: $\sigma_{LBEL} = 3.2 + 2.2 \log_{10}(f_{GHz})$, as can readily be seen in Fig. 140. Such a regression makes more physical sense than the linear relationship with frequency used in the 3GPP model, i.e.: $\sigma_{dB} = 4 + k_\sigma f_{GHz}$.

FIGURE 137

BEL data (stars) collected with the transmit antenna at 1.5 m and computed median BEL (solid lines). Predicted median BEL (3GPP model) are also presented (dotted lines) at 13, 26, 38 and 61 GHz

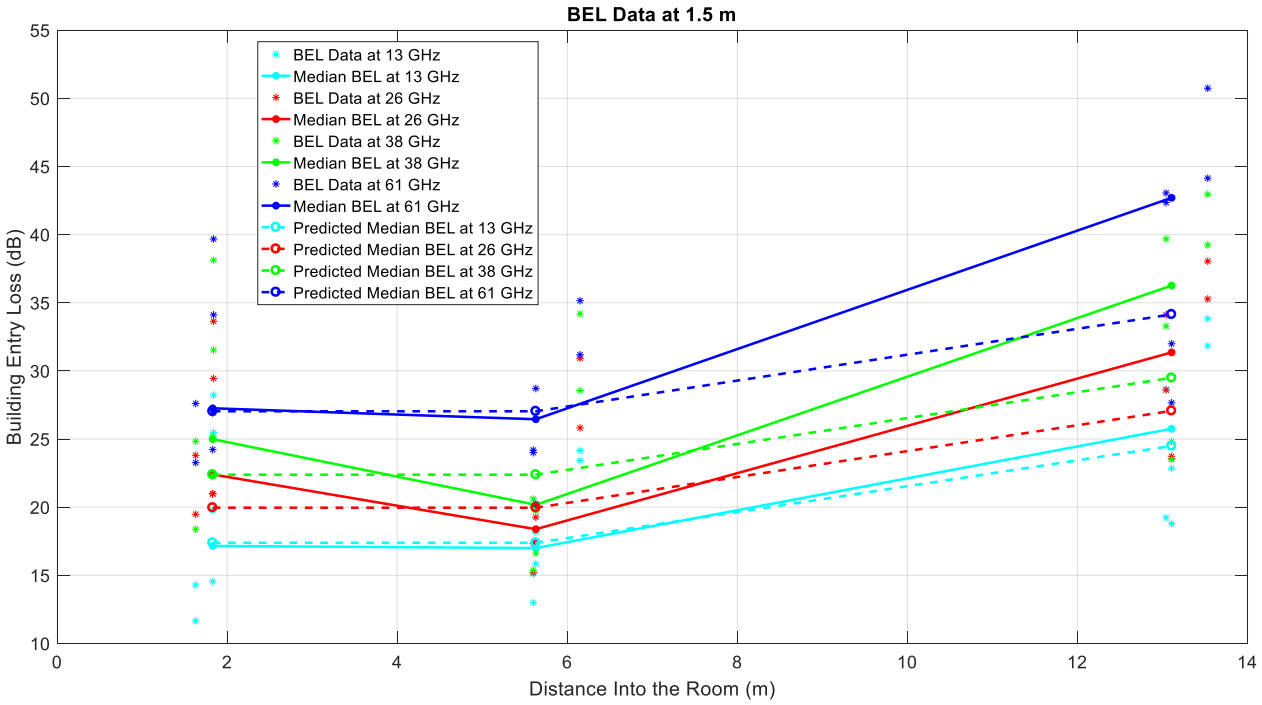

TABLE 48

Mean and standard deviation of the fitted lognormal distribution to the shadowing data shown in Figs 138-139

Frequency (GHz)	Modelled Mean μ_{LBEL} (dB)	Modelled Standard Deviation σ_{LBEL} (dB)
13	1.08	5.68
26	1.38	5.82
38	0.57	7.40
61	0.040	6.81

FIGURE 138

Variability of the BEL data shown in Figure 137 at 138 and 26 GHz, plotted on a Gaussian scale. These distributions are approximately Gaussian, although slightly skewed to the right

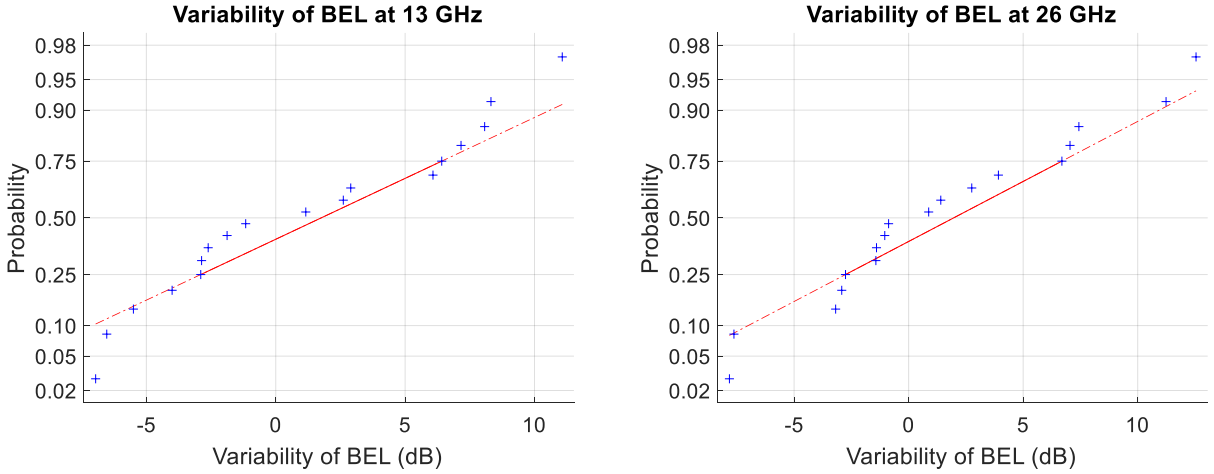

FIGURE 139

Variability of the BEL data in Figure 137 at 163 and 61 GHz, plotted on a Gaussian scale. These distributions are approximately Gaussian

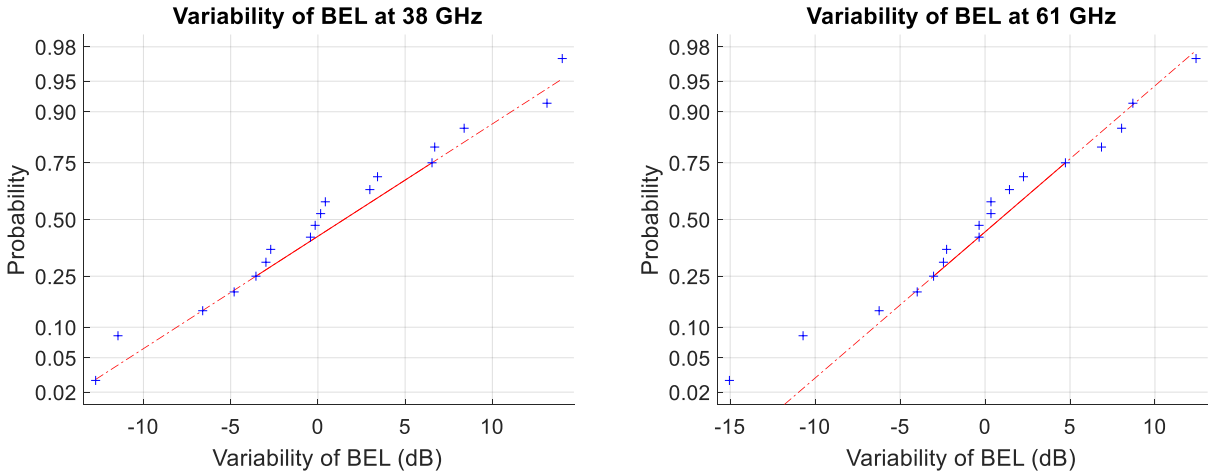

FIGURE 140

Modelling of the location variability of the BEL data at 1.5 m shown in Figure 137

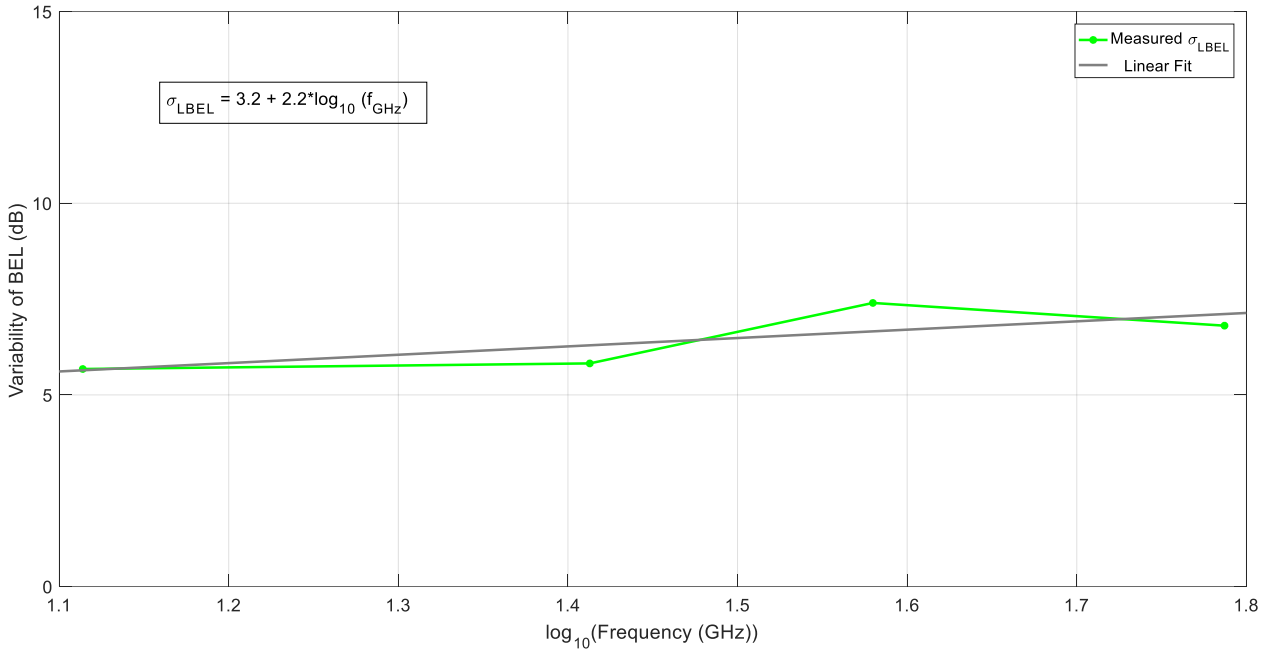

19.6 Description of building material loss measurements in the anechoic chamber

Building material loss measurements clearly play an important role in the modelling of BEL. For this purpose, the free-space method is the method of choice to estimate the transmission coefficient of each building material in both vertical and horizontal polarization.

The CRC channel sounder was deployed in an anechoic chamber, however. The transmit and receive antennas were positioned on opposite sides of a rotating orbit fitted with a frame designed and built to support a sample of building material under test, as shown in Fig. 141. The distance between each set of antennas and the material under test (1 m) satisfies the far field condition and ensures that less than 25% of the area of the material is illuminated in the higher frequency bands.

FIGURE 141

The CRC channel sounder deployed in the anechoic chamber. The wooden tripod is 1.5 m AGL. The material under test is a complete wall section (1.22 m x 1.22 m) held in place with a supporting frame made of PVC, which can also be filled with insulation or wood (see Table 48). The case of normal incidence (θ = 0°) is shown

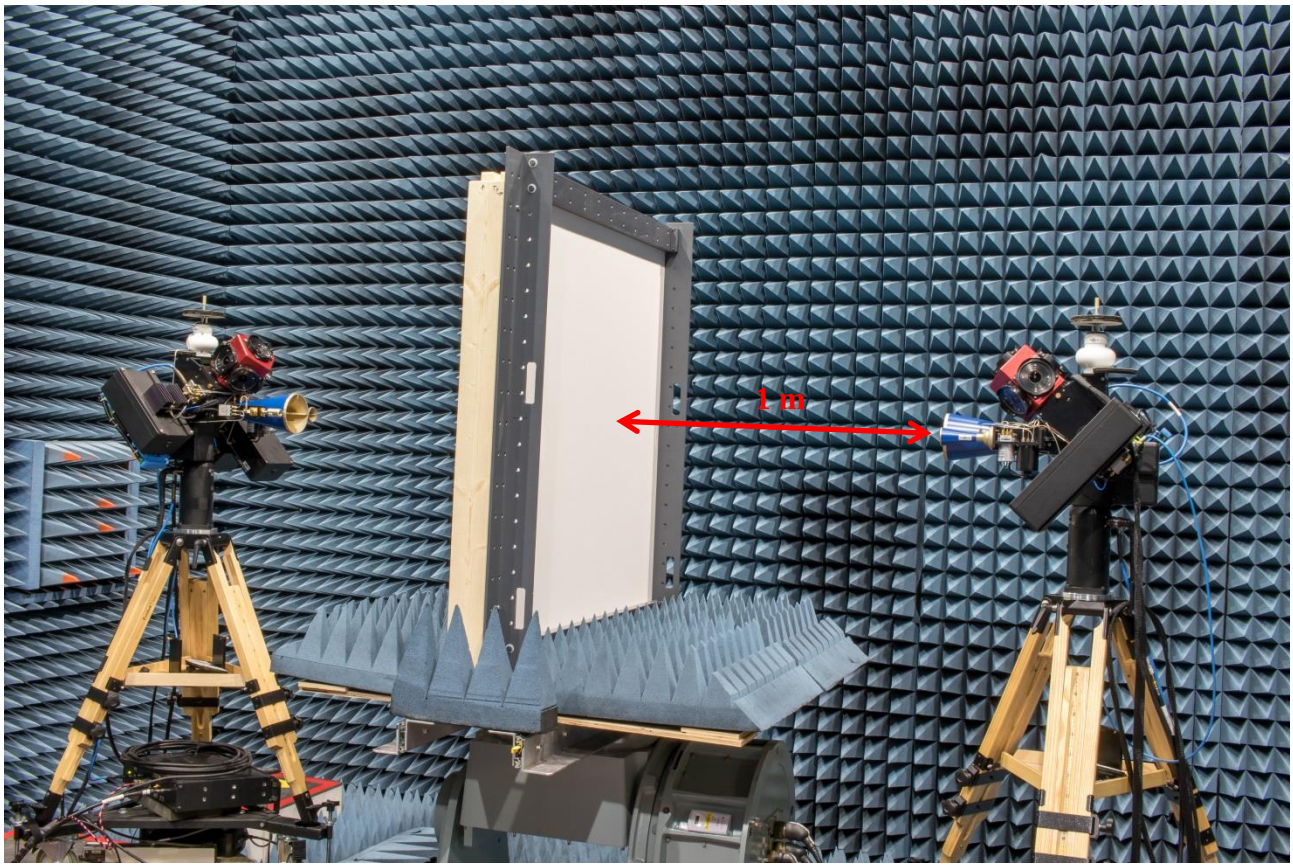

For each of material sample, estimates of the transmission coefficient $L_t(\theta)$ were obtained across the seven frequency bands by measuring the complex channel impulse responses in the time domain with the building material sample, immediately followed by a calibration measurement with the frame empty, thus creating an unobstructed propagation path. The basic idea is to use the calibration measurements in order to isolate the effect of the material sample itself in the absence of extraneous variables such as the distance between antennas or slight variations in the characteristics of the measurement system over time. The transmission coefficient $L_t(\theta)$ is estimated by computing the ratio in dB of the peak amplitude of the impulse response with the material under test to the peak amplitude of the impulse response with the frame empty. The measurement scheme involved four steps for each angular position: first, a reference phase measurement in vertical polarization was conducted with the transmit and receive antennas aiming at a large mirror in the left end of the chamber, far away from the test rig; second, the building material (or empty frame) was illuminated with vertically-polarized waves; third, the building material (or empty frame) was illuminated again, this time with horizontally-polarized signals; the cycle ended with another reference phase measurement. Small variations in the channel sounder system gain over time (tenths of dB) were compensated for by using these reference measurement data. Phase correction was also applied to the data collected across the three highest bands using these reference measurements, but only with limited success.

The dependence of $L_t(\theta)$ on incidence angle was tested for all materials by horizontally turning the sample secured in the frame away from perpendicular in steps of 10°, while leaving the antennas in the exact same location and orientation. It was found that the incidence angle θ could not be increased beyond 70 or 80° without parts of the frame other than the sample itself obstructing the direct

propagation path. The elevation angle at both ends of the channel sounder was set to 0° (see Fig. 141) in all cases.

19.7 Some key building material loss results suitable for BEL modelling

Some representative results of simple or composite building materials over the full incidence angle range (−80° to 80°) are shown in Figs 142-146. The frequency-selective behaviour of transmission loss through regular two-pane glass is likely caused by multiple internal reflections in the glass.

FIGURE 142

Transmission loss L_t as a function of incidence angle (θ) for regular, double-pane window, similar to the ones found in CRC building 76 (Fig. 126)

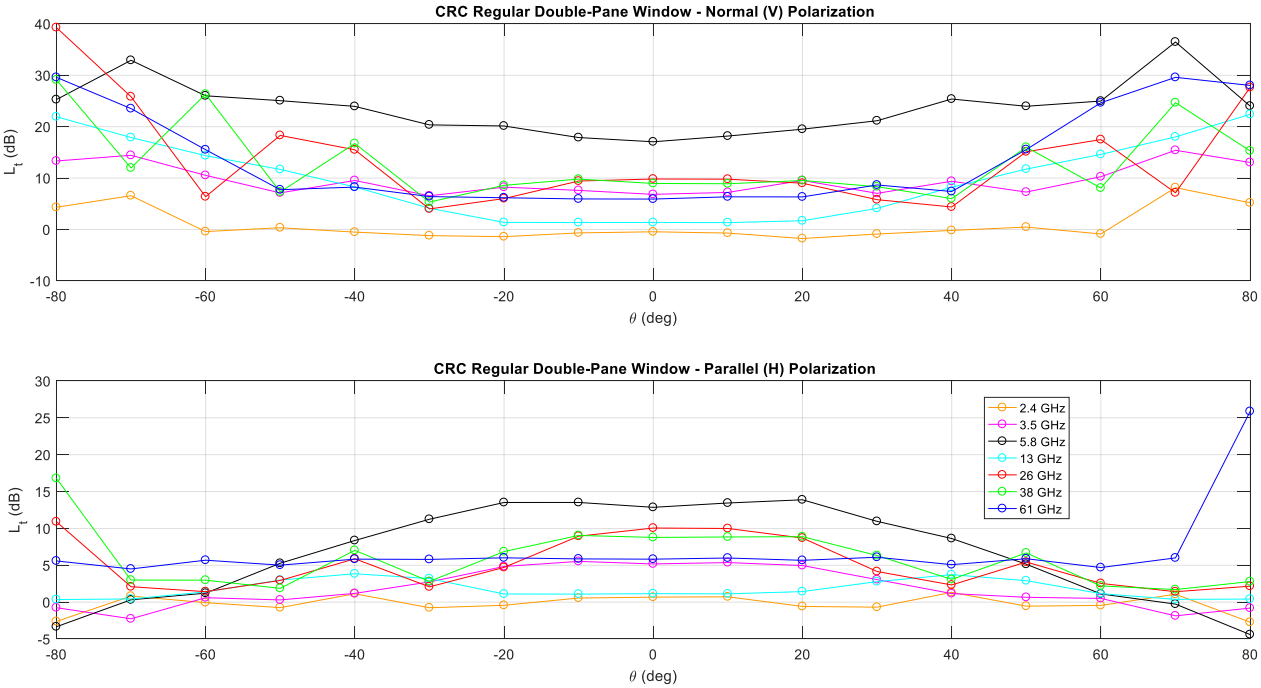

FIGURE 143

Transmission loss L_t as a function of θ for a "ceiling" made of 2½ tiles taken from CRC Building 76 (Fig. 130)

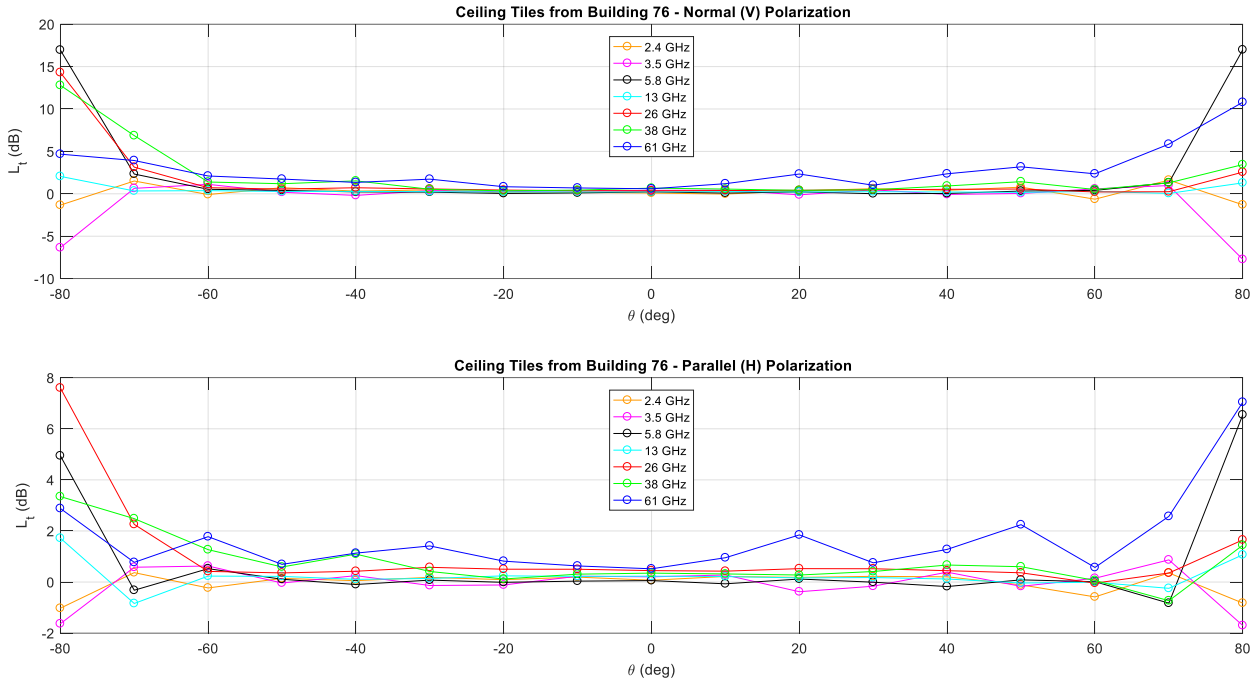

FIGURE 144

Transmission loss L_t as a function of incidence angle (θ) for a cubicle partition taken from Building 76 (Fig. 130)

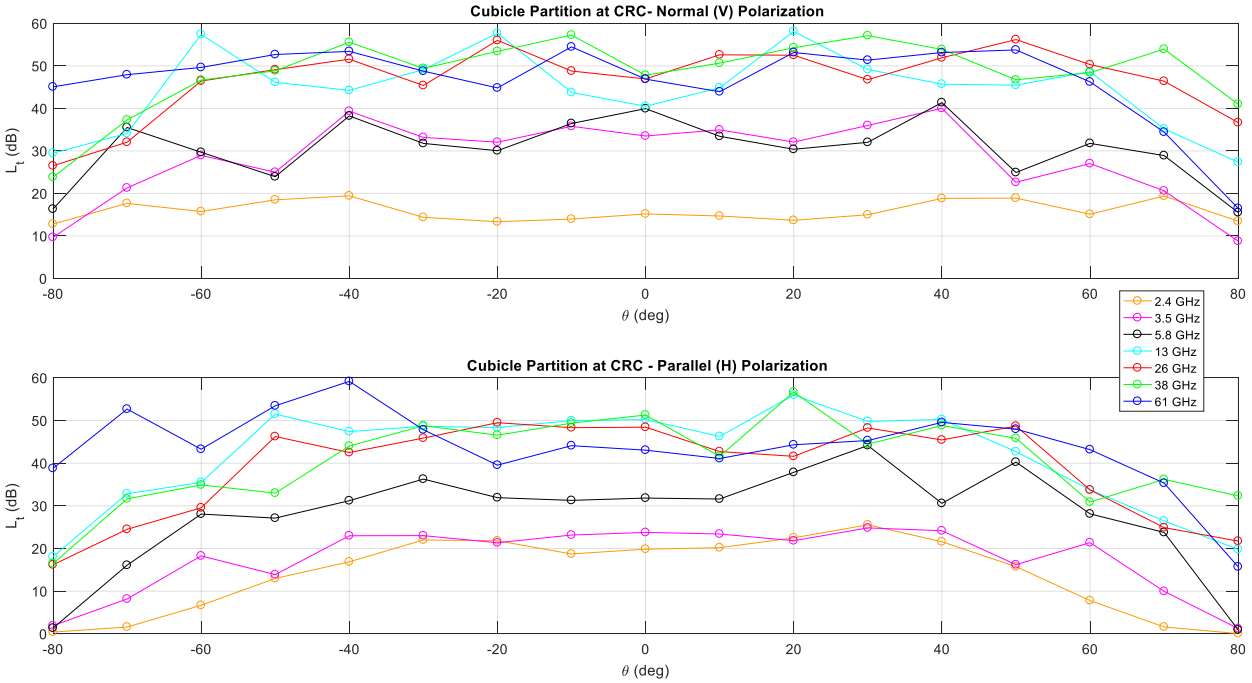

FIGURE 145

Transmission loss L_t as a function of incidence angle (θ) for the hollow wall section (Fig. 141)

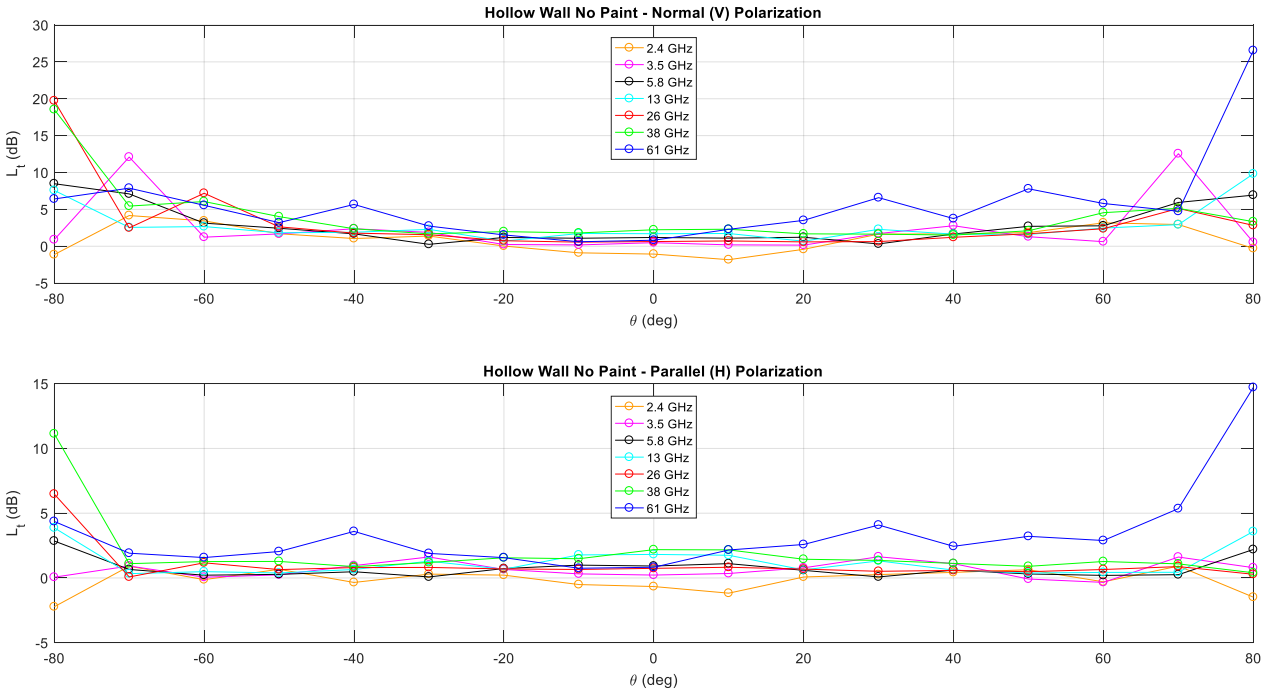

FIGURE 146

Transmission loss L_t as a function of incidence angle (θ) for the wall section (Fig. 141) filled with Roxul insulation

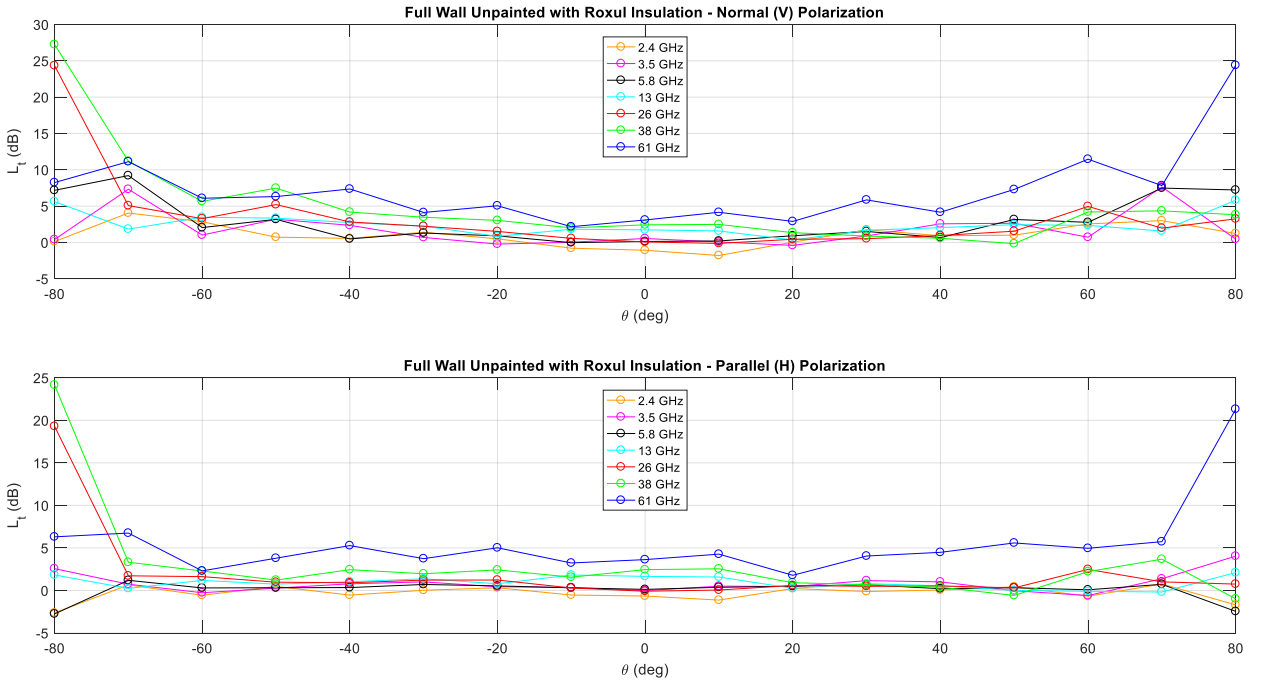

On the one hand, the transmission loss of a “floating ceiling” - as wide as two and a half acoustic tiles deployed side by side but *without* metal frames - is indeed very low across the seven bands (see Fig. 143). Moreover, edge effects are visible at $\theta = \pm 80°$ in Fig. 143. On the other hand, the cubicle partition taken from Building 76 (see Fig. 130 again) has cloth-covered metal sheets on both sides and a cardboard spacer in the middle, which make it very reflective - with up to 59 dB of transmission at 61 GHz (Fig. 144).

Figures 145-146 show that a complete, but hollow wall section (see Fig. 141 again) suffers only modest transmission loss, even when filled with mineral wool insulation.

Table 49, starting on the next page, shows transmission loss for normal incidence across the seven bands for the various building materials; the bulk of these were 1.22 m wide by 1.22 m long. Some small negative L_t (0) values were collected for weakly dissipative materials, such as extruded polysterene rigid insulation in the lower frequency bands (≤ 13 GHz). Note that unlike the ceiling tiles used in Building 76, those used in the refurbished Buildings 2A and 2C are *not* transparent to mm waves, with up to 10 dB losses at 61 GHz (see page 23).

Sizable differences in L_t (0) values between V and H polarization were measured for composite materials, even for this degenerate case ($\theta = 0°$). For example, the same unpainted wall section (pictured in Fig. 141) filled with two layers of wood (called 2”x8” in Canada and the USA) set vertically suffers up to 52 dB of transmission loss in vertical polarization compared to 30 dB in horizontal polarization.

Moreover, inspection of the wall section data listed in Table 49 reveals that the effect of primer or regular paint at millimetric wavelengths is not conclusive. The potential impact of a surface finish on building material losses at millimetric wavelengths came to our attention through reading § 7 of Rec. ITU-R P.1238-7.

TABLE 49

Transmission loss for perpendicular incidence (θ = 0°) for the various building materials tested at CRC. Note that 2”x8” refers to a piece of solid wood (5 cm x 20.3 cm, approximately)

Material	Polarization	Frequency (GHz)						
		2.4	3.5	5.8	13	26	38	61
Sign Board	Vertical	17.290	23.084	32.750	57.738	39.879	45.950	69.292
	Horizontal	17.576	21.857	45.619	55.023	43.746	51.458	69.438
Plywood Mahogany	Vertical	0.263	0.572	0.914	1.156	1.327	1.484	2.701
	Horizontal	0.242	0.346	0.833	1.098	0.672	0.927	1.950
Oriented Strand Board (OSB)	Vertical	0.766	1.209	1.753	1.475	1.638	3.319	5.870
	Horizontal	0.784	0.836	1.763	1.784	1.788	4.314	6.210
Unpainted Hollow Wall Section	Vertical	-1.061	0.483	1.190	1.702	0.637	2.234	0.817
	Horizontal	-0.662	0.223	0.923	1.818	0.743	2.186	0.827
Wall Section, no paint 2”x8” inside wall	Vertical	0.376	1.363	6.270	10.587	23.628	27.985	41.158
	Horizontal	0.113	0.913	2.767	6.556	21.049	14.838	24.078
Interior Gypsum Wallboard	Vertical	0.485	0.910	0.562	0.425	1.033	0.659	0.921
	Horizontal	0.555	0.603	0.281	0.436	1.142	0.299	1.068
Textured Cement Board	Vertical	1.514	2.216	2.852	3.174	4.092	6.269	10.030
	Horizontal	1.309	1.499	2.342	2.966	3.959	5.791	9.789
Cement Board	Vertical	1.391	1.820	1.941	2.724	3.176	4.720	6.297
	Horizontal	1.372	1.406	1.590	2.684	3.426	4.552	6.410
Plywood	Vertical	0.870	1.178	1.501	1.435	3.101	5.259	6.793
	Horizontal	0.888	1.209	1.292	1.410	3.069	5.375	6.853
Standard Spruce Plywood	Vertical	0.422	0.840	0.970	1.250	2.251	3.823	4.883
	Horizontal	0.325	0.651	0.589	1.717	2.238	3.223	5.348
Medium Density Fibreboard (MDF)	Vertical	0.612	1.151	1.058	1.591	1.995	3.253	4.050
	Horizontal	0.593	0.788	0.719	1.659	2.081	2.896	4.163
Chip Board With Wood Grain Melamine	Vertical	0.781	0.904	1.136	2.532	3.240	5.522	7.202
	Horizontal	0.943	0.982	1.008	2.463	3.339	5.231	8.241
Chip Board With White Melamine	Vertical	0.854	1.099	1.207	2.350	3.002	5.102	8.580
	Horizontal	0.893	0.793	0.912	2.304	3.002	4.891	7.856
Corrugated Plastic	Vertical	0.064	0.083	0.012	0.025	0.058	0.574	-0.077
	Horizontal	0.033	-0.005	-0.031	0.036	0.072	0.340	0.185
Extruded Polysterene Rigid Insulation	Vertical	0.012	-0.103	-0.026	-0.004	0.032	0.062	0.075
	Horizontal	0.060	-0.128	0.008	-0.002	0.070	0.076	0.125
Full Wall Unpainted with Mineral Wool Insulation	Vertical	-1.075	0.541	0.133	1.730	0.069	2.425	3.094
	Horizontal	-0.656	-0.015	0.129	1.659	-0.089	2.451	3.629
Full Wall Unpainted Two Layers of 2”x8”	Vertical	2.803	4.006	9.927	13.675	22.493	37.480	52.499
	Horizontal	1.232	2.478	6.977	8.048	12.498	19.922	30.258
Aluminium Sheet	Vertical	22.397	24.775	34.117	56.274	41.795	46.724	64.255
	Horizontal	15.892	27.307	39.676	58.231	42.426	46.779	72.197

TABLE 49 (*continued*)

Material	Polarization	Frequency (GHz)						
Two Ceiling Tiles from CRC Buildings 2A and 2C	Vertical	0.194	0.452	0.407	0.812	1.789	4.416	8.369
	Horizontal	0.261	0.421	0.176	0.957	1.931	4.685	10.328
2 ½ Ceiling Tiles from CRC Building 76	Vertical	0.089	0.404	0.231	0.230	0.358	0.672	0.590
	Horizontal	0.071	0.204	0.056	0.229	0.447	0.349	0.518
Cubicle Partition at CRC (Bottom Part)	Vertical	15.179	33.506	39.945	40.514	46.931	47.802	46.881
	Horizontal	19.843	23.766	31.816	50.212	48.423	51.276	43.041
Hollow Wall with a Coat of Primer Each Side	Vertical	-1.232	0.313	1.120	1.750	0.615	2.371	0.833
	Horizontal	-0.748	0.281	0.936	1.840	0.771	2.292	0.887
Wall with a Coat of Primer on Each Side Plus 2"x8" Side by Side Laid Vertically Inside	Vertical	-0.057	0.713	4.477	6.863	16.770	33.379	25.634
	Horizontal	-0.193	0.386	3.181	4.398	14.236	19.774	15.789
Wall with a Coat of Primer on Each Side with Two Rows of 2"x8" Side by Side	Vertical	2.642	3.275	9.012	12.595	30.483	38.321	53.844
	Horizontal	1.093	2.244	6.051	6.107	17.924	26.049	34.065
Wall with a Coat of Primer on Each Side with Mineral Wool Insulation	Vertical	-0.996	0.551	0.021	1.444	0.575	2.217	1.315
	Horizontal	-0.580	0.150	-0.079	1.453	0.562	1.546	1.358
Acrylic Panel From Cubicle Door Panel	Vertical	0.080	0.206	0.410	0.863	0.404	0.293	0.333
	Horizontal	0.146	0.170	0.349	0.848	0.410	0.224	0.363
Tempered Glass Panel	Vertical	1.916	4.510	3.275	3.194	2.937	2.091	4.530
	Horizontal	1.394	3.337	3.571	3.187	2.975	1.807	4.457
CRC Double-pane Window	Vertical	-0.450	6.829	17.059	1.367	9.818	8.951	5.916
	Horizontal	0.676	5.184	12.862	1.150	10.052	8.779	5.828
Empty Wall with a Coat of Primer and a Coat of Paint on Each Side	Vertical	-1.055	0.236	1.153	1.617	0.789	2.117	2.437
	Horizontal	-0.741	0.193	0.902	1.755	0.923	1.660	1.922
Wall with a Coat of Primer and a Coat of Paint Plus One Layer of 2"x8" Inside the Wall Laid Vertically	Vertical	0.050	0.787	4.359	6.508	16.045	22.820	26.333
	Horizontal	-0.243	0.445	2.964	3.995	15.791	14.450	17.620
Wall with a Coat of Primer and a Coat of Paint Plus Two Staggered Layers of 2"x8" Inside Laid Vertically	Vertical	2.479	3.001	8.876	12.380	25.740	38.361	47.687
	Horizontal	0.933	2.137	6.059	6.205	16.374	26.129	33.634

19.8 References

[1] S. Stavrou, and S.R. Saunders, "Factors influencing outdoor to indoor radio propagation," Proc. IEE 12th Int. Conf. on Antennas and Propagation (ICAP 2003), Exeter, U.K., March-April 2003, pp. 581-585.

[2] L. Barclay, *Propagation of Radiowaves*, 2nd edition. London, UK, the Institution of Electrical Engineers, 2003, Chap. 11.

20 BEL measurements at 3, 10, 17 and 60 GHz frequencies from Orange

20.1 Measurement campaign

This section describes the scenarios considered, presents the setup parameters and the procedures employed to perform the measurements.

A. Scenario description

The measurement scenario, displayed in Fig. 147 (which also displays the transmitting (TX) module and the TX antennas), describes the O2I propagation scenario where the TX antenna is located outside and mounted on top of the white van (2.5 m above ground level). The receiver (RX) was located inside the building (Orange Labs premises in Belfort, France) marked out by the double-ended orange arrow at different location points where the measurement data were collected. The RX antenna height was kept at mobile user level (1.5 m). The distance between the TX and the exterior walls of the building was around 10 m.

FIGURE 147

a) O2I Scenario; b) TX module; c) Omnidirectional antenna at 3 GHz; d) 90° HPBW antenna at 17 GHz; e) 50° HPBW antenna at 60 GHz

Figue 148 shows the building layout. Each number *i* (*i = 1…38*) corresponds with an RX position. Different RX locations were considered during the measurement. These included large offices (LO1, LO2), corridors (Co), a break-room (BR) and a residential flat (Fl).

FIGURE 148

Building Layout. a) Co; b) and c) Fl; d) BR; e) LO1or LO2

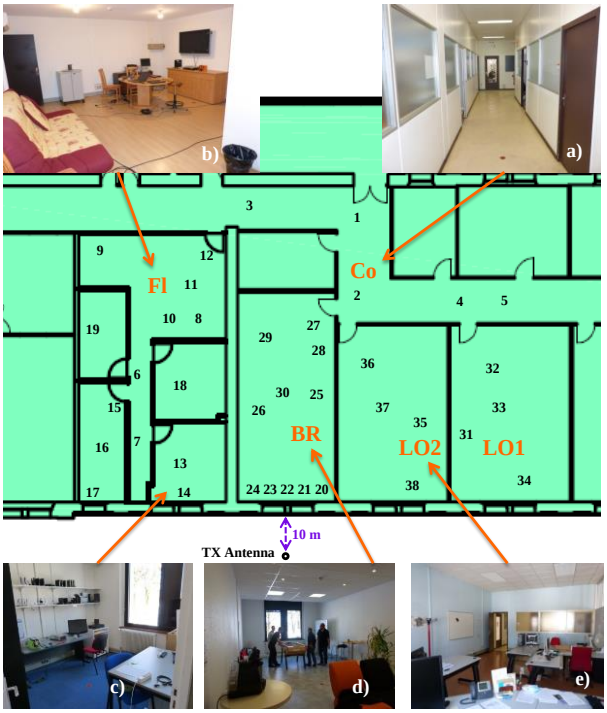

B. Setup and procedure

The measurement campaign was conducted using a wideband channel sounding system [5]. The distance between the TX and the RX units was a few meters (10 to 25 m). An arbitrary waveform generator (AWG) produced successive 8192-length wideband sequences at 1 Gbps-rate with a 125 MHz channel bandwidth. The RX measurement equipment is shown in Fig. 149.

FIGURE 149

RX Equipment. a) 3, 10 and 17 GHz Omnidirectional antennas; b) 90° HPBW antenna at 17 GHz; c) 20° and 90° HPBW antennas at 60 GHz

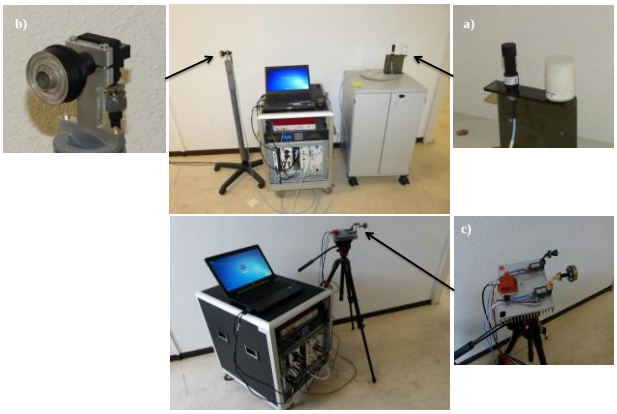

The measurement data were collected in three distinctive setups depending on the RX antenna radiation patterns (see Table 50). As path-loss increases with frequency, RX antennas with narrower beams but larger gains were used at higher frequencies. Therefore, ***"Setup 1 (S1)"*** used omnidirectional (Omni.) antennas at 3, 10 and 17 GHz; ***"Setup 2 (S2)"*** used directional antennas with 90° HPBW at 17 and 60 GHz; "***Setup 3 (S3)***" used highly-directional antennas with 20° HPBW at 60 GHz.

TABLE 50

Measurement setup parameters

Setup Parameters	**3 GHz**	**10 GHz**	**17 GHz**	**60 GHz**
Frequency bands [GHz]	3.6-3.725	10.5-10.625	17.3-17.425	59.875-60.125
Bandwidth	125 MHz			
TX Power [dBm]	from 20 dBm (60 GHz) to 30 dBm (3 GHz)			
RX Antenna Gain [dBi] HPBW [°]	***S1***: 1 dBi Omni.	***S1***: 0dBi Omni.	***S1***: 0 dBi Omni. ***S2***: 7 dBi 90°	***S2***: 6 dBi 90° ***S3***: 20 dBi 20°
TX Antenna Gain [dBi] HPBW [°]	1 dBi Omni.	0 dBi Omni.	7 dBi 90°	10 dBi 50°
Polarization	Vertical			

For ***"S1"***, the omnidirectional RX antenna was mounted on a rotating arm describing a circular trajectory during the measurement. The radius of the trajectory was 2λ, 4λ and 6λ at 3, 10 and 17 GHz respectively. λ is the wavelength.

For ***"S2"***, the 90° HPBW RX antenna was pointed towards 4 different directions with 90° (antenna HPBW) angular step partitioning the space into 4 sectors. In each sector, the antenna remained static while the data were collected.

For ***"S3"***, the 20° HPBW RX antenna was mounted on a panoramic tripod head, manually moved by the operator, describing a 3-D trajectory during the measurement. The azimuth and elevation angles were recorded by an inertial unit. A 3-D "cloud" of channel impulse responses (CIRs) with a non-regular step in the azimuth and elevation dimension was collected. The gap between two consecutive azimuth/elevation points was about 2 to 3°.

20.2 Data processing

In this section, we describe the data processing and define channel metrics such as the building penetration losses L_{O2I} and the channel delay spread *DS*, assuming omnidirectional RX antennas for each setup. The TX and RX antenna maximum gains are subtracted from all measured CIRs.

For ***"S1"***, let $h_n(\tau)$ be the n^{th} CIR recorded during the measurement, N the total number of CIRs and τ the relative delay. N is approximately 400 to 500. The omnidirectional *PDP* is the average power associated with each delay (25).

$$PDP(\tau) = \frac{1}{N}\sum_{n=1}^{N}|h_n(\tau)|^2 \tag{25}$$

For ***"S2"*** and ***"S3"*** the omnidirectional *PDPs* need to be synthesized from the measurements performed using directional RX antennas. The synthesizing procedure presented in [6] and described below is the approach adopted in this paper. In this approach, CIRs are first measured at different angular orientations with a step equal to the RX antenna HPBW. The omnidirectional *PDP* is obtained by summing the received powers from all pointing angles since an angular step equal to the antenna HPBW ensures that the gain of the synthesized omnidirectional antenna is the directional antenna maximum gain.

Therefore, for ***"S2"***, let us note $h_k(\tau)$ the CIR measured in the k^{th} sector and K the total number of sectors ($K=4$). The omnidirectional *PDP*, given in (26), is obtained by summing the received powers from all K sectors.

$$PDP(\tau) = \sum_{k=1}^{K} |h_k(\tau)|^2 \tag{26}$$

For ***"S3"***, a regularly spaced $P \times Q$ grid of CIRs, with a 20° step in the azimuth and elevation domain, is synthesized from the "cloud". P and Q are the number of azimuth and elevation pointing angles respectively, where $P=18$ and $Q=6$ correspond with an azimuth range from –180 to 180° and an elevation range from −50 to 50° respectively. For a specific azimuth-elevation couple indexed by (p, q), $h_{p,q}(\tau)$ is defined. The CIR in the "cloud", whose angular orientation is the closest to the orientation indexed by (p, q), is assigned to $h_{p,q}(\tau)$. The omnidirectional *PDP*, given in (27), is obtained by summing the received powers from all $P \times Q$ pointing angles.

$$PDP(\tau) = \sum_{q=1}^{Q} \sum_{p=1}^{P} |h_{p,q}(\tau)|^2 \tag{27}$$

The *PDP* resulting from this synthesizing procedure is identical to the *PDP* directly obtained with omnidirectional RX antennas. Fig. 150 and Fig. 151 are typical examples showing this agreement between the omnidirectional *PDPs* at 17 GHz and 60 GHz respectively.

FIGURE 150

***PDPs* ("*S1*" and "*S2*") at 17 GHz at location 26**

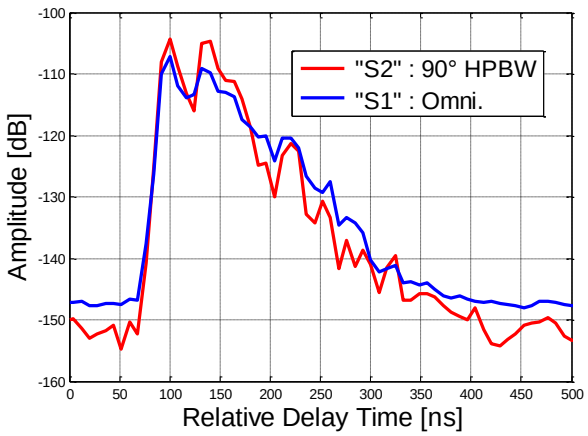

FIGURE 151

***PDPs* (*"S2"* and *"S3"*) at 60 GHz at location 31**

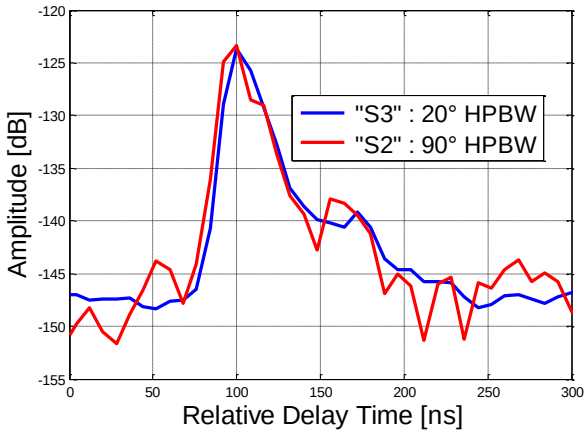

With the *PDPs* computed for each setup, the channel average attenuation A_{av}, expressed in dB, is defined in (28).

$$A_{av} = -10 \cdot log_{10}\left(\int_{\tau} PDP(\tau) \cdot d\tau \right) \tag{28}$$

We define in (29) the building penetration losses L_{O2I}, expressed in dB, as an additional attenuation compared to the theoretical free-space path-loss (FSPL) L_{FS}. L_{O2I} expresses the attenuation due to the penetration through external walls/windows and also the losses caused by the elements present in the indoor propagation environment.

$$\begin{aligned} L_{O2I} &= A_{av} - L_{FS} \\ L_{FS} &= -147.5 + 20 \cdot \log_{10}(f_c) + 20 \cdot \log_{10}(d) \end{aligned} \tag{29}$$

L_{FS} is expressed in dB, f_c the carrier frequency in Hz and d, the distance between TX and RX, in m.

Finally, we quantify in (30) the channel delay spread *DS*.

$$DS = \sqrt{\frac{\int_{\tau} (\tau_{mean} - \tau)^2 \cdot PDP(\tau) \cdot d\tau}{\int_{\tau} PDP(\tau) \cdot d\tau}} \; ; \; \tau_{mean} = \frac{\int_{\tau} \tau \cdot PDP(\tau) \cdot d\tau}{\int_{\tau} PDP(\tau) \cdot d\tau} \tag{30}$$

20.3 Measurement results and analysis

This section presents the penetration losses L_{O2I} and the delay spread *DS* of the propagation channel for the 4 frequency bands and the 38 different RX positions, when the CIR instantaneous dynamic range is at least 20 dB.

A. Penetration losses

The computed L_{O2I} values from the measurement campaign for the different scenarios are summarized in Table 51. *Ri* refers to the RX position *i* represented in Fig. 148.

TABLE 51

Penetration loss values

L_{O2I} [dB]	S1			S2		S3
	3 GHz	10 GHz	17 GHz		60 GHz	
Corridor (Co)						
R1	18	18	18	22	×	28
R2	20	19	22	21	×	×
R3	18	20	21	17	×	×
R4	21	22	23	23	×	×
R5	21	22	21	23	×	×
Average	**20**	**20**	**21**	**21**	**×**	**×**
Flat (Fl)						
R6	27	31	33	31	▫	×
R7	28	32	35	36	▫	×
R8	29	30	33	37	▫	▫
R9	25	29	33	33	▫	▫
R10	28	31	×	34	▫	×
R11	27	26	31	29	▫	×
R12	25	29	32	27	▫	▫
R13	26	29	35	38	▫	37
R14†	27	30	35	36	▫	36
R15	27	31	35	37	▫	×
R16	24	31	37	▫	▫	×
R17†	27	28	33	40	▫	×
R18	29	31	33	38	▫	×
R19	26	31	32	34	▫	▫
Average	**27**	**30**	**34**	**35**	**▫**	**×**
Break room (BR)						
R20‡	17	16	16	12	17	13
R21†	7	4	2	3	4	5
R22‡	12	6	15	10	20	18
R23†	7	5	3	0	5	4
R24‡	20	22	18	20	18	20
R25	5	3	2	▫	4	5
R26	19	18	17	14	23	23
R27	9	4	2	▫	5	4
R28	11	6	7	2	4	6
R29	12	12	8	9	18	18
R30	5	6	0	▫	6	3
Average	**11**	**9**	**8**	**9**	**11**	**11**
Large office 1 (LO1)						
R31	17	21	22	19	22	26
R32	14	19	19	19	18	19
R33	17	20	22	▫	27	22
R34†	8	8	8	17	5	11
Average	**14**	**17**	**18**	**18**	**17**	**20**

L_{O2I} [dB]	S1			S2		S3
	3 GHz	10 GHz	17 GHz	60 GHz		
Large office 2 (LO2)						
R35	20	19	22	▫	×	×
R36	18	20	17	16	21	23
R37	20	24	19	▫	×	×
R38†	23	25	27	32	×	×
Average	**20**	**22**	**21**	**24**	**×**	**×**

† RX behind windows, ‡ RX behind walls, ▫ Not performed, × Low Dynamic Range

Table 51 shows strong variation of L_{O2I} values depending on the room where the RX is located. The most significant results are those from Fl composed of double-layered glass windows with a silver coating and BR whose windows are simply double-layered without a silver coating. These two rooms are separated by a bearing wall and also have similar incidence angle from the TX.

Non-coated glass windows in BR favour radio signal propagation (L_{O2I} around 5 dB). In this room, attenuation behind the windows (R21, R23) is lower than the attenuation when the RX is placed behind the walls (R20, R22 and R24). Also, for the RX positions which are located deeper inside the room (R25 to R30), L_{O2I} values are lower than the values observed just behind the walls. It is thus likely that the radio channel viewed by RX positions from R25 to R30 is dominated by the direct path and/or single-bounce reflections, while at R20, R22 and R24 the propagation may occur through multiple bounces.

Coated glass windows in Fl result however in very high L_{O2I} values (up to 40 dB). In this scenario, particularly at 3, 10 and 17 GHz, RX positions facing the windows exhibit L_{O2I} values similar to the other positions. However at 60 GHz, for the most part, the measured CIRs do not have enough dynamic range despite the use of high gain RX antennas. Therefore, the attenuation was not quantifiable for RX positions deeper inside Fl.

In LO1, L_{O2I} values behind the non-coated glass windows remain relatively low (10 dB), although higher than in BR. This increase could be associated with the different incidence angles between these two rooms. L_{O2I} values recorded in LO2, which is composed with coated glass windows, and Co are relatively high (15 – 30 dB) but overall lower than the values in Fl. The electromagnetic waves propagating into BR certainly pass through the partition walls that separate the latter from LO2 and Co. The transmission through these walls causes additional attenuation which could also explain the scarcity of L_{O2I} values at 60 GHz at these locations, as in Fl. An analysis based on the directions of arrival is ongoing in order to confirm these preliminary physical and geometrical interpretations.

There is hardly any frequency-dependence of L_{O2I} with the non-coated glass windows in BR or LO1 whereas this parameter increases with the frequency in the case of coated glass windows in Fl, especially from 3 to 17 GHz. This is shown in Fig. 152, which summarizes L_{O2I} values for RX positions just behind the building exterior walls and windows. In Co and LO2, the trend is the same as in BR where their main propagation paths most likely come from.

The high L_{O2I} values recorded in Fl have been underlined in the literature [2], [7] as characteristic of energy-efficient glass windows, as opposed to standard glass windows, where L_{O2I} remains low and constant irrespective of the frequency, as observed in BR.

FIGURE 152

Building Entry Losses across the four bands

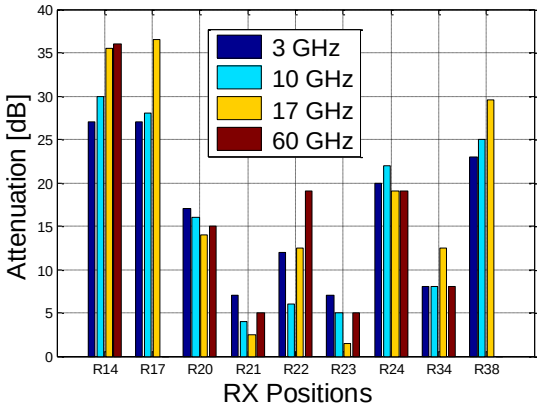

B. Delay spread

Table 52 below shows the *DS* values, computed with a 20 dB (minimum dynamic range) threshold on the *PDPs*.

TABLE 52

Delay spread values

***DS* [ns]**	**S1**			**S2**	**S3**	
	3 GHz	**10 GHz**	**17 GHz**	**60 GHz**		
Corridor (Co)						
Average	19	19	19	18	×	×
Flat (Fl)						
Average	21	19	19	20	▫	×
Break room (BR)						
Average	18	16	20	21	13	13
Large office 1 (LO1)						
Average	13	15	16	16	13	14
Large office 2 (LO2)						
Average	27	27	24	28	×	×

▫ Not performed, × Low Dynamic Range

The *DS* values (< 30 ns) seem weakly correlated with the frequency. Figure 153 provides a typical example of *PDPs* which display similar shapes for the 4 different frequency bands.

FIGURE 153

***PDPs* at 3, 10, 17 and 60 GHz at location 25**

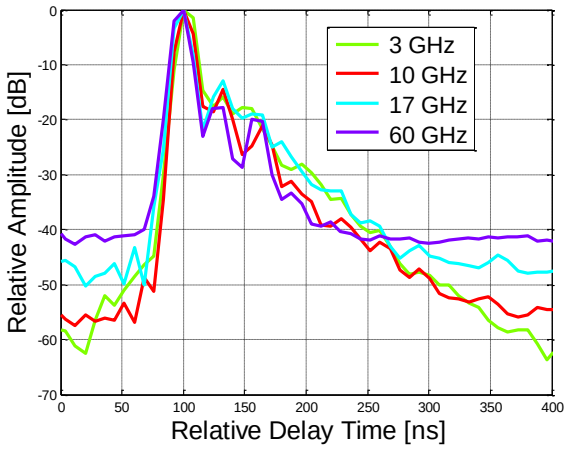

20.4 Conclusion

In this annex, the propagation channel properties at 3, 10, 17 and 60 GHz have been studied. For an O2I scenario, building penetration losses and channel delay spread values have been determined for various RX positions in different rooms. The results reveal a strong variation in signal attenuation (5-40 dB) depending on the window material composition. Two major tendencies have emerged. A relatively low and non-frequency-dependent attenuation (around 5 dB) is observed for non-coated glass windows while a high attenuation (30 dB), increasing with the frequency, is recorded for coated glass windows. The estimated delay spread values are relatively low (below 30 ns for all the measurements) and more or less uniformly distributed across the different frequency bands. Future work will focus on the study of directions of arrival at the mobile station in order to refine some of the conclusions drawn in this paper.

References

[1] R. J. Weiler, M. Peter, W. Keusgen, and M. Wisotzki, “Measuring the Busy Urban 60 GHz Outdoor Access Radio Channel,” IEEE International Conference on Ultra-Wideband (ICUWB), 2014.

[2] I. Rodriguez, H. C. Nguyen, N. T. K. Jorgensen, T. B. Sorensen and P. Mogensen, “Radio Propagation into Modern Buildings: Attenuation Measurements in the Range from 800 MHz to 18 GHz,” IEEE, 2014.

[3] C. Larson, F. Harrysson, B.-E. Olsson and J.-E. Berg, “An Outdoor-to-Indoor Propagation Scenario at 28 GHz,” IEEE European conference on antennas and Propagation (EuCAP), 2014.

[4] P. Okvist, H. Asplund, A. Simonsson, B. Halvarsson, J. Medbo and N. Seifi, “15 GHz Propagation Properties Assessed with 5G Radio access Prototype,” IEEE on Personal , Indoor and Mobile Radio Communications (PIMRC), 2015.

[5] J.-M. Conrat, P. Pajusco, and J. Y. Thiriet, "A Multibands Wideband Propagation Channel Sounder from 2 to 60 GHz," in *Instrumentation and Measurement Technology Conference (IMTC)*, Sorrento, 2006.

[6] S. Sun, G. R. MacCartney, M. K. Samimi, and T. S. Rappaport, “Synthesizing Omnidirectional Antenna Patterns, Received Power and Path Loss from directional Antennas for 5G Millimeter-Wave Communications,” in 2015 IEEE Global Communications Conference (GLOBECOM), Dec. 2015, pp. 3948-3953.

[7] H. Okamoto, K. Kitai and S. Ichitsubo, “outdoor-to-Indoor Propagation Loss Prediction in 800-MHz to 8-GHz Band for an Urban Area,” IEEE Transactions on Vehicular Technology, vol. 58, no. 3, March. 2019.

21 Some zero elevation angle BEL measurement results in China

21.1 Measurement scenarios

Three typical office buildings in China are measured, named as building A, building B and building C, which have different structure and material.

21.1.1 Building A

Building A is with reinforced concrete shear wall and the glass of windows is with one-way transparent glass, which is with a thin metal coating. The thickness of the bearing wall is 35 cm ~ 38 cm. In addition, the building's exterior wall is being equipped with thermal insulation material whose structure is the foam polyethylene sheet and metal reflective layer. The scenes of Building A are shown in Figs 154-156. And Table 53 presents the coordinates of the receiving points and transmitting points.

FIGURE 154

The building A scene of satellite overlooking

FIGURE 155

The transmitting points indoor and the receiving points outdoor on the 4th floor, Building A

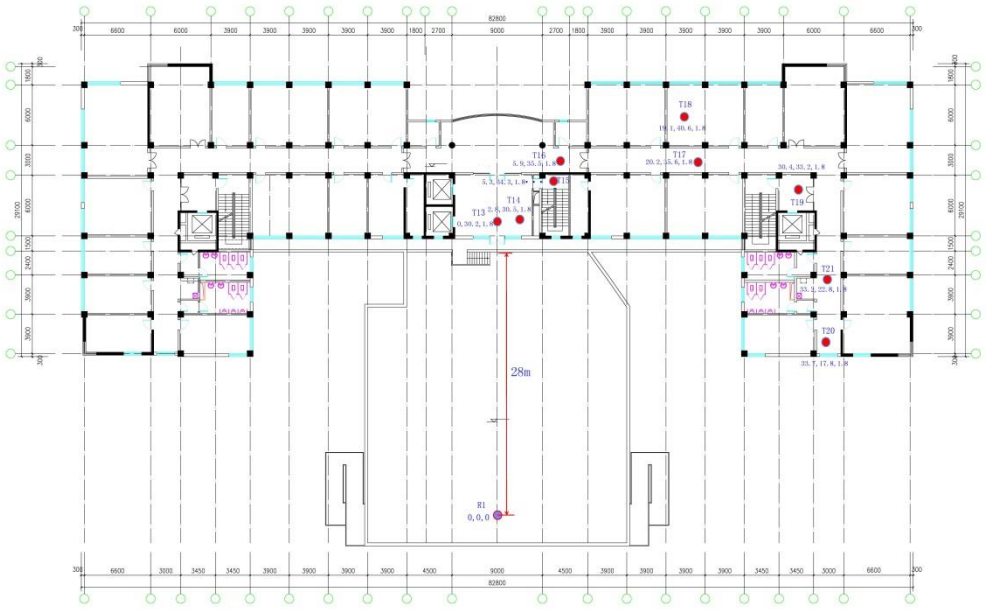

FIGURE 156

The transmitting points indoor on the 5th floor, Building A

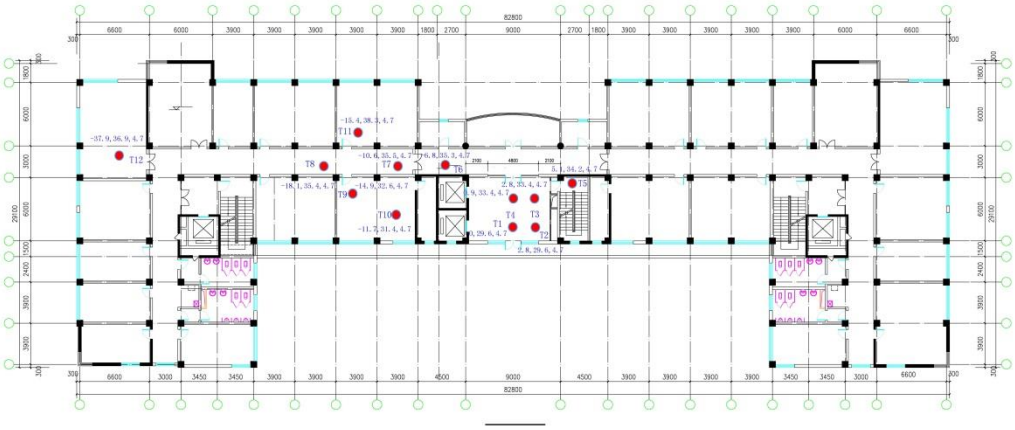

TABLE 53

The coordinates of the receiving points and transmitting points in building A (unit: m)

Points	x	y	z
R2	0	0	0
T1	0	29.6	4.7
T2	2.8	29.6	4.7
T3	2.8	33.4	4.7
T4	0.9	33.4	4.7
T5	5.1	34.2	4.7
T6	-6.8	35.3	4.7
T7	-10.6	35.5	4.7
T8	-18.1	35.4	4.7
T9	-14.9	32.6	4.7
T10	-11.7	31.4	4.7
T11	-15.4	38.3	4.7
T12	-37.9	36.9	4.7
T13	0	30.2	1.8
T14	2.8	30.5	1.8
T15	5.3	34.3	1.8
T16	5.9	35.5	1.8
T17	20.2	35.6	1.8
T18	19.1	40.6	1.8
T19	30.4	33.2	1.8
T20	33.7	17.8	1.8
T21	33.2	22.8	1.8

Some typical measured points' pictures in building A are shown in Figs 157-159.

FIGURE 157

Typical measured point picture in building A

FIGURE 158

Typical measured point picture in building A

FIGURE 159

Typical measured point picture in building A

21.1.2 Building B

Building B is a modern building combined the toughened glass with the reinforced concrete. The toughened glass is laid in the wall which is known as a common toughened glass without a metal coating. Part of exterior wall is equipped with a brown ceramic tile. There is a parking lot outside the building, the length of which is about 35 m. In order to avoid the influence of vehicle movement, the method is:

– The test is taken at the weekend to make sure there are few vehicles and staffs.

– Make sure the receiving antenna be away from the vehicle.

– The height of the receiving antenna is set to 2.3 m to ensure that the connection between the transmitting antenna and the receiving antenna is not blocked by vehicles.

FIGURE 160

The building B scene of satellite overlooking

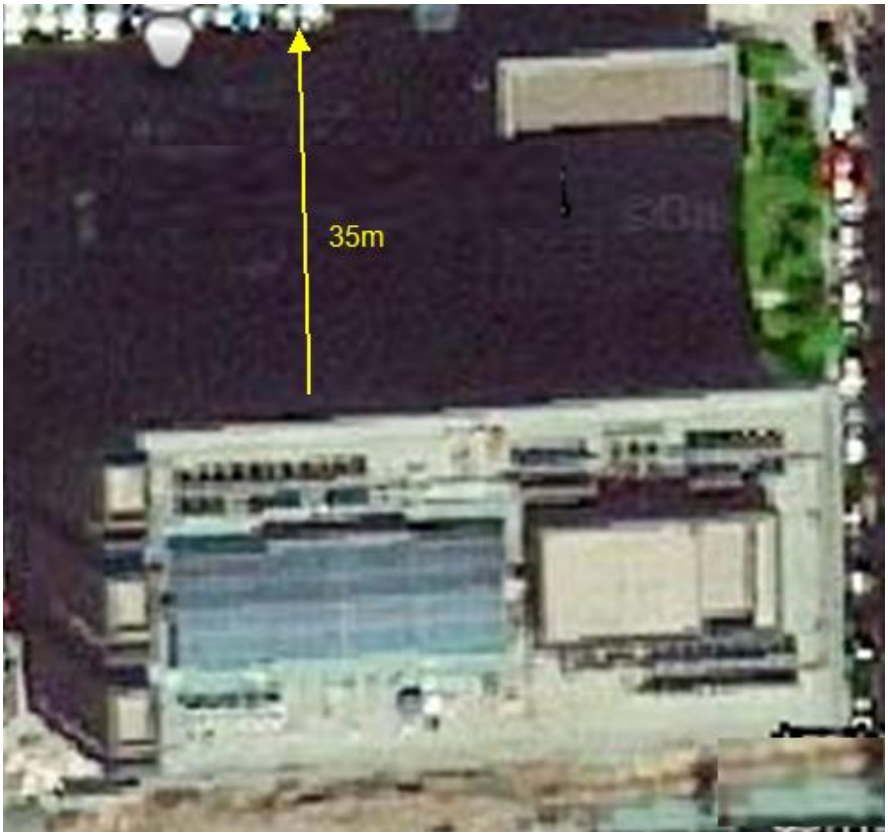

In building B, the positions of Tx and Rx are shown in Figs 161-162. And Table 54 presents the coordinates of the receiving points and transmitting points.

FIGURE 161

The transmitting points indoor on the 2th floor, Building B

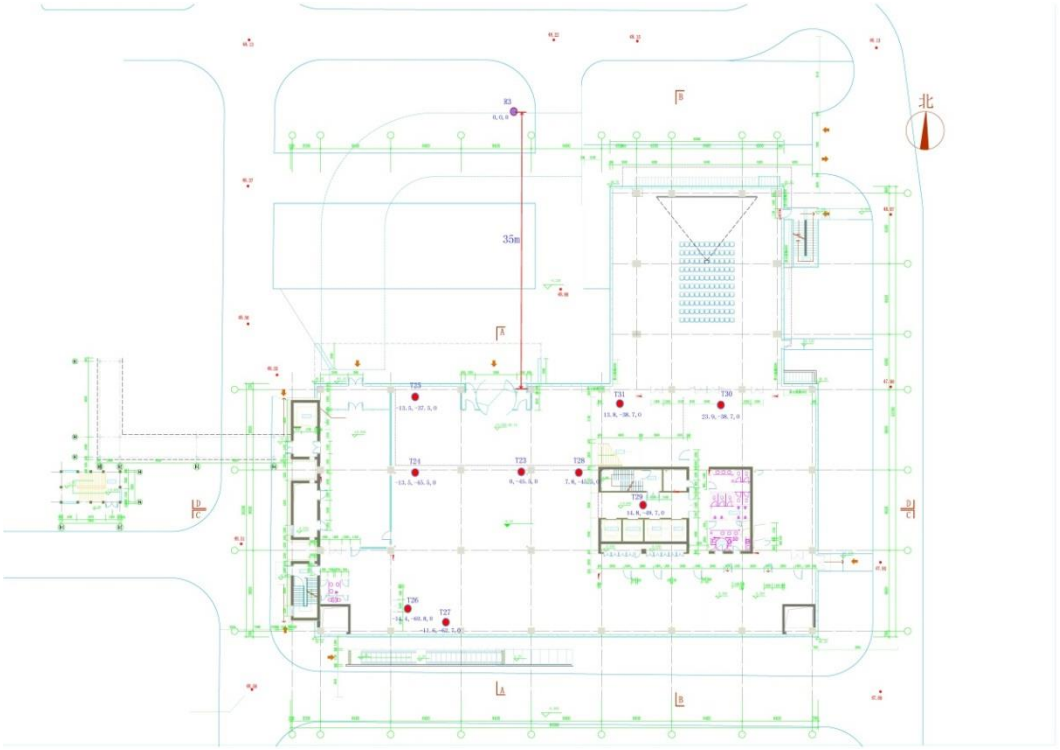

FIGURE 162

The transmitting points indoor on the 3th floor, Building B

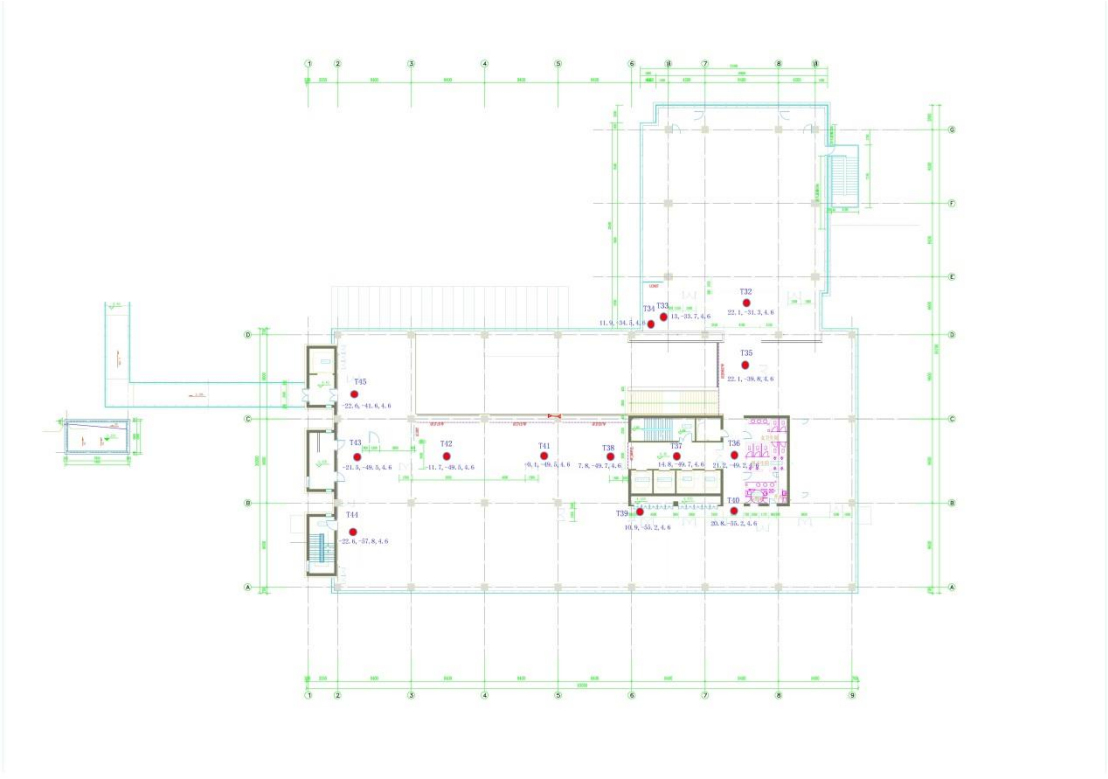

TABLE 54

The coordinates of the receiving points and transmitting points in building B (unit: m)

Points	x	y	z
R3	0.0	0.0	0.0
T23	0.0	-45.5	0.0
T24	-13.5	-45.5	0.0
T25	-13.5	-37.5	0.0
T26	-14.4	-60.8	0.0
T27	-11.6	-62.7	0.0
T28	7.8	-45.5	0.0
T29	14.8	-49.7	0.0
T30	23.9	-38.7	0.0
T31	13.8	-38.7	0.0
T32	22.1	-31.3	4.6
T33	13.0	-34.7	4.6
T34	11.9	-34.5	4.6
T35	22.1	-39.8	4.6
T36	21.2	-49.2	4.6
T37	14.8	-49.7	4.6
T38	7.8	-49.7	4.6
T39	10.9	-55.2	4.6
T40	20.8	-55.2	4.6
T41	-0.1	-49.5	4.6
T42	-11.7	-49.5	4.6
T43	-21.5	-49.5	4.6
T44	-22.6	-57.8	4.6
T45	-22.6	-41.6	4.6
T46	7.1	-35.5	7.6
T47	12.0	-44.1	7.6
T48	11.6	-55.2	7.6
T49	17.9	-55.2	7.6
T50	27.5	-55.3	7.6
T51	20.9	-57.0	7.6
T52	21.2	-49.2	7.6
T53	24.3	-43.6	7.6
T54	14.8	-49.2	7.6

Some typical measured points' pictures in building B are shown in Figs 163-165.

FIGURE 163

Typical measured point picture in building B

FIGURE 164

Typical measured point picture in building B

FIGURE 165

Typical measured point picture in building B

21.1.3 Building C

Building C is an old four-story building with brick wall structure and ordinary glass, as shown in Fig. 166.

FIGURE 166

The building C scene of satellite overlooking

In building C, the positions of Tx and Rx are shown in Fig. 167. And Table 55 presents the coordinates of the receiving points and transmitting points.

FIGURE 167

The transmitting points indoor and the receiving points outdoor on the 2th floor, Building C

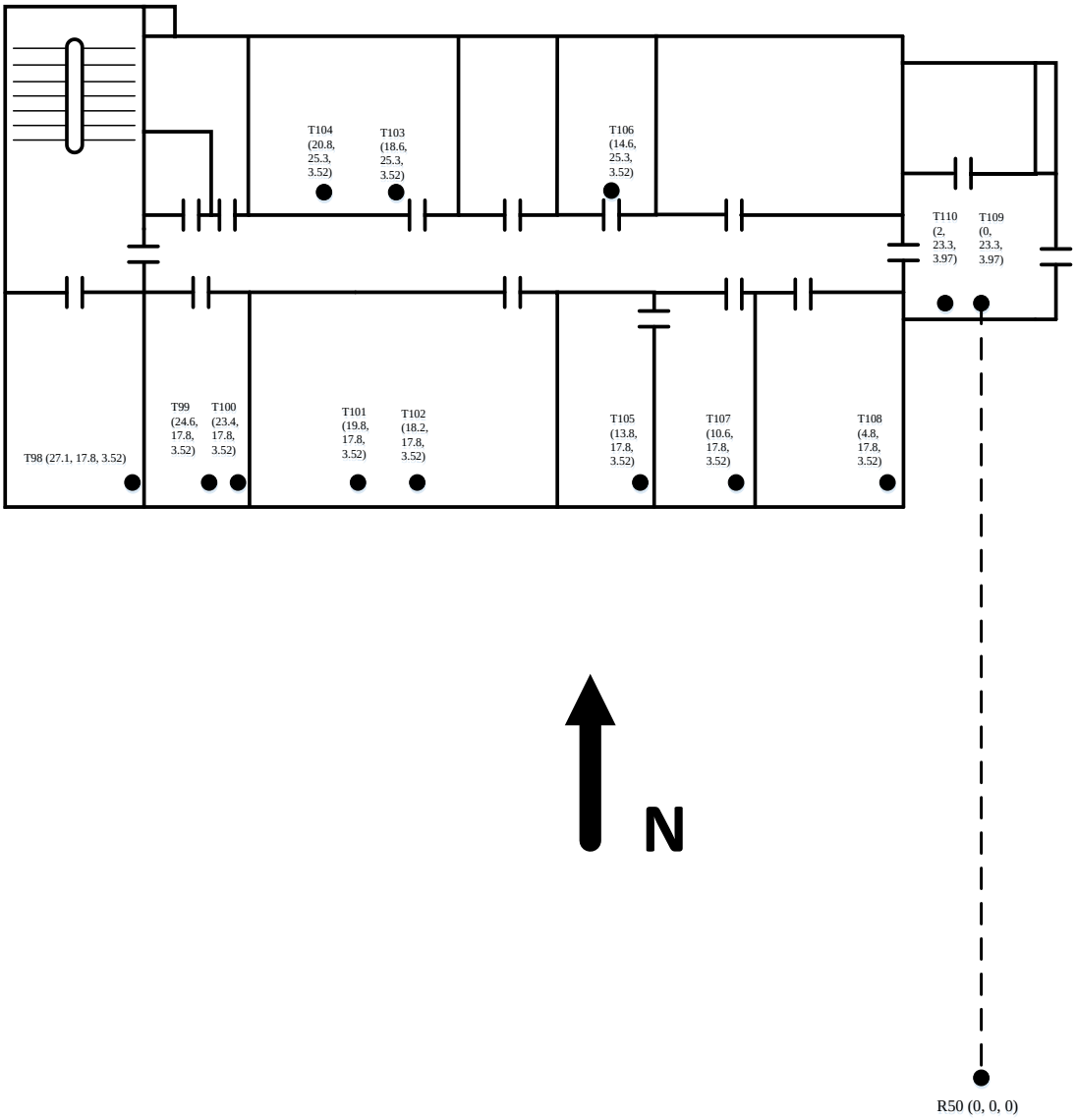

TABLE 55

The coordinates of the receiving points and transmitting points in building C (unit: m)

Points	x	y	z
R50	0	0	0
T90	0	23.29	7.518
T91	9.2	23.29	7.068
T92	16.8	23.29	7.068
T93	28.4	23.69	7.068
T94	9.2	17.79	7.068
T95	10.2	17.79	7.068
T96	11.6	25.3	7.068
T97	10.2	25.3	7.068
T98	27.1	17.8	3.52
T99	24.6	17.8	3.52
T100	23.4	17.8	3.52
T101	19.8	17.8	3.52
T102	18.2	17.8	3.52
T103	18.6	25.3	3.52
T104	20.8	25.3	3.52
T105	13.8	17.8	3.52
T106	14.6	25.3	3.52
T107	10.6	17.8	3.52
T108	4.8	17.8	3.52
T109	0	23.3	3.97
T110	2	23.3	3.97

Some typical measured points' pictures in building A are shown in Figs 168-170.

FIGURE 168

Typical measured point picture in building C

FIGURE 169

Typical measured point picture in building C

FIGURE 170

Typical measured point picture in building C

21.2 Test methodology

In building A, B and C, 11 frequency points are selected in every frequency band during the test.

In building A, 4 frequency bands are selected: 3.5 GHz±100 MHz, 27 GHz±250 MHz, 32 GHz±250 MHz and 39 GHz±250 MHz.

In building B, 4 frequency bands are selected: 3.5 GHz±100 MHz, 28 GHz±250 MHz, 31 GHz±250 MHz and 39 GHz±250 MHz.

In building C, 4 frequency bands are selected: 3.5 GHz±100 MHz, 27 GHz±250 MHz, 32 GHz±250 MHz and 39 GHz±250 MHz.

21.2.1 Measuring system and instrument

The devices of measuring system are shown in Table 56.

TABLE 56

Test instruments and equipment

Equipment	Description
Agilent E8267D signal generator	Frequency Range 9 kHz~40 GHz
Coaxial line	6 dB loss
Agilent E4447 signal analyzer	Test sensitivity>-130 dBm
Omni-directional.	Frequency Range 9 kHz~40 GHz, the gain of which is 2 dBi, linear polarization.
Horn antenna	18 GHz ~ 40 GHz double ridge horn antenna, the gain of which is 10 dBi ~ 17 dBi.
RF power amplifier	The output power in the test is set to 43 dBm ranges 26 GHz to 40 GHz
laser distance measuring instrument	Red laser

We have developed an automatic program in order to remotely control instruments and record test data by LAN. In each location and frequency points, 500 continuous reading is got which will cost about 8 ~10 seconds.

21.2.2 Calculation method of BEL

The free space loss can be calculated as:

$$L_{\mathrm{f}} = 32.45 + 20\lg d\left[\mathrm{m}\right] + 20\lg f\left[\mathrm{GHz}\right] - G_{\mathrm{t}} - G_{\mathrm{r}} \tag{31}$$

Where d is distance between Tx and Rx, f is carrier frequency in GHz. Set transmitted power be *Pt* (dBm) and received power be *Pr* (dBm), the BEL is expressed as:

$$L_{\mathrm{E}} = \left(P_{\mathrm{t}} - P_{\mathrm{r}}\right) - L_{\mathrm{f}} \tag{32}$$

21.3 Conclusion

Through the analysis of CDF curves we can see that the distribution of entry loss probability is relative to the buildings' structure.

22 BEL measurements for two office buildings in the frequency range 800 MHz-28 GHz from Nokia

22.1 Introduction

This chapter provides BEL measurement data for two office buildings (one traditional and one modern) for different frequency bands in the range 800 MHz-28 GHz. From the presented measurement results, which can directly contribute to the existing measurement database, a number of observations are derived and related to existing literature and models in pro of easing the establishment of dependencies between different parameters in future modelling activities.

22.2 Measurement description

In [1], a measurement campaign of outdoor-to-indoor propagation in the frequency range 800 MHz-28 GHz is reported. The measurements results presented here were obtained at two different office building locations (Figs 171 and 172) with main characteristics described in Table 57.

TABLE 57

Summary of building compositions.

Façade elements	Traditional building (STV)	Modern Building (AAU)
Wall	10 cm thick made of light concrete and brick.	45 cm thick multi-layer composed of reinforced-concrete, brick and other isolation layers
Windows	Single-layered clear glass windows with wooden frames.	2-layered energy-efficient (metal-coated) windows with metal frame

FIGURE 171

Traditional office building (STV)

FIGURE 172

Modern office building (AAU)

Measurements were performed in a practical scenario where an omni-directional antenna was deployed outside the buildings at 7 m height, emulating a lamppost-mounted microcell base station (BS). Measurements were executed at diverse positions inside the buildings with omni-directional antennas located at approximately 1.75 m above ground level. Different indoor clutter conditions were considered (e.g. indoor measurements were performed inside a first row of offices, in an intermediate corridor, and in a second row of offices in deep indoor positions). Outdoor reference measurements were obtained as well, in different positions as close as possible to the external façade and following a parallel line to building. Figure 173 presents a simplified overview of the measurement scenario.

FIGURE 173

Overview of the measurement positions (grey: outdoor reference, green: indoor, orange: intermediate corridor, red: deep indoor)

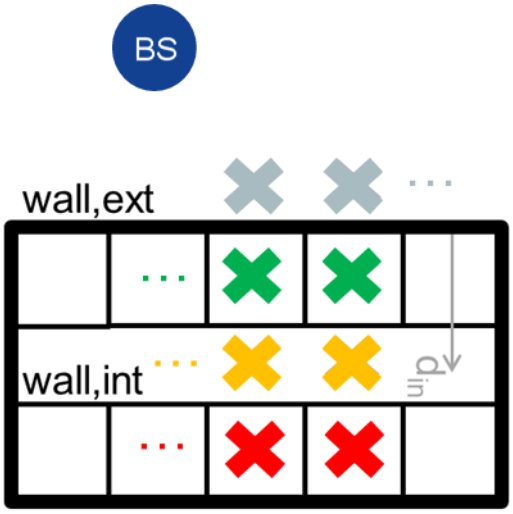

With distances (in perpendicular direction) between the microcell BS and the building of approximately 17 m and 25 m, for the traditional building scenario and the modern building scenario, respectively, the measurements explore non-perpendicular horizontal incidence close zero elevation. The geometrical horizontal incidence angle across the outer wall ranges from -30 and +75 degrees in the traditional building scenario and from −31 to +50 degrees for the modern building.

A few more details on the measurement setup, overview of the scenarios, measurement procedures and data processing is presented in [1-2] and has been summarized in the Annex.

22.3 Measurement results

Figures 174 and 175 present the BEL estimated from the measurements at the traditional and modern offices buildings, respectively. BEL samples are calculated as the difference in dB between the received power at the indoor measurement positions and the correspondent outdoor reference, and thus represent a mixture of external wall attenuation, indoor propagation and indoor wall attenuation (when applicable). The plots show as well the average BEL measured at the different levels of indoor penetration (indoor, intermediate corridor and deep indoor), as well as the average values for all positions for the frequency bands 800 MHz, 2 GHz, 3.5 GHz, 5.2 GHz, 10 GHz, 18 GHz and 28 GHz.

Table 58 summarizes the average BEL and standard deviation (STD) values per frequency band and building[14].

[14] Penetration loss at 28 GHz was computed using the indoor and intermediate corridor only, since the deep indoor measurements at 28 GHz were not possible due to dynamic range (*).

TABLE 58

Summary of BEL values for the two office buildings considering all indoor measurement positions

	Traditional Office Building		Modern Office Building	
Frequency	**Mean**	**STD**	**Mean**	**STD**
800 MHz	14.3	5.4	21.8	5.4
2 GHz	14.7	7.1	25.9	5.9
3.5 GHz	17.8	7.4	28.9	6.3
5.2 GHz	17.7	6.0	37.0	6.9
10 GHz	22.3	7.9	39.1	6.5
18 GHz	21.9	8.9	49.9	6.8
28 GHz	26.4	9.5	39.0*	3.9*

Three main aspects can be observed by comparing the measurement results from both buildings:

- The modern building presents BEL values approximately 7-28 dB higher than the traditional building.
- BEL presents a stronger frequency-dependent behaviour at the modern building than at the traditional building.
- As observed from the frequency trends at the different levels of indoor penetration (especially in the modern building), the outer wall seems to be the main contributor to BEL.

22.4 Normal incidence

Digging a bit more into the previous observations, it is possible to relate this different BEL values and frequency trends to the ones from the elements of the external facades of the two buildings (e.g. walls and windows).

In [3], a set of "controlled" measurements with highly-directional antennas is reported, characterizing the attenuation at normal incidence of the different façade elements for the frequency range 800 MHz – 18 GHz. The original measurements with a frequency resolution of 1 GHz, were later validated by means of an extensive second measurement considering an increased resolution of 100 MHz. The results of the different controlled measurements with directional antennas and normal incidence are plotted in Fig. 176, combined with the results from a third measurement which targeted the frequency range 400 MHz – 800 MHz in 25 MHz steps[15].

[15] The measurement results for the frequency range 400 MHz – 800 MHz have not been published yet.

FIGURE 174

BEL measurement results for the traditional office building

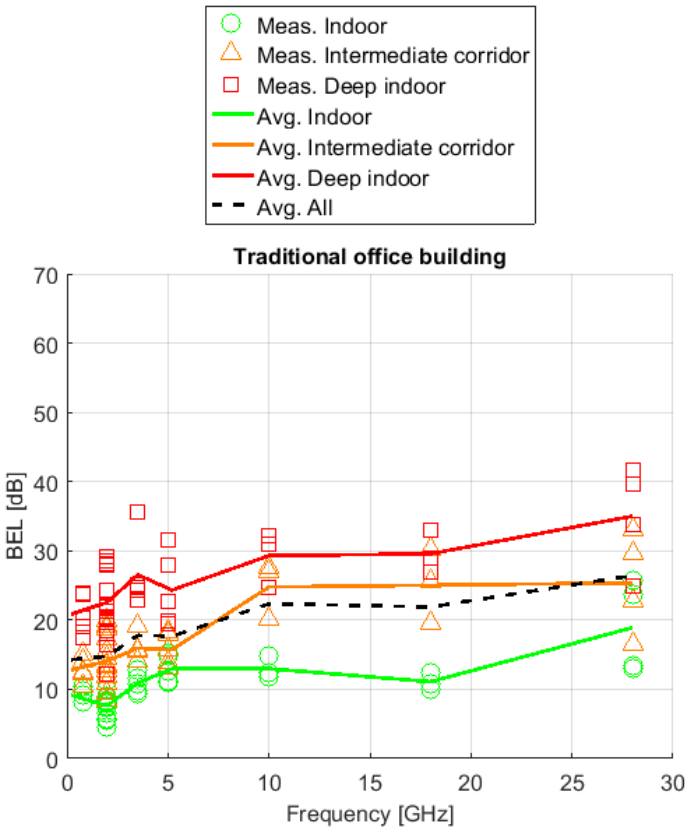

FIGURE 175

BEL measurement results for the modern office building

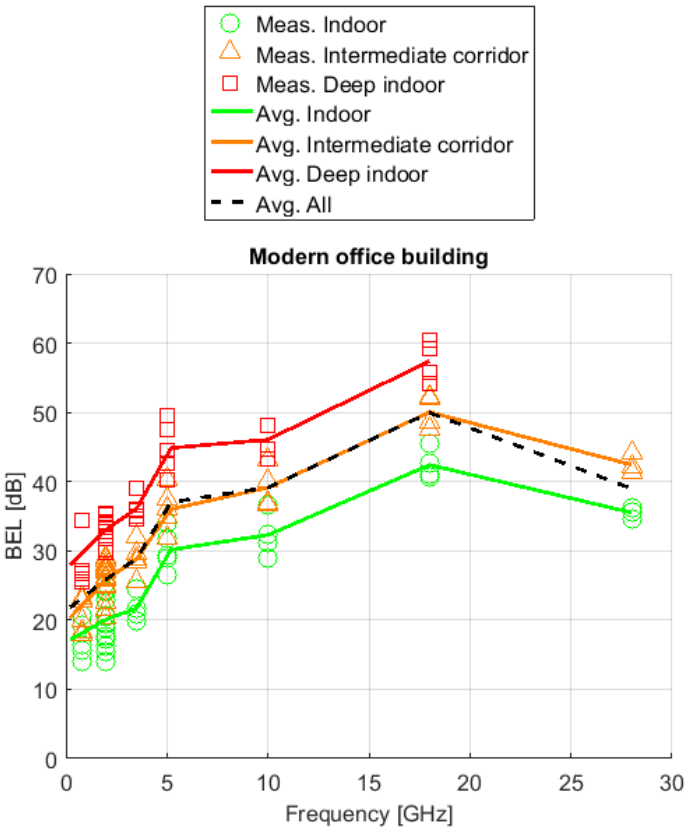

FIGURE 176

Normal incidence attenuation measurement results and associated linear models for the frequency range 400 MHz - 18 GHz, considering the frequency in linear scale (a) and logarithmic scale (b)

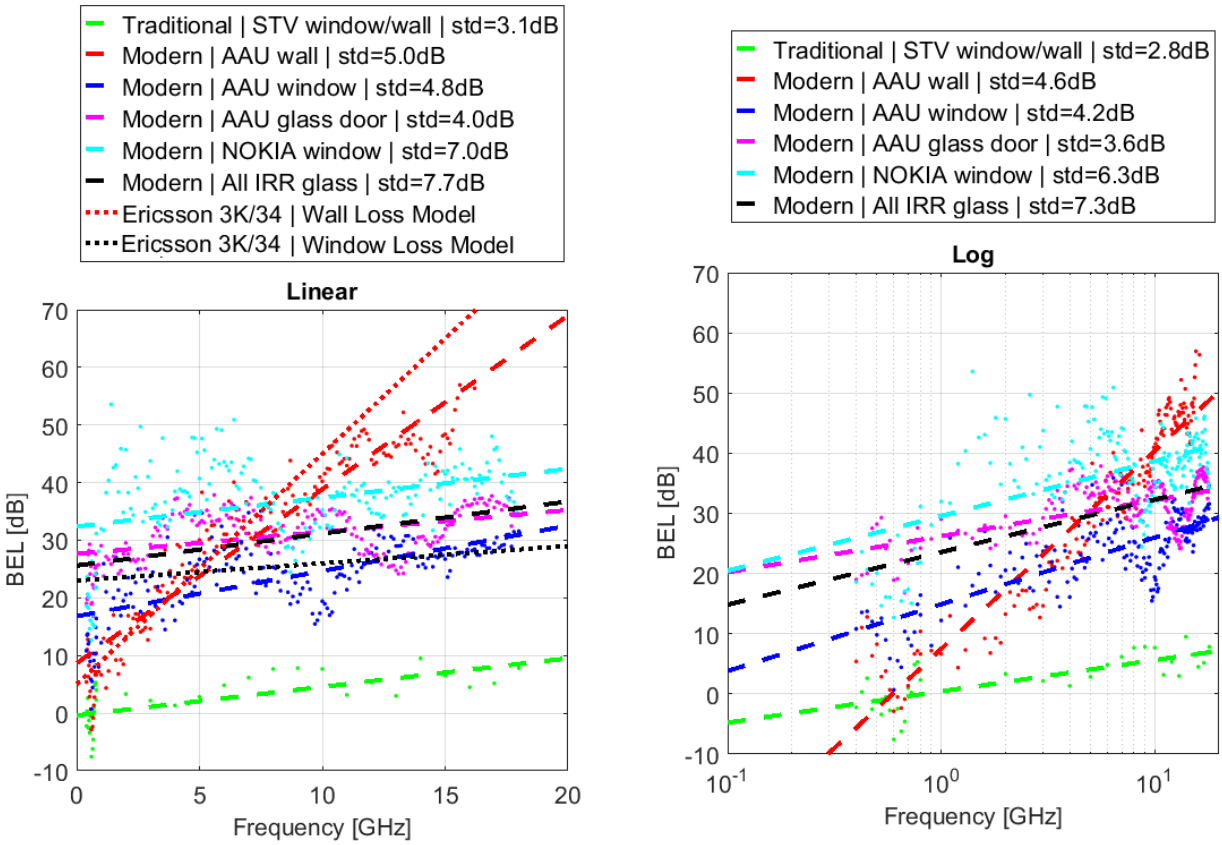

By specifically looking at the results in Fig. 175 (BEL in the modern building) and Fig. 176 a (attenuation introduced by the different AAU modern building façade elements separately: red dots for the external wall and dark blue dots for the windows), it can be seen how the effective BEL follows the trend of the external wall for the low frequencies up to approximately 5 GHz, and the one from the windows attenuation above that frequency. This fact suggests that the signals in this case, penetrate the building through the façade element with lower attenuation.

In the case of the traditional STV building, it was not possible to discriminate the attenuation of the wall and the window with the controlled measurements, and thus the combined attenuation is shown (green dots) in Fig. 176.a. However, one of the previous observations still applies as the normal incidence attenuation shapes the frequency behaviour of the effective BEL inside of the building reported in Fig. 174.

It is worth noting as well, that the normal incidence attenuation values measured are consistently lower than the effective BEL in both buildings, which clearly suggests that these attenuation values may serve as a lower bound in modelling.

22.6 Summary

This chapter presents BEL measurement results in the frequency range 800 MHz – 28 GHz for two different types of buildings: traditional building and modern building. The following aspects are observed:

- The modern building presents higher BEL than the traditional building (approximately 7-28 dB higher).
- BEL presents a stronger frequency-dependent behaviour at the modern building than at the traditional building.
- The outer wall seems to be the main contributor to BEL.
- Signals penetrate the building through the façade element (different types of windows/walls) with lower attenuation.
- The normal incidence attenuation values measured are consistently lower than the effective BEL in both buildings. This clearly suggests that these attenuation values may serve as a lower bound in the BEL modelling, with elevation and azimuth effects, as well as indoor propagation (directly proportional to building dimensions) adding on top of the lower bound.

Acknowledgements

Nokia Corporation would like to thank Aalborg University for providing the measurement data and corresponding analysis reported in [1]-[3].

References

[1] I. Rodriguez, H.C. Nguyen, I.Z. Kovács, T.B. Sørensen and P. Mogensen, “An Empirical Outdoor-to-Indoor Path Loss Model from below 6 GHz to cm-Wave Frequency Bands”, IEEE Antennas and Wireless Propagation Letters (AWPL), vol. PP, no. 99, 2016.

Available: http://dx.doi.org/10.1109/LAWP.2016.2633787

[2] I. Rodriguez, H.C. Nguyen, N.T.K. Jørgensen, T.B. Sørensen, J. Elling, M.B. Gentsch and P. Mogensen,” Path Loss Validation for Urban Micro Cell Scenarios at 3.5 GHz Compared to 1.9 GHz”, IEEE GLOBECOM, 2013.

Available: http://dx.doi.org/10.1109/GLOCOM.2013.6831689

[3] I. Rodriguez, H.C. Nguyen, N.T.K. Jørgensen, T.B. Sørensen and P. Mogensen, “Radio Propagation into Modern Buildings: Attenuation Measurements in the Range from 800 MHz to 18 GHz”, IEEE Vehicular Technology Conference (VTC-Fall), 2014.

Available: http://dx.doi.org/10.1109/VTCFall.2014.6966147

22.A1 Attachment 1: Measurement Scenarios

22.A1.1 Traditional Office Building (STV)

80x20 m (first row of offices 8 m, intermediate corridor 4 m, second row of offices 8 m)

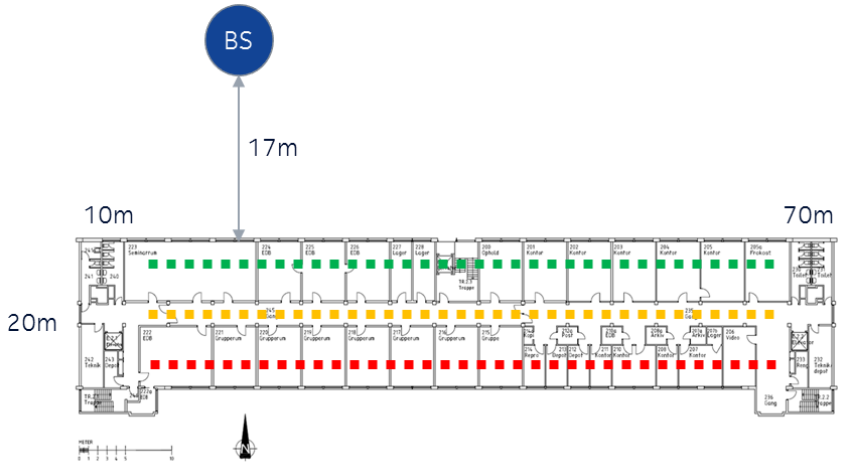

22.A1.2 Modern Office Building (AAU)

45x15m (first row of offices 6 m, intermediate corridor 3 m, second row of offices 6 m)

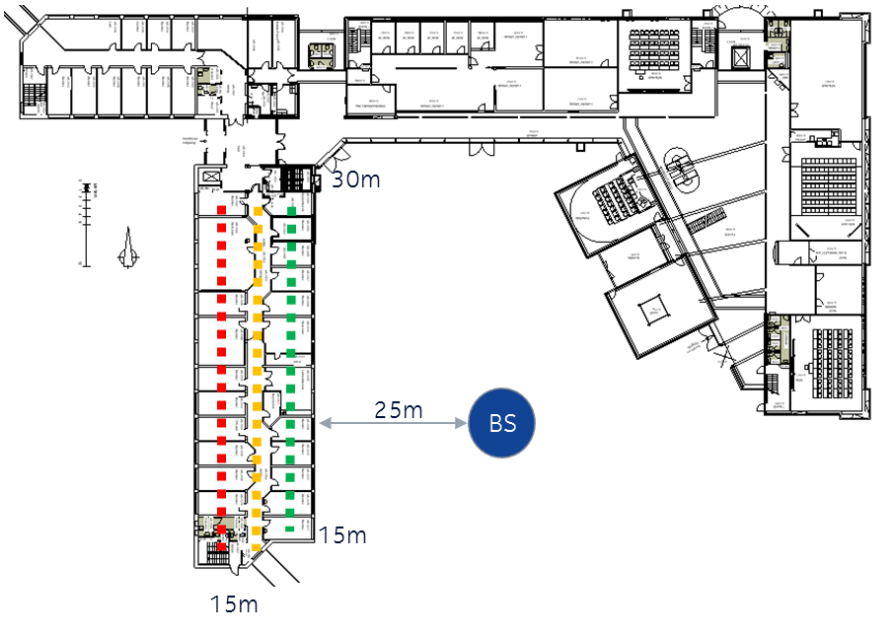

22.A2 Attachment 2: Methodology

22.A2.1 Measurement Setup

Measurement procedures and calibration are described in [1-2].

Practical microcell setup with omnidirectional antennas.

TX: lamppost-like, 7 m

RX: trolley-mounted, 1.75 m

22.A2.2 Measurement Procedures and Data Processing

Measurements with external reference

BEL_indoor [dB] = power_RX_indoor [dBm] - power_RX outdoor_ref [dBm]

BEL_corridor [dB] = power_RX corridor [dBm] - power_RX outdoor_ref [dBm]

BEL_deep_indoor [dB] = power_RX deep_indoor [dBm] - power_RX outdoor_ref [dBm]

22.A3 Attachment 3: Measurements at Normal Incidence

“Controlled measurements over practical scenarios”

Measurement procedures and calibration are described in [3].

Spectrum analyser + yagi (400-800 MHz)/horn(0.8-18 GHz) directional antennas.

Building	Element	Description	Picture
Traditional (STV)	Wall/Window	10 cm thick made of light concrete and brick Single-layered clear glass windows with wooden frames	
Modern (AAU) 	Wall	45 cm thick multi-layer composed of reinforced-concrete, brick and other isolation layers	
	Window	2-layered energy-efficient (metal-coated) windows with metal frame	
	Glass door	2-layered energy-efficient (metal-coated) glass door with metal frame	
Modern (NOKIA)	Window	2-layered energy-efficient (metal-coated) windows with metal frame	

23 BEL: Measurements covering 25 to 73 GHz frequency range in the United Kingdom

23.1 Introduction

Measurements have been made to investigate BEL. These measurements were carried out at the Building Research Establishment (BRE) campus in the UK in February 2017. Data were collected for frequencies between 400 MHz and 73 GHz in four dwellings, representative of traditional and modern (thermally efficient) construction methods. This document includes the BEL statistics for 25 to 73 GHz. The results of measurements below 6 GHz will be submitted at a future date. This work was jointly undertaken by Ofcom and Durham University.

23.2 Overview of BEL measurement campaign

Statistics are presented between 25 GHz and 73 GHz based on the results of a measurements campaign carried out at the Building Research Establishment (BRE) campus in the UK. BRE is a leading multi-disciplinary building science centre aiming to improve buildings through research and knowledge generation. The centre's facilities include a large number of buildings, mainly residential dwellings built between early 19th century to the most recent innovative and thermally efficient construction methods and materials, thereby providing an ideal place to select and conduct BEL measurements that closely represent the current and future house stock of the UK.

Two of the key findings of the majority of the BEL campaigns are:

i) Observed losses show little or no frequency dependency especially for higher frequencies.

ii) Significantly higher losses are recorded where "modern", thermally-efficient building methods (such as metallised glass, foil-backed panels, and cavity wall insulation) are used as compared to 'traditional" buildings without such materials.

These trends are further confirmed by the results of this recent measurement campaign at BRE as illustrated by the cumulative distribution functions (CDFs) of BEL and statistics summarised in Fig. 177 and Table 59, respectively.

FIGURE 177

BEL CDFs for traditional and modern (thermally efficient) buildings
(a) for each frequency (26 GHz, 50 GHz and 70 GHz), (b) for the combined frequencies

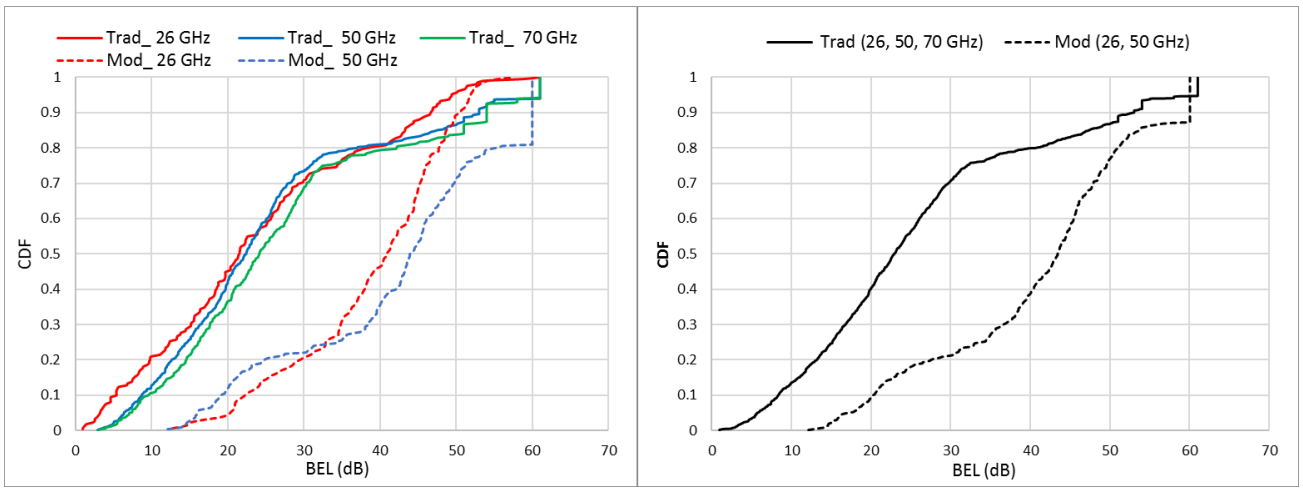

(a) **(b)**

In Fig. 177(a), the CDFs represent modern (Mod_x GHz) and traditional (Trad_x GHz) buildings where in each case the data from two such buildings were merged for each of the three measured frequency ranges (25.5-28.5 GHz, 51-57 GHz and 67-73 GHz). Figure 177(b) represents the CDFs from the combined frequencies for each type of build. The 70 GHz was not measured in one of the modern houses taking into account the dynamic range of the measurement equipment used and the high loss observed in the 50 GHz, hence not included in the summary results.

In Table 59, the statistics obtained from the CDFs are presented for both the 50% and the 1% value with the corresponding standard deviation (SD) for each frequency and from the combined frequencies for both types of build.

From these high level results, it can be summarised that the BEL is dependent on the type of build where the median value for the modern build is more than 20 dB higher than the traditional build. It also indicates that the BEL increases by 3-4 dB across the frequency range 25-73 GHz that might be due to differences in spreading loss between 26, 50 and 70 GHz.

TABLE 59

BEL statistics for traditional and modern (thermally efficient) buildings

		26 GHz	50 GHz	70 GHz	All (26, 50, 70 GHz)
Traditional	**CDF-50%**	21.55	22.45	24.17	22.89
	CDF-1%	1.05	3.86	4.08	3.02
	SD	14.58	15.63	15.80	15.54
Modern	**CDF-50%**	40.95	44.10	-	43.38
	CDF-1%	13.34	14.00	-	14.21
	SD	10.13	14.03	-	12.93

In general, one of the main challenges in carrying out BEL measurements and presentation of loss distributions are the treatment of locations where observed loss exceeds the dynamic range of measurement equipment. Ideally, measured locations inside the building should be statistically significant and spatial positions should be selected to cover the complete depth, rooms, floors and etc., thereby providing a meaningful BEL distribution of the complete building.

Where possible, the same approach of statistically significant measurement locations has been considered in this measurement campaign. In the analysis phase, the locations which did not have a detectable signal were assigned the highest observed loss value for respective frequency and building to ensure that all measured locations are used in the CDFs. The number of undetectable data points may still provide an underestimation of maximum or above 85% values, especially for 50 GHz and 70 GHz. However, it is also noted that the maximum or even above 50% of BEL statistics may not be appropriate for sharing studies.

The rest of this chapter is organised as follows. Section 3 provides brief information on the measurement campaign and the methodology used. Section 4 expands on the summary results, providing BEL statistics for individual houses and the observed variability between traditional and modern houses. Finally, § 5 provides concluding remarks.

23.3 Measurement methodology and equipment

The method for BEL measurements adopted in this campaign follows the recommendations given in § 4 of Recommendation ITU-R P.2040-1 where BEL measurements are defined as the difference (expressed in dB) between the spatial median of the signal level outside the illuminated face of a building and the spatial median of the signal level inside the building at the same height above ground.

For all scenarios, directional transmit antennas on a telescopic mast were used and placed at a sufficient distance (10-15 m) and height (2.1-2.6 m) required to illuminate the building façade. Omni receive antennas were used inside the buildings which were mounted on tripod stands. All floors inside the buildings were marked to ensure the same number and exact locations were used for wideband measurements of considered frequency ranges. Outdoor reference measurements were made as close to the building as possible (1-2 m).

The measurements were performed with the multi-band high time delay resolution sounder custom designed by Durham University [1].

For below 6 GHz, the sounder is capable of generating frequencies between 250 MHz-1 GHz, 2.1-2.9 GHz, 4.4-5.9 GHz. In the higher frequencies, the sounder can generate a waveform with a bandwidth up to 1.5 GHz in a programmable IF unit in the frequency range between 12.5-18 GHz.

The higher frequency ranges between 25-73 GHz are then generated from the IF signal using frequency multipliers giving a maximum bandwidth of 3 GHz in the frequency range 25-30 GHz and 6 GHz in the 50-75 GHz. Dual band measurements in the frequency range 25.5-28.5 GHz and 51-57 GHz, were enabled via splitters and an IF switch at the transmitter using two frequency multipliers and parallel receivers.

TABLE 60

Measurement data collection and post processing parameters

Frequency Range (GHz)	0.25-1	2.1-2.9	4.4-5.9	25.5-28.5	51-57	67-73
Frequencies (GHz)*	0.4, 0.7, 0.9	2.1, 2.4, 2.6	5.1, 5.4, 5.8	26	52, 56	68, 72
Analysis BW (MHz)**	125	150	150	1000	2000	2000
e.i.r.p (dBm)	23-30					
Tx (Beamwidth)	Dir (> 35°)	Dir (60°)	Dir (50°)	Dir (33°)	Dir (50°)	Dir (40°)
Rx Ant. (Beamwidth)	Omni					
Ant. Heights	Tx: 2.1-2.6 m, Rx: 1.1 m					
Ant. Polarisation	V-V					

The data from each frequency range was further sub-divided into sections* based on the analysis bandwidth** given in Table 60 and processed to obtain a power delay profile (PDP) from each second of collected data at each position. The received power was computed from the area under each PDP as in Recommendation ITU-R P.1407-5. The BEL for each frequency section was then estimated by taking the difference between the received power and the median power of the reference locations measured outside each building. Table 60 summarises the key parameters of this measurement campaign.

23.4 Campaign results

The measurement campaign was carried out at the BRE campus in the UK where the following four dwellings were selected for the data collection. The first two can be classified as traditional, built with the construction methods used before 2000's and more representative of the current house stock in the UK. Measurements were also conducted in two other modern dwellings which have been built by using highly innovative and thermally efficient construction methods, however these may represent just 1% of current house stock.

– Traditional - House B 50.2
– Traditional - Victorian Mansion
– Modern - Userhaus
– Modern - Wienerberger E4

Detailed information on the construction material used for all measured buildings has been included with the intention of providing quantitative information on thermal efficiency (measured in U-value) and will be included in later submission.

Table 61 summarises the measured frequencies and respective sections for each house covered in this campaign. This description concentrates on 25 GHz. Since the observed differences in BEL between 52, 56 GHz and 68, 72 GHz frequency sections were minimal; the respective ranges have been merged to improve readability and help with the presentation of results.

In all the results presented in this sections, the terms 26 GHz, 50 GHz and 70 GHz refer to 25.5-28.5 GHz, 51-57 GHz and 67-73 GHz, respectively. The 70 GHz was not measured in Wienerberger E4 house considering the dynamic range of the measurement equipment used and the high loss observed in the 50 GHz. For the other houses, consistent and complete datasets are available and have been used.

TABLE 61

Measurement frequencies in four dwellings at BRE campus

Frequency range (GHz)	Measured houses			
	Traditional		Modern	
	House B 50.2	Victorian mansion	Userhaus	Wienerberger-E4
0.2-1	0.4, 0.7 0.9	0.4, 0.7 0.9	0.4, 0.7 0.9	-
2-3	2.1, 2.4, 2.6	2.1, 2.4, 2.6	2.1, 2.4, 2.7	-
4.9-5	5.1, 5.4, 5.8	5.1, 5.4, 5.8	5.1, 5.4, 5.8	-
25.5-28.5	26	26	26	26
51-57	52, 56	52, 56	52, 56	52, 56
67-73	68, 72	68, 72	68, 72	-

23.4.1 Traditional build houses

23.4.1.1 House B 50.2

This property is a 3-bedroom detached domestic house which was built in the early 1990's and represents the construction type of many homes within the UK. The house is of brick construction comprising of 103 mm thick Ibstock Trafford multi-rustic facing bricks for the external walls and 130 mm thermalite block work for the inner walls. A 75 mm cavity exists between both walls which is filled with Rockwool insulation. The inner walls are dry lined with plaster boards and finished off with a plaster coat.

The roof is constructed using wooden trusses at a 35° pitch and finished with concrete tiles. The roof is insulated with 150 mm Rockwool. The first floor is suspended using 150 mm joists which is insulated with Styrofoam and then laid with a 22 mm chipboard floor covered with carpet. The ground floor is constructed using timber joists to create a suspended floor which is insulated and covered with 22 mm chipboard board and carpet. The house occupies a total floor area of 84 m^2.

FIGURE 178

House B 50.2 floor plans and pictures. Numbers on plans refers to exact positions where the receive antennas were placed and measurements made. R1-R7 denote the outdoor reference points

This house has standard single glazed windows with no metallised coating. The house provides an option to add secondary windows to built-in frames. These secondary units (thin framed glass panes) are normally used to reduce traffic noise and improve some level of thermal efficiency, however not efficient as double or triple glazed windows.

Two datasets were collected in this house, one with standard single glazed windows and the other with secondary windows installed. The CDFs of BEL and its statistics with the corresponding SD for each and combined frequencies are given in Fig. 179 and Table 62, respectively.

FIGURE 179

BEL CDFs for house B 50.2 with single glazed and single glazed plus secondary windows

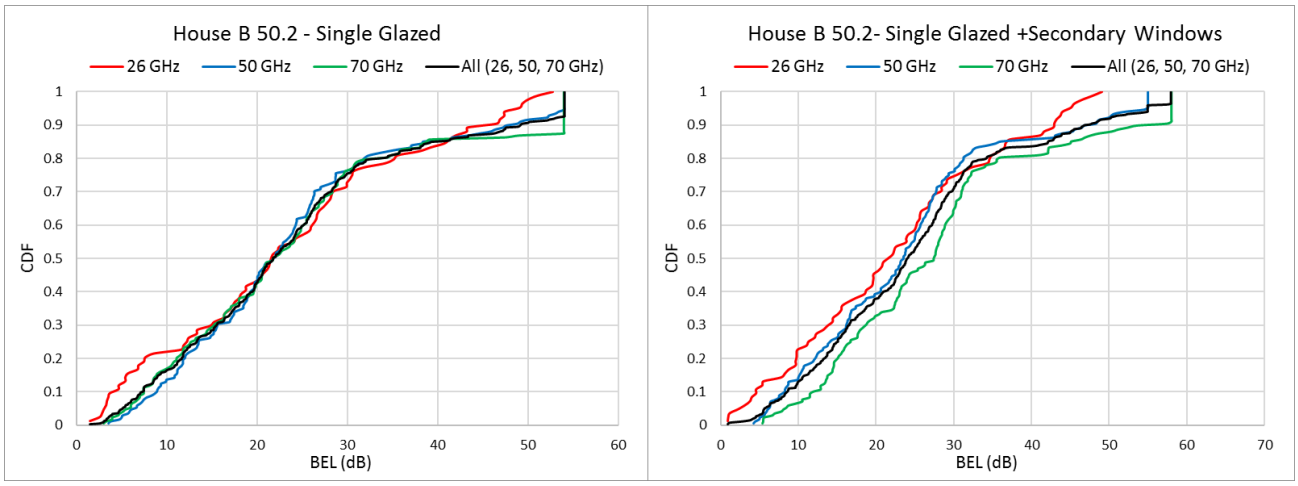

The addition of secondary windows creates some level of frequency dependency on the BEL CDFs. However negligible differences between the two scenarios can be noticed and for the 50% value, the loss increases by just 2-5 dBs for the 50 GHz and 70 GHz. Contrarily, the overall 1% loss values for standard single glazed windows are roughly the same or slightly higher. This can be explained by the measurements made in the hallway (least observed losses for points 8-14) where the main entrance door leading to these points had the standard single glazed glass in both scenarios (ref. Hallway picture in Fig. 178).

TABLE 62

BEL statistics for house B 50.2 with single glazed and single glazed plus secondary windows

		26 GHz	50 GHz	70 GHz	All (26, 50, 70 GHz)
Single Glazed	**CDF-50%**	21.65	21.90	21.87	21.75
	CDF-1%	2.32	3.70	3.21	3.02
	SD	14.11	13.48	14.64	14.05
Secondary Windows	**CDF-50%**	21.86	23.53	27.48	24.12
	CDF-1%	1.02	4.38	5.50	2.50
	SD	13.05	13.40	14.31	13.86

23.4.1.2 1800's Victorian mansion

This family mansion was built in the 1870's using Victorian construction methods of the period. Houses built with similar methods represent one of the pre-1914's house styles and a significant number of such smaller and terraced dwellings can typically be found in the suburbs of towns and cities in the UK. A property of this period will have been of solid wall construction using stone. The wall thickness is approximately 600 mm. A building of this age has no insulated cavity and the windows are traditional timber framed with thick single paned glass and solid wooden internal and external doors.

This building currently houses BRE offices and only a large conference room and main hallway were made available for the campaign (ref. Figure 180). However, roughly 85 m^2 of floor area was covered which is comparable to the spatial area covered by measurements in the House B 50.2.

The CDFs of BEL and its statistics for the Victorian mansion are given in Fig. 181 and Table 61, respectively. A sharp increase in loss for all frequencies can be observed around the 60% value and this happens when the receiver(s) move from the conference room into the hallway (points 34-46).

These receive locations are obstructed by two solid stone walls of roughly 600 mm thickness each. The 26 GHz CDF is not affected by the dynamic range of the measurement equipment however the majority of the hallway points for 50 GHz and 70 GHz suffer and have been assigned the maximum loss observed for the detectable hallway points of respective frequency bands. The CDF curves show some level of frequency dependency with both 3% and 50% value reporting slightly higher loss with increasing frequency ranges.

FIGURE 180

Victorian mansion floor plan and pictures. Numbers on plan refers to exact positions where the receive antennas were placed and measurements made. R1-R5 denote the outdoor reference points

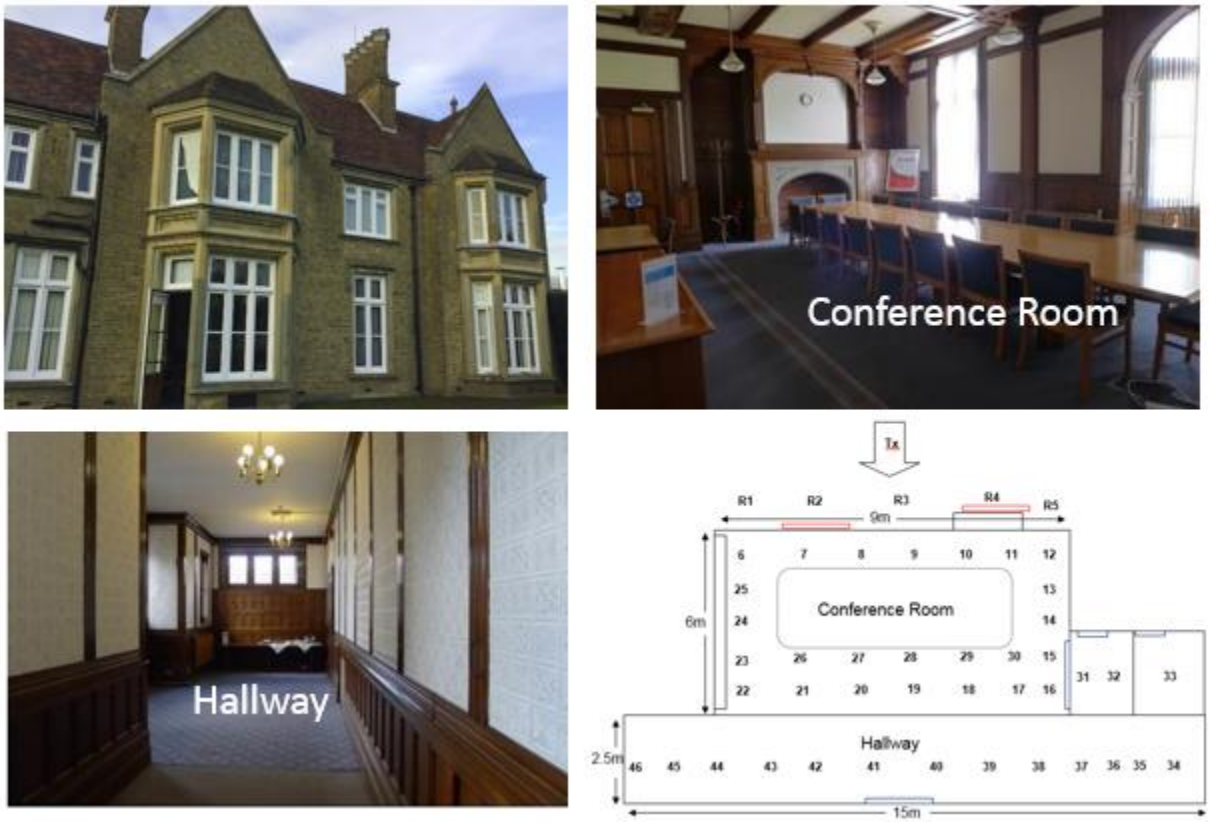

FIGURE 181

BEL CDFs for traditional Victorian mansion

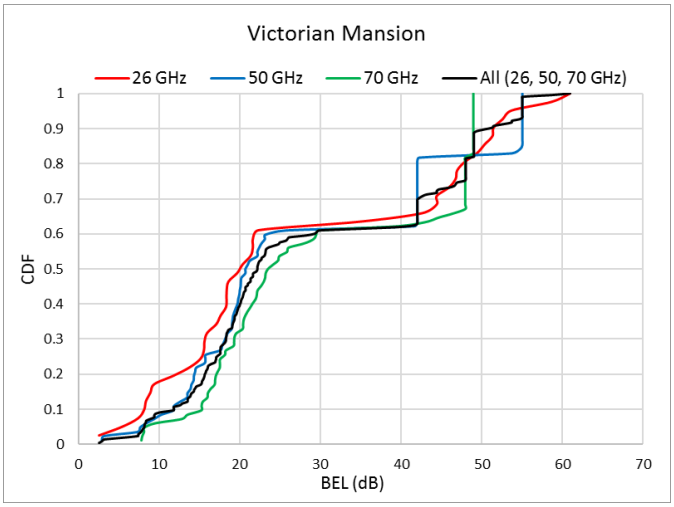

TABLE 63

BEL statistics for traditional Victorian mansion

	26 GHz	50 GHz	70 GHz	All (26, 50, 70 GHz)
CDF-50%	20.36	20.86	23.85	22.19
CDF-3%	3.30	5.27	8.08	7.47
SD	17.74	16.39	14.68	15.97

23.4.1.3 Traditional build BEL variability

Figure 182 shows a comparison of BEL variability of traditional build for all frequencies combined (26, 50 and 70 GHz). It may not be a fair comparison as only a portion of the Victorian property was covered by measurements; however, it is highly unlikely for the CDF curve to significantly change if more measurements were made where the receiver(s) are obstructed by one and two solid stone walls. Interestingly, the median loss values for both traditional houses are between 22-24 dB.

FIGURE 182

Traditional build BEL comparison

23.4.2 Modern Construction Houses

23.4.2.1 Userhaus modular construction house

This house is built around an ultra-modern modular construction technique with each floor module being brought to site fully assembled and fitted into position by a lifting crane (ref. Fig. 183). The external walls are formed of timber frame to which a mix of coloured mono-crystalline photovoltaic cladding panels are attached. A cavity void exists between the outside cladding and the foil backed polyisocyanurate (PIR), insulation which forms part of the pre-assembled modules. Foil backed PIR boards are used for the floor and ceiling as well as the sides for thermal efficiency. The roof uses terracotta thin film building-integrated photovoltaics (BIPV) technology. The windows are double glazed Munster joinery uPVC and come fitted with the modules.

The CDFs of BEL and their statistics are given in Fig. 184 and Table 62, respectively. The measured BEL ranges between 12 and 50 dB and none of the statistics were limited by dynamic range issues which was quite surprising considering the foil backed cladding used in the modular construction of this house.

The measured losses for both 50% and 3% values are about 32 dB and 15 dB, respectively which is approximately 12 dB higher than measured in the traditional houses. Little can be said on the frequency dependence of BEL in this house.

FIGURE 183

Userhaus floor plan and pictures. Numbers on plan refers to exact positions where the receive antennas were placed and measurements made. R1-R4 denote the outdoor reference points

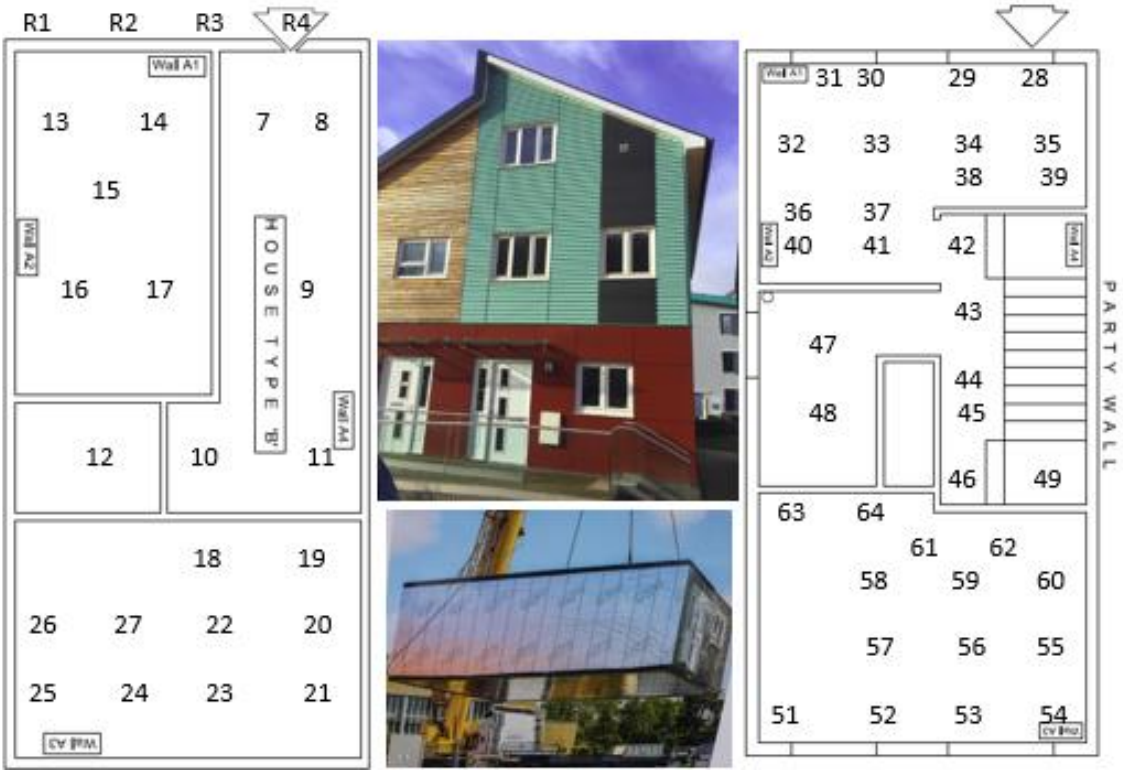

FIGURE 184

BEL CDFs for modern Userhaus modular house

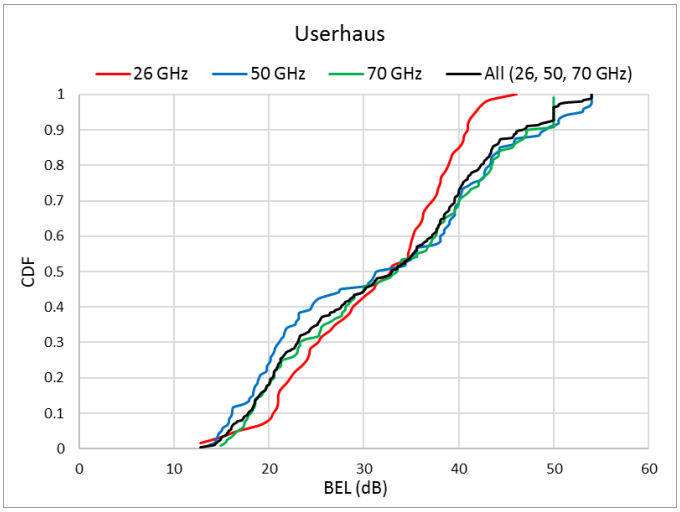

TABLE 64

BEL statistics for modern Userhaus modular house

	26 GHz	50 GHz	70 GHz	All (26, 50, 70 GHz)
CDF-50%	32.92	32.11	33.52	33.02
CDF-3%	14.61	14.49	15.88	14.98
SD	8.23	12.32	11.04	11.07

23.4.2.2 Wienerberger E4 House

This building represents the typical modern thermally efficient and low energy usage home constructed at new housing developments in the UK. The build is based around the thermal properties of clay. The inner walls are constructed using the porotherm clay block walling system with a cavity between the inner wall and external wall comprising of an air gap void and thermal insulating wool wall slabs. The external wall is of conventional 103 mm thick modern brick. The roof is of 40^{o} pitch and covered with Wienerberger Sandtoft tiles. The floor is made from ply wood board. The ground floor is constructed using beams and blocks for good thermal performance and building practice. The windows manufactured by NorDan are extremely thermally efficient and consist of a powder coated aluminium frame which has a softwood internal frame with double glazed glass.

The initial measurements for 26 GHz and 50 GHz revealed losses of more than 40 dB just inside the property and even at locations where the line of sight between the outside transmitter antennas and the receive antennas was blocked by just the windows. Few locations reported smaller losses of approximately 10-15 dB and refer to measurements made in the hallway where the main entrance door leading to these points had a different\ordinary double glazed small glass as compared to the superior glazing used in all other windows of this house.

The CDFs of BEL and their statistics are given in Fig. 186 and Table 63, respectively. The measured losses for both 50% and 3% values are approximately 45 dB and 35 dB, respectively and about 24 and 32 dB higher than measured in traditional houses. Clear frequency dependency can be noticed in the CDF curves.

FIGURE 185

Wienerberger-E4 house pictures

FIGURE 186

BEL CDFs for modern Wienerberger E4 house

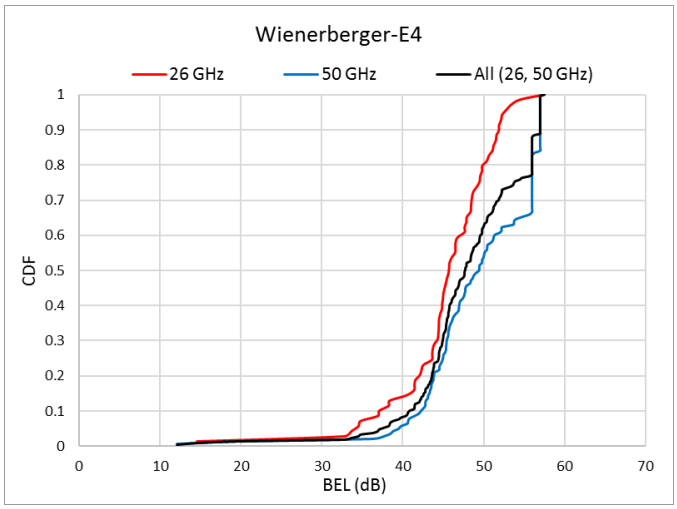

TABLE 65

BEL statistics for modern Wienerberger - E4 house

	26 GHz	50 GHz	All(26, 50 GHz)
CDF-50%	45.11	49.46	47.75
CDF-3%	32.88	37.82	34.61
SD	6.33	7.11	7.09

23.4.2.3 Modern build BEL variability

Figure 187 shows a comparison of BEL variability of modern build for combined 26 GHz, and 50 GHz). Huge differences can be observed between the two modern houses where the Wienerberger

E4 house shows more than 20 dB of loss as compared to the other modern Userhaus house and most probably due to the superior glazed windows used in this house.

FIGURE 187

Modern build BEL comparison

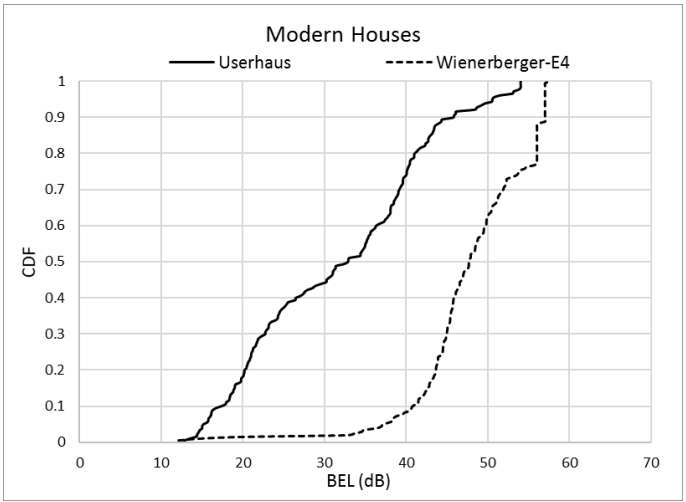

23.5 Concluding remarks

The results of this measurement campaign further reiterate the complexity, variability and unpredictability of modelling BEL, both within a given building and between different buildings. Classification of build type such as traditional and modern helps in simplifying the question; however, these are quite subjective terms where the definitions and actual construction methods for traditional and modern buildings and associated entry losses may vary hugely for different countries and around the world.

One of the other challenges are the huge dynamic range of the measurement equipment required to carry out such measurements. The setup used in this campaign had a reasonable range of 150 dB and covers 0° elevation angles, clearly not enough for one of the modern and traditional houses being measured. This becomes even more important for higher elevation angle measurements where entry loss may increase with increasing elevation angles.

23.6 References

[1] Salous, Sana, Feeney, Stuart, Raimundo, Xavier & Cheema, Adnan (2016). Wideband MIMO channel sounder for radio measurements in the 60 GHz band. *IEEE Transactions on Wireless Communications* **15**(4): 2825-2832.

24 BEL from 5-39 GHz in the United States

24.1 Introduction

This chapter presents measurements of outdoor-to-indoor propagation from 5-39 GHz. This work is a continuation of the work described in Annex 13 of Report ITU-R P.2346. For this exercise a total of five buildings were measured, three of which were measured previously using different techniques. The first is a newer building (built in 2009) that is similar in construction to a modern residential home in the United States. The second is an older commercial office building (built in 1945). The third building is a very new (2014) commercial office building built using modern "green" building techniques. The fourth and fifth buildings are an older commercial office buildings (both built around 1966). These five buildings allow for the measurement of propagation losses through both modern and older materials; such as glass/windows and exterior block and siding. The excess loss (with free space losses removed) for all of the buildings is presented in the document.

The purpose of re-evaluating some buildings that were previously studied is to have a common baseline with which to compare these results as the type of receive antenna used was changed from a directional to an omni-directional antenna.

24.2 Experimental setup

The signals used during this experiment were continuous wave (CW) at 5, 12, 20, 25, 30, and 39 GHz.

The antenna used the transmitter was a dual ridge horn antenna (MVG Model Number: SH4000), this is the same antenna that was used in the previous study (Doc. 3M/59). The receive antenna was a wide band omni-directional antenna (Electro-Metrics Model Number ME-6758).

The outdoor transmitter consisted of a signal generator (Anritsu MG3690C) connected to the dual ridge horn antenna. The receiver consisted of an omni-directional antenna with a wide-band amplifier connected to a spectrum analyser (Agilent E4446A).

24.2.1 Building descriptions

The first building that was measured is a recently constructed building similar to a modern US residential building. The building's exterior is made up of vinyl siding followed by plywood sheeting with metal studs with fiberglass insulation in-between covered by final layer of drywall. The windows in the building are standard double pane low-emissivity windows used in most modern US construction.

The second building is an older commercial office building. The exterior walls are composed of 10.2 cm of brick on top of 20.3 cm of concrete block followed by 2.5 cm furring strips and 1.9 cm layer of plaster. The windows are older and made of double pane glazed glass with aluminum frames.

The third building is a new building that was constructed with a focus on environmental factors, e.g. a lot of recycled/energy efficient material and low E glass windows.

There also is a reflective thermal coating on the windows to help keep the building cool in the summer and warm in the winter. This coating as well as the low E glass seems to have a large effect on the transmission of signals into/out of the building, as will be shown in the results that follow.

The fourth and fifth building were older commercial office buildings both built around 1966. The exterior walls are composed concrete block followed by wooden furring strips and fiberglass insulation and topped with drywall. The windows are older and made of double pane glazed glass with aluminum frames.

FIGURE 188

Photograph of the front of Building 1 (left), Building 2 (right), Building 3 (middle) and Building 4 (bottom left) and Building 5 (bottom right)

24.2.2 Testing locations

For each building the transmitter was positioned at a fixed point centred on the building from left to right and at a sufficient distance to provide nominally uniform illumination across the face of the building. The omni-directional receiver was then used to measure the reference power level across the face of the building. After the reference power levels were obtained the receiver was positioned at various locations inside the building to measure the received power inside. The height of the transmitter and receiver were matched to eliminate any changes in the received signal level due gain deviations in the antenna patterns.

The testing locations were chosen to be somewhat uniformly distributed and to ensure that all of the unique aspects of the building were sampled (e.g. windows, doors, large wall sections, hallways, etc.). Spatial density in terms of number of testing locations within each of the buildings is given in the following table:

TABLE 66

Spatial density of measurements

Building number	Point density
1	1 point / 4 m2
2	1 point / 10 m2
3	1 point / 9 m2
4	1 point / 9 m2
5	1 point / 9 m2

24.3 Results

The following sections contain the results of the measured building loss from each building. The results are analysed and presented in several different ways, including: tabulated, as a function of frequency and depth and also and statistically.

24.3.1 Tabulated results

TABLE 67

Tabulated building loss results for building 1

Frequency [GHz]	Minimum [dB]	Mean [dB]	Maximum [dB]	Standard deviation [dB]
5	4.23	14.85	31.83	5.65
12	1.3	12.91	29.50	6.11
20	1.53	12.69	24.63	5.99
25	3.13	14.50	31.43	6.42
30	0.73	12.19	33.33	7.06
39	2.73	18.24	35.13	7.30

TABLE 68

Tabulated building loss results for building 2

Frequency [GHz]	Minimum [dB]	Mean [dB]	Maximum [dB]	Standard deviation [dB]
5	1.16	22.67	53.86	10.00
12	0.56	21.00	54.16	10.94
20	0.52	25.83	60.02	13.17
25	2.36	29.81	60.46	12.91
30	2.38	23.61	52.08	12.69
39	1.10	27.97	50.70	12.04

TABLE 69

Tabulated building loss results for building 3

Frequency [GHz]	Minimum [dB]	Mean [dB]	Maximum [dB]	Standard deviation [dB]
5	9.60	34.92	70.10	12.94
12	8.15	29.97	57.15	12.37
20	13.90	41.62	68.20	13.74
25	8.90	33.67	57.00	12.35
30	12.40	38.29	52.50	11.05
39	4.40	33.54	57.80	13.55

TABLE 70

Tabulated building loss results for building 4

Frequency [GHz]	Minimum [dB]	Mean [dB]	Maximum [dB]	**Standard** deviation [dB]
5	1.50	18.86	35.90	8.51
12	.60	16.59	47.00	10.86
20	.80	17.10	37.80	9.99
25	.50	21.00	44.80	12.27
30	1.70	18.76	45.40	11.92
39	2.25	19.04	55.55	12.66

TABLE 71

Tabulated building loss results for building 5

Frequency [GHz]	Minimum [dB]	Mean [dB]	Maximum [dB]	**Standard** deviation **[dB]**
5	4.70	25.71	42.30	8.85
12	3.90	18.80	42.10	10.37
20	6.50	23.59	49.00	10.45
25	10.60	30.02	46.70	9.81
30	1.50	18.57	37.80	9.95
39	3.90	22.72	56.10	12.12

It is important to note that all of the buildings presented a multipath rich environment. This created a substantial amount of variation in the received signal as a function of position. Multipath has the potential to be both constructive and destructive. When considering any single spatial point, the contribution of multipath should be taken into account, and therefore some of the minimum (and maximum) values in the above tables are likely influenced by multipath.

24.3.2 BEL vs depth

The next five figures (Figs 189-193) show the relationship between the BEL and the depth inside the building. Note that the all of the free space loss has been removed.

FIGURE 189

BEL vs depth for building 1

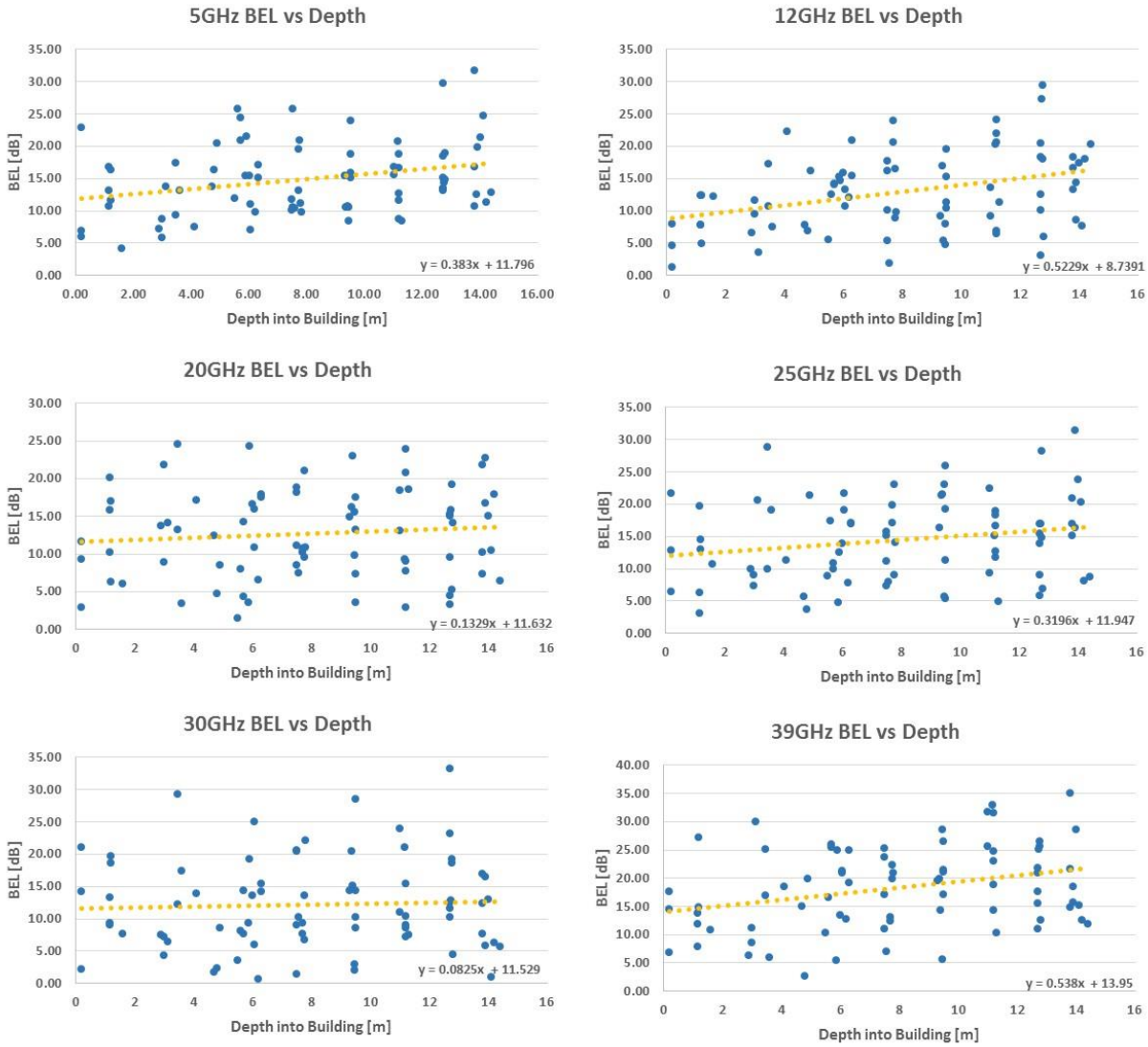

FIGURE 190

BEL vs depth for building 2

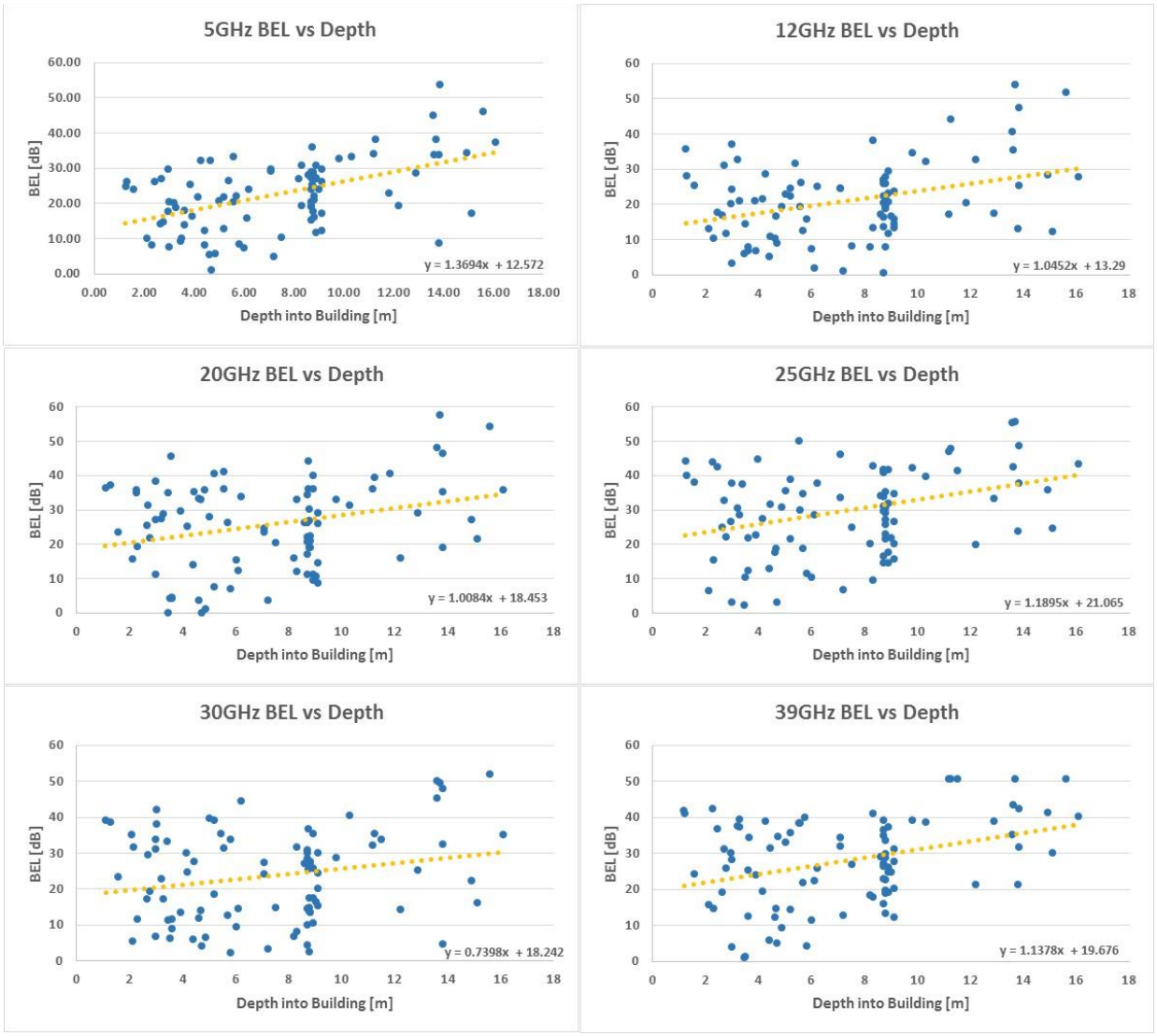

FIGURE 191

BEL vs depth for building 3

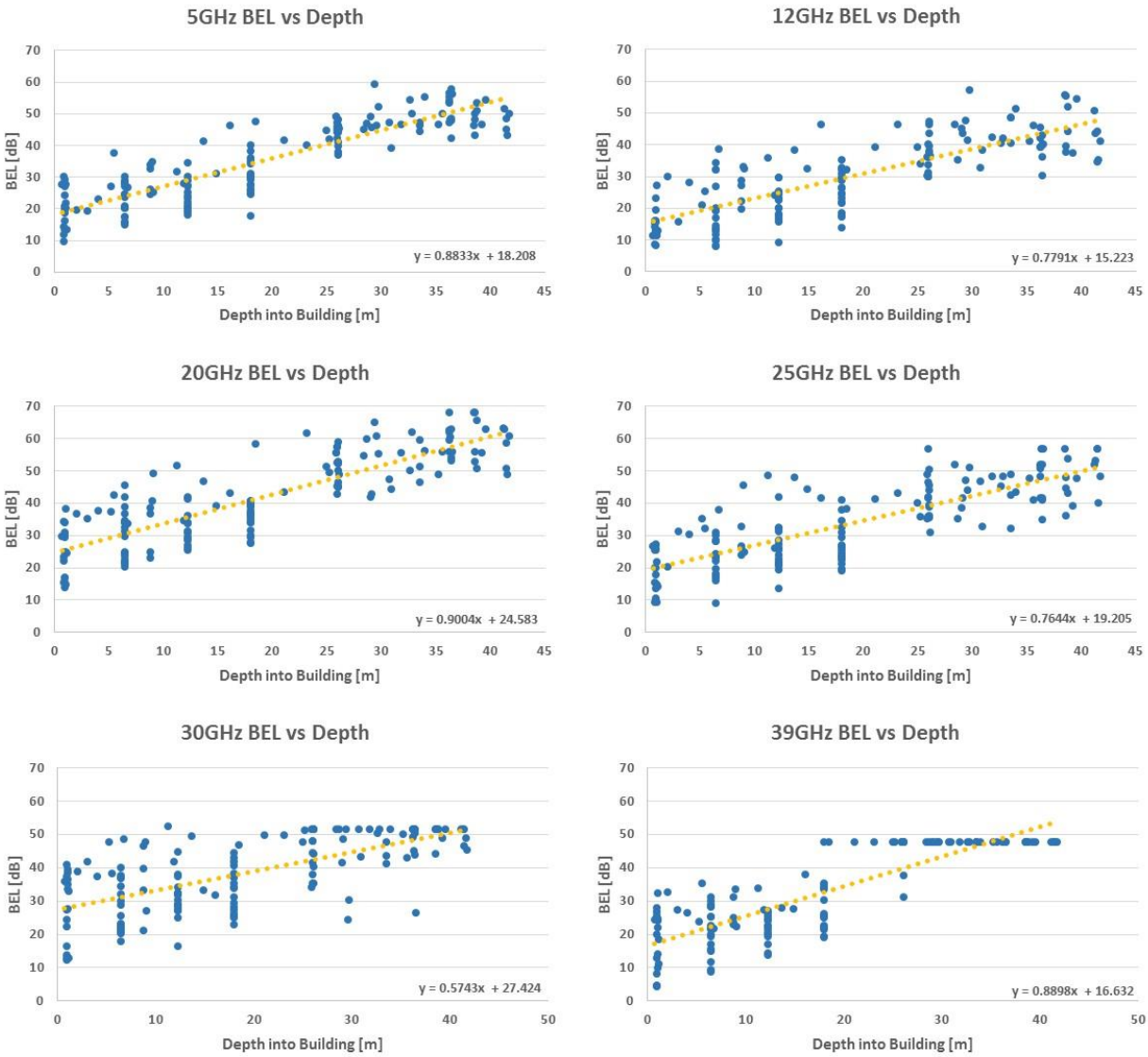

FIGURE 192

BEL vs depth for building 4

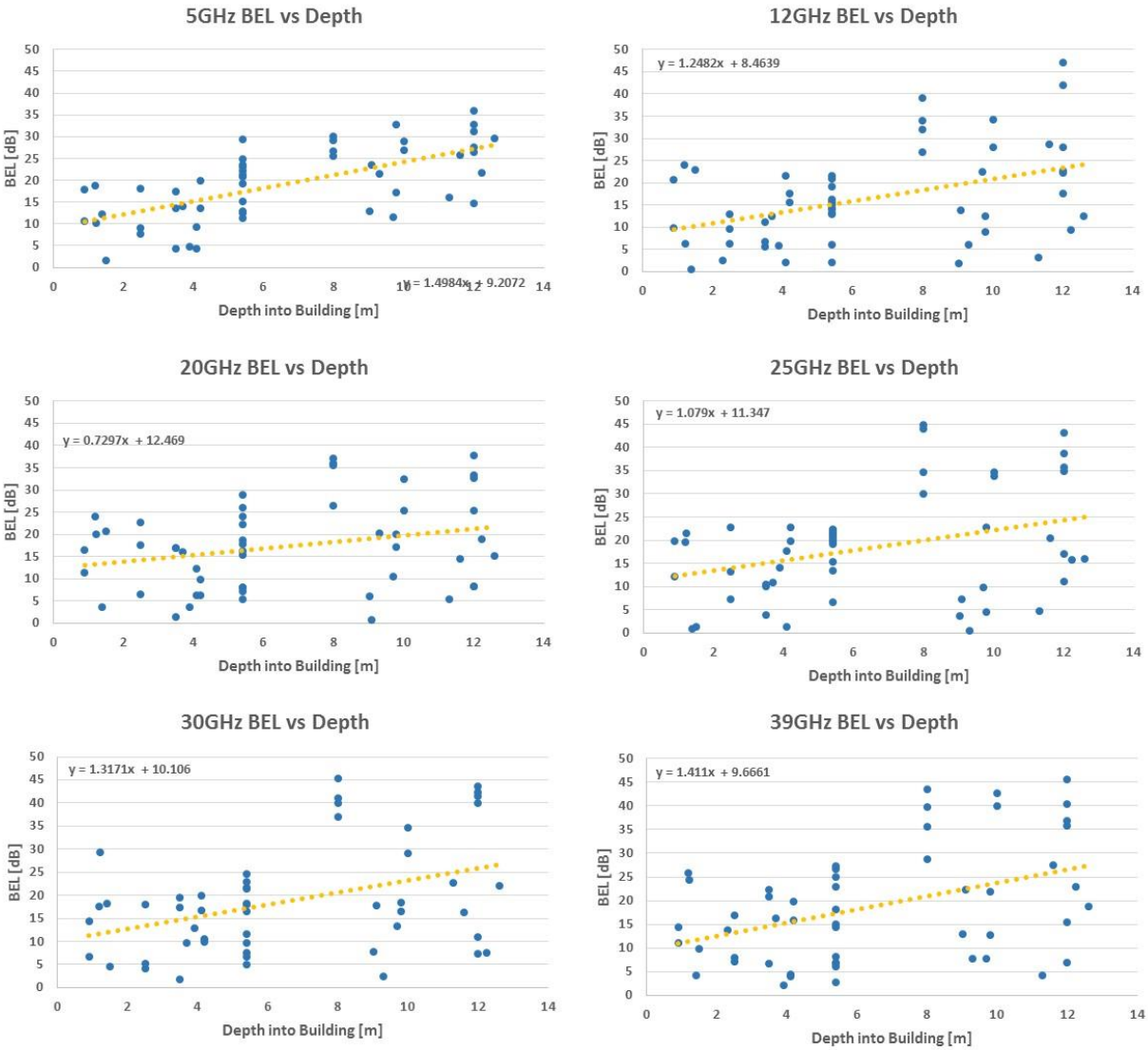

FIGURE 193

BEL vs depth for building 5

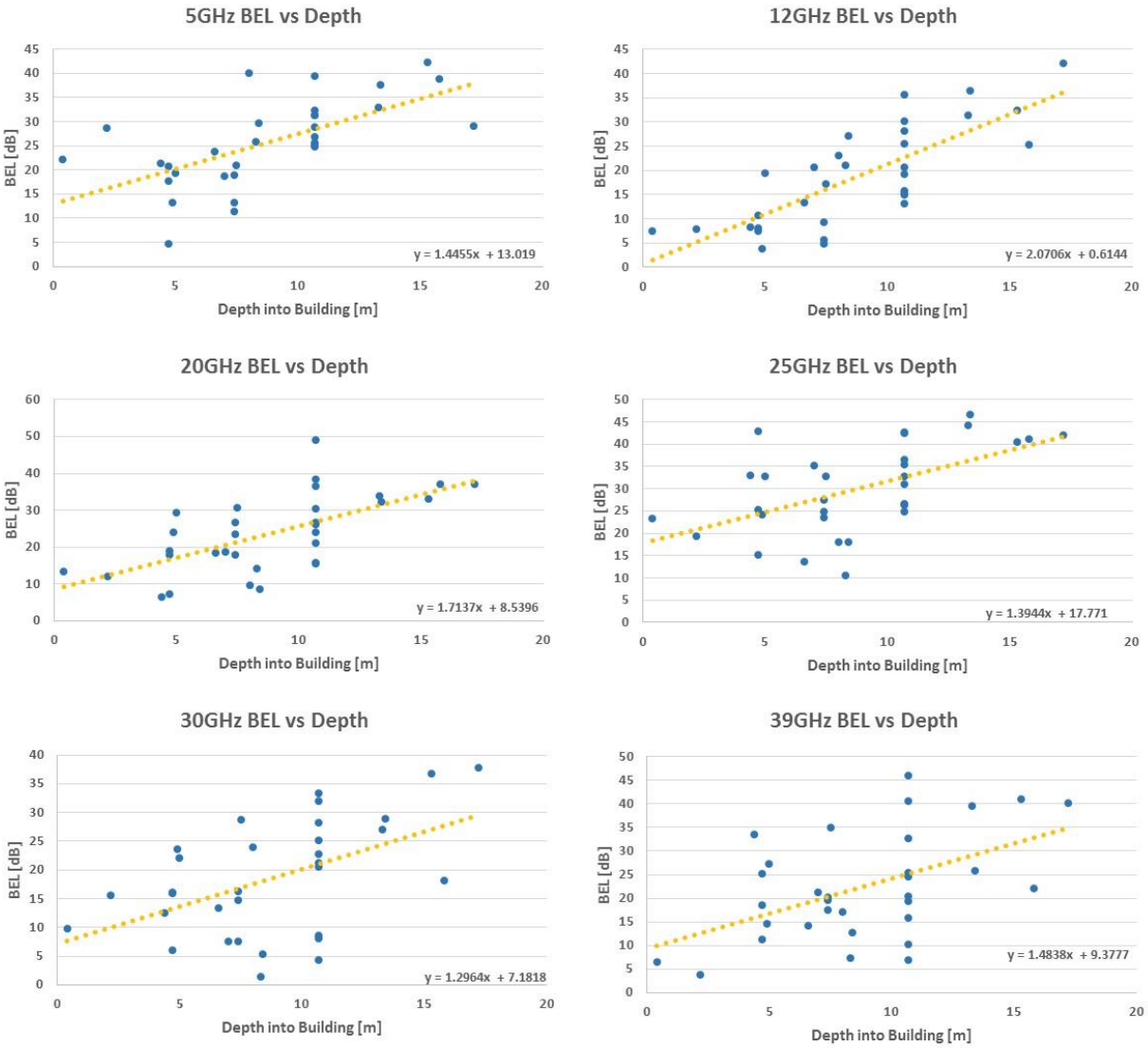

There does appear to be a consistent increasing trend of BEL as a function of depth inside the building. On average the BEL increases by 0.8-1.5 dB/m.

24.3.3 PDF distributions

Next the probability density functions (PDFs) of the data sets are considered.

FIGURE 194

BEL PDFs for building 1

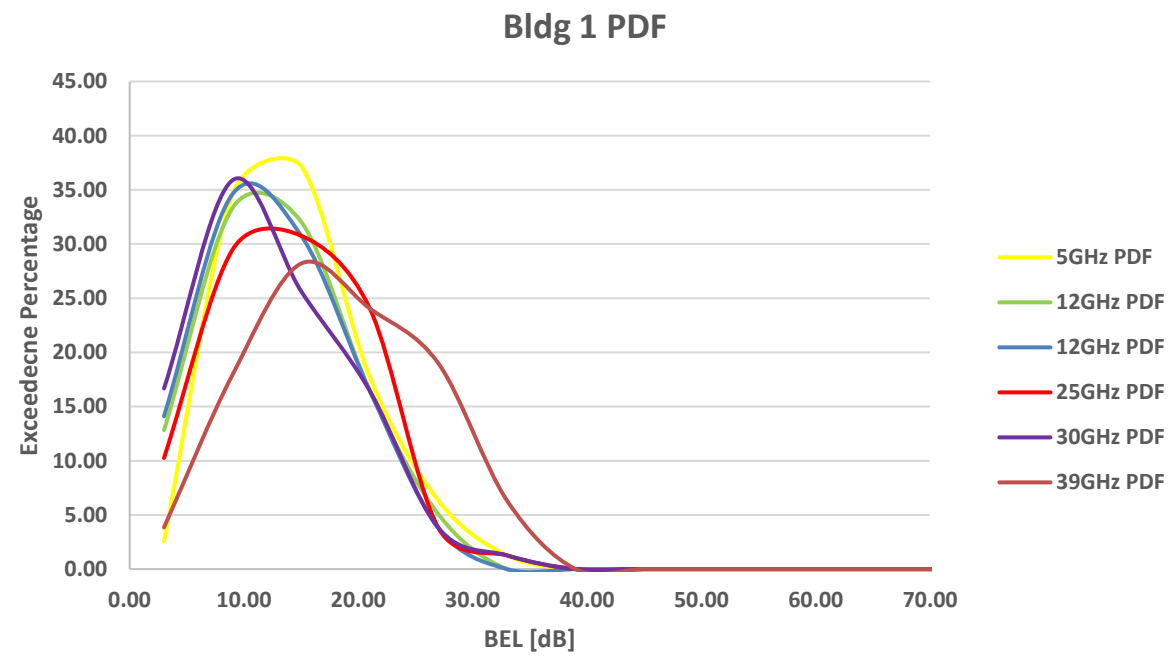

FIGURE 195

BEL PDFs for building 2

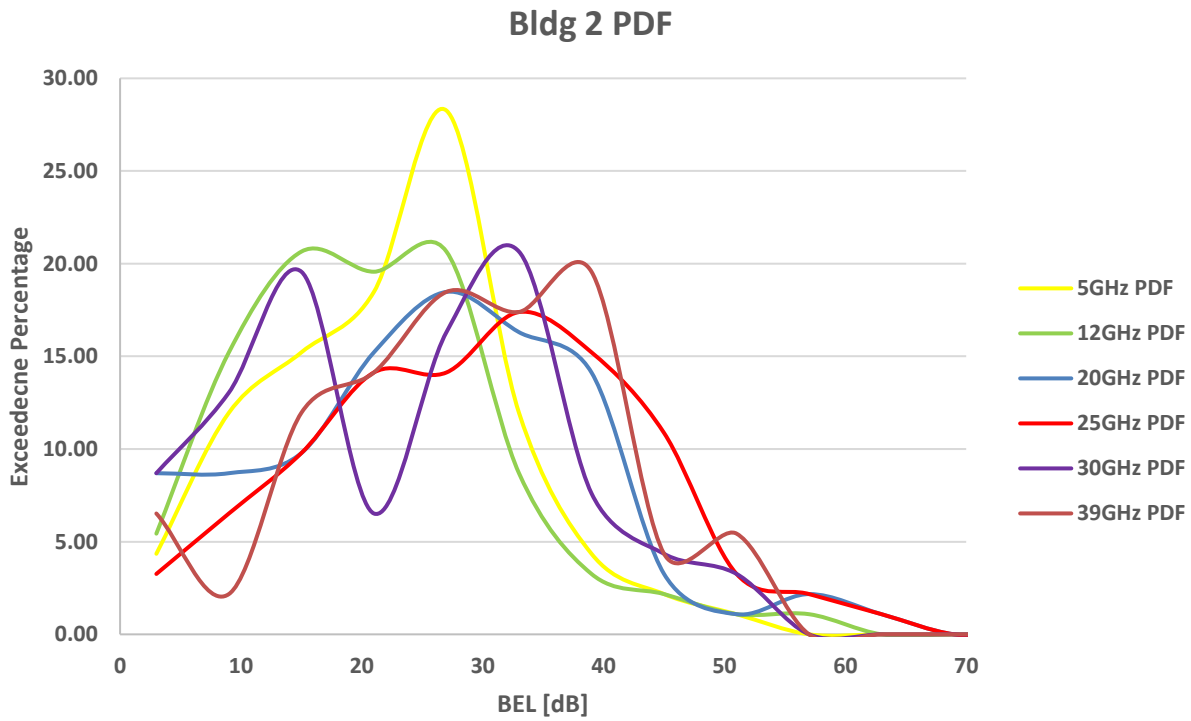

FIGURE 196

BEL PDFs for building 3

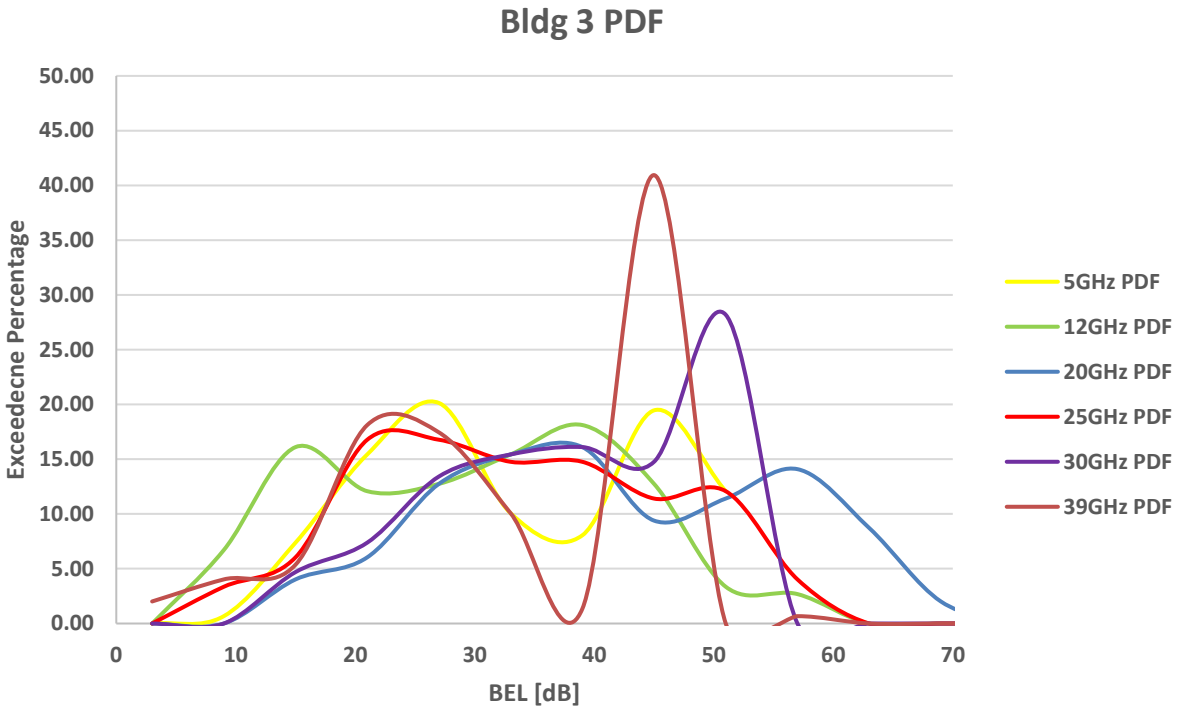

FIGURE 197

BEL PDFs for building 4

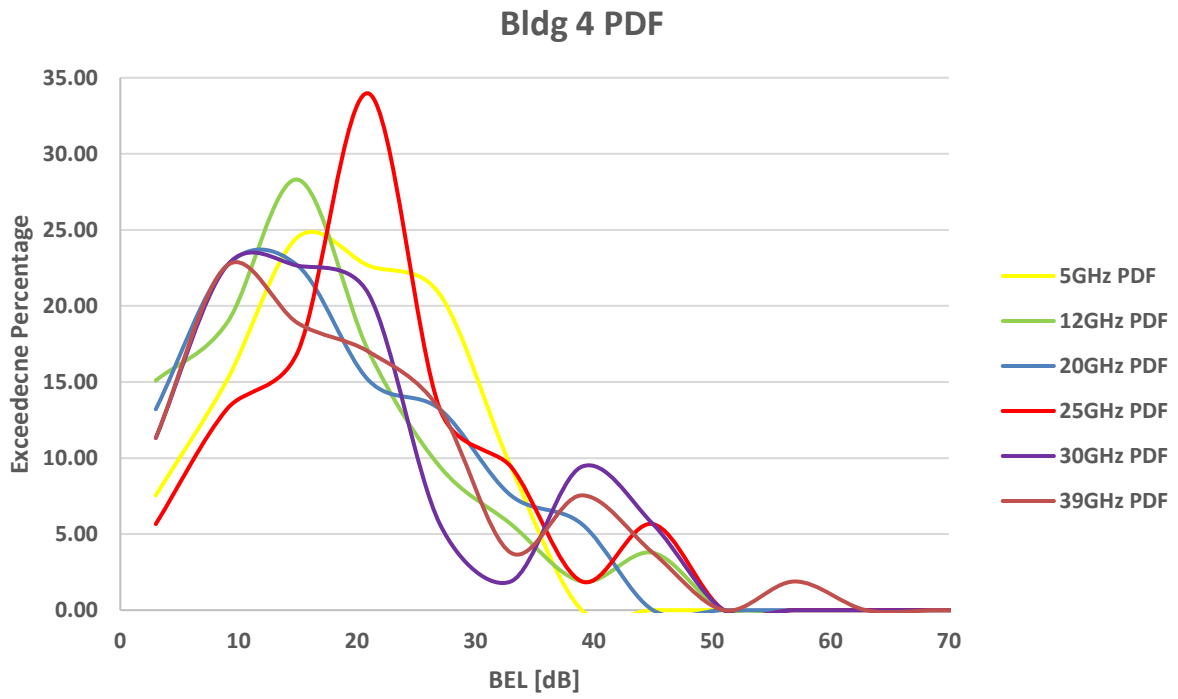

FIGURE 198

BEL PDFs for building 5

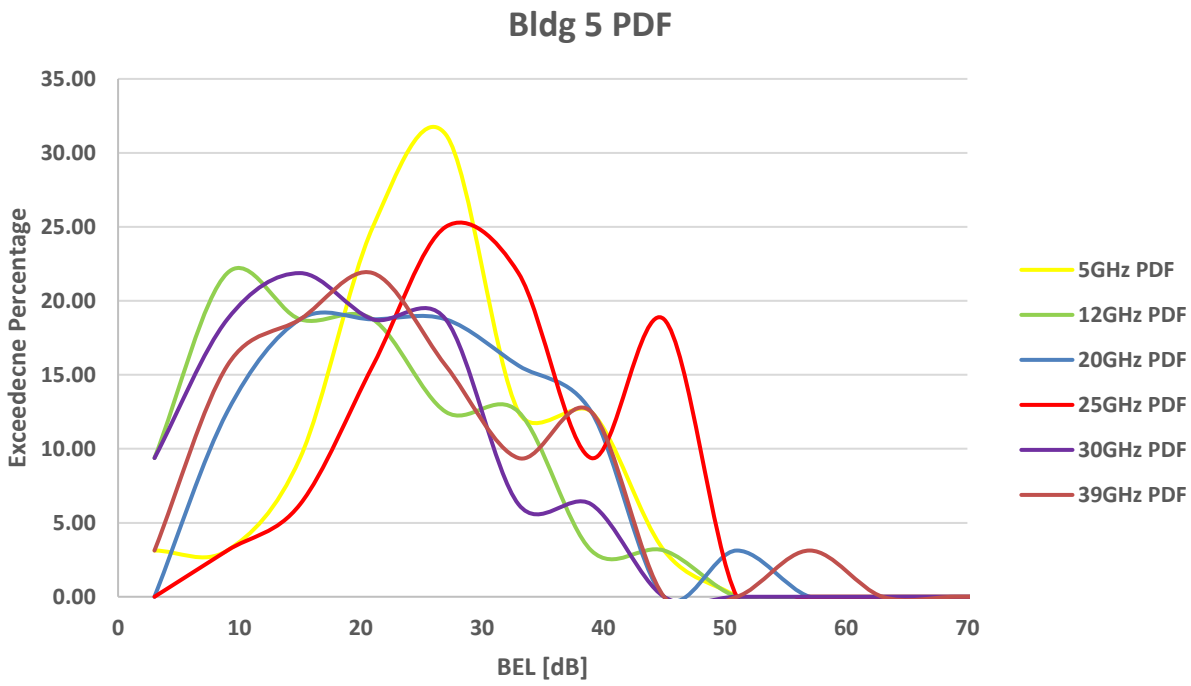

24.3.4 CDF Distributions

Next the probability density functions (PDFs) of the data sets are considered.

FIGURE 199

BEL CDFs for building 1

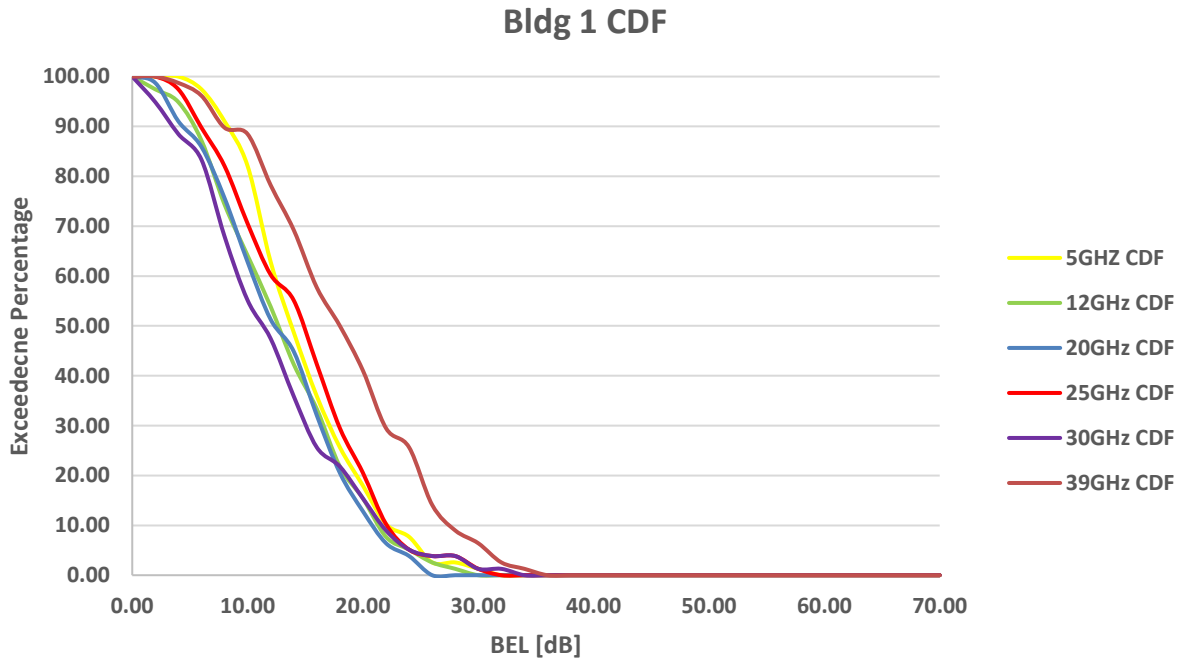

FIGURE 200

BEL CDFs for building 2

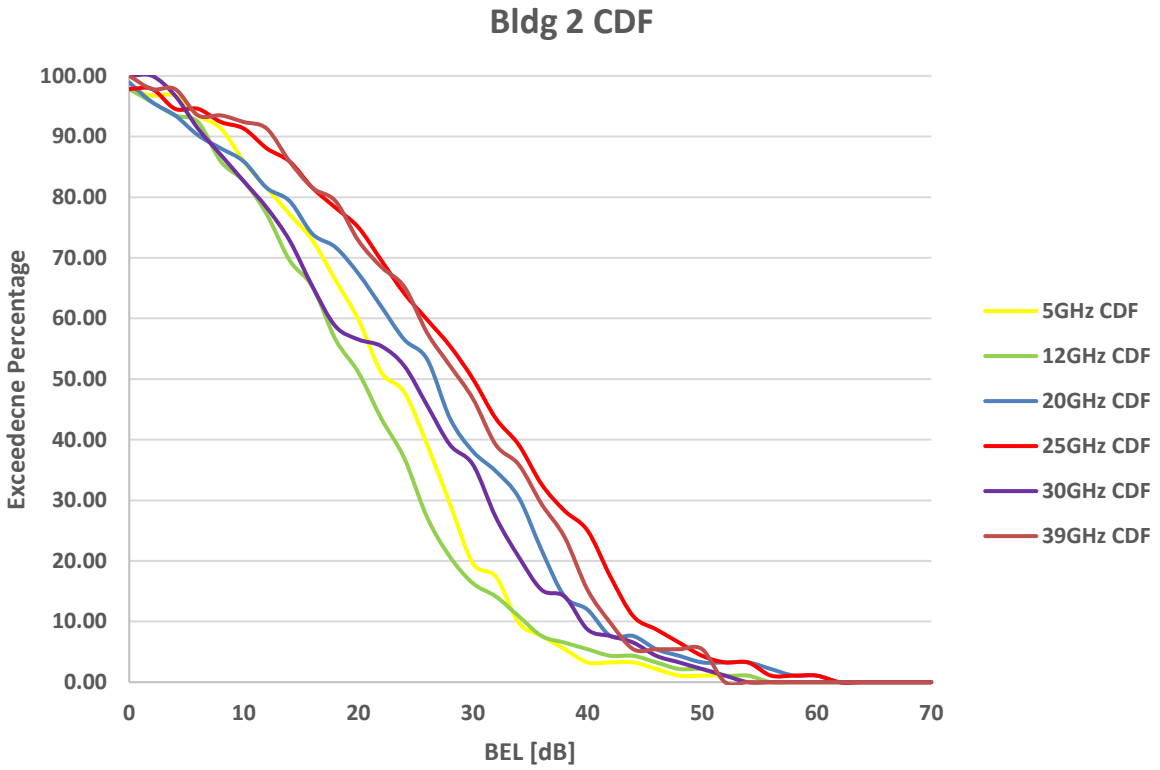

FIGURE 201

BEL CDFs for building 3

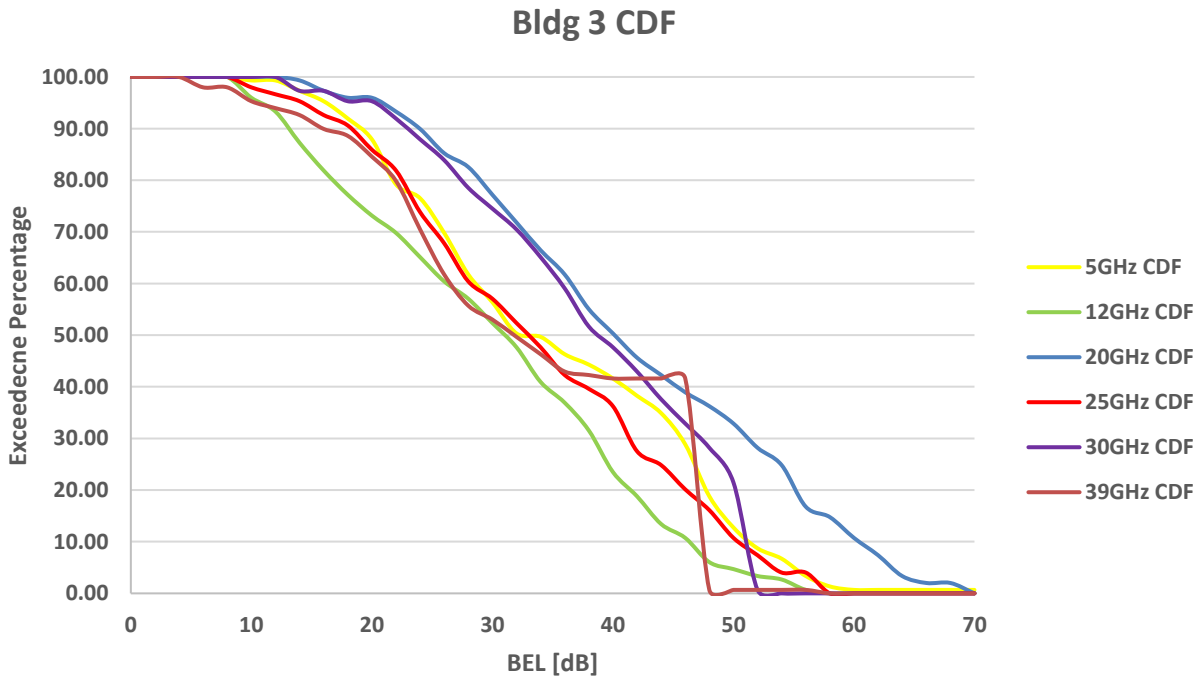

FIGURE 202

BEL CDFs for building 4

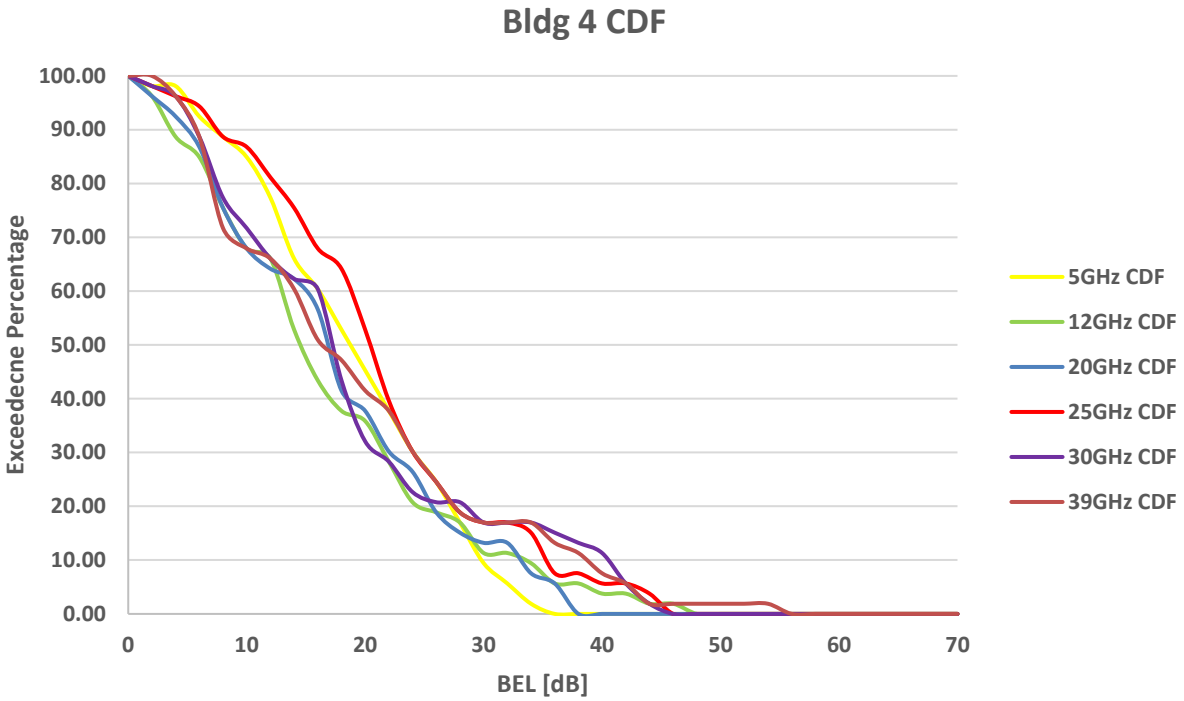

FIGURE 203

BEL CDFs for building 5

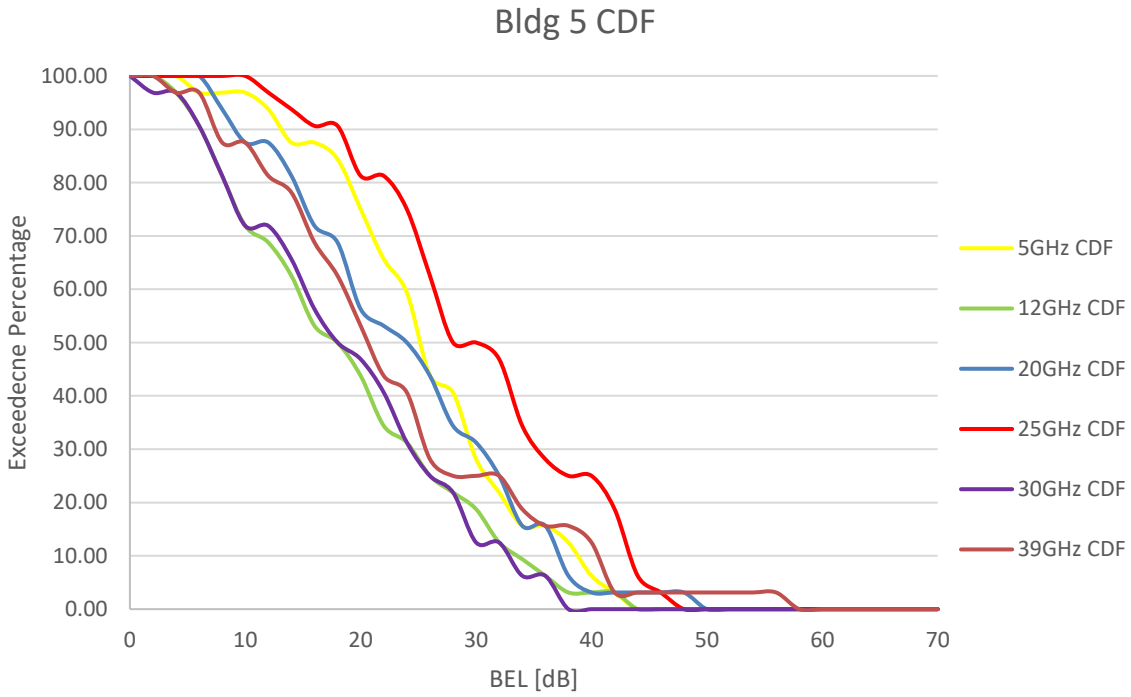

24.3.5 BEL vs frequency

Next the frequency dependence of the BEL is examined.

FIGURE 204

Frequency dependence of BEL

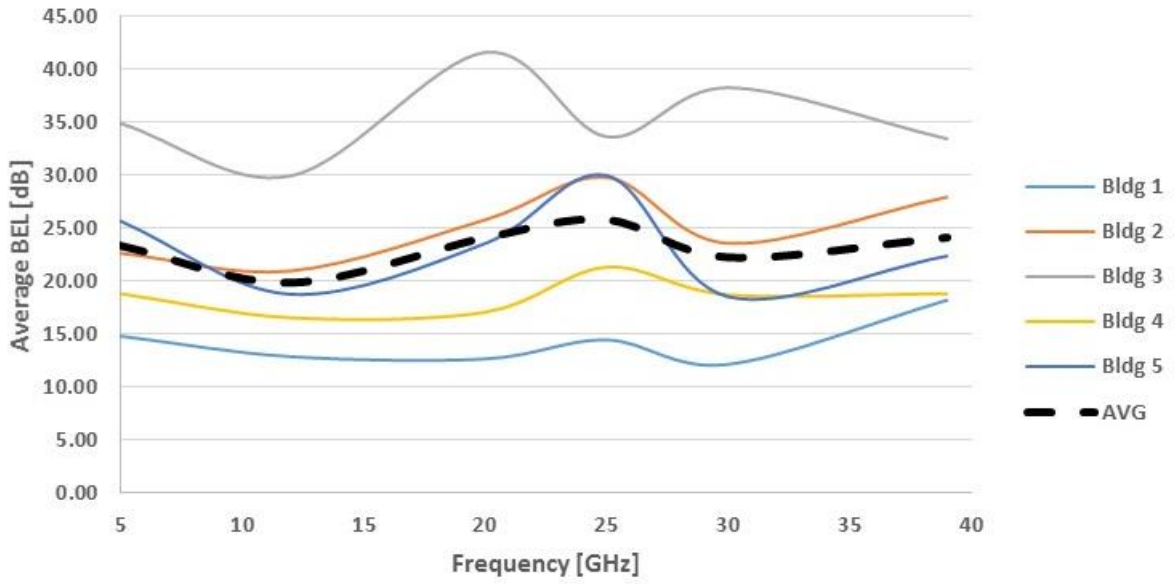

24.4 Conclusion

This chapter presented the BEL characterization of 5 different building; each represented different construction periods with a variety of different building materials. There are many variables which must be considered when evaluating BEL and this experiment sought to eliminate as many variables as possible and focus only of the actual loss introduced by the building itself.

25 Measurements on slant-path BEL in bands around 24 GHz from Telstra

25.1 Introduction

This chapter outlines the results of a measurement campaign on slant-path building-entry loss undertaken in Melbourne Australia. The objective of this campaign was to determine the additive losses due to the building structure and materials as experienced by IMT-2020 signals in bands around 24 GHz. This measurement campaign was undertaken in early-2017 by a research team from Victoria University[16] with funding support provided by Telstra Corporation Ltd.

25.2 Approach

The measurement campaign was undertaken on the campus of Victoria University in Melbourne, Australia. The target building is comprised of steel-reinforced concrete for structure and floors, with double-brick external walls and a mix of double-brick and stud-and-plaster internal walls, topped by a near-flat zinc-coated ribbed-steel roof. The windows are single-glazed and set into aluminium frames. The general structural situation of the buildings under test is shown below, including the two transmitting antennas (Tx1 and Tx2):

[16] Dr Shabbir Ahmed, Mr Saurav Dahal, Dr Mike Faulkner.

FIGURE 205

General view of measurement scenario – from Tx site (Building G, roof)

The buildings might generally be considered as ‘traditional masonry construction’ with minimal thermal efficiency measures. Further details of the building layouts and surrounds are provided in Appendix 1.

Two calibrated horn antennas were mounted on the parapet of Building G, to illuminate two of the target Building E tower sections. Each antenna was individually down-tilted and adjusted for boresight illumination of the particular target floor within Building E, and the different target floors providing a range of slant-angles of incidence. The general physical layout of the measurement environment is illustrated in Appendix 1, and detailed illumination areas and the specific slant-angles of incidence for each floor are illustrated in Appendix 2.

Each of the transmitting horn antennas was connected to a transmitter providing a continuous-wave (CW) narrow-band signal. Each of the antennas was pointed at different sections of the building-under-test.

The ‘mobile’ receiver consisted of a calibrated standard horn antenna connected to two low-noise-amplifiers (in series) that provided an aggregate gain of 55.0 dB (including connecting cables), and fed into a swept-frequency spectrum analyser with resolution bandwidth set to 50 kHz. This setup resulted in an effective noise-floor of −71.5 dBm (in 50 kHz) at the input of the spectrum analyser. The 50 kHz resolution bandwidth of the spectrum analyser is taken to be the effective Rx noise bandwidth.

Further details of the transmitter and receiver system set-up are given in the following Table:

TABLE 72

Test equipment key parameters

Parameter	Value
Tx height above RefGL (m)	23.5
Nominal Tx frequency: Tx #1 Tx #2	 24.002 GHz 24.000 GHz
Tx emission level (at output): Tx #1 Tx #2	 11.5 dBm 8.5 dBm
Tx antenna type	Calibrated horn
Tx antenna gain	17 dBi
Tx antenna beamwidth (3dB)	20^0
Tx antenna down-tilt (range)	$32\text{-}54^0$
Rx height above RefGL (m)	1.5 m
Rx antenna type	Calibrated horn
Rx antenna gain	9.6 dBi
Rx antenna beamwidth (3dB)	47.5^0

For each measurement azimuth/elevation data point, the spectrum analyser made 10 sweeps and recorded the average received power over these sweeps, and this process repeated 3 times. Thus, the overall average power for each data point is derived from a total of 30 sweeps (over a period of 1-2 seconds). This, together with small perturbations in the physical positioning of the receiver antenna at each measurement location (as elevations were adjusted) was assumed sufficient at this frequency to randomise the phasing of the multipath components.

To establish external incident signal level reference values, a series of measurements were taken at several locations immediately outside of the target Building E. Within the building, a series of measurements was made, which included locations near to windows and central locations within each room. To account for potential external/internal reflections, and direct bore-sight components (if any), measurement data-sets were developed for various up/down-tilt angles and in 7^o azimuth increments (resulting in over 400 measurements per location, and about 24,000 overall).

Two approaches were adopted in relation to determining the effective received signal power: a) measurement of the received power in the strongest multipath cluster – that is, the highest receive power over all the measured pointing directions (azimuth and elevation), and termed the “peak” received power; and b) measurement of the received power that would be received by a reference isotropic antenna – that is, the aggregate (or sum) received power integrated over all directions, and termed the “omni” received power.

Throughout the measurement campaign, the weather was fine with typical temperature (20^0C) and humidity (40%) for the spring period in south-eastern Australia.

The detailed graphical results for each of the measurement locations can be found in Appendices 3, 4 and 5 to this chapter.

25.3 Observations & Results

To more conveniently characterise the BEL, these studies sought to determine the deviation from the free-space path loss (FSPL) caused by the building structure, and based on determining d_o and α in the generic formula:

$$PL_d = FSL_{d_0} + 10log\left(\frac{d}{d_0}\right)^{\propto}$$

Where:

d = linear (laser) distance between Tx and the respective Rx measurement point

d_0 = FSPL intercept point for line-of-best-fit

α = path loss exponent for line-of-best-fit

FSL_{d0} = free space path loss at best-fit intercept point.

The method of *minimum mean square error* (MMSE) was used to determine the effective 'line of best fit' for the BEL factor for each floor level and encompassing the relevant indoor measurement data points.

While the measured data also indicates that aggregate path loss increases as the measurement locations move deeper inside the building, the increasing loss with internal depth does not appear to be a linear function of distance – suggesting the existence of a more complex multipath environment within the building depending on specific internal walls, wall angles, and possible furniture/other items.

However, in considering the line-of-best-fit, we can observe a notable and incremental BEL factor over FSPL (versus distance between Tx and Rx), that is generally characterised by the FSPL intercept point (d_0) and the BEL path loss exponent (PLE).

A cumulative distribution function (CDF) was also created of the differential path loss compared to FSPL for each floor, which reveals several apparent trends:

- There is an almost uniform 4 dB difference between the 'peak' and 'omni' path loss factors, for every floor.
- The BEL generally decreases with floor height (AGL) - thought to be due to lower angle-of arrival and decreasing internal floor/ceiling reflections and thus lower internal multipath complexity.
- The variance of measured levels on each room also generally decreases with floor height (AGL) – again thought to be associated with lower angle-of-arrival, greater fraction of power from the direct signal, along with lower internal multipath complexity.

A summary of the key results for each floor are provided in the following Tables:

TABLE 73

Summary of measured BEL results – Tx2 (Frequency 2)

Floor level	Angle of Arrival (elev) (Tx2)	Mean BEL (peak) compared to FSPL (dB)	Mean BEL (omni) compared to FSPL (dB)	Line-of-best fit (peak/omni)		
				Intercept with FSPL (d_0) (m)	Path Loss Exponent (α)	Std Deviation (dB)
1 (Grnd)	54.0^0	41.80	37.84	15.83 15.43	15.39 13.70	7.82 6.33
2	49.5^0	39.23	35.22	11.01 12.37	11.25 11.43	6.03 5.30
3	39.0^0	35.29	30.98	9.28 10.50	9.38 9.30	8.88 7.59
4	37.0^0	34.44	30.22	14.00 14.75	15.36 14.85	4.19 4.13

And similar results were obtained for Tx1 (Frequency 1):

TABLE 74

Summary of measured BEL results – Tx1 (Frequency 1)

Floor level	Angle of Arrival (elev) (Tx1)	Mean BEL (peak) compared to FSPL (dB)	Mean BEL (omni) compared to FSPL (dB)	Line-of-best fit (peak/omni)		
				Intercept with FSPL (d_0) (m)	Path Loss Exponent (α)	Std Deviation (dB)
1 (Grnd)	49.2^0	44.15	40.28	19.89 21.29	21.26 22.18	6.97 6.54
2	44.5^0	36.88	32.07	20.09 20.86	19.94 18.94	5.69 5.29
3	44.0^0	*[Insufficient measurement data]*				
4	32.5^0	32.50	26.85	17.26 18.22	17.78 16.73	4.73 3.79

More particularly, considering the measured results for each floor the following observations are offered:

- Overall additive BEL (compared to FSPL) for this ‘traditional’ style building at 24 GHz, varies over the range **30-42 dB**, depending on floor height (AGL) and angle-of-incidence:
  - Lower floors and/or higher angle-of-incidence exhibit higher BEL values.
- The derived PLE is higher as the measuring location recedes deeper inside the building – thought to be due to increasing complexity of the scattering environment.

25.4 Conclusions

Subject to the angle-of-arrival, realistic values for BEL for conventional/traditional masonry buildings with no special thermal efficiency measures appear to be in the range **30-40 dB** – and for ground-level rooms experiencing angles-of-arrival of greater than 39^0, a typical BEL value of around **40 dB** seems to be reasonable.

It is suggested that these building types are relatively common in many countries, and that such BEL values might be expected to be applicable to many urban and suburban scenarios.

25.A1 Attachment 1: General Building Layout – Buildings G and E, Victoria University, Melbourne, Australia

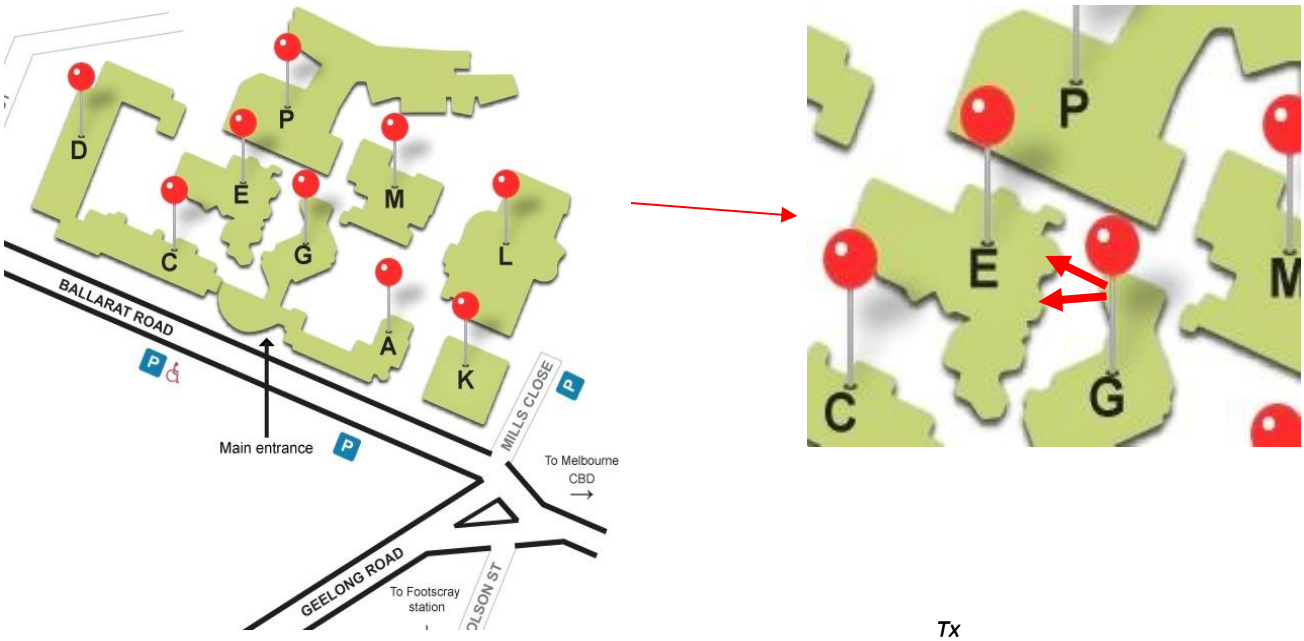

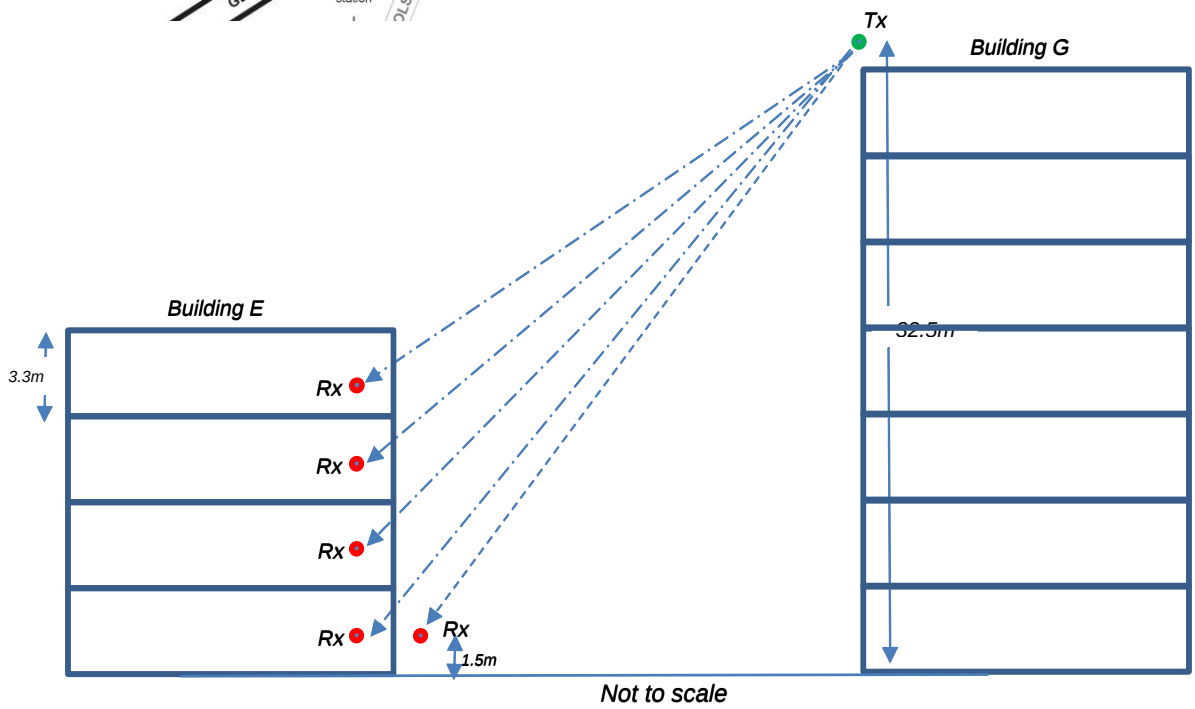

25.A2 Attachment 2: Detailed building illumination plans

2.1 Building E – Level 1 (Ground level)

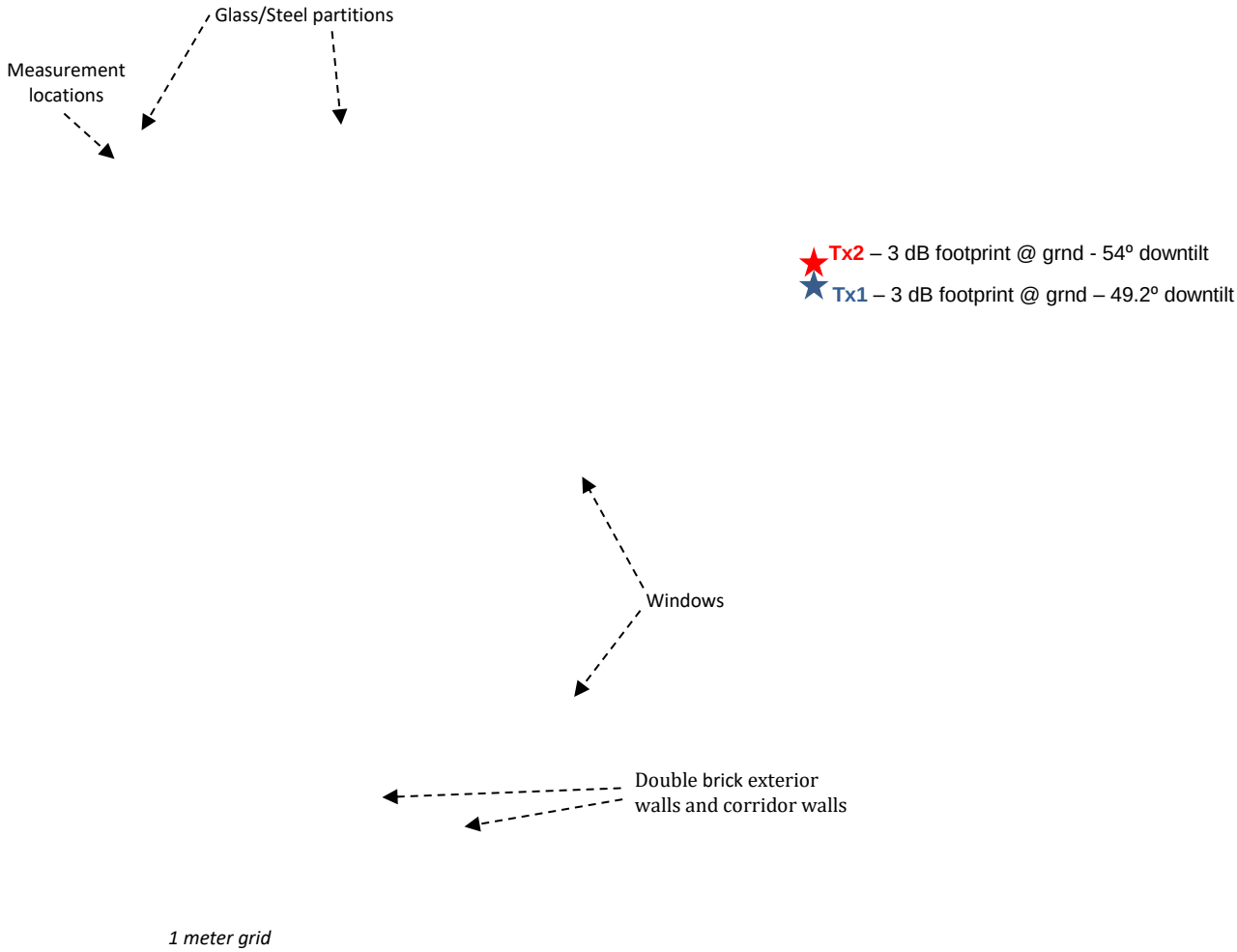

2.2 Building E – Level 2

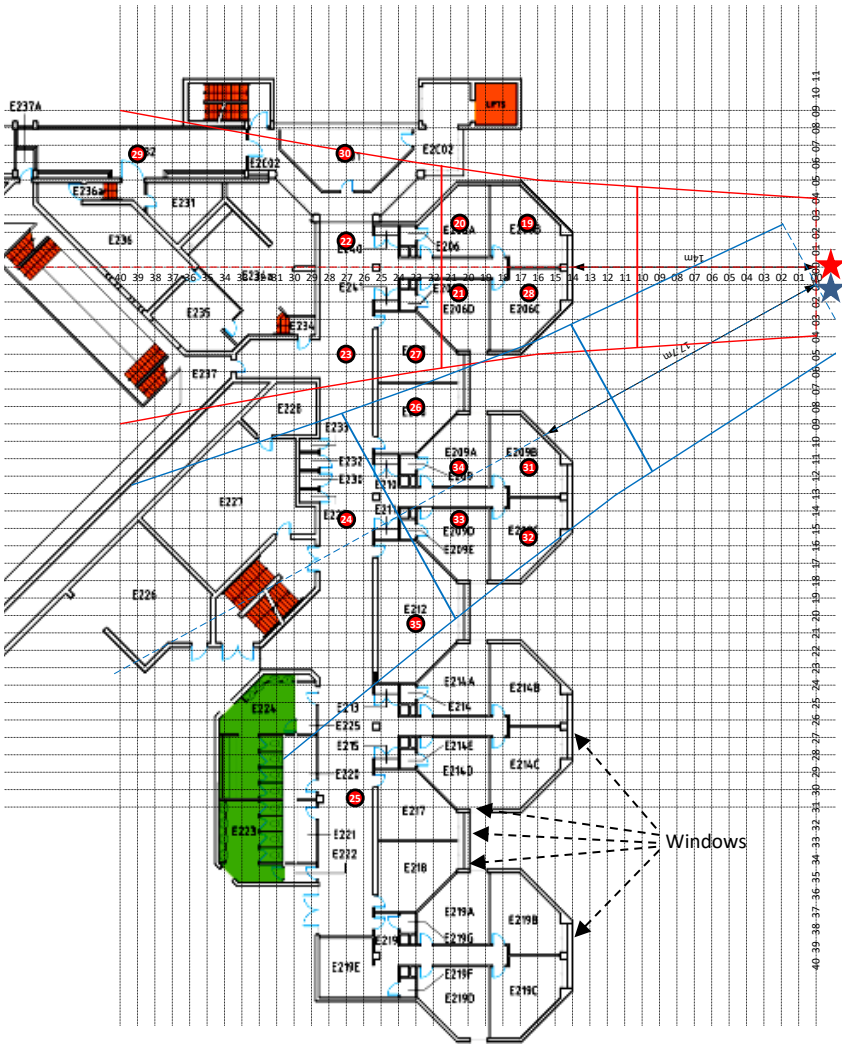

2.3 Building E – Level 3

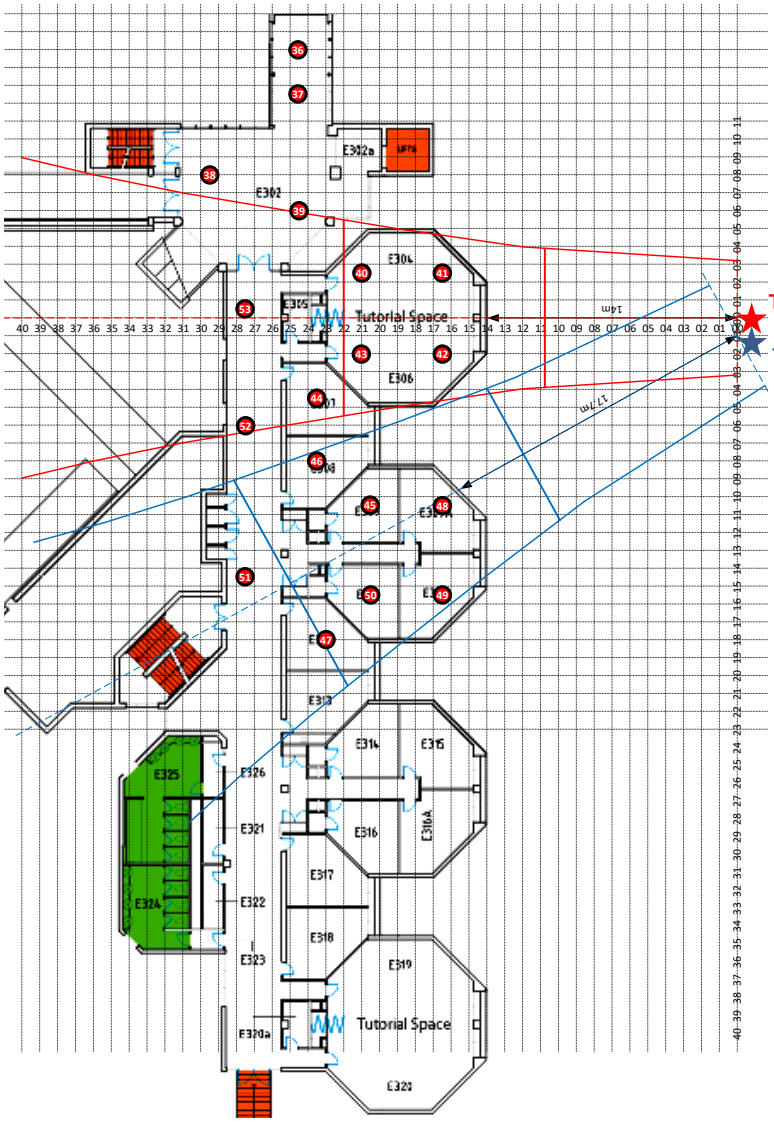

Tx2 – 3 dB footprint @ level3 – 44º downtilt

Tx1 – 3 dB footprint @ level3 – 39º downtilt

2.4 Building E – Level 4

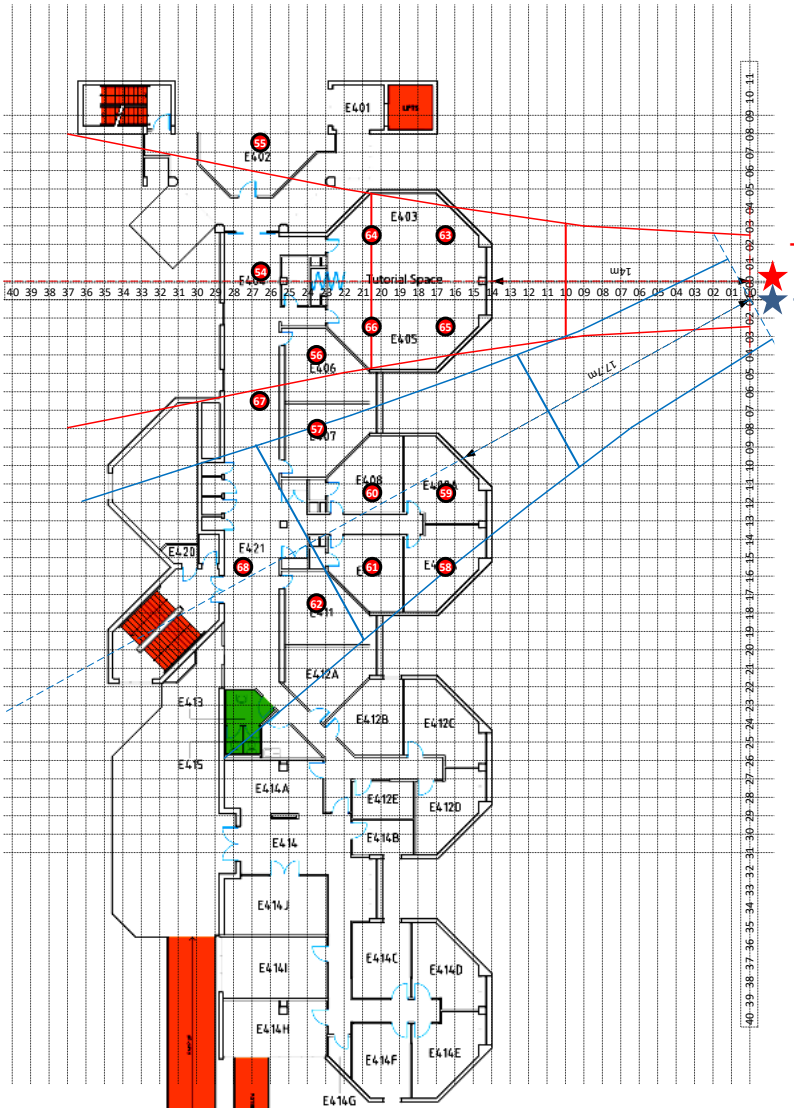

Tx2 – 3 dB footprint @ level4 – 37º downtilt

Tx1 – 3 dB footprint @ level4 – 32.5º downtilt

25.A3 Attachment 3: Detailed measurement results (Tx2 – Frequency 2)

Example measurements on Tx2 signal

3.1 Building E – Level 1 (Ground level)

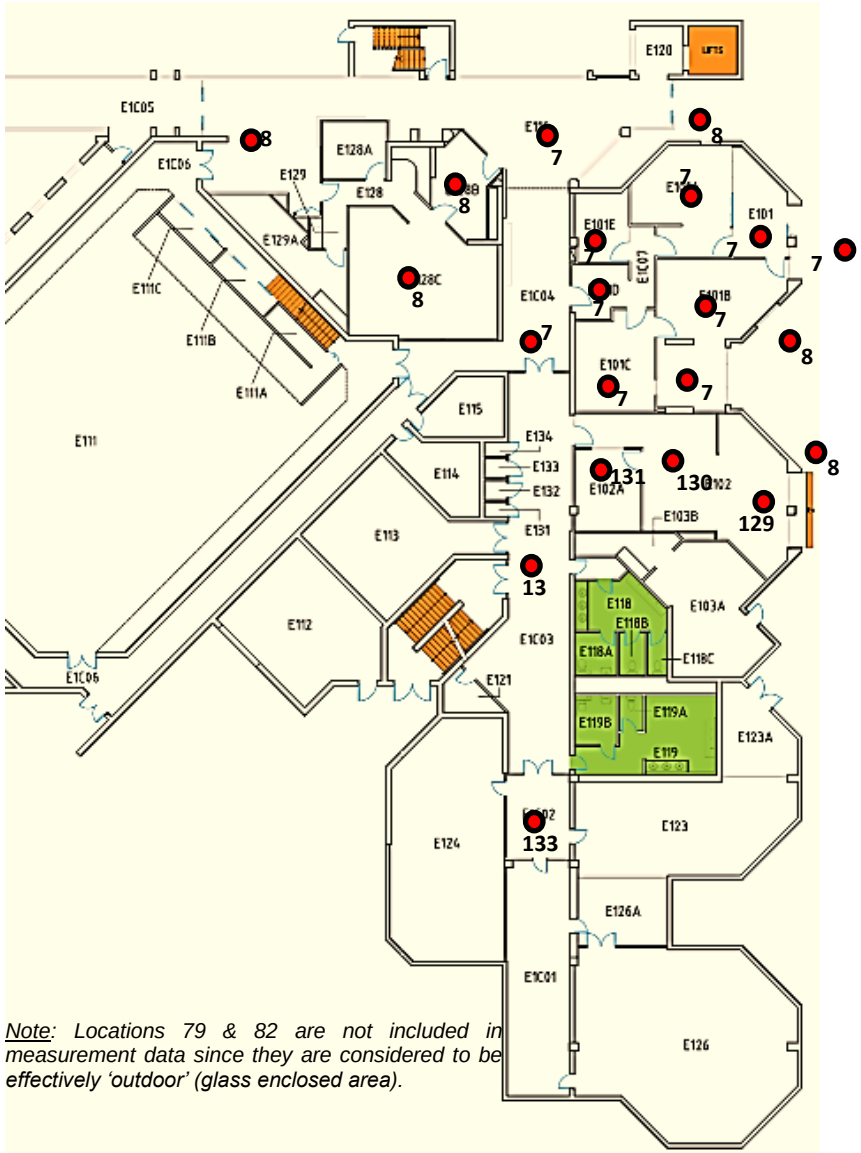

Note: Locations 79 & 82 are not included in measurement data since they are considered to be effectively 'outdoor' (glass enclosed area).

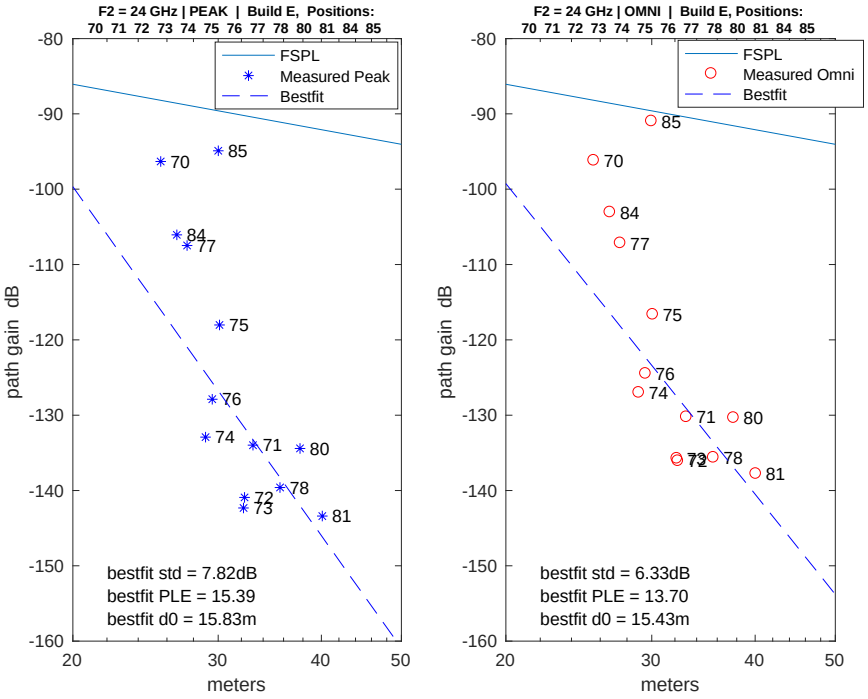

NOTE: Best-fit lines include only the indoor measurement points

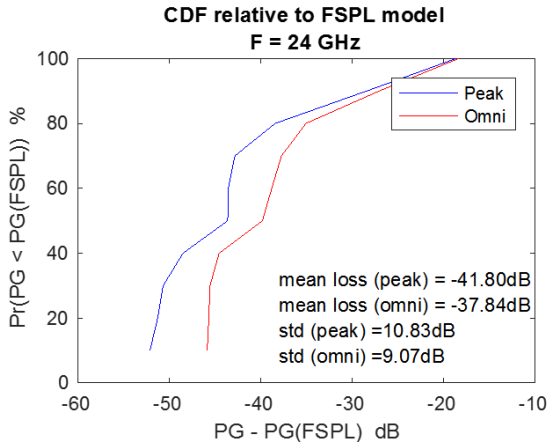

3.2 Building E – Level 2 (Tx2 – Frequency 2)

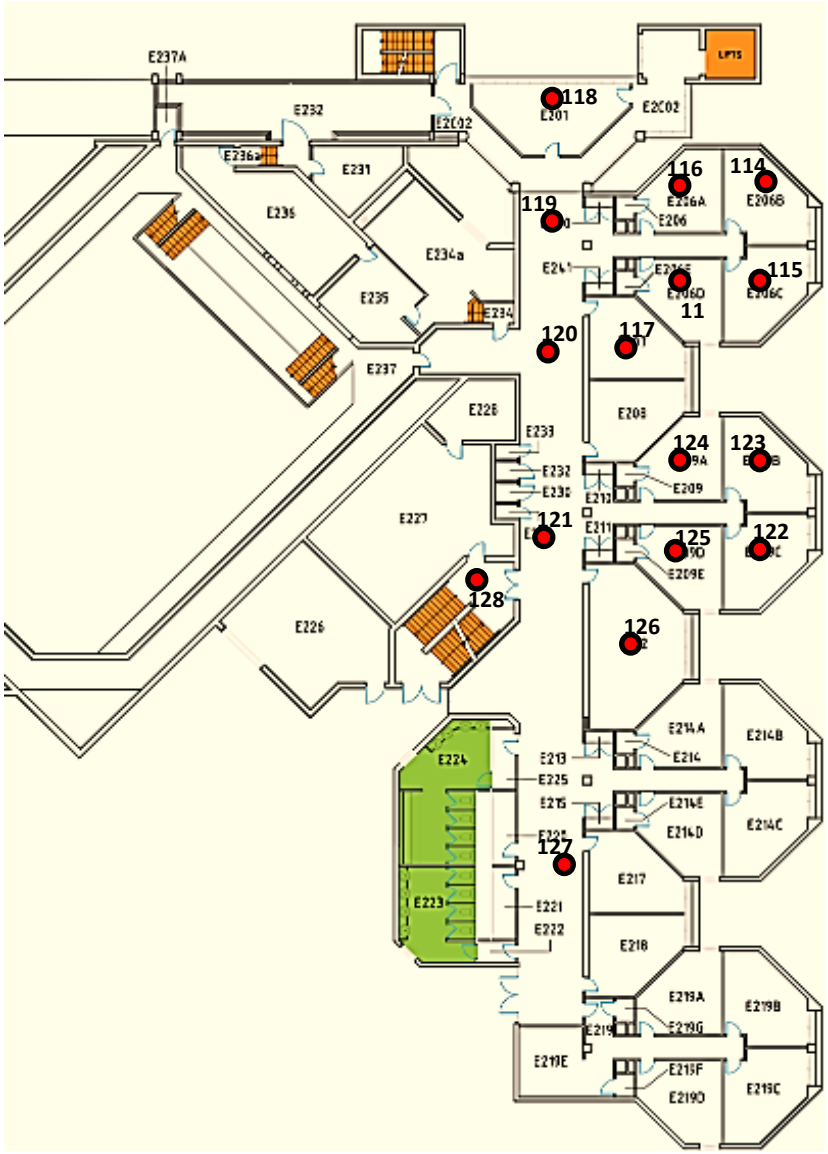

Example measurements on Tx2 signal

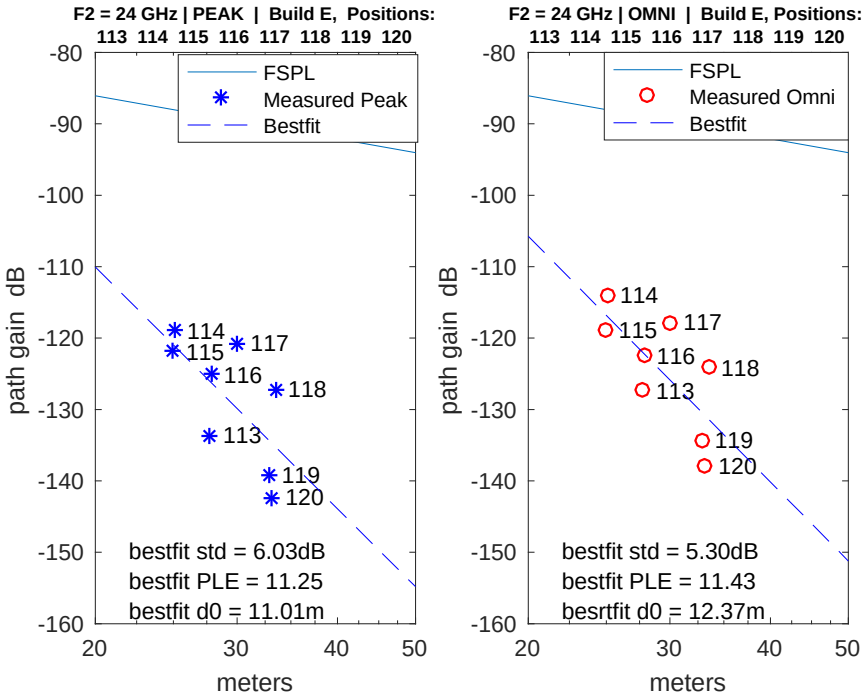

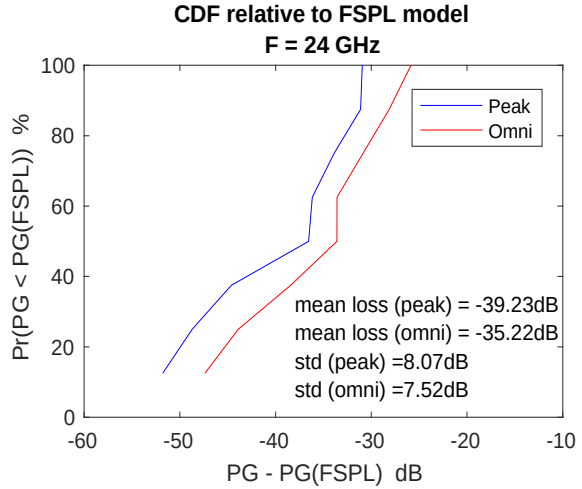

3.3 Building E – Level 3 (Tx2 – Frequency 2)

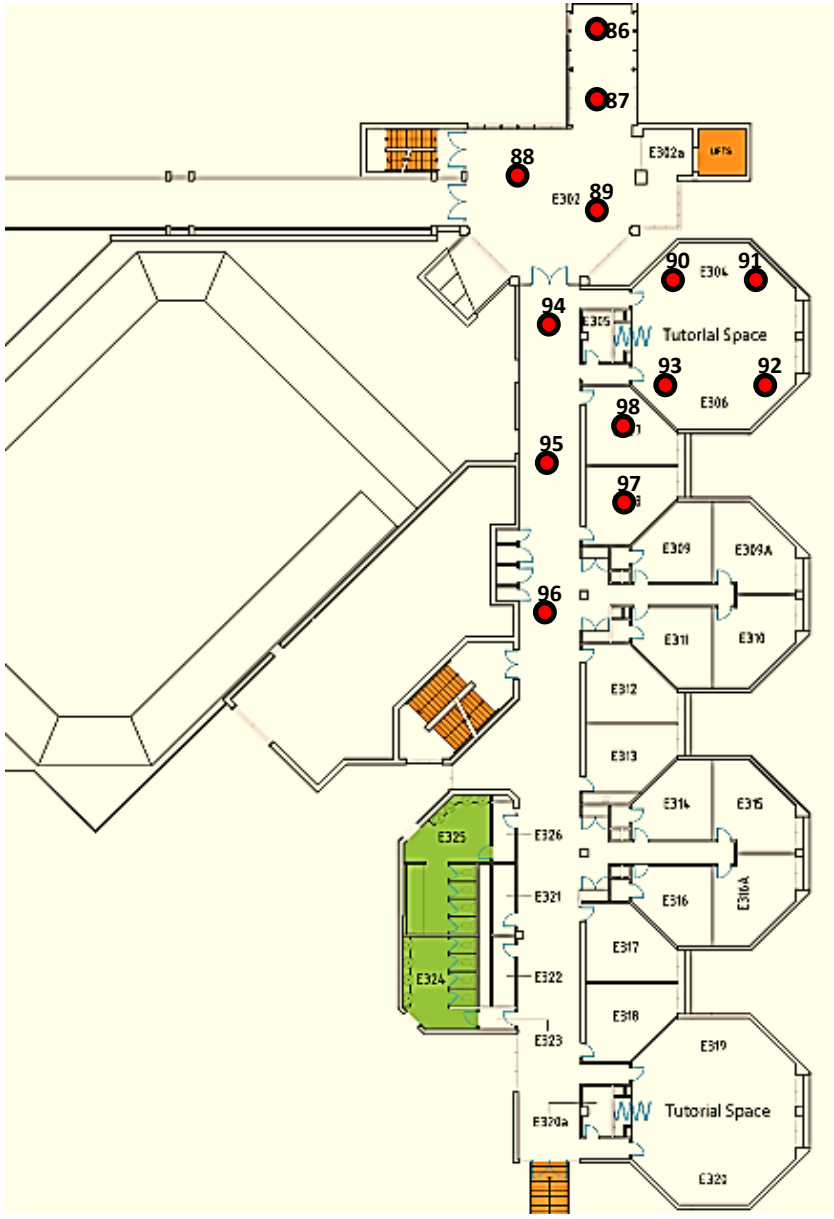

Example measurements on Tx2 signal

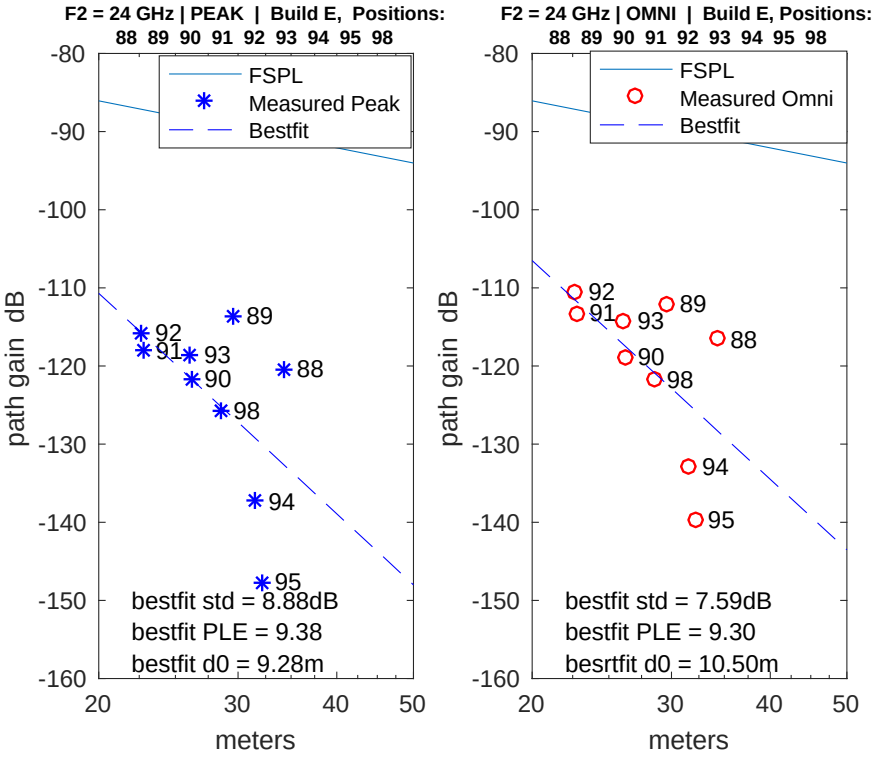

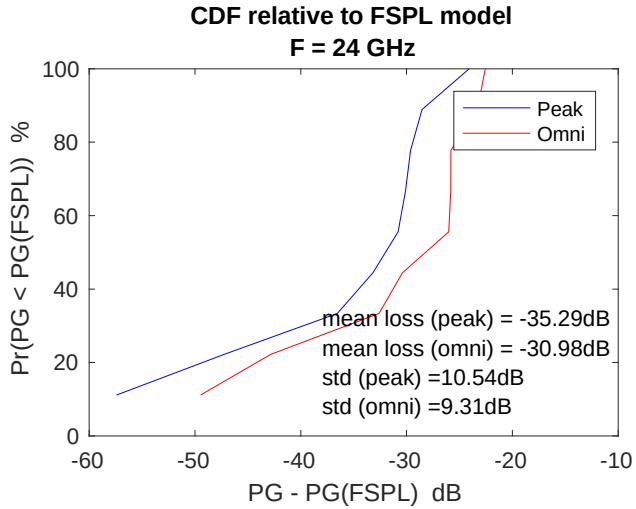

3.4 Building E – Level 4 (Tx2 – Frequency 2)

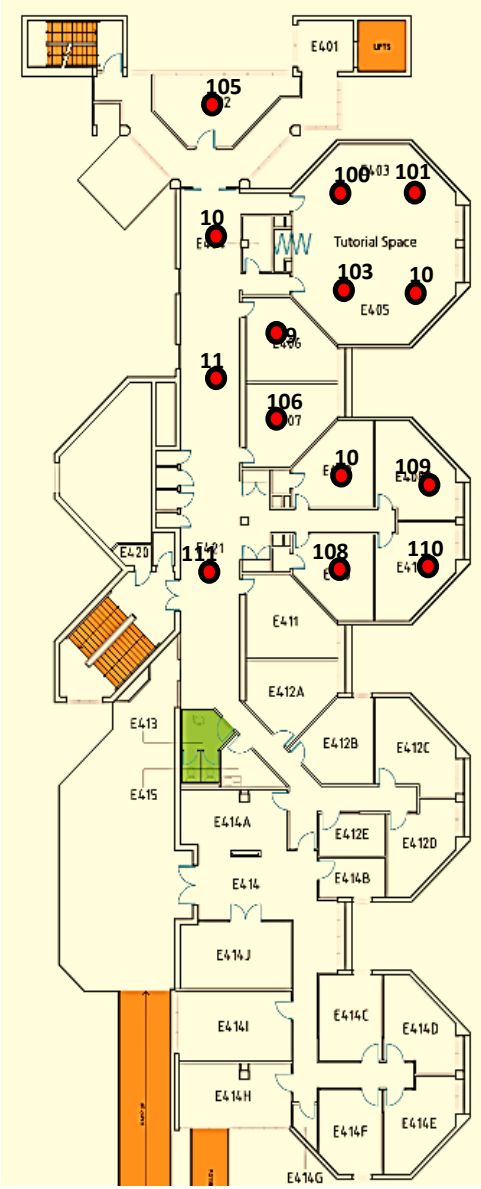

Example measurements on Tx2 signal

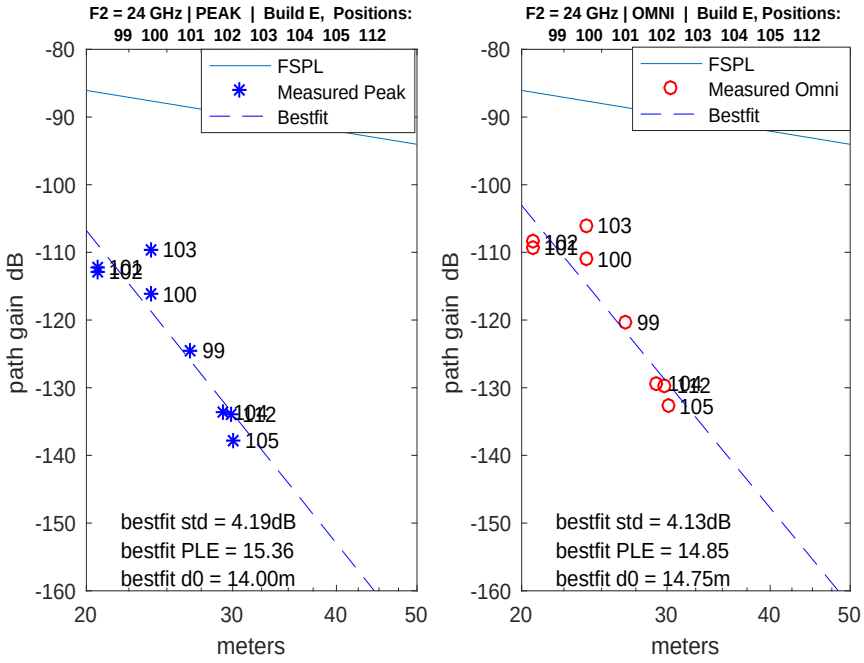

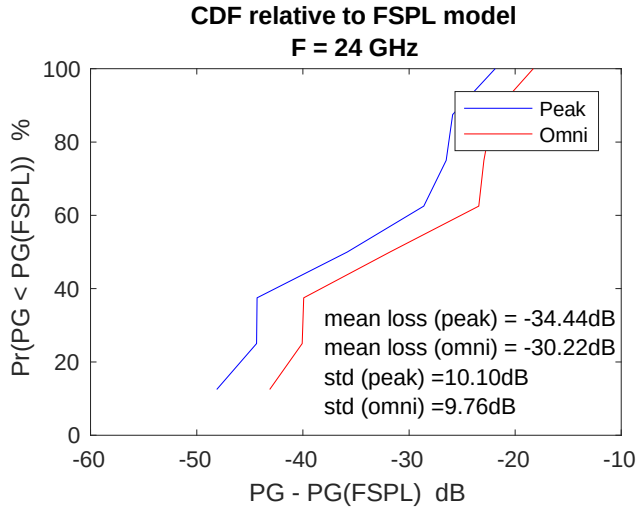

25.A4 Attachment 4: Detailed measurement results (Tx1 – Frequency 1)

4.1 Building E – Level 1 (Ground level)

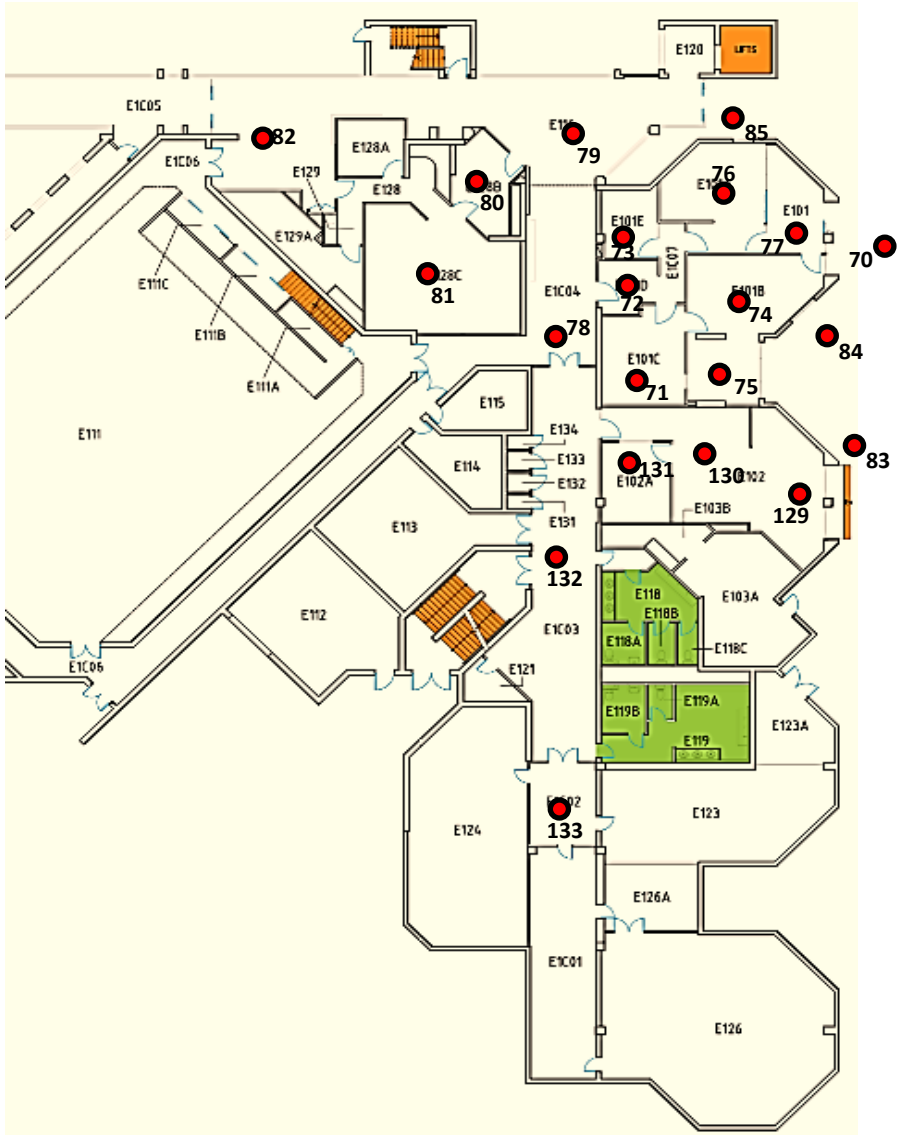

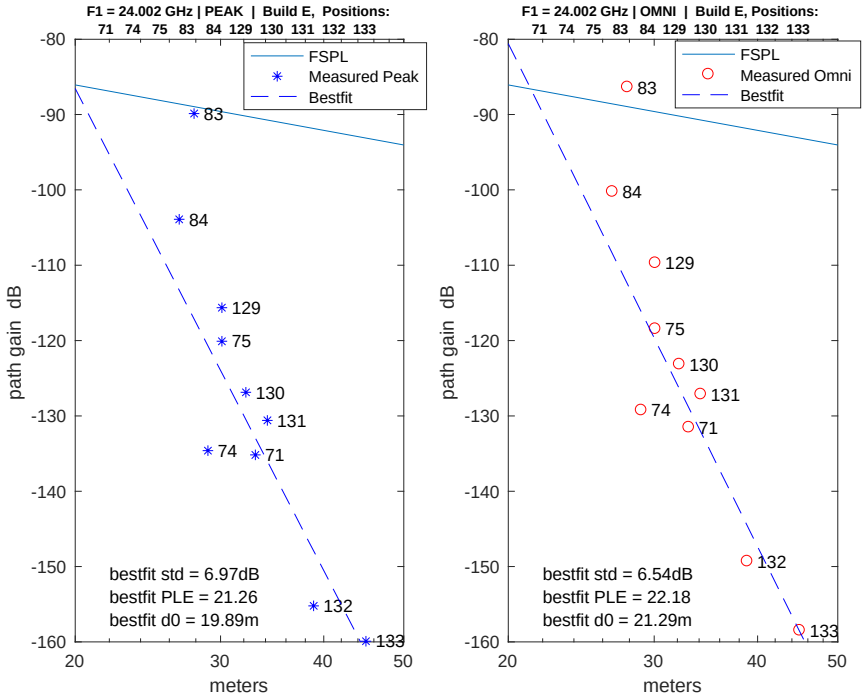

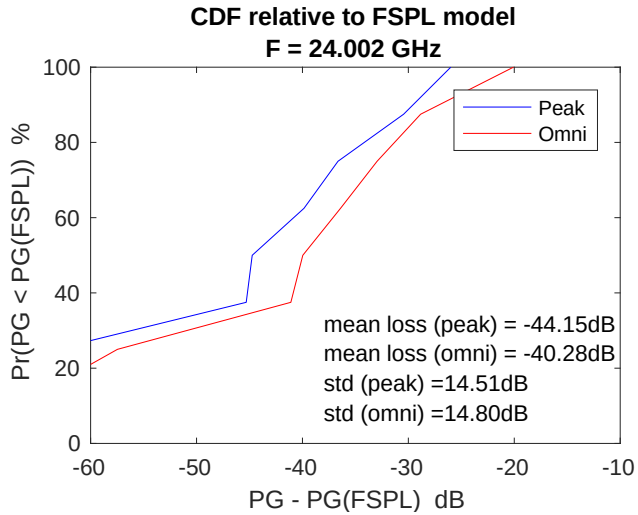

4.1 Building E – Level 2 (Tx1 – Frequency 1)

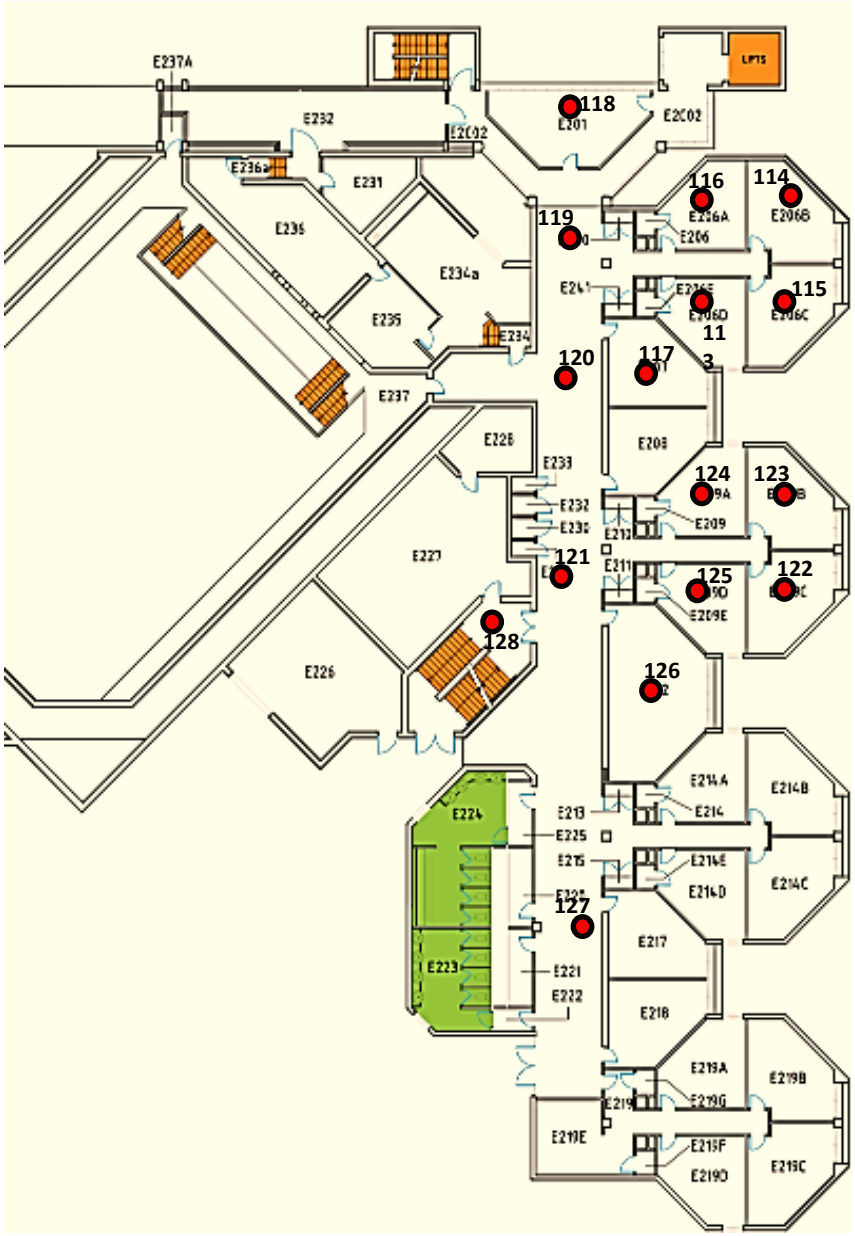

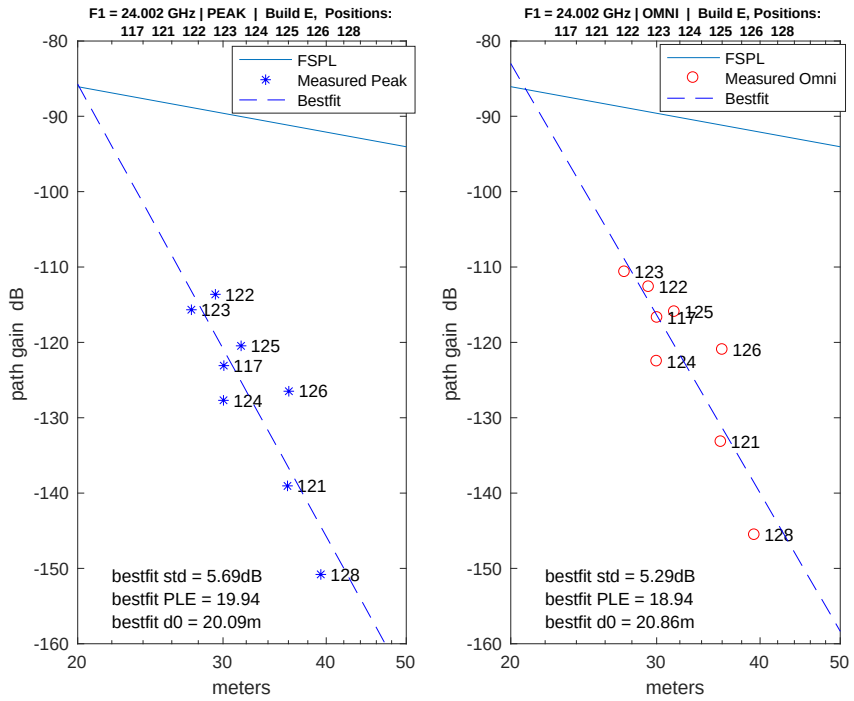

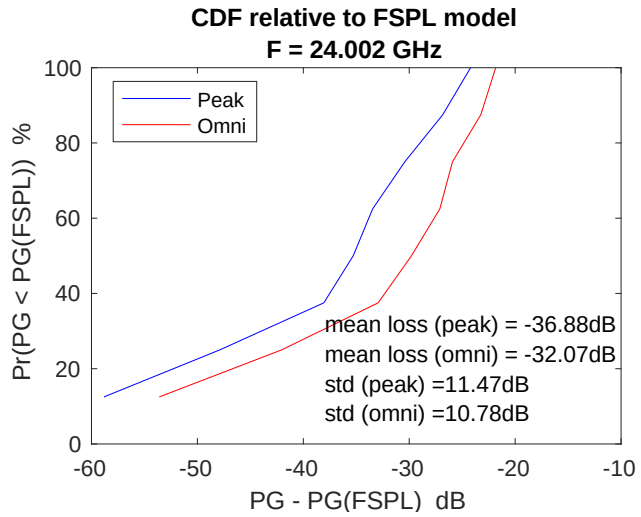

4.1 Building E – Level 3 (Tx1 – Frequency 1)

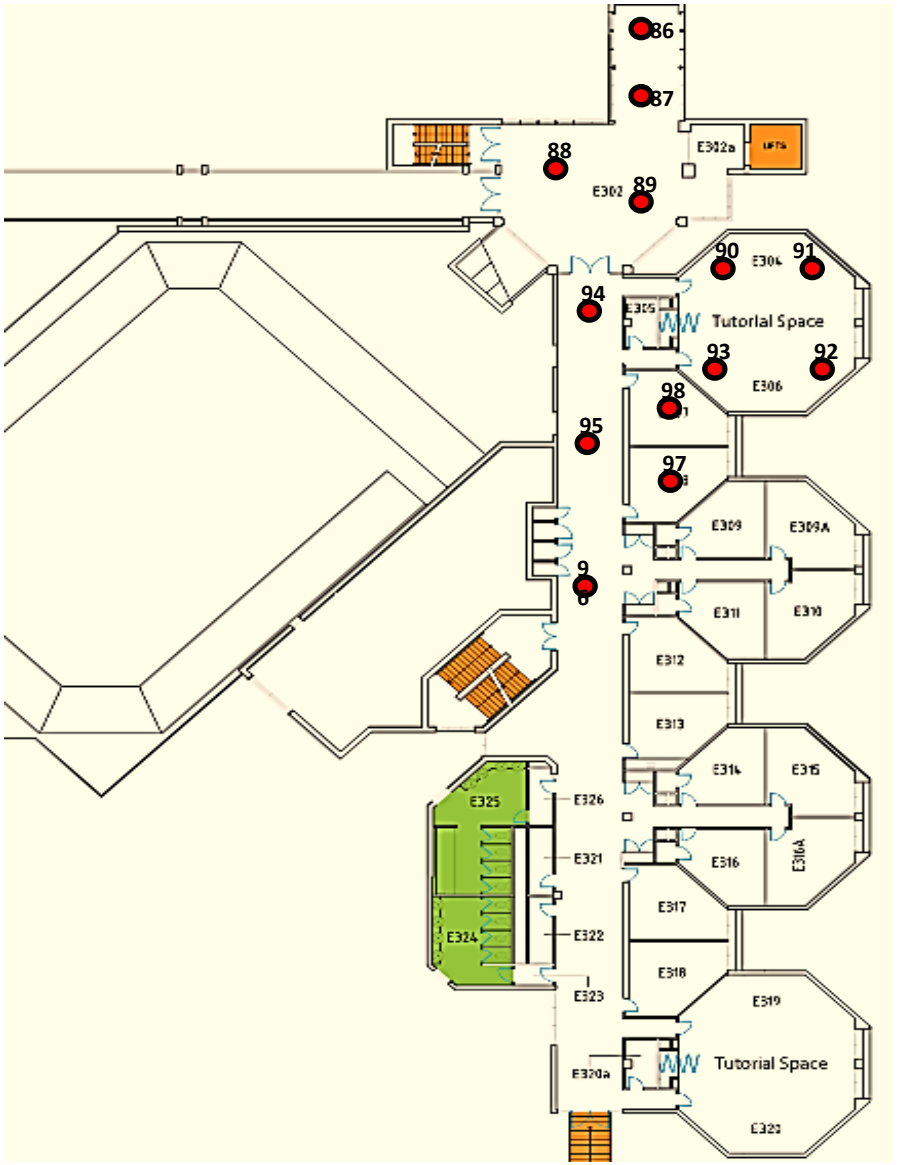

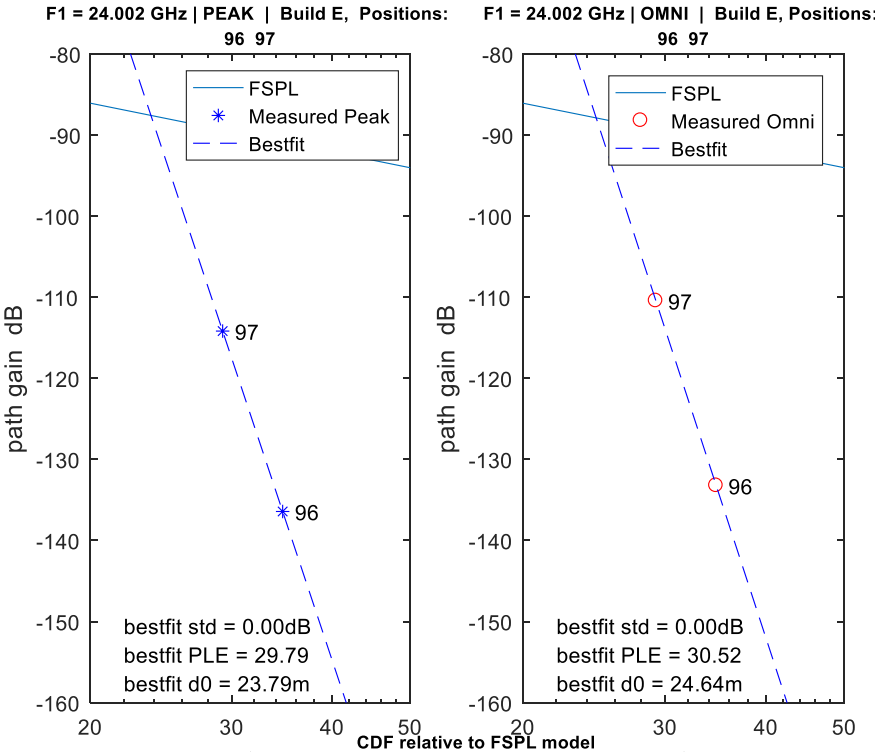

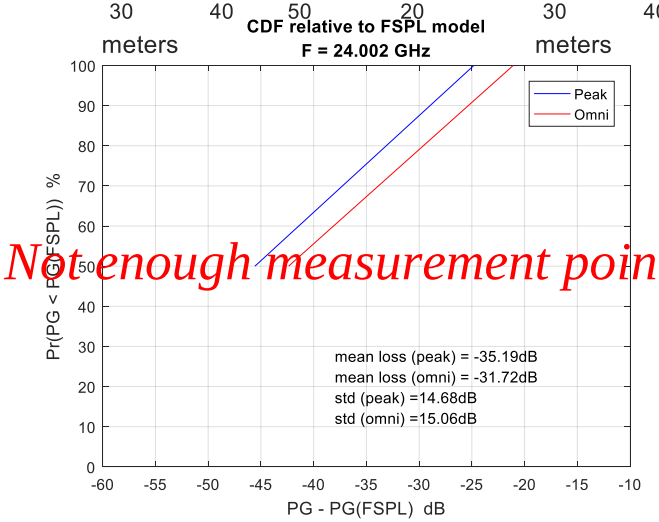

Not enough measurement points

4.1 Building E – Level 4 (Tx1 – Frequency 1)

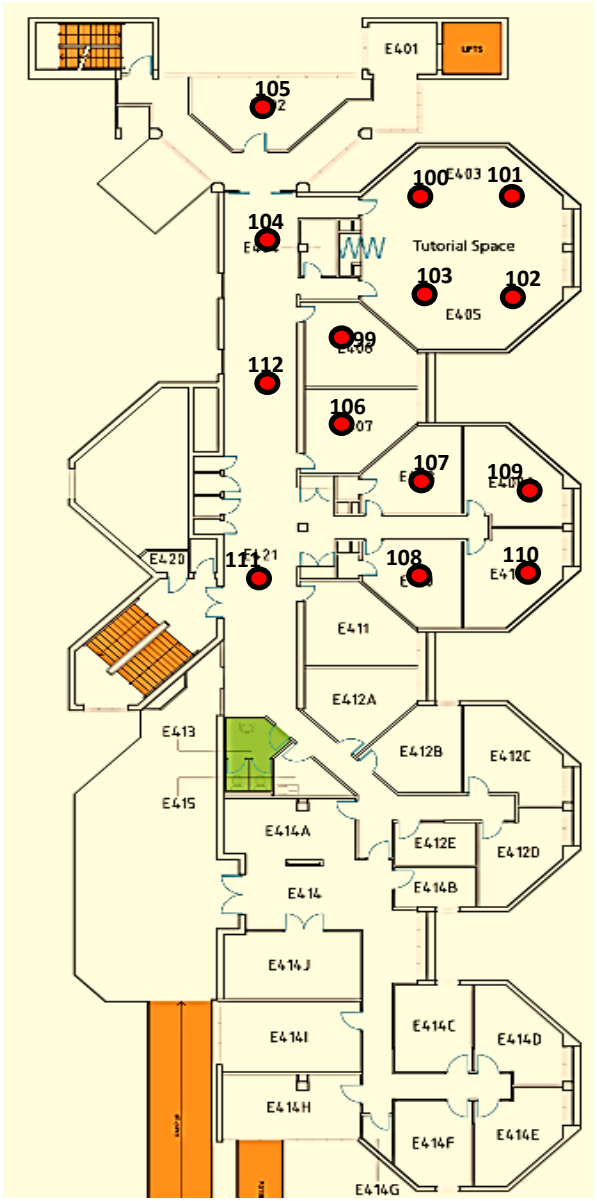

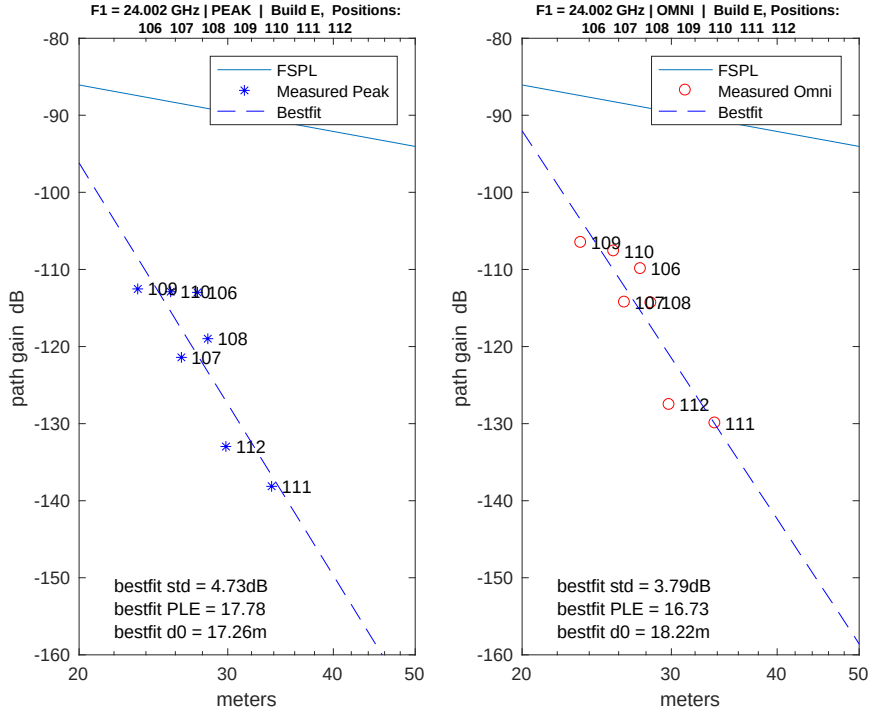

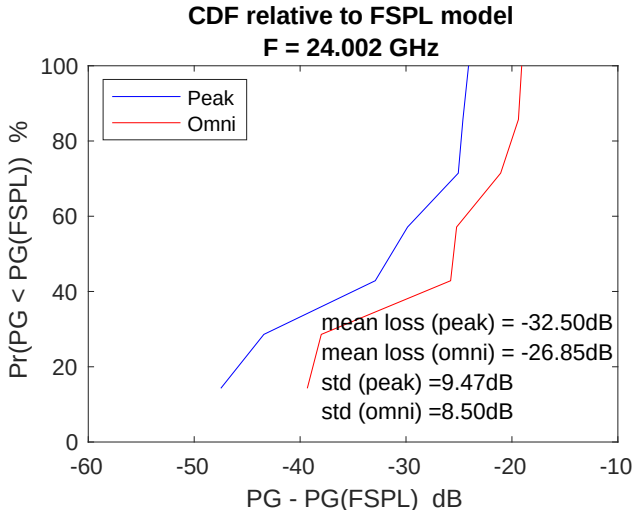

25.A5 Attachment 5: Mean BEL vs AoA

5.1 Building E – Tx2 'peak' and 'omni' cases

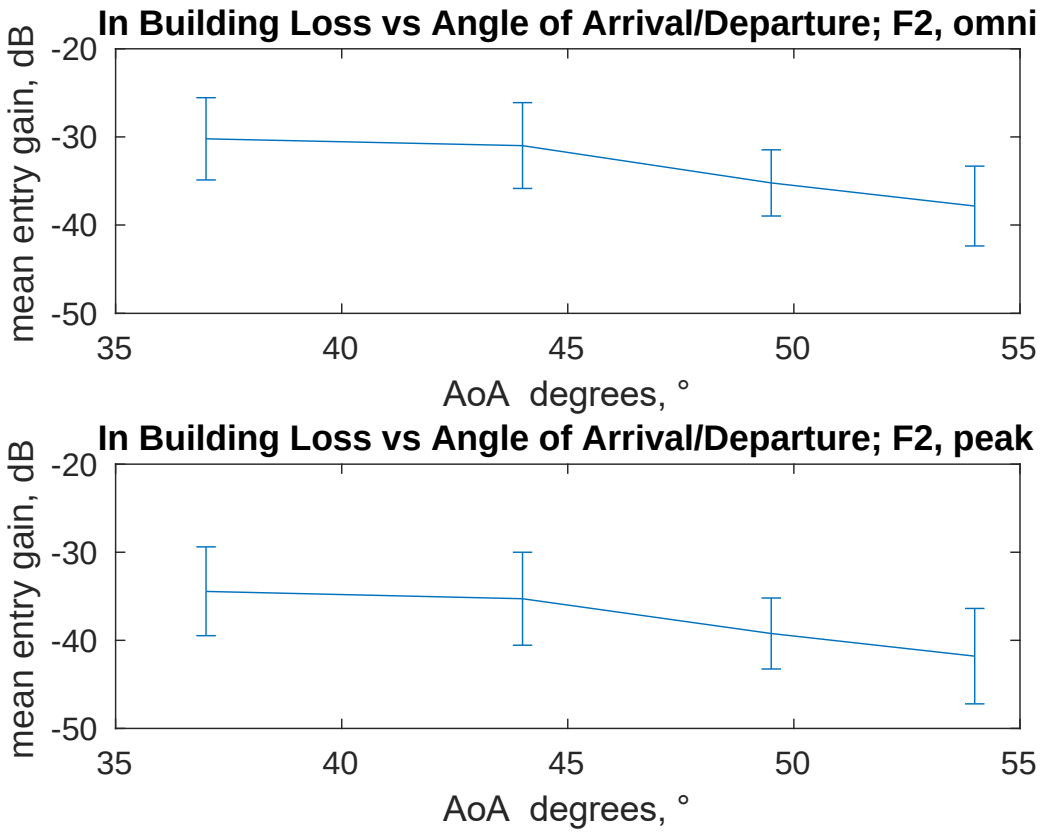

NOTES:

– Error bars illustrate 95% level [2x SD/sqrt(#points)]

– BEL clearly appears to increase with AoA.

5.2 Building E – Tx1 'peak' and 'omni' cases (Frequency 1)

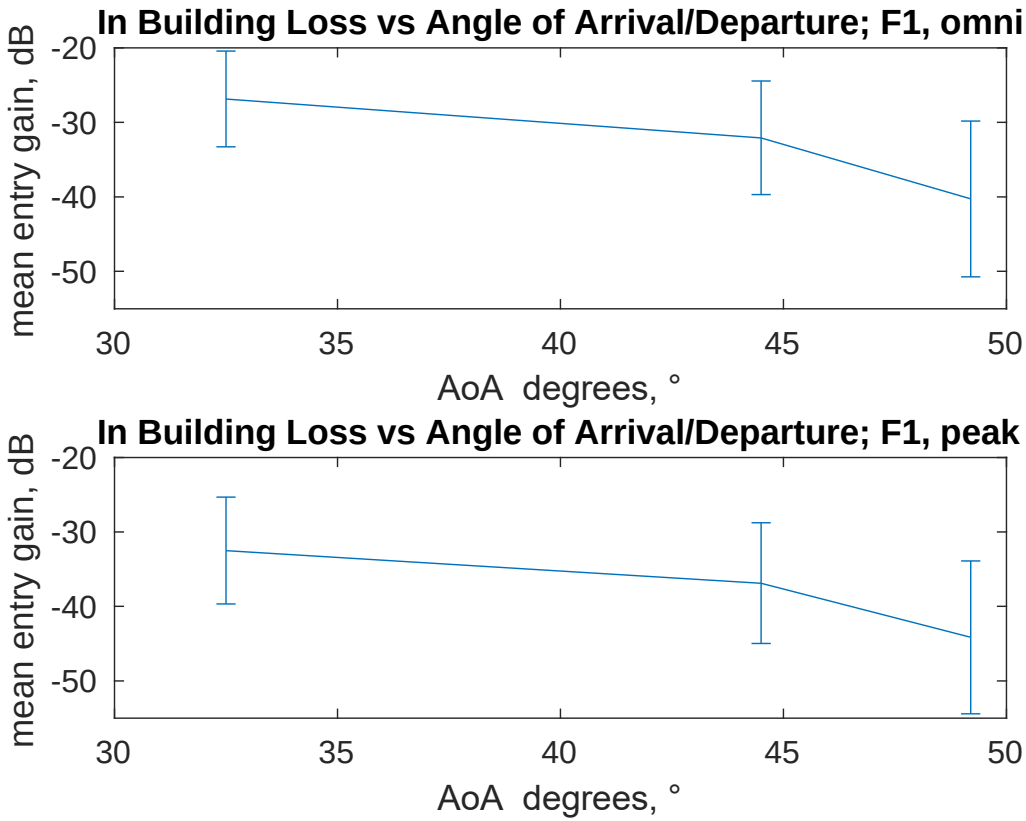

NOTES:

– Error bars illustrate 95% level [2x SD/sqrt(#points)]

– BEL clearly appears to increase with AoA.

25.A6 Attachment 6: Selected Polar Plots

6.1 Building E – Position 84

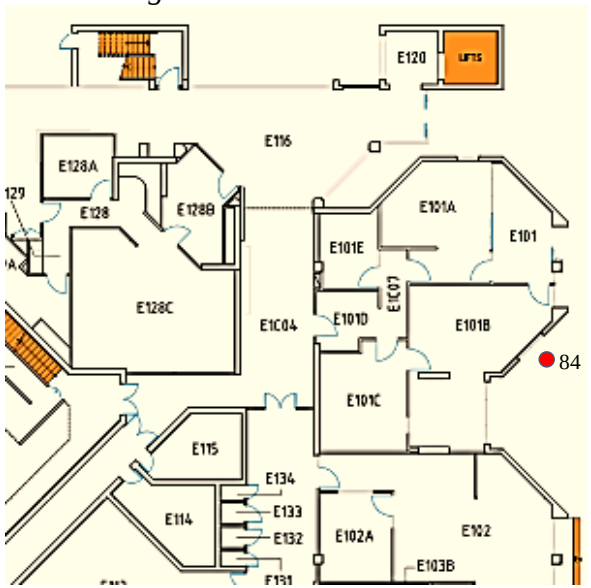

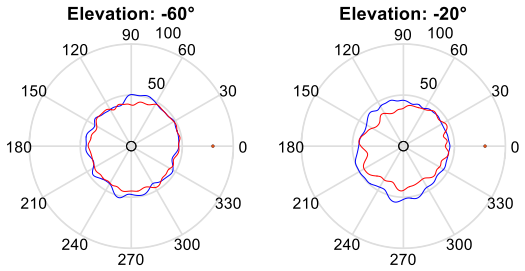

Noise floor = -71.5 dBm

Red = Tx2
Blue = Tx1

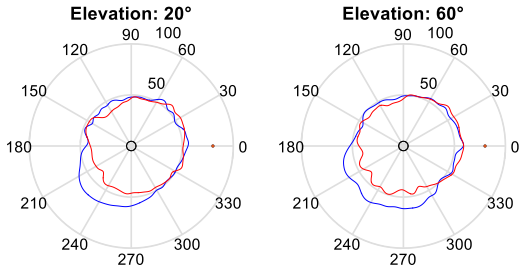

LHS = Tx2 *RHS =*

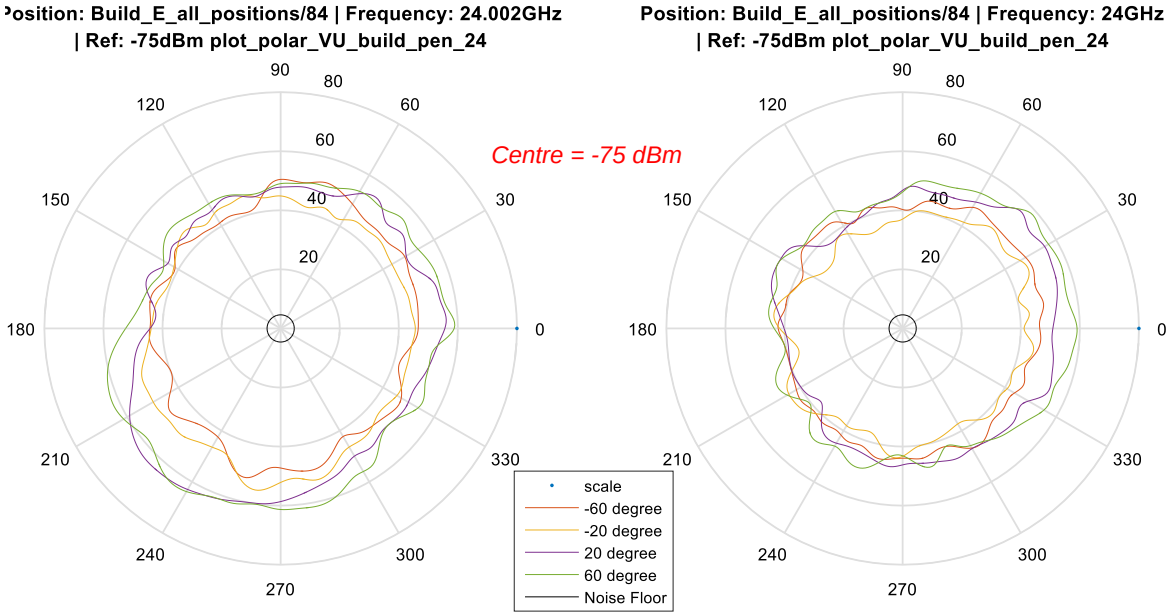

Back reflections off E block

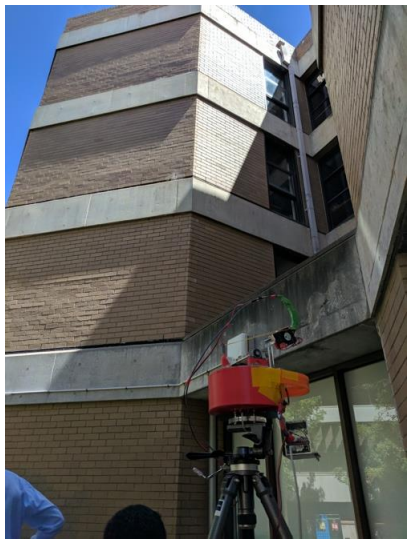

Tree blockage to Tx

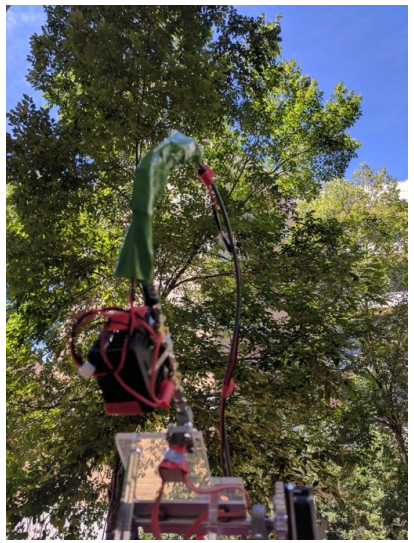

6.2 Building E – Position 85

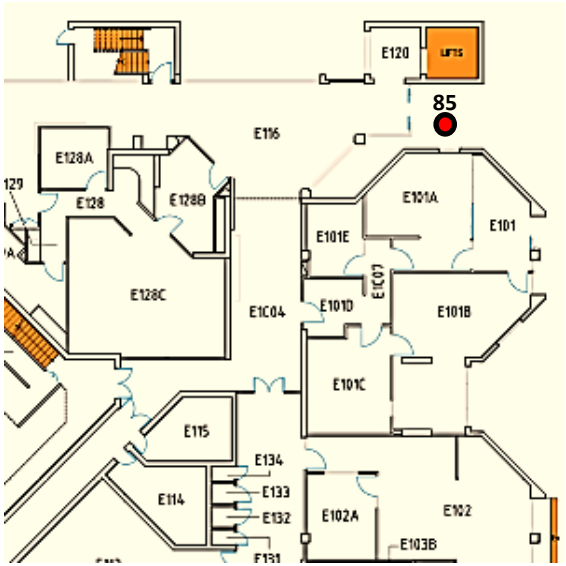

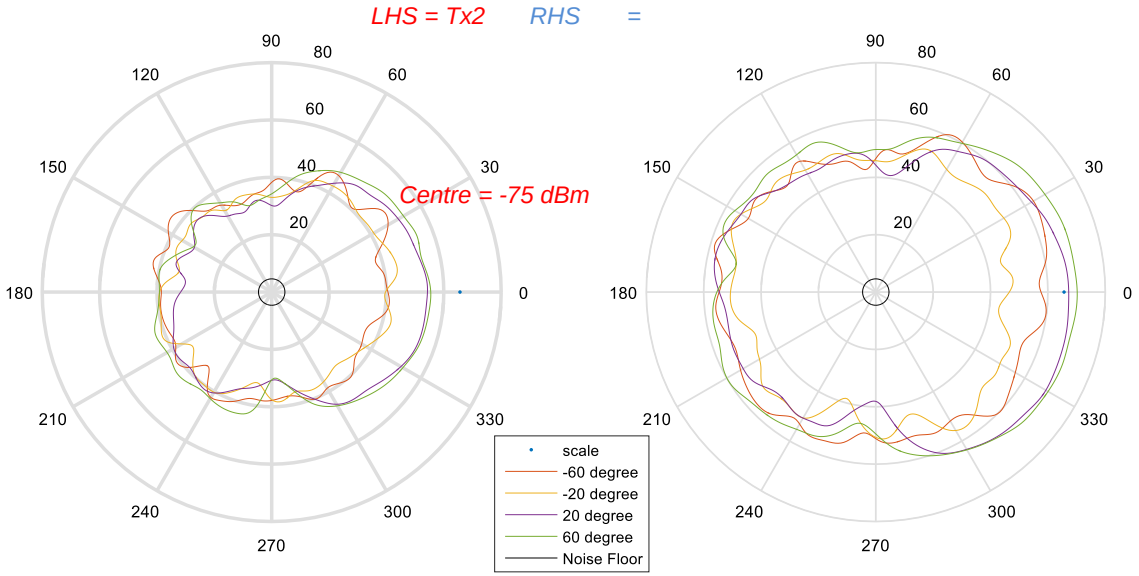

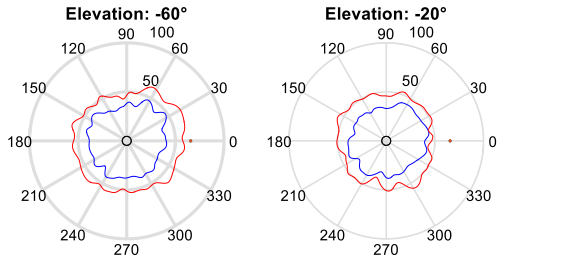

Noise floor = -71.5 dBm

Red = Tx2
Blue = Tx1

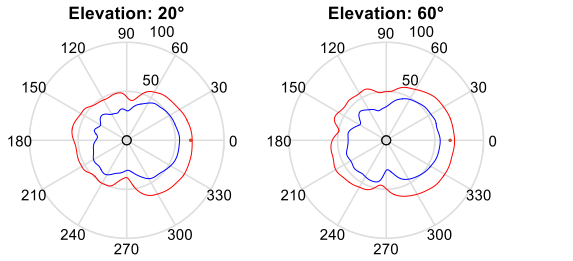

6.3 Building E – Position 92

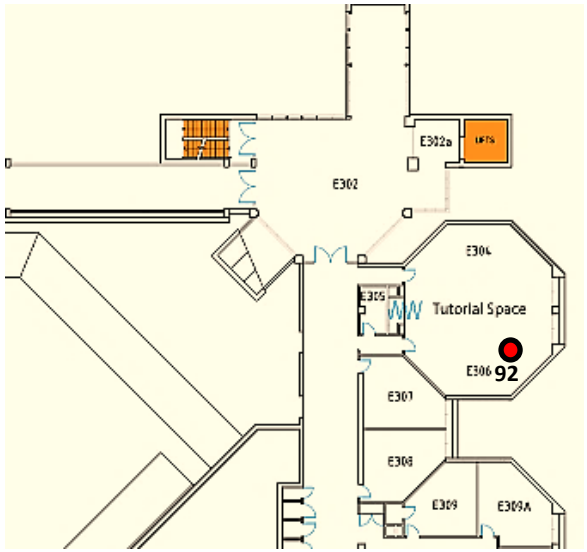

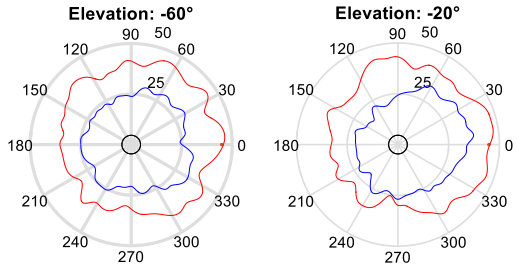

Noise floor = -71.5 dBm

Red = Tx2
Blue = Tx1

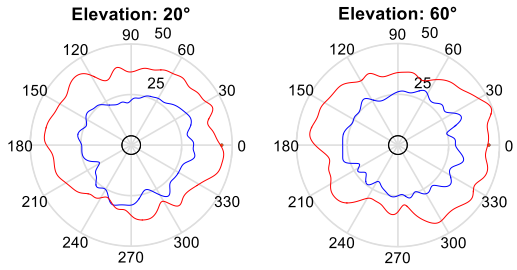

LHS = Tx2 *RHS =*

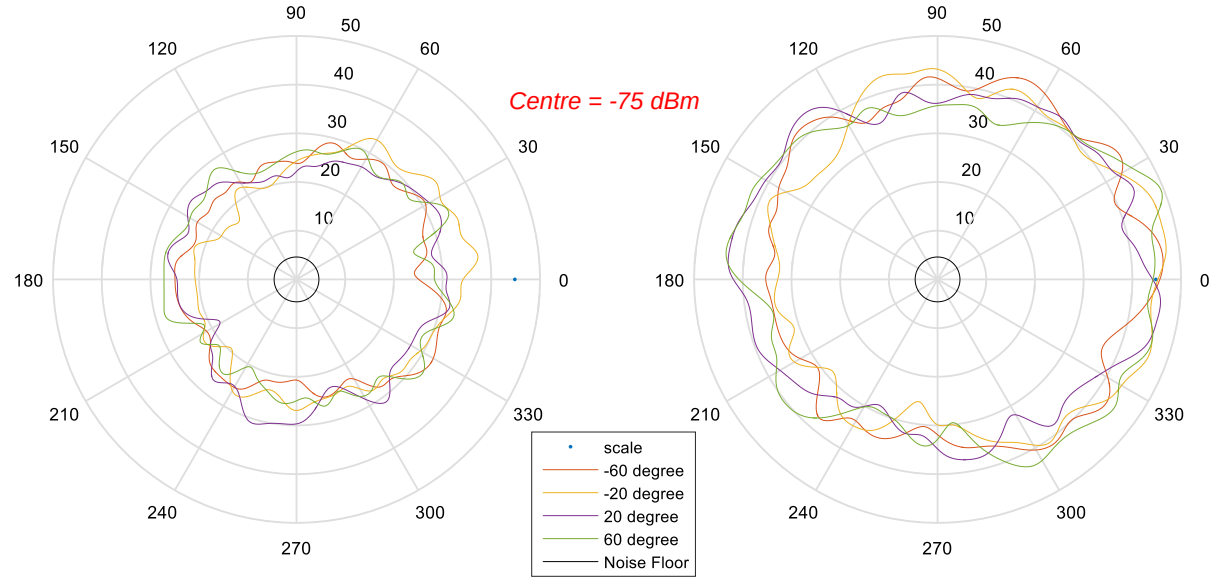

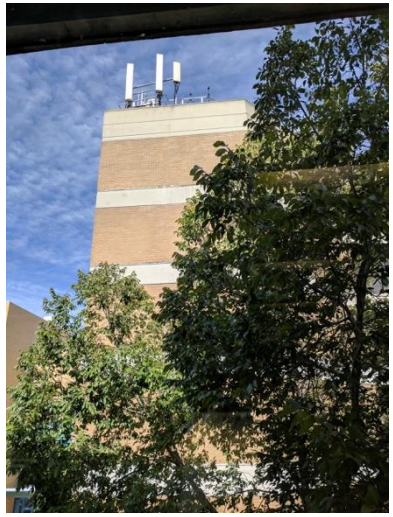

6.4 Building E – Position 93

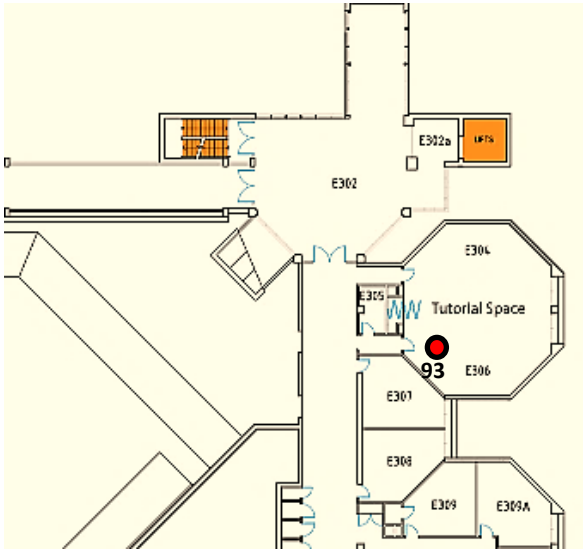

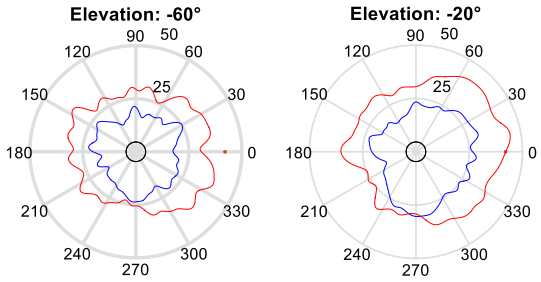

Noise floor = -71.5 dBm

Red = Tx2
Blue = Tx1

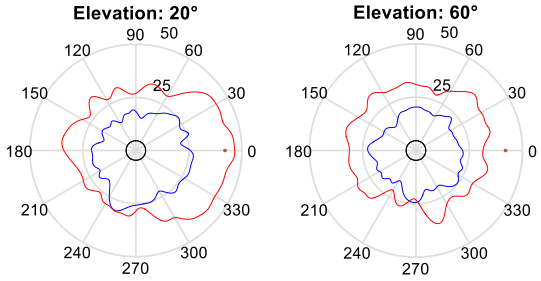

LHS = Tx2 *RHS =*

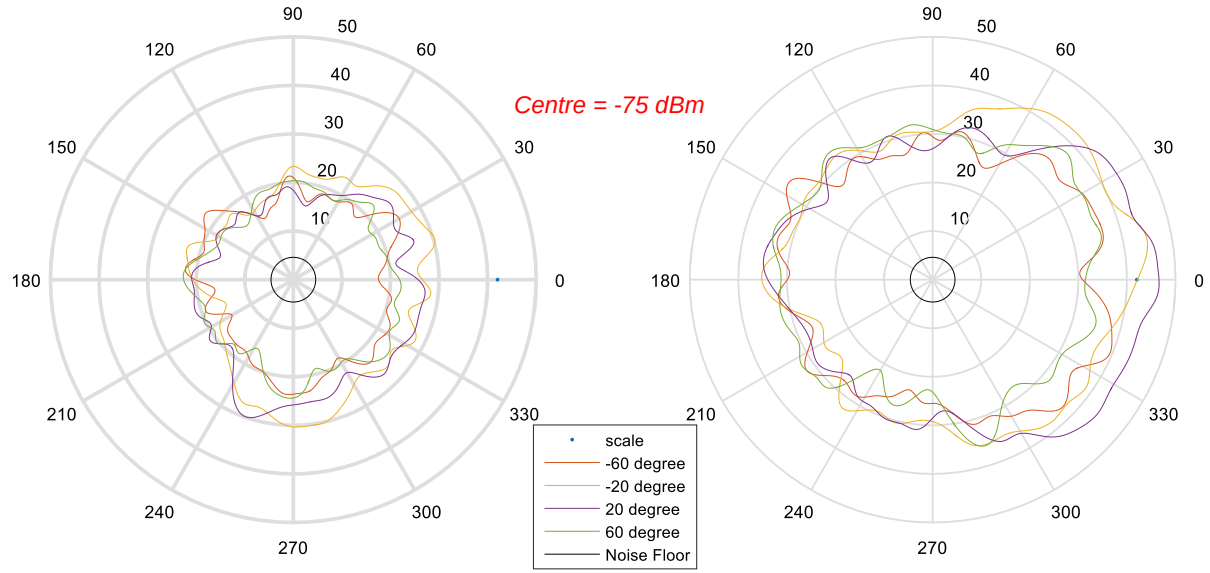

6.5 Building E – Position 94

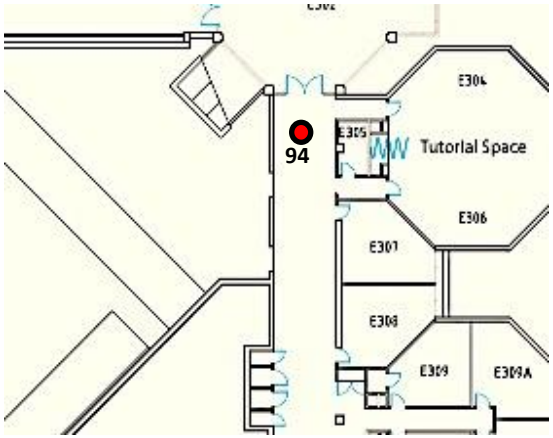

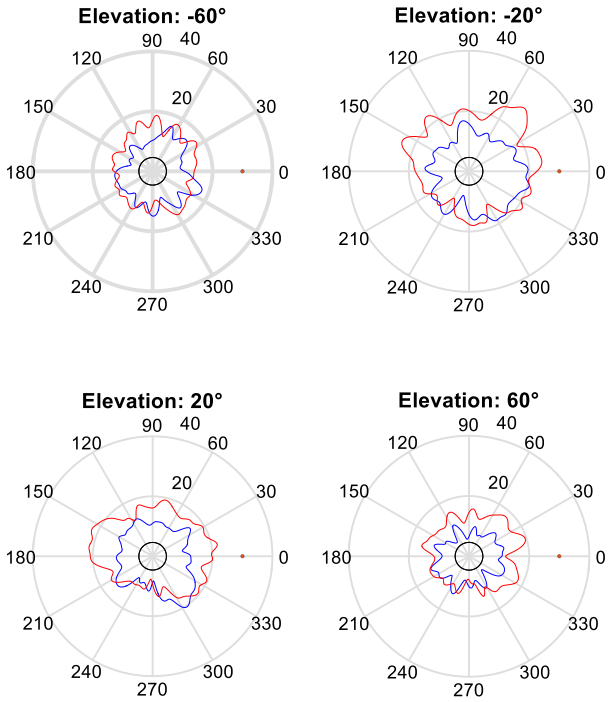

LHS = Tx2 *RHS =*

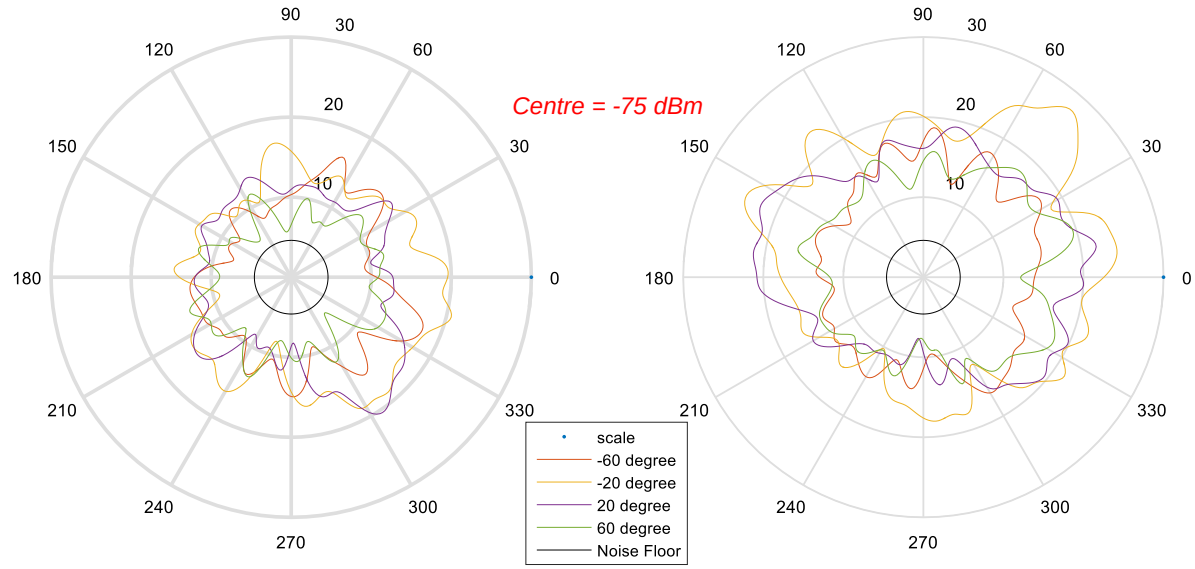

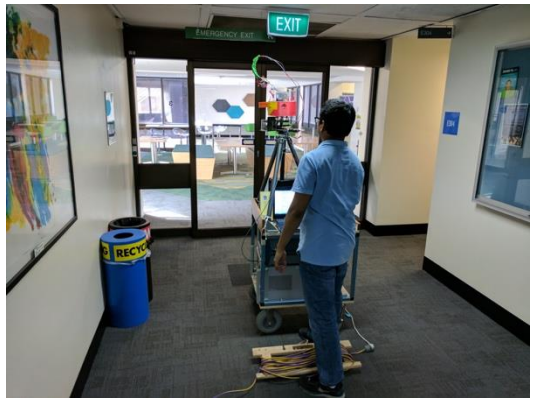

26 BEL measurement results and modelling vary with elevation incident angle in China

26.1 Introduction

This chapter focuses on determining the building entry penetration loss varied with incident elevation angle in the band 3.5 GHz±100 MHz, 27 GHz±250 MHz, 32 GHz±250 MHz, 39 GHz±250 MHz for different typical office buildings. There are three buildings and building A is modern, thermally-efficient building, building B is a common modern building with big glass windows, and building C is 'traditional' lower BEL buildings. Our preliminary study results can be found in Annex 1. Through the measurements results, we can see that the distribution of BEL probability is relative to the buildings' structure, material and incident angle.

The BEL varied with incident angle is given by:

$$BEL(\theta) = K - m10\lg(|\cos\theta|) \tag{33}$$

where θ is the angle between the incident direction, see Fig. 206 and the normal line of the obstacle, the coefficient *K* and m are related to the type of building, as shown in Table 75. And it exhibited model error RMS.

FIGURE 206

Measurement environment diagram

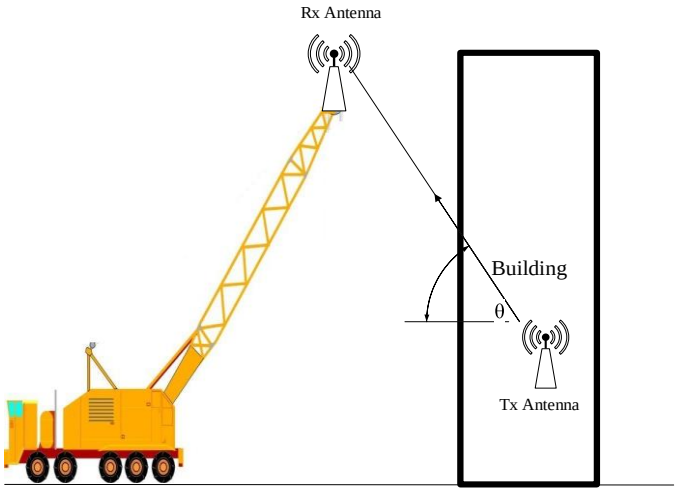

TABLE 75

The parameters of penetration loss with incident angle

Obstacle	Frequency	*K* (dB)	*m*	Modelling error RMS (dB)
Building A with one-way transparent glass	3.5 GHz±100 MHz	22.99	5.0	1.06
	27 GHz±250 MHz	25.18	8.0	3.78
	32 GHz±250 MHz	29.02	5.0	3.81
	39 GHz±250 MHz	27.12	5.0	4.37
Building A with thermal insulation material	3.5 GHz±100 MHz	40.94	5.0	3.67
	27 GHz±250 MHz	46.48	5.0	4.01
	32 GHz±250 MHz	51.74	4.0	4.90
	39 GHz±250 MHz	52.58	5.0	1.79
Building B with a layer of reinforced concrete walls	3.5 GHz±100 MHz	37.91	5.0	2.49
	27 GHz±250 MHz	43.63	8.0	0.34
	32 GHz±250 MHz	46.46	5.0	1.86
	39 GHz±250 MHz	45.97	5.0	2.16
Building B with two layers of reinforced concrete walls	3.5 GHz±100 MHz	45.62	8.0	2.01
	27 GHz±250 MHz	53.33	8.0	1.22
	32 GHz±250 MHz	56.41	8.0	1.60
	39 GHz±250 MHz	58.29	8.0	2.87
Building C with brick wall	3.5 GHz±100 MHz	9.35	10.0	1.38
	27 GHz±250 MHz	38.65	0.0	1.45
	32 GHz±250 MHz	46.53	0.0	1.60
	39 GHz±250 MHz	42.35	0.0	2.63
Building C with ordinary glass	3.5 GHz±100 MHz	6.09	20.0	1.58
	27 GHz±250 MHz	7.91	30.0	3.38
	32 GHz±250 MHz	6.88	30.0	1.02
	39 GHz±250 MHz	9.40	30.0	2.03

26.A Attachment: BEL measurement

26.A.1 Measurement scenarios

Three typical office buildings in China are measured, named as building A, building B and building C, which have different structure and material.

26.A.1.1 Building A

Building A is with reinforced concrete shear wall and the glass of windows is with one-way transparent glass, which is with a thin metal coating. The thickness of the bearing wall is 35 cm ~ 38 cm. In addition, the building's exterior wall is being equipped with thermal insulation material whose structure is the foam polyethylene sheet and metal reflective layer.

The scenes of Building A are shown in Figs 207 and 208. Table 76 presents the coordinates of the receiving points and transmitting points.

FIGURE 207

The scene of building A with thermal insulation material

FIGURE 208

The transmitting points indoor and the receiving points, Building A

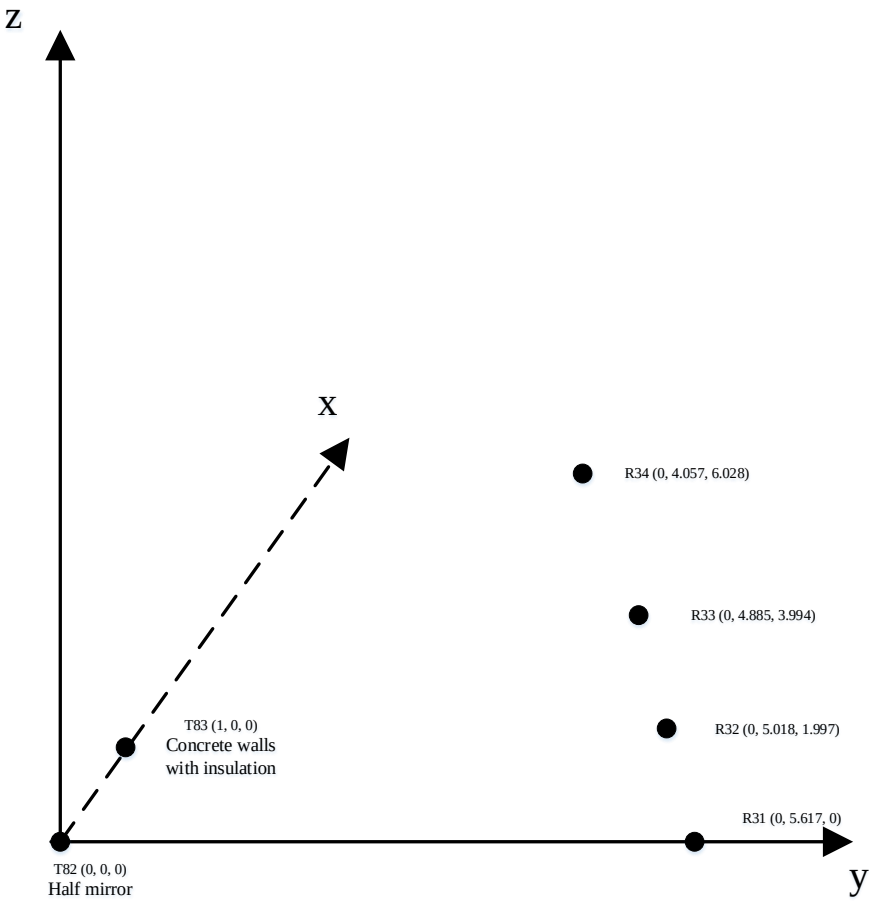

TABLE 76

The coordinates of the receiving points and transmitting points in building A (unit: m)

Points	x	y	z
T82	0	0	0
T83	1	0	0
R31	0	5.617	0
R32	0	5.018	1.997
R33	0	4.885	3.994
R34	0	4.057	6.028

Typical measured points' pictures in building A are shown in Fig. 209.

FIGURE 209

Typical measured point picture in building A

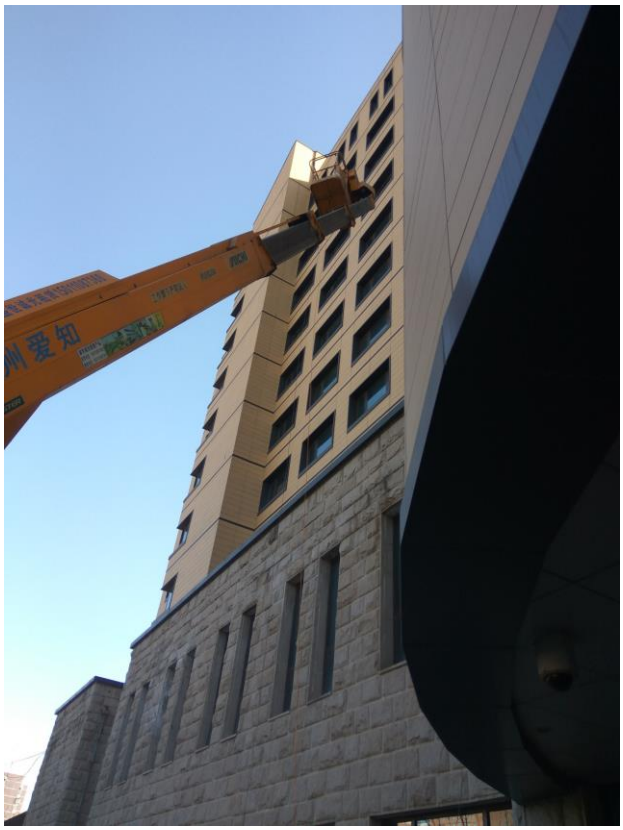

26.A.1.2 Building B

Building B is a modern building combined the toughened glass with the reinforced concrete. The toughened glass is laid in the wall which is known as a common toughened glass without metal coat. Part of exterior wall is equipped with a brown ceramic tile. There is a parking lot outside the building, the length of which is about 35m. In order to avoid the influence of vehicle movement, the method is:

– The test is taken at the weekend to make sure there are few vehicles and staffs.
– Make sure the receiving antenna be away from the vehicle.
– The height of the receiving antenna is set to 2.3 m to ensure that the connection between the transmitting antenna and the receiving antenna is not blocked by vehicles.

FIGURE 210

The scene of building B

In building B, the positions of Tx and Rx are shown in Fig. 211. Table 77 presents the coordinates of the receiving points and transmitting points.

FIGURE 211

The transmitting points indoor and the receiving points, Building B

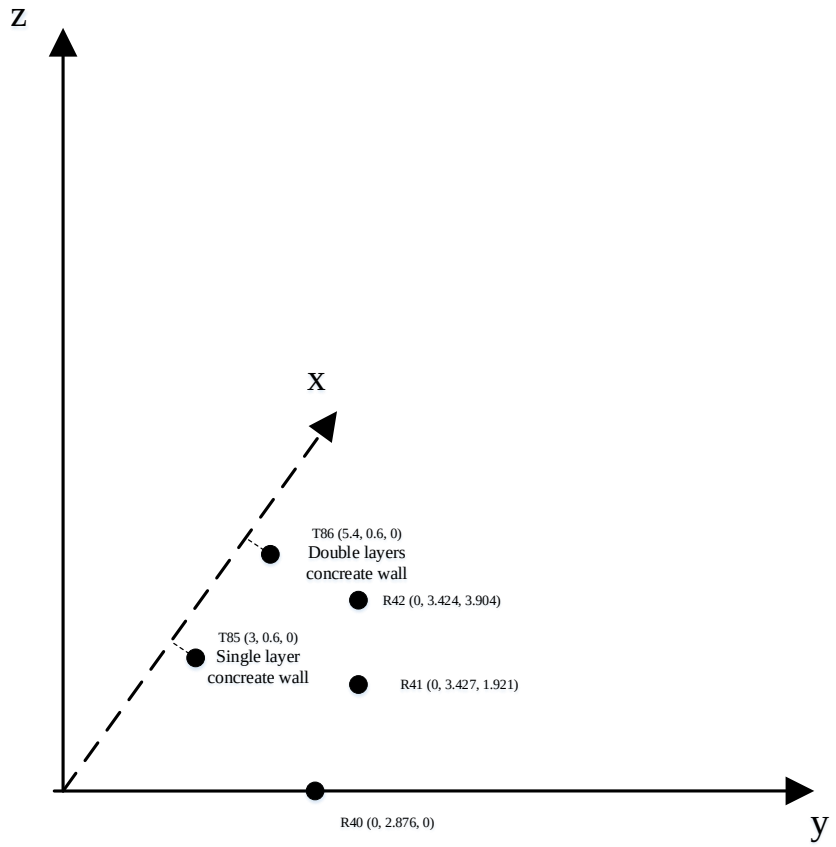

TABLE 77

The coordinates of the receiving points and transmitting points in building B (unit: m)

Points	x	y	z
T85	3	0.6	0
T86	5.4	0.6	0
R40	0	2.876	0
R41	0	3.427	1.921
R42	0	3.424	3.904

Some typical measured points' pictures in building B are shown in Fig. 212.

FIGURE 212

Typical measured point picture in building B

26.A.1.3 Building C

Building C is an old four-story building with brick wall structure and ordinary glass, as shown in Fig. 213.

FIGURE 213

The scene of building C

In building C, the positions of Tx and Rx are shown in Fig. 214. Table 78 presents the coordinates of the receiving points and transmitting points.

FIGURE 214

The transmitting points indoor and the receiving points, building C

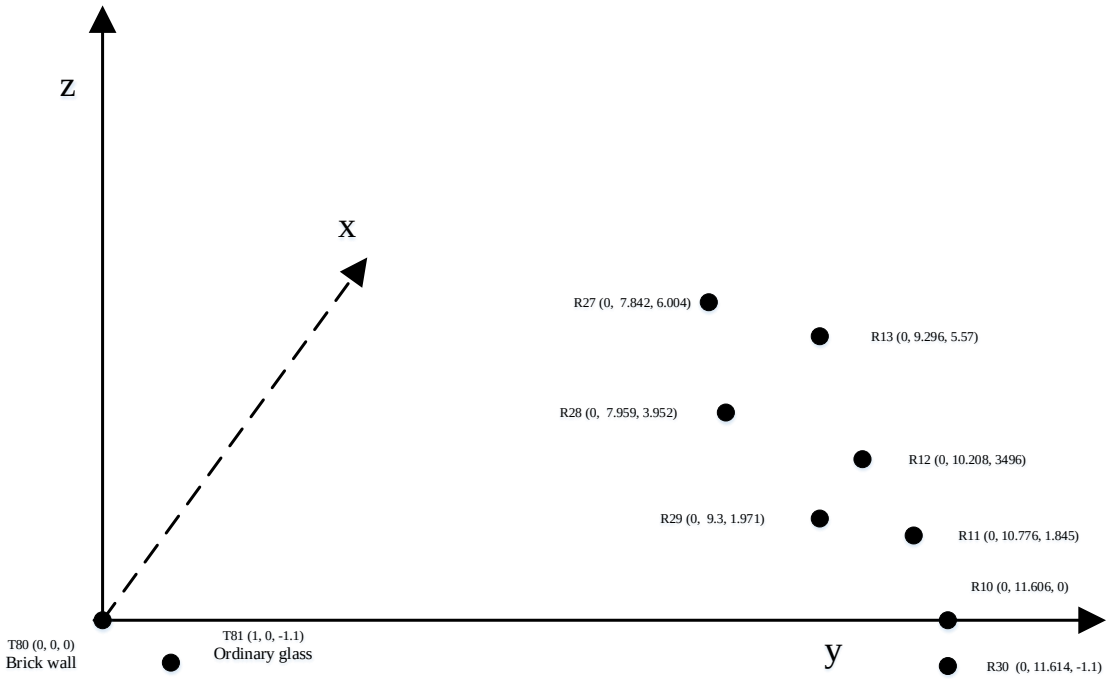

TABLE 78

The coordinates of the receiving points and transmitting points in building C (unit: m)

Points	x	y	z
T80	0	0	0
T81	1	0	-1.1
R10	0	11.606	0
R11	0	10.776	1.845
R12	0	10.208	3.496
R13	0	9.296	5.57
R27	0	7.842	6.004
R28	0	7.959	3.952
R29	0	9.3	1.971
R30	0	11.614	-1.1

Some typical measured points' pictures in building C are shown in Fig. 215.

FIGURE 215

Typical measured point picture in building C

26.A.2 Test methodology

In building A, B and C, 11 frequency points are selected in every frequency band during the test.

4 frequency bands are selected: 3.5 GHz±100 MHz, 27 GHz±250 MHz, 32 GHz±250 MHz, 39 GHz±250 MHz.

26.A.2.1 Measuring system and instrument

The devices of measuring system are shown in Table 79.

TABLE 79

Test instruments and equipment

Equipment	Description
Agilent E8267D signal generator	Frequency Range 9 kHz~40 GHz
Coaxial line	/
Agilent E4447 signal analyzer	Test sensitivity>-130 dBm
Ultra wideband Omni-directional antennas	Frequency Range1.6 GHz~50 GHz , the gain of which is about 2.15 dBi, linear polarization.
RF power amplifier	The output power in the test is over 43 dBm in ranges 26 GHz to 40 GHz
laser distance measuring instrument	Red laser

An automatic program has been developed in order to remote instruments and record test data by LAN. Sinusoidal continuous wave are used in measurements, as well as highly sensitive spectrum

analyser, and open the pre-amplifier at receiver, and RBW are set to a smaller value, in order to improve the sensitivity, more importantly, In each location and frequency points, 500 continuous reading is got which will cost about 11 seconds just as showed in Fig. 216 and then got the median value, It effectively suppresses the influence of the receiver noise, obtains the effective value at the low receiving level, and improves the confidence of the measurement result under the low receiving level condition. During the measurement process, the antenna polarization direction is constant, and both the transmitting and receiving antennas are vertically polarized, the antennas is showed in Fig. 217. In the measurement we observe and do adjustment, so that the crane platform does not block the Tx and Rx antenna direct path.

FIGURE 216

Building A. Entry Loss: Incident angle=21.7 deg, Half mirror, 3.601 GHz

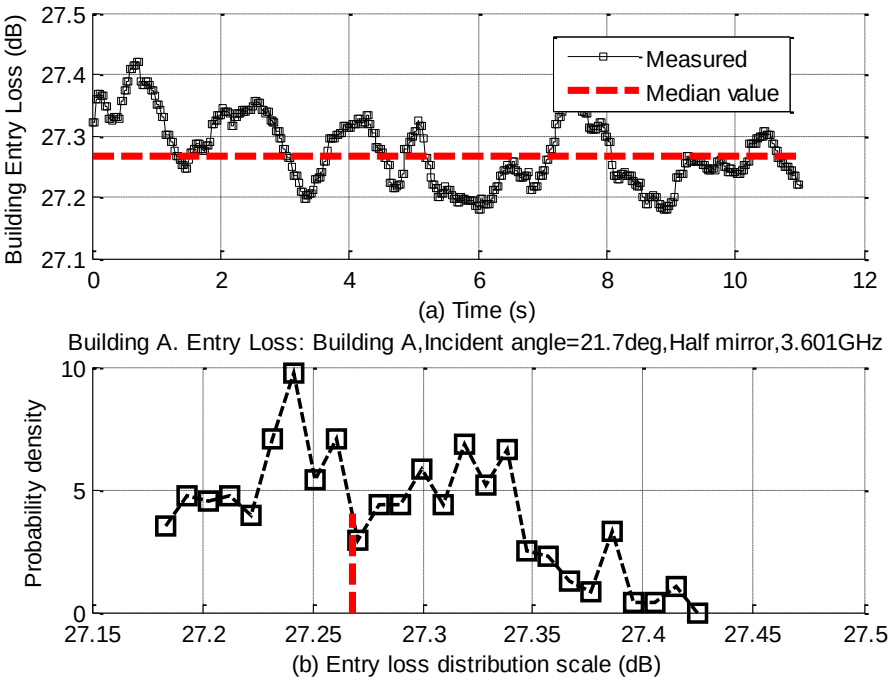

FIGURE 217

1.6GHz~50GHz Ultra wideband Omni-directional antennas, linear polarization

We measured 11 frequencies in one band and then averaged the median of BEL at 11 frequencies, it will reduce the effect of multipath by averaging. This process is shown in Fig. 217.

FIGURE 218

500 continuous reading->Median value of BEL at 11 frequencies->Average of Median value

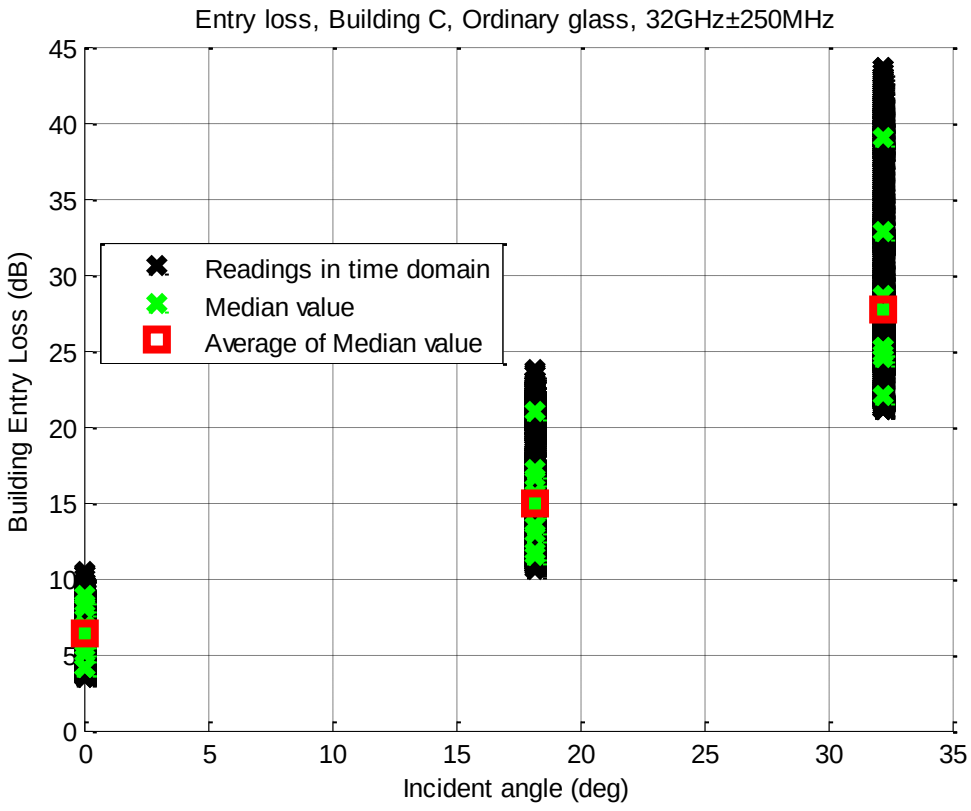

26.A.2.2 Calculation method of BEL

In the measurement, the Omni-directional antennas were carried, the radiation pattern of which is similar to the half-wave dipole antenna:

$$F(\theta) = \cos\theta \tag{34}$$

Take the cable loss 6 dB, the free space loss can be calculated as:

$$L_f = 32.45 + 20\lg D[m] + 20\lg F[GHz] - \left[4.3 + 10\lg\left(\cos^4\theta\right)\right] \tag{35}$$

Where d is distance between Tx and Rx, f is carrier frequency in GHz. Set transmitted power be *Pt* (dBm) and received power be *Pr* (dBm), the BEL is expressed as:

$$L_E = (P_t - P_r) - L_f \tag{36}$$

26.A.3 Measurement results

26.A.3.1 Measurement results and analysis of building A scenario

26.A.3.1.1 Building A with one-way transparent glass

TABLE 80

Measurement of penetration loss with incident angle, building A with one-way transparent glass

Frequency/Incident angle (deg)	0.00	21.70	39.27	56.06
3.5 GHz±100 MHz	24.58	23.67	28.88	34.66
27 GHz±250 MHz	31.43	24.16	31.79	45.03
32 GHz±250 MHz	31.25	27.32	30.54	46.76
39 GHz±250 MHz	25.17	35.01	27.08	41.03

TABLE 81

The parameters of penetration loss with incident angle, building A with one-way transparent glass

Frequency	*K (dB)*	*m*	Modelling error RMS (dB)
3.5 GHz±100 MHz	22.99	5.0	1.06
27 GHz±250 MHz	25.18	8.0	3.78
32 GHz±250 MHz	29.02	5.0	3.81
39 GHz±250 MHz	27.12	5.0	4.37

FIGURE 219

Entry loss, Building A, Half mirror

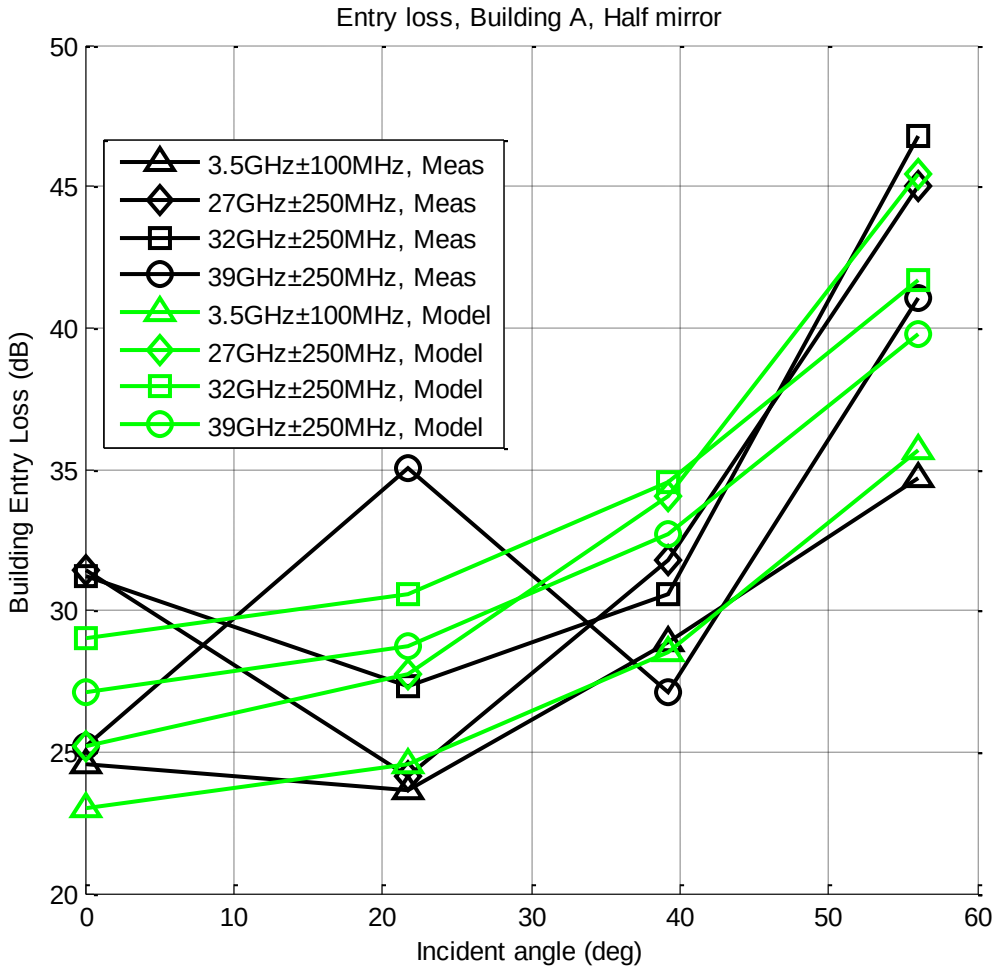

26.A.3.1.2 Building A with Concrete walls with insulation

TABLE 82

Measurement of penetration loss with incident angle, building A with thermal insulation material

Frequency/ Incident angle(deg)	0.00	21.32	38.70	55.28
3.5 GHz±100 MHz	42.94	46.73	45.71	47.54
27 GHz±250 MHz	52.31	45.91	46.93	59.91
32 GHz±250 MHz	58.58	51.09	49.47	63.12
39 GHz±250 MHz	52.40	56.25	55.21	65.61

TABLE 83

The parameters of penetration loss with incident angle, building A with thermal insulation material

Frequency	*K (dB)*	*m*	Modelling error RMS (dB)
3.5 GHz±100 MHz	40.94	5.0	3.67
27 GHz±250 MHz	46.48	5.0	4.01
32 GHz±250 MHz	51.74	4.0	4.90
39 GHz±250 MHz	52.58	5.0	1.79

FIGURE 220

Entry loss, building A, Concrete walls with insulation

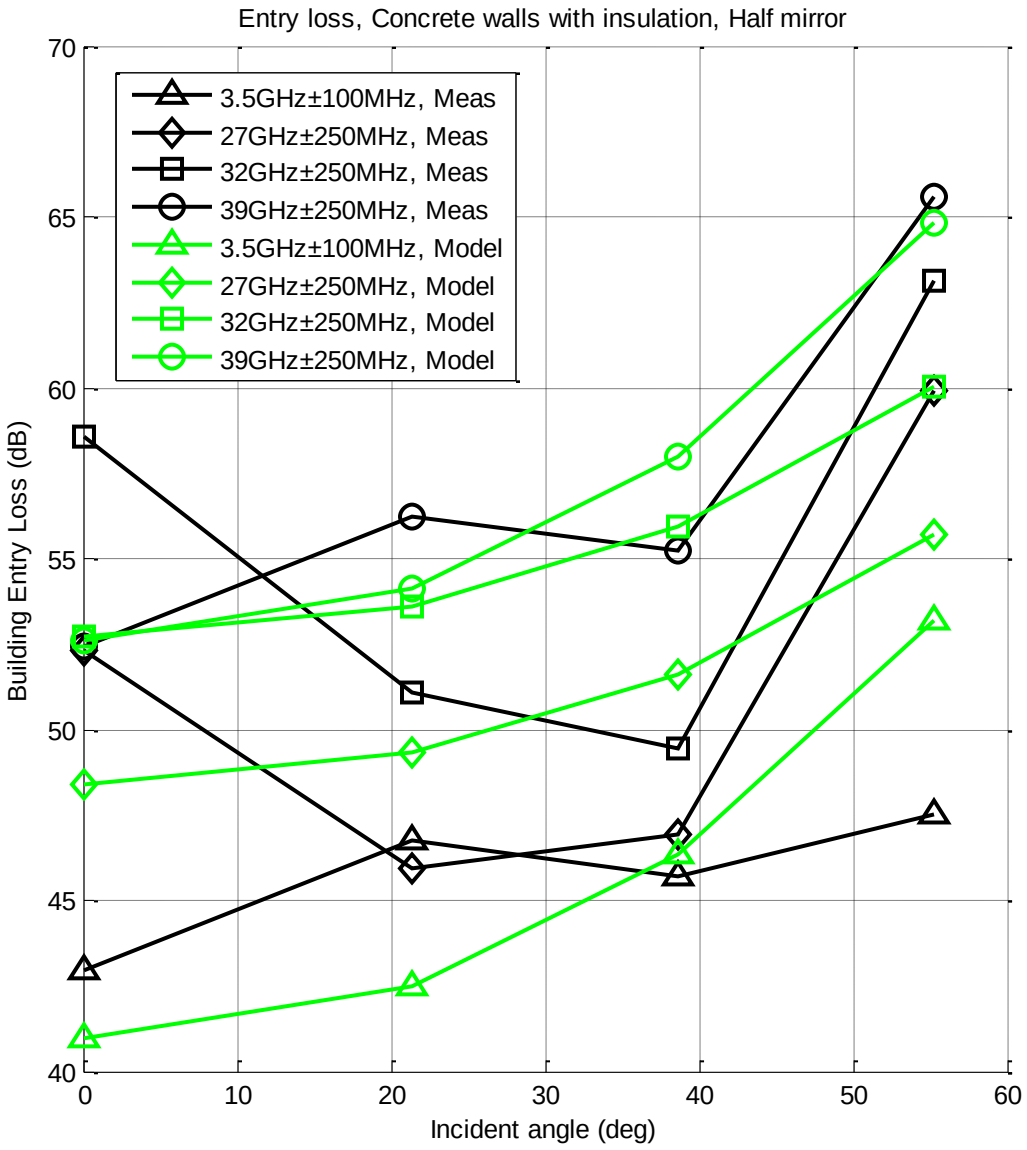

26.A.3.2 Measurement results and analysis of building B scenario

26.A.3.2.1 Building B with a layer of reinforced concrete walls

TABLE 84

Measurement of penetration loss with incident angle, building B with a layer of reinforced concrete walls

Frequency /Incident angle (deg)	0.00	24.99	43.46
3.5 GHz±100 MHz	35.84	43.54	43.44
27 GHz±250 MHz	43.26	47.49	54.69
32 GHz±250 MHz	45.94	51.09	51.43
39 GHz±250 MHz	44.01	51.12	51.89

TABLE 85

The parameters of penetration loss with incident angle, building B with a layer of reinforced concrete walls

Frequency	*K* (dB)	*m*	Modelling error RMS (dB)
3.5 GHz±100 MHz	37.91	5.0	2.49
27 GHz±250 MHz	43.63	8.0	0.34
32 GHz±250 MHz	46.46	5.0	1.86
39 GHz±250 MHz	45.97	5.0	2.16

FIGURE 221

Entry loss, Building B, Single layer concrete wall

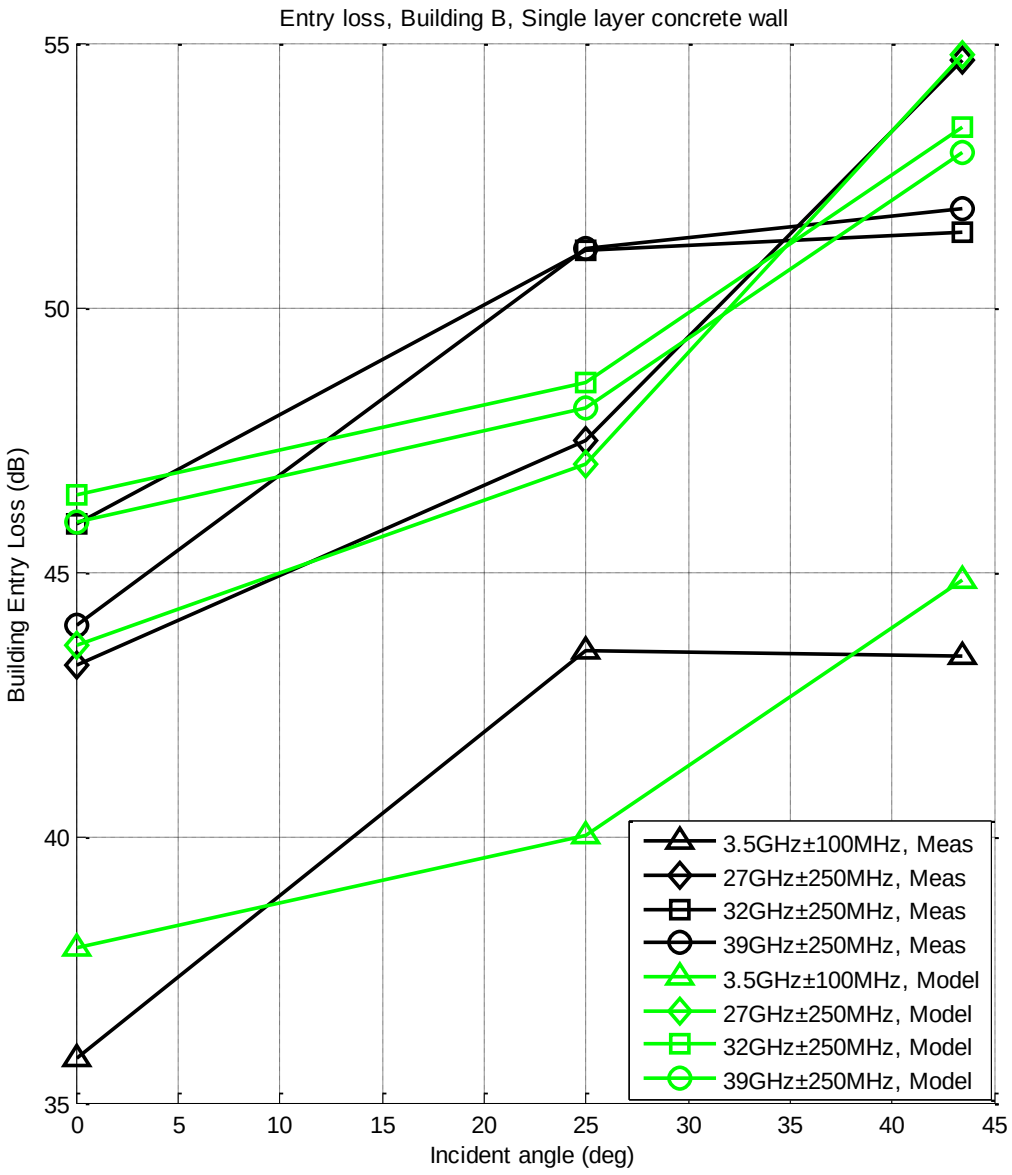

26.A.3.2.2 Building B with two layers of reinforced concrete walls

TABLE 86

Measurement of penetration loss with incident angle, building B with two layers of reinforced concrete walls

Frequency/Incident angle (deg)	0.00	17.49	32.65
3.5 GHz±100 MHz	45.79	49.65	49.06
27 GHz±250 MHz	54.95	54.70	57.97
32 GHz±250 MHz	58.68	56.88	61.30
39 GHz±250 MHz	61.68	56.30	64.51

TABLE 87

The parameters of penetration loss with incident angle, building B with two layers of reinforced concrete walls

Frequency	*K* (dB)	*m*	Modelling error RMS (dB)
3.5 GHz±100 MHz	45.62	8.0	2.01
27 GHz±250 MHz	53.33	8.0	1.22
32 GHz±250 MHz	56.41	8.0	1.60
39 GHz±250 MHz	58.29	8.0	2.87

FIGURE 222

Entry loss, Building B, Double layers concrete wall

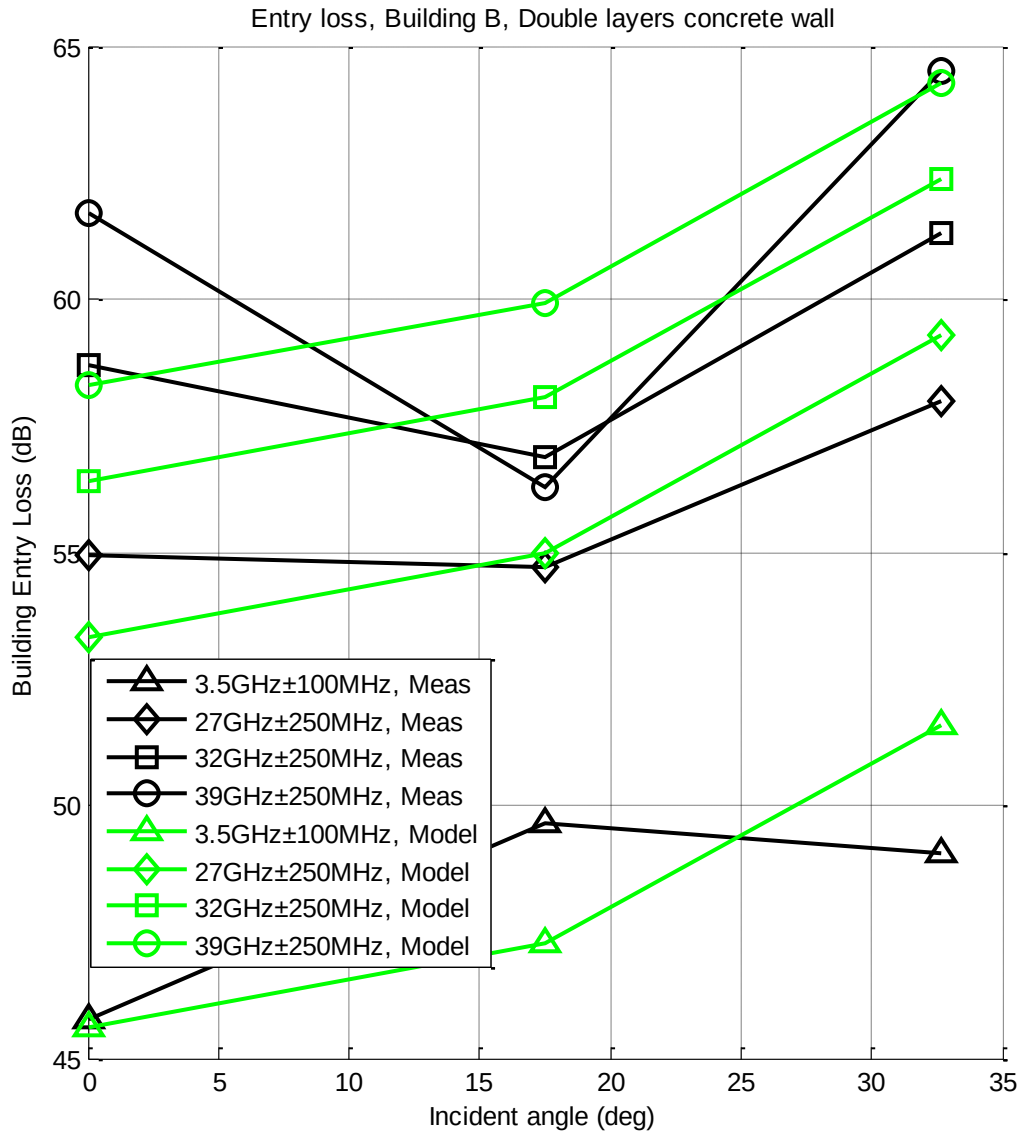

26.A.3.3 Measurement results and analysis of building C scenario

26.A.3.3.1 Building C with brick wall

TABLE 88

Measurement of penetration loss with incident angle, building C with brick wall

Frequency/Incident angle (deg)	0.00	9.72	18.91	30.93
3.5 GHz±100 MHz	9.98	9.95	9.57	17.58
27 GHz±250 MHz	37.83	37.73	37.88	41.15
32 GHz±250 MHz	46.64	45.85	49.00	44.63
39 GHz±250 MHz	41.05	45.98	43.42	38.94

TABLE 89

The parameters of penetration loss with incident angle, building C with brick wall

Frequency	*K* (dB)	*m*	Modelling error RMS (dB)
3.5 GHz±100 MHz	9.35	10.0	1.38
27 GHz±250 MHz	38.65	0.0	1.45
32 GHz±250 MHz	46.53	0.0	1.60
39 GHz±250 MHz	42.35	0.0	2.63

FIGURE 223

Entry loss, Building C, Brick wall

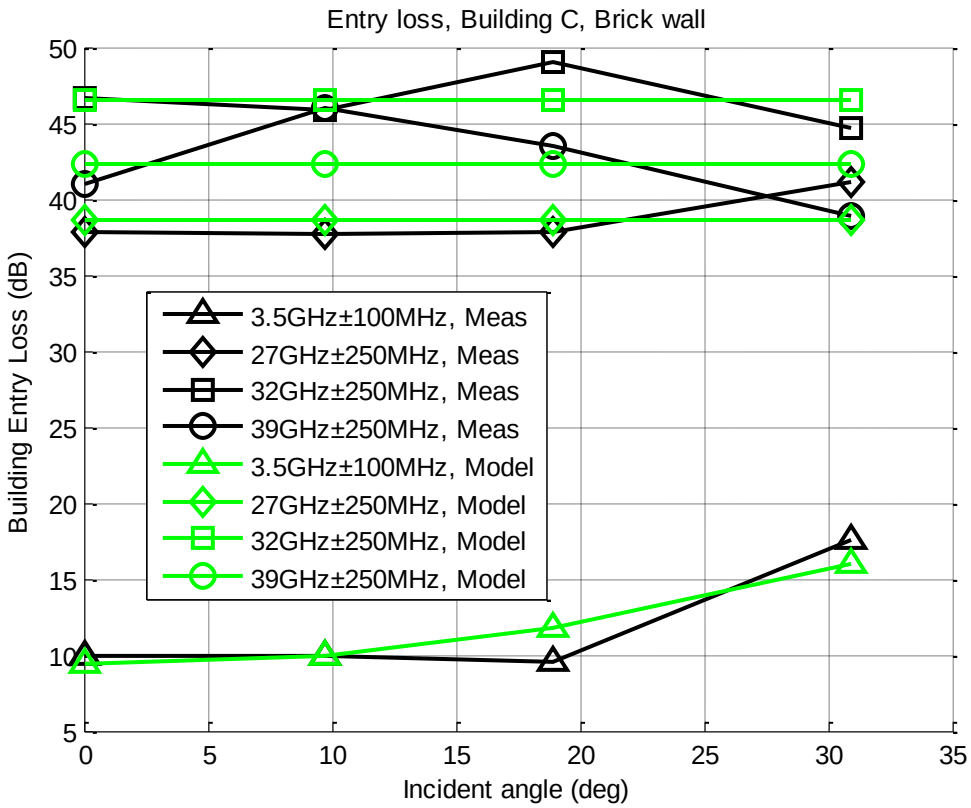

26.A.3.3.2 Building C with ordinary glass

TABLE 90

Measurement of penetration loss with incident angle, building C with ordinary glass

Frequency/Incident angle (deg)	0.00	18.18	32.21
3.5 GHz±100 MHz	5.78	12.61	18.85
27 GHz±250 MHz	11.92	10.32	29.93
32 GHz±250 MHz	6.36	14.98	27.74
39 GHz±250 MHz	10.62	13.21	32.81

TABLE 91

Parameters of penetration loss with incident angle, building C with ordinary glass

Frequency	*K* (dB)	*m*	Modelling error RMS (dB)
3.5 GHz±100 MHz	6.09	20.0	1.58
27 GHz±250 MHz	7.91	30.0	3.38
32 GHz±250 MHz	6.88	30.0	1.02
39 GHz±250 MHz	9.40	30.0	2.03

FIGURE 224

Entry loss, Building C, Ordinary glass

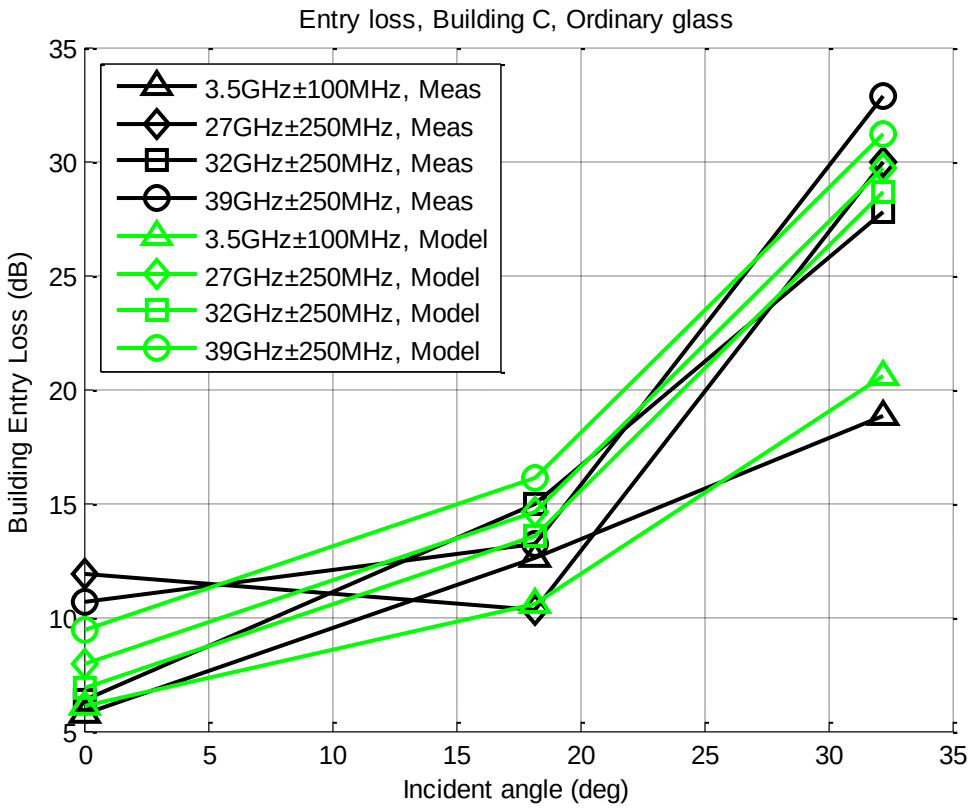

26.A.4 Conclusion

Through the analysis, we can see that the Entry loss is relative to the buildings' structure， materials and incident angle. As can be seen from the measurement data, from the statistical point of view, the larger the incident angle is, the greater the BEL is. In addition, we must realize that the structure and material of modern buildings have a complex effect on the propagation of radio waves. Even if the same building, such as the wave propagation path through the different materials, the change rule of BEL with the incident angle are different. Overall, the building in the band above 27 GHz can reach a considerable BEL, in particular, we need to point out that the one-way transparent glass and the traditional glass is different, for it will cause a much larger BEL.

27 BEL measurement and modelling results on elevation angle dependence from Ericsson

27.1 Introduction

Extensive measurement data have been provided supporting BEL modelling in ITU-R in the frequency range subject for WRC-19 agenda item 1.13 studies (24-86 GHz). This data accounts mainly for paths entering buildings horizontally. In order to provide proper modelling for e.g. earth space sharing scenarios it is essential to account for any dependence of BEL on the elevation angles which corresponding paths may have entering the buildings. This chapter provides measured BEL for a 'traditional' type of building (having non-coated type window glass) for different elevation angles and radio frequencies in the range 2-60 GHz.

The research leading to these results received funding from the European Commission H2020 programme under grant agreement no 671650 (mmMAGIC project).

27.2 Measurement campaign

A BEL measurement campaign has been performed in a 'traditional' type of office building in the Kista area of Stockholm, as depicted in Fig. 225. The receiver antenna (Rx) is located about 1 m outside an open window at floors 4, 7 and 8 and the transmit antenna (Tx) is located about 1.8 m above the floor on floor 4. The measurements were performed with both horizontal and vertical orientation of the Tx and Rx antennas. At floor 8 the elevation angle is around 70 degrees. Consequently, the Rx antenna has to be horizontally oriented for both the vertical and the horizontal polarizations (outside floor 4 at the exterior wall) in order to point the antenna lobe towards the exterior wall segment outside floor four. For Rx locations at floors 4 and 7 the antenna orientations are the same as corresponding polarisations. For both vertical and horizontal polarisations, the Tx antenna is oriented to maximize the received power. For the vertically polarized Rx antenna at floor 8 the Tx antenna orientation for maximum power is horizontal close to the wall (Tx points 1-5) and vertical for the rest locations (Tx points 6-13).

TABLE 92

Basic data of measurement setup

Carrier frequency	**2.44 GHz**	**5.8 GHz**	**58.68 GHz**
Bandwidth	80 MHz	150 MHz	2 GHz
Transmit power	10 dBm	10 dBm	10 dBm
Antenna Tx	Electric dipole 2dBi	Electric dipole 2dBi	Electric dipole 2dBi
Antenna Rx	Electric dipole 2dBi	Electric dipole 2dBi	Electric dipole 2dBi
Tx Antenna height	1.8 m (ref : indoor floor)		
Rx Antenna height	1.0 m (ref : indoor floor)		

FIGURE 225

Outdoor to indoor measurement scenario (left). The indoor Rx locations at floors 4, 7 and 8 are marked with blue-filled circles and the Tx locations at floor 4 are marked with a red-filled circles. On the right hand side, a photograph of the building is shown

27.3 Analysis

The elevation angle is determined as follows. First the point where the line connecting the Rx and Tx intersects the exterior wall is found. This point is projected vertically down to the wall segment at floor four. The elevation angle is now given by the line connecting this point to the Rx antenna. The elevation angle θ is the complement ($\theta = 90 - \phi$) of the polar angle ϕ used in spherical coordinate systems.

The measurements are calibrated by free space measurements accounting for any antenna pattern effects at Rx due to the elevation angle. The antenna gain elevation angle variation was found to be within 1 dB. In Fig. 226 the BEL is shown for the different elevation angles and frequencies (corresponding cumulative distributions are shown in Fig. 227). Points p1, p8 and p11 are omitted as the elevation angle is ambiguous for these points. Maximum, median and minimum loss are presented in three separate graphs.

It was found that the elevation dependent loss L_{el} may be modelled with a simple linear expression:

$$L_{el} = k \text{ abs } (\theta) \text{ (dB)}$$

where k (dB/ 90º) is a model parameter and θ is the elevation angle. This function has been fitted to the measurement data assuming that k is frequency independent. The model parameter k ranges from 24 dB/90º to 31 dB/90º. The standard deviation between model and measurements is in the range 1.35 to 2.22 dB.

FIGURE 226

Measured BEL (loss in excess of free space loss) versus elevation angle for the different frequencies together with the fitted linear model. The top graph corresponds to minimum loss (2.5% level); the middle graph corresponds to median loss; and the bottom graph to maximum loss (97.5% level)

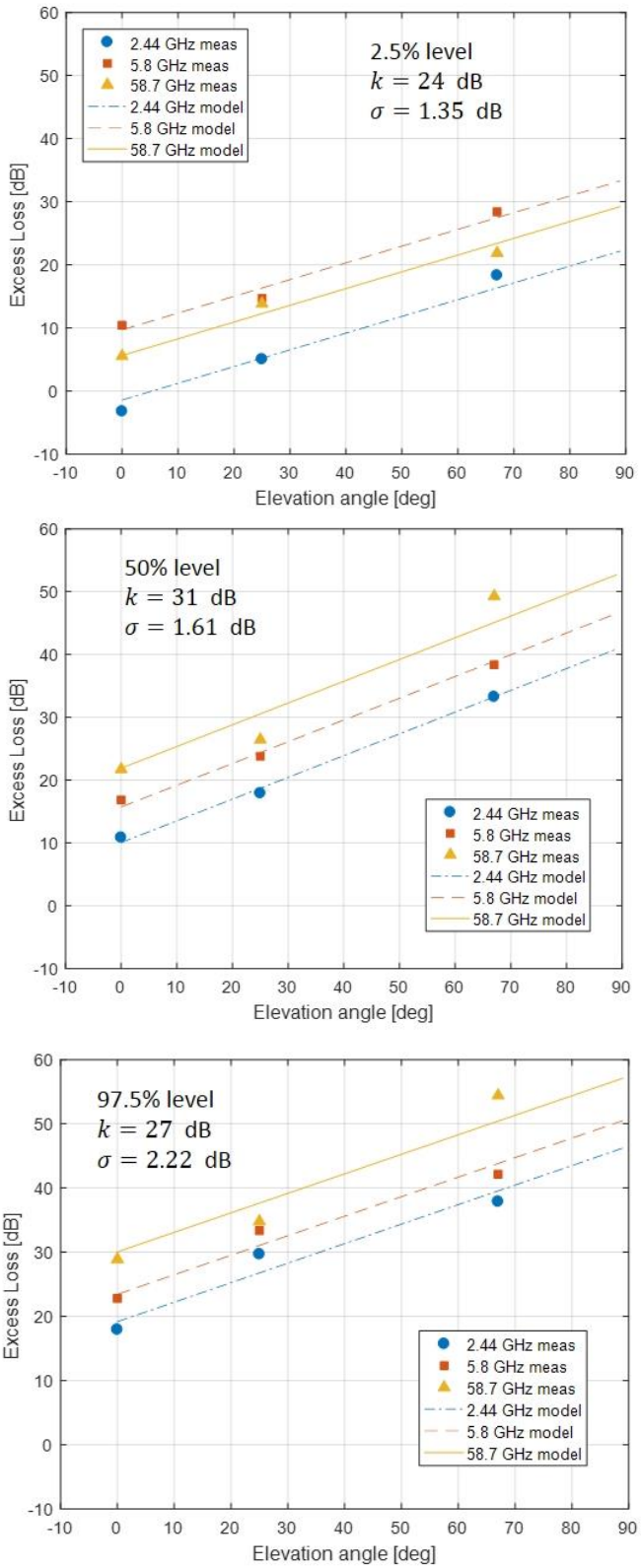

FIGURE 227

Cumulative distribution functions of measured BEL for the different elevation angles and radio frequencies. The left hand graphs show distributions where Tx locations p1, p8 and p11 are excluded.
The right hand graphs show distributions for all Tx locations

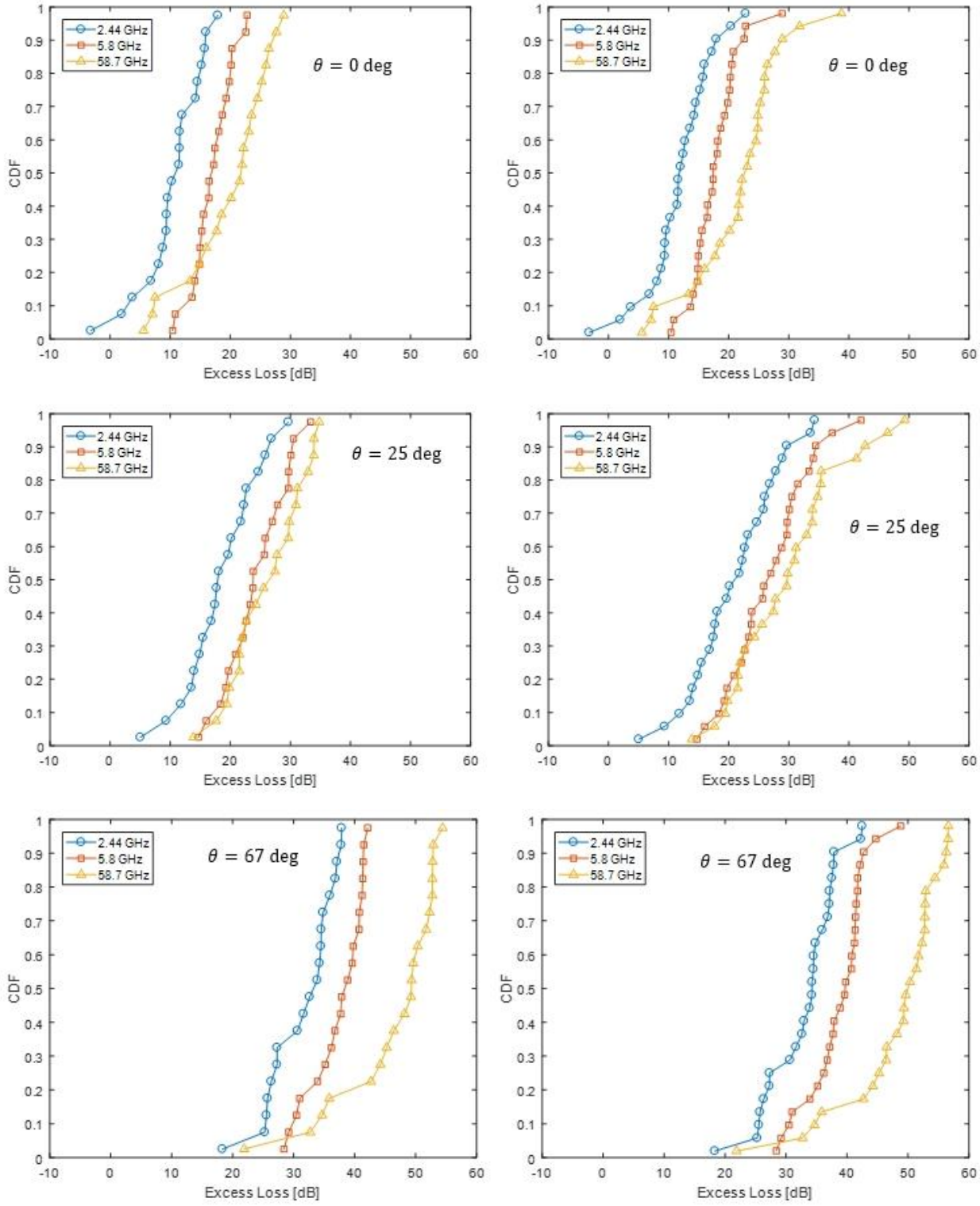

28 BEL measurements for three buildings in the frequency range 800 MHz-5.2 GHz with varying elevation incident angle from Nokia

28.1 Introduction

This chapter provides BEL measurement data with varying elevation incident angle for three buildings and different frequency bands in the range 800 MHz-5.2 GHz. The presented measurement results, which can directly contribute to the existing measurement database, are compared to predictions made with a simple geometrical knife-edge diffraction (KED)-based height gain (HG) model.

28.2 Measurement overview

In [1], a simple geometrical HG model based on KED for urban microcells is presented. As part of the validation, the model was tested against multi-frequency (800 MHz - 5.2 GHz) measurement results from a campaign of outdoor-to-indoor propagation performed in Aalborg, Denmark.

Measurements were performed in a practical scenario where an omni-directional antenna was deployed outside the buildings at 7 m height, emulating a lamppost-mounted microcell BS. Measurements were executed at diverse positions inside the buildings (e.g. different floors) with omni-directional antennas located at approximately 1.75 m above floor level.

A selection of measurements results for three different buildings is presented as part of this chapter. An overview of the considered building scenarios is shown in Figs 228, 229 and 230, and the main characteristics are summarized in Table 93.

FIGURE 228

AAL1 building

FIGURE 229

AAL2 building

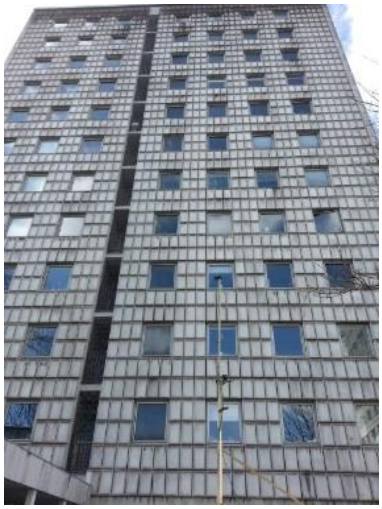

FIGURE 230

AAL3 building

TABLE 93

Summary of different building measurement scenarios

	Building type	TX/RX heights	BS-building distance	Azimuth angle (at façade / at RX)	Indoor distance
AAL1	Traditional	TX: 7m RX: 1.6-37.7 m (floors 0-12)	~3 m	54º / 66º	2 m
AAL2	Modern	TX: 7m RX: 1.6-35.6 (floors 0-11)	~3 m	33º / 18º	3 m
AAL3	Modern	TX: 7m RX: 1.6-48.7 (floors 0-16)	~2 m	27º / 12º	2.5 m

Further details on the measurement setup, overview of the scenarios, measurement procedures and data processing are presented in [1] and some have been summarized in the Attachment.

28.3 Measurement results and comparison with KED-based model

Figure 231 present the BEL measurement samples, estimated by subtracting the free space path loss (PL) from the calibrated path loss measurement samples, plotted against the different elevation angles (θ) for all the considered scenarios and frequencies. As it can be seen, the results present an irregular behaviour but, the general trends, indicate that BEL increases with absolute elevation incidence angle and frequency. It is also noticeable that different buildings present different BEL absolute magnitude. As the BS antennas were relatively closer to the ground level (in relation to the overall height range explored) it is not possible to derive any clear conclusion on the symmetry of BEL with positive and negative elevation angles.

The model presented in [1] provides physical and geometrical explanations to the described behaviours. By assuming that at the considered frequencies, penetration into the buildings (especially in modern buildings) occurs through the windows, the model splits the overall experienced PL into 3 different and independent components: outdoor PL (propagation from the BS to a window), outdoor-to-indoor PL (penetration into the building through the window) and indoor PL (propagation from the window to the indoor terminal).

FIGURE 231

BEL vs elevation incidence angle for all the scenarios and frequencies

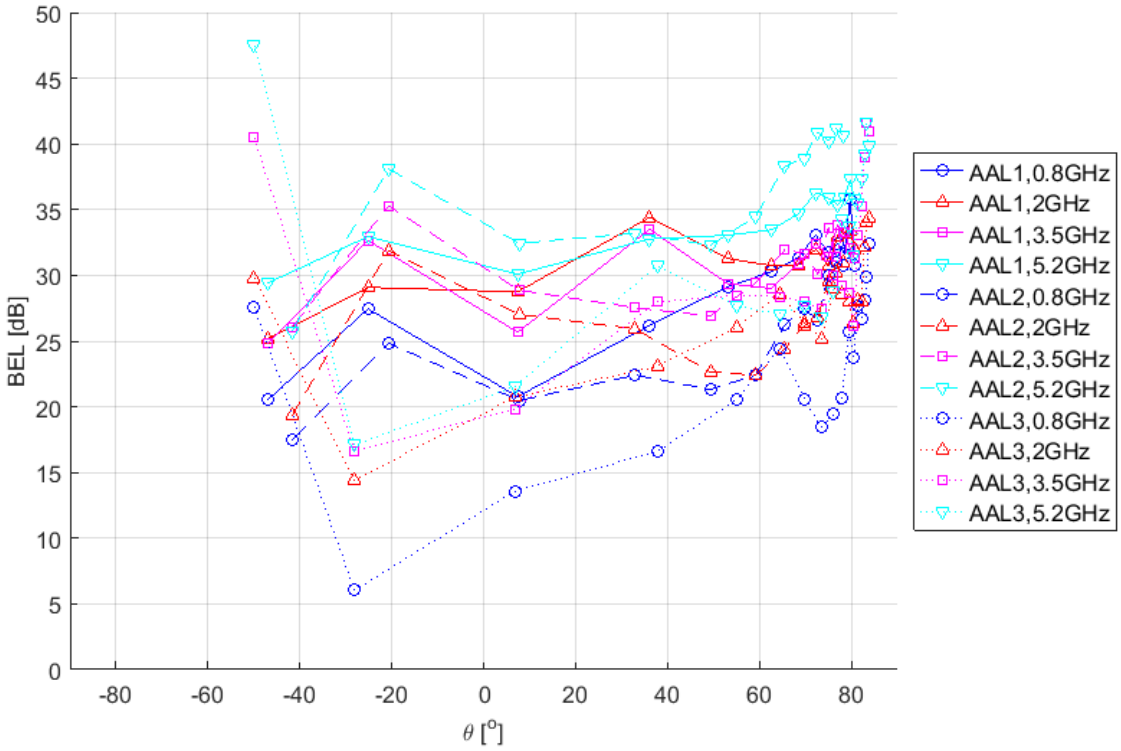

The key part of the model, which drives all the dynamics of the model is the outdoor-to-indoor PL computation, assumes diffraction at the frame and attenuation by the glass of the window. The overall outdoor-to-indoor loss is modelled as the normal incidence attenuation value of the glass (which is the only external input parameter to the model) plus a diffraction loss term. This term is computed by means of simple geometrical KED calculations for both the azimuth and elevation domains. By explicitly considering the exact geometry of the scenario, the model is able to discriminate for example, users closer to the external wall and deep indoor users. A very extensive geometrical validation is also reported in [1] for 3.5 GHz. The frequency dependence in the model is implicitly introduced by the KED computation, so no further compensation is needed.

Figures 232, 233 and 234 present the measurement results (calibrated path loss at different RX height/floor) for buildings AAL1, AAL2 and AAL3, respectively. As it can be seen, the model is in good agreement with the measurements. It should be noted that in this case is not BEL as such, but the overall PL loss (outdoor PL+ outdoor-to-indoor PL + indoor PL) what it is considered in the figures.

As aforementioned, the only external information that the model needs is the attenuation value of the external glass at normal incidence. As it can be seen in the Figures, the values assumed to fit the model to the measurements are realistic, according to the different type of construction (traditional or modern) and frequency bands [2].

FIGURE 232

Path loss measurement results in AAL1

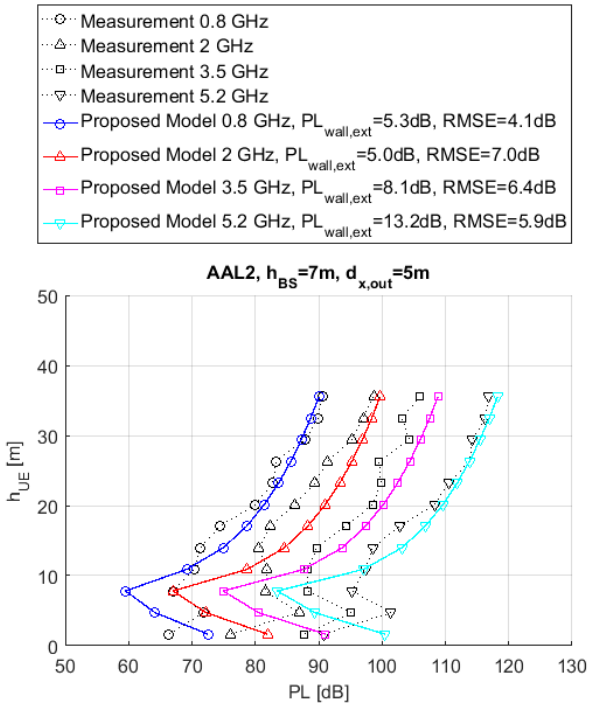

FIGURE 233

Path loss measurement results in AAL2

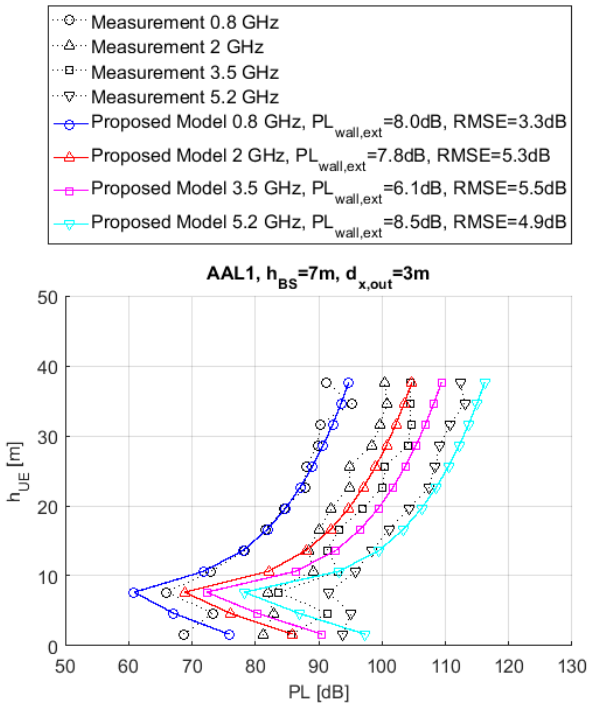

FIGURE 234

Path loss measurement results in AAL3

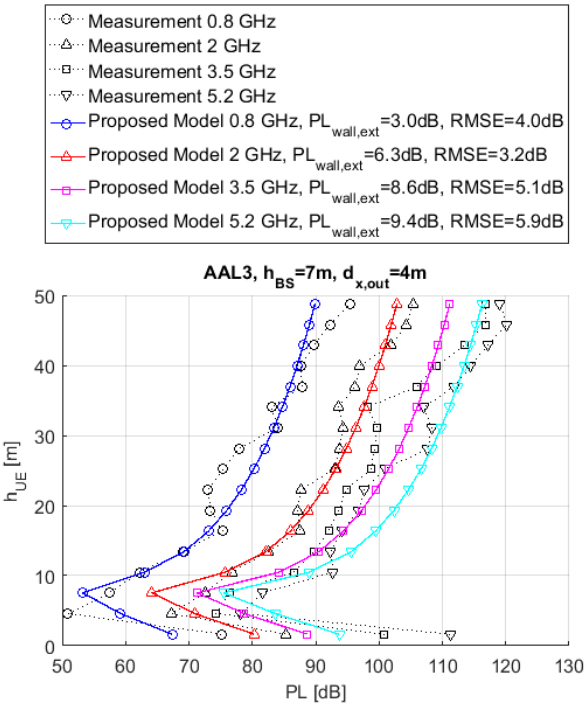

28.4 Summary

This section presented BEL measurement results with varying incident angle in the frequency range 800 MHz – 5.2 GHz for three different buildings. The following aspects are observed:

- BEL presents, in general, an irregular behaviour, although some trends are present:
  - BEL increases with absolute elevation incidence angle and frequency.
- Different buildings experience different BEL, due to the different composition of the external façade.
- Different indoor positions inside a building experience different BEL.
- Acknowledgement

Nokia Corporation would like to thank Aalborg University for providing the measurement data and corresponding analysis reported in [1]-[2].

References

[1] I. Rodriguez, H.C. Nguyen, T.B. Sørensen, Z. Zhao, H. Guan, and P. Mogensen, “A Novel Geometrical Height Gain Model for Line-of-Sight Urban Micro Cells Below 6 GHz”, IEEE International Symposium on Wireless Communication Systems (ISWCS), 2016.

Available: http://dx.doi.org/10.1109/ISWCS.2016.7600935

[2] I. Rodriguez, H.C. Nguyen, N.T.K. Jørgensen, T.B. Sørensen and P. Mogensen, “Radio Propagation into Modern Buildings: Attenuation Measurements in the Range from 800 MHz to 18 GHz”, IEEE Vehicular Technology Conference (VTC-Fall), 2014.

Available: http://dx.doi.org/10.1109/VTCFall.2014.6966147

28.A Attachment: Methodology

28.A.1 Measurement Setup

Practical microcell setup with omnidirectional antennas.

TX: lamppost-like, 7 m

RX: trolley-mounted, 1.75 m

28.A.2 Measurement Procedures and Data Processing

Each sample inside the building is a local average over ~2 sqm.

Calibrated link budget

Antenna compensation: Elevation pattern at BS, Effective gain at RX.

29 Building entry loss measurements at 3.5, 6, 10, 18, and 24 GHz frequencies in the Republic of Korea[17]

29.1 Introduction

In this section, in order to analyse the dominant factor in the frequency dependence of the BEL, window penetration loss (WPL) was investigated by on-site measurement and two BEL measurement scenarios were used. First, a transmitter (Tx) was placed on the façade of the building and the BEL characteristics were analysed by moving the receiver (Rx) to the office rooms and corridor inside the building. In order to eliminate the influence of BEL due to the complex structure inside the building, the Tx was located on a lateral building and the BEL was analysed while moving the Rx in the

[17] Sharing studies carried out by ITU-R on different agenda items of WRC-19 were based on the text of this Report which was inforce at the time of these activities or at the time which the activity was carried out.

corridor. The Republic of Korea provided WPL-dependent BEL measurement results for a traditional office building in the frequency range 3.5-24 GHz in the Republic of Korea.

29.2 Measurement methods

BEL measurements were performed in a traditional office building in Chosun university campus (Gwangju, in the Republic of Korea), as depicted in Fig. 235. The building is 10 stories tall with reinforced concrete shear walls whose thickness is 35 ~ 38 cm. In an exterior wall, a double glazed window (6 mm thick glass separated by an air gap of 12 mm) is mounted inside the 113 mm × 120 mm metal frame. Five windows are connected horizontally continuously on the exterior wall of the office room. The interior wall is being equipped with plasterboards and foam polyethylene sheet and its thickness is around 12.5 cm. There is a road on a hill approximately 43 meters away in front of the building and its height corresponds to that of the 5th floor of this building.

Figures 235 and 236 show photographs around the office building and the BEL measurement scenario. The signals used for this BEL measurement were continuous wave (CW) at 3.5, 6, 10, 18 and 24 GHz. Tx and Rx antennas were omnidirectional ones and their gain was frequency dependent (0.9-4.0 dBi). There are two measurement scenarios depending on Tx locations.

– In the first measurement scenario, the Tx is located at the façade of the building, the received power is measured in a complex structure inside the building.
– In the second measurement scenario, the Tx is placed at the lateral of the building, the received power is measured in a simple structured corridor.

For the first measurement scenario, a Tx 1 antenna at the façade of the building is located on the road. An indoor Rx 1 was on the 6th floor (6th F) and measured a received power while moving from the window to the inside of the building. The Tx 1 antenna was set up on a pole with a height of 2.5 m above ground, equal to the height of the Rx 1 antenna. There are seven sections and each section has four measurement locations such as Reference, Window, Middle, and Corridor. Window, Middle, and Corridor were marked on the floor and were 1.0, 5.0, and 10.2 m away from the exterior wall, respectively.

For the second measurement, the Tx 2 is located at a distance of about 44 m at the lateral of the building and the indoor Rx 2 on the 6th F corridor measures the received power by moving inward from the window of the corridor. The Tx 2 antenna is installed on a mast on a truck roof and is 12 m high above the ground, in order to be equal to the height of the Rx 2 antenna on the 6th F corridor. The Rx 2 measured the power radiated from the Tx 2 every 5 m in the 100 m long corridor inside the building. The reference power was also measured at the same distance from the exterior wall. The Rx 1 and 2 were the same system and its antenna was set up on a handcart inside the building. The antenna height was 1.5 m above the floor. The reference power outside the building was measured at a distance of 1.6 m from the exterior wall.

FIGURE 235

Photographs of the building for the BEL measurement. Tx positions on the road and Rx movement routes inside the building (a), facade view of the building (b), lateral view of the building (d), and the canyon (d)

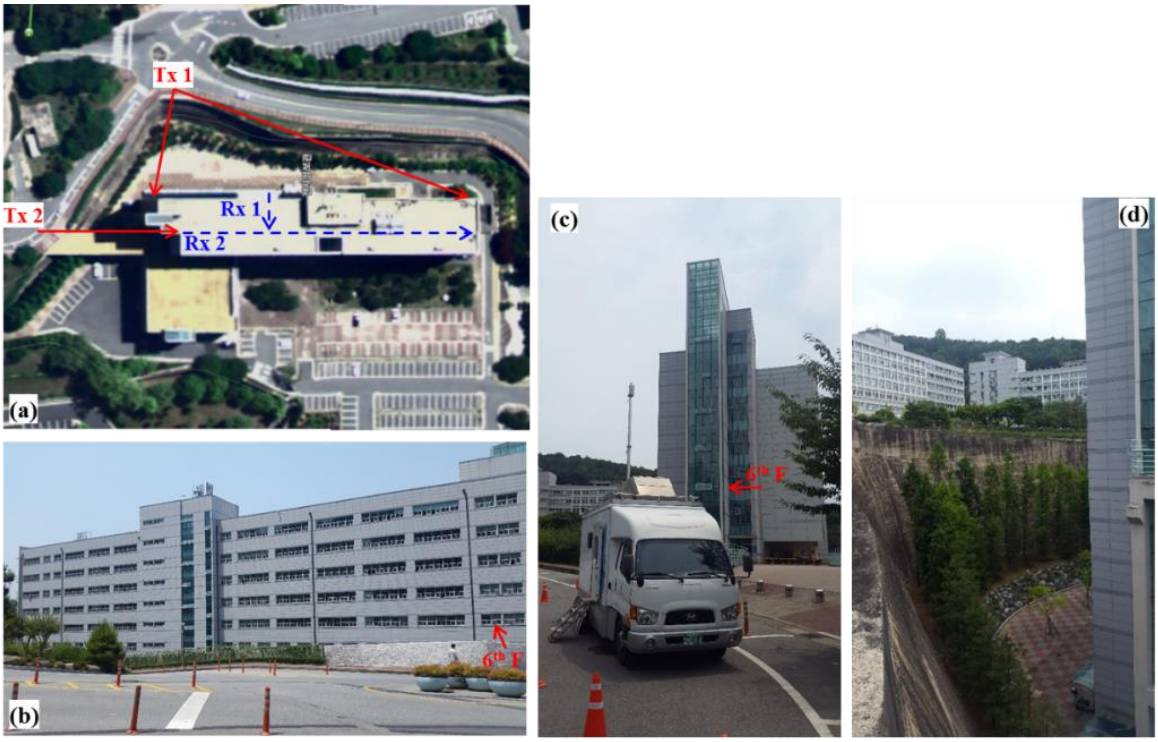

FIGURE 236

BEL measurement scenario [Tx and Rx locations, Photos of laboratory (a), seminar room (b), corridor (c) inside the building]

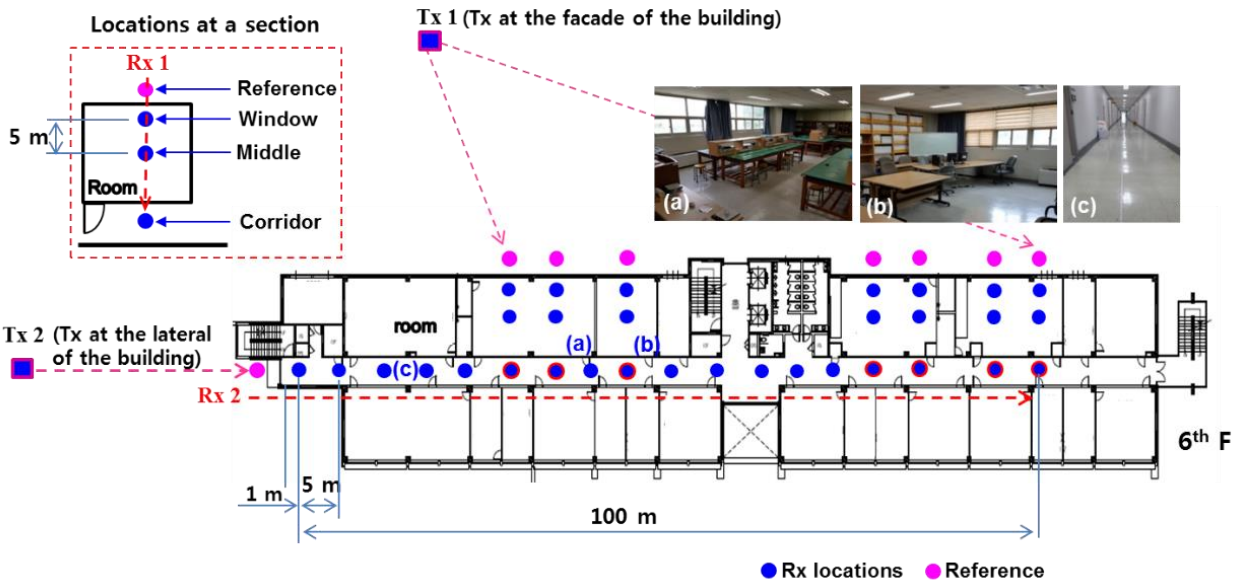

29.3 Measurement results

29.3.1 Window penetration loss (WPL) characteristics

Prior to the investigation of BEL, first, window penetration loss (WPL) was measured using two omnidirectional antennas, which were identical to those used for BEL measurements. These antennas were connected with a vector network analyser (VNA) and were placed inside and outside the outer

wall window, respectively. These were installed at a height of 1.5 m above the floor. The distance between two antennas was 2 m. S12 was measured according to the opening and closing of the window from 1 to 25 GHz.

Figure 237(a) shows the measured loss characteristics through window. WPL is frequency dependent; there is little loss at 3.5, 10, and 24 GHz. In particular, WPL at 6 and 18 GHz is 14 and 5.8 dB, respectively. It is consistent with recent published WPL research results [1-3]. That is, the WPL was particularly high in the 5-6 GHz band [1-3] and little loss in the 10-13 GHz band [3]. Oscillatory dependence of loss on frequency is due to a resonance phenomenon of the dielectric multilayer structure of the double or triple glazed window. At 24 GHz, however, two signals were overlapped due to fading effects. In order to demonstrate WPL at 18 and 24 GHz, the measurements were repeated using horn antennas (ETS-LINDGREN, model 3160-0). In Figure 237(b), WPL at 18 and 24 GHz is 3.24 and 1.32 dB, respectively. It is proven that these results show the same tendency as the results of omnidirectional antennas. Figure 237(c) presents WPL characteristics using the omnidirectional antennas at frequencies for BEL measurements.

FIGURE 237

Measured penetration loss characteristics through window using omnidirectional antennas (a) [insets: the window between the antennas was open (top) and closed (bottom)], horn antennas (b) [the insets: photos of the open (left) and closed (right) window], and WPL characteristics based on using omnidirectional antennas

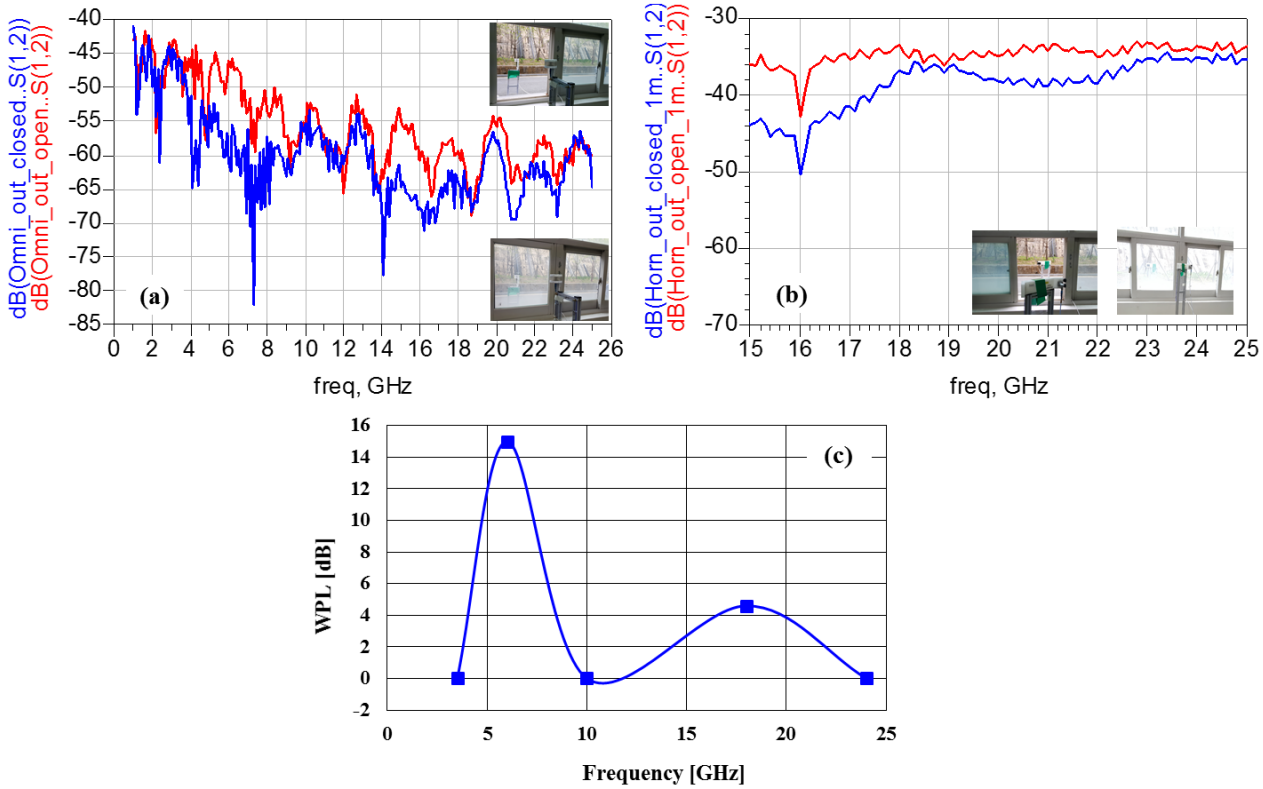

29.3.2 BEL characteristics

The BEL has been calculated by using the recommendations given in § 4 of Recommendation ITU-R P.2040-1 where its definition is the difference (in dB) between the median of the measured reference power and the received power measured inside the building.

Figure 238 presents cumulative distribution function (CDF) characteristics of the BEL based on the results of the first measurement. As the Rx moved deep inside the building, it is clear that the BEL increases. However, the CDF spread at the Window, Middle, and Corridor is reduced from 50.45 dB to 41.66 dB and 39.31 dB, respectively. That means that scattered and reflected energy becomes more

uniformly distributed. At all measurement locations, the BEL at 18 GHz was larger than at 24 GHz due to high WPL.

Figure 239 shows frequency and location dependency of the BEL at 10, 50, and 90 percentile levels of the CDF. As the Rx 1 moves from the Window to the inside of the building (Middle and Corridor), the BEL is also increased. In the Middle, BEL is equal or decreased compared to the BEL at the Window. This phenomenon indicates that many rays are received by multiple reflections. Despite the presence of internal walls and many clutters causing multi-reflections, the frequency characteristics of the BEL in the corridor show the same tendency as WPL. At 6 GHz, the BEL was equal to or slightly larger than that at 10 and 24 GHz. Similar results were observed in the measurement results reported in Report ITU-R P.2346-2. That is, the BEL is higher at 5.8 GHz and 8.5 GHz, which are one of the frequency bands of high WPL [1, 4, 5].

FIGURE 238

CDF characteristics of the BEL in terms of depth within the building and frequency

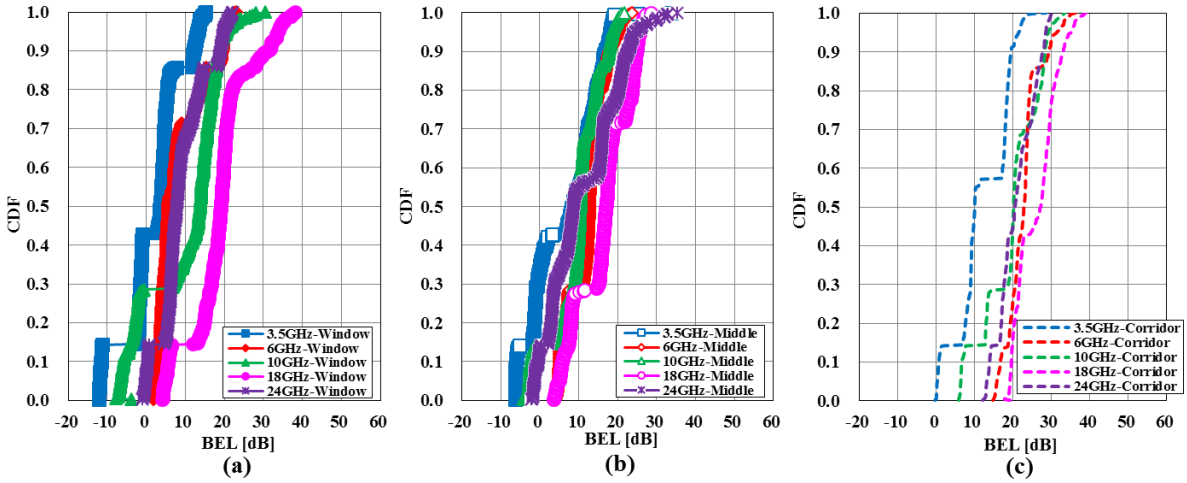

FIGURE 239

Frequency and location dependency of BEL at 10, 50 and 90 percentile levels of CDF

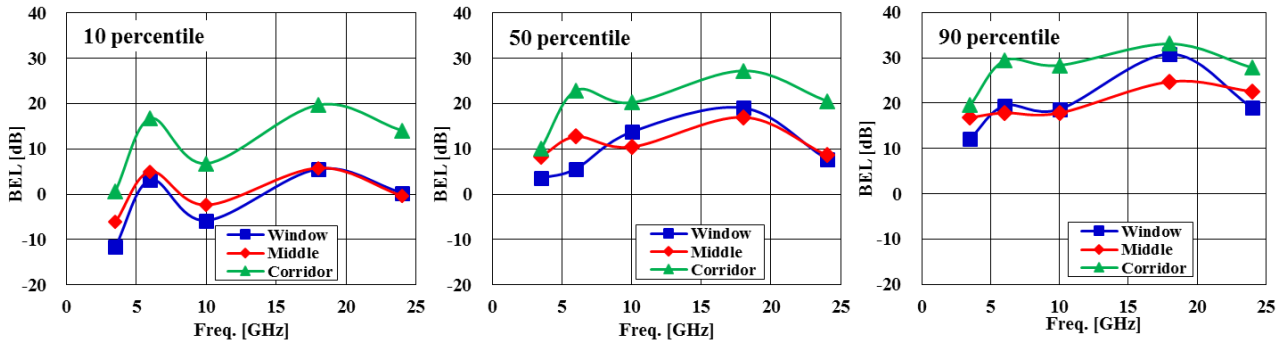

FIGURE 240

CDF characteristics of the BEL (left) and frequency dependency of BEL at 10, 50 and 90 percentile levels (right) for all locations [SD: the standard deviation]

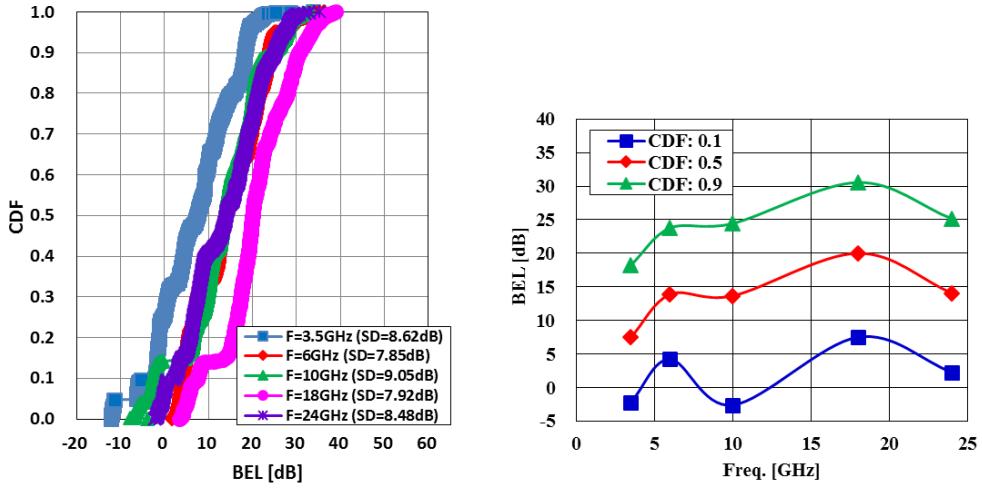

For the first measurement scenario, the CDF of the BEL measured at all locations and its frequency dependency at 10, 50 and 90 percentile levels are shown in Fig. 240. As the frequency increases, the BEL tends to increase. However, the BEL is low at 3.5, 10 and 24 GHz because of low WPL. It is clear that the BEL frequency dependence of the traditional building is directly affected by the WPL of the external window.

FIGURE 241

BEL characteristics as function of distance from the exterior wall

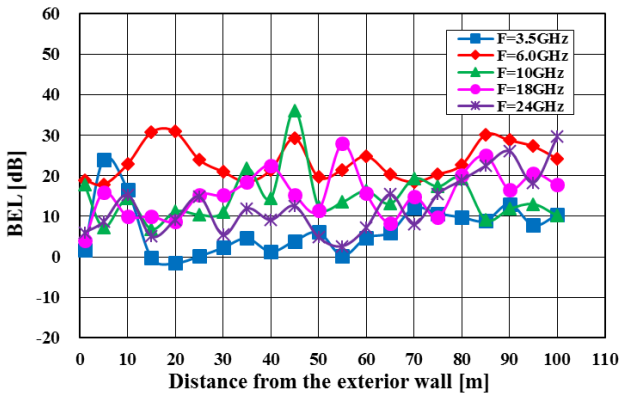

For the second measurement campaign, BEL characteristics were investigated as function of distance from the exterior wall which is in LOS with respect to the Tx 2. The results are presented in Fig. 241. As the distance increases, the BEL increases gradually and BEL fluctuation from 40 to 60 m is presumably due to the complicated corridor structure such as stairs, elevator, and toilet. The BEL at 6 GHz was larger than that at 10, 18 and 24 GHz, and the BEL at 24 GHz was similar to one at 10 and 18 GHz except for a fluctuation interval. These BEL characteristics are similar to the WPL.

FIGURE 242

Comparison of BEL measurement scenarios on the façade and lateral of a building [CDF (left) and its 10, 50 and 90 percentile levels as a function of frequency (right)]

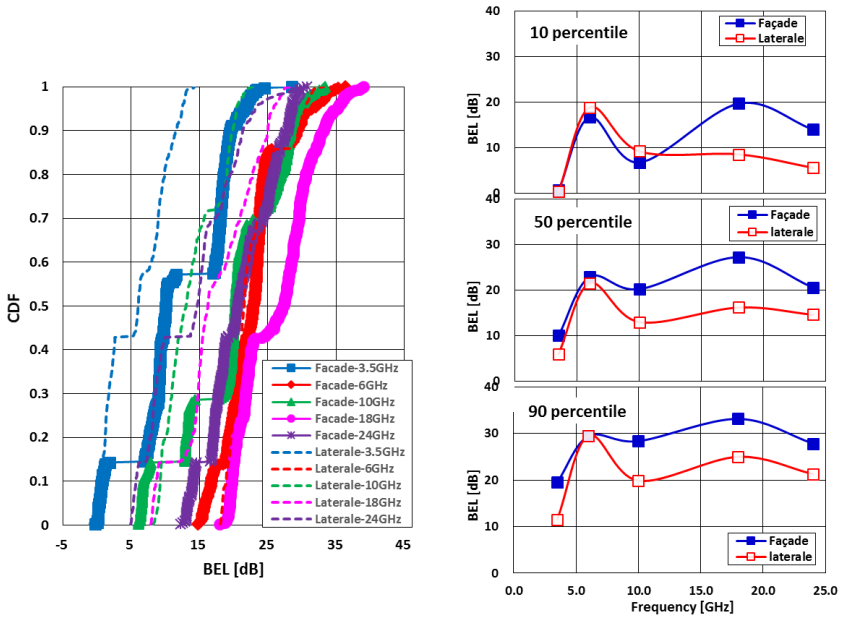

For the first and second measurements, BEL measured in the same seven locations in the corridor was investigated. Their CDF and frequency dependency at 10, 50 and 90 percentile levels of CDF are shown in Fig. 242. For the first measurement (facade) case, BEL increases overall due to interior wall penetration losses. The BEL difference due to frontal and lateral radiation from Txs is 8 dB above 10 GHz and the inner wall penetration loss is estimated to be less than 8 dB. It is also clear that the frequency dependency of the BEL is similar to that of the WPL.

29.4 Summary of the results

In these BEL measurements, in order to analyse the dominant factor in the frequency characteristics of the BEL, the window penetration loss (WPL) of the double glazed window was measured. The first BEL measurement scenario, which passes through the windows and the complex internal structures of the building, and the second BEL measurement scenario, which only penetrates the external windows, were performed for a traditional office building in the frequency range 3.5-24 GHz in the Republic of Korea. The WPL at 4-9 GHz bands and 13-18 GHz band is high, but one at 10-13 GHz band and 23-25 GHz bands is negligible due to a resonance phenomenon of the dielectric multilayer structure of the double glazed window. These WPL frequency characteristics are directly reflected in the BEL frequency dependency. In the first BEL measurement scenario, from the window, to the middle of the office and the corridor inside the building, the frequency characteristics of the BEL were the same as those of the WPL. In the second BEL measurement scenario, the BEL at 6 GHz was larger than that at 10, 18, and 24 GHz, and the BEL at 24 GHz was similar to one at 10 and 18 GHz. These BEL characteristics are also similar to WPL. As measurement results of the WPL and two BEL scenarios, it is clear that the BEL frequency dependence of the traditional building is directly affected by the WPL of the external window.

References

[1] Aki Karttunen, Sinh Le Hong Nguyen, Pasi Koivumäki, Katsuyuki Haneda, Tuomo Hentilä, Ari Asp, Arto Hujanen, Ismo Huhtinen, Matti Somersalo, Seppo Horsmanheimo, and Jouko Aurinsalo, “Window and Wall Penetration Loss On-Site Measurements with Three Methods,” IEEE European conference on antennas and propagation (EuCAP), 2018.

[2] Rudd, R., Craig, K., Ganley, M., and Hartless, R. "Building materials and propagation," Final Report, Ofcom, 2604 2014.

[3] ITU, "Compilation of measurement data relating to building entry loss" Report ITU-R P.2346-2, pp. 138-158.

[4] ITU, "Compilation of measurement data relating to building entry loss" Report ITU-R P.2346-2, pp. 97-101.

[5] ITU, "Compilation of measurement data relating to building entry loss" Report ITU-R P.2346-2, pp. 133-138.

30 Effect of antenna beamwidth on building entry loss (Republic of Korea, 32.4 GHz)[18]

30.1 Introduction

Recommendation ITU-R P.2109 – Prediction of Building Entry Loss, makes the assumption of omnidirectional antenna reception. Guidance is required for the case where directional antennas are deployed. To address this issue, BEL measurement campaigns were conducted with various directional antennas and developed an antenna beamwidth-dependent BEL model.

30.2 Measurement overview

The system parameters and specifications of the sounder are listed in Table 94.

TABLE 94

ETRI's 32 GHz channel sounder specification

Centre frequency	32.4 GHz
Bandwidth	500 MHz
Max Tx power	22 dBm
PN code length	4095
AGC dynamic range	60 dB
Sounding architecture	Sliding correlation

With this new sounder, BEL measurements were conducted with the four antennas listed in Table 95.

TABLE 95

RX antenna information

Antenna (HPBW)	Antenna gain
10° horn antenna	27.0 dBi
30° horn antenna	15.6 dBi
60° horn antenna	9.7 dBi
Omnidirectional antenna	5.8 dBi

[18] Sharing studies carried out by ITU-R on different agenda items of WRC-19 were based on the text of this Report which was inforce at the time of these activities or at the time which the activity was carried out.

The BEL measurements were conducted in two office buildings in ETRI campus as shown in Figs 243 and 244. The exterior walls of both buildings were constructed with concrete blocks and glass windows. Since Building A uses regular glass, Building A is classified as a traditional building according to Recommendation ITU-R P.2109-0. Building B is classified as thermally-efficient since the windows are dual-layer with an interior metallic coating. Building A is six stories with a planar dimension of 72 m × 25 m, while Building B is five stories with a dimension of 58 m × 27 m.

FIGURE 243

BEL measurements for Building A (traditional type)

FIGURE 244

BEL measurements for Building B (thermally-efficient type)

Figure 245 shows the BEL measurement setup. The antenna height of RX and that of TX are the same above the ground (aligned with a laser pointer), i.e. $h_{TX} = h_{RX'}$, and these heights are sufficiently high to avoid clutter (trees, vehicles, humans, etc.) between the building and TX (As shown in Figs 243 and 244, a lift was utilized to adjust the TX height). In Building A, the measurements were collected on the 2nd floor (following the European convention of floor level count, i.e. the ground level is the 0th floor) and $h_{TX}(= h_{RX'}) = 11.7$ m, $h_{RX} = 1.5$ m, $d_{TX\text{-building}} = 33$ m. In Building B, the measurements were on the 3rd floor and $h_{TX}(= h_{RX'}) = 14.7$ m, $h_{RX} = 1.5$ m, $d_{TX\text{-building}} = 38$ m.

FIGURE 245

BEL measurement setup

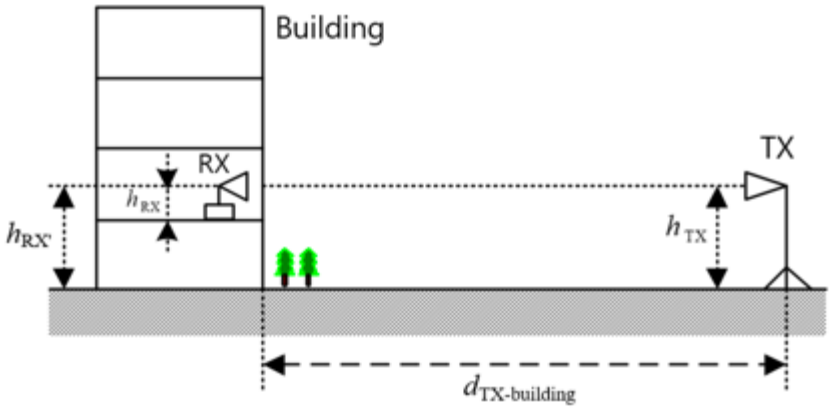

To consider near perpendicular incidences on the building, an effort was made to move the position of TX along with the position RX. However, the TX was not moved for every individual RX point. IT was moved when the region of RX was changed. The concept of the RX region is shown in Fig. 246.

FIGURE 246

TX positions for near perpendicular incidences

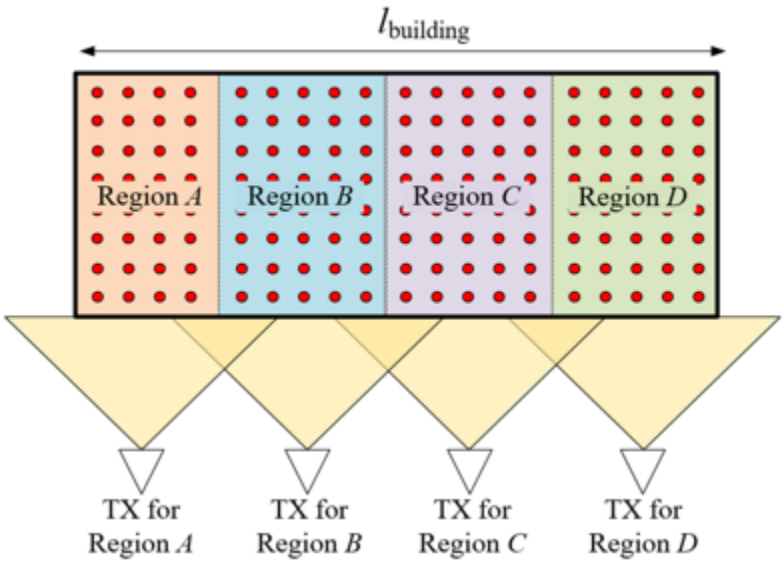

Figures 247 to 250 show RX measurement environments for a corridor, a conference room, a computer lab and an open-space office, respectively.

FIGURE 247

Corridor measurement

FIGURE 248

Conference room measurement

FIGURE 249

Computer lab measurement

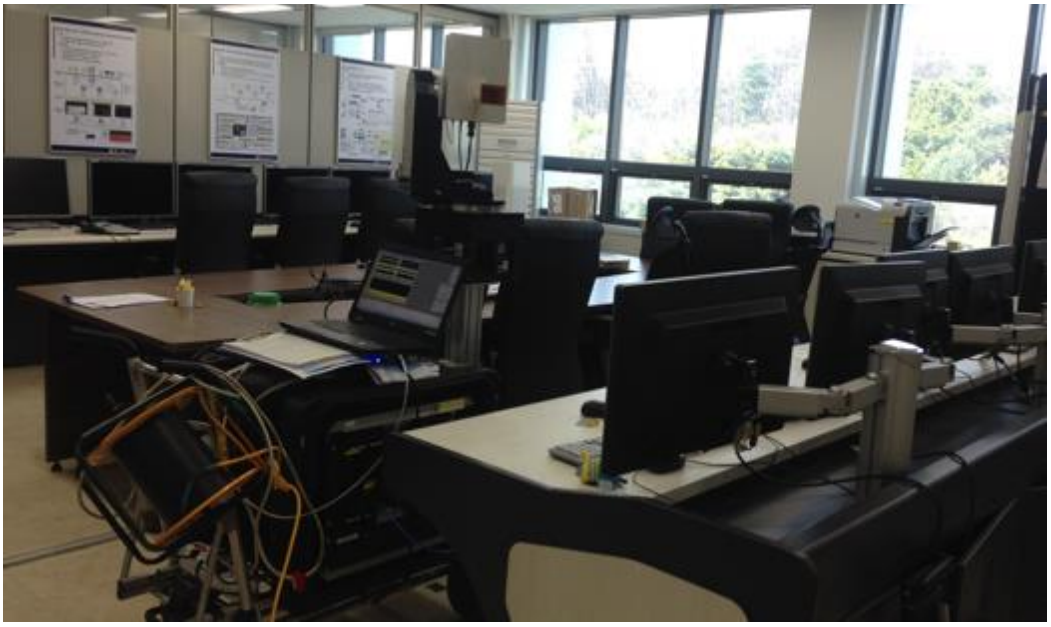

FIGURE 250

Open space office measurement

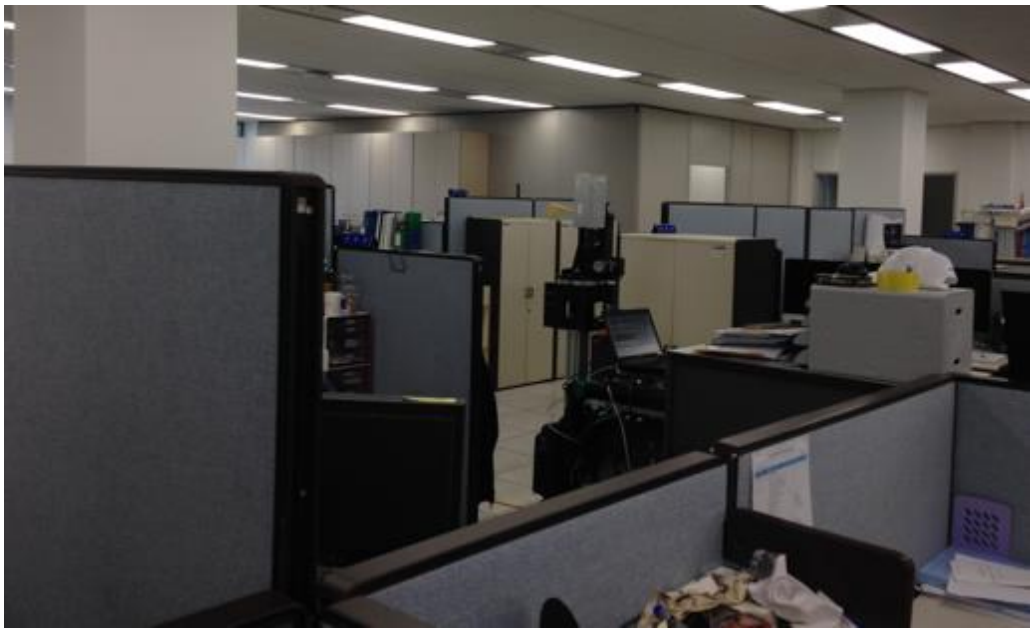

Figures 251 and 252 show measurement points for Buildings A and B, respectively.

FIGURE 251

Measurement points for Building A

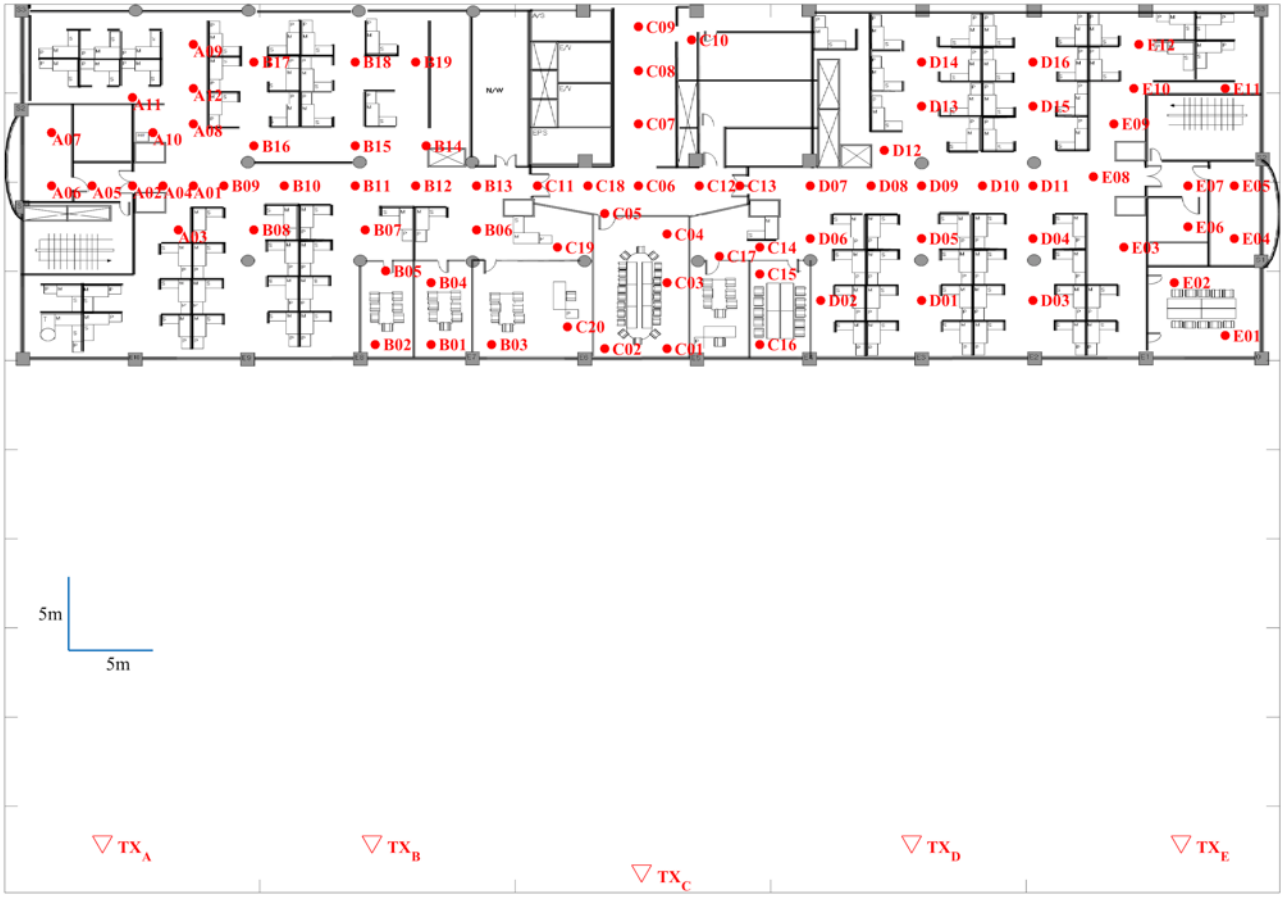

FIGURE 252

Measurement points for Building B

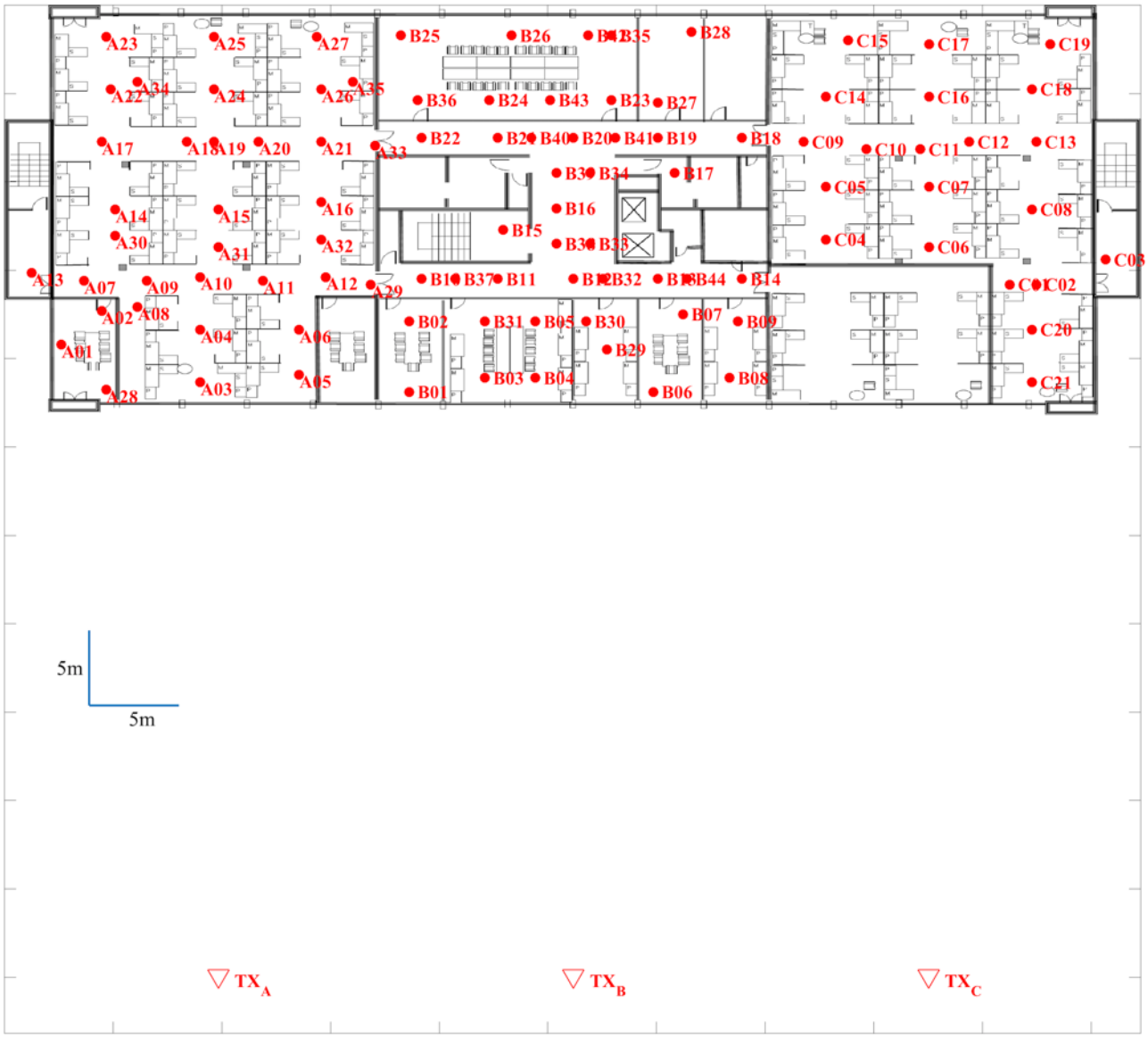

30.3 Measurement results

Figures 253 and 254 show graphical illustrations of BEL measurements at every RX point in Building A. Figure 253 illustrates rotational BEL measurements collected with the 10° horn antenna and Fig. 254 illustrates omnidirectional BEL measurements collected with the omnidirectional antenna. Among the Rx points in the figures, outages occurred at the points marked with "×".

FIGURE 253

Rotational BEL measurements with 10° horn antenna in Building A

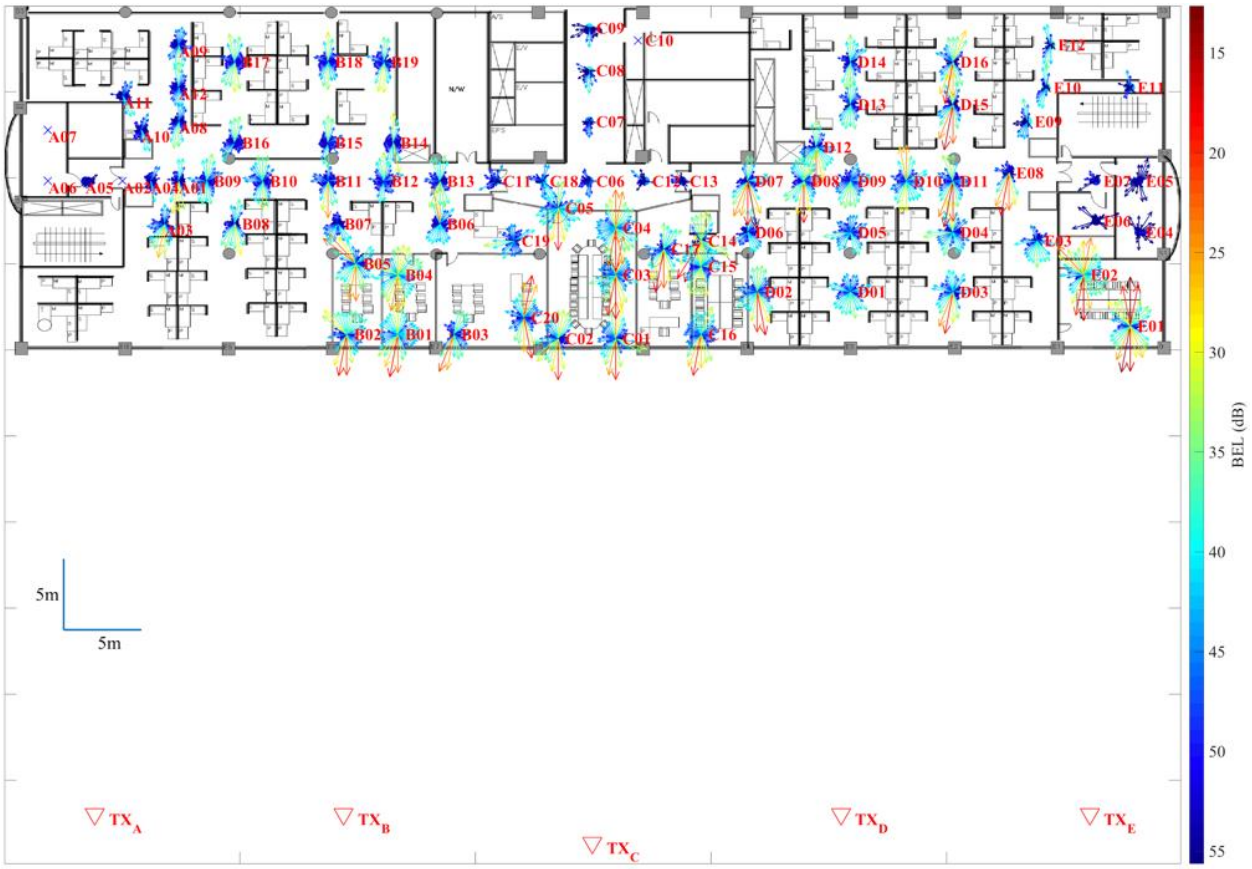

FIGURE 254

Omnidirectional BEL measurements in Building A

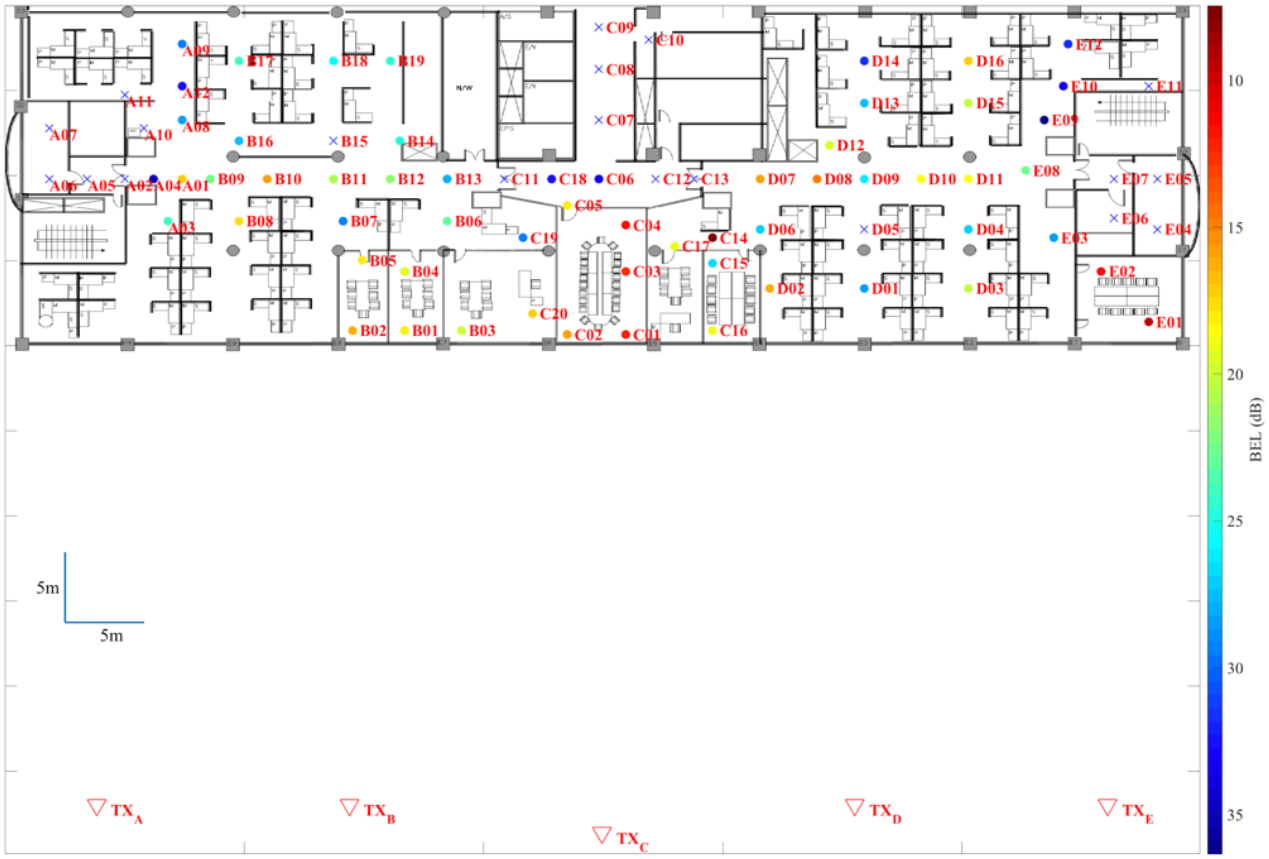

Figures 255 and 256 show graphical illustrations of 10º horn antenna and omnidirectional antenna BEL measurements collected in Building B, respectively.

FIGURE 255

Rotational BEL measurements with 10° horn antenna in Building B

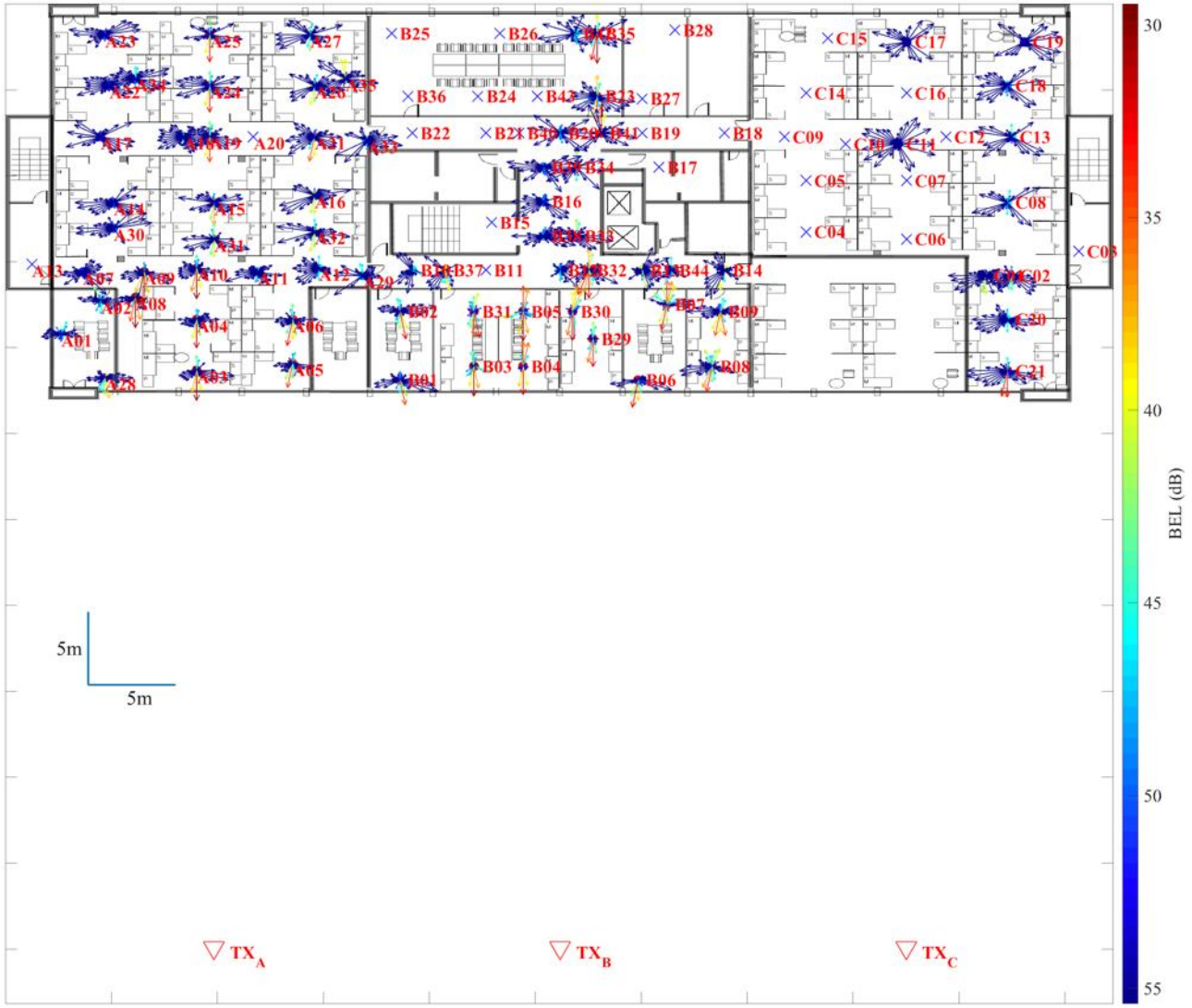

FIGURE 256

Omnidirectional BEL measurements in Building B

Although measurements were conducted with several beamwidth antennas such as 10º, 30º, 60º and omnidirectional antennas, the beamwidth-dependent BEL analysis was performed with beamwidth-synthesized data from the 10º horn antenna measurement data based on the procedures in Recommendation ITU-R P.1407. This is because the 10º horn antenna measurement data have fewer outage points than the wider-beamwidth antennas. Note that the outage points were assigned to the highest observed loss value to ensure all measurement locations are used in the CDFderivation.

Figure 257 shows the 10º horn antenna directional BEL and the omnidirectional BEL statistics compared to the BEL model in Recommendation ITU-R P.2109-0. As can be seen, the CDFs from the omnidirectional BEL measurements are close to those in the Recommendation, which the measurement environments (building materials and building inside environments) and the environments in the Recommendation are in agreement. It can be seen that the 10º beamwidth directional BEL statistics are clearly different from the omnidirectional BEL statistics for both traditional and thermally-efficient buildings. That is, the existing BEL model in the Recommendation does not provide accurate BEL information depending on the antenna beamwidth. Note that all the other beamwidth (from 10º to omnidirectional) directional BEL statistics are in between the 10º beamwidth BEL statistics and omnidirectional BEL statistics.

FIGURE 257

Comparison of BEL measurements to the existing Rec. ITU-R P.2109 models

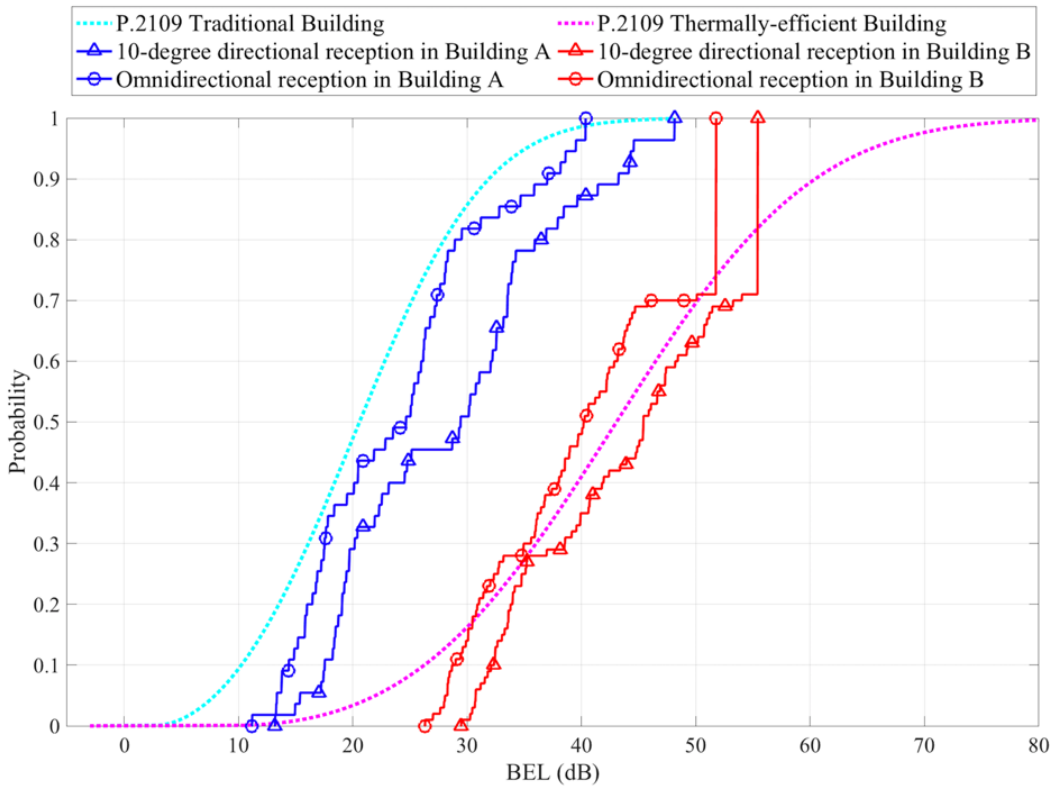

Figure 258 shows the BEL variation with respect to the antenna beamwidth when the probability $P = 0.5$ from Fig. 257. The BEL difference between the 10º directional reception and the omnidirectional reception is 5.27 dB and 5.23 dB for Building A and Building B, respectively. IT can also be seen that the BEL in Fig. 258 is dependent on the antenna beamwidth.

FIGURE 258

BEL variation with respect to antenna beamwidth for *P*=0.5

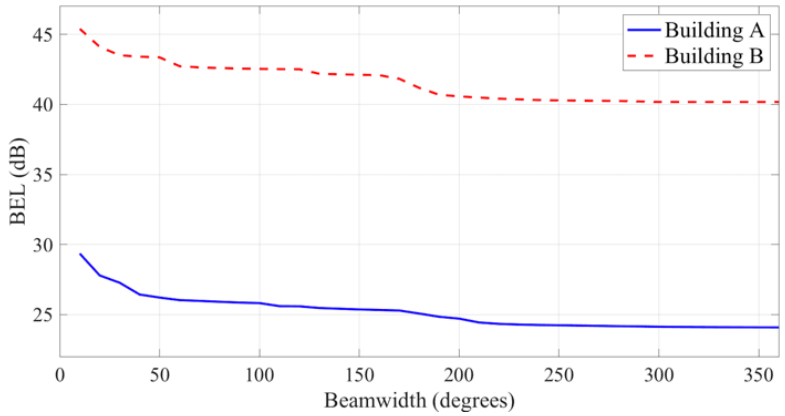

30.4 Model development

To reflect the antenna beamwidth effect on the BEL model in Recommendation ITU-R P.2109-0, the overall beamwidth-dependent BEL model was considered as given below:

$$L_{BEL}^{narrow}(W_\phi) = L_{BEL}^{omni} + \Delta L_{BEL}(W_\phi) \quad \text{(dB)} \tag{37}$$

where W_ϕ denotes the antenna half-power beamwidth, L_{BEL}^{omni} denotes the omnidirectional BEL that can be obtained with the existing BEL model in the Recommendation and ΔL_{BEL} denotes the additional loss due to the antenna beamwidth effect.

In equation (37), ΔL_{BEL} can be obtained by measurement data fitting. By examining the measurement data, it was found that ΔL_{BEL} is inversely proportional to the beamwidth. By fitting the following model to the measurement data, the fitting parameter as in Table 97 was obtained.

$$\Delta L_{BEL}(W_\phi) = \eta\left(\frac{1}{W_\phi} - \frac{1}{360^\circ}\right),\ 10^\circ \le W_\phi \le 360^\circ \tag{38}$$

As can be seen in Table 96 (as illustrated in Fig. 259), the difference of the constant parameter η between Building A and Building B is not significant. This is because the beamwidth effect is relevant to the surrounding indoor environment inside the buildings; while L_{BEL}^{omni} will capture the building-type differences. A single constant η was obtained by fitting both Buildings A and B measurement data simultaneously as in Table 96. As can be seen in Fig. 259, the combined parameterised model does not deviate much from the individually parameterised models.

TABLE 96

Constant η for W_ϕ-beamwidth directional BEL

Building	η	RMSE (dB)
A	62.11	1.08
B	54.90	0.86
A & B combined	58.00	0.94

FIGURE 259

Additional BEL in terms of antenna beamwidth

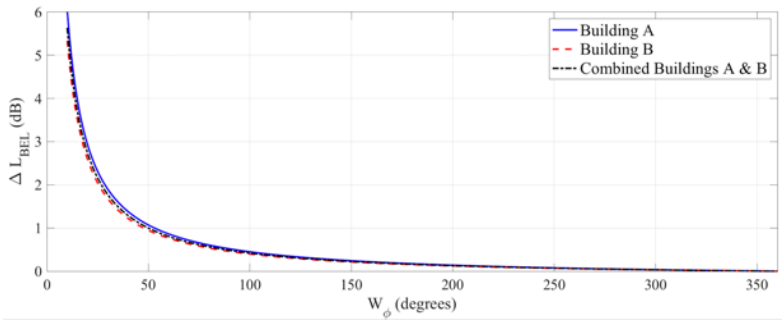

31 New measurements of domestic buildings (UK, 169 MHz – 60 GHz)[19]

31.1 Introduction

A campaign of measurements has recently been completed in the UK to gather further data on building entry loss to domestic buildings of contrasting construction type. These measurements were carried out at the Building Research Establishment (BRE) campus in the UK in 2017. Measurements were made at frequencies between 169 MHz and 60 GHz in four dwellings, representative of both

[19] Sharing studies carried out by ITU-R on different agenda items of WRC-19 were based on the text of this Report which was inforce at the time of these activities or at the time which the activity was carried out.

traditional and modern (thermally efficient) construction methods. The work was sponsored by Telefonica UK.

It is hoped that this new independent data set be useful in the validation of the existing models and in the development of new site-specific models.

31.2 Measurement method

31.2.1 Target buildings

The test houses used are shown in Figs 260 and 261 below.

The 'UserHuus' is an example of modular off-site construction. It consists of separate 4.9 m × 11.4 m unit blocks which are then assembled onsite. There are two connected semi-detached houses on site. The external walls are formed of timber frame to which cladding panels are attached. A cavity void exists between the outside cladding and the foil backed insulation which forms part of the pre-assembled modules. Foil backed PIR boards are used for the floor and ceiling as well as the sides for thermal efficiency. The windows are double glazed and come fitted with the modules.

The Wienerberger house is a modern, thermally efficient, version of a conventional brick built house. It has large windows which provide a lot of sunlight during the days and has a large open plan kitchen and living room. The inner walls are constructed of clay block with a cavity between the inner wall and external wall comprising of an air gap void and thermal insulating wool wall slabs. The external wall is of conventional 103 mm thick modern brick. The windows are extremely thermally efficient and consist of a powder coated aluminium frame which has a softwood internal frame with double glazing.

FIGURE 260

'Modern' test houses: UserHuus (left) and Wienerberger E4 (right)

The Mansion was built in the 1870's using typical Victorian construction methods. The external walls are of solid construction. It has no insulated cavity, the windows are traditionally timber-framed with thick single paned glass and the internal and external doors are solid wood.

FIGURE 261

'Traditional' test house: The mansion

31.2.2 Measurement equipment

The need to make measurements on a wide range of frequencies, coupled with a requirement for the use of a wideband test signal, led to the use of a software-defined radio approach for the measurement system. The platform used was the Ettus 'B200mini' transceiver, which covers 70 MHz to 6 GHz with up to 56 MHz bandwidth.

To remove multipath fading effects, a simple pseudo-noise (PN) sequence sounding signal is used, clocked at 20 MHz. The software receiver consisted of a correlator matched to the transmitted sequence. The output of this correlator gives the time-domain response of the channel, but this is not required in the present work; furthermore, the temporal resolution available at the bandwidths used is too low to give useful data on the short paths being examined here. The impulse response data was not, therefore, retained.

At the lower frequencies, a linear power amplifier (mini circuits type ZHL-42+) was used to raise the output of the B200 SDR from the nominal +10 dBm to around +30 dBm. The receiver software aggregates all impulse response peaks that exceed the noise floor by 10 dB, and saves the result to file. In the version of the software used below 6 GHz, these received power values are logged continuously, and are also added to a plot showing the cumulative distribution of received power which is updated continuously. This display allows the operator to judge the point at which the statistics gathered have become stationary.

For the lower millimetre-wave bands (27 and 38 GHz), the B200 transceivers were used at an intermediate frequency around 2 GHz, with custom-built up- and down-converters used to achieve the final frequency. At these frequencies, link-budget limitations mean that it is not feasible to collect data continuously by sampling the room with an omnidirectional antenna. Furthermore, the use of such an antenna would be unrealistic, as real systems would exhibit significant directionality.

FIGURE 262

mm-wave downconverter on azimuth-scanning mount

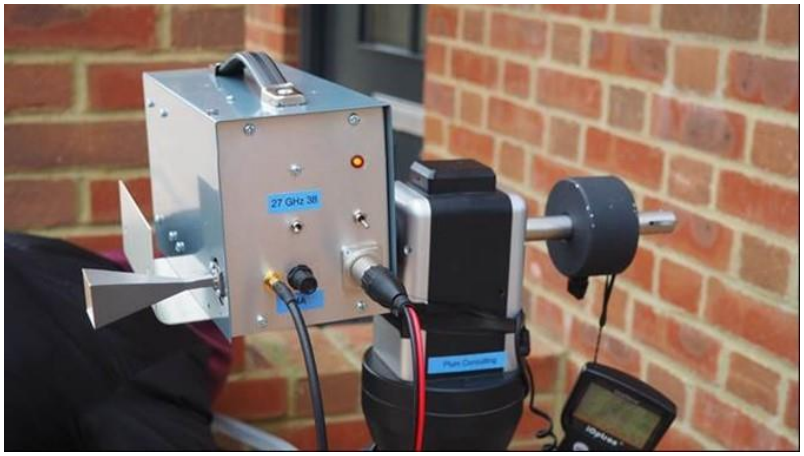

For measurements at the highest frequency, development modules from Pasternack Inc were used in conjunction with the same SDR equipment. These measurements were constrained by the link budget available and are not reported in the present contribution.

The measurement bandwidths used for each frequency are shown in Table 97.

TABLE 97

Measurement frequencies and bandwidths

Frequencies	Bandwidth
169 MHz and 458.5 MHz	1 MHz
700 MHz, 2.3 GHz and 3.5 GHz.	20 MHz
27 GHz, 38 GHz, 60 GHz	20 MHz

31.2.3 Procedure

The BEL calculations compared indoor measurements with external reference measurements made approximately 1 m in front of each property. At frequencies below 6 GHz, the reference measurements were made at ground floor level by walking backwards and forwards across the front of the house with a receive antenna height of 1.7 m above ground. The median value of the received power was taken as the reference, the intention being to remove any multipath effects from the estimate of the power flux incident on the building. Measurements were also made at first floor and second floor (for UserHuus only) heights by holding the receive antenna out of upstairs windows.

At higher frequencies, the use of directional antennas and the small Fresnel zones makes it possible to use the maximum measured power directly as the reference. The ground floor reference was used for all BEL calculations as this was a more accurately controlled measurement.

31.2.4 Data processing

The measurements made above or below 6 GHz were processed differently due to the different ways the measurements were made. Cumulative distribution function (CDF) graphs were generated for individual rooms and whole house results; for the <6 GHz measurements, these represent the entirety of the continuous data gathered with omnidirectional antennas. At above 6 GHz, the primary CDF plots relate to measurements made with the directional antennas aligned for maximum received power. Plots are also included showing the statistical distribution of power over all azimuths; these

latter statistics would be relevant for predictions of interference where arbitrary antenna orientation can be assumed.

31.3 Results

31.3.1 Median BEL results averaged over all rooms

Figures 263 and 264 show the variation in the median BEL with frequency for each house, averaged over all rooms, for two different incidence angles.

The cross-over of the Wienerberger plot above the UserHuus plot at higher frequencies may be due to the type of low E glazing used; if both houses used the same glazing the results may have tended to merge at higher frequencies as the behaviour of apertures comes to dominate as wall attenuation increases.

FIGURE 263

BEL for all houses averaged over all rooms at normal incidence

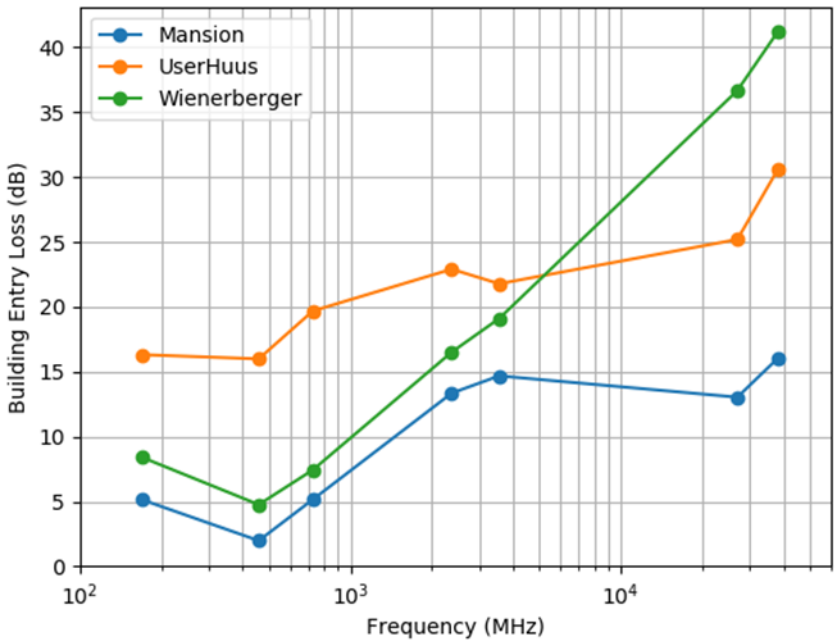

FIGURE 264

BEL for all houses averaged over all rooms at 45° incidence

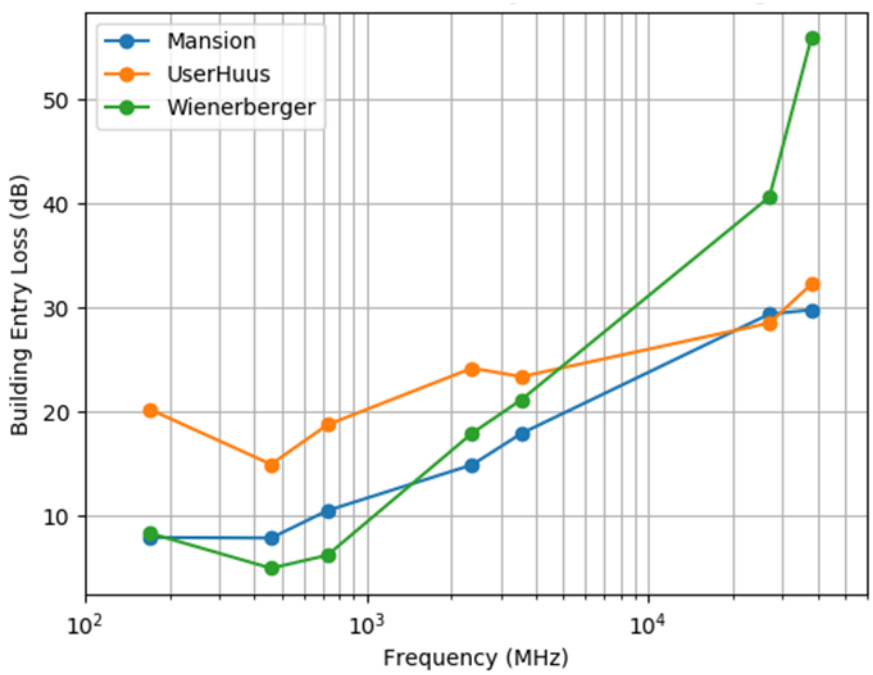

31.3.2 Median BEL results for each room in each house

For each antenna height and incident angle the relative BEL for each of the rooms in the Mansion follows a pattern that would be expected. The rooms 002 and 004 are on the ground at the back of the Mansion with no directly visible windows, with signals needing to penetrate the external wall and at least one internal wall. Room 101 has no directly visible external window. These rooms have the highest BEL as expected. Room 002 and room 101 both have an external side window although this is not directly visible for an incident angle of 90°. However, at an incident angle of 45° this side window is partially visible, and this does appear to reduce the BEL of room 002 compared to room 004 at higher frequencies, whilst the BEL of room 101 is considerably reduced over all frequencies.

The hallways and room 102 have windows of plain glass, giving a line of sight to the external terminal.

FIGURE 265

BEL for all rooms in Mansion at normal incidence

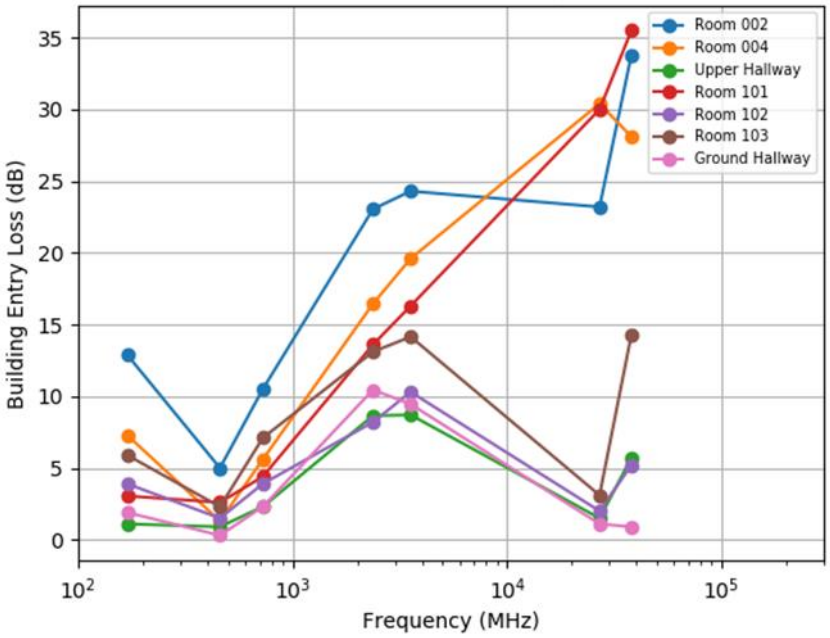

FIGURE 266

BEL for all rooms in Mansion at 45° incidence

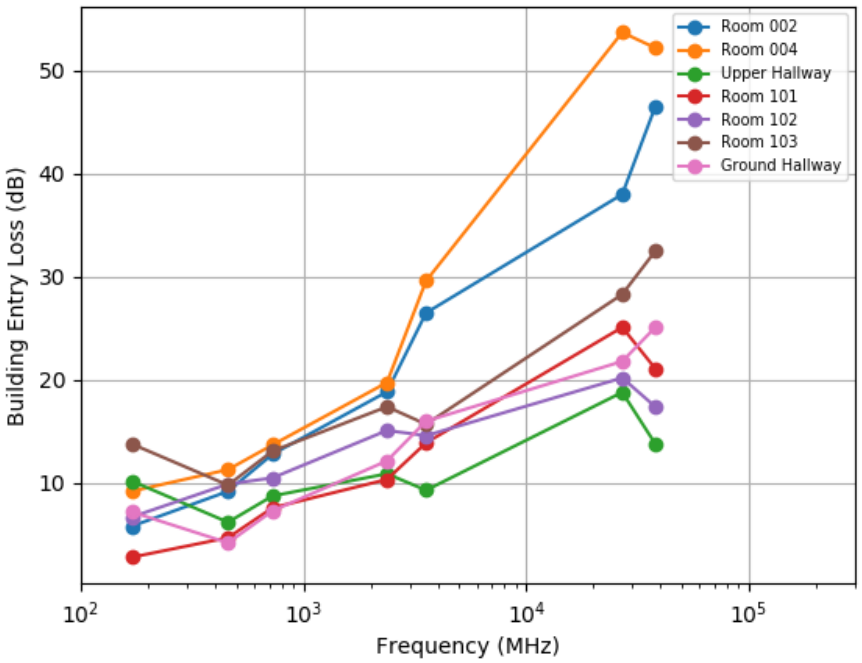

FIGURE 267

BEL for all rooms in UserHuus at normal incidence

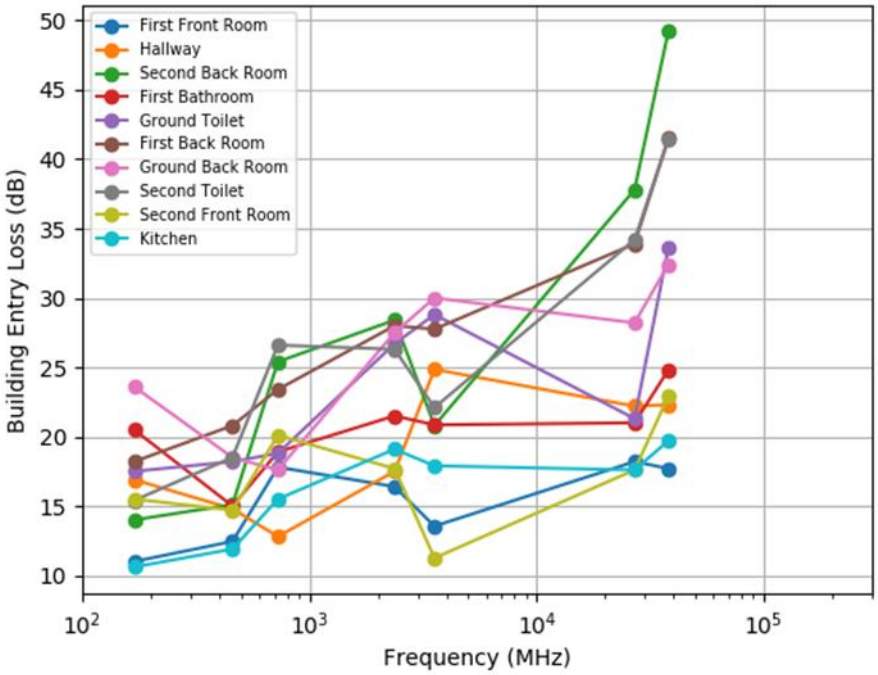

FIGURE 268

BEL for all rooms in UserHuus at 45° incidence

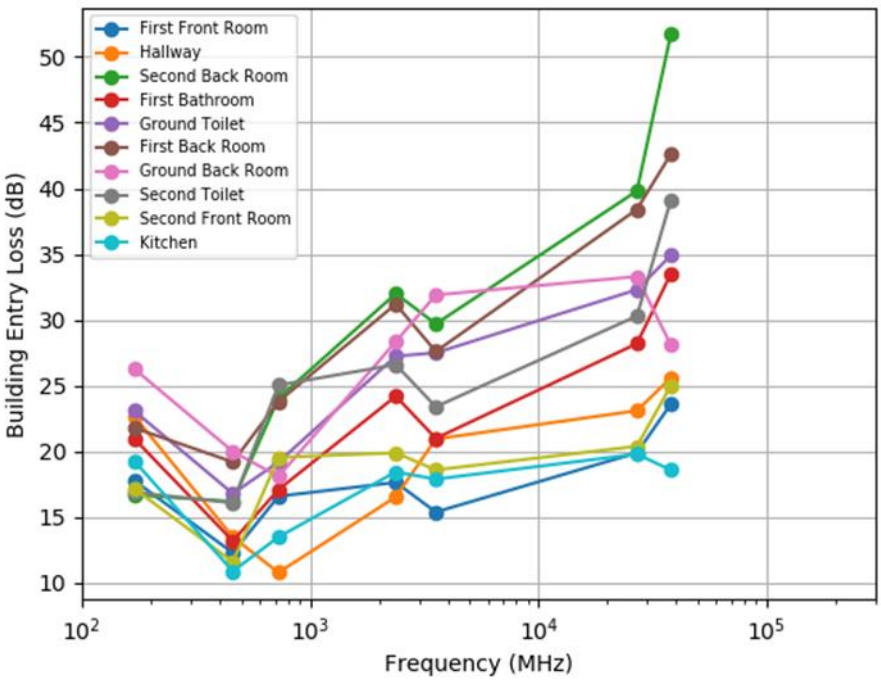

FIGURE 269

BEL for all rooms in Wienerberger at normal incidence

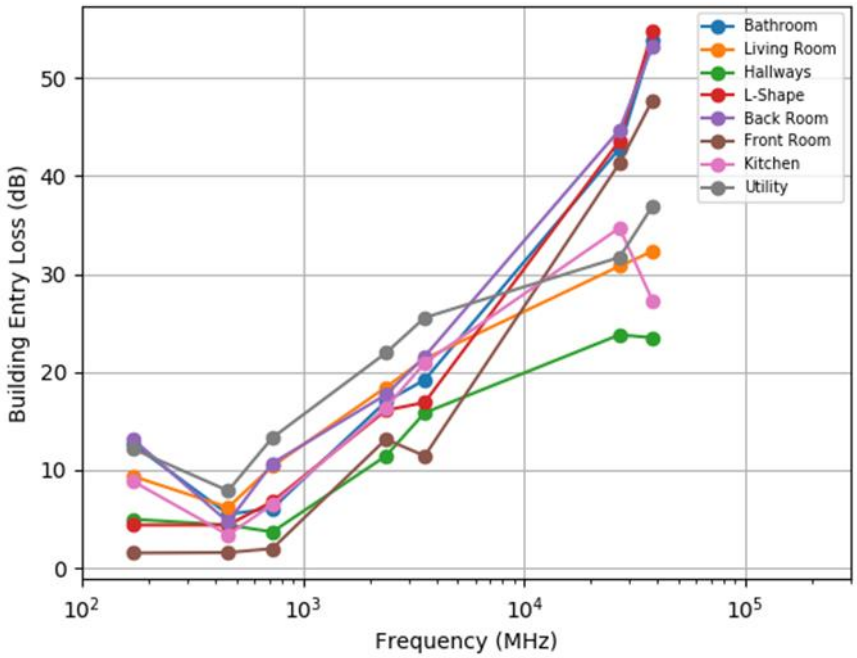

FIGURE 270

BEL for all rooms in Wienerberger at 45° incidence

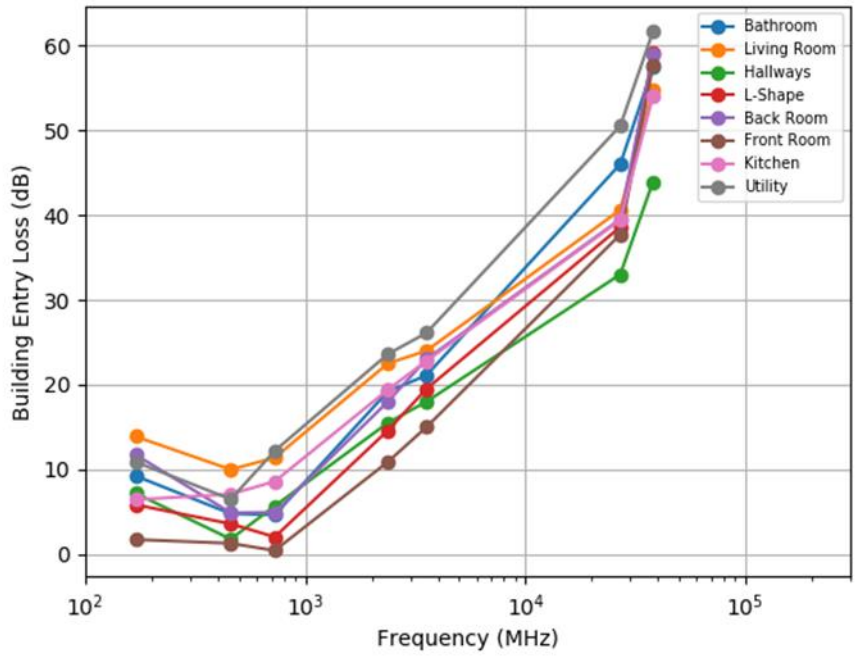

31.3.3 Cumulative distributions of BEL

This section shows CDF graphs across all frequencies except 60 GHz for each house, transmit antenna height and incident angle.

It should be noted that, unlike the results above, these statistics include data gathered at all orientations of the mm-wave antennas. The CDFs for these frequencies cannot, therefore, be directly compared with the model of Recommendation ITU-R P.2109.

FIGURE 271

BEL CDF for Mansion rooms (including antenna pattern, LHS 90°, RHS 45°)

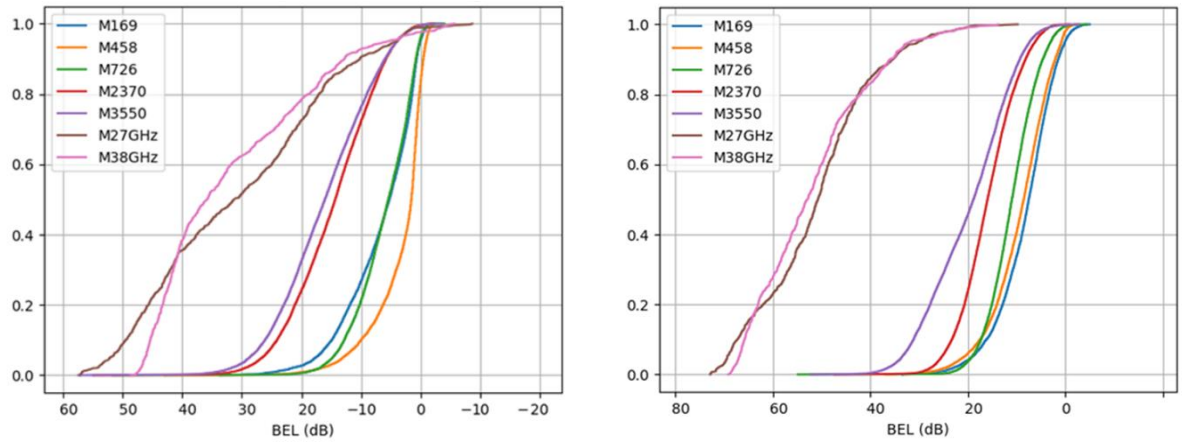

FIGURE 272

BEL CDF for UserHuus rooms (including antenna pattern, LHS 90°, RHS 45°)

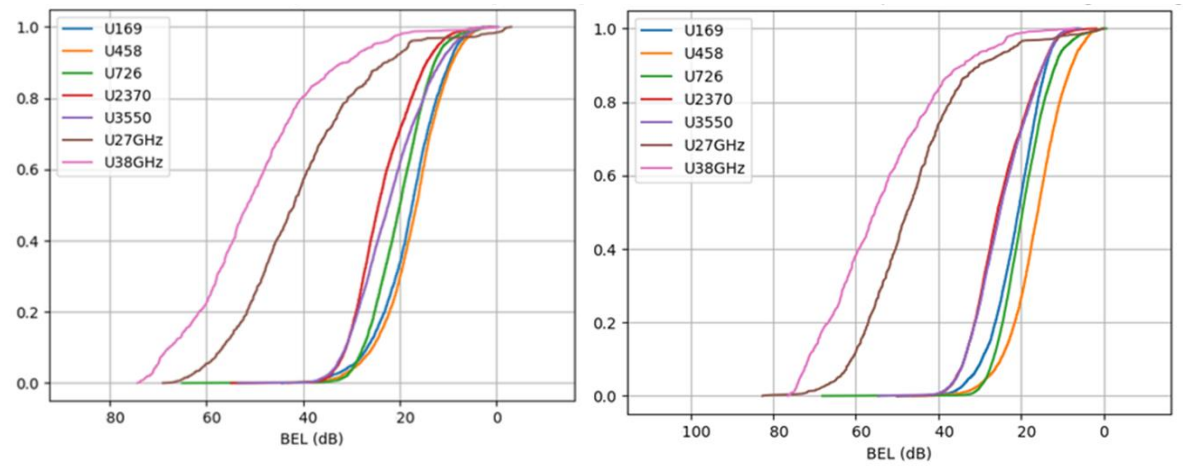

FIGURE 273

BEL CDF for Wienerberger rooms (including antenna pattern, LHS 90°, RHS 45°)

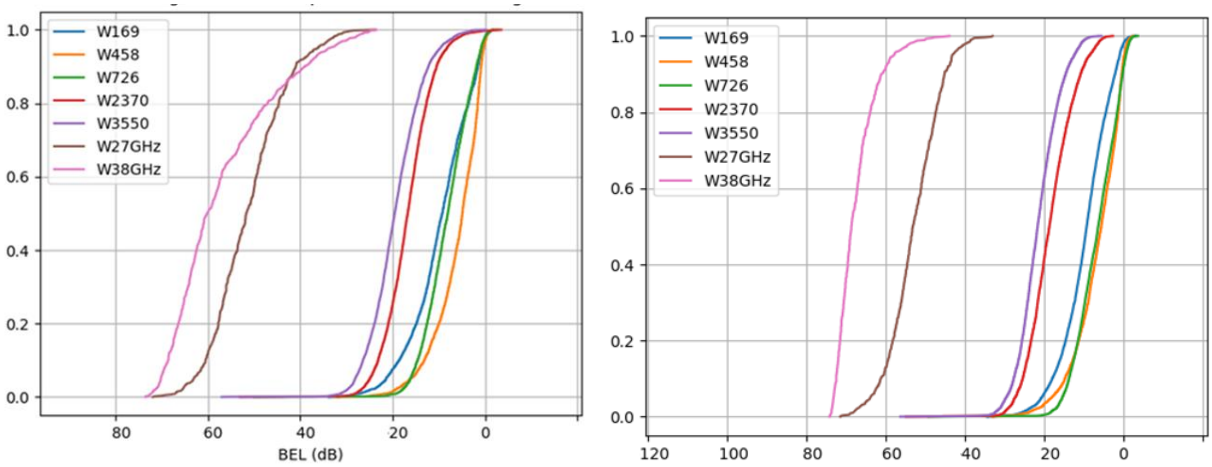

31.3.4 Comparison with Recommendation ITU-R P.2109 model

Figure 274 plots the values of median measured loss for the three houses on the same axes as predicted median BEL given by the Recommendation ITU-R P.2109 model (in the legend, the mansion is referred to as '*Brick, traditional*', the Wienerberger House as '*Brick modern'* and the UserHuus as '*Modern Construction*').

FIGURE 274

BEL results by generic house type compared to the Recommendation ITU-R P.2109 model

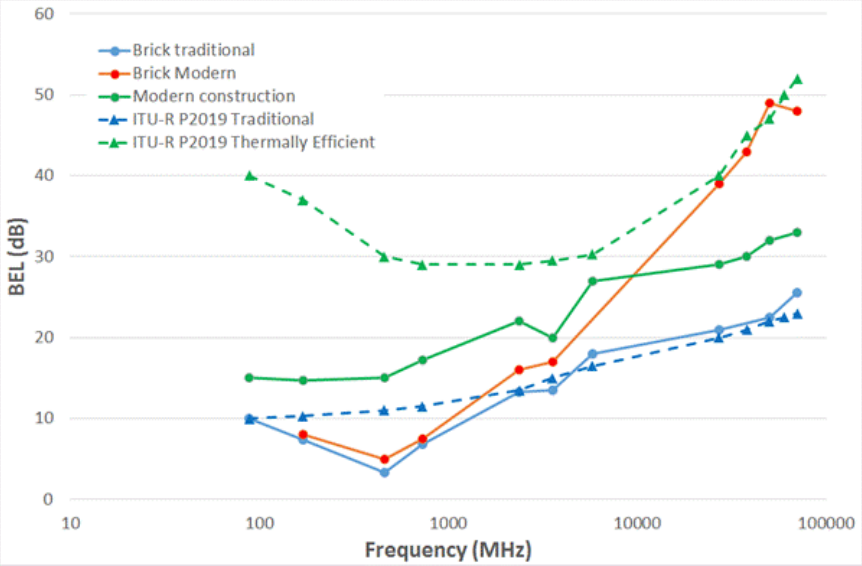

The model compares very well to the traditional brick measurement. The "thermally efficient" model gives BEL values much higher than measurements at lower frequencies and does not fully take into account the differences between the "Brick modern" (e.g. Wienerberger house) and "Modern Construction" (e.g. UserHuus) type houses

These difference may be due to the fact that much of the data underlying the ITU-R model was derived from larger buildings and the different types of low-E glazing used in the two modern houses.

31.4 Summary of results

The new measurements have served to confirm many of the results seen in earlier studies, including the tendency for median values of BEL to fall to a minimum at low UHF frequencies.

The large variation in BEL seen as a result of differences in building materials, particularly glazing, is particularly clear.

It is intended that the data submitted with this contribution will aid the validation of the existing model in Recommendation ITU-R P.2109 and the development of new, site-specific, BEL models.

32 Independent and joint statistics of clutter loss and building entry loss – initial measurements (UK, 100 MHz – 100 GHz)[20]

32.1 Introduction

Accurate propagation models are essential, not only for the planning of specific radio services, but also for assessing the compatibility between different users or systems when making national or international spectrum assignments.

The ITU-R has recently published two new Recommendations, one [1] giving a method for the estimation of building entry loss (BEL) at frequencies between 100 MHz and 100 GHz and the other an empirical model for the additional transmission loss due to local terminal clutter [2]. In the case of the BEL model, a necessary simplifying assumption in model development was that the building can be considered in isolation from its immediate environment.

While each model gives appropriate predictions for the specific loss cases in isolation, the general requirement is to predict the overall loss in cases where a building is surrounded by other buildings, trees and similar local clutter.

A simplistic approach would be to assume that the losses due to clutter and BEL would be multiplicative (i.e., that the overall excess loss would be the sum, in dB, of the individual losses). Brief consideration suggests that this is unlikely to be the case. Once a certain level of screening is reached due to attenuation on one path geometry, it is likely that other geometries will provide lower loss coupling mechanisms. For instance, the lowest clutter loss to a building façade might be via rooftop diffraction from the building opposite and the lowest loss into the building might be via a brick wall. Taken together, however, these losses might be greater than that due to a specular reflection from a third building coupling into the building of interest via a side window. It is therefore likely that the combined loss will tend to an asymptotic value.

Unfortunately, there appears to be little or no empirical data currently available that would allow this issue to be investigated in a quantitative manner. A set of pilot measurements has therefore been undertaken and is reported here.

32.2 Experimental arrangement

Measurements were made in and around two conveniently located buildings (‘Arts A’ and the ‘Meeting House’) on the campus of the University of Sussex (Fig. 275).

[20] Sharing studies carried out by ITU-R on different agenda items of WRC-19 were based on the text of this Report which was inforce at the time of these activities or at the time which the activity was carried out.

FIGURE 275

Measurement geometry (image data: © 2018 Google)

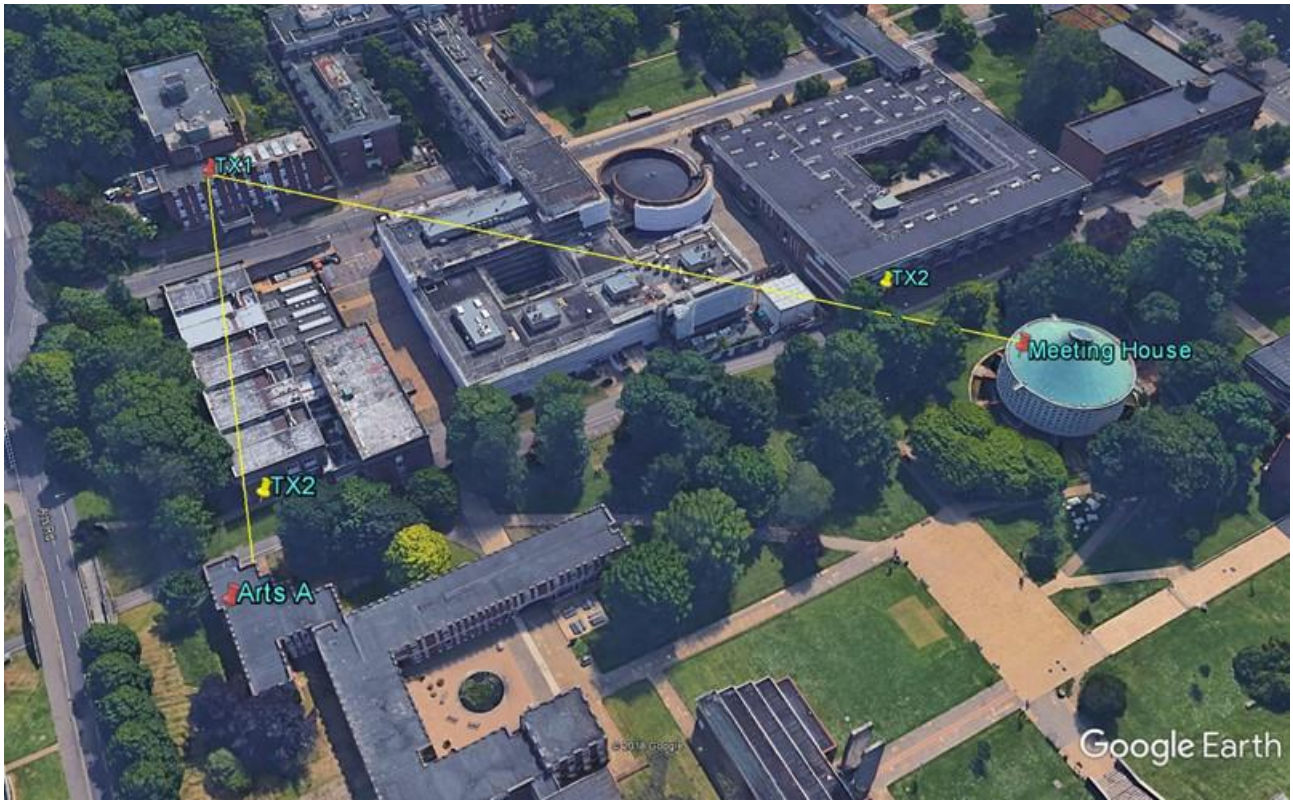

The aim of the measurements was to gather three sets of statistical data for each location investigated:

– Building entry loss (BEL, in isolation)

– Clutter loss (to façade of building)

– Overall loss (clutter and BEL combined).

A rooftop transmitter site (‘TX1’ in Fig. 275) was chosen to give paths obstructed by clutter to both test locations. With the transmitter at this location, measurements were made of the fields immediately outside, and inside, the buildings.

The transmitter was then moved to locations (‘TX2’) that were line of sight to each building, and the outdoor and indoor measurements repeated.

The Meeting House (Fig. 276) is a circular building, with offices and a quiet area on the ground floor and a chapel above. The external wall of the quiet area is mostly of glass.

FIGURE 276

Meeting House, from direction of test transmitter locations

The ‘Arts A’ building houses offices and seminar rooms and is of outwardly traditional construction.

FIGURE 277

‘Arts A’ building, from direction of test transmitter locations

32.2.1 Measurement equipment

The eventual need to make measurements on a wide range of frequencies, coupled with a requirement for the use of a wideband test signal, suggested the adoption of a software-defined radio approach to the measurement system. This allowed simple re-configuration of the system and flexibility in transmitted waveform, with a minimum of hardware.

The platform used is the Ettus ‘B200mini’ device which covers 70 MHz to 6 GHz with 56 MHz bandwidth. This hardware is combined with the software-defined radio (SDR) framework of the open-source GNUradio project (www.gnuradio.org). To minimise the processing overhead, a simple pseudo-noise (PN) sequence sounding signal is used, clocked at 2 MHz. A power amplifier allowing operation at up to 20W and a flat-plate antenna with 12 dBi gain were used at the transmitter.

The receiver consists of a correlator matched to the transmitted sequence. The output of this correlator gives the time-domain response of the channel, but this is not required in the present work; furthermore, the temporal resolution available at the bandwidths used is too low to give useful data on the short paths being examined here. The impulse response data is not, therefore, retained.

The receiver software aggregates all impulse response peaks that exceed the noise floor by 10 dB and saves the result to file. The received power values are logged continuously, at around 5 samples/second and are also added to a plot showing the cumulative distribution of received power which is updated continuously. This display allows the operator to judge the point at which the statistics gathered have become stationary. An omnidirectional, colinear antenna was used, with a 10 dBi gain.

FIGURE 278

View from 'cluttered path' transmitter site towards the Meeting House

32.2.2 Procedure

The measurements procedure sought only to characterise the statistics of signal variation within individual rooms of each building. It was found, by following a semi-random path within each room, that independent measurements could reproduce the cumulative loss distribution to within 1 dB.

The building entry loss distributions shown below are derived in line with the method given in Recommendation ITU-R P.2040 [4], with the indoor measurements normalised on the basis of the median field measured immediately outside the building.

32.3 Results

32.3.1 Building loss in isolation

The BEL measurements made with the transmitter in line of sight to the buildings (i.e. 'TX2' positions) follow the method used in the measurements underlying the model of [1] and described in Annex 2 of [4].

FIGURE 279

'Meeting House BEL' (local TX)

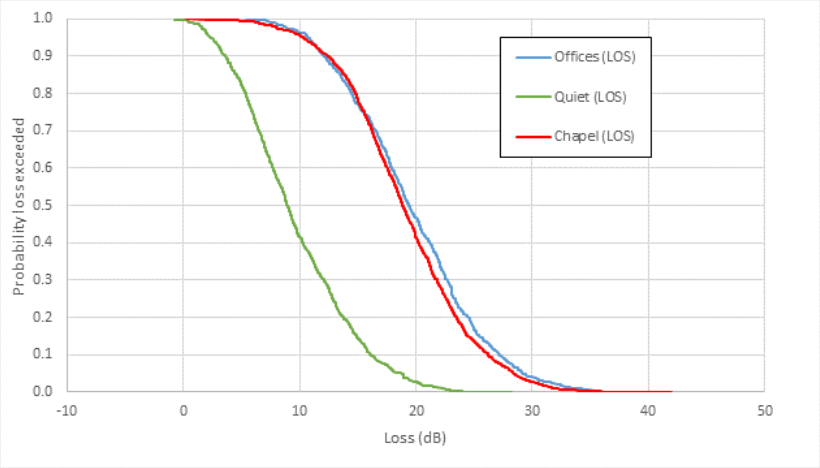

FIGURE 280

'Arts A' BEL (local TX)

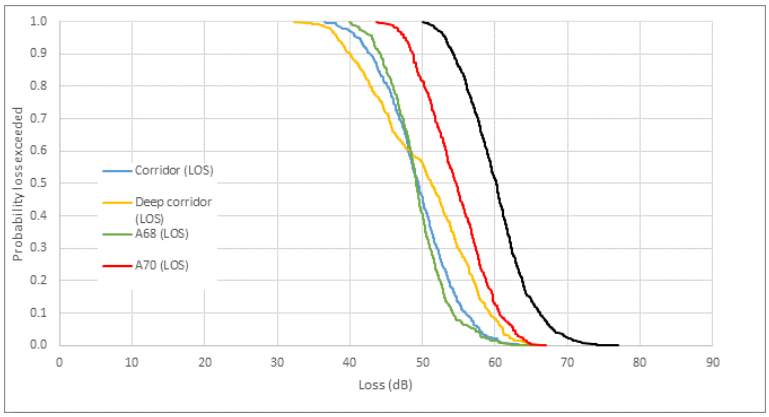

Figures 279 and 280 show contrasting loss distributions; those for the 'Meeting House' are typical of results for traditional buildings with light masonry walls and plain glass windows, while those for the 'Arts A' building are high even by the standards of thermally-efficient buildings using a high proportion of metallised material in their construction.

32.3.2 Building loss measured over a cluttered path

BEL statistics measured with a cluttered path to the transmitter ('TX1') were derived in the same way as those above, with the indoor measurements normalised to the field measured immediately outside the building in the direction of the test transmitter as described in Annex 2 of [4].

The median clutter losses in excess of the free space loss were estimated by comparing the median received field measured at the building façade with the predicted free space field strength.

TABLE 98

Estimated clutter loss on paths to building façades

Path	Path length	Excess loss wrt free space
Meeting House	168 m	42.9 dB
Arts A	104 m	31.9 dB

The BEL values derived using cluttered path data (Figs 281 and 282) were significantly smaller than those using uncluttered test transmitters, by some 10 dB in the case of the 'Meeting House' and around 30 dB in the case of the 'Arts A' building.

FIGURE 281

'Meeting House BEL' (cluttered TX)

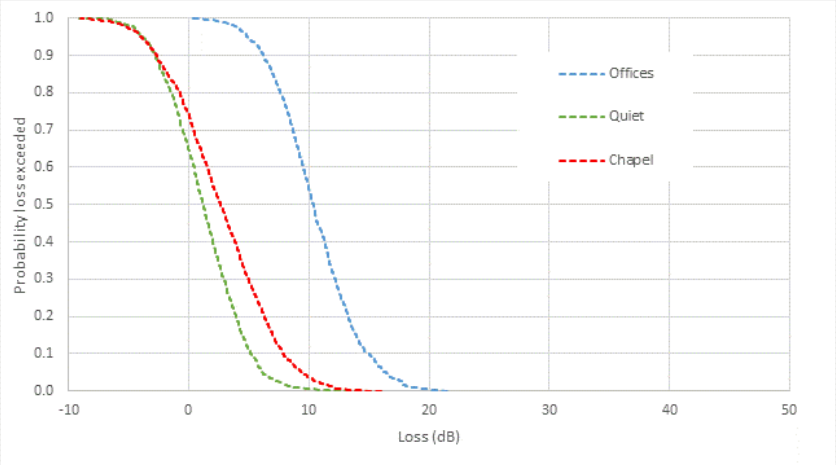

FIGURE 282

'Arts A' BEL (cluttered TX)

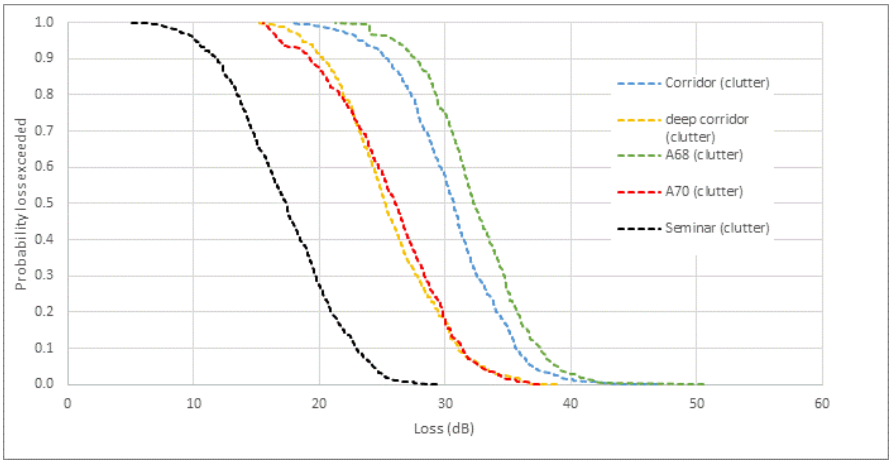

32.4 Summary of the results

These initial results tend to confirm the presumption made above, namely that building entry loss and clutter loss cannot be treated as multiplicative, and that the ultimate combined loss will tend to an asymptotic value determined by the details of building geometry and the surrounding environment.

To confirm these initial observations, and to lay the ground for a quantitative statistical model will require a significant measurement campaign in varying environments at the frequencies of current industrial and regulatory interest.

Given the time-consuming nature of such measurements, it would be very valuable to investigate whether detailed ray-tracing models might be used to investigate the relevant coupling mechanisms, and thus to run virtual measurement campaigns. Given the large dynamic range involved, and hence the sensitivity to apparently minor modelling artefacts, such an approach would not be trivial.

32.5 References

[1] "Prediction of Building Entry Loss", Recommendation ITU-R P.2109-0, Geneva, 2017.

[2] "Prediction of Clutter Loss", Recommendation ITU-R P.2108-0, Geneva, 2017.

[3] "The development of the new ITU-R model for building entry loss, Richard Rudd *et al*., 12th European Conference on Antennas & Propagation 2018 (EuCAP 2018), London, April 2018.

[4] "Effects of building materials and structures on radiowave propagation above about 100 MHz", Recommendation ITU-R P.2040-1, Geneva, 2015.

33 Building entry loss measurements in an urban environment at 27.5 and 39.5 GHz (China)[21]

33.1 Introduction

5G cellular systems will need to use millimetre-wave (mmW) links to meet rising numbers of subscribers using more mobile data. Over the world, several 5G project groups are trying to finish the research and designing on new media access controller and physical layer chips, and are also shooting for a target that the industry can deploy the system in 2020. According to the World Radio Conference (WRC) 2015 in November 2015, ITU-R has extensively given the suitable frequency bands for 5G, such as 24.25 to 27.5, 37 to 40.5, 42.5 to 43.5 and 45.5 to 47 GHz. In addition, it has been proved that the coverage of mmW communication system is limited due to large attenuation. Thus, in order to study its performance in outdoor-to-indoor (O2I) scenario, it is critical to evaluate the building entry loss (BEL) at these candidate mmW frequency bands.

This contribution focused on providing a compilation of empirical data on BEL in a typical urban environment at 27.5 and 39.5 GHz, which can be intended to support the material in Recommendation ITU-R P.2040. The BEL is an additional loss in large-scale channel model, which is irrelevant to the propagation distance and just depends on building materials and structures. Thus, an improved time domain channel sounder was designed to support larger bandwidth and enough dynamic range for O2I measurements. In this report, receivers were allocated in indoor office and corridor to receive the signal from the roof of another building. According to the measurement results, statistical analyses for BEL at 27.5 and 39.5 GHz are reported as followed.

33.2 Measurement environment

A typical O2I measurement campaign in urban environment was promoted in building A3 and A5, China Wireless Valley (CNV, in No. 9, East Mozhou Road, Jiangning District, Nanjing City, Jiangsu Province, 211100, P. R. China) using new designed time domain channel sounder from January to March 2018 as shown in Figure33-1. These two buildings are modern commercial office building, where the exterior walls are composed of brick followed by a layer of plaster. The windows are made of double pane glazed glass with aluminium frames. During the measurement, the transmitter was fixed and mounted on the roof of Building A3, marked red in Fig. 283(a), while 23 and 13 receiver locations were selected in 3rd and 4th floor in Building A5, respectively.

BEL reflects the influence of building materials on propagation without the free space transmission loss. Thus, it is critical to calculate the free space transmission loss using Friis equation, in which the distance between Tx and Rx is related to their coordinates.

---

[21] Sharing studies carried out by ITU-R on different agenda items of WRC-19 were based on the text of this Report which was inforce at the time of these activities or at the time which the activity was carried out.

FIGURE 283

O2I measurement scenario

(a)

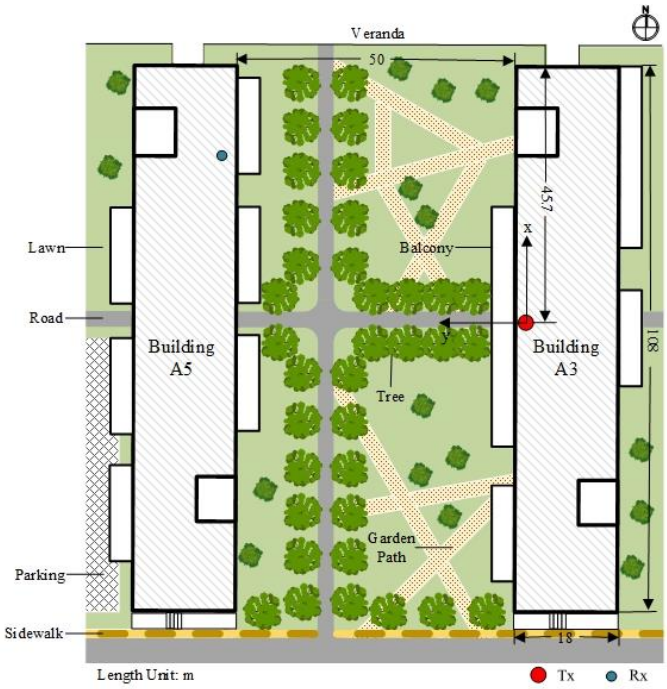

(b)

33.2.1 Indoor office environment (3rd floor in Building A5)

As shown in Fig. 284, 15 receiver positions are located in office and 8 receiver positions are located in corridor outside the office with the windows and composite door closed, while these two parts were separated by glass wall. In addition, the overall window to wall ratio is close to 2:1. During the measurement, receiving antennas were moved from one position to another. The coordinates are listed in Table 99.

FIGURE 284

Indoor office receiver locations

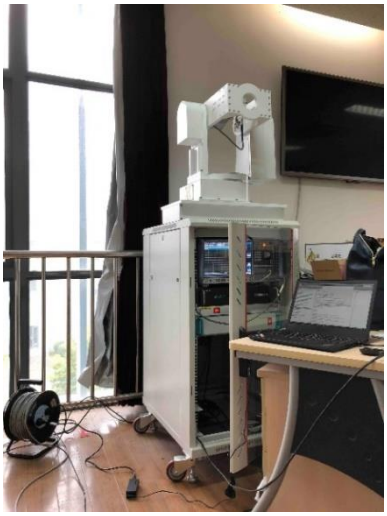

(a)

(b)

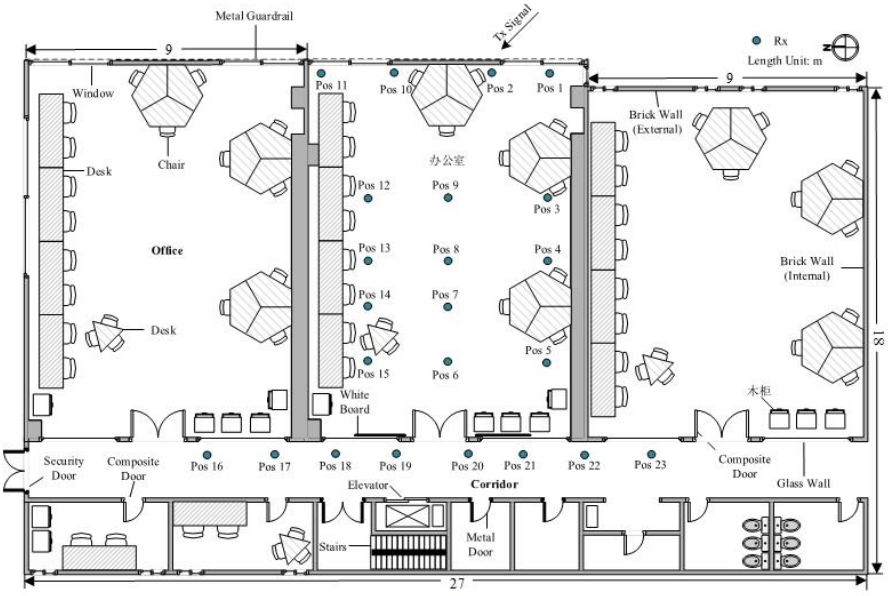

(c)

TABLE 99

The coordinates of the receiving points in 3rd floor (unit: m)

Rx	*x*	*y*	*z*	Rx	*x*	*y*	*z*
Pos 1	29.06	48.23	-9.10	Pos 13	34.06	53.93	-9.10
Pos 2	31.06	48.23	-9.10	Pos 14	34.06	55.94	-9.10
Pos 3	28.71	51.93	-9.10	Pos 15	34.06	57.94	-9.10
Pos 4	28.71	53.93	-9.10	Pos 16	39.09	60.01	-9.10
Pos 5	28.71	57.94	-9.10	Pos 17	37.09	60.01	-9.10
Pos 6	32.35	57.94	-9.10	Pos 18	35.09	60.01	-9.10
Pos 7	32.35	55.94	-9.10	Pos 19	33.09	60.01	-9.10
Pos 8	32.35	53.93	-9.10	Pos 20	31.09	60.01	-9.10
Pos 9	32.35	51.93	-9.10	Pos 21	29.09	60.01	-9.10
Pos 10	34.07	48.23	-9.10	Pos 22	27.09	60.01	-9.10
Pos 11	36.07	48.23	-9.10	Pos 23	25.09	60.01	-9.10
Pos 12	34.06	51.93	-9.10				

33.2.2 Corridor environment (4th floor in Building A5)

As shown in Fig. 285, 13 receiver positions are located in corridor outside the office with the composite door closed during the measurement. Different from previous measurement at 3rd floor, the Rx positions were close to the brick wall, rather than the glass wall. In addition, the overall window-to-wall ratio is much less than 3rd floor scenario. Thus, the received signal went through at least two walls with larger attenuation compared with the BEL at 3rd floor. The coordinates are listed in Table 100.

FIGURE 285

The receiver locations in corridor environment

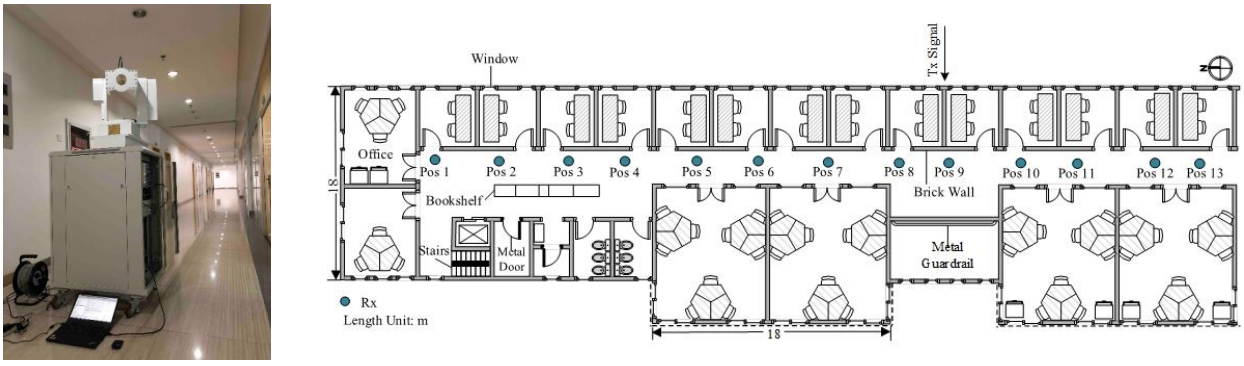

(a) (b)

TABLE 100

The coordinates of the receiving points in 3rd floor (unit: m)

Rx	*x*	*y*	*z*	Rx	*x*	*y*	*z*
Pos 1	35.71	57.46	-4.90	Pos 8	0.71	57.46	-4.90
Pos 2	30.71	57.46	-4.90	Pos 9	-4.29	57.46	-4.90
Pos 3	25.71	57.46	-4.90	Pos 10	-9.29	57.46	-4.90
Pos 4	20.71	57.46	-4.90	Pos 11	-14.29	57.46	-4.90
Pos 5	15.71	57.46	-4.90	Pos 12	-19.29	57.46	-4.90
Pos 6	10.71	57.46	-4.90	Pos 13	-24.29	57.46	-4.90
Pos 7	5.71	57.46	-4.90				

33.3 Measurement setup and procedure

33.3.1 Principles of time domain measurement method

Two widely used mmW channel sounding approaches consist in frequency and time domain. The vector network analyser (VNA) based frequency domain sounders, a reference signal must be transmitted to port A with finite length cable or increase the length of coaxial cable to transmitting antenna, whereas reduce the quality for exceed line loss. Thus VNA based campaigns were usually performed in indoor environments where the dimension within their range. In addition, this frequency-sweeping method does not fully describe the characteristic of wideband channel, especially when frequency-dispersive parameters are in consideration. On the contrary, time domain method transmits wideband signal where receivers are totally detached with generator, and suits for outdoor measuring requirements.

In order to employ a genuine broadband sounding technique, it is prior to transmit high bandwidth signal which need to design new generator. And then use wideband signal analyser to obtain raw channel data, including the gain of measuring devices and cables. Consider the autocorrelation function of input signal $s(t)$:

$$R_{ss}(\tau) = \int_{-\infty}^{\infty} s(t)s(t-\tau)d\tau \tag{39}$$

Followed by a correlator, its output is defined as cross correlation function of $r(t)$ and $s(t)$, given as the function of autocorrelation property shown in

$$R_{rs}(\tau) = \int_{-\infty}^{\infty} h(\lambda)R_{ss}(\tau-\lambda)d\lambda = h(\tau) * R_{ss}(\tau) \tag{40}$$

The ideal correlation property in equation (40) is generally difficult to realize. Thus usually design the waveform that has correlation properties either close to the ideal impulse function or to the more practical triangular function with obvious peak. Figure 286 shows the block diagram of the time domain channel sounder.

FIGURE 286

Block diagram of channel response with the details of correlator in dashed line

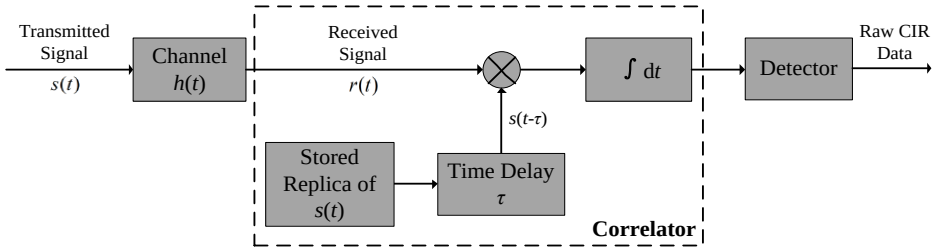

33.3.2 Measurement system and measurement instruments

Figure 287 shows the new designed mmW time domain channel sounder using commercial-off-the-shelf instruments. A vector signal generator (Rohde & Schwarz SMW200A) and a spectrum analyser (Rohde & Schwarz FSW50) which support higher frequency bands up- or down-conversion respectively without the external are used. A maximal length of 4 096 Golay complementary codes were transmitted to replace pseudorandom noise (PN) sequence, which has been proved this sequence performs well as for periodic auto-correlation property and increase the accuracy of CIR data when doing the relevant operation with raw data stored from spectrum analyser.

Furthermore programmable controlled multi-dimension positioners which can remote in arbitrary azimuth and elevation directions are used in transmitter and receiver for installing high gain horn antennas with a small half power beamwidth (HPBW). Therefore a directional-scanning-sounding (DSS) method can be used by rotating the antenna towards different directions in such a way that the spatial channel can be scanned step by step. These directional observations can be reproduced to omni-directional channel characteristics by synthesis process.

In order to guarantee a quasi-static environment, two wireless routers were used to connect all measurement instruments in a local area network (LAN) and complete auto-measurement. Additionally, two GPS disciplining rubidium clocks were added to provide precise reference clock signals, which can not only keep frequency synchronization between Tx and Rx, but also realize the synchronization trigger and data acquisition.

As the result of using multi-function positioners, Tx and Rx antennas were set to rotate in the range of 60˚ and 360˚ in azimuth and several fixed elevation angle in Table 101 for more details. The horn antenna was stepped in 10˚ (depending on its HPBW) increment to simulate equivalent omnidirectional antenna. Calibration is particularly critical for sounders before the measurement to not only remove the impulse response of instruments and cables, but also calculate transmitting delay caused by trigger signal to obtain absolute transmission delay. Complete configuration of sounder is listed in Table 101.

FIGURE 287

Time domain channel sounding system

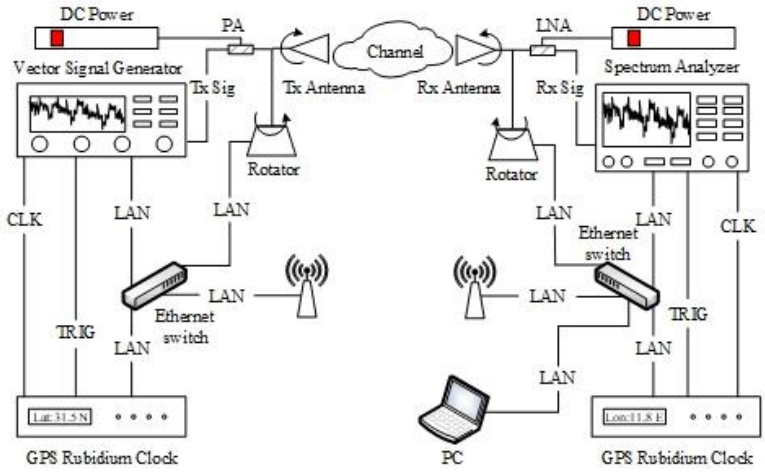

(a)

(b)

(c)

TABLE 101

System configurations of time domain channel measurements

Measured environments:	3rd floor	4th floor
Centre frequency	27.5, 39.5 GHz	
RF Bandwidth	200 MHz	
Transmitted sequence length	4 096 (complex Golay complementary sequences)	
Time resolution	5 ns	
Tx antenna transmitted power	12 dBm	
Power amplifier (gain)	27.5 GHz: MWG203C (20 dB) 39.5 GHz: MWG201C (18 dB)	
Low noise amplifier	27.5 GHz: MWL003C (33 dB) 39.5 GHz: MWL004C (35 dB)	

TABLE 101 (*end*)

Antenna (Gain)	27.5 GHz: HD-260SGAH25K (26.04 dBi) 39.5 GHz: HD-400SGAH25+V (25.84 dBi)	
Antenna polarization	V-V	
Tx antenna rotation range in azimuth	[115˚: 10˚: 175˚]	[150˚: 10˚: 210˚]
Tx antenna elevation angles	-10˚	-5˚
Rx antenna rotation range in azimuth	360˚ step with 10˚ increment	
Rx antenna elevation angles	0˚, 10˚	0˚, 10˚

According to the previous illustration, the O2I measurement procedures for using mechanically-steerable highly-directional horn antennas are shown in Fig. 288.

FIGURE 288

Flowchart of BEL measurements in urban environments

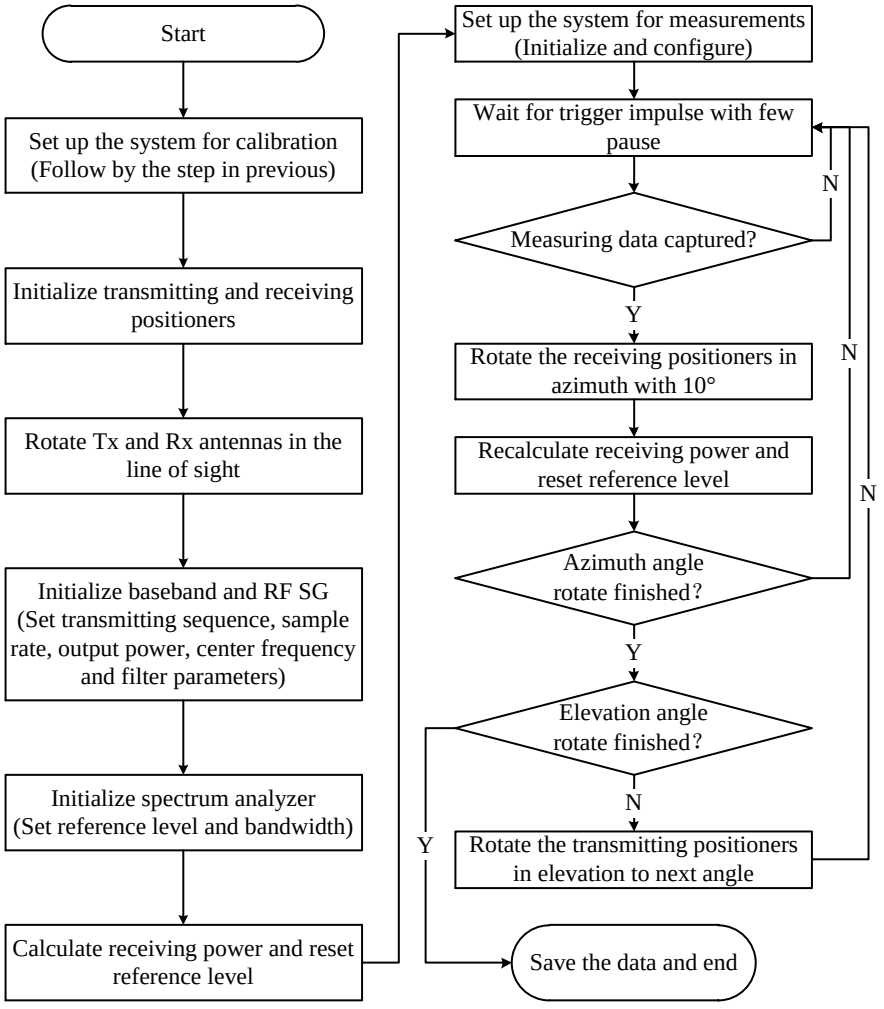

33.4 Data processing

The BEL is defined as the additional loss due to a terminal being inside a building, which is the difference between the spatial median of the signal level outside the illuminated face of a building and the spatial median of the signal level inside the building at the same height above ground.

However, it should be noticed that the receivers are far from the ground and exist obvious line-of-sight (LoS) path between Tx and the exterior wall of building. Thus, BEL can be calculated by:

$$BEL = PL - PL_{FS} \tag{41}$$

where PL is the total propagation loss and satisfies

$$P_r = P_t + G_t + G_r + G_s - PL \tag{42}$$

where P_t and P_r are transmitted and received power, respectively. G_t and G_r are transmitted and received antenna gain, G_s is the gain of measurement system, which is obtained by calibration data. L_{FS} is free space transmission loss calculated by Friis equation:

$$L_{FS} = 20\lg d + 20\lg f - 147.56 \tag{43}$$

where d is the distance between TRx antennas in meter, f is the centre frequency in Hz. When using directional-scan-sounding method, received power P_r is defined as:

$$P_r = \sum_t |h(t)|^2 \tag{44}$$

where omni-directional channel impulse response $h(t)$ is obtained as followed

$$h(t) = \sum_{\vec{\Theta}} \sum_{\vec{\Phi}} h\left(t, \vec{\Theta}, \vec{\Phi}\right) \tag{45}$$

where $\vec{\Theta}$ and $\vec{\Phi}$ represent 3D angle of departure and arrival, respectively. In equation (45), it needs to sum in time, where its interval is determined by noise floor according to the definition in Recommendation ITU-R P.1407.

33.5 Measurement results and analysis

Based on the definitions in § 33.3, the BEL for the 3rd and 4th floor at 27.5 and 39.5 GHz were calculated using the CIR data from different directions in azimuth and elevation. As shown in Fig. 289, it is observed that the BEL is much smaller when Rx positions are close to the window for about 20 dB. However, the BEL for other Rx in the office is very similar due to LoS path blocked by windows. As for the receivers outside the office, larger BEL indicates that glass wall and composite door cause at least 10 dB additional loss. Compared the results in Fig. 289 (a) and (b), minor differences exist between 27.5 and 39.5 GHz. Table 102 shows the statistical results in 3rd floor. Figure 290 and Table 103 show the measurement results in corridor environment at 4th floor of Building A5. It is obvious that the BEL at 4th floor is larger than the results at 3rd, due to multilayer brick walls obstruction. Compared the measured results in corridor environments at these two floors, the mean value of BEL at 4th floor is 3 dB larger than the others with larger standard deviation. It is speculated that this result is related to the window-to-wall ratio of exterior wall (2:1 and 1:2) and the building materials of partition wall (glass wall and brick wall), where stronger signal can be received at 3rd floor. Figure 291 illustrates the CDF of measured BEL, which all follow normal distribution.

FIGURE 289

BEL for omni-directional channel in indoor office environment at 3rd floor

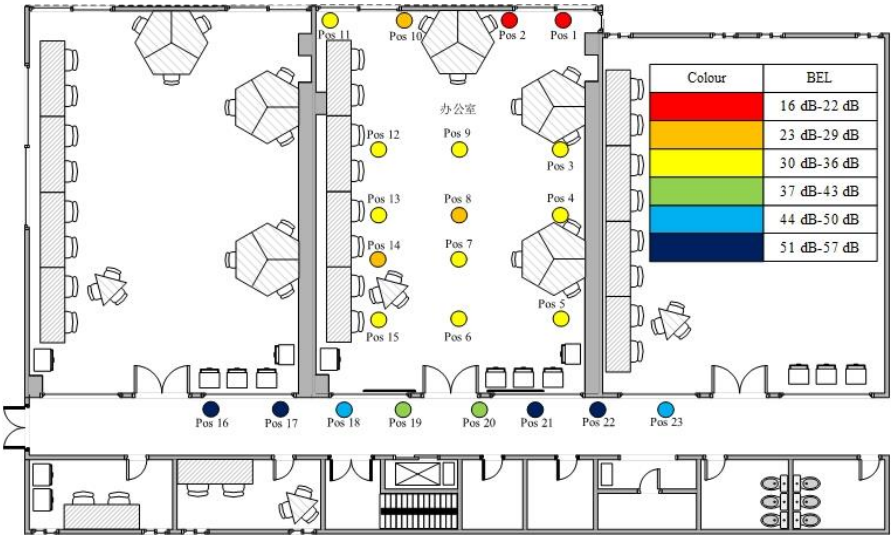

(a) 27.5 GHz

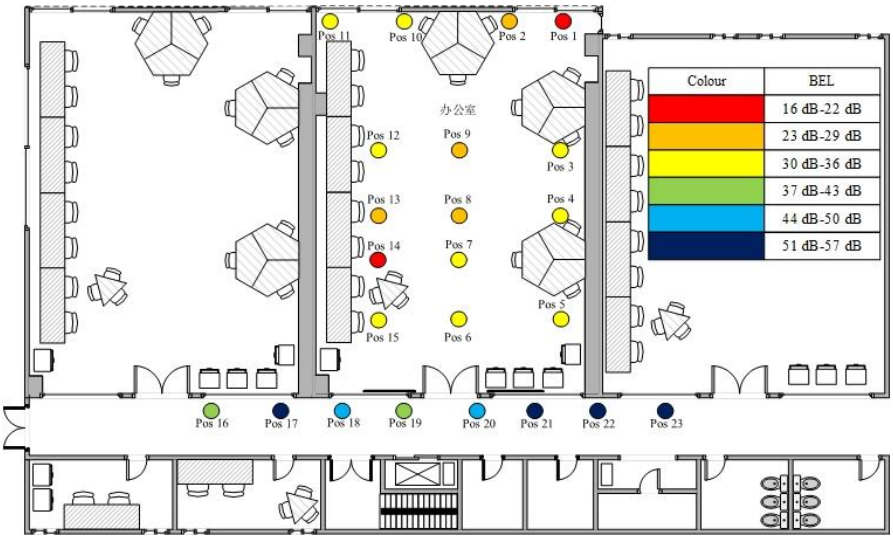

(b) 39.5 GHz

TABLE 102

BEL values for 3rd floor measurement

Configuration		Parameters			
Freq. (GHz)	**Scen.**	**Max. (dB)**	**Min. (dB)**	**Mean (dB)**	**Std. (dB)**
27.5	Office	35.26	17.66	29.23	5.21
	Corridor	54.41	39.32	47.55	5.46
39.5	Office	34.27	16.02	28.73	4.67
	Corridor	54.22	39.39	48.07	5.15

FIGURE 290

BEL for omni-directional channel in corridor environment at 4th floor

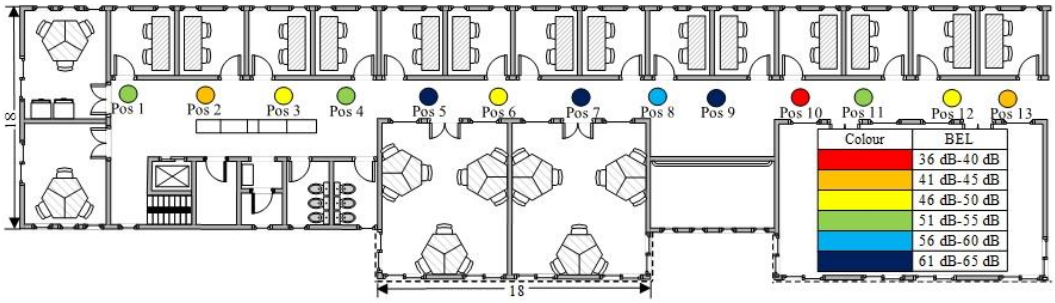

(a) 27.5 GHz

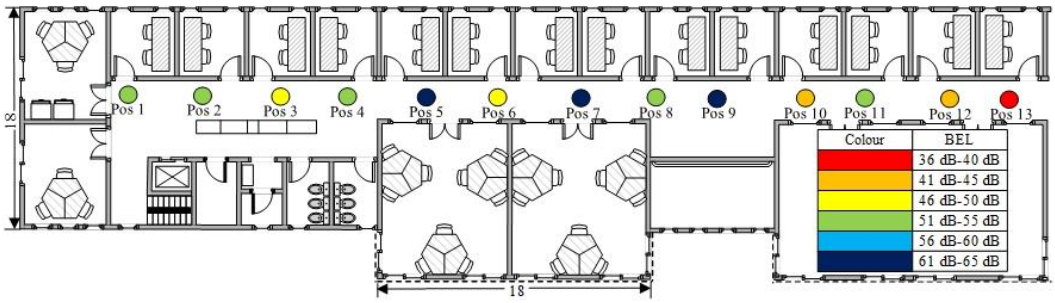

(b) 39.5 GHz

TABLE 103

BEL values for 4th floor measurement

Configuration		Parameters			
Freq. (GHz)	**Scen.**	**Max. (dB)**	**Min. (dB)**	**Mean (dB)**	**Std. (dB)**
27.5	Corridor	64.57	38.94	51.41	8.02
39.5	Corridor	64.29	36.63	50.96	7.88

FIGURE 291

CDF distribution of measured BEL in urban environments

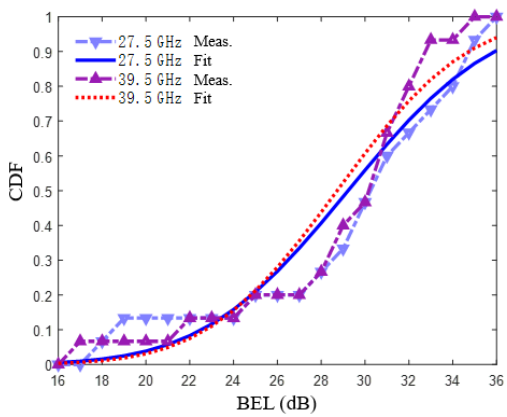

(a) office @3rd floor

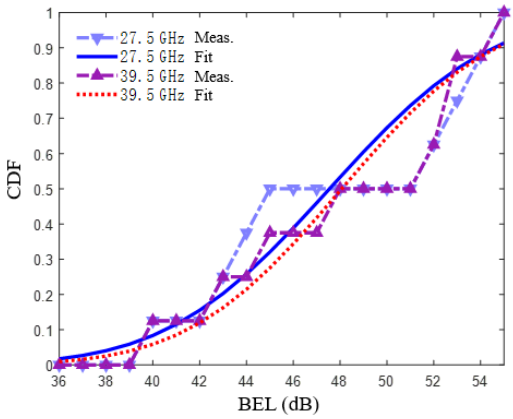

(b) corridor @3rd floor

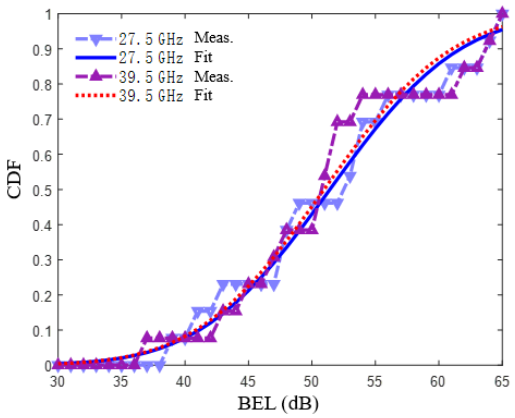

(c) corridor @4th floor

33.6 Summary of the results

In this Report, the BEL in a modern urban environment was measured to study the coverage of a mmW system at 27.5 and 39.5 GHz. In corridor environments, the building entry loss at the 3rd floor was substantially smaller than the case for the receivers at the 4th floor, which was determined by the building material and structure. Eliminated the free space basic transmission loss, median entry loss was at the same level and irrelevant to the depth within the building. Furthermore, the receivers in the corridor experienced 20 dB additional loss, which indicates that outdoor mmW signals only can penetrate through the external wall of a building with a large window-to-wall ratio. And also, the BEL was found to vary non-monotonically with frequency compared the measurement results at 27.5 and 39.5 GHz. Finally, the measurement data in this report can be used to build a large scale channel model and help to allocate mmW communication systems in urban environments.

34 Effect of azimuth incidence angle on building entry loss (Republic of Korea)[22]

34.1 Introduction

Recommendation ITU-R P.2109-0 provides prediction methods for building entry loss. Regardless of the azimuth incidence angle, the recommendation provides identical predictions. However, ITU-R measurements (see for information Document 3J/186 (a.k.a. 3K/238 or 3M/312) (UK, 2018)) illustrate building entry loss changes between the normal incidence and 45° incidence. Based on the analysis of measurement data for 0° (perpendicular incidence), 15°, 30°, 45° and 60° azimuth angle incidences, this section proposes a draft revision of Recommendation ITU-R P.2109-0 to reflect the effect of azimuth incidence angle on building entry loss.

34.2 Incidence angle dependency in other standard models

The COST-231 model [1] includes an incidence angle dependency, in that the additional loss due to non-perpendicular angle incidence to the building façade is given by

$$\Delta L = A(1 - \cos\phi)^2 \tag{46}$$

[22] Sharing studies carried out by ITU-R on different agenda items of WRC-19 were based on the text of this Report which was inforce at the time of these activities or at the time which the activity was carried out.

where ϕ is the angle deviation of the TX beam from the perpendicular incidence, which can be understood as the azimuth angle deviation as illustrated in Fig. 292. Constant *A* in (1) is about 20 dB [1].

FIGURE 292

Definition of azimuth incidence angle deviation, ϕ

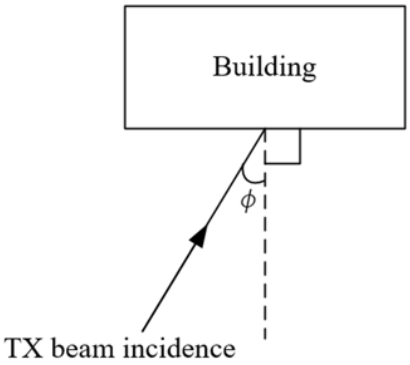

34.3 Measurement overview

To investigate the effect of azimuth incidence angle dependency, additional building entry loss measurements were conducted on top of the previous building entry loss measurement (see for information Document 3J/181 (a.k.a. 3K/225 or 3M/306)). Regarding the measurement equipment and the antenna, see for information Document 3K/181 (a.k.a. 3K/225 or 3M/306).

To locate the TX sounder for different azimuth angles without difficulty, a different lift was used from that in other ITU-R measurements (see for information Document 3K/181 (a.k.a. 3K/225 or 3M/306)) as illustrated in Figs 293 and 294.

FIGURE 293

BEL measurement photo 1

FIGURE 294

BEL measurement photo 2

Figure 295 illustrates the RX measurement points. Since numerous measurements were collected at a single point (different RX beamwidth antennas and different TX beam incidence angles), the measurement data were not collected throughout the whole building area.

FIGURE 295

BEL measurement setup (planar view)

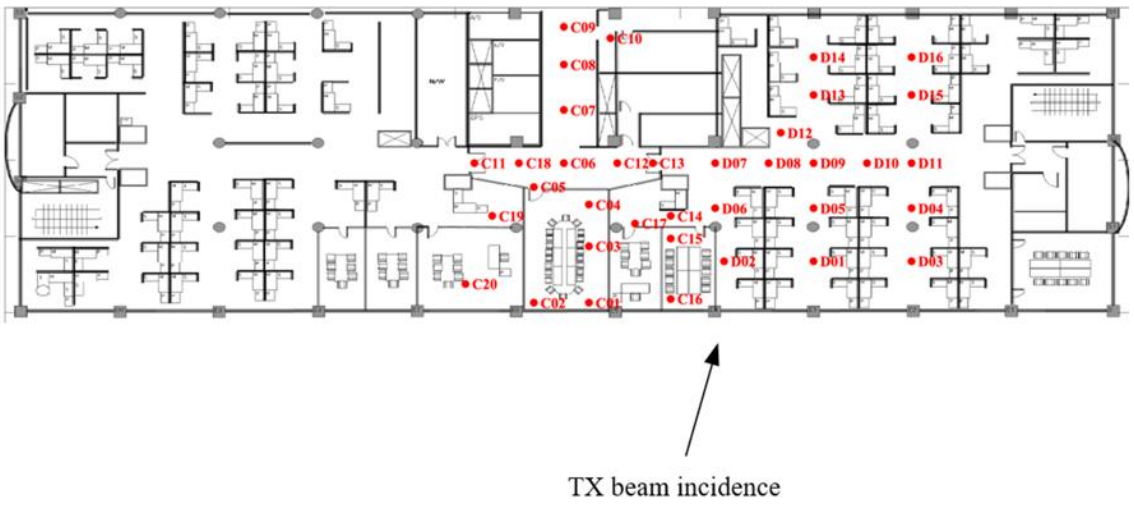

34.4 Analysis

Based on the measurement data analysis, Fig. 296 shows the CDFs of the overall BEL for different incidence angles. Figure 297 shows the median behaviour of the additional loss due to incidence angle (i.e. the additional loss is calculated by subtracting from the loss at perpendicular incidences) compared to the COST 231 model. From the Figure, it can be seen that the additional loss agrees reasonably well with the COST model.

FIGURE 296

CDF of BEL measurement

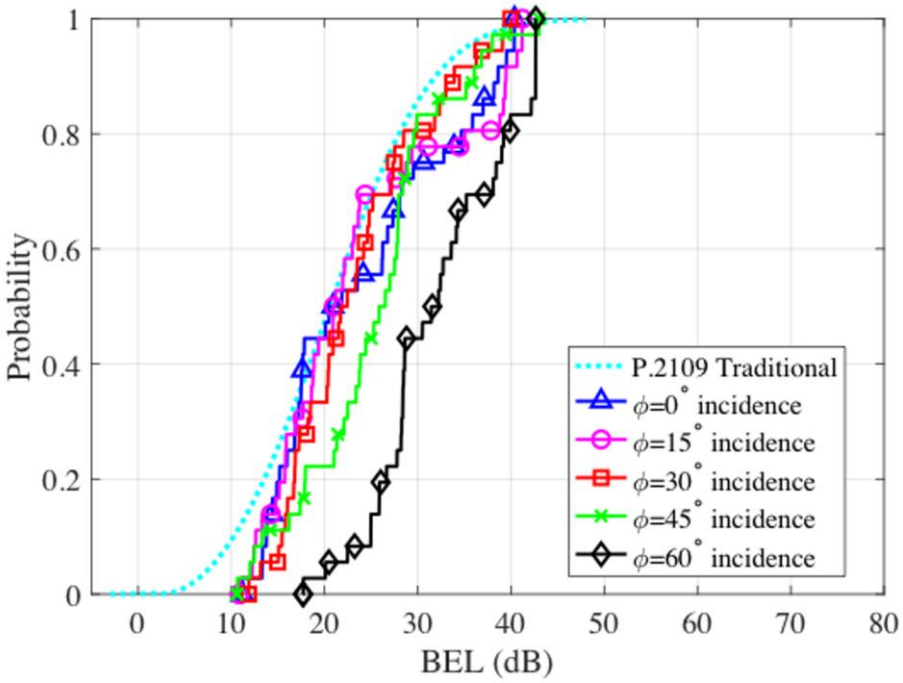

FIGURE 297

Incidence angle dependency

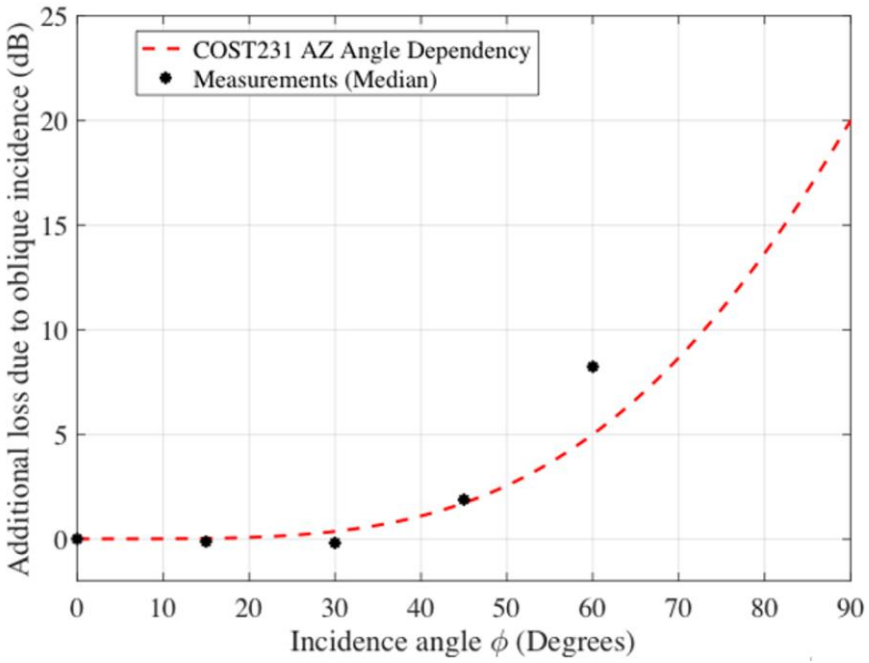

34.5 References

[1] COST Action 231, Digital Mobile Radio towards Future Generation Systems, Final Report, EUR 18957, 1999.

35 Building entry loss measurements for heavy industry factory at 3, 6, 10, 18 and 24 GHz (Republic of Korea)[23]

35.1 Introduction

To provide a model for general building entry loss (BEL), measurement data for various buildings are required. However, recently reported BEL measurements are mostly limited to offices and residential houses. Therefore, a multi-frequency BEL measurement was conducted in a heavy industry factory in the Republic of Korea in the frequency range 3–24 GHz. Measurement results are compared with the BEL model for traditional buildings in Recommendation ITU-R P.2109-0. In industrial regions, for frequencies in the range 3 GHz, measurement results are in good agreement with those obtained using the BEL model for traditional buildings, while for higher frequencies, in the range 6-24 GHz, different results are obtained.

35.2 Measurement environment

BEL measurements were performed in a heavy industry factory in Mokpo National Maritime University (Mokpo, Republic of Korea). The factory is a traditional building; the exterior consists of reinforced concrete and glass windows as shown in Fig. 298. Both upper and lower windows are present, and the lower windows are fenced with a security metal. Utilities and trees cover the front and left regions of the building; further, cars are parked in front of the factory.

Figure 299 shows that a transmitter was positioned 22 m from the factory. Continuous wave (CW) signals at 3, 6, 10, 18 and 24 GHz are used for BEL measurements. Identical omnidirectional antennas were used at transmitting and receiving ends with a gain of −1-5 dBi at 3-24 GHz. The transmitter consists of a signal generator (SMB100A) along with the omnidirectional antenna, which is positioned at a height of 2 m. The receiver for the outdoor reference and insides of the factory consist of the omnidirectional antenna also positioned at a height of 2 m along with the kerb, low noise amplifier and signal analyser (FSQ40). The outdoor receiver for the reference measurement was positioned in direct line-of-sight (LOS) 19.5 m from the transmitter. Measurement parameters are listed in Table 11. The measurement systems for the transmitter and receiver are shown in Fig. 300.

The outdoor reference measurement was taken at four different locations – R1, R2, R3 and R4 – as shown in Fig. 300. The indoor BEL measurement was taken at 20 different locations within the 17.2 m × 19.3 m factory, where uniformly distributed testing locations considering all of the unique aspects of the factory, are chosen. Various heavy machinery and equipment such as milling machines, ship engines, workbenches and other utilities are installed in the factory. The interior of the factory is shown in Fig. 301 and the heavy machinery and equipment sizes are shown in Fig. 302.

[23] Sharing studies carried out by ITU-R on different agenda items of WRC-19 were based on the text of this Report which was inforce at the time of these activities or at the time which the activity was carried out.

FIGURE 298

Building images of the left, front and right views

FIGURE 299

BEL measurement scenario. Heavy industry factory (red box) (a) and depiction of measurement setup (b)

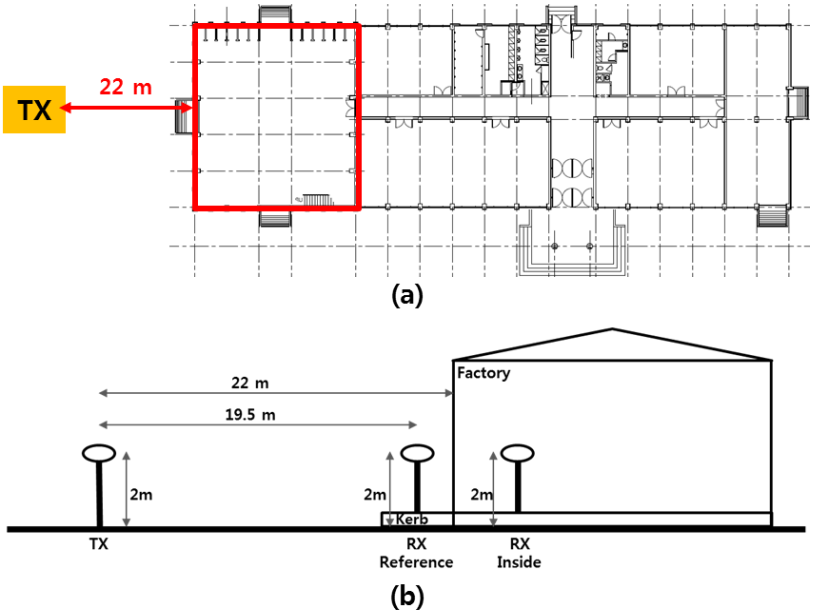

TABLE 104

Measurement parameters

Parameters	Transmitter	Receiver
Frequency	3, 6, 10, 18, 24 GHz	
TX Power	8 dBm (CW)	-
Antenna (gain)	Omni (-1–5 dBi)	
Antenna Height	2 m	

FIGURE 300

Factory floor plan, BEL measurement points of the receiver, various machinery and equipment, transmitter and receiver

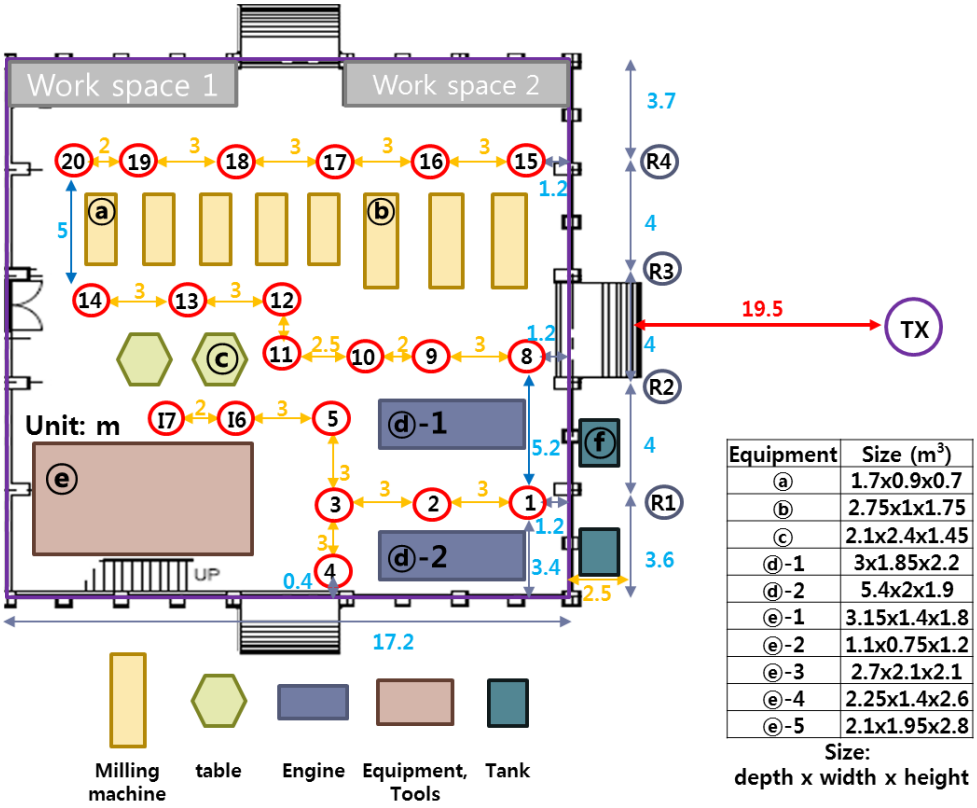

Equipment	Size (m^3)
ⓐ	1.7x0.9x0.7
ⓑ	2.75x1x1.75
ⓒ	2.1x2.4x1.45
ⓓ-1	3x1.85x2.2
ⓓ-2	5.4x2x1.9
ⓔ-1	3.15x1.4x1.8
ⓔ-2	1.1x0.75x1.2
ⓔ-3	2.7x2.1x2.1
ⓔ-4	2.25x1.4x2.6
ⓔ-5	2.1x1.95x2.8

Size:
depth x width x height

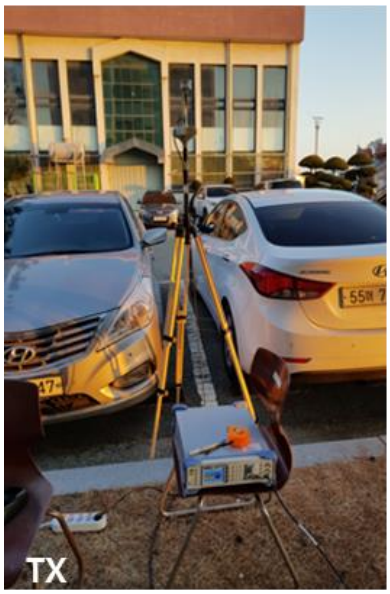

FIGURE 301

Factory interior images from various points

FIGURE 302

Various heavy machinery and equipment in the factory

35.3 Measurement results

35.3.1 Outdoor reference measurements

Prior to the investigation of BEL, outdoor reference measurements were obtained at four different locations in front of the factory, where the reference receiver was in direct LOS, 19.5 m from the transmitter and 2.5 m from the factory. The measured outdoor reference power for each of the measurement frequencies was determined using a median signal level. Figure 303 shows the measured and ideal reference received powers, where free space basic transmission loss is used for ideal reference received power. A difference less than 2 dB is obtained between measured and ideal results.

FIGURE 303

Measured and ideal reference received powers

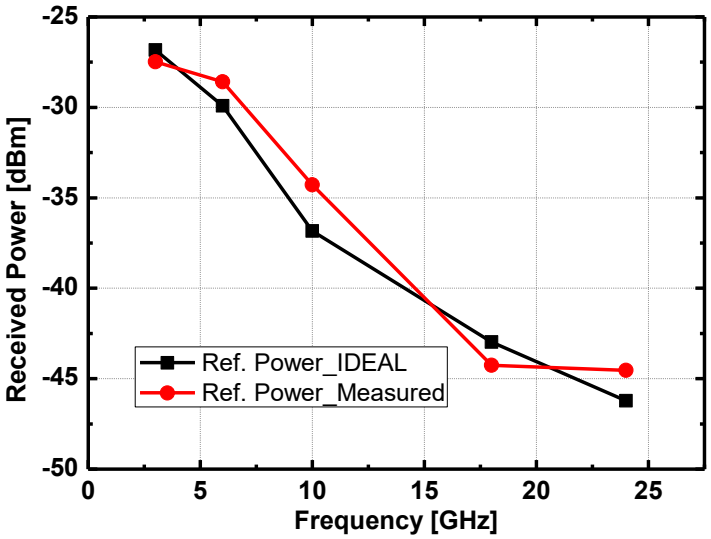

35.3.2 BEL characteristics

The BEL was calculated using the difference between the measured received power inside the factory and the measured outdoor reference power satisfying Recommendation ITU-R P.2040-1.

Figure 304 shows the median BEL measurement results for each position (1-20 in Fig. 300) at 3, 6, 10, 18 and 24 GHz, where each position at a single frequency has 90 measured samples. As it can be seen, the median BEL increases as the receiver moves further inside of the building. However, the receiver locations of 8–10 in Fig. 300 show higher median BEL, because the signal is blocked by huge steel door at the centre of front view in Fig. 299.

FIGURE 304

Location dependency of median BEL in dB scale at 3, 6, 10, 18 and 24 GHz

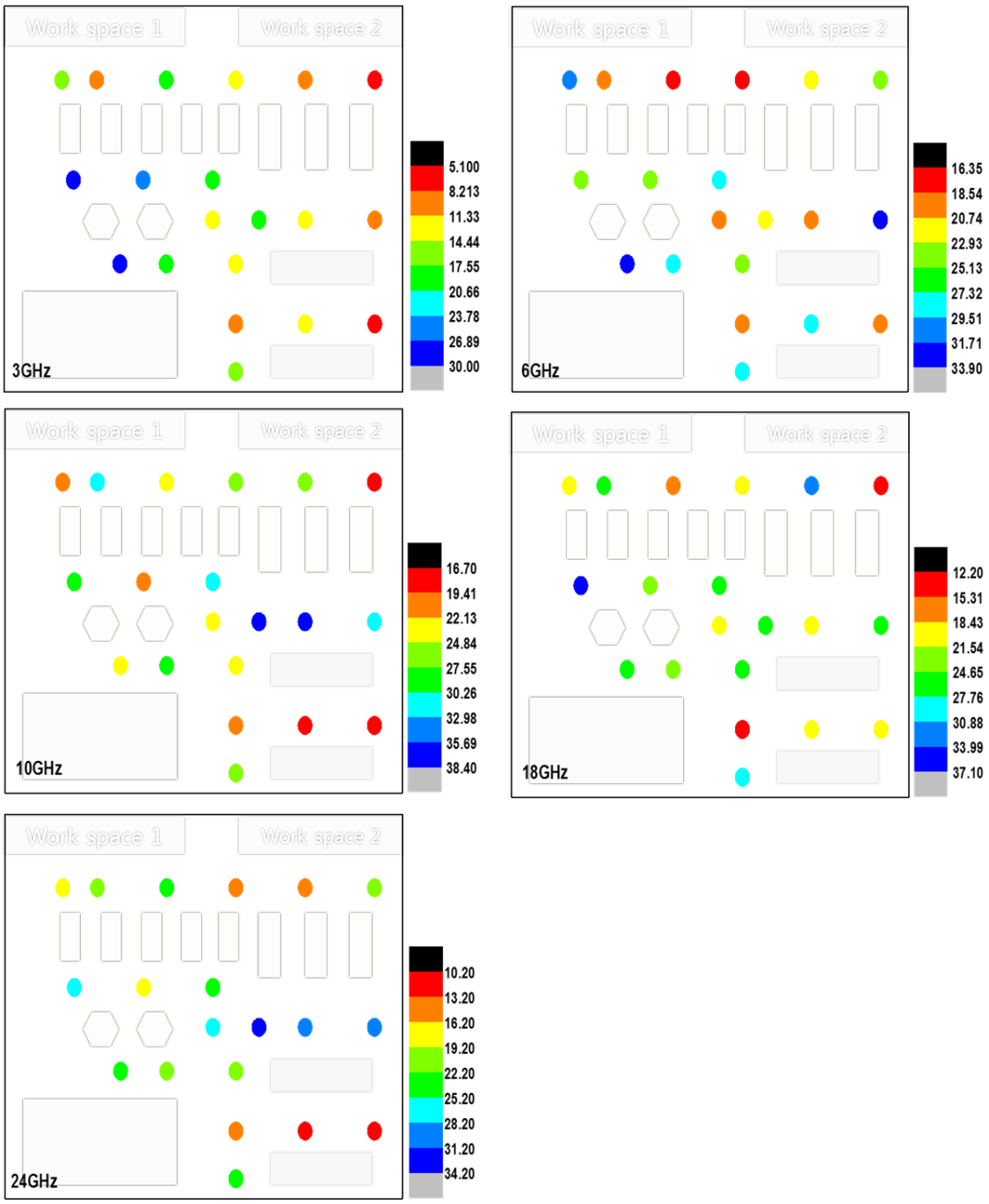

Figure 305 shows cumulative distribution function (CDF) characteristics for all the BEL measurement results in all the 20 locations, where each CDF at a single frequency has 1 800 measured samples. All the measured CDF results at each frequency are compared with those obtained from the traditional building BEL model in Recommendation ITU-R P.2109-0. Standard deviations of the measured BEL in the factory are 6.82, 4.99, 6.11, 6.15 and 6.26 dB at 3, 6, 10, 18 and 24 GHz, respectively. Measured median BELs are 14.75, 22.01, 22.99, 24.27 and 19.47 dB at 3, 6, 10, 18 and 24 GHz, respectively. These values are -0.74, 5.37, 5.32, 5.23 and -0.3 dB higher than the traditional building BEL model in Recommendation ITU-R P.2109-0 at 3, 6, 10, 18 and 24 GHz, respectively. The measured CDF result at 3 GHz is similar to that of the traditional building BEL model, while the measured CDF results at 6, 10, 18 and 24 GHz are different from the traditional building BEL model.

FIGURE 305

CDF characteristics of the BEL in terms of frequency

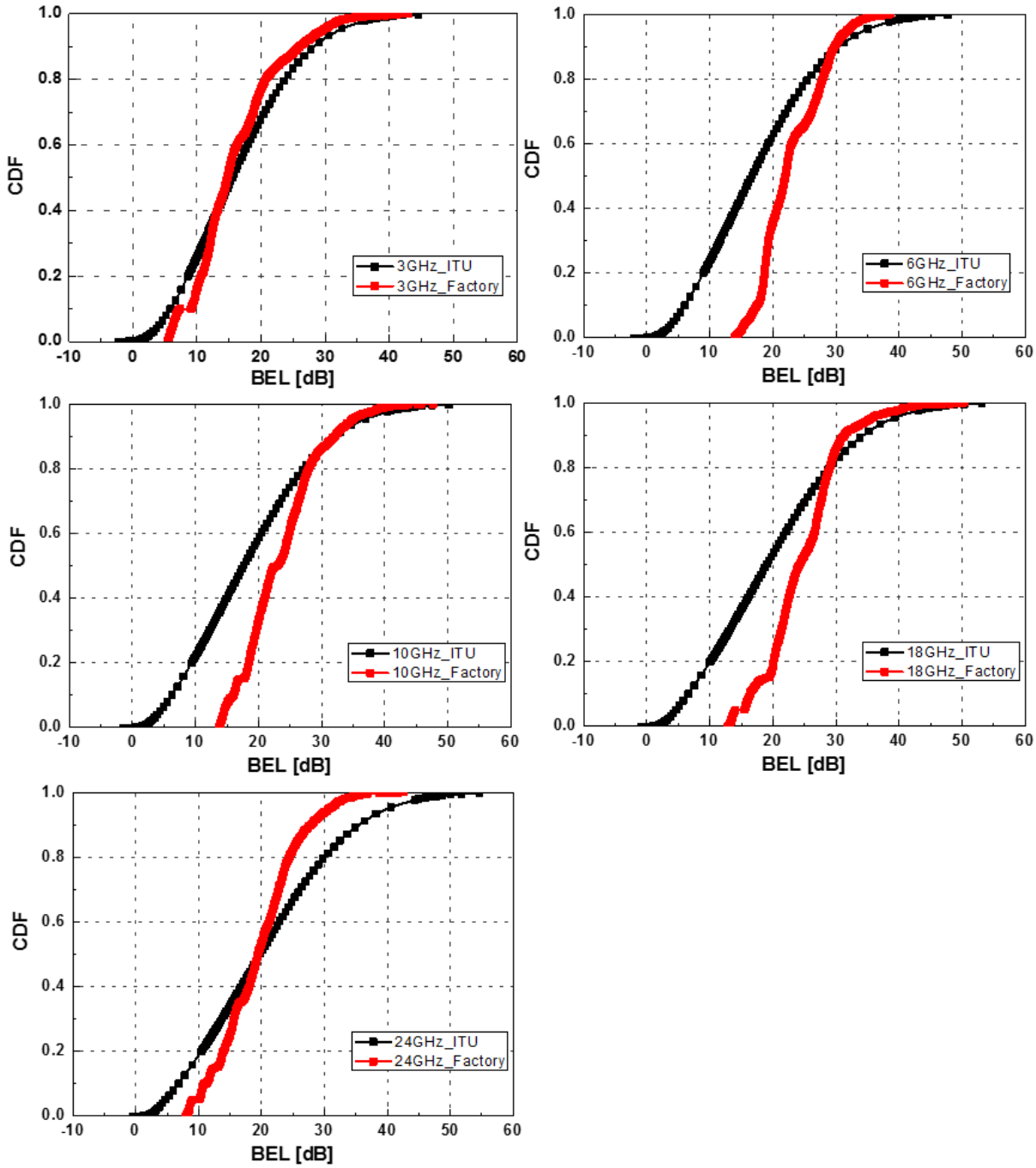

35.4 Summary of the results

To investigate a model for BEL in an industrial environment, multi-frequency BEL measurements in a heavy industry factory in the Republic of Korea were conducted for the frequency range 3-24 GHz. Measurement results reveal that BEL for the heavy industry factory is different from that of the traditional building as the frequency increases.

36 Measurements for building entry loss into a basement at frequency 1.5 GHz and 3 GHz (Republic of Korea)[24]

36.1 Introduction

The definition of building entry loss was established by the International Telecommunication Union (ITU-R) [1]–[2], which also indicated that additional loss is prevented by the interior of the building when radio waves are transmitted through the building. The materials used to construct the building are important, and several studies have reported greater building entry losses with higher numbers of stories [3]. Although there is some literature on building ground loss for high-rise buildings, definitions and measurements of building loss due to basements are scarce. Overall, there is a lack of research on building loss during propagation.

36.2 Measurement of building entry loss

36.2.1 Measurement campaign

As shown in Fig. 306, the propagation path was predicted for the case of a building in Chosun University (Gwangju, Republic of Korea), for which measurements could be obtained in the basement. There are four direct propagation paths to the basement. Only propagation paths between the ground and basement floors are considered here; other propagation paths are shown in the next section.

FIGURE 306

Measurement setup

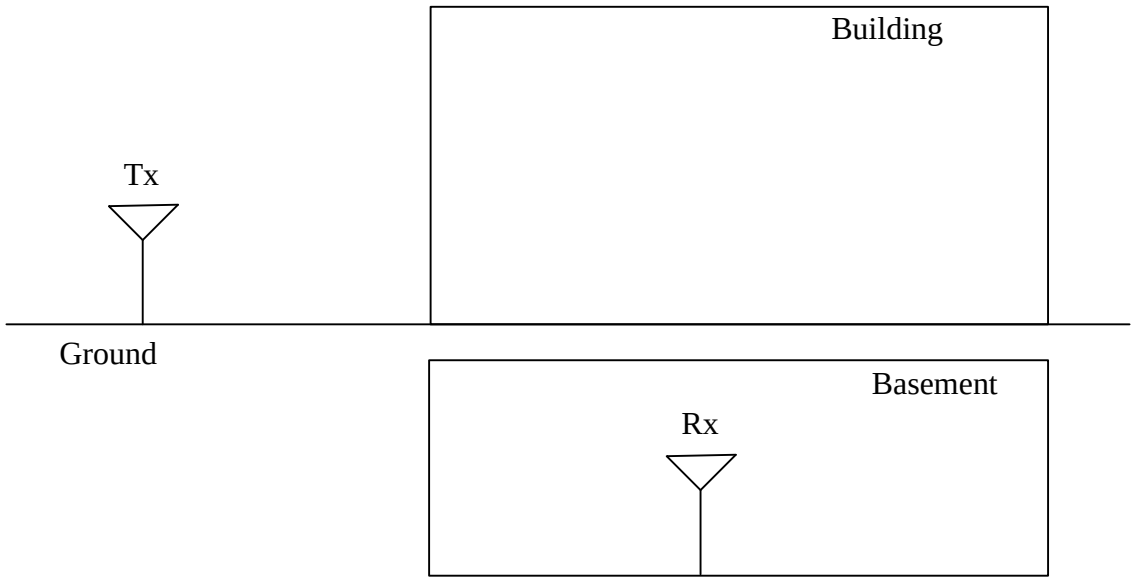

Figure 307 shows the building, which contains a basement parking lot. Figure 307(a) shows front and side views of the building, respectively. Figure 307(b) shows a photograph of the indoor basement parking lot. As shown in Fig. 307(b), a vehicle access road is located on the left side of the building. This building has three entrances, including one main entrance and two side entrances. The outdoor wall around the main entrance is composed of glass and those around the side entrances are concrete. The basement is concreted down from the first floor, and there are three conduits between the first

[24] Sharing studies carried out by ITU-R on different agenda items of WRC-19 were based on the text of this Report which was inforce at the time of these activities or at the time which the activity was carried out.

floor and the basement, containing an emergency stairwell, an elevator and the access road, respectively. The basement space is not closed, as the access road is open to vehicles at all times; however, the experimental transmitter (Tx) points were located in front of the main entrance, and the distance between the access road and the main entrance is large. Measurements towards the entrance in the basement were performed using a horn antenna, as described in § 3.3. The measurement frequencies were 1.5 and 3 GHz.

FIGURE 307

The study building in Chosun University (Gwangju, Republic of Korea): (a) front view, (b) basement parking lot

(a)

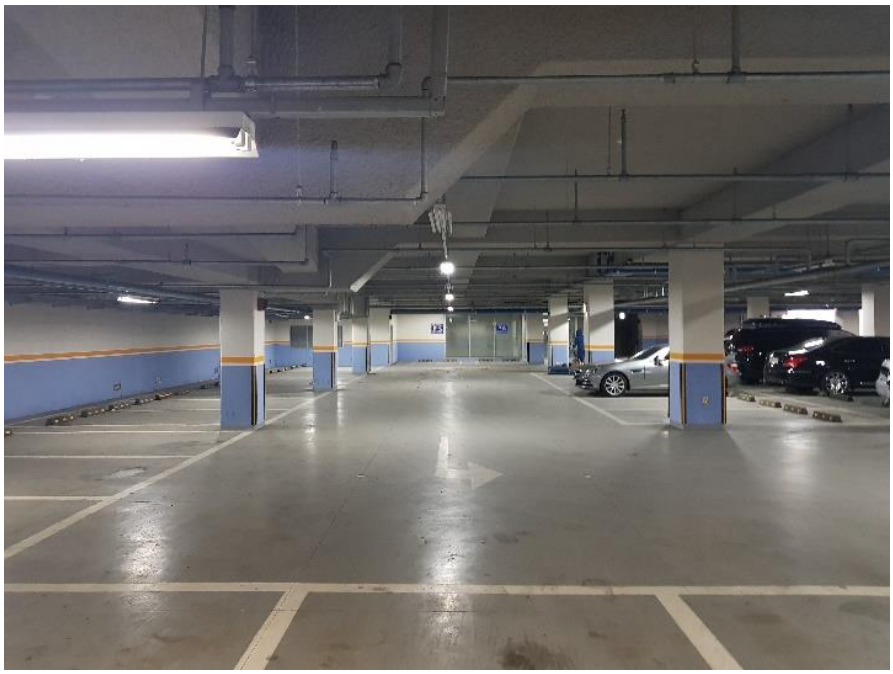

(b)

The Tx and receiver (Rx) systems can be seen in the photos in Fig. 308. The transmission system consists of a signal generator, power amplifier and direct current (DC) power supply for the operation of the amplifier. The transmission system consists of a spectrum analyser, low noise amplifier, and DC power supply for the operation of the amplifier. A laptop was used to control the spectrum

analyser. Measurements were conducted using omnidirectional bi-conical antennas with a sinusoidal signal at frequencies of 1.5 and 3 GHz. The detailed parameters of each frequency for the link budget are shown in Table 105.

FIGURE 308

The transmitter (Tx) and receiver (Rx) systems for measurement of building entry loss in a basement:(a) Tx, (b) Rx

(a) (b)

TABLE 105

System parameters

Parameters	Value	
Frequency (GHz)	1.50	3.00
Tx power (dBm)	0	0
Tx amplified gain (dB)	20.61	33.75
Rx amplified gain (dB)	52.83	52.00
Tx cable loss (dB)	0.86	1.10
Tx cable2 loss (dB)	0.60	0.82
Rx cable loss (dB)	1.11	1.54
Rx cable2 loss (dB)	0.30	0.45
Omnidirectional gain (dBi)	−6.27	−3.67

Accurate assignment of an origin was required to create a grid of points. The assigned position of x = 0 was the inner wall of the basement, and that of y = 0 was the centre of the elevator, as shown in Fig. 309. The elevator has equivalent positions in both the first floor and the basement, and is thus

useful for accurate assignment of grid points. The position of the inner wall of the basement was measured from outside the building, as shown in Fig. 309.

Reference points for measuring building entry loss were marked at intervals of 1 m from the inner wall of the basement. Rx measurement points were arranged in rows of six and marked with red circles in Fig. 309. The heights of the Tx and Rx antennas were both 1.8 m, i.e. half of the basement height (distance from the floor to the ceiling).

FIGURE 309

The Tx and Rx measurement points for building entry loss in the basement

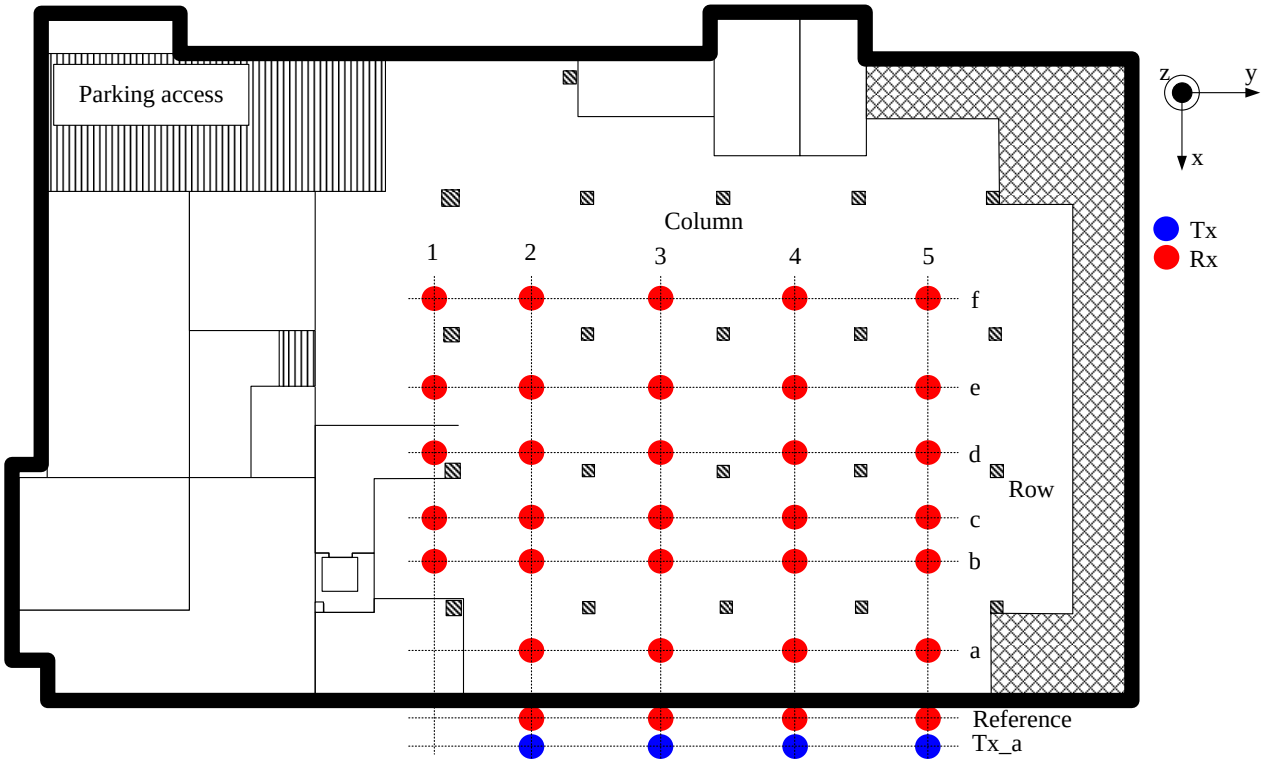

36.2.2 Measurement results of building entry loss in the basement

A total of 51 received powers were measured with the spectrum analyser; graphs of median ground and basement floor penetration losses, excluding the maximum and minimum values, are shown in Fig. 310. Analysis of the cumulative distribution function shown in Fig. 310 (b) revealed 50% losses of 58 dB and 68 dB at 1.5 and 3 GHz, respectively. Hence, the building entry loss at 3 GHz is around 10 dB higher than that at 1.5 GHz.

Building column 2 exhibited a lower building entry loss than the other columns. Column 2 is located in front of the main entrance of the building on the first floor, and hence most likely represents the location at which waves enter the basement via the first floor, adding to the waves that directly enter the basement. The results for the row of measurement points in this location were similar. This row of measurement points is closest to the wall of the building and was hence expected to exhibit the lowest building entry loss; however, the BEL here was higher than in other rows. In contrast, row A in column 2 shows similar results to the other rows for this column, but the results for row A differ from those of the other measurement rows at columns 3–5. This is likely because there is a café on the first floor of the building along the path of columns 3–5; the physical environment of the first floor thus influences building entry loss in the basement.

FIGURE 310

Results for measurement point rows a–f in the basement: (a) BEL at 1.5 GHz, (b) BEL at 3 GHz, (c) CDF

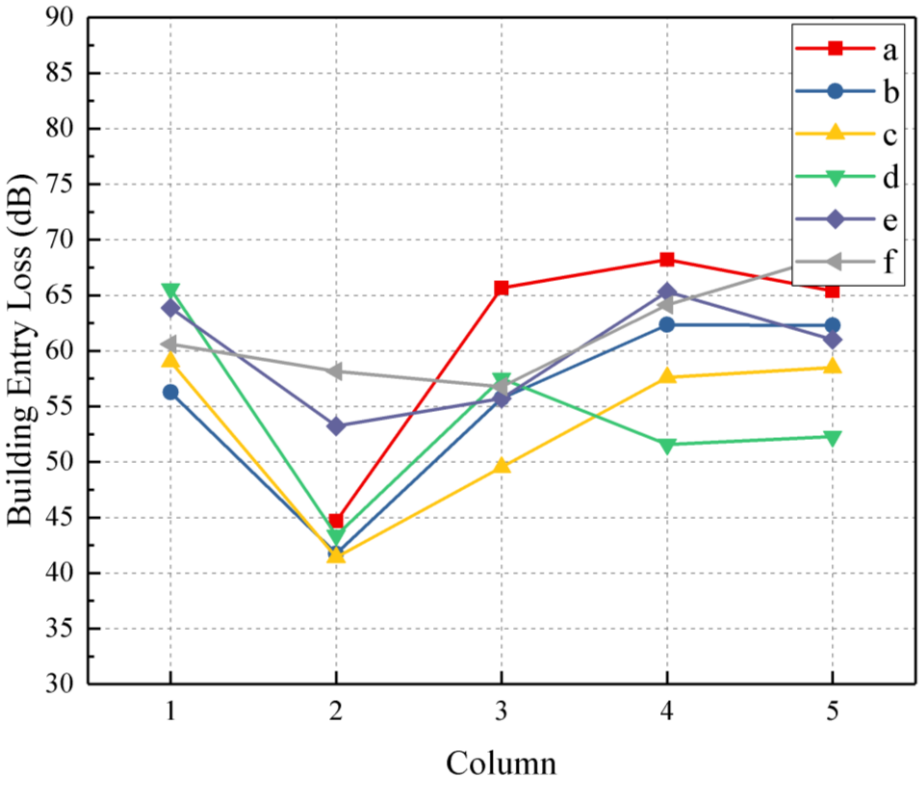

(a)

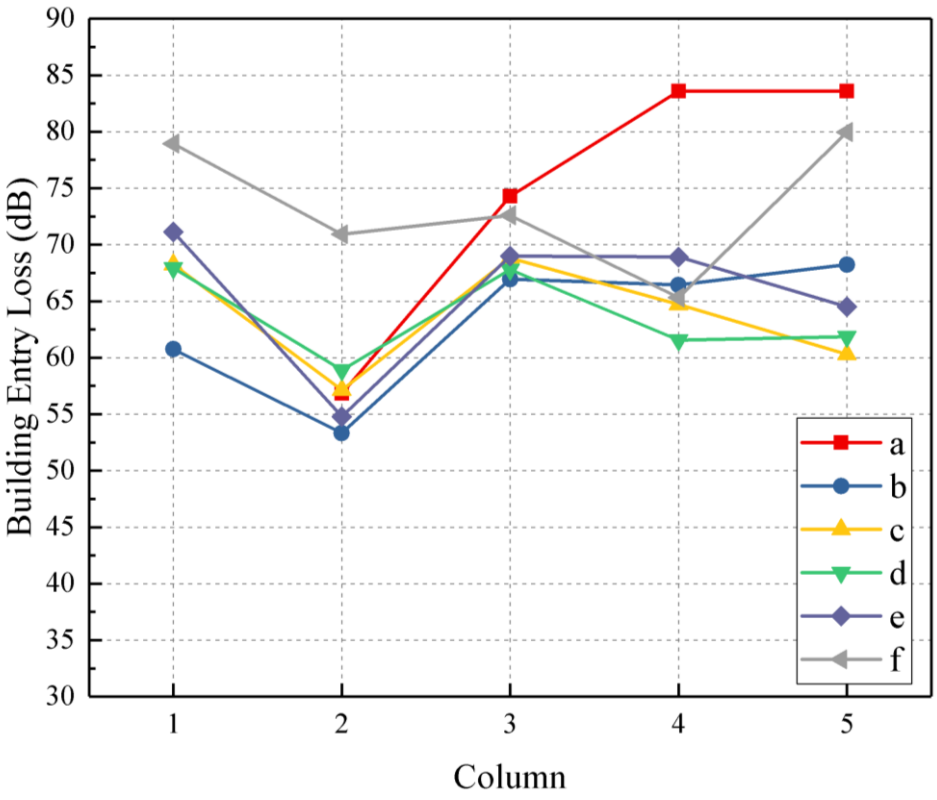

(b)

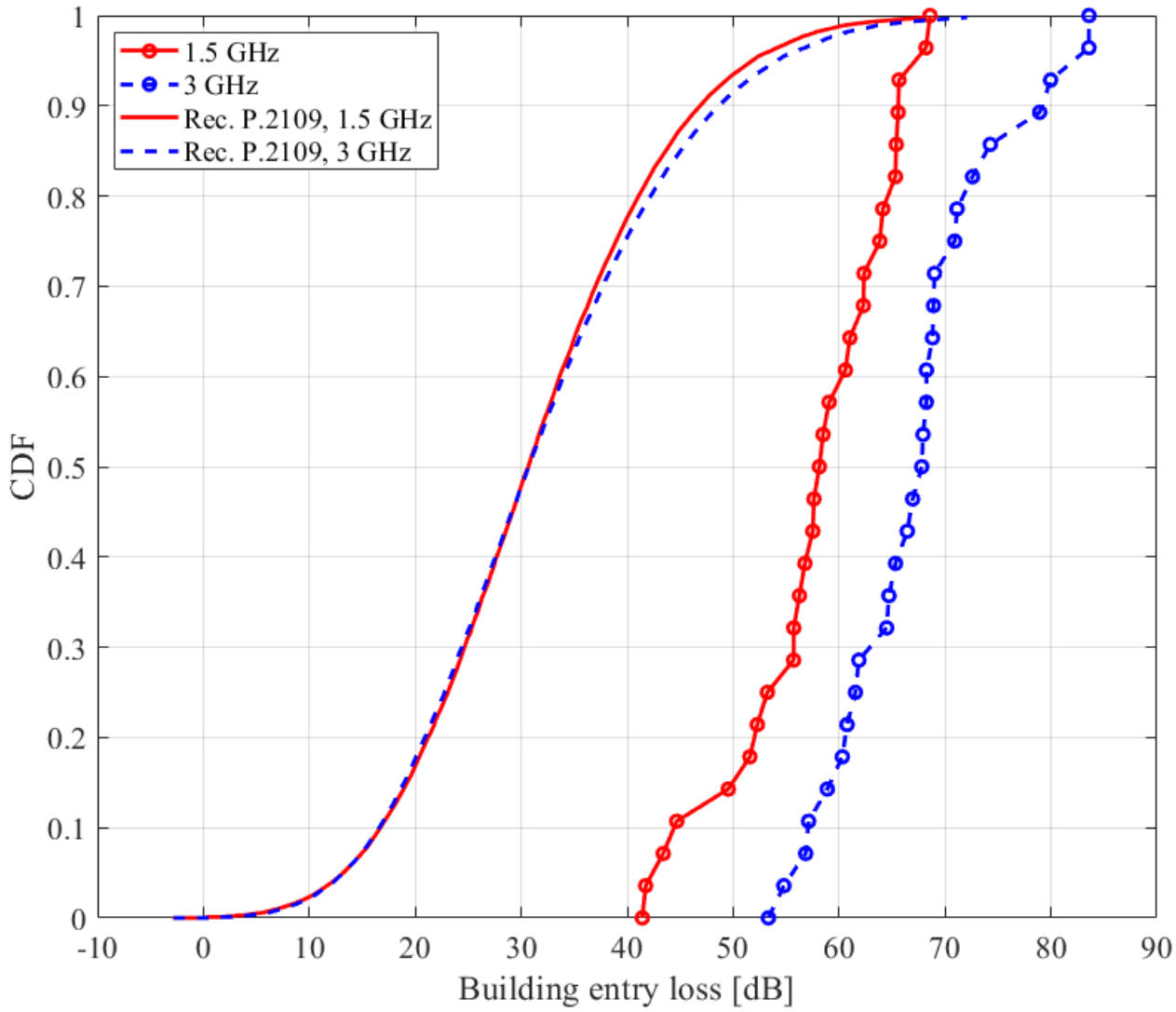

(c)

36.3 Analysis of propagation path between the ground and basement floors

The measurement results for the BEL in the basement indicate that it is significantly affected by the physical environment of the first floor. Additional measurement scenarios should be explored to verify the relationship between the BEL in the basement and the environment of the first floor. Therefore, three measurement scenarios, including the propagation path on the first floor, the loss between the first floor and the basement, and the arrival angle in the basement, were devised. The scenario models are shown in Fig. 311. In § 3.1, environmental measurements obtained on the first floor based on outdoor Tx measurements are discussed; then, penetration losses along a perpendicular incident wave from the first floor to the basement are described, and finally, the incident wave propagating from the open space in the basement is discussed.

FIGURE 311

The analysis setup for measuring the propagation path from outside of the building into the basement

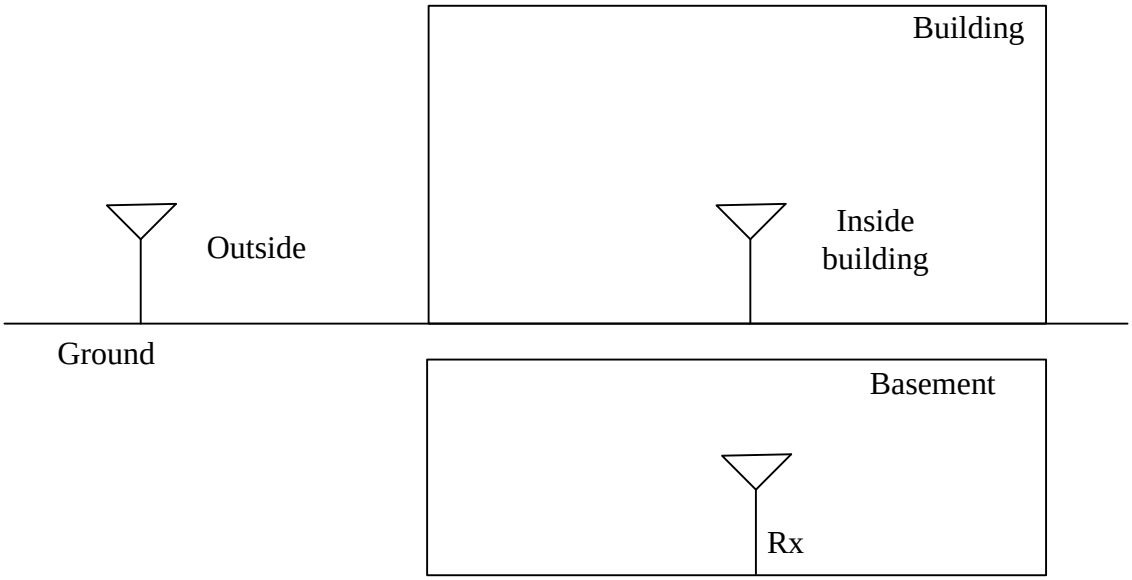

36.3.1 Measurement of the propagation path on the first floor

A received power from outdoor wave outdoor and indoor of first floor was measured to export the propagation paths before incident to the basement. A possibility that paths of the propagation wave pass through the inside of building and into the basement should be verified. The measurement site on the first floor was classified in three cases such as from the main entry of building to the corridor, a lobby and from an outside building to the entry of parking lots. Points was marked like Fig. 312, each point kept a distance of 1 m. The measurement was performed using an antenna with an omni-direction pattern at 3 GHz.

FIGURE 312

Measurements points for determining the propagation paths on the first floor

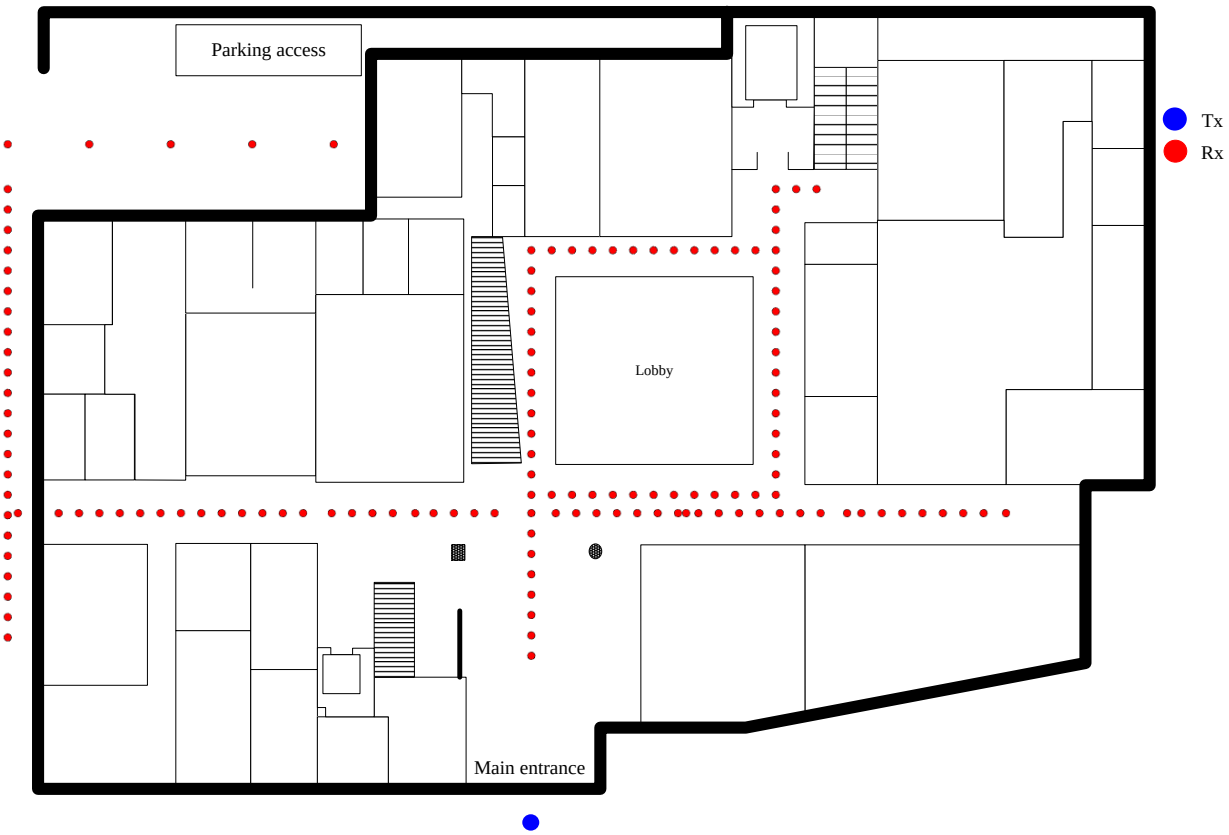

Figure 313 shows a scatter graph of the measurement points depicted in Fig. 313, based on the received power at each point. The received power in the section from the main entrance to the corridor exhibited the highest value. In practice, this cause of results shows the lower measured BEL as d2 points of Fig. 310 (b) compared with other rows. This is also the section with the highest received power among all sections on the first floor. The reason for the high received power measured at this location is that it is where the reflected wave that penetrates through the ground on the first floor is received; the high received power here also indicates that the transmitted wave enters the basement in front of this point.

The measurement results obtained outside the building showed that the building received a significant proportion of the transmitted wave. However, the received power decreases upon entry to the parking lot. It is therefore likely that the transmitted wave in front of the main entrance to the building does not affect the measurement of BEL obtained in the basement.

FIGURE 313

The received power of propagation paths on the first floor

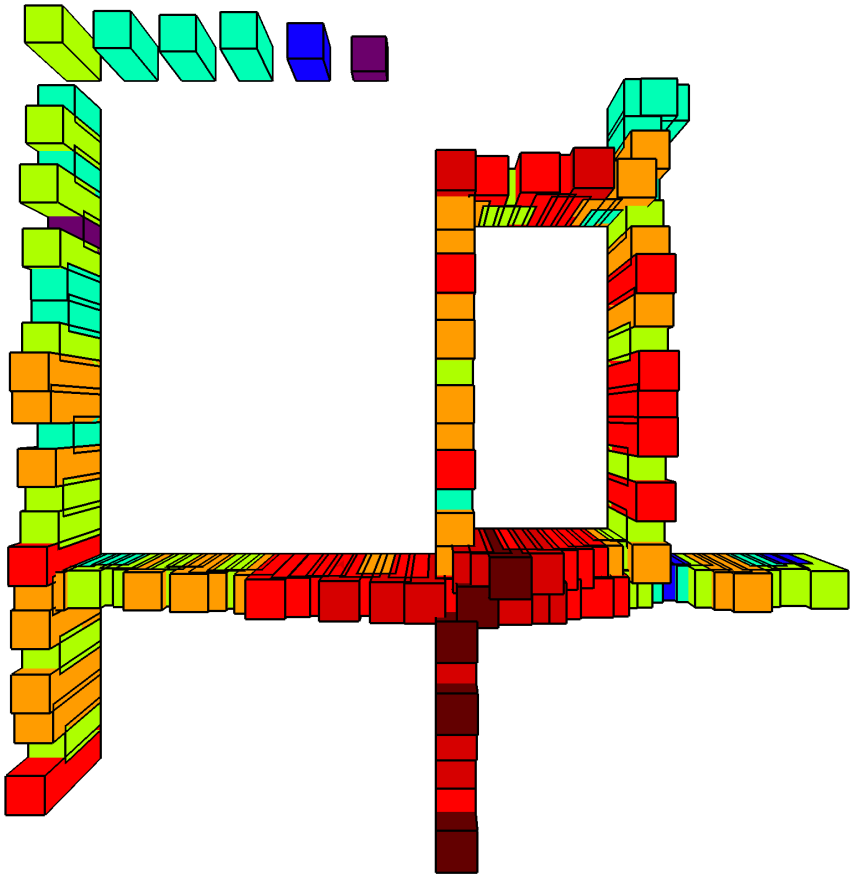

36.3.2 Propagation loss between the first floor and the basement

This scenario measures the proportion of radio waves that penetrate the first floor to enter the basement. The optimal points for this measurement are those in measurement row d, i.e., just below the corridor on the first floor, as shown Fig. 314. The system was constructed with a horn antenna to exclude other propagation paths, as shown in Fig. 315.

FIGURE 314

The Tx and Rx points for measuring penetration loss between the first floor and the basement: (a) basement, (b) first floor

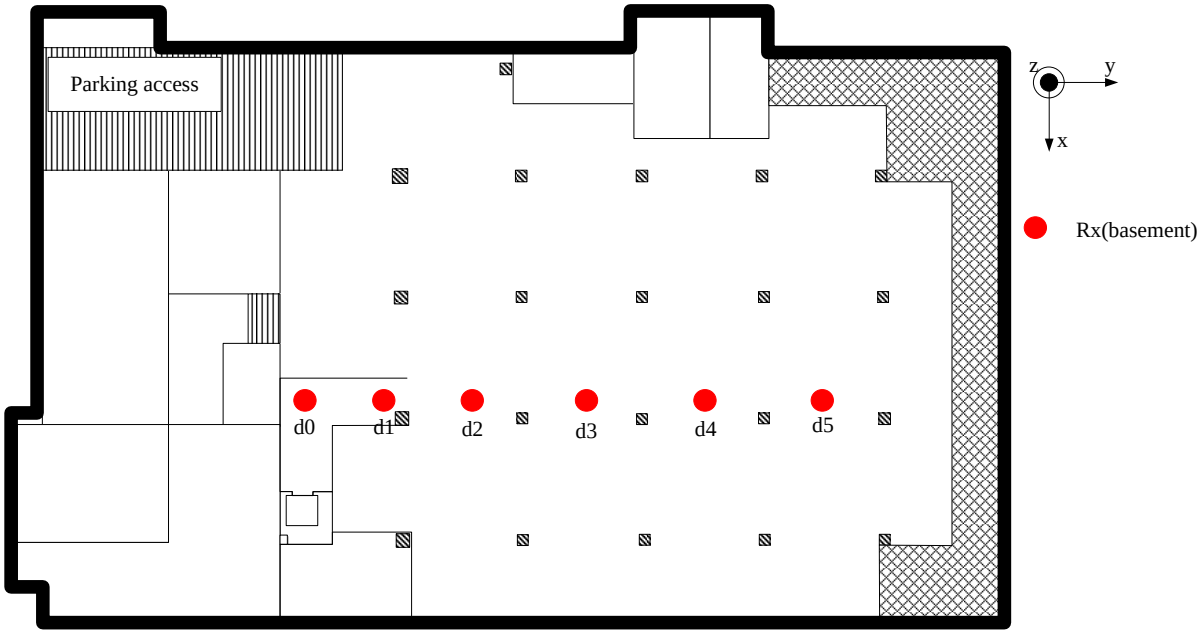

(a)

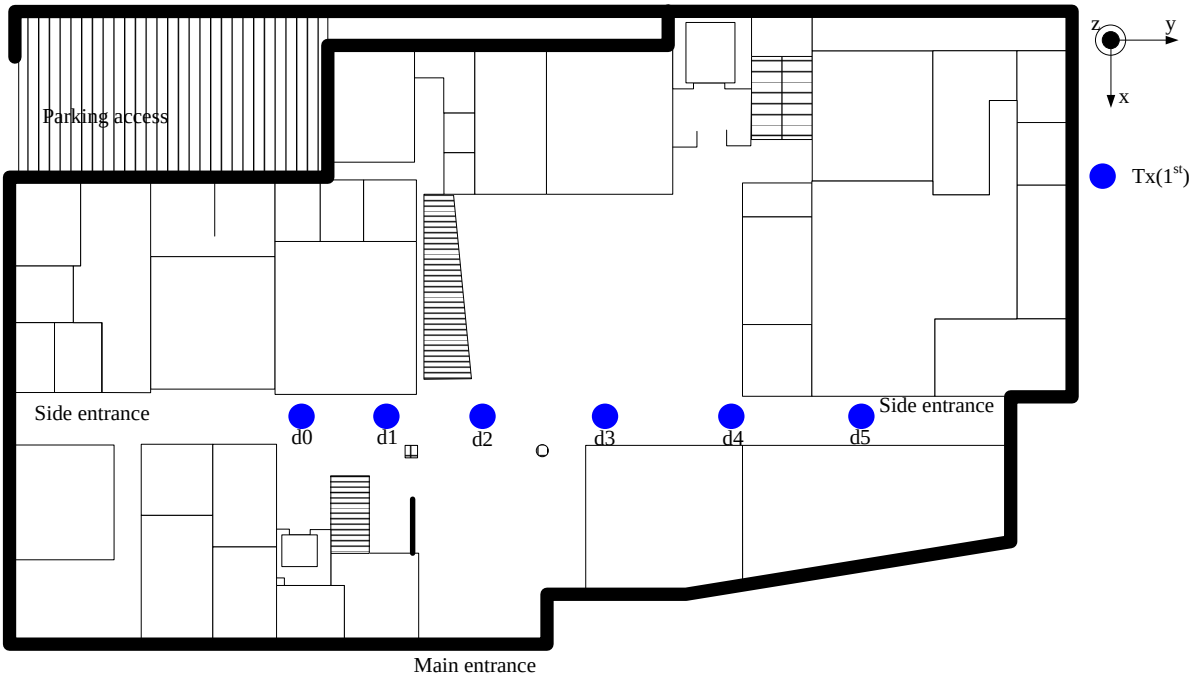

(b)

FIGURE 315

Tx and Rx systems for measuring penetration loss between the first floor and the basement: (a) Tx, (b) Rx

(a) (b)

Figure 316 shows the measured penetration loss between the first floor and the basement. The highest amount of penetration loss occurred at point d0, because this point is located underneath an aluminium ceiling, as shown in Fig. 316 (a).

The results show higher loss than basement entry loss; the waves penetrating into the basement had a largely oblique propagation path rather than a perpendicular propagation path.

FIGURE 316

Penetration loss between the first floor and the basement.

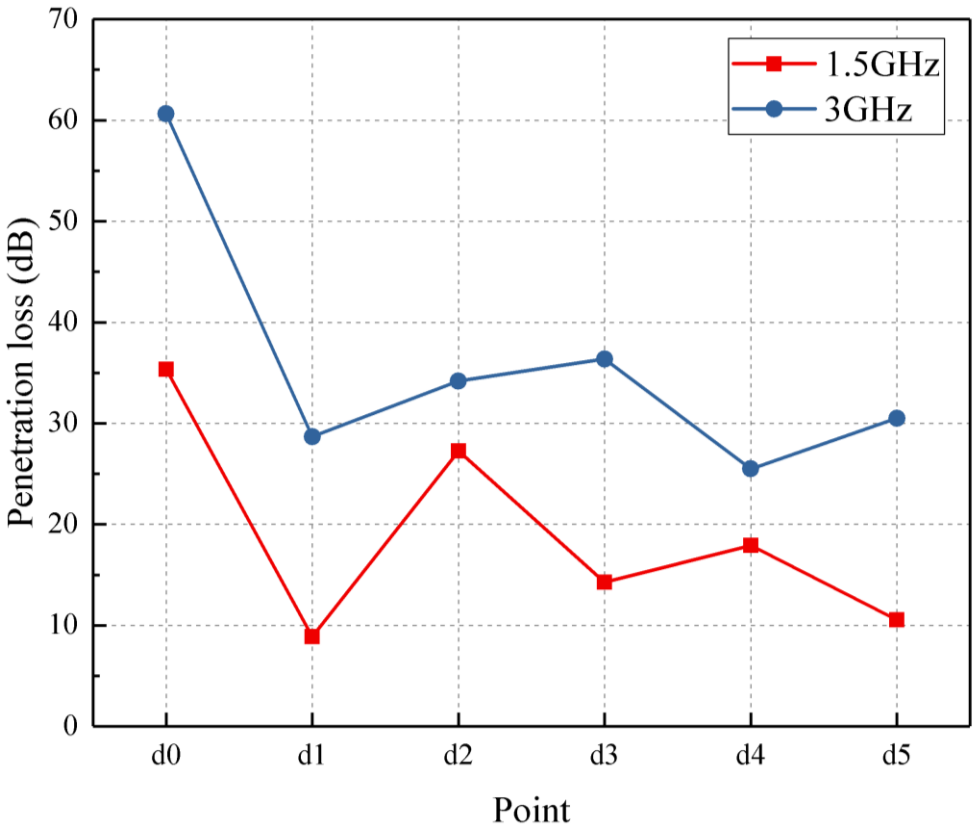

36.3.3 Comparison of the propagation path from the open entrance with direct propagation

Normally, parking lots have an open entrance. In the present case, the BEL measurement location was open at all times, and omnidirectional antennas were used for both the Tx and Rx measurements. Therefore, propagation paths from the open entrance were also considered.

The propagation path measurements from the open entrance to the basement focus on the loss determined by aligned horn antennas, for both Tx and Rx, at a frequency of 3 GHz. The e horn antennas were either aligned toward the wall or toward the open entrance, as shown in Fig. 317.

FIGURE 317

Measurement points and alignment of the horn antennas (toward the wall or toward the open entrance)

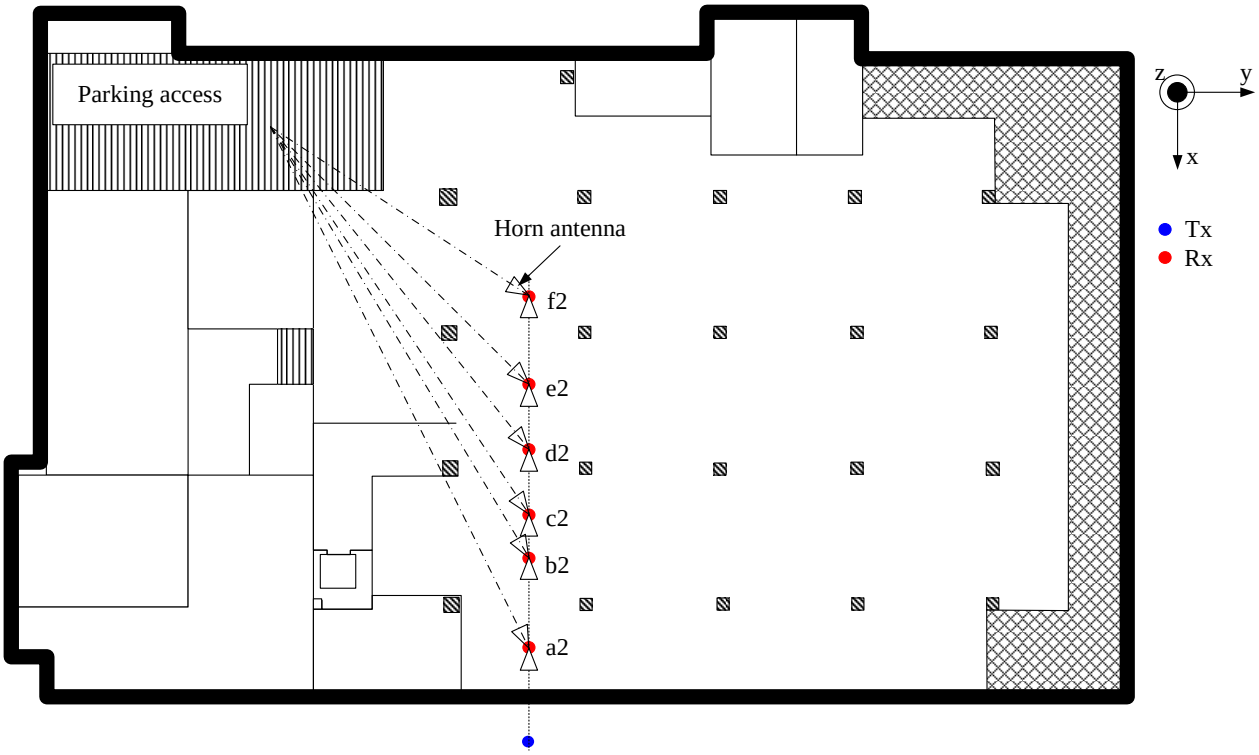

The received power measurement results for the various angles are shown in Fig. 318. Each point of measurement results has the difference received power from 20 dBm to 40 dBm. The entrance to the parking lot is located to the side of the measurement site, at a large distance from Tx. Hence, the incident wave propagating from the entrance to the parking lot is too small to affect the BEL measurement. Therefore, the wave entering the basement is almost entirely due to the direct penetration of the ground and wave reflection, with no contribution from outdoor of the building.

FIGURE 318

The results of received power for toward the wall and toward entry in the basement

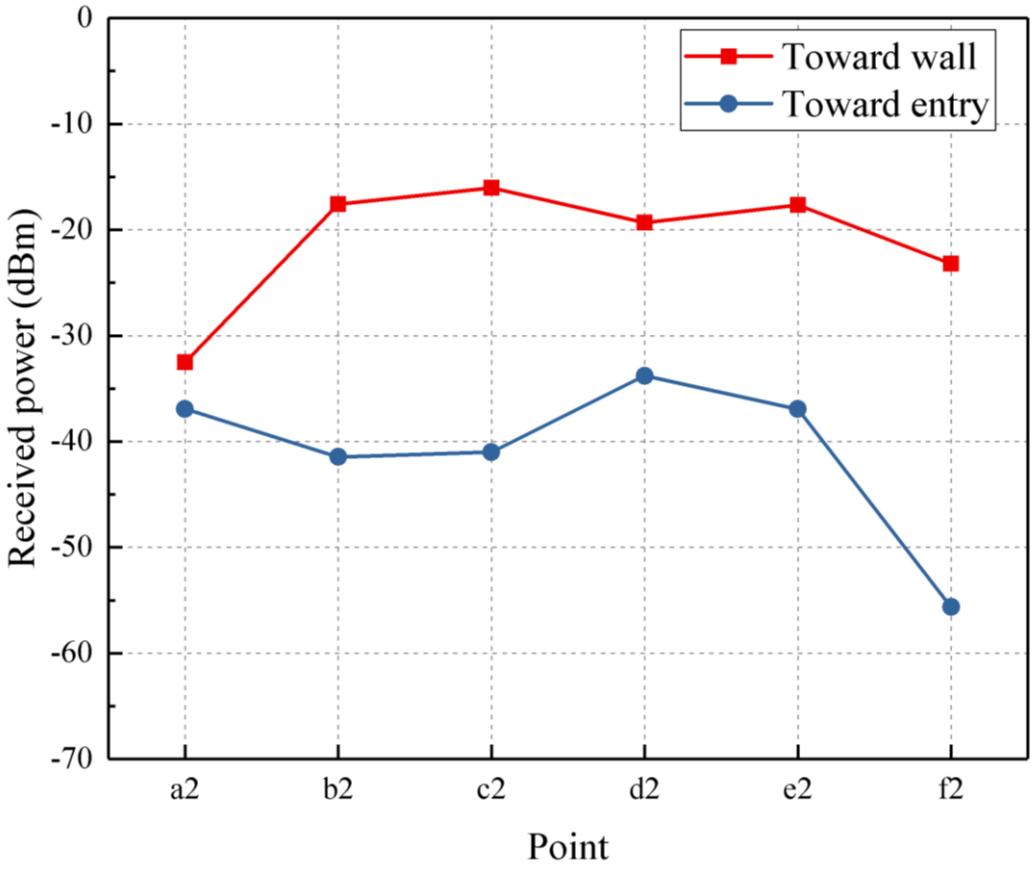

36.4 Summary of the results

In this study, BEL measurements were performed for the basement of a building, to aid in the development of future industrial applications based on wave propagation. The entry of radio waves into the basement was predicted under two scenarios, and the BEL of the direct propagation path (into the basement) was measured. The BEL of the direct path was found to be 58 dB and 68 dB at 1.5 GHz and 3 GHz, respectively. The measurement results were affected by the physical environment of the first floor.

To establish the influence of the first floor environment, three scenarios were developed to determine propagation paths on the first floor, loss between the first floor and the basement, and arrival angle in the basement. By measuring the propagation path on the first floor, it was verified that radio waves enter the basement via the main entrance to the building, and that the BEL was not greatly affected by the wave transmitted from outside the building to the entrance of the parking lot. The losses between the first floor and the basement were 19 dB and 35 dB at 1.5 GHz and 3 GHz, respectively. Therefore, an oblique transmitted wave penetrates further than a perpendicular transmitted wave. Finally, it was demonstrated that the contribution of transmitted waves passing through the first floor, to wave energy entering the basement, is greater than that of the wave transmitted from the building entrance to the parking lot.

These results could aid predictions of the path of radio waves entering a basement space from outside the building, thus contributing to better utilization of radio waves in basement spaces

References

[1] Rec. ITU-R P.2040-1, *Effects of building materials and structures on radiowave propagation above about 100 MHz*, vol. 2015 P-Series, 2015.

[2] Rec. ITU-R P.2109, *Prediction of building entry loss*, vol. 2017 P-Series, 2017.

[3] Rep. ITU-R P.2346-2, *Compilation of measurement data relating to building entry loss*, vol. 2017 P-Series, 2017.

37 BEL measurements in a line-of-sight (LoS) and cluttered path[25]

37.1 Introduction

In general, in outdoor-to-indoor propagation environments, radio waves propagate into the building through reflection and diffraction from surrounding clutters, such as buildings and trees. Therefore, the overall excess loss should be predicted. To do this, it is important to predict individual losses such as clutter loss and building entry loss (BEL).

To confirm the relevant coupling mechanisms, the quantitative variation in BEL according to the surrounding environments of the building of interest should be analysed. In the cluttered path, BEL characteristics were measured according to presence or absence of the major clutter (a huge structure) behind the building and the results are compared with those measured in the LoS path.

37.2 Measurement overview

Measurements were performed at Mokpo National Maritime University (Mokpo, in the Republic of Korea), as depicted in Fig. 319. A building (Building A) for BEL measurements is located 32 m away from the seaside port and a training ship is anchored at the port. Building A comprises an engine training factory, offices and laboratories. BEL measurements were performed in and around the engine training factory.

The BEL was measured in the two paths between a transmitter (Tx) and receiver (Rx), when the ship was anchored in the port and when it is not:

– Path 1: Line-of-sight path (LoS).

– Path 2: Cluttered path (CLTP).

[25] Sharing studies carried out by ITU-R on different agenda items of WRC-19 were based on the text of this Report which was inforce at the time of these activities or at the time which the activity was carried out.

FIGURE 319

Measurement geometry (a), buildings in measurement paths (b, c and d) and paths (image data: https://map.naver.com/)

The transmitter is located at location ‘Tx 1’, which is 60 m away from the factory entrance in Building A, as shown in Figure 1. The path between Tx and Rx in this location is LoS (path 1) and the received power is measured both inside and outside the factory.

In the case of path 2, the transmitter is placed on the roof of Building B. It is located 310 m from Building A and is denoted by Tx2. The path between the Tx and Rx is a CLTP and there are two main clutters (Buildings C and D), as shown in Figure 1. Measurements are repeated inside and outside the factory in this site as well.

To investigate the effect of reflections due to a major clutter around Building A, the measurements were performed when the ship was anchored at the harbour and when it departed and the results were compared.

The height of the main buildings in the CLTP is shown in Fig. 320. The length and height of the training ship are 103 m and 33.2 m, respectively. It serves as the main structure for reflection at the rear side of Building A with a size of 62 m × 20 m × 12 m.

FIGURE 320

Height of main buildings [measured based on the outside ground of Building A]

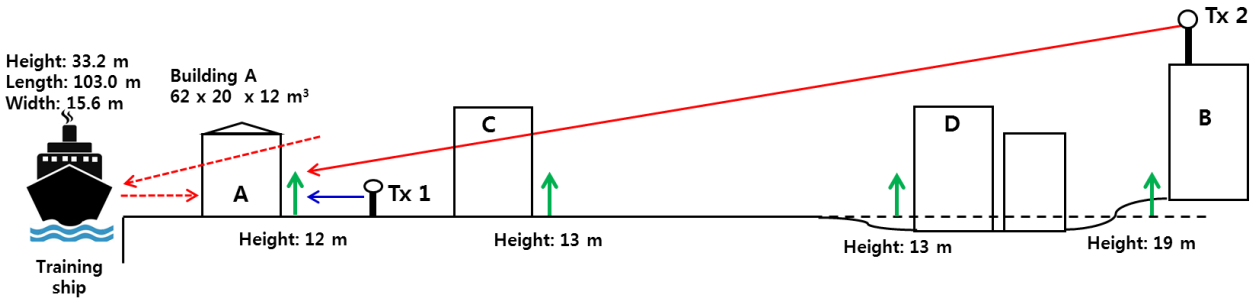

FIGURE 321

Front (from the direction of location Tx1) and rear (from the direction of the ship) sides of Building A, the front, lateral and rear sides of the factory and the indoor of the factory

Building A is a traditional construction consisting of a factory, offices and laboratories. The factory has glass windows on three sides. Security metal fences are installed outside the window. There are utilities and trees on the lateral and rear sides of the factory, respectively. Cars are parked in the parking lot on the lateral side of the factory. Machinery such as milling machines, engines, workbenches and utilities are installed inside the factory.

FIGURE 322

Outdoor and indoor measurement scenarios for two paths: locations for reference (circles) and reflection measurements (squares)

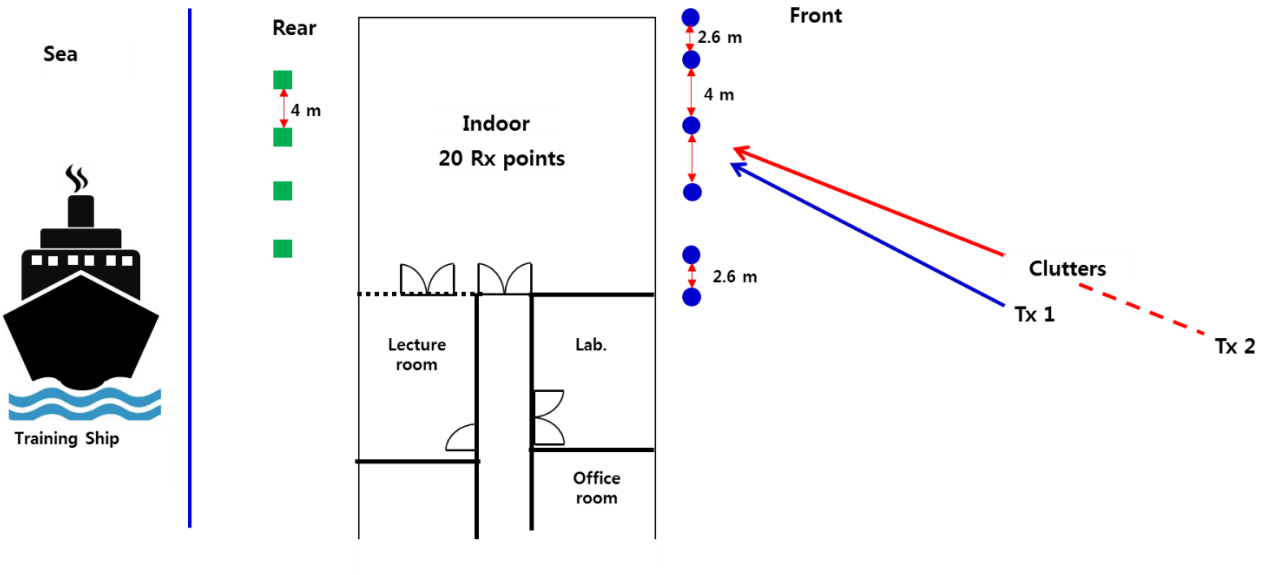

37.2.1 Measurement scenario

A BEL measurement scenario is presented in Fig. 322. Reference measurements were performed at six locations on the front side of the factory and they are marked with circles. The received power was measured at 20 points inside the factory in a 20 m × 20 m area. To analyse the amount of power reflected from the ship located behind the building, the received power was additionally measured at four points between the factory and ship and they are denoted by squares, as shown in Fig. 322.

The above measurements were performed with and without the ship at the port. Figure 323 shows the images when the ship is anchored at the port and when it is not. When the ship was docked, the difference in ship height between high and low tide was 2 m from the ground.

FIGURE 323

Images when the ship is anchored at the port and when it is not.

37.2.2 Measurement systems

These measurements were performed using a continuous wave (CW) of 6 GHz. For the transmitter (Tx), a signal generator (SG) was connected with an antenna using a cable with a loss of 5.1 dB. The output of the SG was 8 dBm. The receiver system consisted of a spectrum analyser (SA), a low-noise amplifier (LNA) and an antenna. The loss of the two connecting cables was 1.6 dB. The details of the measurement systems are provided in Table 106.

TABLE 106

Basic details of measurement set-up

Items	Transmitter (Tx)	Receiver (Rx)
Frequency	6 GHz	
Tx Power	8 dBm	NA
Antenna, Gain	Omni (3.0 – 24 GHz), 2.5 dBi @ 6 GHz	
Amplifier Gain	NA	LNA 38.7 dB @ 6 GHz

FIGURE 324

Images of the transmitter and receiver at each location

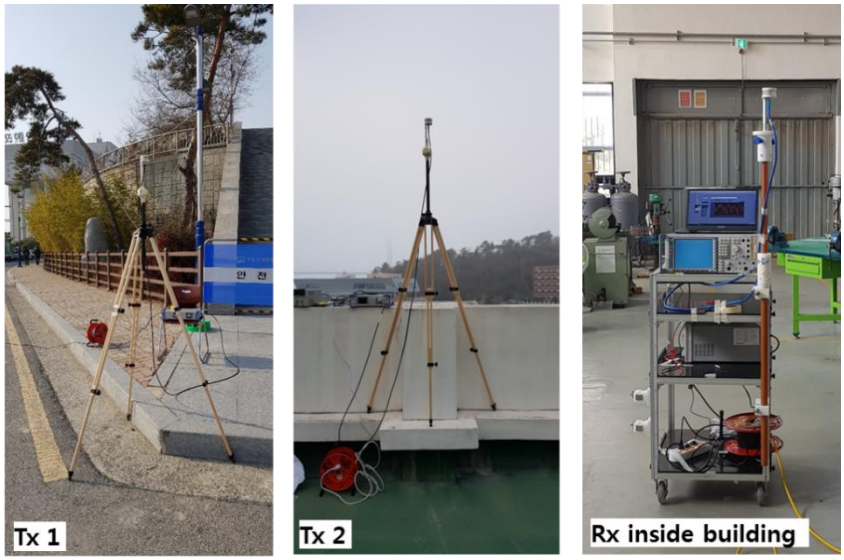

The transmitter and receiver at each location are shown in Fig. 324. The height of the antenna at the location of Tx 1 and Tx 2 is 2.0 m and 2.7 m from the ground and rooftop floor, respectively. The equipment of the receiver were mounted in the handcart. The received power was measured inside and outside the factory by using this handcart. The height of the antenna from the floor was 1.8 m.

37.3 Measurement results

37.3.1 BEL characteristics

The cumulative distribution function (CDF) data of all the measured BEL values are shown in Fig. 324 and their median values are listed in Table 107. When the ship is anchored (with the ship, W-ship), the BEL values in the CLTP are significantly lower than those in the LoS path and the difference is 16.96 dB. However, when the ship is not anchored at the port (without the ship, W/O-ship), the BEL values in the CLTP increases by 10.49 dB, from 9.15 to 19.64 dB. However, the BEL values are almost constant in the LoS path, regardless of whether the ship is anchored at the port or not.

FIGURE 325

CDF characteristics of measured BEL

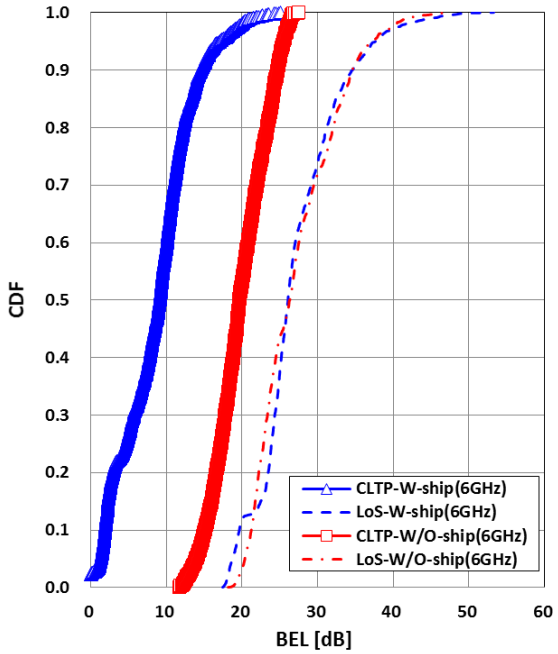

TABLE 107

Median values of calculated BEL for each measurement path

Items	CLTP	LoS	Difference (LoS-CLTP)
	BEL (dB)	BEL (dB)	
With the ship (W-ship)	9.15	26.11	16.96
Without the ship (W/O-ship)	19.64	26.34	6.70
Difference (W/O-W-ship)	10.49	0.23	

FIGURE 326

Received power measured at the front, inside and rear sides of the building for CLTP (left) and LoS path (right)

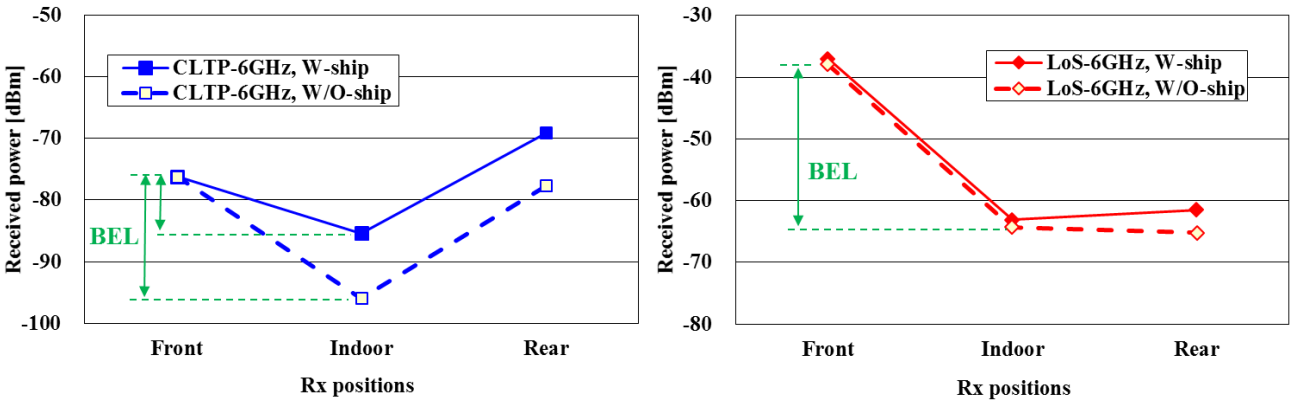

FIGURE 327

Conceptual illustration of the effect of reflections for CLTP

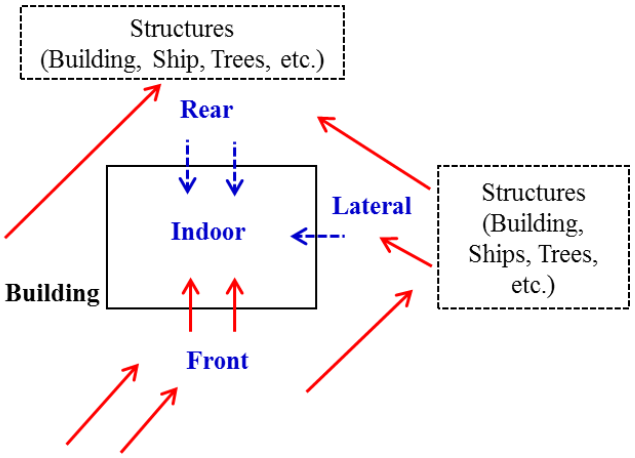

37.3.2 Received power analysis

To analyse how the power reflected from structures located behind the building affects the indoor environment, the received powers at the front, inside and rear sides of the building are measured and their median values are presented in Fig. 326. The values at the rear side of the factory are median values measured at four points, as shown in Fig. 327. The difference in powers measured in the front side of the building and indoor is the BEL.

In CLTP, when the ship is located in the port (W-ship), the received power at the rear side of the building is 8.5 dBm higher than that in the front side of the building. In the absence of the ship at the port (W/O-ship), the difference in received power between the front and rear sides of the building is 1.5 dBm and the received power on the inside of the building decreases by 10.5 dBm. This result indicates that the power around the building is uniform if there is no structure for reflection around the building.

For the LoS path, regardless of the presence or absence of the ship, the received power does not change in the front side of the building and indoors. In the absence of the ship, the received power at the back of the building decreases by 3.6 dBm, which would have been reflected from the building next to the factory building.

These results imply that most of the radio waves are reflected by the structure (ship) located on the rear side of the building that enter the building again. This is the reason why the BEL is decreasing in the CLTP, as shown in the conceptual illustration in Fig. 327.

37.4 Summary of the results

In environments where waves are reflected from surrounding clutters of a building, they enter the building again, the BEL in the CLTP is lower than that in the LoS path. Therefore, the BEL may change depending on the external environments surrounding the building.

References

[1] United Kingdom of Great Britain and Northern Ireland, “Independent and joint statistics of clutter loss and building entry loss – Initial measurements”, see Document 3J/187-3K/239-3M/313 (2018) for information

38 On joint statistics of clutter loss and building entry loss at frequency 3 GHz and 24 GHz[26]

38.1 Introduction

According to an ITU-R document [1], the clutter loss of the receiver inside a building is reported to be unequal to the sum of clutter loss and building entry loss (BEL). However, in this experiment, a value similar to the total excess loss was obtained by adding the clutter loss and BEL from equation (47).

As shown in Fig. 328, a transmitter (Tx) was installed in Gwangju Metropolitan City, which had a helicopter landing area. As actual satellite radio waves cannot be used, a transmitter was set up at a height, similar to the radio wave model, with a receiver path in a building for the radio waves. The distance between the transmitter and receiver buildings was 447 m; each building had a BEL path, inside building clutter loss (BEL+clutter loss) path, and outside building clutter loss path. The aim was to determine whether the BEL+clutter loss was equal to the sum of the clutter loss outside the building and BEL by measuring the received power of each path.

$$\text{Clutter loss for Rx of inside building (BEL + clutter loss)} = \text{Clutter loss for Rx of outside building} + \text{BEL} \quad (47)$$

FIGURE 328

Configuration of measurements of power received of BEL, Clutter loss and BEL+clutter loss paths

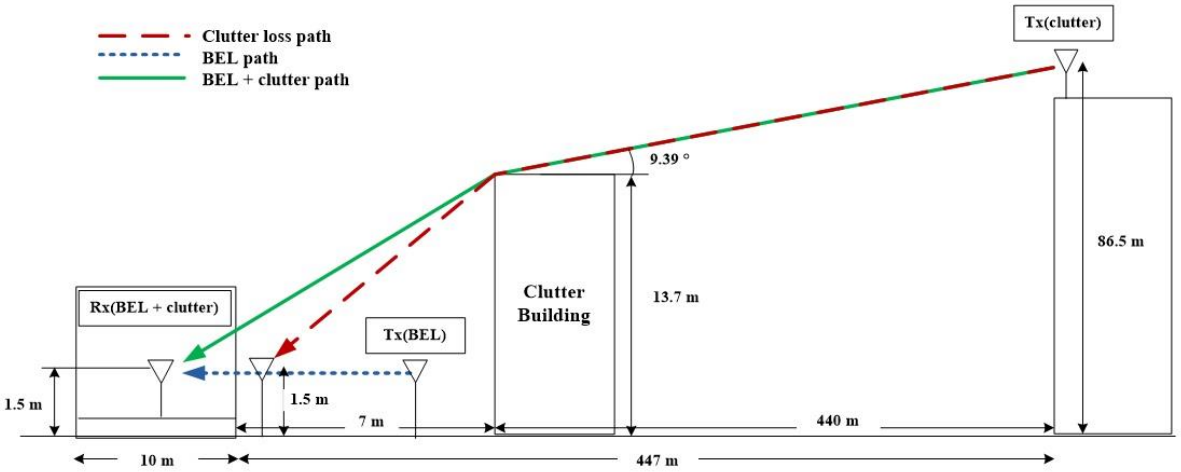

[26] Sharing studies carried out by ITU-R on different agenda items of WRC-19 were based on the text of this Report which was inforce at the time of these activities or at the time which the activity was carried out.

38.2 Experimental arrangement

FIGURE 329

Measurement geometry (image data: © 2019 Daum)

Figure 329 shows a side view of the overall measurement scheme. The horizontal distance between the transmitter and clutter building was approximately 440 m. Figure 329 shows that the straight distance from the transmitter to receiver is nearly 458 m. The non-line of sight (NLOS) is the distance from the transmitter (Tx1 clutter) to the receiver that is used to exclude the free space loss from the measured received power. To measure the path of the BEL, the transmitter (Tx2 BEL) was set up in front of the building and the receiver (Rx) inside the building as shown in Fig. 2. The measured received power is $P_{rcv,in}$ of equation (38-2) given below:

$$\text{BEL} = P_{rcv,ref} - P_{rcv,in} \tag{48}$$

where:

$P_{rcv,ref}$: received power in front of building from Tx2

$P_{rcv,in}$: received power in the building from Tx2

BEL : building entry loss.

Figure 330 shows the measurement site for clutter and BEL+clutter loss of a suburban area. The measurement site is located close to surrounding clutter buildings. Such an environment is considered to have a larger effect on the clutter building rather than the reflection effect of the buildings at the measurement points.

FIGURE 330

Measurement site of suburban area

The equipment used for the measurement is shown in Fig. 331. The transmitter located at a height is composed of a biconical antenna and signal generator, as shown in Fig. 331(a). The receiver consists of a biconical antenna, low noise amplifier (LNA), filter, spectrum analyser and data acquisition PC, as shown in Fig. 331(b).

FIGURE 331

Configuration of measurement equipment (a) Transmitter (b) Receiver

(a) **(b)**

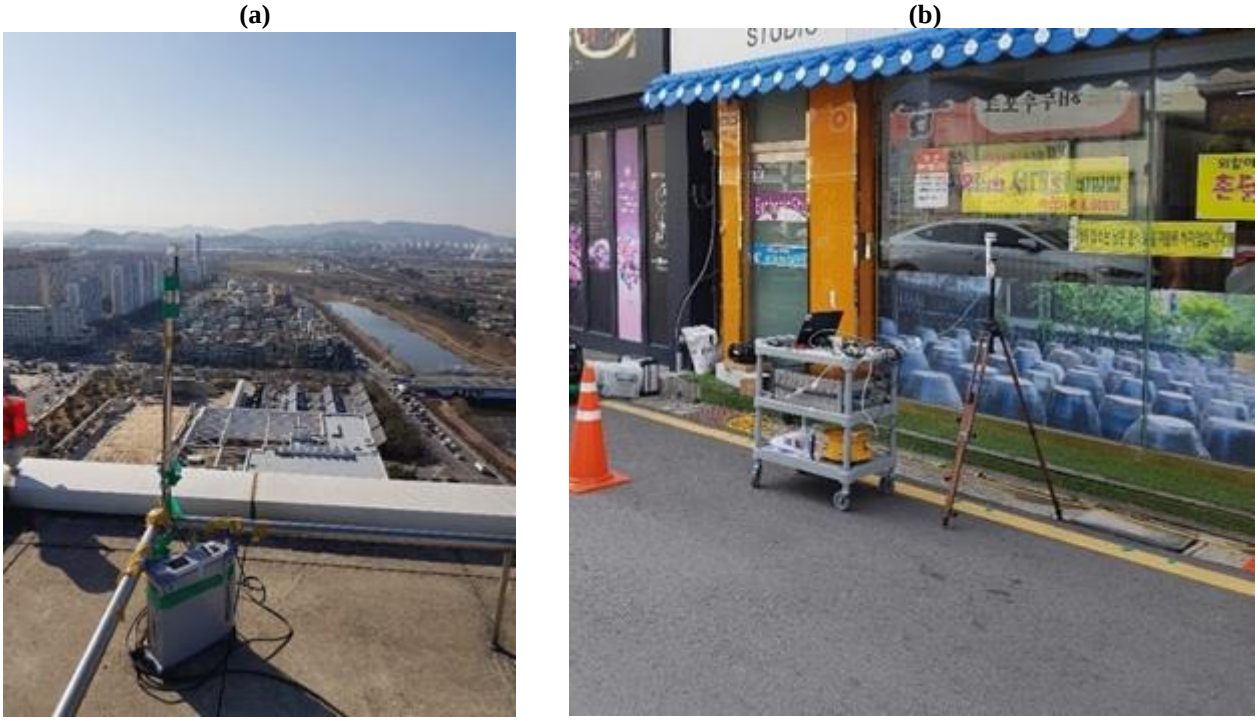

Figure 332 shows the measurement environment of the transmitter and receiver. Figure 332 (a) shows the transmitter for clutter loss, Fig. 332 (b) shows the inside the building measurement environment.

FIGURE 332

Measurement environment (a) Tx for clutter loss (b) Rx for clutter loss(inside)

(a) **(b)**

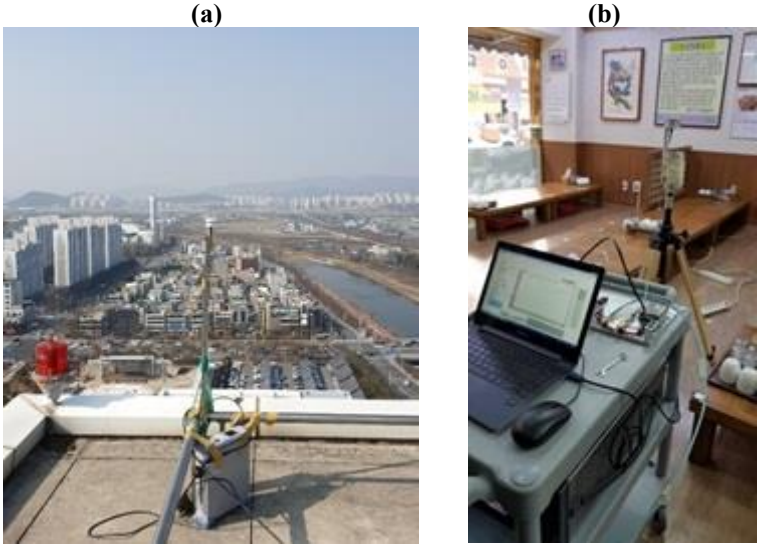

Table 108 shows the receiver and transmitter parameters for the measuring instruments, which were used to compensate the clutter loss and BEL from the measured received power by using equation (49). In the equation, free space loss is a basic transmission loss for 458 m, which is the straight distance from the transmitter to the receiver.

TABLE 108

Equipment parameter of transmitter & receiver

Contents		**3 GHz**	**24 GHz**
Tx	Output power	5 dBm	0 dBm
	Cable loss	1.34 dB	3.89 dB
	Antenna gain	−1.65 dBi	5.16 dBi
Rx	Antenna gain	−2.02 dBi	5.15 dBi
	Cable loss	1.50 dB	5.01 dB
	Filter insertion loss	1.54 dB	0.43 dB
	3 GHz LNA 1 gain	41.16 dB	–
	3 GHz LNA 2 gain	27.07 dB	–
	24 GHz LNA gain	–	51.96 dB
	Cable loss	0.44 dB	2.18 dB

$$\text{Clutter Loss} = P_t - P_r + G_r + G_t + G_{LNA} - cable\ loss - free\ space\ loss \quad (49)$$

Figure 333 shows the measurement points for the clutter loss and BEL. The clutter loss and BEL+clutter loss were measured on the same line from line indexes **a** to **e** for determining the BEL. The received power of BEL and clutter loss was measured by moving the receiver through distances of approximately 1 m in the building.

FIGURE 333

Measurement points (a) clutter (b) BEL + clutter

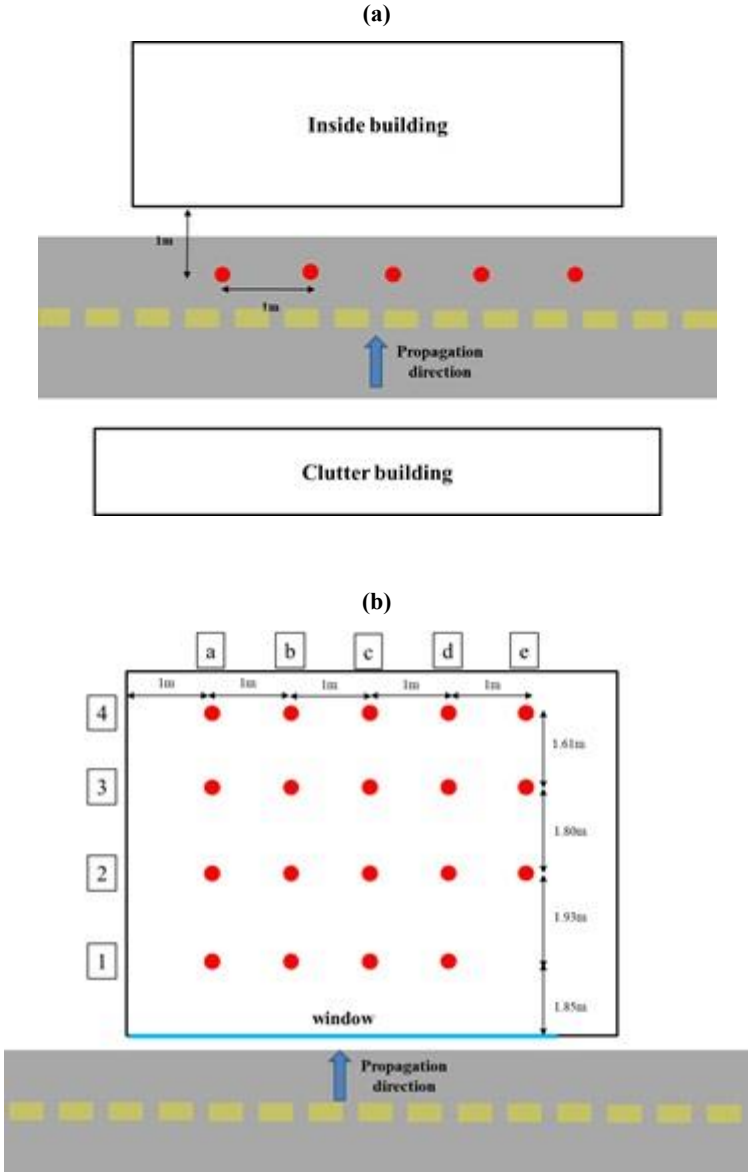

38.3 Results

The received power was measured over 5 m in step-by-step intervals of 1 m and the result of the excess loss was calculated using equation (49) to compensate for the equipment parameters in the measured values. The results of the calculations are shown in Fig. 334. Figure 334(a) shows the results of the BEL measurement and has median values of 13.12 dB at 3 GHz and 14.2 dB at 24 GHz. Figure 334(b) shows the result of measuring the BEL + clutter inside the building. At 3 GHz and 24 GHz, the BEL+clutter loss are 27.79 dB and 26.36 dB, respectively.

FIGURE 334

Results of calculation of clutter loss and BEL (a) BEL (b) BEL+clutter loss

(a)

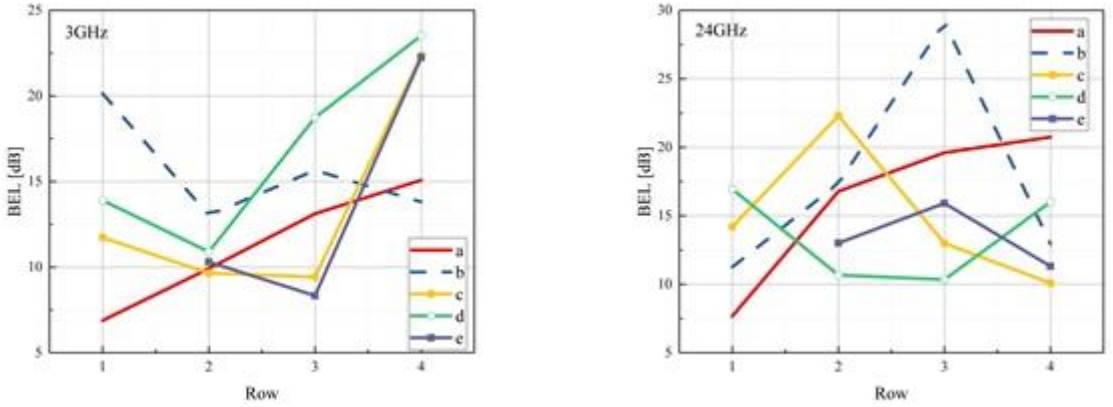

(b)

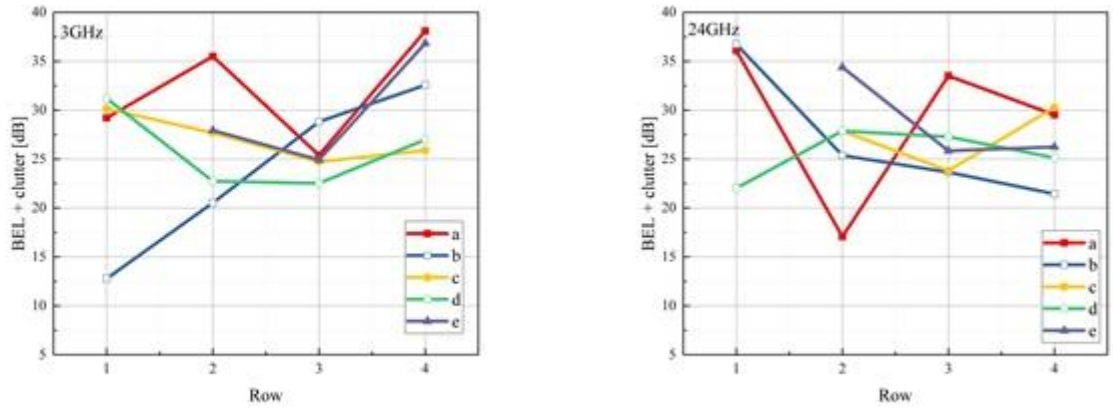

Figures 335 and 336 show the BEL and BEL+clutter loss calculated at 3 GHz and 24 GHz for each path as cumulative distribution functions. The cumulative distribution function is a probability function that signifies the extraction of the excess loss value. A probability of 0.5 in the BEL is 13.12 dB and 14.2 dB at each frequency, respectively; the probability of 0.5 in the BEL+clutter loss is 27.6 dB and 26.13 dB at each frequency, respectively; the probability of 0.5 in the clutter loss is 10.25 dB and 17.75 dB at each frequency, respectively. The straight distance between the transmitter and inside building of receiver is 458 m. The BEL+clutter loss measured inside the building is 27.55 dB at 3 GHz and 26.12 dB at 24 GHz, the difference is −4.19 dB and 5.82 dB respectively.

FIGURE 335

3 GHz BEL & BEL+clutter loss

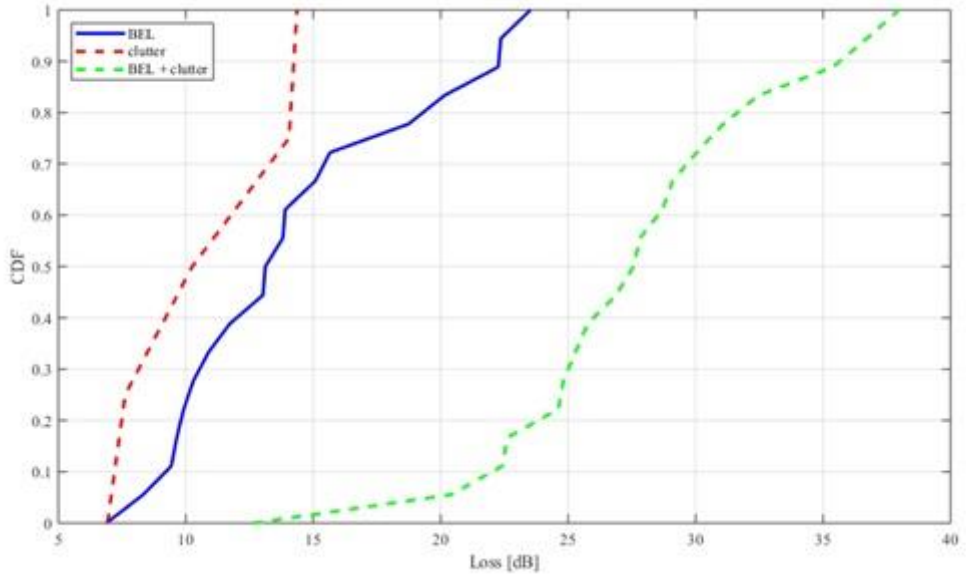

FIGURE 336

24 GHz BEL & BEL+clutter loss

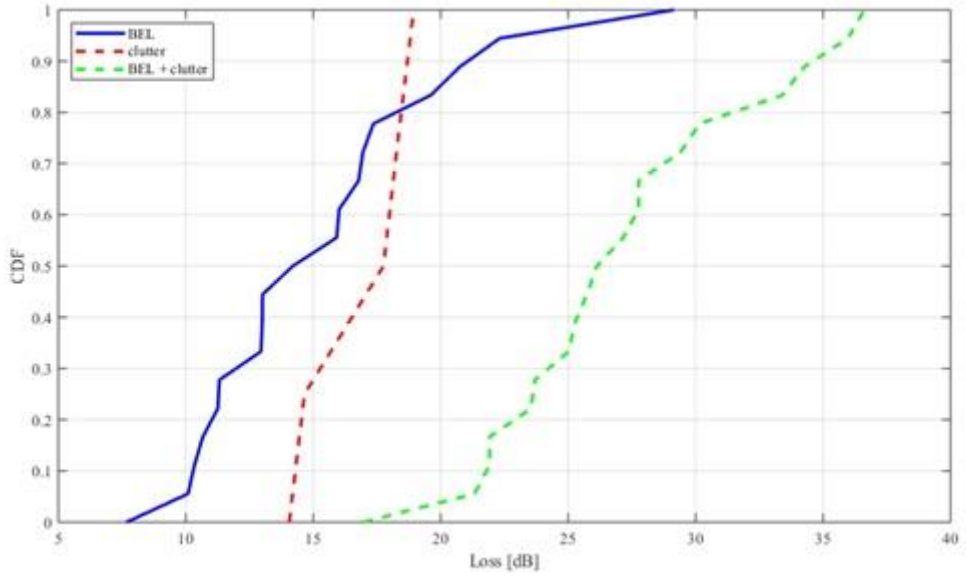

Table 109 shows the measured clutter loss, BEL and BEL+clutter loss values at 3 GHz and 24 GHz. The difference is compared with the BEL+clutter loss measured by combining clutter loss and BEL. The sum of the clutter loss and BEL inside building is 23.36 dB and 31.94 dB at 3 GHz and 24 GHz respectively. In the building, the BEL+clutter loss difference at 3 GHz is −4.19 dB and that at 24 GHz is 5.82 dB.

TABLE 109

Median value of clutter loss, BEL and BEL+clutter loss

	Contents	3 GHz	24 GHz
①	Clutter loss	10.24 dB	17.74 dB
②	BEL	13.12 dB	14.20 dB
③	BEL+Clutter loss	27.55 dB	26.12 dB
① + ② - ③	Difference	−4.19 dB	5.82 dB

38.4 Summary of the results

This study was conducted to examine whether the sum of the clutter loss and BEL in a suburban environment was equal to the total excess loss and to determine the differences. The satellite model of satellite radio waves was assumed and calculated and compared the clutter loss and BEL at 3 GHz and 24 GHz. The measured received power was calculated by calibrating the parameters of the equipment used and the calculated values were compared. The results showed that the excess loss of clutter loss and BEL was similar to the sum of the clutter loss and BEL.

38.5 References

[1] "Independent and Joint Statistics of Clutter Loss and Building Entry Loss-Initial Measurements", see Document 3K/239, June 2018 for information.

[2] "Prediction of Clutter Loss", Recommendation ITU-R P.2108-0, Geneva, 2017.

[3] "Prediction of Building Entry Loss", Recommendation ITU-R P.2109-0, Geneva, 2017.

39 Combined and independent statistics of clutter loss and building entry loss measurements at 26 GHz[27]

39.0 Introduction

In sharing studies, BEL and clutter loss (CL) are treated as multiplicative, i.e., the overall excess loss would be the sum in dB of the individual losses.

In this section, results of measurements are presented, which characterise BEL and CL separately and BEL over a cluttered path. The results come from three different measurement campaigns in the same site but with different experimental setups summarised in Table 110.

[27] Sharing studies carried out by ITU-R on different agenda items of WRC-19 were based on the text of this Report which was inforce at the time of these activities or at the time which the activity was carried out.

TABLE 110

Measurement campaigns and experimental setups

Campaign	Experimental setup	Losses characterized
Measurements 2019	Durham University Channel sounder	BEL over cluttered path BEL isolated building Clutter loss
Measurements 2018	CW + downconverter	BEL isolated building
Measurements 2017	CW at 26 GHz	Clutter loss

39.1 Measurement campaign 2019

39.1.1 Scenario

The measurements were performed at the JRC site in Ispra, Italy using the multiband, wideband channel sounder of Durham University [3-5]. The site corresponds to the suburban scenario category, with two or three storey buildings having an average building height of 12 metres, parking zones, green areas, squares and office centres. Figure 337 shows the scenario where the measurements were performed.

FIGURE 337

Measurement scenario

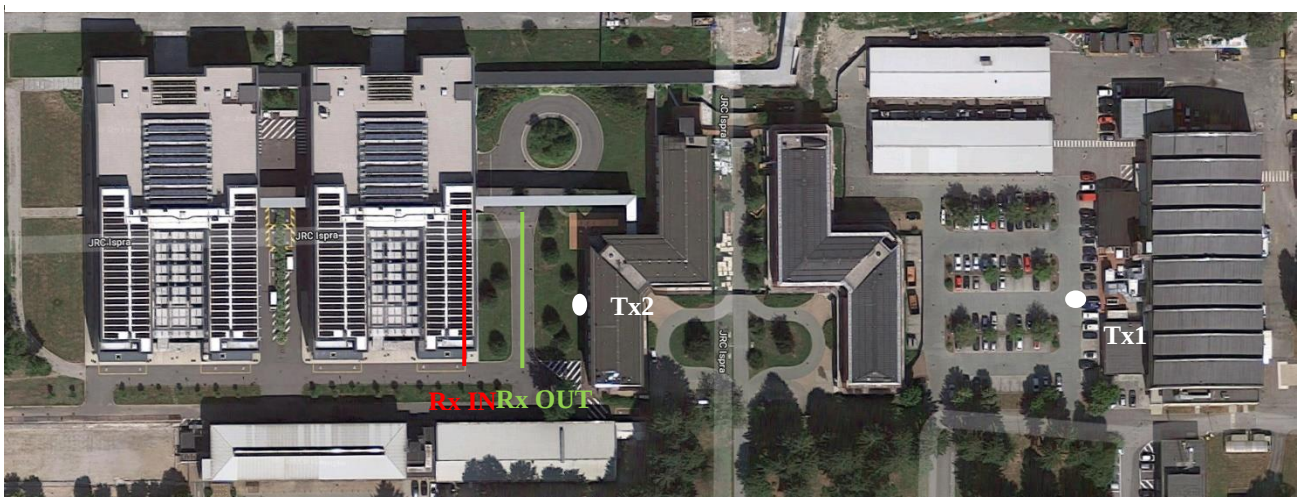

The transmitter used a standard-gain horn antenna, was mounted on a cherry picker at a 25 m height in location *Tx1* and 7 m height in location *Tx2*, as shown in Fig. 338.

The receiver was mounted on a trolley, was fitted with an omnidirectional antenna placed at a 1.5 m height above ground level. It was used to record data inside a modern building, *Rx IN* path, where measurements were done in the offices and in the corridor closest to the illuminated façade of the building. Measurements were performed outside the building on a street canyon, *Rx OUT* path, registering data every 1 m.

FIGURE 338

Tx1 position, Tx2 position and Rx IN path with receiver on the trolley

39.1.2 Location of the measurement points

Having the accurate location of the receiver measurement points and transmitter position is very important for calculating distances, azimuth and elevation angles. Especially when the transmitter is at close distances to the receiver. These parameters are then used in the data processing for calculating free space loss and antenna gain corrections, to finally obtain BEL and CL.

Due to the presence of nearby buildings and trees, the use of a single GNSS receiver provided poor accuracy in the position. To improve the position accuracy, a total station (Leica PTS1200) was used to measure vertical and horizontal angles as well as the lope distance from the instrument to a given point. To coordinate the measurements, the station was set over a known point and its orientation was fixed using an additional known point (back sight). These reference points were selected in open-sky areas and their coordinates were determined beforehand using GNSS data. About 15 minutes of data were collected at each of these points using a triple-frequency multi-constellation GNSS receiver (AsteRx-m2 UAS), with a geodetic grade antenna (Trimble Zephyr 3 base antenna). The data were then processed in RTK mode using as a base station a receiver installed on the highest building on the JRC Ispra campus, enabling to determine the coordinate of these points with centimetre-level accuracy.

Using these points to set up the total station and the back sight, it was then possible to coordinate the points of measurements, even between buildings as illustrated in Fig. 339.

FIGURE 339

Survey results

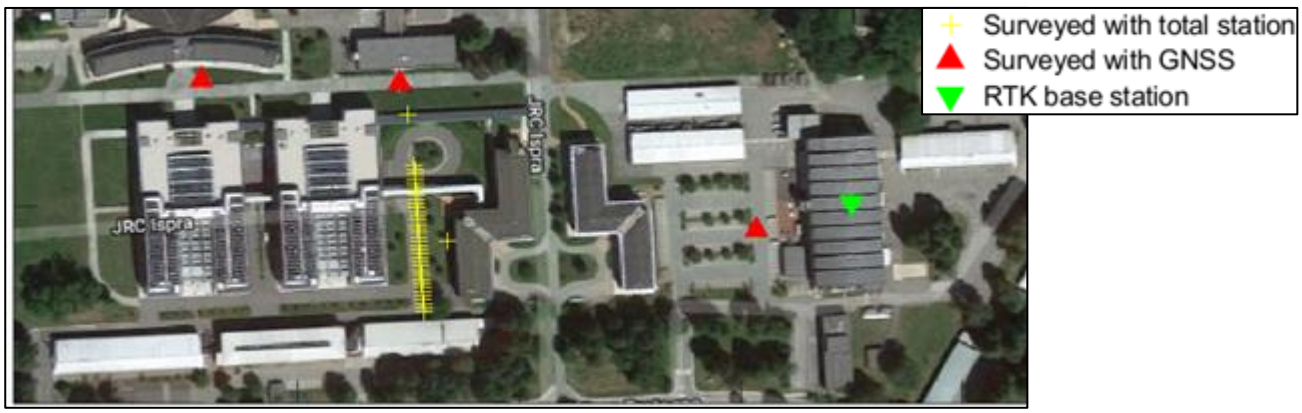

39.1.3 Experimental setup

The measurements were carried out with a Durham University channel sounder at 26 GHz [3].

The Durham sounder uses the chirp (FMCW) technique with heterodyne detection and covers a number of frequency bands with 3 GHz bandwidth between 25.5-28.5 GHz, 6 GHz bandwidth in the 50-75 GHz band and a maximum of 9 GHz in the 60-90 GHz band. The time delay window is on the order of 819.2 μs, which gives 1.2 kHz Doppler coverage for a single input single output configuration. Configurations in the 25.5-28.5 GHz bands include eight transmit by eight receive. To conduct the current measurements, a new single channel RF head was set up for transmission with a high gain power amplifier of 40 dB giving an output power of 30 dBm and a standard horn antenna with 18 dB gain and a 3 dB beamwidth of 20°. At the receiver, a single channel receiver was used with a 30 dB gain LNA for the clutter loss measurements and a 56 dB gain LNA for the clutter and building entry loss measurements. The receive antenna was omni-directional in all the measurements except for the combined clutter and building entry loss measurements.

The measurements were conducted with a 3 GHz bandwidth, and processed with a 2 GHz bandwidth, to obtain power delay profiles (PDP). Figure 4 shows examples of PDP. Each PDP was then used to estimate the noise floor and a threshold above the noise floor was set and then the received power was estimated from the PDP. Only PDPs, which met a minimum of 10 dB SNR, were used in the estimated power. Calibration files were obtained over the air for distances between 25 m to 45 m in 5 m steps in a line of sight (LOS) scenario in a non-cluttered environment. The received power at these distances was then compared to free space loss to determine the linearity of the sounder and the overall calibration factor. For example, at 30 m and 40 m distances, the free space loss at 26 GHz is 90.28 dB and 92.78 dB respectively. The received power with the sounder was -36.7 dB and -39.1 dB, which gives a 2.4 dB difference in comparison to a 2.5 dB theoretical value which is difference of 0.1 dB.

These files were then used to calibrate the received power and the corresponding excess loss. In all scenarios, the equivalent isotropic radiated power, e.i.r.p. was 48 dBm. Table 111 gives the configuration used in the different scenarios.

TABLE 111

Configuration of measurements

Tx antenna	Rx antenna	LNA	Measurement scenario
horn	Omni	No LNA	Outside building for BEL
			Outside building for clutter loss
		LNA 50	Inside building for BEL
	horn	LNA 50	Inside building with clutter

FIGURE 340

Examples of PDP (a) Clutter loss, (b) BEL on ground floor

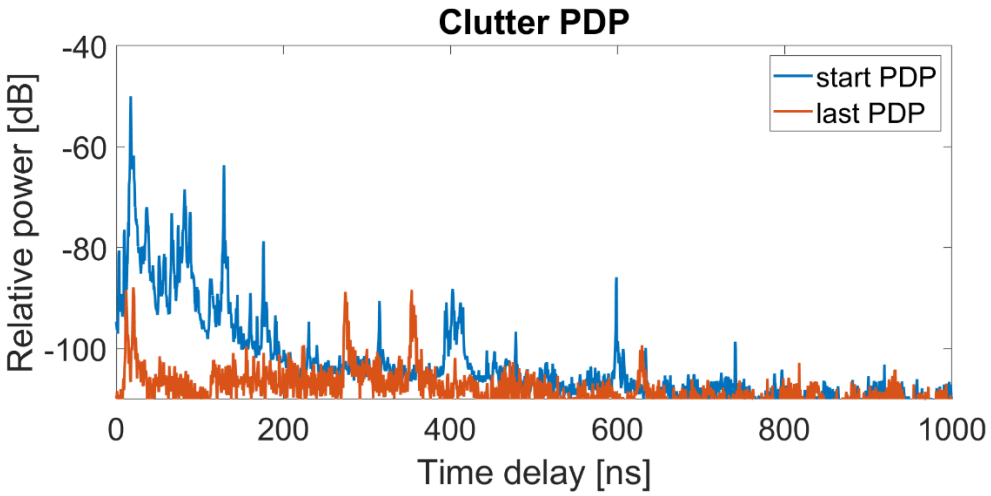

(a) PDP for the start and last locations

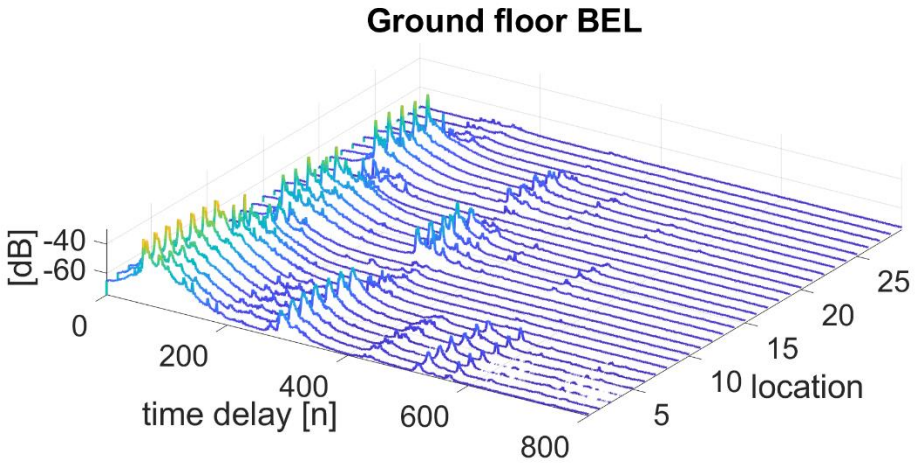

(b) PDP for all the locations on the ground floor

39.1.4 Building entry loss over cluttered path measurements

To characterize building entry loss over a cluttered path, the transmitter was placed at Tx1 position on a cherry picker at 25 m height. There was no line-of-sight between the outdoor terminal and the face of the building under test.

First, measurements were performed in *Rx OUT* path every 1 m, to characterize the clutter loss. Then, measurements were carried out inside the building on different floors inside the offices and corridor closest to the illuminated façade of the building, *Rx IN*, to characterize the building entry loss over a cluttered path.

Figure 341 shows the side view of the scenario. Figure 342 shows the scenario top view with the 3 dB antenna beam width coverage plotted in orange. It can be observed that *Rx OUT* and *Rx IN* paths were inside the 3 dB beam width, and that the measurements done outside were in front of the offices used in the measurement inside.

Figure 343 shows the *Rx IN* path, with the measurement locations on the offices and corridor closest to the illuminated façade of the building and the *Rx OUT* path just in front of the offices used for the inside measurements.

FIGURE 341

Scenario side view

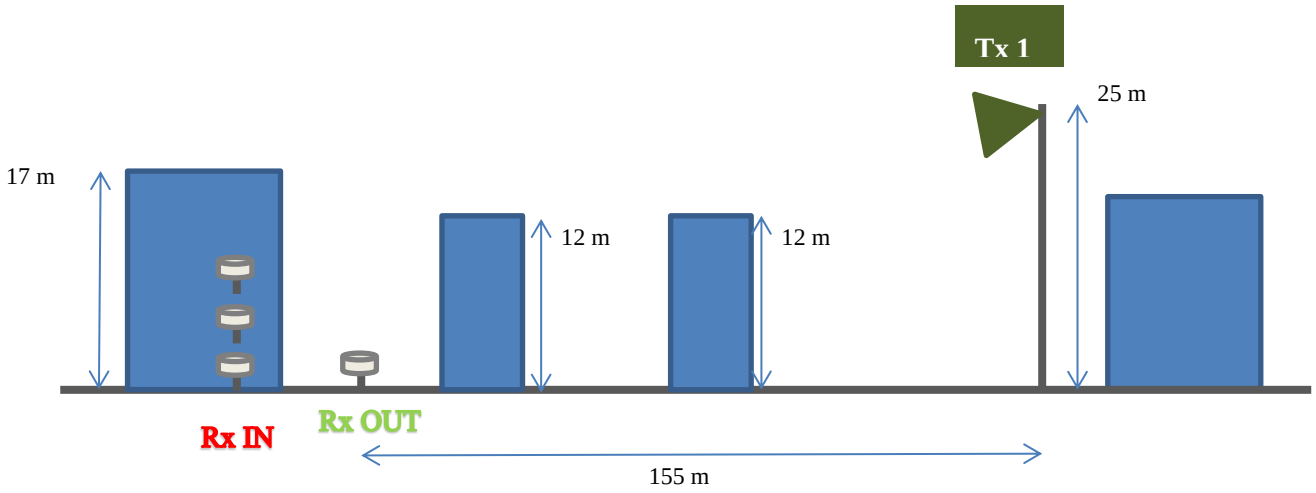

FIGURE 342

Scenario top view with 3 dB antenna beam width coverage

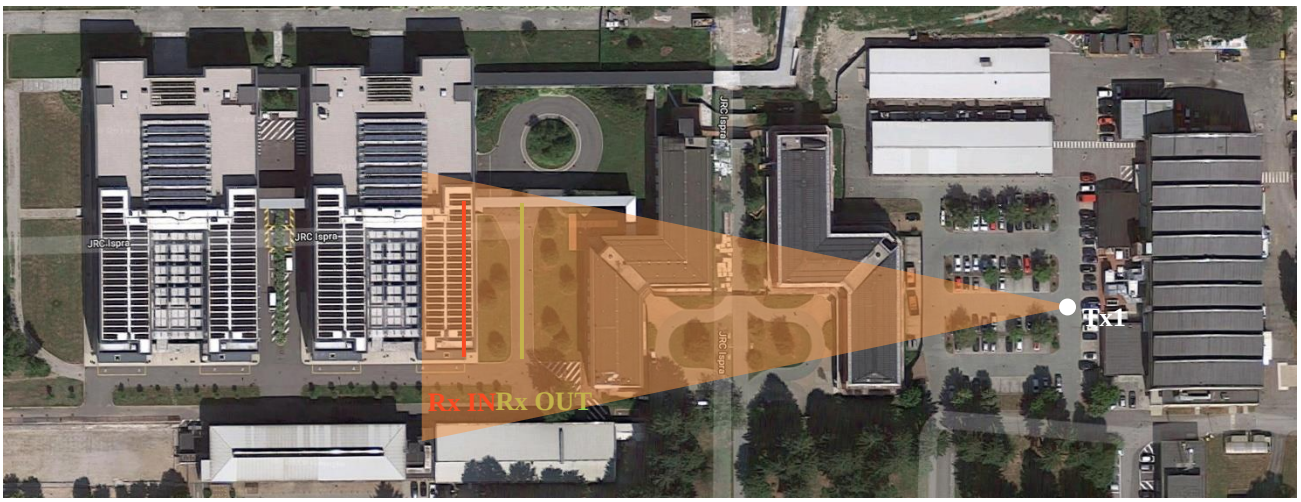

FIGURE 343

Rx IN path in ground floor, Rx OUT in front of offices

39.1.5 Building entry loss isolated building measurements

To characterize the building entry loss effect alone, the transmitter was placed at Tx2 position on the cherry picker with a height of 7 m. The outdoor terminal is in LOS with the face of the building under test. The distance from the transmitter to the building is 30 m.

First, measurements were performed inside the building on different floors, *Rx IN*. Then, measurements were performed in *Rx OUT* path to obtain LOS values. Measurements were carried out in the same locations as in building entry loss over cluttered path case, shown in Fig. 343.

Figure 344 shows the side view of the scenario. Figure 345 shows the scenario top view with the 3 dB antenna beam width coverage plotted in orange. It can be observed that part of *Rx OUT* and *Rx IN* paths were not inside the 3 dB beam width. In this case, the transmitter antenna gain compensation was taking into account when processing the data.

FIGURE 344

Scenario side view

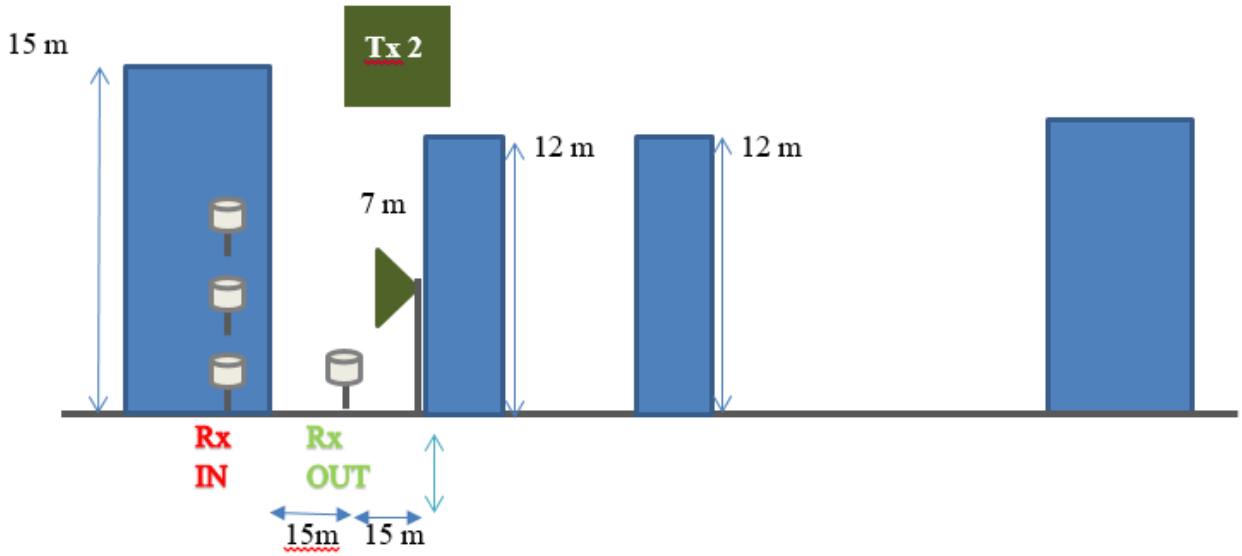

FIGURE 345

Scenario top view with 3 dB antenna beam width coverage

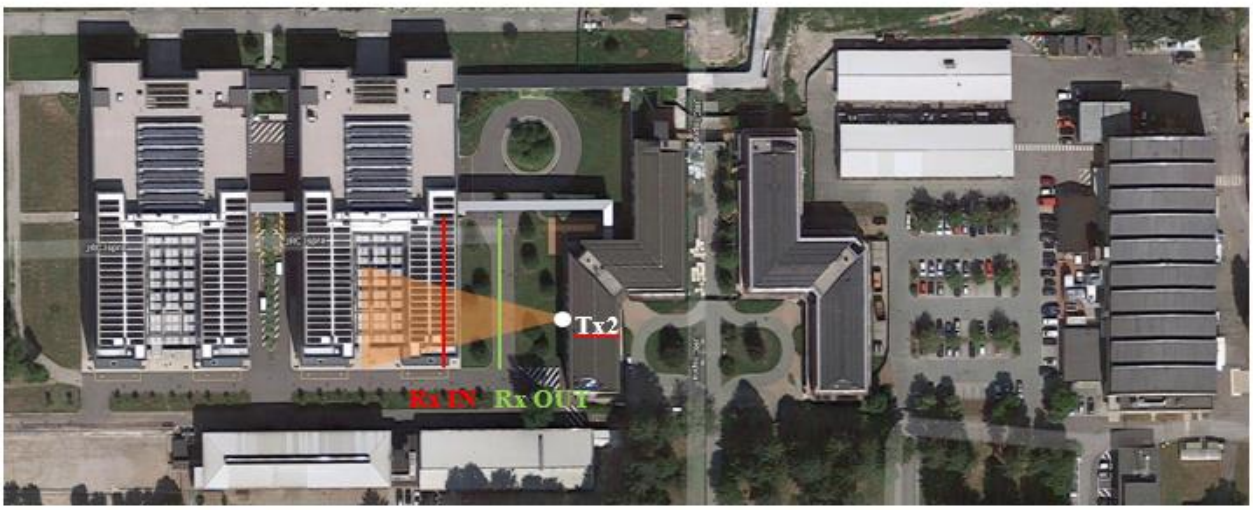

39.1.6 Data analysis

The data were analysed to estimate the building entry loss and clutter loss.

Building entry loss was estimated according to the building-entry-loss recommendation, Recommendation ITU-R P.2140.

Clutter loss was estimated using the agreed methodology and the definition given in Recommendation ITU-R P.2108.

39.1.6.1 Building entry loss analysis

Building entry loss was estimated as the difference between the spatial median of the signal level outside the illuminated face of a building and the spatial median of the signal level inside the building.

For the BEL where the transmitter was located outside the building in LOS, it was estimated by taking the difference between the spatial median of the signal level outside the illuminated face of the building and the spatial median of the signal level inside the building. Similarly, for the BEL over the cluttered path in NLOS, the spatial median of the measurements taken outside the building was subtracted from the spatial median inside the building.

The BEL was estimated first without considering the transmitter antenna gain compensation, and then considering the compensation.

Figures 346 and 347 correspond to the non-compensated transmitter antenna gain.

Figure 346 shows the CDF of the received power for outside the building from both *TX1*, over the cluttered path, and *TX2*.

Figure 347 shows the building entry loss from TX2 for each floor and for the three floors combined.

Figure 348 shows the building entry loss from TX1, over the cluttered path, for each floor and for the three floors combined.

The CDFs in Fig. 349 median values are 45.8 dB for TX2 and 44 dB for TX1.

Table 112 shows the BEL estimated from both methods, outdoor terminal in LOS and NLOS, and also without and with the compensation for the transmitter antenna gain. It can be observed that the results are very close: there is a difference of 1.8 dB without Gtx compensation and 0.3 dB with Gtx compensation. This indicates that for the estimation of building entry loss either method is valid, i.e. the outdoor terminal is in LOS or NLOS with the face of the building under test, and processing the data without and with Gtx compensation, as long as measurements outside of the building are just in front of the offices used for the inside measurements.

TABLE 112

BEL from cluttered path and isolated building

	No Gtx compensation	**Gtx compensation**
BEL over cluttered path	44.03 dB	42.6 dB
BEL	45.8 dB	42.9 dB

FIGURE 346

CDF of received power outside the building from TX1 (over cluttered path) and TX2 (BEL)

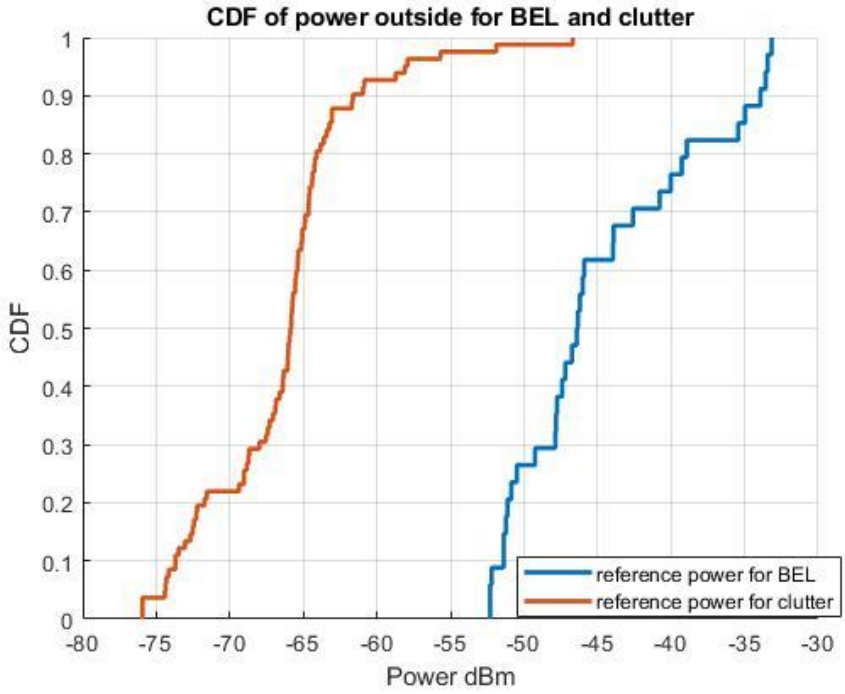

FIGURE 347

BEL estimated from TX2

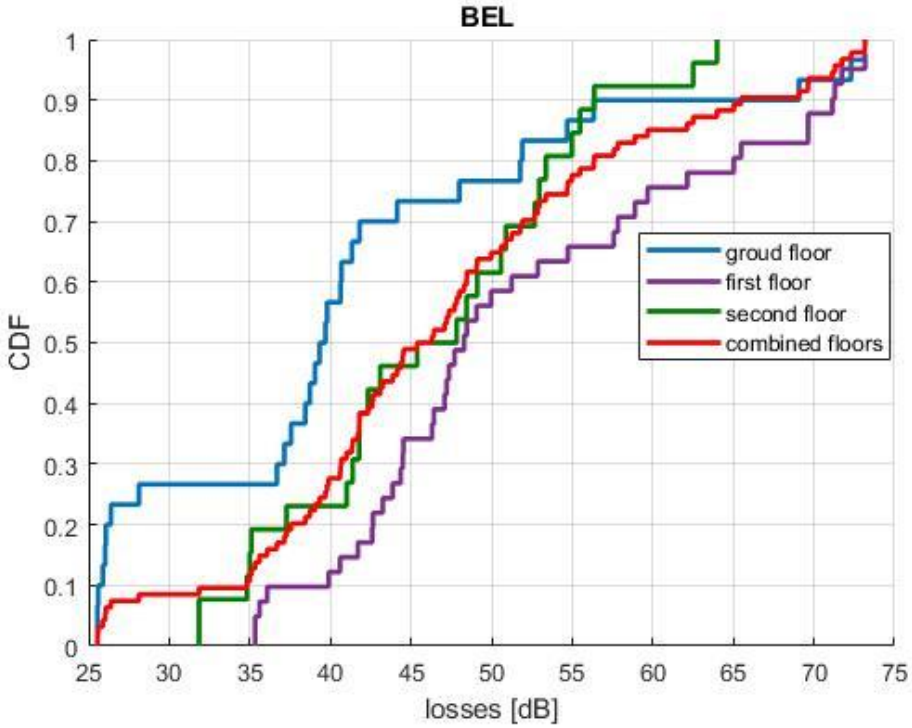

FIGURE 348

BEL estimated from TX1 (over cluttered path)

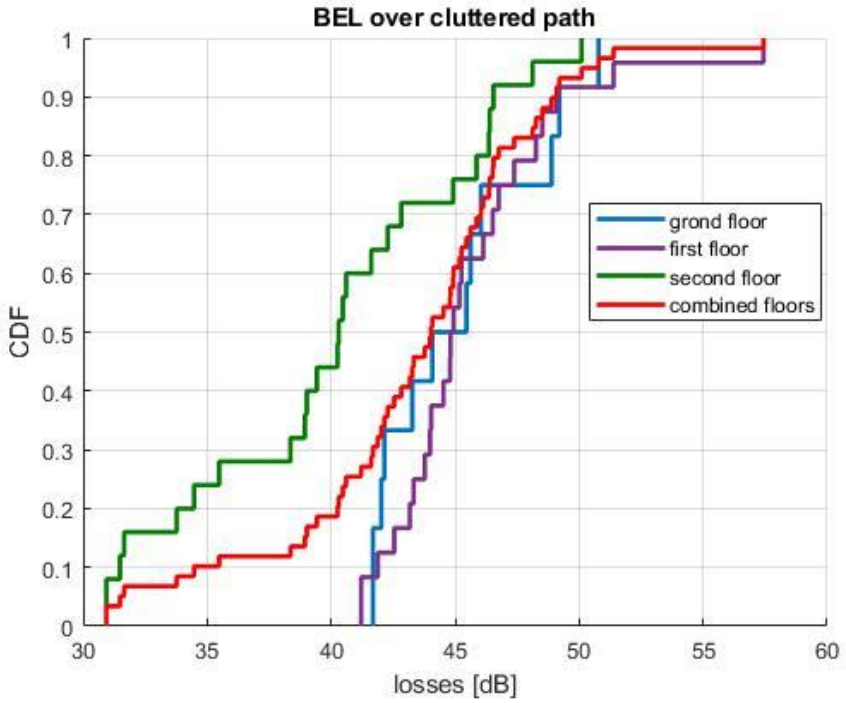

FIGURE 349

BEL estimated from TX1(clutter) and TX2 (BEL)

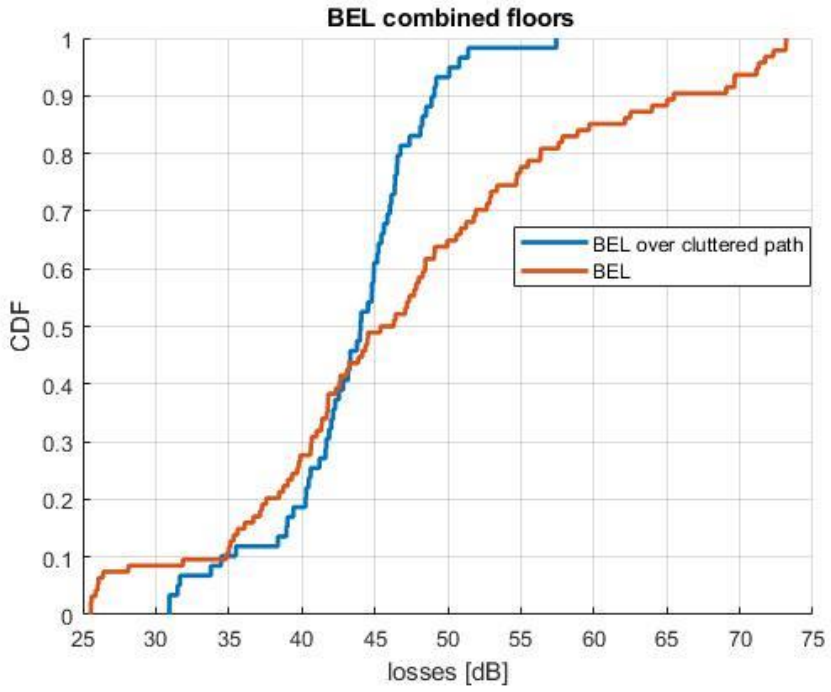

39.1.6.2 Clutter loss analysis

The data were used to estimate the clutter loss by taking the difference between the theoretically predicted free space basic transmission loss, (Recommendation ITU-R P.525) and the measured basic transmission loss.

Figure 350 shows the clutter loss with respect to elevation angle.

Figure 351 displays the CDF of the clutter loss, which has a median loss value of 18 dB.

FIGURE 350

Clutter loss from 2019 measurements

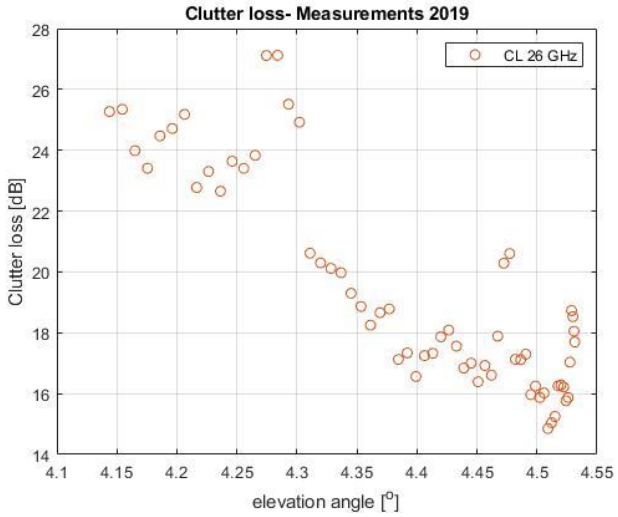

FIGURE 351

Clutter loss CDF

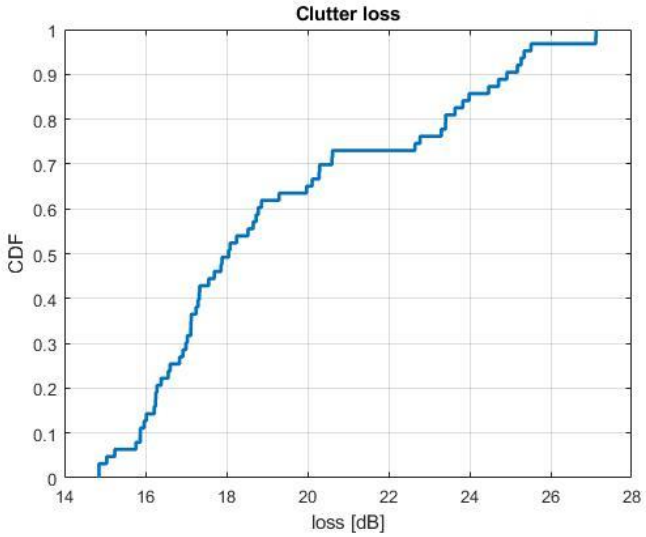

39.2 BEL from 2018 experimental campaign

During a previous campaign, BEL measurements were performed by placing the transmitter at 100 m far from the building, and at 25 m height, as it is shown in Fig. 352. The building used for the measurements in 2018, is a twin of the building used in 2019, with the same construction materials, same inside distribution, but in 2018 the *Tx3* was placed on the side where there were no buildings.

The receiver registered first measurements outside the building, following *RX OUT* path, and then inside the building in different floors in offices and corridor closest to the illuminated façade of the building, *RX IN* as shown in Fig. 353. *Rx OUT* path just is in front of the offices used for the inside measurements.

FIGURE 352

Scenario top view for BEL measurements 2018

FIGURE 353

Tx on cherry picker and receiver on the trolley

FIGURE 354

Experimental measurement setup

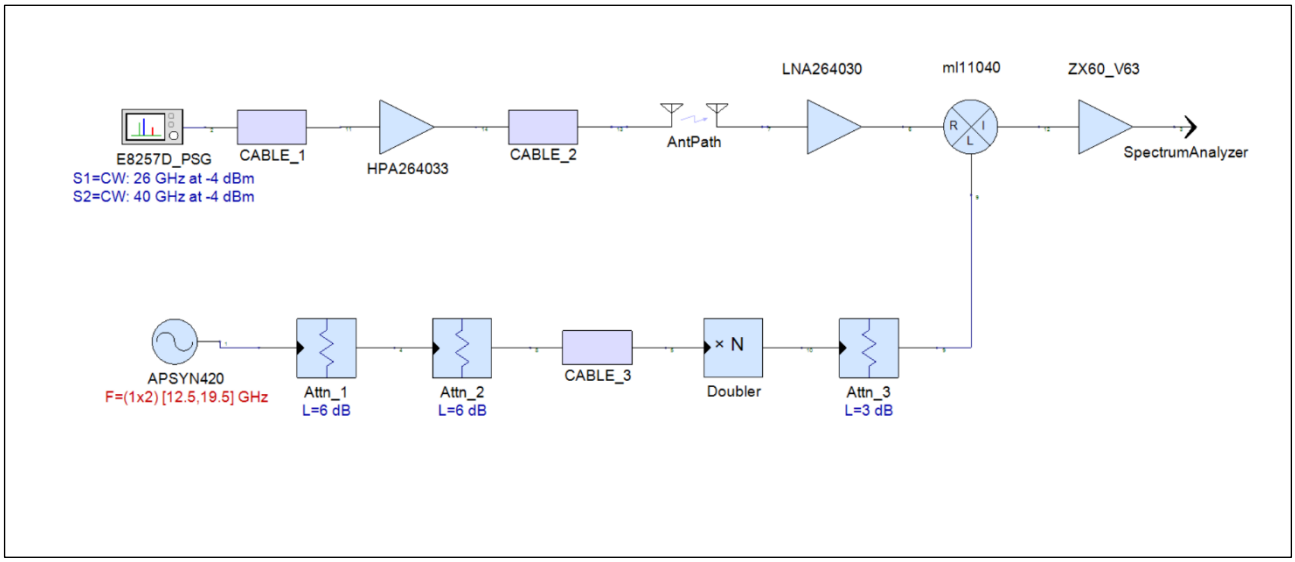

For these measurements, the measurement setup shown in Fig. 354 was used. The transmitter side, was mounted on a cherry picker. The transmitter comprises a signal generator delivering a continuous wave at 26 GHz. Its output signal, which was set to −4 dBm feeds a high power amplifier of 40 dB gain and the same standard-gain horn antenna as in the measurement campaign in 2019 through low loss coaxial cables. The e.i.r.p. was 49 dBm.

The receiver was mounted on a trolley at 1.5 m height. The receiver side, includes a Ka band sub-harmonic down converter feeding a spectrum analyser. The Rx consists of an omni-directional antenna followed by a low noise amplifier connected to the RF port (R) of a double-balanced mixer. Its local oscillator is generated by a frequency synthesizer set to 12.5 GHz followed by a frequency doubler. A set of attenuators adapt the amplitude range of the different components. By setting the reference frequency to 25 GHz, an intermediate frequency 1 GHz is obtained. The intermediate frequency port (I) is connected to a low noise amplifier whose output forms the intermediate frequency output (IF out) of the down converter. Finally, the IF out is connected to a spectrum analyser.

Calibration measurements were carried out in the anechoic chamber to verify and check the operating range of all components, to estimate the cables and connector losses, the overall calibration factor and the dynamic range of the system. The e.i.r.p., minimum received power at the receiver, *Prx*, dynamic range and calibration factor, *CF*, values showed in Table 113.

TABLE 113

e.i.r.p., Prx, Dynamic range values

Frequency (GHz)	e.i.r.p. (dBm)	Grx (dBm)	Prx minimum (dBm)	Dynamic range (dB)	Calibration factor (dB)
26	49	44.1	−148.9	197.9	46.9

At each location, 30 measurements were recorded and the median of the measurements was calculated.

FIGURE 355

CDF of power measured outside and inside

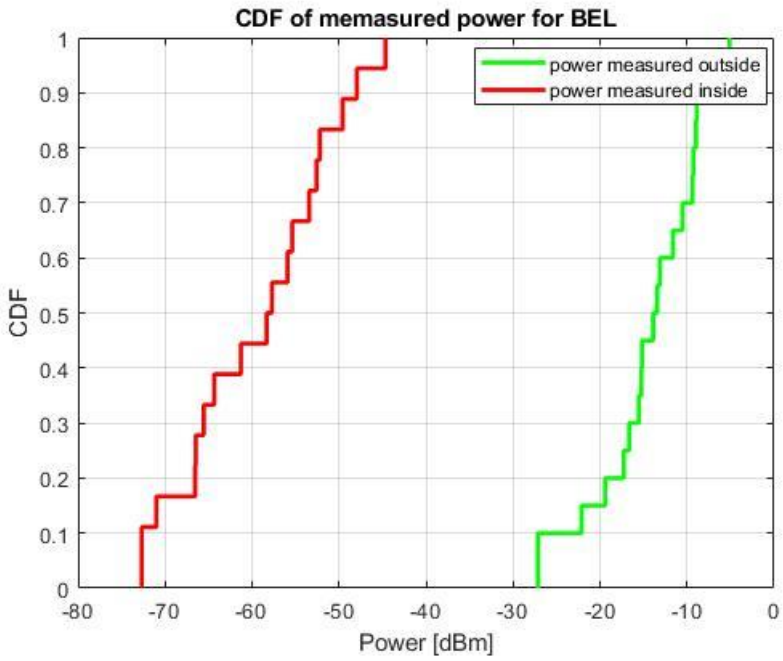

The BEL was estimated by taking the difference between the spatial median of the signal level outside the illuminated face of the building and the spatial median of the signal level inside the building. The CDF of the measured power is shown in Fig. 355.

The median value of the measurements taken outside the building is −13.43 dBm, and the median value of the measurements taken inside the building is −57.7 dBm. The building entry loss is 44.27 dB. In this case, the compensation of the transmitter antenna gain was not applied.

TABLE 114

BEL from 2018 measurements

	Outside building	**Inside building**
Median value (dBm)	−13.43	−57.7
BEL (dB)	44.27	

39.3 Clutter loss from 2017 experimental campaign

JRC presented in Geneva meeting in 2017 the first findings of a measurement campaign carried out in 2017 inside the Ispra site to characterize clutter loss at 26 GHz and 40 GHz.

The data from the same experimental campaign were reanalysed following the agreed methodology and the definition given in Recommendation ITU-R P.2108.

Figure 356 shows a Google picture with a top view of the area where the measurements were done. Several paths were identified for the measurements. All the paths include buildings with a mean height of 12 metres between the transmitter and the receiver. Paths are marked with different colours in the picture: light blue (Path1), green (Path2) and red (Path3). The transmitter position is marked in the picture with a dark blue square.

FIGURE 356

Scenario top view for clutter loss measurements 2017

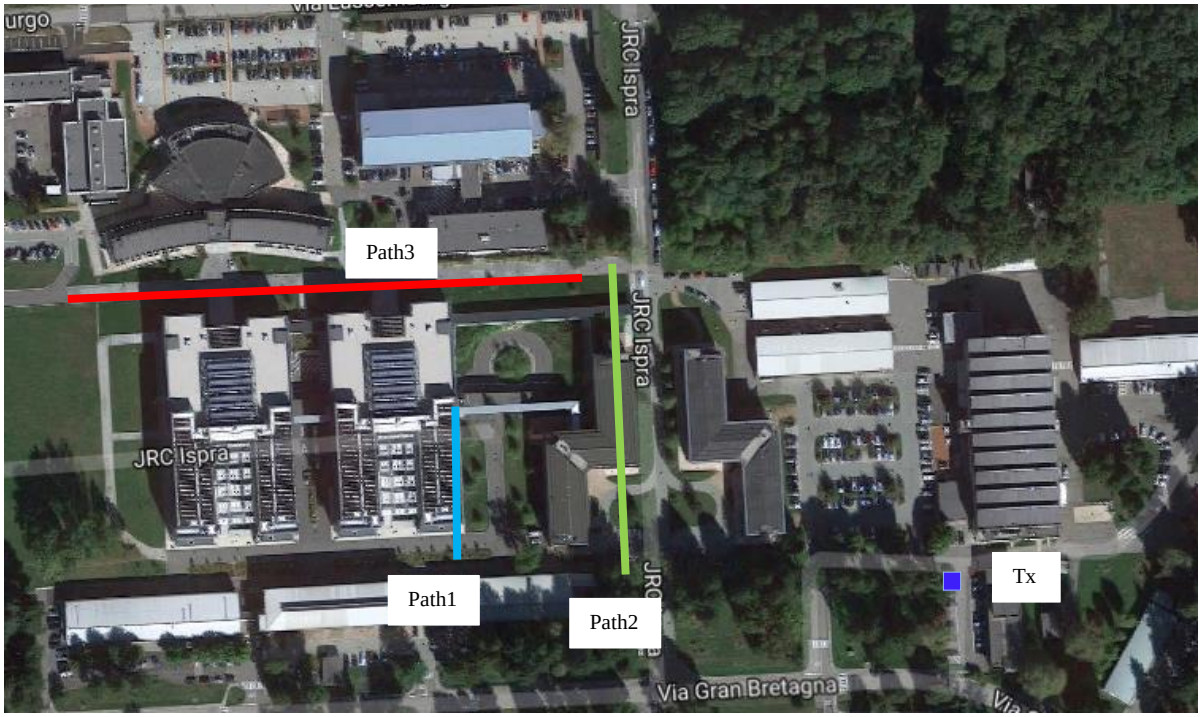

The transmitter (Tx) used was the same as in the measurements 2018. It was installed on an adjustable height mast on the roof of a building. Transmit antenna heights of 15 m and 22 m above ground level were used during the measurements.

The Tx antenna was tilted to point towards the measurement location to ensure it remains inside the main beam of the tx antenna.

The receiver, Rx, was mounted on a trolley, with an omnidirectional antenna at a height of 1.5 m. Measurements were registered every 4 metres. At each position, around 30 measurements were taken.

FIGURE 357

Measurement set up

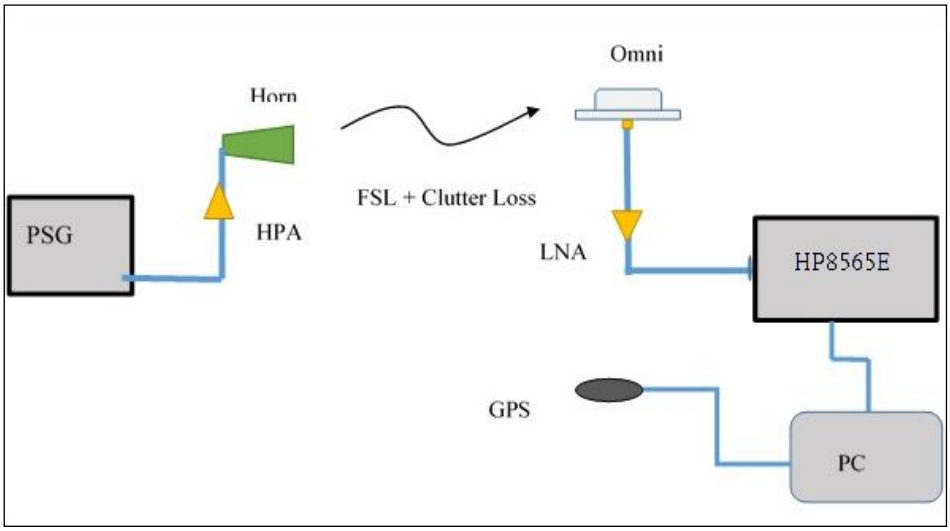

The measurement setup is shown in Fig. 357.

The transmitter used a signal generator for transmitting a CW, a high power amplifies with 40 dB gain and a standard-gain horn antenna with 18 dB gain and a 3 dB bandwidth of 20°.

The receiver's chain consists of: omnidirectional antenna, a low noise amplifier with 30 dB, a spectrum analyser and a GPS receiver connected to a laptop to register the measured data and the position of the receiver.

Calibration measurements were carried out in the anechoic chamber to verify and check the operating range of all components, to estimate the cables and connector losses, the overall calibration factor and the dynamic range of the system. The equivalent isotropic radiated power, e.i.r.p., minimum received power at the receiver, *Prx*, dynamic range and calibration factor, *CF*, values showed in Table 115.

TABLE 115

e.i.r.p., Prx, Dynamic range values

Frequency (GHz)	e.i.r.p. (dBm)	Prx minimum (dBm)	Dynamic range (dB)	Calibration factor (dB)
26	48.2	−124.5	172.7	74.7

Range distances covered during the measurements were between 120 m and 350 metres.

Figure 358 shows the clutter loss with respect to elevation angle for the 26 GHz for measurements from 2017 in blue, and 2019 in red. For both measurements, compensation of transmitter antenna gain was applied.

As in 2017, more paths had been measured, and two different heights had been used for the Tx, 15 m and 22 m, and estimated the clutter loss for 0° to 4.5° elevation angle.

In 2019, only a single path was measured with only one height for the Tx, 25 m, obtaining only clutter loss values from 4.1° to 4.55°.

If clutter loss from the two different campaigns is compared for the elevation angles 4.1° to 4.55°, median clutter loss values of 18 dB are obtained, as shown in Table 116.

TABLE 116

Clutter loss 2017 and 2019

Measurements	Median CL (4.1°-4.55°)
2019	18
2017	18.21

FIGURE 358

Clutter loss measurements 2019 and 2017

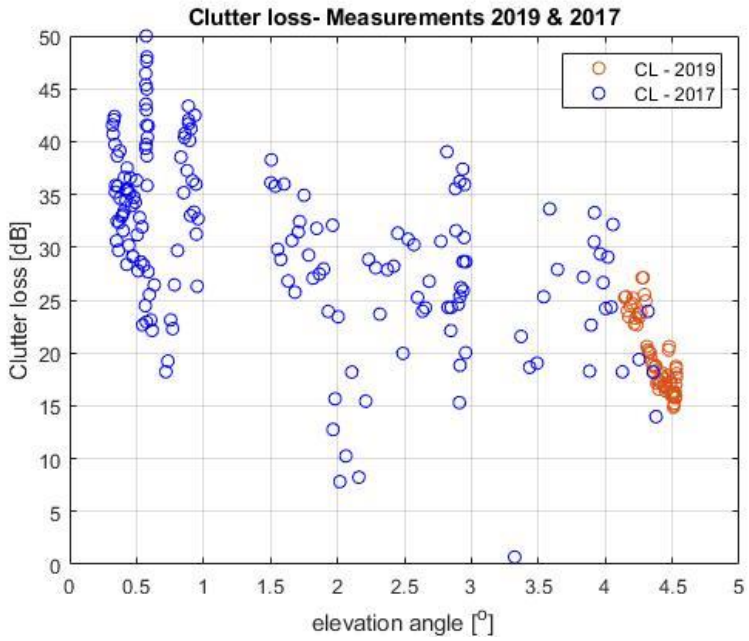

39.4 Summary of the results

Data sets at 26 GHz from three different measurement campaigns in the same site but with different experimental setups were used to characterize clutter loss, building entry loss in isolated building and building entry loss over a cluttered path.

TABLE 117

Measurement campaigns, experimental setups and results

Campaign	Experimental setup	Losses characterized	Measured values [dB]	
			No Gtx correction	Gtx correction
Measurements 2019	Durham University Channel sounder	BEL over cluttered path, NLOS	44.03	42.6
		BEL isolated building, LOS	45.8	42.9
		Clutter loss	18.07	18.07
Measurements 2018	CW + downconverter	BEL isolated building, LOS	44.27	
Measurements 2017	CW at 26 GHz	Clutter loss		18.21

Measurements were performed to estimate building entry loss by placing the transmitter: in front of the building on a street canyon, in front of the building on an open field, or at a high level in a cluttered environment with NLOS.

The data were processed to estimate median values of the building entry loss. From the three sets of data and a difference of less than 1.8 dB between the BEL estimations was found between the measurements performed in 2018 and 2019.

The difference between the estimation of BEL from a transmitter placed outside in LOS to the façade of the building or from a transmitter above a cluttered environment with NLOS gave values which differ by less than 1.8 dB which indicates that either method can be used for estimating the BEL. In all cases, measurements done outside have to be in front of the offices used in the measurement inside. Data were processed with and without transmitter antenna gain compensation, and results were very similar.

The clutter loss estimated from two different data sets are 18 dB, which confirms that both experimental setups and the methodology are valid for this kind of measurements.

With these results, it can be concluded that at 26 GHz, BEL and CL can be treated as multiplicative, i.e. the overall excess loss is the sum in dB of the individual losses.

39.5 References

[1] Recommendation ITU-R P.2109 – Prediction of building entry loss

[2] Recommendation ITU-R P.2108 – Prediction of clutter loss

[3] S. Salous, “Radio Propagation Measurement and Channel modelling”, Wiley

[4] Xavier Raimundo, Saied El-Faitori, and Sana Salous, Multi-band outdoor measurements in a residential environment for 5G networks, European Conference on Antennas and Propagation, EUCAP 2018

[5] Jack Lewis Towers, Sana Salous, Xavier Raimundo, and Adnan Cheema, Building entry loss for traditional and thermally efficient houses between 0.4 and 73 GHz, European Conference on Antennas and Propagation, EUCAP 2018

[6] B. Montenegro-Villacieros *et al.*, “Clutter loss measurements in suburban environment at 26 GHz and 40 GHz”, European Conference on Antennas and Propagation, EuCAP 2018

Annex 1

BEL in point-to-area applications below 3 GHz

The following information has been found helpful in planning broadcast and other point-to-area radio services.

For *indoor reception* two important parameters must also be taken into account. The first is the BEL and the second is the variation of the BEL due to different building materials. The standard deviations, given below, take into account the large spread of BEL but do not include the location variability within different buildings. It should be noted that there is limited reliable information and measurement results about BEL. Provisionally, BEL values that may be used are given in Table 118.

TABLE 118

BEL[(1)], L_{be}, σ_{be}

F	**Median value, L_{be} (dB)**	**Standard deviation, σ_{be} (dB)**
0.2 GHz	9	3
0.6 GHz	11	6
1.5 GHz	11	6

(1) These values may have to be updated when more experimental data become available.

For frequencies below 0.2 GHz, L_{be} = 9 dB, σ_{be} = 3 dB; for frequencies above 1.5 GHz, L_{be} = 11 dB, σ_{be} = 6 dB. Between 0.2 GHz and 0.6 GHz (and between 0.6 GHz and 1.5 GHz), appropriate values for L_{be} and σ_{be} can be obtained by linear interpolation between the values for L_{be} and σ_{be} given in Table 7 for 0.2 GHz and 0.6 GHz (0.6 GHz and 1.5 GHz).

The field-strength variation for indoor reception is the combined result of the outdoor variation, σ_L, and the variation due to building attenuation, σ_{be}. These variations are likely to be uncorrelated. The standard deviation for indoor reception, σ_i can therefore be calculated by taking the square root of the sum of the squares of the individual standard deviations.

$$\sigma_i = \sqrt{\sigma_L^2 + \sigma_{be}^2} \quad \text{dB} \tag{50}$$

where σ_L is the standard deviation of location variability.

For example, for digital emissions with bandwidth greater than 1 MHz, at VHF, where the signal standard deviations are 5.5 dB and 3 dB respectively, the combined value is 6.3 dB. In Band IV/V, where the signal standard deviations are 5.5 dB and 6 dB, the combined value is 8.1 dB.